Introduction to Dusty Plasma Physics

Series in Plasma Physics

Series Editors:

Professor Peter Stott, CEA Cadarache, France
Professor Hans Wilhelmsson, Chalmers University of Technolgy, Sweden

Other books in the series

The Theory of Photon Acceleration
J T Mendonça

Laser-Aided Diagnostics of Plasmas and Gases
K Muraoka and M Maeda

Reaction–Diffusion Problems in the Physics of Hot Plasmas
H Wilhelmsson and E Lazzaro

The Plasma Boundary of Magnetic Fusion Devices
P C Stangeby

Transport and Structural Formation in Plasmas
K Itoh, S-I Itoh and A Fukuyama

Tokamak Plasmas: A Complex Physical System
B B Kadomstev

Electromagnetic Instabilities in Inhomogeneous Plasma
A B Mikhailovskii

Instabilities in a Confined Plasma
A B Mikhailovskii

Physics of Intense Beams in Plasma
M V Nezlin

Collective Modes in Inhomogeneous Plasma: Kinetic and Advanced Fluid Theory
J Weiland

Forthcoming titles in the series

Microscopic Dynamics of Plasmas and Chaos
D F Escande and Y Elskens

Inertial Confinement Fusion
S Pfalzner

Series in Plasma Physics

Introduction to Dusty Plasma Physics

P K Shukla

Ruhr-Universität Bochum, Germany and Umeå University, Sweden

A A Mamun

Jahangrinagar University, Dhaka, Bangladesh

Institute of Physics Publishing
Bristol and Philadelphia

British Library Cataloguing-in-Publication Data

A catalogue record for this book is available from the British Library.

ISBN 0 7503 0653 X

Library of Congress Cataloging-in-Publication Data are available

Commissioning Editor: John Navas
Production Editor: Simon Laurenson
Production Control: Sarah Plenty
Cover Design: Victoria Le Billon
Marketing Executive: Laura Serratrice

Published by Institute of Physics Publishing, wholly owned by The Institute of Physics, London

Institute of Physics Publishing, Dirac House, Temple Back, Bristol BS1 6BE, UK

US Office: Institute of Physics Publishing, The Public Ledger Building, Suite 1035, 150 South Independence Mall West, Philadelphia, PA 19106, USA

Typeset in LaTeX 2_ε by Text 2 Text, Torquay, Devon
Printed in the UK by MPG Books Ltd, Bodmin, Cornwall

Contents

Preface

This book presents an up-to-date account of collective processes in dusty plasmas. This is a new frontier in applied physics and modern technology. A dusty plasma is a complex system because of the variation of the dust grain charge, mass and size with space and time. It exhibits new and unusual behaviour, and provides a possibility for modified or entirely new collective modes of oscillation, instabilities as well as coherent nonlinear structures. A particularly interesting aspect of a dusty plasma is that it can be strongly coupled, i.e. the interaction potential energy between the dust grains can exceed their kinetic energy. As a result, grain–grain correlations become important; for strong enough coupling, the dust grains can condense into a dusty plasma crystal configuration. It turns out that the dynamics of dust particles produces phenomena on such a long time scale that they can even be seen with the naked eye.

This book is designed for students and scientists who possess a rudimentary working knowledge of wave motions in plasmas and fluids at the graduate level. It can be used for learning and teaching the essentials of dusty plasma physics and its applications to low-temperature laboratory and space environments.

Since the early 1990s there has been a great deal of interest in studying the physics of dusty plasmas which has now become a new discipline in plasma science. A large number of dusty plasma papers has appeared within the ten years following the discovery of dust acoustic waves and dusty plasma crystals. Several conference proceedings have summarized the progress that has been made in dusty plasma research. However, the existing materials on collective processes in dusty plasmas are scattered, and there is a need for their unification. It is, therefore, timely to present an up-to-date, comprehensive and coherent description of dusty plasma physics in the form of an introductory book that, we hope, should be useful to readers who wish to learn and teach its essentials and to familiarize themselves with the progress that has recently been made. This is the objective of the present book.

This book has grown out of the research work on topics on which the authors have spent a considerable amount of time and thought. We have dealt with the basic properties of dusty plasmas, the charging of dust grains and their dynamics under the action of numerous forces, as well as various aspects of collective interactions including waves, linear and nonlinear instabilities, coherent nonlinear structures, new attractive forces, dust crystals, etc. The book is divided into eight chapters covering the above-mentioned topics which have wide-ranging applications to laboratory and space dusty plasmas. CGS units are used throughout the book. The references included here are somewhat selective and designed to be representative of original ideas set forth on a particular theme.

The book is organized as follows. In chapter 1, we start with a rudimentary introduction to dusty plasma physics and point out how this differs from that of the usual electron–ion plasma. Conditions for defining weakly and strongly correlated dusty plasmas are illustrated in terms of the Coulomb coupling parameter. The dust grain charging processes, which are amongst the main ingredients of dusty plasma physics, are described in chapter 2. Numerous forces and dust grain dynamics are examined in chapter 3.

Chapter 4 deals with various types of waves in both unmagnetized and magnetized dusty plasmas. Here, we have focused on low-frequency dust acoustic (DA), dust ion-acoustic (DIA) and dust lattice (DL) waves in an unmagnetized plasma, while a great variety of waves appears when an external magnetic field is applied to a uniform and non-uniform dusty plasma. The dust charge fluctuations provide a novel damping mechanism for the DA and DIA waves. The effects of the plasma boundaries and the dust–neutral as well as the dust–dust interactions on the propagation of the DA and DIA waves are also examined. When the spacing between the dust grains is of the order of the dusty plasma Debye radius, the dust grains interact with each other via the Debye–Hückel repulsive force. In such a situation, there arise DL waves due to lattice vibrations. Theoretically predicted dispersion properties of DA, DIA and DL waves are now experimentally verified. The presence of both a magnetic field and plasma non-uniformities introduces new types of dusty plasma waves, in addition to modifying the existing ion-cyclotron and Alfvén wave dispersion properties.

Chapter 5 presents various instabilities that drive low-frequency waves at non-thermal levels in dusty plasmas. In addition to discussing the well known instabilities in infinite and bounded systems, we also present studies of some new instabilities which involve ionization, the ion drag force, the dust charge gradient, the self-gravitation of dust grains, etc. Furthermore, we have also considered several examples of parametric instabilities in weakly and strongly coupled dusty plasmas.

Chapter 6 is concerned with the electrodynamics and dispersion properties of a dusty plasma containing elongated and rotating dust grains that are of finite size. Expressions for the dust charge and dust current densities are developed by including the dust dipole moment and the dust grain rotation. The dust rotational energy can excite different wave modes. Finally, studies of the dust grain vibration and rotation in the presence of electromagnetic fields are carried out.

Chapter 7 is devoted to coherent nonlinear structures in dusty plasmas. We consider DA and DIA solitons and shocks as well as double layers in an unmagnetized dusty plasma. The coherent nonlinear structures produced by non-Maxwellian trapped particle distributions are also presented. Furthermore, we discuss the topic of self-organization in the form of coherent vortices. The focus is then on the stationary solutions of the nonlinear equations that govern the dynamics of low-frequency electrostatic and electromagnetic dispersive waves in a non-uniform dusty magnetoplasma.

Chapter 8 deals with the formation of dust crystals and the associated attractive forces. The latter can come from overlapping Debye spheres, ion focusing and wakefields, dipole–dipole interactions, and shadowing effects. Also presented are experimental demonstrations of the dust crystal formation and phase transitions in strongly coupled radio-frequency and glow discharges. Some results for the particulate dynamics under microgravity conditions are included as well. Finally, we have discussed the formation of multiple Mach cones in a two-dimensional dusty plasma crystal. Evidently, the dusty plasma crystal opens a new area for the study of strongly coupled Coulomb systems. A detailed study of Coulomb crystal structures is expected to advance the research and growth of an atomic crystal, as well as the analysis of forces acting on them, which is useful for the development of the control of dust in processing plasmas.

We are grateful to Professor Lennart Stenflo and Dr Horst Fichtner who kindly read the entire book and offered valuable suggestions for improvements. We have greatly benefited from many enlightening discussions with a number of physicists including Professors Robert Bingham, Alan Cairns, John Dawson, Umberto de Angelis, Ove Havnes, Asoka Mendis, Frank Melandsø, Jose Tito Mendonça, Gregor Morfill, Mitsuhiro Nambu, Nagesha Rao, David Resendes, Marlene Rosenberg, Mohammed Salimullah, Lennart Stenflo, David Tskhakaya, Ram Varma and Frank Verheest. A A Mamun thanks the Alexander von Humboldt Foundation for financial support. This work could not have been completed without the substantial help and constant encouragement of our wives Ranjana Shukla and Khurshida Khayer Mamun.

P K Shukla and A A Mamun
May 2001

Chapter 1

Introduction

1.1 Historical Background

About 70 years ago Tonks and Langmuir (1929) first coined the term 'plasma' to describe the inner region (remote from the boundaries) of a glowing ionized gas produced by means of an electric discharge in a tube. The term plasma represents a macroscopically neutral gas containing many interacting charged particles (electrons and ions) and neutrals. It is likely that 99% of the matter in our universe (in which the dust is one of the omnipresent ingredients) is in the form of a plasma. Thus, in most cases a plasma coexists with the dust particulates. These particulates may be as large as a micron. They are not neutral, but are charged either negatively or positively depending on their surrounding plasma environments. An admixture of such charged dust or macro-particles, electrons, ions and neutrals forms a 'dusty plasma'.

The history of dusty plasmas is quite old (Mendis 1997). A bright comet observed by our distant ancestors is an excellent cosmic laboratory for the study of dust–plasma interactions and their physical and dynamical consequences. The other manifestations of dust-laden plasmas observed by the ancients would have been the zodiacal light (a triangular glow rising above the horizon shortly after Sunset or before Sunrise), the Orion Nebula (faintly visible to the naked eye as a star in the sword of the hunter in the Orion constellation), the noctilucent clouds (observed at the Earth's polar summer mesopause), etc. An almost incredible number of images of astrophysical objects (e.g. the Eagle Nebula, planetary rings, etc) have recently been obtained by the Hubble Space Telescope and spacecraft.

Observations of dust-laden plasmas in the terrestrial laboratory were also available in the remote past. The fact that an ordinary flame is considered as a plasma may come as a surprise due to the high-level of collisionality within it. However, strictly it is not: what makes it close to being a plasma is the presence of minute ($\sim$100 Å) particles of unburnt carbon (soot). While the yellow light emitted by typical hydrocarbon flames (namely candles) is due to incandescence of these small particulates heated to well over 1000 °C, the thermionic emission of electrons from them elevates the degree of ionization within the flame several orders of magnitude above what is given by the Saha equation for air at that temperature. Thus, it is amazing that the ancients thought of fire as a fourth state of matter (other than earth, water and air), while we have given this designation to a plasma only about 70 years ago.

There are a number of more recent examples of dust-laden plasmas in the terrestrial environments. These are rocket and space shuttle exhausts, thermonuclear fireballs, processing plasmas used in device fabrications (e.g. microchips for computers), dusty plasmas created in laboratories for studying basic collective processes, plasma crystals, etc.

1.2 Characteristics of Dusty Plasmas

A dusty plasma is loosely defined as a normal electron–ion plasma with an additional charged component of micron- or submicron-sized particulates. This extra component of macro-particles increases the complexity of the system even further. This is why a dusty plasma is also referred to as a 'complex plasma'. Dusty plasmas are low-temperature fully or partially ionized electrically conducting gases whose constituents are electrons, ions, charged dust grains and neutral atoms. Dust grains are massive (billions times heavier than the protons) and their sizes range from nanometres to millimetres. Dust grains may be metallic, conducting, or made of ice particulates. The size and shape of dust grains will be different, unless they are man-made. However, when viewed from afar, they can be considered as point charges.

A plasma with dust particles or grains can be termed as either 'dust in a plasma' or 'a dusty plasma' depending on the ordering of a number of characteristic lengths. These are the dust grain radius (r_{d}), the average intergrain distance (a), the plasma Debye radius (λ_{D}) and the dimension of the dusty plasma. The situation $r_{\mathrm{d}} \ll \lambda_{\mathrm{D}} < a$ (in which charged dust particles are considered as a collection of isolated screened grains) corresponds to 'dust in a plasma', while the situation $r_{\mathrm{d}} \ll a < \lambda_{\mathrm{D}}$ (in which charged dust particles participate in the collective behaviour) corresponds to 'a dusty plasma'. When we consider a plasma with isolated dust grains ($a \gg \lambda_{\mathrm{D}}$), we should take into account the local plasma inhomogeneities. On the other hand, when we consider the opposite situation ($a \ll \lambda_{\mathrm{D}}$), we should treat dust grains as massive charged particles similar to multiply charged negative or positive ions. However, in studies of collective dusty plasma behaviour, we should also take into account the dust particle charging processes (which we describe in chapter 2). The basic differences between a dusty plasma and an electron–ion (or multi-ion) plasma are pointed out in table 1.1. The table shows that there exists some distribution for the dust grain charge–mass ratio ($q_{\mathrm{d}}/m_{\mathrm{d}}$). The interaction between dust grains is screened by the background electrons and ions. The presence of charged dust grains does not only modify the existing low-frequency waves

Table 1.1. The basic differences between electron–ion and dusty plasmas.

Characteristics	Electron–ion plasma	Dusty plasma
Quasi-neutrality condition	$n_{\mathrm{e}0} = Z_{\mathrm{i}} n_{\mathrm{i}0}$	$Z_{\mathrm{d}} n_{\mathrm{d}0} + n_{\mathrm{e}0} = Z_{\mathrm{i}} n_{\mathrm{i}0}$
Massive particle charge	$q_{\mathrm{i}} = Z_{\mathrm{i}} e$	$\lvert q_{\mathrm{d}} \rvert = Z_{\mathrm{d}} e \gg q_{\mathrm{i}}$
Charge dynamics	$q_{\mathrm{i}} =$ constant	$\partial q_{\mathrm{d}}/\partial t =$ net current
Massive particle mass	m_{i}	$m_{\mathrm{d}} \gg m_{\mathrm{i}}$
Plasma frequency	ω_{pi}	$\omega_{\mathrm{pd}} \ll \omega_{\mathrm{pi}}$
Debye radius	λ_{De}	$\lambda_{\mathrm{Di}} \ll \lambda_{\mathrm{De}}$
Particle size	uniform	dust size distribution
$\boldsymbol{E} \times \boldsymbol{B}_0$ particle drift	ion drift at low B_0	dust drift at high B_0
Linear waves	IAW, LHW, etc	DIAW, DAW, etc
Nonlinear effects	IA solitons/shocks	DA/DIA solitons/shocks
Interaction	repulsive only	attractive between grains
Crystallization	no crystallization	dust crystallization
Phase transition	no phase transition	phase transition

(e.g. ion-acoustic waves (IAW), lower hybrid waves (LHW), ion-acoustic (IA) solitons/shocks, etc), but also introduces new types of low-frequency dust-related waves (e.g. dust acoustic waves (DAW), dust IA waves (DIAW), dust ion-acoustic (DIA) solitons/shocks, dust acoustic (DA) solitons/shocks, etc) and associated instabilities (to be described in chapters 4–7). To understand the characteristics of a dusty plasma properly, we have to re-examine some basic characteristics, such as macroscopic neutrality, Debye shielding, characteristic frequencies, Coulomb coupling parameter, etc. In the following few sections, we shall elaborate these basic characteristics and numerous notations.

1.2.1 Macroscopic neutrality

When no external disturbance is present, like an electron–ion plasma a dusty plasma is also macroscopically neutral. This means that in an equilibrium with no external forces present, the net resulting electric charge in a dusty plasma is zero. Therefore, the equilibrium charge neutrality condition in a dusty plasma reads

$$q_{\mathrm{i}} n_{\mathrm{i}0} = e n_{\mathrm{e}0} - q_{\mathrm{d}} n_{\mathrm{d}0} \tag{1.2.1}$$

where n_{s0} is the unperturbed number density of the plasma species s (s equals e for electrons, i for ions and d for dust grains), $q_{\mathrm{i}} = Z_{\mathrm{i}} e$ is the ion charge (we note that the ion charge state $Z_{\mathrm{i}} = 1$ will be used in the rest of the book), $q_{\mathrm{d}} = Z_{\mathrm{d}} e$ ($-Z_{\mathrm{d}} e$) is the dust particle charge when the grains are positively (negatively) charged, e is the magnitude of the electron charge and Z_{d} is the number of charges residing on the dust grain surface. Typically, a dust grain acquires one thousand to several hundred thousand elementary charges and $Z_{\mathrm{d}} n_{\mathrm{d}0}$ could be comparable to n_{i0}, even for $n_{d0} \ll n_{i0}$. However, in many laboratory and space plasma situations, most of the background electrons could stick onto the dust grain surface during the charging processes and as a result one might encounter a significant depletion of the electron number density in the ambient dusty plasma. Accordingly, for negatively charged dust grains equation (1.2.1) is then replaced by

$$n_{i0} \approx Z_d n_{d0}. \tag{1.2.2}$$

It should be noted here that a complete depletion of the electrons is not possible, because the minimum value of the ratio between the electron and ion number densities turns out to be the square root of the electron to ion mass ratio when electron and ion temperatures are approximately equal and the grain surface potential approaches zero.

1.2.2 Debye shielding

It is well known that a fundamental characteristic of a plasma is its ability to shield the electric field of an individual charged particle or of a surface that is at some non-zero potential. This characteristic provides a measure of the distance (called the Debye radius) over which the influence of the electric field of an individual charged particle (or of a surface that has a non-zero potential) is felt by other charged particles inside the plasma. The Debye shielding in an electron–ion plasma is well explained in most standard textbooks (e.g. Chen 1974, Bittencourt 1986). The Debye shielding in a dusty plasma is explained below.

Let us assume that an electric field is applied by inserting a charged ball inside a dusty plasma whose constituents are electrons, ions and positively or negatively charged dust particles. The ball would attract particles of opposite charges, i.e. if it is positive, a cloud of electrons and dust particles (if they are negatively charged) would surround it, and if it is negative, a cloud of ions and dust particles (if they are positively charged) would surround it. We also assume that recombination of the plasma particles does not occur on the surface of the ball. If the plasmas were cold (i.e. there were no agitations of charged particles), there would be just as many charges in the cloud as in the ball. This case corresponds to a perfect shielding, i.e. no electric field would be present in the body of the plasma outside the cloud. On the other hand, if the temperature is finite, those particles which are at the edge of the cloud (where the electric field is weak) would have enough thermal energy to escape from the cloud. The edge of the cloud then occurs at the radius where the potential energy is approximately equal to the thermal energy $k_B T_s$ of the particles (where k_B is the Boltzmann constant and T_s is the temperature of the plasma species s). This corresponds to an incomplete shielding and a finite electric potential exists there.

We now calculate an approximate thickness of such a charged cloud (sheath). We assume that the potential $\phi_s(r)$ at the centre ($r = 0$) of the cloud is ϕ_{s0}. We also assume that the dust–ion mass ratio m_d/m_i is so large that the inertia of the dust particles prevents them from moving significantly. The massive dust particles form only a uniform background of negative charges. The electrons and ions are assumed to be in local thermodynamic equilibrium, and their number densities, n_e and n_i, obey the Boltzmann distribution, namely

$$n_\mathrm{e} = n_\mathrm{e0} \exp\left(\frac{e\phi_s}{k_\mathrm{B} T_\mathrm{e}}\right) \tag{1.2.3}$$

and

$$n_\mathrm{i} = n_\mathrm{i0} \exp\left(-\frac{e\phi_s}{k_\mathrm{B} T_\mathrm{i}}\right) \tag{1.2.4}$$

where n_e0 and n_i0 are, respectively, the electron and ion number densities far away from the cloud. For our present dusty plasma situation, Poisson's equation can be written in the form

$$\nabla^2 \phi_s = 4\pi(en_\mathrm{e} - en_\mathrm{i} - q_\mathrm{d} n_\mathrm{d}) \tag{1.2.5}$$

where n_d is the dust particle number density. According to our assumption, the dust particle number density is the same both inside and outside the cloud, i.e. $q_\mathrm{d} n_\mathrm{d} = q_\mathrm{d} n_\mathrm{d0} = en_\mathrm{e0} - en_\mathrm{i0}$. Substituting equations (1.2.3) and (1.2.4) into equation (1.2.5) and assuming $e\phi_s/k_\mathrm{B} T_\mathrm{e} \ll 1$ and $e\phi_s/k_\mathrm{B} T_\mathrm{i} \ll 1$, we have

$$\nabla^2 \phi_s = \left(\frac{1}{\lambda_\mathrm{De}^2} + \frac{1}{\lambda_\mathrm{Di}^2}\right)\phi_s \tag{1.2.6}$$

where $\lambda_\mathrm{De} = (k_\mathrm{B} T_\mathrm{e}/4\pi n_\mathrm{e0} e^2)^{1/2}$ and $\lambda_\mathrm{Di} = (k_\mathrm{B} T_\mathrm{i}/4\pi n_\mathrm{i0} e^2)^{1/2}$ are the electron and ion Debye radii, respectively. It should be noted here that the approximations $e\phi_s/k_\mathrm{B} T_\mathrm{e} \ll 1$ and $e\phi_s/k_\mathrm{B} T_\mathrm{i} \ll 1$ may not be valid near the region $r = 0$. However, this region (called the sheath), where the potential ϕ_s falls very rapidly, does not contribute much to the thickness of the cloud. Assuming $\phi_s = \phi_{s0} \exp(-r/\lambda_\mathrm{D})$, we obtain from equation (1.2.6) the dusty plasma Debye radius

$$\lambda_\mathrm{D} = \frac{\lambda_\mathrm{De}\lambda_\mathrm{Di}}{\sqrt{\lambda_\mathrm{De}^2 + \lambda_\mathrm{Di}^2}}. \tag{1.2.7}$$

The quantity λ_D is a measure of the shielding distance or the thickness of the sheath. For a dusty plasma with negatively charged dust grains, we have $n_\mathrm{e0} \ll n_\mathrm{i0}$ and $T_\mathrm{e} \geq T_\mathrm{i}$, i.e. $\lambda_\mathrm{De} \gg \lambda_\mathrm{Di}$. Accordingly, we have $\lambda_\mathrm{D} \simeq \lambda_\mathrm{Di}$. This means that the shielding distance or the thickness of the sheath in a dusty plasma is mainly determined by the temperature and number density of the ions. However, when the dust particles are positively charged and most of the ions are attached onto the dust grain surface, i.e. when $T_\mathrm{e} n_\mathrm{i0} \ll T_\mathrm{i} n_\mathrm{e0}$, we have $\lambda_\mathrm{De} \ll \lambda_\mathrm{Di}$. This corresponds to $\lambda_\mathrm{D} \simeq \lambda_\mathrm{De}$. This means that in a dusty plasma with positively charged dust grains, the shielding distance or the thickness of the sheath is mainly determined by the temperature and density of the electrons.

1.2.3 Characteristic frequencies

Similar to the usual electron–ion plasma, an important dusty plasma property is the stability of its macroscopic space charge neutrality. When a plasma is instantaneously disturbed from its equilibrium, the resulting internal space charge field gives rise to collective particle motions which tend to restore the original charge neutrality. These collective motions are characterized by a natural frequency of oscillations known as the plasma frequency ω_{p}. We now explain how one can define the plasma frequency ω_{p} in a uniform, cold, unmagnetized dusty plasma. The electrostatic oscillations of the electrons, ions or dust particles, which are due to the internal space charge field are described by the continuity equation

$$\frac{\partial n_s}{\partial t} + \nabla \cdot (n_s \boldsymbol{v}_s) = 0 \tag{1.2.8}$$

the momentum equation

$$\frac{\partial \boldsymbol{v}_s}{\partial t} + (\boldsymbol{v}_s \cdot \nabla)\boldsymbol{v}_s = -\frac{q_s}{m_s}\nabla\phi \tag{1.2.9}$$

and Poisson's equation

$$\nabla^2\phi = -4\pi \sum_s q_s n_s \tag{1.2.10}$$

where, for simplicity, we have neglected sources and sinks as well as the pressure gradient forces. We now assume that the amplitude of the oscillations is so small that the terms containing higher powers of the amplitude can be neglected (i.e. the linear theory is valid) and that at the equilibrium all plasma particles (electrons, ions and dust particles) are at rest and no equilibrium space charge field is present. Therefore, assuming $n_s = n_{s0} + n_{s1}$, where $n_{s1} \ll n_{s0}$, we can linearize equations (1.2.8)–(1.2.10), and combine them to obtain

$$\frac{\partial^2}{\partial t^2}\nabla^2\phi + 4\pi \sum_s \frac{n_{s0} q_s^2}{m_s}\nabla^2\phi = 0. \tag{1.2.11}$$

Integrating equation (1.2.11) over the space $\boldsymbol{r}(x, y, z)$ twice under the appropriate boundary condition [namely $\phi = 0$ at equilibrium ($r = 0$)], and replacing $\partial/\partial t$ by $\mathrm{d}/\mathrm{d}t$ we can rewrite equation (1.2.11) as

$$\frac{\mathrm{d}^2\phi}{\mathrm{d}t^2} + \omega_{\mathrm{p}}^2\phi = 0 \tag{1.2.12}$$

where

$$\omega_{\mathrm{p}}^2 = \sum_s \frac{4\pi n_{s0} q_s^2}{m_s} = \sum_s \omega_{ps}^2 \tag{1.2.13}$$

and $\omega_{ps} = (4\pi n_{s0} q_s^2/m_s)^{1/2}$ represents the plasma frequency associated with the plasma species s. Equation (1.2.12) indicates that the internal space charge potential oscillates with a characteristic frequency $\omega_{\rm p}$. This can be interpreted as follows. When the plasma particles are displaced from their equilibrium positions, a space charge field will be built up in such a direction as to restore the neutrality of the plasma by pulling the particles back to their original positions. But because of their inertia, they will overshoot and will be again pulled back to their original positions by the space charge field of the opposite polarity. Again, because of their inertia they will overshoot and thus continuously oscillate around their equilibrium positions. The frequency of such oscillations will, of course, not be the same for electrons, ions and dust grains, but will depend on the mass and the charge of the plasma particles. For example, electrons oscillate around ions with the electron plasma frequency $\omega_{\rm pe} = (4\pi n_{\rm e0}e^2/m_{\rm e})^{1/2}$, ions oscillate around charged dust grains with the ion plasma frequency $\omega_{\rm pi} = (4\pi n_{\rm i0}e^2/m_{\rm i})^{1/2}$ and dust particles oscillate around their equilibrium positions with the dust plasma frequency $\omega_{\rm pd} = (4\pi n_{\rm d0}Z_{\rm d}^2e^2/m_{\rm d})^{1/2}$.

The other important characteristic frequencies are associated with the collisions of the plasma particles (electrons, ions and dust grains) with stationary neutrals. These are the electron–neutral collision frequency $\nu_{\rm en}$, the ion–neutral collision frequency $\nu_{\rm in}$, and the dust–neutral collision frequency $\nu_{\rm dn}$, respectively. The collision frequency ν_{sn} for scattering of the plasma species s by the neutrals is

$$\nu_{sn} = n_{\rm n}\sigma_s^n V_{{\rm T}s} \tag{1.2.14}$$

where $n_{\rm n}$ is the neutral number density, σ_s^n is the scattering cross section (which is typically of the order of 5×10^{-15} cm^2 and depends weakly on the temperature T_s) and $V_{{\rm T}s} = (k_{\rm B}T_s/m_s)^{1/2}$ is the thermal speed of the species s. The collisions of the plasma particles with stationary neutrals tend to damp their collective oscillations and gradually diminish their amplitudes. The oscillations will be slightly damped only when the collision frequency ν_{sn} is smaller than the plasma frequency $\omega_{\rm p}$, i.e.

$$\nu_{\rm en}, \nu_{\rm in}, \nu_{\rm dn} < \omega_{\rm p}. \tag{1.2.15}$$

1.2.4 Coulomb coupling parameter

One other important special characteristic of a dusty plasma is its Coulomb coupling parameter which determines the possibility of the formation of dusty plasma crystals. To explain this characteristic, let us consider two dust grains (both having the same charge $q_{\rm d}$) separated from each other by a distance a. The dust Coulomb potential energy (including the shielding effect) is

$$\mathcal{E}_{\rm c} = \frac{q_{\rm d}^2}{a}\exp\left(-\frac{a}{\lambda_{\rm D}}\right) \tag{1.2.16}$$

and the dust thermal energy is $k_{\rm B}T_{\rm d}$. Thus, the Coulomb coupling parameter $\Gamma_{\rm c}$ (defined as the ratio of the dust potential energy to the dust thermal energy) is represented by

$$\Gamma_{\mathrm{c}} = \frac{Z_{\mathrm{d}}^2 e^2}{a k_{\mathrm{B}} T_{\mathrm{d}}} \exp\left(-\frac{a}{\lambda_{\mathrm{D}}}\right). \tag{1.2.17}$$

A dusty plasma is a weakly coupled system when $\Gamma_{\mathrm{c}} \ll 1$, while it is strongly coupled when $\Gamma_{\mathrm{c}} \gg 1$. Thus, the number of charges residing on the grain surface (Z_{d}), the ratio of the intergrain distance to the Debye screening radius (a/λ_{D}) and the dust thermal energy ($k_{\mathrm{B}} T_{\mathrm{d}}$) play decisive roles in deciding whether a dusty plasma will be strongly coupled or weakly coupled. It can easily be shown that in several laboratory dusty plasma systems, massive dust grains are strongly coupled because of their huge electric charge, low temperature and small intergrain distance.

1.3 Dusty Plasmas in Space

Dusty plasmas are rather ubiquitous in space (Verheest 2000). There are a number of well known systems in space, such as interstellar clouds, circumstellar clouds, solar system, etc where the presence of charged dust particles has been well established.

The interstellar space (the space between the stars) is filled with a vast medium of gas and dust. The gas content of the interstellar medium continually decreases with time as new generations of stars are formed during the collapse of giant molecular clouds. The collapse and fragmentation of these clouds give rise to the formation of stellar clusters. The presence of dust in interstellar or circumstellar clouds has been known for a long time (from star reddening and infrared emission). The dust grains in interstellar or circumstellar clouds are dielectric (ices, silicates, etc) and metallic (graphite, magnetite, amorphous carbons, etc). Typical parameters of dust-laden plasmas in interstellar clouds are $n_{\mathrm{e}} = 10^{-3}$–10^{-4} cm^{-3}, $T_{\mathrm{e}} \simeq 12$ K, $n_{\mathrm{d}} \simeq 10^{-7}$ cm^{-3}, $r_{\mathrm{d}} \simeq 0.2$ μm, $n_{\mathrm{n}} \simeq 10^4$ cm^{-3} and $a/\lambda_{\mathrm{D}} \leq 0.3$.

We now focus our attention on dusty plasmas in our solar system which is, in fact, full of dust. The existence of dust in the early solar nebula has long been advocated by the Nobel Laureate Hannes Alfvén (1954). The coagulation of the dust grains in the solar nebula would have led to ‘planetesimals’ from where comets and planets have been formed. The physical properties (such as size, mass, density, charge, etc) of such dust grains vary depending on their origin and surroundings. The origins of the dust grains in the solar system are, for example, micrometeoroids, space debris, man-made pollution, lunar ejecta, etc. We now present a few sections to explain briefly some important characteristics of the dust particles and their plasma environments in a number of different regions of our solar system, namely interplanetary space, comets, planetary rings, Earth’s atmosphere, etc.

1.3.1 Interplanetary space

The interplanetary space is full of dust known as 'interplanetary dust'. The existence of interplanetary dust particles was known from the zodiacal light. The zodiacal light is due to dust grains distributed throughout the inner solar system, with strong contributions from the asteroid belt. These have probably originated from decay by collisional fragmentation of debris from comets, which are known to release between 0.25 tonnes s^{-1} (in the case of short-period comets) and 20 tonnes s^{-1} (in the case of long-period comets) dusty gases in the solar system (de Angelis 1992). The other important sources of the interplanetary dust are asteroids that produce most of their dust during mutual collisions in the asteroid belt. Through the combined effects of solar wind drag and the Poynting–Robertson light drag (a loss of orbital angular momentum by gyrating particles associated with their absorption and re-emission of the solar radiation), all particles smaller than $\sim$1 cm gradually spiral into the Sun on timescales ranging from thousands to millions of years. It has been estimated that the accretion of interplanetary dust (received by the Earth) is roughly 40 000 tonnes per year. For the past two decades NASA has routinely collected interplanetary dust in the stratosphere using high-altitude research aircrafts. The dust particles are collected at altitudes of 18–20 km by inertial impacts onto plastic plates coated with highly viscous silicone oil. The size of most dust particles found on the collectors are 5–20 mm. The interplanetary dust particles often have very fragile, fluffy appearance. The outside and inside of such interplanetary dust particles are shown in figures 1.1 and 1.2, respectively. Some of these particles are so fragile that they disintegrate into dozens or hundreds of fragments when they impact the collector surface. The interplanetary dust particles are usually very rich in carbon. Otherwise, they are usually composed of submicrometre mineral grains (hydrous or anhydrous), and some grains have abundant glassy modules (GEMS), proposed to be interstellar silicates. Typical parameters of dust-laden plasmas in the zodiacal dust disc are $n_e \simeq 5\ \mathrm{cm}^{-3}$, $T_e \simeq 10^5$ K, $n_d \simeq 10^{-12}\ \mathrm{cm}^{-3}$, $r_d = 2 - 10\ \mu$m and $a/\lambda_D \simeq 5$. There are many particles that appear to contain abundant pre-solar molecular cloud material, marked by isotopic anomalies in H and N (Messenger 2000).

1.3.2 Comets

Comets are small, fragile, irregularly shaped bodies composed of an admixture of non-volatile grains and frozen gases. They have highly elliptical orbits that bring them very close to the Sun and swing them deeply into the space. The comet structures are diverse and very dynamic, but they all develop a surrounding cloud of diffuse material, called a coma that usually grows in size and brightness as the comet approaches the Sun. There is a small, bright nucleus (less than 10 km in diameter) in the middle of the coma. The coma and the nucleus together constitute the head of the comet. As comets approach the Sun, they develop enormous tails

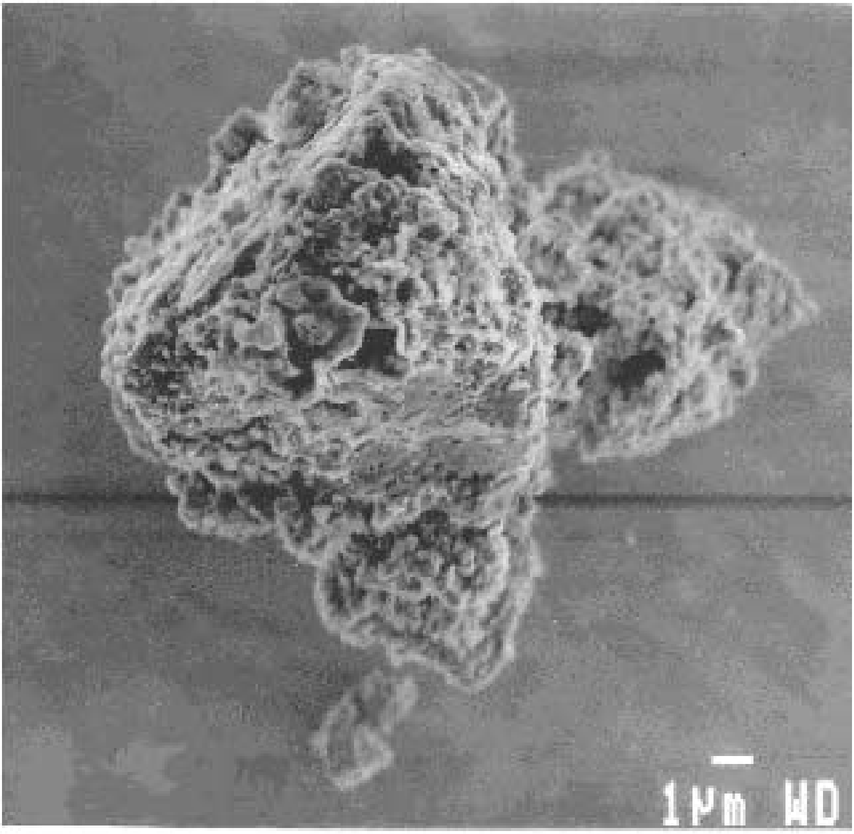

Figure 1.1. The appearance of interplanetary dust particles (courtesy of Dr Scott Messenger, Washington University).

of luminous material that extend for millions of kilometres in the anti-sunward direction from the head. When far from the Sun, the nucleus is very cold and its material is frozen solid within the nucleus. When a comet approaches within a few AU of the Sun, the surface of the nucleus begins to warm, and the volatiles evaporate. The evaporated molecules boil off and carry small solid particles with them, forming the comet's coma of gas and dust. When the nucleus is frozen, it can be seen only by reflected Sunlight. However, when a coma develops, dust reflects still more Sunlight, and gas in the coma absorbs ultraviolet radiation and begins to fluorescence. At about 5 AU from the Sun, fluorescence usually becomes more intense than reflected light. As the comet absorbs ultraviolet light, chemical processes release hydrogen that escapes the comet's gravity and forms a hydrogen envelope. This envelope cannot be seen from the Earth because its light is absorbed by our atmosphere, but it has been detected by spacecraft. The Sun's

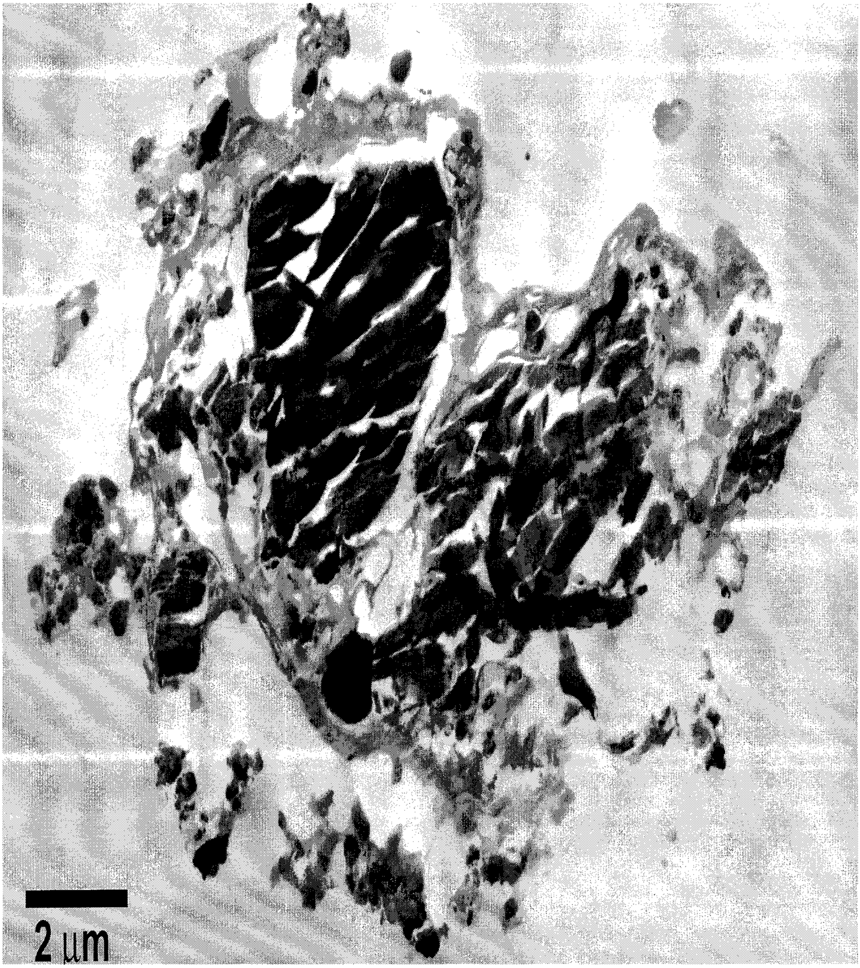

Figure 1.2. Typical interior view of anhydrous interplanetary dust viewed by transmission electron microscopy (courtesy of Dr Lindsay Keller, Johnson Space Center).

radiation pressure and the solar wind accelerate materials away from comet's head at different velocities according to the size and mass of the materials. Thus, relatively massive dust tails are accelerated slowly and tend to be curved. The ion tail is much less massive, and is accelerated so much that it appears as a nearly straight line extending away from the comet opposite to the Sun. Figure 1.3, a view of comet Hale-Bopp, shows two distinct tails. The thin blue plasma tail is made of gases and the broad white tail is made of macroscopic dust particles. The data from the Vega and Giotto spacecraft have provided much more information about cometary dust particles. A large number of very small grains (VSG) have

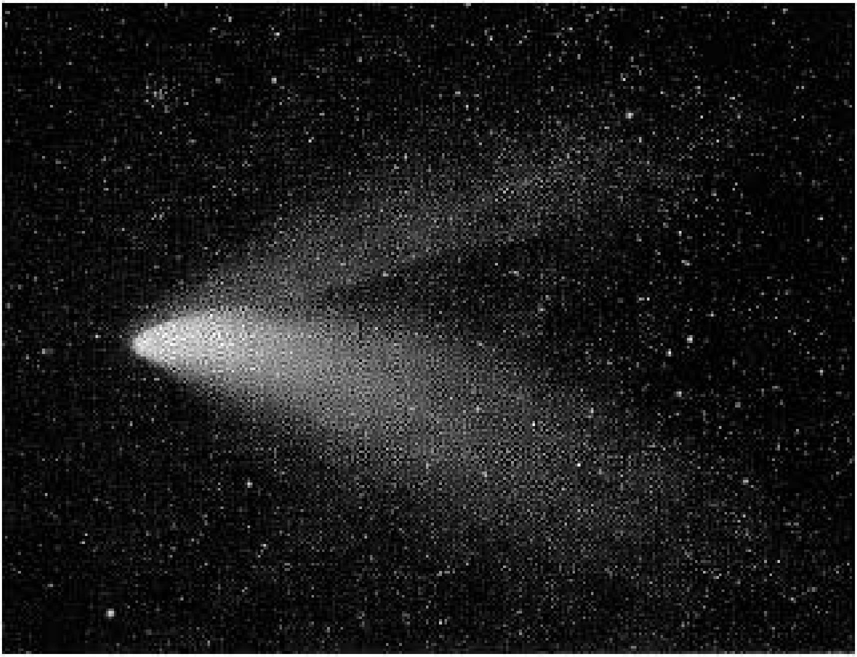

Figure 1.3. A view of comet Hale-Bopp showing two distinct tails, namely a thin blue plasma tail and a broad white dust tail (after Wurden *et al* 1999 and courtesy of Dr G Wurden, LANL, Los Alamos).

Table 1.2. Typical parameters of a dust-laden plasma in Halley's comet.

Characteristics	Inside ionopause	Outside ionopause
n_{e} (cm^{-3})	10^3–10^4	10^2–10^3
T_{e} (eV)	≤ 0.1	~ 1
n_{d} (cm^{-3})	10^{-3}	10^{-8}–10^{-7}
r_{d} (μm)	0.1–10	0.01–10
n_{n} (cm^{-3})	10^{10}	—
a/λ_{D}	≥ 1	≥ 10

been found with a size distribution fitted by a power law, i.e. $n(r_{\mathrm{d}}) \simeq r_{\mathrm{d}}^{-s}$, where s varies from 3.3 (for Vega 2) to 4.1 (for Giotto). Table 1.2 shows typical plasma parameters of a dust-laden plasma inside and outside the ionopause (a plasma boundary which separates the region of smoothly/cold outward flowing cometary ions) of Halley's comet.

1.3.3 Planetary rings

It is now well established that most of the rings of the outer giant planets (such as Jupiter, Saturn, Uranus, Neptune) are made of micron- to submicron-sized dust particles. Below we provide a brief description for understanding the origin of dust particles in planetary rings.

1.3.3.1 Jupiter's ring system

The ring of Jupiter was discovered by Voyager 1 (by taking a single image) that was targeted specifically to search for a faint ring system. A more complete set of images were finally taken by Voyager 2. Jupiter's ring is now known to be composed of three major components, namely the main ring, the halo and the gossamer ring. The main ring is about 7000 km wide and has an abrupt outer boundary about 129 000 km from the centre of the planet. The main ring encompasses the orbits of the two small moons, Adrastea and Metis, which may act as the source for the dust that makes up most of the ring.

1.3.3.2 Saturn's ring system

The rings of Saturn have puzzled astronomers since they were first discovered by Galileo in 1610 using his first telescope. The puzzles have only significantly increased since Voyagers 1 and 2 imaged the ring system extensively in 1980 and 1981. The rings have been given letter names in the order of their discovery. The main rings (from the outward direction) are known as C, B and A. The Cassini Division is the largest gap in the rings and separates the rings B and A. Recently, a number of fainter rings have also been discovered. The D ring is exceedingly faint and closest to the planet. The F ring is narrow and just outside the A ring. There are two other far fainter rings named G and E. The particles in Saturn's rings are composed primarily of ice and range from microns to metres in size. One of the most interesting features observed in Saturn's ring system by both Voyagers 1 and 2 was the nearly radial spokes (Smith *et al* 1981, 1982) which (more than anything else) provided the impetus for the study of dust–plasma interactions in planetary magnetospheres. These spokes are confined to the dense central B ring with the inner edge at about $1.52R_{\mathrm{s}}$ (R_{s} is the radius of Saturn) and the outer edge at about $1.95R_{\mathrm{s}}$. They have an inner boundary at $\sim 1.72R_{\mathrm{s}}$ and an outer boundary at approximately the outer edge of the B ring. A typical spoke pattern is seen in figure 1.4. The spokes exhibit a characteristic wedge shape. The spoke model is based on the assumption that the spokes contain electrostatically levitated micron- and submicron-sized dust grains and that the thin radial elongation is due to the rapid radial motion of dense plasma clouds whose radii are of the order of several thousand kilometres. The characteristics of dust and plasma varies from one ring to another. Table 1.3 shows the dust and plasma characteristics of the E ring, the F ring and the spokes of Saturn.

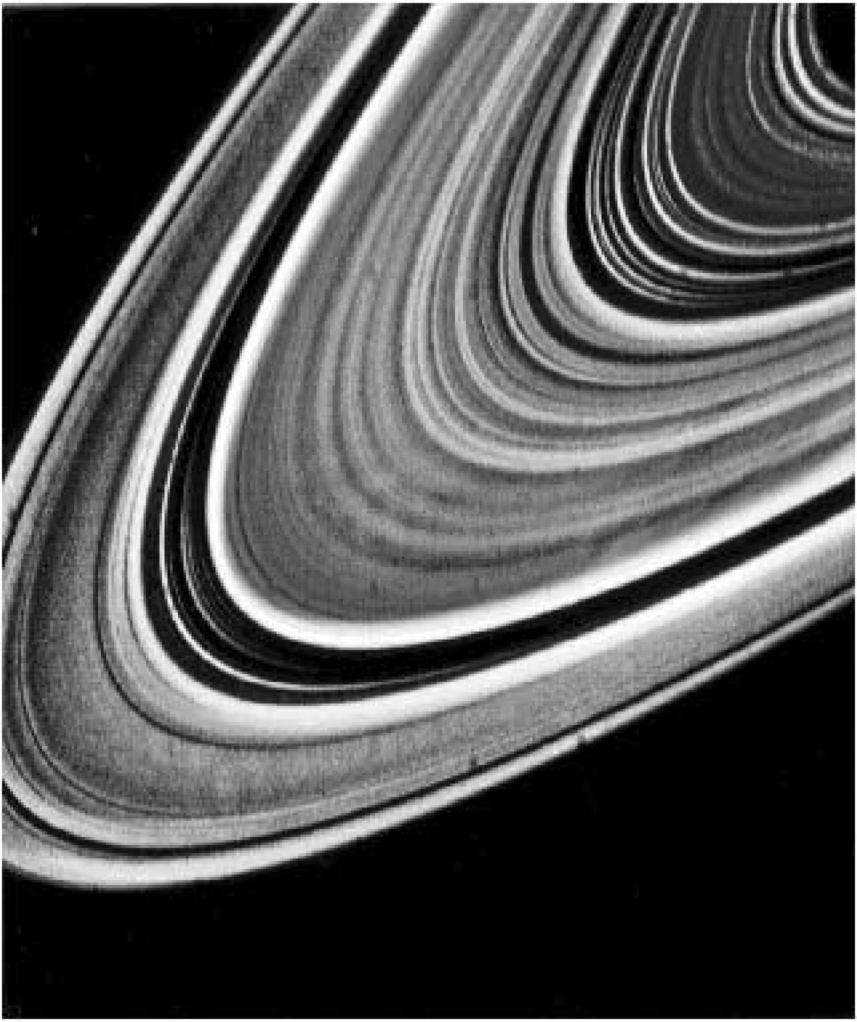

Figure 1.4. A view of the nearly radial spokes in Saturn's B ring. The azimuthal width of a spoke is typically a few thousand kilometres, which in the electrostatic levitation model corresponds to the size of the meteoric-impact-produced plasma cloud (courtesy of Jet Propulsion Laboratory (JPL)).

1.3.3.3 Uranian ring system

The Uranian ring system was discovered in 1977 during observations of a stellar occultation by the planet. The star was observed to blink out briefly five times before the planet and again five times afterwards, indicating that the planet was

Table 1.3. Typical parameters of a dust-laden plasma in Saturn's rings.

Characteristics	E ring	F ring	Spokes
n_e (cm^{-3})	$\sim$10	$\sim$10	0.1–10^2
T_e (K)	10^5–10^6	10^5–10^6	$\sim 10^4$
n_d (cm^{-3})	10^{-7}	$\leq$10	$\sim$1
r_d (μm)	$\sim$1	1	$\sim$1
a/λ_D	0.1	$\leq 10^{-3}$	$\leq 10^{-2}$

encircled by five narrow rings. However, a number of Earth-based observations indicated that there were actually nine major rings. These (from the outward direction) are 6, 5, 4, α, β, η, γ, δ and ϵ. A number of images, which provide additional occultations of the ring system, were taken by the Voyager spacecraft in 1986. The Voyager cameras also detected a few additional rings and showed that the nine major rings are surrounded by the belts of fine dust particles. A narrow ring named 1986U1R or λ, which has been found to be different from the others, was discovered in the backscattered Voyager images. These rings observed in a single Voyager image at high angles were found to be much brighter than their environment. This indicates that the main constituent of these rings is dust. One other ring named 1986U2R, which is interior to all other rings, is also visible in a single Voyager image at a phase angle of 90°. Although it is not possible to obtain sufficient information about the particle properties of this ring from a single view, a predominance of dust is strongly suspected. To study the characteristics of the constituents of Uranian rings, Ockert *et al* (1987) made a photometric analysis and showed that the brightness distribution is dominated by backscattering. This indicates that the rings mainly consist of macroscopic dust grains.

1.3.3.4 Neptune's ring system

Neptune also has an external ring system. Earth-based observations showed only faint arcs instead of complete rings. However, in the year 1989 Voyager 2's images showed them to be complete rings with bright clumps. One of the rings (out of four) appears to have a curious twisted structure. Like those of Jupiter and Uranus, Neptune's rings are very dark. The plasma wave instruments on board the Voyager 2 spacecraft detected small micrometre-sized dust particles. Observations revealed a power law distribution (with an index 4) for the dust grains. The dust radius was in the range 1.6–10 μm. The number density of the dust is very low (e.g. $n_d \simeq 10^{-8}$–10^{-7} cm^{-3}). The dust material is dirty ice, although other compositions (such as silicates) cannot be ruled out. Further study is required to determine more accurately the mass and size distributions of dust grains as well as charges residing on them. The data also revealed that at each ring plane there is an intense broadband burst of noise, extending from below 10 Hz to above 10 KHz. The presence of charged dust grains might be contributing to these low-frequency noises in Neptune's atmosphere which has oddly oriented magnetic fields. The latter are presumably generated by motions of conductive fluids (probably water) in its middle layer.

1.3.4 Earth's atmosphere

The most important part of our Earth's environment, where the presence of charged dust particles are observed (Cho and Kelley 1993, Havnes *et al* 1996a), is the polar summer mesopause located between 80 and 90 km in altitude. The most significant phenomenon observed in the polar summer mesopause is the formation of a special type of cloud known as 'noctilucent clouds' (NLCs). The NLCs were reported for the first time in 1885 (Backhouse 1885) and were, from the beginning, recognized as being different from other clouds. Rocket grenades launched during the International Geophysical Year of 1957–1958 revealed another peculiarity of the polar mesopause: it was much colder in the summer than in the winter. This observation supported speculations that the NLCs were composed of ice that formed at extremely low temperatures (even below 100 K). There also occur some other important phenomena, such as the polar mesospheric summer echoes (PMSE), and strong radar backscatter that has been observed at frequencies from 50 MHz to 1.3 GHz. At the heights of the PMSE there also exist layers of electron density depletion and positive ion density enhancement, which are elaborately discussed in some review articles (Thomas 1991, Cho and Kelley 1993).

A number of more recent theories involve heavy ion clusters or charged dust particles with total charge density that is significant compared with the electron or ion component (Havnes *et al* 1996a). A high charge density on the dust may, in principle, be the result of comparatively few and large highly charged dust particles. A high charge on a dust particle can be possible only if the dust is positively charged by photoemission. On the other hand, if the photoelectron emission is negligible and the dust grain charging is only due to collection of plasma particles, the charge on each dust particle will be low (typically a few unit charges or less) and negative (Havnes *et al* 1996a). Typical parameters of dust-laden plasmas in NLCs are $n_\mathrm{e} \simeq 10^3$ cm^{-3}, $T_\mathrm{e} \simeq 150$ K, $n_\mathrm{d} \simeq 10$ cm^{-3}, $r_\mathrm{d} \simeq 0.1$ μm, $n_\mathrm{n} \simeq 10^{14}$ cm^{-3} and $a/\lambda_\mathrm{D} \simeq 0.2$.

One of the most significant sources of dust in the Earth's atmosphere is man-made pollution (terrestrial aerosols). These have been found to be mainly (90%) in the form of aluminium oxide (Al_2O_3) spheroid in sizes that range from 0.1 μm to 10 μm. Their origin is from rocket and space shuttle exhausts (Bernhardt *et al* 1995).

Recent measurements from balloon and aircraft collection have provided some basic properties (such as constituents, size, density, etc) of dust particles in our Earth's surroundings. These are listed in table 1.4. The characteristics of the

Table 1.4. Composition, size and density of dust particles in our Earth's surroundings.

Origin	Composition	Radius (μm)	Density (cm^{-3})
Shuttle exhausts	dirty ice	5×10^{-3}	3×10^{4}
Terrestrial aerosol	Al_2O_3 spheroid	0.1–10	10^{-10}–10^{-6}
Micrometeoroid	60% chondritic, 30% iron–sulfur–nickel, 10% silicates	5–10	10^{-10}–10^{-9}
Industrial contamination	magnetite spherules	$\sim$10	$\sim 10^{-5}$

Table 1.5. Approximate values of some parameters of a dust-laden plasma in rocket exhausts and flames.

Characteristics	Rocket exhausts	Flames
n_{e} (cm^{-3})	10^{13}	10^{12}
T_{e} (K)	3×10^{3}	2×10^{3}
n_{d} (cm^{-3})	10^{8}	10^{11}
r_{d} (μm)	0.1	0.01
n_{n} (cm^{-3})	10^{18}	10^{19}
a/λ_{D}	≤ 5	≤ 1

plasma and dust particles vary depending on the situation we consider. Table 1.5 shows the characteristics of the plasma and dust particles in rocket exhausts and flames.

1.4 Dusty Plasmas in Laboratories

The extensive literature on dust in space and astrophysical plasmas (discussed in the preceding section) is a terrific starting point for the understanding of laboratory dusty plasmas. However, there are two distinctive features of laboratory dusty plasmas which differ significantly from those of space and astrophysical dusty plasmas. First, laboratory discharges have geometric boundaries whose structure, composition, temperature, conductivity, etc influence the formation and transport of the dust grains. Second, the external circuit, which maintains the dusty plasma, imposes spatiotemporally varying boundary conditions on the dusty discharge. We will now discuss how dust may occur in laboratory devices, particularly in direct current (dc) and radio-frequency (rf) discharges, plasma processing reactors, fusion plasma devices, solid-fuel combustion products, etc.

1.4.1 dc and rf discharges

While dust particles are found in dc discharges, they are usually observed in larger quantities for the same gases under conditions of rf excitations. An obvious question may first arise: how do the dust particles originate? The dust particles may originate from the plasma chemistry in the gas phase (e.g. carbon monoxide or silane containing discharges) or from the sputtering of electrodes (e.g. most metals, graphite, etc). It is found that the dust particles occur more rapidly in electronegative gas mixtures or in a gas mixture where a substrate (such as silicon or carbon) is present. By the process of sputtering both silicon and carbon yield electronegative free radicals. To satisfy ambipolarity, the dust particles will, therefore, be negatively charged. The rf discharge is a very efficient trap for negative ions and for macroscopic, negatively charged dust particles. The electrodes acquire a negative dc bias due to the much higher mobility of the electrons compared with that of the positive ions. The ambipolar electric fields, which occur in the radial direction because of the mobility effect, also trap negative ions and dust particles. The physical properties (such as growth, charge, position, temperature, etc) of the dust particles, which are formed in dc or rf discharges, depend on various physical and chemical processes/parameters involved. These are pointed out as follows (Garscadden *et al* 1994).

(i) Growth: radicals and ion fluxes, bonds, temperature, desorption, surface charge, sputtering, etc.
(ii) Charge: floating potential, electron and ion fluxes, electron affinity and work function, electrostriction, field and thermionic emission, photoelectric charging, etc.
(iii) Position: electrostatic–gravitational balance, collisional drag from ions and neutrals, ensemble polarizability, mass, etc.
(iv) Temperature: surface radical recombination, surface electron–ion recombination, surface quenching of energetic species, thermionic emission, pyrolysis, radiation, Knudsen or continuum cooling, etc.

1.4.2 Plasma processing reactors

The common use of low-pressure plasma processing reactors and the easy availability of laser light scattering diagnostics showed that many of these discharges produced and trapped large quantities of macroscopic dust grains. Scanning electron micrographs (SEMs) of the dust using a low-energy probe reveal narrow size distributions and a morphology reminiscent of the microscopic cauliflowers shown in figure 1.5. The low-voltage SEMs are essential if one is to resolve the surface texture of low atomic number materials. The low-voltage

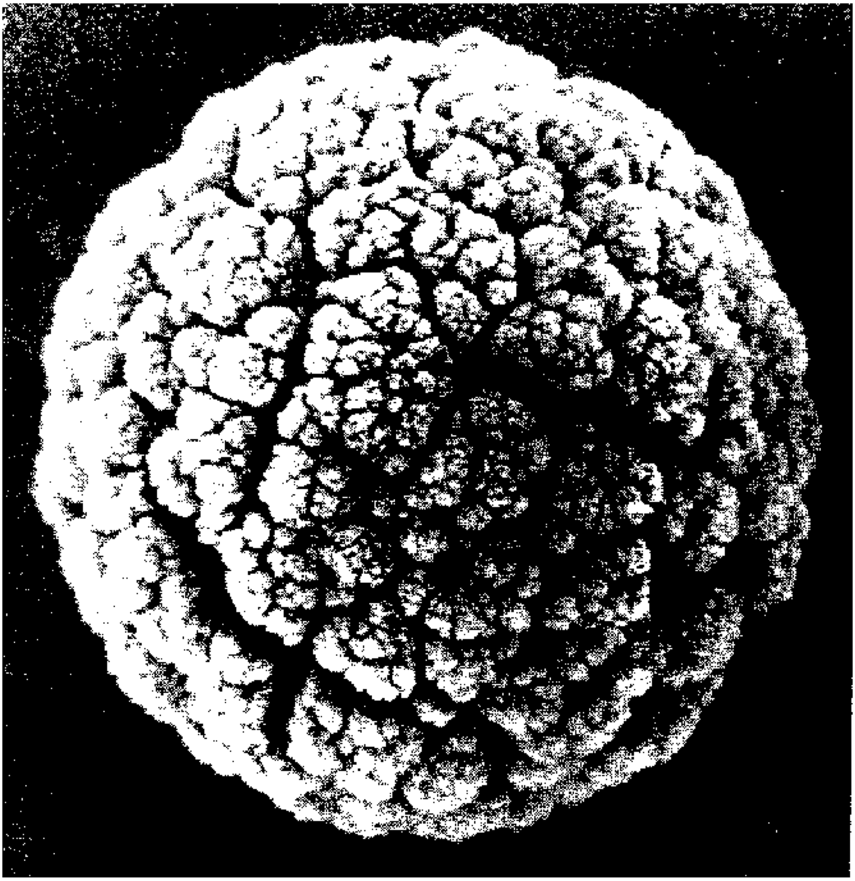

Figure 1.5. Low-voltage high-resolution SEM of a typical dust particle (of diameter 650 nm) grown from a 1 Torr 15 kHz He plasma with graphite electrodes (after Garscadden *et al* 1994).

and low-current probe also permits one to examine uncoated samples without beam damage. The transmission electron micrographs (TEMs) of whole grains and thin sections show radial, columnar microstructures, a lack of morphology and surface texture and a lack of crystallinity in domains as small as 200 Å. The fractal morphology and surface texture are similar to those encountered in sputtered coatings where the surface temperature is less than half of the melting temperature of the deposited material. The morphology of the particle permits insights into the nature of the fluxes from which homogeneously nucleated grains are built.

1.4.3 Fusion plasma devices

The presence of dust particles in fusion devices has been known for a long time. However, their possible consequences for plasma operation and performances have become a topic of recent interest (Tsytovich 1997, Winter 1998, 2000). The plasmas in fusion devices (for example, tokamaks, stellarators, etc) are more or less contaminated by elements (impurities) heavier than the hydrogen isotopes which are the fuel in fusion reactors. The impurities (dust particles) are generated by a number of processes, such as desorption, arcing, sputtering, evaporation and sublimation of thermally overloaded wall material, etc. It is well known that in the case of graphite wall components, in addition to C atoms, a significant amount of $C_1, C_2, C_3, \ldots, C_n$ clusters are liberated. The other generation mechanism for the formation of impurities (dust particles) is the spallation and flaking of thin films of redeposited material or of films which were grown intentionally for wall conditioning purposes. The films from wall conditioning, which have a thickness of a few 100 nm, can be the source of thin flakes. The redeposited layers from tokamak operation may have thicknesses up to several 100 μm. They may have a stratified structure due to the superposition of consecutive discharge events. They tend to be mechanically unstable for thicknesses exceeding a few μm.

When we consider fusion devices operating with DT, additional processes such as the formation of ^{3}He due to the decay of T, the formation of ^{4}He due to neutron-induced spallation reactions of low-Z wall material, the ejection of dust particles due to α-particle-induced embrittlement of the near-surface region, etc may become important. The dust particles are likely to be formed during He-glow discharge cleaning and during thin film deposition for wall conditioning (carbonization, boronization, siliconization). All particles that have been formed will fall to the bottom at the end of a fusion plasma discharge. However, the lighter ones can be re-ejected into the fusion plasma either by magnetic effects or by electrostatic charging when they are in contact with the edge of the plasma. They may then be levitated close to the wall.

Recently, different types of dust particles were collected from the TEXTOR-94 which is a medium-sized tokamak with $\sim$4 MW ICRF and $\sim$4 MW neutral beam injection heating and capable of full-performance plasma pulses with durations up to 10 s (Winter 1998). The dust was collected by means of a vacuum cleaner from the bottom porthole areas of TEXTOR-94. The coarse particles were removed from the sticky bag of the vacuum cleaner by shaking them off (coarse fraction). The main part of the coarse fraction consisted of dark or whitish particles of typically 0.1–0.5 mm size with irregular shapes. An interesting point is that about 15% of these coarse particles are ferromagnetic. A representative fraction of the magnetic coarse fraction is shown in figure 1.6. The coarse particles are found to be of different types and sizes, such as metal cuttings, spheres of diameters between 0.01 and 0.1 mm, irregularly formed pieces, etc.

The non-magnetic coarse particles, which appear like pieces of rock and with a composition of about 70% Si, 11% Al, 10% S, 7% Ca and 0.6% Fe, were also

Figure 1.6. An SEM image of magnetic coarse fraction showing metal cuttings, various spheres and irregularly formed particles (after Winter 1998).

observed. These particles do not show the typical signatures of redeposited and flaked-off particles. They were probably formed during Si-ICRF conditioning or in test-limiter experiments with silane gas puffing, either by plasma-induced growth or by pyrolysis and agglomeration in the plasma, or arc chipping from very thick local deposits (e.g. the test limiter). The co-deposited flaked-off films constitute another part of the coarse non-magnetic fraction and resemble closely that of their magnetic counterparts with the exception of a lower metal content. The third group of non-magnetic big particles was graphite grains with size of $\sim$0.1 mm, composed of well established graphite grains with typical diameters of 1–10 μm. These clearly originate from fatigued graphite armour tiles.

The particles from solvents (with suspended particles) taken immediately after ultrasonic stir-up and those taken after 2 h of settlement differed in the size distribution. The particles taken after 2 h settlement were significantly smaller on average than the others. The smallest ones were partly ferromagnetic. A number of particles of submicron size, which themselves are agglomerates of individual particles of about 100–300 nm diameter, were found to exist. The agglomerates are not always closely packed but have a woolly open structure. The size and structure of these small particles are consistent with what one would expect from plasma-induced growth. The SEM investigations of nano-particles formed in processing plasmas show similar sizes and a diffuse cauliflower-like structure (shown in figure 1.5).

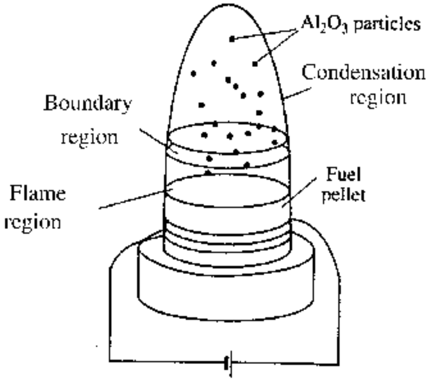

Figure 1.7. Diagram of the main zones of the solid-fuel combustion product plasma (after Samaryan *et al* 2000).

Table 1.6. Typical parameters of different regions in a solid-fuel combustion product plasma (Samaryan *et al* 2000).

Characteristics	Flame region	Boundary region	Condensation region
Gas temperature (K)	$\sim$3000	$\sim$2000	$\sim$600
n_d (cm^{-3})	$\leq 10^2$	10^3–10^8	$\geq 10^4$
Γ_c	$\ll 1$	3–40	$\ll 1$

1.4.4 Solid-fuel combustion products

The presence of micron- or submicron-sized dust particles is experimentally observed in a solid-fuel combustion product plasma. Figure 1.7 shows a diagram of three main regions of a solid-fuel combustion product plasma (Samaryan *et al* 2000) which is produced by the combustion of the aluminium-coated solid fuel. The combustion product plasma consists of electrons, ions and micron-sized dust particles of a condensed dispersed phase. The magnesium-coated solid fuel may also be used to produce such a combustion product plasma. The constituents of dust particles are Al_2O_3 (in the case of aluminium-coated solid fuel) or MgO (in the case of magnesium-coated solid fuel). The number density of alkile metal atoms ranges from $\sim 10^9$ cm^{-3} to $\sim 10^{10}$ cm^{-3}. The size of the dust particles is ~ 0.2 μm. The other dusty plasma parameters in three main regions of the solid combustion product plasma, namely the flame, boundary and condensation regions, are given in table 1.6. It is well known that for a given size and density of dust particles of the condensed dispersed phase the Coulomb coupling parameter Γ_c is determined by the screening of the particles by the plasma component formed as a result of the ionization of alkali-metal

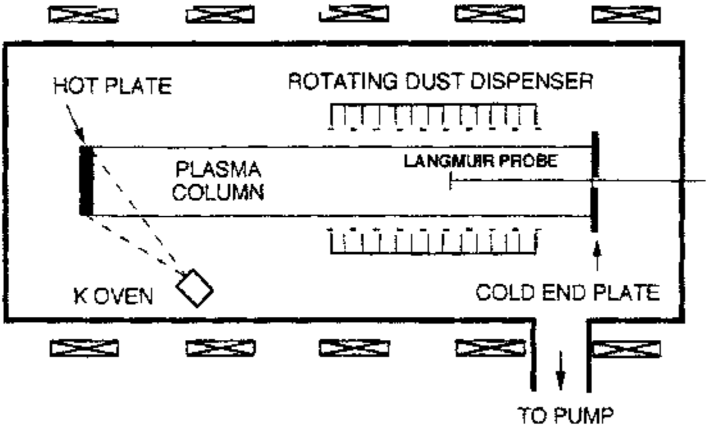

Figure 1.8. Diagram of the Q-machine including the rotating drum and the dust dispenser (after Merlino *et al* 1998).

impurity (Na and K which are always present in the synthetic fuel and end up in the combustion products) atoms. The plasma parameters in the flame and condensation regions of the synthetic solid-fuel combustion product plasma are such that the Coulomb coupling parameter Γ_c is much less than 1. Thus, in these regions ordered structures of dust particles were not observed. The main obstacle for the formation of ordered structures is a large amount of alkali-metal impurities in the fuel samples, i.e. high electron and ion densities in a plasma by ionization. A low density of dust particles of the condensed disperse phase in a high-temperature region was also an inhibiting factor. Ordered structures of particles of the condensed disperse phase were not observed in the condensation zone where the particle density is quite high, but the charge on the dust particles is so low on account of the relatively low temperature of the medium. However, for aluminium-coated solid fuels with a low alkali-metal impurity content, an ordered arrangement of the dust particles of the condensed dispersed phase may be formed in the boundary region between the flame and the condensation zone.

1.5 Production of Dusty Plasmas

To produce/confine dusty plasmas in laboratories, a number of techniques have been developed in the last few years. We now briefly explain some of these techniques/methods.

1.5.1 Modified Q-machine

A simple device for producing dusty plasmas is a dusty plasma device (DPD) which is a single-ended Q-machine modified to allow the dispersal of dust grains over a portion of the cylindrical plasma column (Xu *et al* 1992). A schematic illustration of a DPD is shown in figure 1.8. A singly ionized potassium plasma is produced by surface ionization of potassium atoms on a hot (~2500 K) tantalum plate which provides neutralizing electrons. The plasma column (of ~4 cm diameter and ~80 cm long) is confined radially by a longitudinal magnetic field (~3–4 kG). The basic constituents of the ambient plasma are K^+ ions and electrons with approximately equal temperatures $T_e \simeq T_i \simeq 2300$ K and densities in the range of $\sim 10^5$–10^{10} cm^{-3}. The neutral gas pressure is so low ($\sim 10^{-6}$ Torr) that the mean free paths for ion–neutral and electron–neutral collisions are larger than the machine dimensions. To dispense dust particles into the plasma, the plasma column is surrounded, over a portion of its length, by a dust dispenser (figure 1.8). The dust dispenser consists of a rotating metal cylinder and a stationary screen. The dust particles, initially loaded into the bottom of the cylinder, are carried by a rotating cylinder up to the top and fall onto the screen. A series of stiff metal bristles attached to the inside of the cylinder scrapes across the outer surface of the screen as the cylinder is rotated. This continuous scraping agitates the screen allowing the dust particles to dispense evenly throughout the plasma column. The fallen dust particles that are collected at the bottom of the cylinder are then recycled. A continuous dust recycling takes place provided that there exists a sufficient amount of dust particles within the plasma column.

The dust grains used in such experiments are usually aluminium oxide (Al_2O_3) and kaolin (hydrated aluminium silicate, $Al_2Si_2O_7nH_2O$) of various sizes and shapes. The samples of the dust grains are collected from the vacuum chamber and an analysis can be made of photographs taken with an electron microscope to determine their size distribution.

The dust grain is mainly charged up by the collection of the plasma particles (K^+ ions and electrons). Thus, the situation of a dust grain is similar to that of an electrically floating Langmuir probe which charges up negatively to a potential $V \simeq 4k_B T_e/e$ in a K^+ plasma. To estimate the charge state of a dust grain, one may consider the grain as a small sphere of radius r_d (although a spherical shape is not always common for kaolin dust). A sphere of radius r_d has a capacitance $C = r_d$. Thus, the charge on the dust grain is $q_d = CV \simeq 5.5 \times 10^3 e$ for $r_d = 10$ μm and $T_e = 2300$ K. We now estimate the time τ_c required for an uncharged dust grain to charge up to nearly equilibrium potential. This time τ_c is approximated as $\tau_c = q_d/I_e$, where $I_e \sim -4\pi r_d^2 e n_e V_{Te}$ is the charging current (since $|I_e| \gg I_i$). When $n_e = 10^7$ cm^{-3}, $r_d = 10$ μm and $T_e \simeq 2320$ K, we have $q_d = -5.5 \times 10^3 e$, $I_e = -4 \times 10^{-10}$ A and $\tau_c \simeq 2$ μs. As the fall speed of a dust grain is estimated to be ~100 cm s^{-1} (Xu *et al* 1992), the dust grains attain their equilibrium charge while falling within a very thin layer at the top portion of the plasma column.

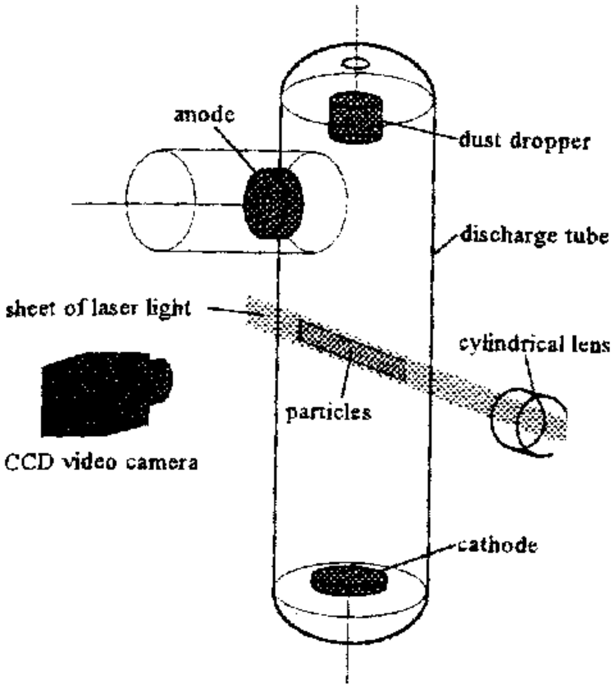

Figure 1.9. Schematic illustration of how dusty plasmas are produced in strata of a dc neon glow discharge (after Fortov *et al* 1997).

1.5.2 dc discharges

Dusty plasmas are produced by suspending micron-sized dust particles in a stratum of a dc neon glow discharge (Fortov *et al* 1997). The discharge is formed in a cylindrical glass tube with cold electrodes. A 3 cm inner diameter and 60 cm long glass tube is positioned vertically. The electrodes are separated by 40 cm. The discharge current is varied from 0.4 to 2.5 mA, the pressure of neon is varied from 0.2 to 1 Torr. These conditions allow the formation of the natural standing strata in between two electrodes as shown in figure 1.9. A few grams of micron-sized particles are placed in a dust dropper in the upper side of the glass tube. The falling particles are trapped and suspended in the strata where the gravitational force $m_{\rm d}g = Z_{\rm d}eE_{\rm s}$ (g is the acceleration due to gravity and $E_{\rm s}$ is the electric field in the strata). Fortov *et al* (1997) used two types of dust grains in their experiments, namely borosilicate glass micro-balloons and alumina particles, both having the mass density 2.3 g cm^{-3}. The other parameters for such dusty plasmas are $T_{\rm e} = (3\text{–}30) \times 10^4$ K, $n_{\rm e} \simeq 10^9$ cm^{-3}, $n_{\rm d} = 10^3\text{–}10^4$ cm^{-3}, $T_{\rm d} = 300$ K (room temperature), $E_{\rm s} \simeq 10$ V cm^{-1}, $r_{\rm d} = 1\text{–}5$ μm and $Z_{\rm d} \sim 10^5$ (for alumina particles), $r_{\rm d} = 50\text{–}65$ μm and $Z_{\rm d} \simeq 10^6$ (for glass particles).

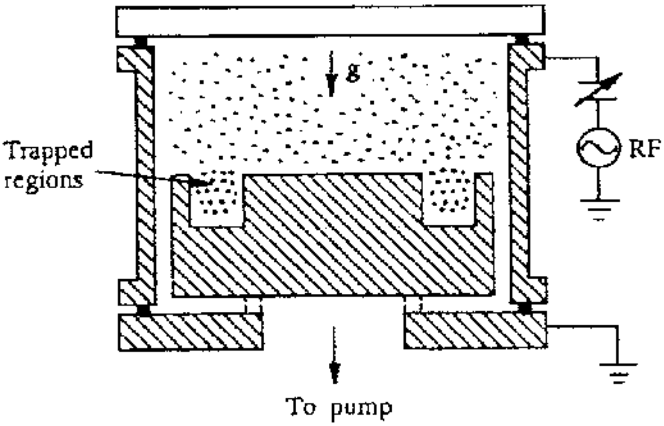

Figure 1.10. Sketch of the side view of the cylindrical discharge system (after Chu and I 1994).

1.5.3 rf discharges

A dusty plasma has been for the first time confined in a cylindrical symmetric rf plasma system (Chu and I 1994). The system, the side view of which is shown in figure 1.10, consists of a hollow outer electrode capacitively coupled to a 14 MHz rf power amplifier, a grounded centre electrode with a ring-shaped groove on the top for particle trapping and a top glass window for observation. A digital video recording system is used to monitor the image of the particles illuminated by a He–Ne laser through an optical microscope mounted on the top of the chamber. The optical axis is parallel to the symmetry axis of the system. The system is pumped by a diffusion pump. O_2 and SiH_4 are introduced into the chamber with 10 mTorr background argon gas. The ratio of the reactive gas flow to the partial pressure is kept 0.2 (cm^3 min^{-1}) mTorr^{-1}. The O_2 and SiH_4 partial pressures are kept equal. The rf power is kept at 30 W. The system total pressure is always kept less than 10 mTorr for the particle generation. An axial magnetic field (50–100 G) is also introduced to increase the generation efficiency. The particle size and number density increase with the reactive gas flow on time and pressure. After the formation of micron-sized particles, the reactive gas flows and the magnetic field is turned off. The particles are then trapped in the toroidal groove. Under the gravitational force, the particle diameter slowly increases with decreasing hight. The size of the particles is almost mono-dispersive within 3 mm along the vertical direction. The rf power precisely controlled by a programmable function generator is the main control parameter. It has been observed in such an experiment that at low rf power the dust particles are in the form of Coulomb crystals. However, as the rf power is increased, such crystals are melted.

The dusty plasma parameters, which are obtained from the micro-image and Langmuir probe measurements, are $n_e \simeq 10^9\ \mathrm{cm}^{-3}$, $n_d = 2 \times 10^5\ \mathrm{cm}^{-3}$, $r_d = 5\ \mu\mathrm{m}$ (SiO_2 particles), $T_e \simeq 23\,200$ K, $T_i \simeq 350$ K and $\Gamma_c = 100$–200.

1.6 Electrostatic Sheath

It is now clear that in all laboratory plasma devices the plasma is confined within finite solid boundaries (walls). The behaviour of the plasma near the walls (which is different from that away from the walls) in a two-component electron–ion plasma is well explained in some standard textbooks (Chen 1974). To understand the behaviour of dusty plasmas near the boundary walls, we consider a one-dimensional model with no appreciable electric field inside the plasma. We assume that the dusty plasma consists of thermal electrons, a cold ion fluid and negatively charged immobile dust grains. If the electrons and ions hit the wall at the same time, they combine and are lost. However, as the electrons have much higher thermal velocities than ions, they are lost faster than the ions and cause the boundary potential to be negative. This potential cannot be distributed over the entire plasma, since the Debye shielding will confine the potential variation to a layer of the order of several Debye lengths in thickness. This layer, which must exist on all cold boundary walls (with which the plasma is in contact), is called an electrostatic sheath.

To examine the exact behaviour of the potential $\phi_s(x)$ in the sheath, we assume that at the plane $x = 0$ the ions are entering the sheath region from the main plasma with a drift speed v_{i0}. These drifting ions are needed to account for the loss of ions to the wall from the region in which they were created by ionization. In steady state, we have for the cold ions

$$n_i v_i = n_{i0} v_{i0} \tag{1.6.1}$$

and

$$\tfrac{1}{2} m_i (v_i^2 - v_{i0}^2) = -e\phi_s \tag{1.6.2}$$

where n_{i0} is the number density of single-charged ions at $x = 0$ (i.e. where ϕ_s is taken to be zero). The electron number density n_e is given by equation (1.2.3). Equations (1.2.3), (1.6.1) and (1.6.2) are completed by Poisson's equation

$$\frac{\mathrm{d}^2\phi_s}{\mathrm{d}x^2} = 4\pi e(n_e + Z_d n_d - n_i) \tag{1.6.3}$$

and the macroscopic charge neutrality condition

$$Z_d n_d = n_{i0} - n_{e0}. \tag{1.6.4}$$

Combining equations (1.6.1) and (1.6.2) we have

$$n_i = n_{i0}\left(1 - \frac{2e\phi_s}{m_i v_{i0}^2}\right)^{-1/2}. \tag{1.6.5}$$

Substituting equations (1.2.3), (1.6.4) and (1.6.5) into equation (1.6.3) we obtain

$$\frac{\mathrm{d}^2\psi_s}{\mathrm{d}\xi^2} = \delta\left(1 + \frac{2\psi_s}{M^2}\right)^{-1/2} - \exp(-\psi_s) - (\delta - 1) \tag{1.6.6}$$

where $\psi_s = -e\phi_s/k_B T_e$, $\xi = x/\lambda_{De}$, $M = v_{i0}/c_s$, $c_s = (k_B T_e/m_i)^{1/2}$ and $\delta = n_{i0}/n_{e0}$. Equation (1.6.6) is the nonlinear equation describing the behaviour of the electrostatic potential in a dusty plasma sheath. Multiplying equation (1.6.6) by $\mathrm{d}\psi_s/\mathrm{d}\xi$ and integrating once, we obtain

$$\frac{1}{2}\left(\frac{\mathrm{d}\psi_s}{\mathrm{d}\xi}\right)^2 + V(\psi_s) = 0 \tag{1.6.7}$$

where $V(\psi_s)$ is given by

$$V(\psi_s) = (\delta - 1)\psi_s - \exp(-\psi_s) - \delta M^2\left(1 + \frac{2\psi_s}{M^2}\right)^{1/2} + C_s \tag{1.6.8}$$

and C_s is an integration constant which takes the value $C_s = 1 + \delta M^2$ for $\psi_s = 0$ and $\mathrm{d}\psi_s/\mathrm{d}\xi = 0$ at $\xi = 0$. Equation (1.6.7) can be regarded as an 'energy integral' of an oscillating particle of pseudo-mass '1', pseudo-position 'ψ_s', pseudo-speed '$\mathrm{d}\psi_s/\mathrm{d}\xi$' and pseudo-potential (also known as the Sagdeev potential) '$V(\psi_s)$'. The nature of ψ_s in the plasma sheath can, therefore, be studied either by analysis of the Sagdeev potential $V(\psi_s)$ or by the numerical solution of equation (1.6.7). Whatever the method one uses, because of the square root term in equation (1.6.8), there is a lower bound $\psi_s = -M^2/2$ for the potential, at which the ion density becomes infinite. Without going into further numerical details of equation (1.6.7), we analyse $V(\psi_s)$ for the small-amplitude limit (i.e. $\psi_s \ll 1$) which provides some useful information about how the nature of ψ_s in a dusty plasma sheath differs from that in an electron–ion (two-component) plasma. For the small amplitude limit, we expand $V(\psi_s)$ in a Taylor series and obtain

$$V(\psi_s) = C_1\psi_s^2 + C_2\psi_s^3 \ldots \tag{1.6.9}$$

where $C_1 = (\delta/M^2 - 1)/2$ and $C_2 = (1/3 - \delta/M^4)/2$. It turns out that the solution of equation (1.6.7) exists if $C_1 < 0$. The latter yields

$$\frac{\delta}{M^2} - 1 < 0. \tag{1.6.10}$$

The condition (1.6.10) is the modified Bohm criterion in the dusty plasma under consideration. It is clear that in the absence of the dust particles, $\delta = 1$ and the Bohm criterion for the electron–ion (two-component) plasma becomes $M > 1$, whereas in the presence of the dust particles we have $\delta > 1$ so that the Bohm criterion becomes $M > M_c$, where $M_c = \sqrt{\delta}$. This clearly explains how the presence of the dust particles modifies the Bohm criterion or the critical Mach number M_c. Since δ is a function of n_{d0} and Z_d, the Bohm criterion is modified by the dust particle number density. We find that as n_{e0} decreases (i.e. n_{d0} or Z_d increase), the critical Mach number M_c increases. The Bohm criterion dictates that ions entering the sheath from the main body of the plasma must have a super ion acoustic speed, which is larger when the dust grains are present.

1.7 Some Aspects of Dusty Plasmas

The physics of dusty plasmas is a topic of growing importance, which has gained more and more interest over the last few years not only from the academic point of view, but also from the view of its new aspects in space and modern astrophysics, semiconductor technology, fusion devices, plasma chemistry, crystal physics, biophysics, etc. In the following sections, we briefly discuss some of these important aspects.

1.7.1 Space science and astrophysics

The basic physics and chemistry of dusty plasmas in space (such as in planetary rings, in cometary tails, in interstellar clouds, etc) is similar to that of low-pressure laboratory dusty plasmas, but we have already shown in sections 1.3 and 1.4 that the plasma conditions for space dusty plasmas can differ from those of laboratory dusty plasmas by huge orders of magnitudes. The first hint that dust particles were charged by the space plasma particles might explain some heavenly features came in October 1980 when Voyager 1 sped past Saturn and sent back pictures of mysterious dark spokes (Smith *et al* 1981) sweeping around the B ring (the planet's largest and brightest ring). It was then proposed by Hill and Mendis (1981a) as well as by Goertz and Morfill (1983) that the spokes might be charged dust and sculpted by electrostatic forces. Hill and Mendis (1981a) argued that electrons hurled into the ring by aurora-like processes near Saturn might have electrified the dust, while Goertz and Morfill (1983) attributed the electrification to the burst of the plasma generated as micrometeoroids pelted the boulder of the ring. Both of these mechanisms would tend to produce spoke-like regions (shown in figure 1.4) of electrification, where electrostatic repulsion between dust particles and the boulders would raise trails of the dust grains.

On the other hand, the way by which tiny dust particles were distributed in the cometary tails could not be explained by gravity or by other forces (associated with Sunlight pressure) acting on uncharged dust grains of this size. The solar radiation pressure should push the dust grains directly outward from the Sun, introducing tail symmetry above and below the cometary orbital plane. But the spacecraft that intercepted Comet Halley found that the smaller dust grains gathered on one side of that plane (Glanz 1994). This can be explained by assuming that the dust particles picked up an electric charge from the solar wind and that the charged dust particles moving through the magnetic field feel a force perpendicular to their direction of travel and to the field direction. As the pressure of the Sunlight is pushing the grains directly away from the Sun and the magnetic field of the solar wind spirals along the ecliptic plane like the grooves in a phonograph record, the charged grains should get pushed either upwards or downwards with respect to the orbital plane of the comet depending on their charge. The calculations of the interaction between the grains and the solar wind plasma showed that it would tend to give the grains a negative charge and the resulting force would push them below the orbital plane—exactly where they were observed.

The different physical and chemical processes become important in these various space dusty plasma situations. For example, the electrostatic equilibrium of a solid grain in the solar system can be affected by the photoelectron emission due to the solar radiation (which we will discuss in detail in chapter 2). It has been shown by Goertz (1989) that this leads to an electrostatic equilibrium of the particles which can be both size and time dependent, with a possible positive charge for larger ($r_{\rm d} \simeq 6~\mu$m) particles and a negative charge for smaller ($r_{\rm d} \simeq 1~\mu$m) particles. These considerations play a key role in several aspects:

(i) The chance of two dust particles combining to form a larger particle following a collision increases when the particles are oppositely charged. This is important in understanding the evolution of the grain-size distribution.

(ii) The grain motion in planetary rings is influenced by electrical forces connected with the grain's charge. The Voyager observations of Saturn's rings revealed the existence of radially elongated ($\sim 10^6$ m) discs with light-scattering properties that suggest that the rings contain small grains (about a micron or less). These spokes are described through a gravito-electrodynamics model which suggests that electrostatic forces may be responsible for the rich structure observed in Saturn's rings via the radial transport of the grains.

One of the other important applications of dusty plasma physics is to understand how ambipolar diffusion and interstellar grains (both charged and neutral) regulate the formation and evolution of proto-stellar cores in interstellar molecular clouds. The dynamics or even the presence of charged dust particles in the interstellar molecular clouds (which is, in fact, a partially ionized dusty plasma with a significant fraction of neutrals) may affect the gravitational contraction process which causes the collapse of the large interstellar clouds. The dust particles, by the process of coagulation, turn out to be a dust ball which serves as a core, and around such cores the gaseous components of the cloud can collapse. Therefore, the presence or the dynamics of charged dust grains essentially plays a vital role in star formation via self-gravitational instability.

Table 1.7. The main plasma processes used in the semiconductor industry (Hopkins and Lawler 2000).

Application	Method	Materials
Deposition	1. Plasma-enhanced chemical vapour deposition	SiO_2, SiN, TEOS, dielectric, etc
	2. Physical vapour deposition	Metal (Al, Cu, etc)
Reactive ion etch	1. Polysilicon etch	Si, SiN, silicide, etc
	2. Dielectric etch	SiO_2, TEOS, K, etc
	3. Metal etch	Al, Ti, TiN, W, etc
Implant	Plasma ion source for doping	AS, B, Sb, P, etc
Ash	Photo-resist and residue removal	AS, B, Sb, P, etc

1.7.2 Semiconductor industry

During the past few decades, the science of high-temperature and collisionless plasmas has grown explosively, fuelled by the challenging problems in magnetic fusion, inertial fusion and space plasma physics. As funds for basic research in fusion and space plasmas dwindle, it is fortunate that a new application of plasma physics has loomed large within the past five years—the application of low-temperature, partially ionized plasmas (dusty plasmas) in the manufacturing of chips and material processing (Chen 1995, Hopkins and Lawler 2000). This aspect of dusty plasma physics may indeed ultimately come to have one of the greatest impacts on our everyday lives. Clear evidence that these dust problems are connected with plasma technologies was first presented in the pioneering work of Roth *et al* (1985) on silane discharges and in Selwyn *et al* (1989) on microelectronics etching or sputtering tools. The number of applications of plasma processing in the industrial environment has accelerated enormously in the last few years. While once they were purely the remit of academic interest, they now form the cornerstones of several economically important industries. The largest of these is the semiconductor industry, which in 1999 represented a global market of 155 billion US dollars (Hopkins and Lawler 2000). We agree that much of the technology developed in this industry lags behind the recent advances in other areas such as micro-mechanical systems, integrated optical communications, etc. The application of plasma processes in manufacturering semiconductor devices can be divided into four main areas, shown in table 1.7.

The largest by far of these are the deposition and etching processes, as devices are basically a series of patterned layers. The deposition technique forms the layers and etching develops the device pattern in these layers formed by the lithography steps. These processes are also an integral part of the lithography steps as they are used to form the reticles/masks used by the photo-lithography process to pattern the device on the silicon wafers. There are two main types of plasma systems used commercially: capacitively coupled and inductively coupled. There are also a number of electron cyclotron resonance sources and helicons, though these are less common.

1.7.3 Plasma chemistry and nanotechnology

The field of dusty plasmas, which is in fact a multi-disciplinary research topic of recent interest, involves not only numerous physical processes, but also deals with fundamental mechanisms and questions that arise in detailed physics and chemistry leading to particle formation. The heterogeneous and homogeneous nucleation phenomena determine the formation of very small (less than nanometre) sized proto-particles. The formation of proto-particles is followed by agglomeration and coagulation processes, as similarly found in other parts of chemistry such as colloidal chemistry.

Basically the formation of powder in a reactive plasma starts with the formation of primary clusters of atoms which grow during a nucleation phase up to a critical number density. The coagulation or agglomeration leads then to macro-particles with size around 50 nm, which finally grow to micrometre-sized particles by accretion of neutrals or ionic monomers, since further agglomeration is prevented by the particle charging (Bouchoule 1999, Perrin and Hollenstein 1999, Gallagher 2000, Hollenstein 2000). The powder formation is observed in most of the popular reactive plasmas that are used for industrial applications (Bouchoule 1999). The powder formation is not only found in hydrocarbon and silane plasmas, but also in plasmas with more complex monomers such as hexamethyldisiloaxane or oxygen plasmas (Perrin and Hollenstein 1999, Hollenstein 2000). At present, the different mechanisms and processes leading to powder formation in these reactive plasmas are far from being elucidated. The behaviour of larger particles (of radius larger than few tens of nanometres) produced in the process of powder formation is more or less well understood. However, on the formation and behaviour of the smaller proto-particles and their chemistry only little is known; this is essentially due to experimental difficulties in detecting and monitoring these small particles in detail. Besides the different physical and chemical processes leading to the formation of these proto-particles or precursors, the nature of the nucleation process plays a primary role. The nucleation process may be driven either by homogeneous or heterogeneous reactions. However, in many cases it is found to be very difficult to distinguish the real origin of the nucleation and much research effort is at present spent on this problem.

It is still believed that homogeneous reactions dominate the powder formation reactions in pure silane rf plasmas. The particle growth in these plasmas is thought to be a consequence of the strong electron-attachment energies of

Si-containing molecules and particles (Perrin and Hollenstein 1999, Gallagher 2000, Hollenstein 2000). Recently, a steady-state homogeneous model of particle growth in silane discharges has been proposed by Gallagher (2000) who assumed that particles grow primarily from SiH_3^- and SiH_m radicals, first into $Si_xH_m^-$ ions and Si_xH_m radicals, then with increasing x into clusters containing multiply bonded silicon, and finally into compact, primarily silicon particles.

A number of experimental investigations (Kushner 1988) has been performed in order to address the powder precursors in these plasmas and the gas-phase reactions leading to large clusters that finally agglomerate to form particles up to a micrometre in size. The neutral radicals have been the candidates for particle precursors since reaction path propagation is supposed to proceed by the insertion of silane radicals into higher-mass saturated molecules (Hollenstein 2000). The positive ions have also been invoked as potential powder precursors, although it has been found that activation barriers exist, preventing the formation of high-mass cations. The negative ions are also experimentally found to exist in silane plasmas (Hollenstein 2000). The experimental anti-correlation between the negative ion intensity and the powder formation and their rf modulation frequency dependence indicate the importance of the anion trapping in this process. At lower rf power modulation frequencies all the negative ions formed leave the discharge volume, but at higher power modulation frequencies the plasma off time is too short to empty completely the discharge of the negative ions. Thus, in the latter case a large fraction of the negative ions remains trapped and they accumulate and grow towards higher and higher masses in a similar way as in the model recently considered by Gallagher (2000). It has been, therefore, proposed that negative ions may be the most possible powder precursors in a pure rf SiH_4 plasma at low or moderate power densities and that the polymerization pathway proceeds via negative ion clustering. The possible path way for SiH_4 addition reactions proposed by Perrin and Hollenstein (1999) is

$$\mathrm{Si}_n\mathrm{H}_m^- + \mathrm{SiH}_4 \longrightarrow (\mathrm{Si}_{n+1}\mathrm{H}_{m'}^-)^* + (\mathrm{H}, \mathrm{H}_2)\ \text{products} \tag{1.7.1}$$

where excited negative ions $(\mathrm{Si}_{n+1}\mathrm{H}_{m'}^-)^*$ may relax either by redistribution of excess energy among internal re-vibrational modes or by stabilizing collisions with a third body with their auto-detachment lifetime

$$(\mathrm{Si}_{n+1}\mathrm{H}_{m'}^-)^* + M \longrightarrow \mathrm{Si}_{n+1}\mathrm{H}_{m'}^- + \mathrm{M}. \tag{1.7.2}$$

The mutual anion–cation recombinations as given by

$$\mathrm{Si}_n\mathrm{H}_m^- + \mathrm{Si}_p\mathrm{H}_q \longrightarrow \mathrm{Si}_{n'}\mathrm{H}_{m'} + (\mathrm{H}, \mathrm{H}_2)\ \text{products} \tag{1.7.3}$$

followed by re-attachment of an electron on the recombined neutral

$$\mathrm{e} + \mathrm{Si}_{n'}\mathrm{H}_{m'} \longrightarrow (\mathrm{Si}_{n'}\mathrm{H}_{m'})^* \longrightarrow \mathrm{Si}_{n'}\mathrm{H}_{m'} \tag{1.7.4}$$

may be a second possible polymerization path as proposed by Haaland (1990). The agglomeration, as often observed in dusty plasmas, is a fundamental process which plays an important role in many parts of physics, chemistry and astrophysics (Horányi and Goertz 1990). After a first phase, where the plasma chemistry dominates, a few nanometre-sized primary particles or proto-particles are formed. They reach a critical number density that triggers a rapid growth or an agglomeration phase. Within a short time the particle size strongly increases up to a few hundred nanometres, whereas the particle number density decreases drastically over several orders of magnitude. The agglomeration and its different forms such as coagulation and flocculation are the basic phenomena in colloidal systems such as aerosols (Bouchoule 1999, Perrin and Hollenstein 1999, Hollenstein 2000). It has been assumed in most of the previous models for agglomeration in dusty plasmas that the agglomerating particles are electrically neutral and so all classes of particles can agglomerate with each other. However, particles in the plasma, especially particles of several nanometres or larger in size are necessarily electrically charged. The particle charging might reduce the agglomeration rate and also influence the limit of the maximum achievable particle size. Recently, a few attempts have been made in order to include the charging into an agglomeration model (Kortshagen and Bhandarkar 1999, Kim and Kim 2000).

1.7.4 Fusion research

We have already discussed in section 1.4.3 the properties of dust grains and their occurrence in fusion devices. The dust is indeed an important safety issue for ITER and future fusion reactors. The dust particles may retain a large fraction of hydrogen (>0.2 H/C) which will lead to considerable tritium inventories (Winter 1998, 2000). Furthermore, these fine dispersed dust particles may be chemically reactive and may spontaneously react with oxygen or water vapour in the case of a vacuum or coolant leak. A further aspect is the migration of dust particles. Due to thermophoretic forces and due to repetitive evaporation and condensation they may accumulate at cold areas of the device. They may block spacings and fill gaps which were introduced for engineering reasons. The heat transfer to actively cooled components may be impeded by a loose dust layer on the surface.

The problem of dust in tokamaks is of growing interest now. The sizes of the dust particles, which are observed in tokamaks TEXTOR, DIII-D, ALCATOR C-MOD, TFTR, etc, range from $\sim$100 nm to $\sim$100 μm (Winter 1998, 2000). The strongest evidence for a self-organized structure (Tsytovich 1997) of the tokamak dust is probably the fractal structures of the cauliflower-like forms shown in figure 1.5.

1.7.5 Crystal physics

The search for ordered many-body Coulomb systems in laboratory devices has been a problem of great interest over the past few decades. The competition between the mutual Coulomb interaction and the background thermal fluctuation

Table 1.8. The basic differences between the solid and dusty plasma crystals.

Characteristics	Solid-state crystal	Dusty plasma crystal
Crystal type	atomic crystals	dust crystals
Interaction energy	a few eV	$\sim$900 eV
Lattice spacing	$\sim$0.1 nm	$\sim$1 mm

plays a key role in determining the degree of ordering of the Coulomb system (Ichimaru 1982, Liu *et al* 1999). As the Coulomb coupling parameter Γ_c increases, the system can be self-organized from a disordered gas phase to a more ordered condensed phase. The Wigner crystals can be formed when Γ_c reaches the order of a few hundred (Wigner 1938).

The formation of Coulomb crystals in dusty plasmas, which widely exists in various systems, such as astro-plasma systems, industrial plasma processing systems, laboratory discharge systems, etc has attracted a great deal of attention during the last few years. It has been found that micron-sized dust particles suspended in a gaseous plasma background of temperature of a few electronvolts can be charged up to 10^4 electrons due to the much higher electron mobility than ion mobility. These large charges of the massive dust particle drastically increase the coupling constant Γ_c by eight orders of magnitude, and the suspended dust clouds can be turned into ordered crystal states even at room temperature and with a submicron lattice constant. The large dust mass slows down the timescale to the order of a second and the proper spatial scales make direct observations of particle trajectories feasible through optical micro-imaging. Therefore, unlike in an atomic-scale system, the macroscopic structure and its dynamical behaviour can be directly studied in real time and space.

Recently, a number of laboratory experiments (e.g. Chu and I 1994, Thomas *et al* 1994, Hayashi and Tachibana 1994, Melzer *et al* 1994) have demonstrated that highly ordered dust structures (known as 'dusty plasma crystals') are formed when $\Gamma_c \geq 170$. The latter was first theoretically predicted by Ikezi (1986). The dusty plasma crystals are, of course, different from the usual solid state crystals. The basic differences between the solid and dusty plasma crystals are pointed out in table 1.8. However, experimental observations reveal that as the temperature of the dust is increased (i.e. Γ_c is decreased), the dust crystals melt and then vaporize so that one encounters the usual weakly coupled ideal Coulomb plasma. Thus, laboratory experiments in such a dusty plasma system, which provide an excellent opportunity for the study of a transition from the strongly coupled to a weakly coupled regime and vice-versa, open up new and interesting aspects of dusty plasma physics (to be described in detail in chapter 8).

Chapter 2

Dust Charging Processes

2.1 Introduction

The central point in the physics of dusty plasmas is to understand the charging of dust grains which are invariably immersed in an ambient plasma with radiative background. The elementary processes that lead to the charging of dust grains are quite complex and depend mainly on the environment around the dust grains. The important elementary dust grain charging processes are (i) interaction of dust grains with gaseous plasma particles, (ii) interaction of dust grains with energetic particles (electrons and ions) and (iii) interaction of dust grains with photons.

When dust grains are immersed in a gaseous plasma, the plasma particles (electrons and ions) are collected by the dust grains which act as probes. The dust grains are, therefore, charged by the collection of the plasma particles flowing onto their surfaces. The dust grain charge q_{d} is determined by $\mathrm{d}q_{\mathrm{d}}/\mathrm{d}t = \sum_j I_j$, where j represents the plasma species (electrons and ions) and I_j is the current associated with the species j. At equilibrium the net current flowing onto the dust grain surface becomes zero, i.e. $\sum_j I_{j0} = 0$, where I_{j0} is the equilibrium current. This means that the dust grain surface acquires some potential ϕ_{g} which is $-2.5k_{\mathrm{B}}T/e$ (where $T = T_{\mathrm{e}} \simeq T_{\mathrm{i}}$) for a hydrogen plasma and $-3.6k_{\mathrm{B}}T/e$ for an oxygen plasma (Northrop 1992). It turns out that the dust grains immersed in a gaseous plasma are usually negatively charged. When energetic plasma particles (electrons or ions) are incident onto a dust grain surface, they are either backscattered/reflected by the dust grain or they pass through the dust grain material. During their passage they may lose their energy partially or fully. A portion of the lost energy can go into exciting other electrons that in turn may escape from the material. The emitted electrons are known as secondary electrons. The release of these secondary electrons from the dust grain tends to make the grain surface positive. The interaction of photons incident onto the dust grain surface causes photoemission of electrons from the dust grain surface. The dust grains, which emit photoelectrons, may become positively charged. The emitted electrons collide with other dust grains and are captured by some of these grains which may become negatively charged. There are, of course, a number of other dust grain charging mechanisms, namely thermionic emission, field emission, radioactivity, impact ionization etc. These are significant only in some different special circumstances.

To explain different important dust grain charging processes, we consider first isolated dust grains and then non-isolated dust grains. We also describe how the dust grain charge (in both isolated and non-isolated cases) can be measured in laboratory experiments. We finally discuss some important consequences of the dust grain charging processes.

2.2 Isolated Dust Grains

It is quite difficult to explain/understand the charging of a dust grain if all the charging processes mentioned above are included simultaneously. We, therefore, consider small isolated dust grains ($r_{\rm d} \ll \lambda_{\rm D} \ll a$) and explain each of the important dust grain charging mechanisms one by one.

2.2.1 Collection of plasma particles

We consider a finite-sized neutral dust particle immersed in an unmagnetized plasma whose constituents are electrons and ions. Since the electron thermal speed is much larger than the ion thermal speed, the electrons reach the dust grain surface much more rapidly than the ions. Thus, the dust grain acquires much more electrons than ions, and as a result its surface potential becomes negative. On the other hand, absorption of the plasma ions tends to make the dust grain charge as well as its surface potential positive. The currents of the primary electrons and ions are, of course, affected by the grain surface potential itself, since they depend on the relative speed between the plasma and the dust grain. When the surface potential is negative, the electrons are repelled and the ions are attracted, i.e. the dust grain current carried by the electrons is reduced and that carried by the ions is increased. On the other hand, if the surface potential is positive, the electrons are attracted and the ions are repelled, i.e. the grain current carried by the electrons is increased and that carried by the ions is reduced.

We now calculate the charging current I_j to the dust grain carried by the plasma particle j by using the orbit-limited motion (OLM) approach (Chen 1965, Allen 1992). We consider (as shown in figure 2.1) that from an infinite distance a plasma particle j is approaching a spherical dust grain of radius $r_{\rm d}$ and charge $q_{\rm d}$. When the plasma particle enters the Debye sphere, it feels the influence of the dust grain and its path changes due to the electrostatic force. We assume that v_j and $v_{{\rm g}j}$ are the speed of the plasma particle before and after its grazing collision with the dust grain. It is obvious that for a fixed velocity, as we decrease the impact parameter b_j, the plasma particle hits the dust grain. The cross section for charging collisions between the dust and the plasma particle j is $\sigma_j^{\rm d} = \pi b_j^2$.

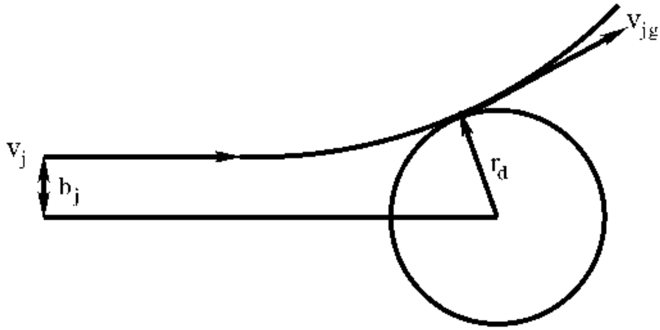

Figure 2.1. Grazing collisions between a plasma particle j and a charged dust particle with $q_j q_{\mathrm{d}} < 0$.

Conservation of momentum and energy requires that

$$m_j v_j b_j = m_j v_{\mathrm{g}j} r_{\mathrm{d}} \tag{2.2.1a}$$

and

$$\frac{1}{2} m_j v_j^2 = \frac{1}{2} m_j v_{\mathrm{g}j}^2 + \frac{q_j q_{\mathrm{d}}}{r_{\mathrm{d}}}. \tag{2.2.1b}$$

The dust grain charge q_{d} is related to the potential difference $\phi_{\mathrm{d}}(= \phi_{\mathrm{g}} - \phi_{\mathrm{p}})$ between the grain potential ϕ_{g} and the plasma potential ϕ_{p}, i.e. $q_{\mathrm{d}} = C\phi_{\mathrm{d}}$, where the capacitance C of the spherical dust grain in a plasma is $C = r_{\mathrm{d}} \exp(-r_{\mathrm{d}}/\lambda_{\mathrm{D}}) \simeq r_{\mathrm{d}}$ for $\lambda_{\mathrm{D}} \gg r_{\mathrm{d}}$. Using the relation $q_{\mathrm{d}} = r_{\mathrm{d}}\phi_{\mathrm{d}}$ and equations (2.2.1a) and (2.2.1b) one can easily express b_j in terms of ϕ_{d}. Thus, σ_j^{d} becomes

$$\sigma_j^{\mathrm{d}} = \pi r_{\mathrm{d}}^2 \left(1 - \frac{2 q_j \phi_{\mathrm{d}}}{m_j v_j^2}\right). \tag{2.2.2}$$

If $f_j(v_j)$ is the velocity distribution of the plasma species j at infinite distance from the dust grain, the dust grain charging current I_j carried by the plasma species j is

$$I_j = q_j \int_{V_j^{\min}}^{\infty} v_j \sigma_j^{\mathrm{d}} f_j(v_j)\, \mathrm{d}\boldsymbol{v}_j \tag{2.2.3}$$

where $V_j^{\min}$ is the minimum value of the plasma particle velocity for which the particle hits the dust grain. To approximate $V_j^{\min}$ we consider two situations, namely $q_j\phi_{\mathrm{d}} < 0$ and $q_j\phi_{\mathrm{d}} > 0$. When $q_j\phi_{\mathrm{d}} < 0$, the plasma particle and the dust grain attract each other and the integration in equation (2.2.3) is to be performed over the complete v_j domain. On the other hand, when $q_j\phi_{\mathrm{d}} > 0$, the plasma particle and the dust grain repel each other and hence $V_j^{\min} > 0$ in order to allow for a collision between the dust grain and the plasma particle. Thus, in this case V_j^{min} becomes

$$V_j^{\mathrm{min}} = \left(-\frac{2q_j\phi_{\mathrm{d}}}{m_j}\right)^{1/2}. \tag{2.2.4}$$

We further assume that the velocity distribution of the plasma species is Maxwellian, i.e.

$$f_j(v_j) = n_j\left(\frac{m_j}{2\pi k_{\mathrm{B}}T_j}\right)^{3/2}\exp\left(-\frac{m_j v_j^2}{2k_{\mathrm{B}}T_j}\right) \tag{2.2.5}$$

where n_j is the plasma particle number density. Substituting equations (2.2.2) and (2.2.5) into equation (2.2.3), expressing the result in spherical polar coordinates and performing the integration, we can write the charging current I_j for attractive ($q_j\phi_{\mathrm{d}} < 0$) and repulsive ($q_j\phi_{\mathrm{d}} > 0$) potentials as

$$I_j = 4\pi r_{\mathrm{d}}^2 n_j q_j\left(\frac{k_{\mathrm{B}}T_j}{2\pi m_j}\right)^{1/2}\left(1-\frac{q_j\phi_{\mathrm{d}}}{k_{\mathrm{B}}T_j}\right) \qquad \text{for } q_j\phi_{\mathrm{d}} < 0 \tag{2.2.6}$$

and

$$I_j = 4\pi r_{\mathrm{d}}^2 n_j q_j\left(\frac{k_{\mathrm{B}}T_j}{2\pi m_j}\right)^{1/2}\exp\left(-\frac{q_j\phi_{\mathrm{d}}}{k_{\mathrm{B}}T_j}\right) \qquad \text{for } q_j\phi_{\mathrm{d}} > 0. \tag{2.2.7}$$

Equation (2.2.7) is valid for any repulsive potential in a Maxwellian plasma as long as the surface potential has a monotonic behaviour outwards from the surface as well as when the streaming speed v_{j0} is much smaller than the thermal speed $V_{\mathrm{T}j}$. Now, we consider a more general dusty plasma situation in which the ions have some finite streaming speed. For such a situation the electron current is as before, but the ion current will be different and can be calculated by using the ion distribution function

$$f_{\mathrm{i}}(v_{\mathrm{i}}) = n_{\mathrm{i}}\left(\frac{m_{\mathrm{i}}}{2\pi k_{\mathrm{B}}T_{\mathrm{i}}}\right)^{3/2}\exp\left[-\frac{m_{\mathrm{i}}(v_{\mathrm{i}}-v_{\mathrm{i}0})^2}{2k_{\mathrm{B}}T_{\mathrm{i}}}\right]. \tag{2.2.8}$$

Thus, following the same procedure as before, we can obtain the ion current I_{i}. For negatively charged dust grains we have (Shukla 1996)

$$I_{\mathrm{i}} = 4\pi r_{\mathrm{d}}^2 e n_{\mathrm{i}}\left(\frac{k_{\mathrm{B}}T_{\mathrm{i}}}{2\pi m_{\mathrm{i}}}\right)^{1/2}\left[F_1(u_0) - F_2(u_0)\frac{e\phi_{\mathrm{d}}}{k_{\mathrm{B}}T_{\mathrm{i}}}\right] \tag{2.2.9}$$

where $F_1(u_0) = (\sqrt{\pi}/4u_0)(1+2u_0^2)\,\mathrm{erf}(u_0) + (1/2)\exp(-u_0^2)$ and $F_2(u_0) = (\sqrt{\pi}/2u_0)\,\mathrm{erf}(u_0)$ are written in terms of the error function $\mathrm{erf}(u_0) = (2/\sqrt{\pi})\int_0^{u_0}\exp(-t^2)\,\mathrm{d}t$ and $u_0 = v_{\mathrm{i}0}/V_{\mathrm{Ti}}$. It is easy to show by Taylor series expansion around $u_0 = 0$ that both the function F_1 and F_2 approach unity as u_0 approaches zero. Thus, it is obvious that for ion streaming speed much less than the ion thermal speed, i.e. for $u_0 \ll 1$, equation (2.2.9) reduces to equation (2.2.7) with $j = i$ and $q_i = e$. On the other hand, if the ion streaming speed is much larger than the ion thermal speed, i.e. if $u_0 \gg 1$, the ion current can be approximated as

$$I_i \simeq \pi r_d^2 e n_i v_{i0} \left(1 - \frac{2e\phi_d}{m v_{i0}^2}\right). \tag{2.2.10}$$

We discussed above the charging current for an orbit-limited sphere. But what will be the corresponding charging current I_j for an orbit-limited cylinder? The answer to this question was provided by Whipple (1981) who considered a Maxwellian distribution of plasma particles (electrons and ions) and showed that the charging current I_j for an orbit-limited cylinder with $q_j\phi_d < 0$ is

$$I_j = 2\pi r_d L_d n_j q_j \left(\frac{k_B T_j}{2\pi m_j}\right)^{1/2} \frac{2}{\sqrt{\pi}} \left[\psi_d + \frac{\sqrt{\pi}}{2} \exp(\psi_d^2)\,\mathrm{erfc}(\psi_d)\right] \tag{2.2.11}$$

where $\mathrm{erfc}(\psi_d)$ is the complementary error function defined as

$$\mathrm{erfc}(\psi_d) = \frac{2}{\sqrt{\pi}} \int_{\psi_d}^{\infty} \exp(-t^2)\,\mathrm{d}t \tag{2.2.12}$$

$\psi_d = (-q_j\phi_d/k_B T_j)^{1/2}$ and L_d is the length of the cylindrical dust grain. The concept of the OLM can be further generalized to include collectors that are less symmetric than spheres and circular cylinders (Laframboise and Parker 1973).

We may also ask ourselves: how can we obtain the charging current that is sheath-limited rather than orbit-limited? When the current is sheath-limited, the range of integration must be determined from the behaviour of the particle trajectories in the sheath. This is, in general, a complicated problem that can only be treated numerically by following particle orbits and by treating the potential distribution self-consistently.

2.2.2 Secondary electron emission

The energetic primary plasma particles falling onto a dust grain surface may cause a release of secondary electrons from the latter. The process of secondary electron emission can occur in two ways: one by electron impact and the other by ion impact. We now briefly discuss these two processes.

2.2.2.1 Electron impact

When an electron approaches a dust grain surface, it has to face any of the following possible situations: it may be scattered/reflected by the dust grain before it enters into the dust grain, it may enter into the dust grain and stop immediately (i.e. stick onto the dust grain surface), it may enter into the dust grain, interact with scattering centres and pass a part or all of the dust material wherein it may lose its energy, and a portion of this energy can go into exciting other electrons which in turn may escape from the grain surface. These situations, namely reflection, absorption, transmission/tunnelling and secondary emission are usually treated as distinct processes. Reflection or absorption is only significant for incident electrons with very low energies. The tunnelling/transmission refers to those electrons which leave the dust grain material with a similar but somewhat lower energy than they had upon entering the dust grain. The tunnelling is experimentally distinguished from the secondary emission primarily by the energy of the emitted electrons. The contribution of the processes of scattering/reflection and absorption/collection of primary plasma particles is described in the previous section. The present section is, therefore, concerned with the processes of tunnelling/transmission and secondary electron emission which directly lead to the charging of the dust grains.

We first discuss how one can obtain the expression for the secondary emission yield from a spherical dust grain surface. The well known Sternglass formula (Sternglass 1954, Jonker 1952) for the secondary emission yield from semi-infinite slabs of material, where the electrons are assumed to escape from only one surface (the side at which the primary electrons enter), cannot be used when dealing with different geometries other than a planar slab. For a situation of spherical dust grains the secondary electrons are not limited to the point of incidence of primary electrons, but may also exit from all points of the grain surface. Thus, the secondary emission yield for spherical dust grains is higher than that determined by the Sternglass formula. Chow *et al* (1993) have modified the yield equation of Jonker (1952) and have derived the modified yield equation for the enhanced secondary emission yield from a very small spherical dust grain.

Chow *et al* (1993) have considered a very small spherical dust grain and have assumed that (i) the energy loss of the primary electrons can be described by Whiddington's law (Whiddington 1912): $E(x) = (E_{\mathrm{p}}^2 - K_{\mathrm{W}}x)^{1/2}$, where $E(x)$ is the energy of the primary electron at a depth x (after entering into the dust grain), E_{p} is the initial energy of the primary electron (just before entering into the dust grain) and K_{W} is Whiddington's constant for energy loss with distance, (ii) the primary electron current density is conserved within the grain, (iii) the production of secondaries is proportional to the energy loss of the primaries, (iv) the secondary electron flux decreases exponentially with distance between the surface and the point of production and (v) the primary electrons are incident normal to the grain. Using these assumptions we can express the current $\mathrm{d}i_{\mathrm{s}}$ associated with the secondary electrons (excited by the primary electrons that have traversed a distance from x to $x + \mathrm{d}x$ beneath the dust grain surface) as

$$\mathrm{d}i_{\mathrm{s}} = -K_{\mathrm{s}}I_{\mathrm{e}}\mathrm{e}^{-\alpha l(x,\theta)}\frac{\mathrm{d}E}{\mathrm{d}x}\,\mathrm{d}x \qquad (2.2.13)$$

where α is the inverse of the absorption length for secondaries, K_{s} represents

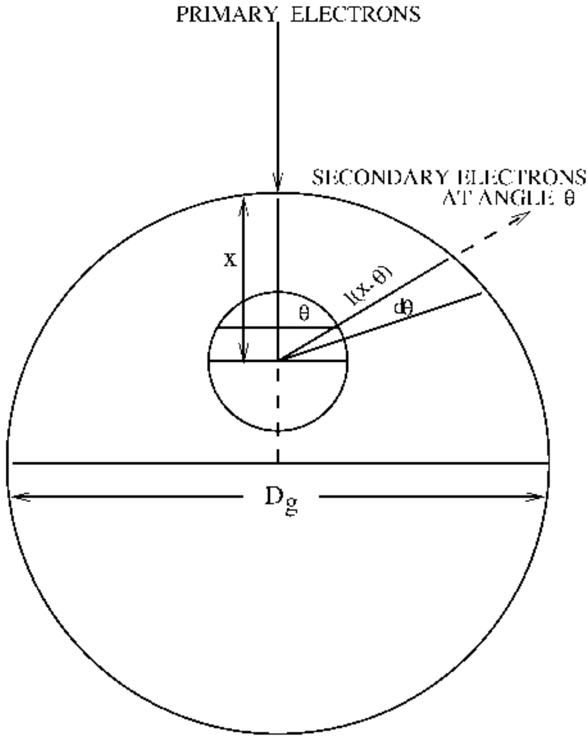

Figure 2.2. The model geometry for the secondary electron emission from a small spherical dust grain (after Chow *et al* 1993).

the efficiency with which the lost primary electron energy is used to excite the secondaries and $l(x,\theta)$ is the distance that a secondary electron must travel to reach the surface from a depth x and along an angle θ from the primary electron path (as shown in figure 2.2). To determine the length $l(x,\theta)$, we neglect the contribution of the scattering process and assume that the secondaries are emitted isotropically in all directions from the point of excitation (Jonker 1952). The geometry for the secondary electron emission shown in figure 2.2 allows us to express $l(x,\theta)$ as

$$l(x,\theta) = [r_{\mathrm{d}}^2 + (r_{\mathrm{d}} - x)^2 - 2r_{\mathrm{d}}(r_{\mathrm{d}} - x)\cos\theta']^{1/2} \tag{2.2.14}$$

where $\theta' = \theta - \sin^{-1}[(r_{\mathrm{d}} - x)\sin\theta/r_{\mathrm{d}}]$. It is easily shown that the ratio of the secondaries emitted at an angle θ in the range θ and $\theta + \mathrm{d}\theta$ to the total number of excited secondaries is $0.5\sin\theta\,\mathrm{d}\theta$. It should be noted that, for a spherical dust grain, θ can vary from 0 to π, whereas, for a planar slab, θ is limited to $\pi/2$. Using Whiddington's law, we can express the current $\mathrm{d}I_{\mathrm{s}}$ associated with the secondary electrons as

$$\mathrm{d}I_{\mathrm{s}} = \tfrac{1}{2} K_{\mathrm{s}} K_{\mathrm{W}} I_{\mathrm{e}} (E_{\mathrm{p}}^2 - K_{\mathrm{W}} x)^{-1/2} f(x)\,\mathrm{d}x \tag{2.2.15}$$

where

$$f(x) = \tfrac{1}{2} \int_0^{\pi} \mathrm{e}^{-\alpha l(x,\theta)} \sin\theta\,\mathrm{d}\theta \tag{2.2.16}$$

with $l(x, \theta)$ given in equation (2.2.14). Since a primary electron excites secondaries along its entire path within the grain, we must integrate equation (2.2.16) from the point of entry ($x = 0$) to either the point of exit ($x = 2r_{\mathrm{d}} = D_{\mathrm{g}}$) or the maximum penetration distance, depending on which one of the two values is smaller. The maximum penetration depth $x_{\max}$ corresponds to the point at which $E(x) = 0$ and can be determined from Whiddington's law. The latter yields $x_{\max} = E_{\mathrm{p}}^2/K_{\mathrm{W}}$. It is obvious that the primary electrons can only escape the grain at the opposite side ($x = D_{\mathrm{g}}$) when the primary electrons have sufficient energy to exceed the diameter of the grain ($x_{\max} > D_{\mathrm{g}}$), i.e. when $E_{\mathrm{p}} > E_{\min} = (K_{\mathrm{W}} D_{\mathrm{g}})^{1/2}$. Thus, the final expression for the secondary yield $\delta_{\mathrm{s}}(E_{\mathrm{p}}) = I_{\mathrm{s}}/I_{\mathrm{e}}$ is

$$\delta_{\mathrm{s}}(E_{\mathrm{p}}) = \tfrac{1}{2} \int_0^{\min[D_{\mathrm{g}}, x_{\max}]} K_{\mathrm{s}} K_{\mathrm{W}} (E_{\mathrm{p}}^2 - K_{\mathrm{W}} x)^{-1/2} f(x)\,\mathrm{d}x. \tag{2.2.17}$$

It should be noted that these escaping electrons will constitute another current leaving the dust grain, which will need to be considered when determining the equilibrium potentials. We also note that equation (2.2.17) more closely matches the expression for the secondary electron yield obtained by Jonker (1952). We can now numerically solve equation (2.2.17) in order to obtain the secondary electron yield δ_{s} as a function of the primary electron energy E_{p} and can compare the present numerical results with those of Jonker (1952). Figure 2.3 shows the secondary electron yield as a function of the primary electron energy E_{p} for different-sized conducting dust grains, in addition to the Jonker yield for semi-infinite slabs. At low primary energies the smaller dust grains have higher yields, because within these smaller grains the excited secondary electrons have shorter distance to travel to reach the surface. However, as the primary energy increases, the yield curves for different-sized grains may cross and larger dust grains may have higher yields than the smaller grains. On the other hand, Whiddington's law for energy loss signifies that the greatest amount of energy is lost at the end of a primary electron's path. Consequently, the majority of secondary electrons are excited just as the primary electrons have lost their last bit of energy and are being stopped. When the energy of a primary electron exceeds $E_{\min}$, the electron tunnels right through the grain and hence does not excite as many secondaries as does a primary electron that stopped within the grain. Thus, it is possible for a larger dust grain to have a higher yield than a smaller grain for two reasons: (i) larger grains will have a larger upper limit of integration in equation (2.2.17) for $E_{\mathrm{p}} > E_{\min}$ and (ii) in the regime, where the primary energy is larger than $E_{\min}$ of the smaller grain but less than $E_{\min}$ of the larger grain, more secondaries will

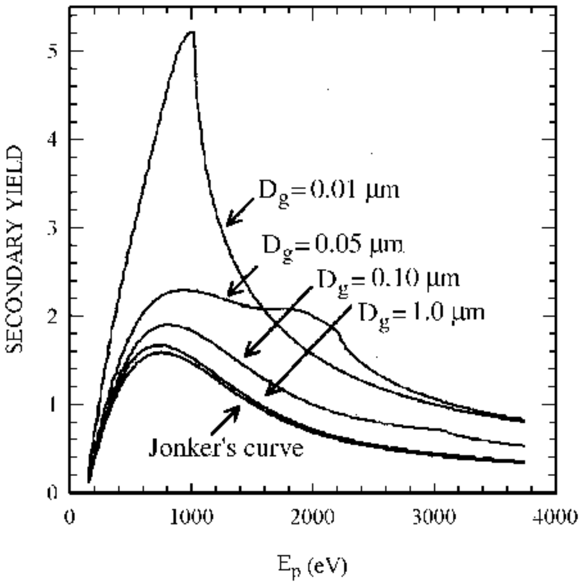

Figure 2.3. Secondary emission yield δ_s as a function of the primary electron energy E_p for different-sized conducting dust grains where $\alpha = 10^6$ cm^{-1}, $K_W = 10^{12}$ V^2 cm^{-1} and $K_s = 0.01$ (after Chow *et al* 1993).

be excited in the larger grain. These two reasons tend to favour larger yields for larger grains. On the other hand, only the fact that excited secondary electrons have shorter distances to travel to reach the surface of the smaller dust grains favour larger yields for the latter. Therefore, the parameters K_W, α and r_d will determine which of these effects will dominate and thus determine whether the yields of larger grains will ever exceed the yields of smaller dust grains.

The currents associated with the secondary electrons I_s are (Meyer-Vernet 1982)

$$I_s = \frac{8\pi^2 r_d^2 e}{m_e^2} \int_0^\infty E\delta_s(E) f_e(E - e\phi_d)\,\mathrm{d}E \tag{2.2.18}$$

for $\phi_d \leq 0$ and

$$I_s = \frac{8\pi^2 r_d^2 e}{m_e^2} \exp\left(-\frac{e\phi_d}{k_B T_{se}}\right)\left(1 + \frac{e\phi_d}{k_B T_{se}}\right) \int_{e\phi_d}^\infty E\delta_s(E) f_e(E - e\phi_d)\,\mathrm{d}E \tag{2.2.19}$$

for $\phi_d \geq 0$, where $k_B T_{se}$ is the thermal energy of the emitted secondary electrons which have been found to have a Maxwellian velocity distribution (Meyer-Vernet 1982, Goertz 1989). It has further been found that the range of $k_B T_{se}$ is quite small (1–5 eV) regardless of the energy of the incoming primaries (Goertz 1989). Assuming that the electrons follow a Maxwellian distribution, i.e. if we express

$f_{\rm e}(E - e\phi_{\rm d})$ as

$$f_{\rm e}(E - e\phi_{\rm d}) = n_{\rm e}\left(\frac{m_{\rm e}}{2\pi k_{\rm B}T_{\rm e}}\right)^{3/2} \exp\left(-\frac{E - e\phi_{\rm d}}{k_{\rm B}T_{\rm e}}\right) \tag{2.2.20}$$

we can rewrite equations (2.2.18) and (2.2.19) as

$$I_{\rm s} = 4\pi r_{\rm d}^2 n_{\rm e} e\left(\frac{k_{\rm B}T_{\rm e}}{2\pi m_{\rm e}}\right)^{1/2} \frac{1}{(k_{\rm B}T_{\rm e})^2} \times \exp\left(\frac{e\phi_{\rm d}}{k_{\rm B}T_{\rm e}}\right) \int_0^\infty E\delta_{\rm s}(E) \exp\left(-\frac{E}{k_{\rm B}T_{\rm e}}\right) {\rm d}E \tag{2.2.21}$$

for $\phi_{\rm d} \le 0$ and

$$I_{\rm s} = 4\pi r_{\rm d}^2 n_{\rm e} e\left(\frac{k_{\rm B}T_{\rm e}}{2\pi m_{\rm e}}\right)^{1/2} \frac{1}{(k_{\rm B}T_{\rm e})^2} \exp\left(\frac{e\phi_{\rm d}}{k_{\rm B}T_{\rm e}}\right) \exp\left(-\frac{e\phi_{\rm d}}{k_{\rm B}T_{\rm e}}\right) \times \left(1 + \frac{e\phi_{\rm d}}{k_{\rm B}T_{\rm e}}\right) \int_{e\phi_{\rm d}}^\infty E\delta_{\rm s}(E) \exp\left(-\frac{E}{k_{\rm B}T_{\rm e}}\right) {\rm d}E \tag{2.2.22}$$

for $\phi_{\rm d} \ge 0$. Equations (2.2.21) and (2.2.22) represent the secondary electron emission charging current for negatively and positively charged dust grains, respectively.

To calculate the tunnel current (i.e. the current associated with the primary electrons with energy $E_{\rm p} > E_{\rm min}$), we assume that the primary electron current density is conserved within the dust grain and that Whiddington's law is valid. The tunnel current $I_{\rm t}$ can, therefore, be expressed as

$$I_{\rm t} = \frac{8\pi^2 r_{\rm d}^2 e}{m_{\rm e}^2} \int_{E_{\rm min}}^\infty E f_{\rm e}(E - e\phi_{\rm d})\, {\rm d}E \tag{2.2.23}$$

for $\phi_{\rm d} \le 0$ and

$$I_{\rm t} = \frac{8\pi^2 r_{\rm d}^2 e}{m_{\rm e}^2} \int_{E_{\rm min}+e\phi_{\rm d}}^\infty E f_{\rm e}(E - e\phi_{\rm d})\, {\rm d}E \tag{2.2.24}$$

for $\phi_{\rm d} \ge 0$. Although the distributions of electrons leaving the grain is not known, we can relate them to the incoming Maxwellian electrons due to the conservation of the current density. Thus, substituting equation (2.2.20) into equations (2.2.23) and (2.2.24) we can finally express the tunnel current $I_{\rm t}$ as

$$I_{\rm t} = 4\pi r_{\rm d}^2 n_{\rm e} e\left(\frac{k_{\rm B}T_{\rm e}}{2\pi m_{\rm e}}\right)^{1/2} \exp\left(\frac{e\phi_{\rm d}}{k_{\rm B}T_{\rm e}}\right) \exp\left(-\frac{E_{\rm min}}{k_{\rm B}T_{\rm e}}\right) \left(1 + \frac{E_{\rm min}}{k_{\rm B}T_{\rm e}}\right) \tag{2.2.25}$$

for $\phi_{\rm d} \le 0$ and

$$I_{\rm t} = 4\pi r_{\rm d}^2 n_{\rm e} e\left(\frac{k_{\rm B}T_{\rm e}}{2\pi m_{\rm e}}\right)^{1/2} \exp\left(-\frac{E_{\rm min}}{k_{\rm B}T_{\rm e}}\right) \left(1 + \frac{E_{\rm min} + e\phi_{\rm d}}{k_{\rm B}T_{\rm e}}\right) \tag{2.2.26}$$

for $\phi_d \geq 0$. Chow *et al* (1993) have numerically analysed the secondary electron emission current given by equations (2.2.21) and (2.2.22) and the tunnel current given by equations (2.2.25) and (2.2.26). They have found that the secondary electron current increases with $k_B T_e$ for $k_B T_e < E_m$ (where E_m is the energy of the primary electrons for which the secondary yield δ_s is maximum) and dominates when $k_B T_e$ is of the order of E_m. It decreases with $k_B T_e$ when $k_B T_e \gg E_m$. On the other hand, the tunnel current will increase indefinitely with increasing $k_B T_e$ and will dominate when $k_B T_e$ is comparable to or larger than $E_{min} = (K_W D_g)^{1/2}$.

2.2.2.2 Ion impact

The ions approaching a dust grain surface at low kinetic energies (below 1 keV) are neutralized by the electrons which, on the other hand, tunnel through the potential barrier to neutralize the ions. The energy released in this process may excite additional electrons which can then be emitted from the dust grain surface. The number of excited electrons depends on the available potential energy (after neutralization) which is determined by the ionization potential energy W_i and the work function W_f of the dust grain material. When a conduction electron is captured by the incident ion, it makes available a maximum energy of $W_i - W_f$. At least W_f of this must be used to free another electron from the material so that the condition for the secondary emission is $W_i > 2W_f$.

When the incident ions have energies above 10 keV, the secondary electron yields due to ion impact can be substantially larger than unity. Draine and Salpeter (1979) showed that the behaviour of such high-energy ions falling on a dust grain surface may be the same as that of the electrons falling on the dust grain surface. This means that, like the electrons (incident on a dust grain surface as we discussed in the previous section), the energetic ions falling on a dust grain may enter into the dust grain and stop immediately (i.e. stick onto the dust grain surface) or may pass through the dust material and thus lose their energy (during their passage through the dust grain material), a portion of which can go into exciting the electrons that in turn may escape from the grain surface. The physical model for the production of the secondary electrons by ion impact (as well as the dust grain charging currents associated with these secondary electrons and tunnelling ions) is similar to that by electron impact discussed in the previous section. The sufficiently high-energy ions can also penetrate and re-emit along with the secondary electrons. However, the fraction of such re-emitted ions is usually quite small and thus one can neglect the secondary ion emission in calculating the dust grain surface potential.

2.2.3 Photoemission

When a flux of photons with energy ($h\nu$) larger than the photoelectric work function (W_f) of the dust grain incidents on the dust grain surface, the latter emits photoelectrons, where $\hbar$ is Planck's constant and ν is the photon frequency. The photoemission of electrons depends on (i) the wavelength of the incident photons, (ii) the surface area of the dust grain and (iii) the properties of the dust grain material. This mechanism contributes to a positive charging current and tries to make the dust grain positively charged. We note that various metals typically have photoelectric work function $W_\mathrm{f} < 5$ eV, such as Ag ($W_\mathrm{f} = 4.46$ eV), Cu ($W_\mathrm{f} = 4.45$ eV), Al ($W_\mathrm{f} = 4.2$ eV), Ca ($W_\mathrm{f} = 3.2$ eV) and Cs ($W_\mathrm{f} = 1.8$ eV). There are also a number of low work function materials, e.g. carbides (binary compounds of carbon and more electropositive metals) with work functions $W_\mathrm{f} \simeq 2.18$–3.50 eV, borides (binary compounds of boron and more electropositive metals) with work functions $W_\mathrm{f} = 2.45$–2.92 eV, oxides of metals with work functions ranging from $W_\mathrm{f} = 1$ eV (Cs) to $W_\mathrm{f} = 4$ eV (zirconium).

The maximum charge on a grain, which in the presence of a photon is assumed to emit photoelectrons, can roughly be estimated as follows. We assume that W_f is the photoelectric work function of the material of the dust grain which is positively charged ($q_\mathrm{d} > 0$). Thus, in order to excite an electron the incoming photons must have energy $h\nu > W_\mathrm{f} + q_\mathrm{d}e/r_\mathrm{d}$. This implies that the maximum dust grain charge is roughly

$$q_\mathrm{d} = (h\nu - W_\mathrm{f})\frac{r_\mathrm{d}}{e}. \tag{2.2.27}$$

As the dust grain surface is positive, i.e. $\phi_\mathrm{d} > 0$, a fraction of the photoelectrons return to the dust grain surface and the most energetic ones overcome the dust grain potential and escape. Thus, the net current is determined by the balance between the photoelectrons returned to the dust grain surface and the photoelectrons escaped from the dust grain surface. The electron photoemission current for a unidirectional photon flux and for $\phi_\mathrm{d} > 0$ is, therefore, roughly (Rosenberg *et al* 1996)

$$I_\mathrm{p} = \pi r_\mathrm{d}^2 e J_\mathrm{p} Q_\mathrm{ab} Y_\mathrm{p} \exp\left(-\frac{e\phi_\mathrm{d}}{k_\mathrm{B}T_\mathrm{p}}\right) \tag{2.2.28}$$

where J_p is the photon flux, Q_ab is the efficiency of the absorption for photons ($Q_\mathrm{ab} \sim 1$ for $2\pi r_\mathrm{d}/\lambda > 1$, where λ is the wavelength of the incident photons), Y_p is the yield of the photoelectrons and T_p is their average temperature. It may be noted that the exponential factor in equation (2.2.28) takes into account that the photoelectrons have sufficient energy to overcome the potential barrier of the positively charged dust grain. It is important to mention that equation (2.2.28) is valid when the photo-emitted electrons follow a Maxwellian distribution with the temperature T_p. However, in order to take into account the energetics of the photoemission processes the assumption of a Maxwellian distribution for the photoemitted electrons may require some modification.

We now consider a dust grain with negative surface potential. As the dust grain potential is negative (i.e. $\phi_\mathrm{d} < 0$), no photoelectron returns to the dust grain surface, i.e. all the photoelectrons emitted by the dust grain surface escape into the plasma. This leads to a constant current $I_\mathrm{p} = \pi r_\mathrm{d}^2 e J_\mathrm{p} Q_\mathrm{ab} Y_\mathrm{p}$.

2.2.4 Other charging processes

There are a number of other dust grain charging mechanisms, namely thermionic emission, field emission, radioactivity, impact ionization, etc. These processes, whose importance for a particular application has to be evaluated individually, may be briefly discussed as follows.

2.2.4.1 Thermionic emission

One of the important charging processes which charge up the dust grains positively is thermionic emission (Sodha and Guha 1971, Rosenberg and Mendis 1995). When a dust grain is heated to a high temperature, electrons or ions may be thermionically emitted from the dust grain surface. The thermionic emission may be induced by laser heating or by thermal infrared (IR) heating or by hot filaments surrounding the dust grain. The thermionic electron emission current $I_{\rm th}$ can be obtained from the Richardson equation which, including the increase in the work function due to the grain electrostatic barrier, can be expressed as (Rosenberg *et al* 1999)

$$I_{\rm th} = 4\pi r_{\rm d}^2 A_{\rm t} T_{\rm d}^2 \exp\left(-\frac{|W_{\rm f} + e\phi_{\rm d}|}{k_{\rm B} T_{\rm d}}\right) \tag{2.2.29}$$

where $A_{\rm t} = 4\pi e m_{\rm e} k_{\rm B}^2/h^3$ is a constant.

We now estimate the laser intensity required to heat the dust grains to a temperature $T_{\rm d}$. We consider an inert gas (e.g. He, Ne, Ar, etc) with dispersed dust grains of low work function material and high boiling point. If I is the intensity of the laser energy flux to heat the grains to a temperature $T_{\rm d}$, the dust grain heating rate $\dot{Q}_{\rm heat}$ due to a unidirectional photon flux is

$$\dot{Q}_{\rm heat} = \pi r_{\rm d}^2 Q_{\rm ab} I. \tag{2.2.30}$$

We consider a gas pressure of about 2 mbar and a grain radius of the order of 10 μm, which correspond to typical parameters of dusty plasma experiments. The mean free path of neutrals in the background gas is of the order of 35 μm and the gas temperature $T_{\rm n}$ is of the order of 300 K. Thus, in this regime the neutral Knudsen number $K_{\rm n}$ (the ratio of the neutral mean free path to the grain size) is much larger than one. The dust grain loses heat in the gas due to conduction and radiation. The conduction loss rate $\dot{Q}_{\rm cond}$ in the free molecular regime ($K_{\rm n} \gg 1$) with an accommodation coefficient of the order of unity is

$$\dot{Q}_{\rm cond} = \pi r_{\rm d}^2 n_{\rm n} V_{T{\rm n}} k_{\rm B}(T_{\rm d} - T_{\rm n}) \tag{2.2.31}$$

where $V_{T{\rm n}} = (k_{\rm B} T_{\rm n}/m_{\rm n})^{1/2}$ is the thermal speed of the background neutral gas. The blackbody radiative loss rate is

$$\dot{Q}_{\rm rad} = \pi r_{\rm d}^2 \varepsilon_{\rm E} \sigma_{\rm sb}(T_{\rm d}^4 - T_{\rm n}^4) \tag{2.2.32}$$

where ε_E is the emissivity of the grain and σ_{sb} is the Stefan–Boltzmann constant. We now consider an example and assume that the dust grains are heated to a temperature of $T_d \simeq 1700$ K and that the temperature and the number density of the neutral gas (Ne) are $T_n \simeq 300$ K and $n_n \simeq 5 \times 10^{16}$ cm^{-3}, respectively. For this case one can approximate that the radiative loss is about twice as large as the conductive loss (i.e. $\dot{Q}_{rad} \simeq 2\dot{Q}_{cond}$). Therefore, using equations (2.2.30)–(2.2.32) in $\dot{Q}_{heat} = \dot{Q}_{cond} + \dot{Q}_{rad}$, the intensity I of the laser energy flux can be approximated as 300 W cm^{-2}. This intensity can practically be achieved by a low-power IR laser or even perhaps by a series of incandescently hot filaments surrounding the dust grain.

2.2.4.2 Field emission

There are some special circumstances when micron- or submicron-sized dust grains may acquire a very high negative (or positive) potential and emit electrons (or ions) as field emission. The onset of electron field emission from a dust grain surface occurs when its surface electric field is in between 10^6 V cm^{-1} and 10^7 V cm^{-1} (Whipple 1981). The field 10^6 V cm^{-1} corresponds to an emission flux of 10^5 cm^{-2} s^{-1} for a work function of 3.5 eV. As the surface electric field of a small spherical dust grain is approximately ϕ_d/r_d, the surface potential ϕ_d (in volts) corresponding to the surface electric field of 10^6 V cm^{-1} is approximately $10^6 r_d$ (where r_d is in cm). This means that field emission is important for the dust grains of radii (or the surface with radii of curvature) of the order of a micron. The dust grain potential is limited by the electron (ion) field emission for negatively (positively) charged dust grains.

2.2.4.3 Radioactivity

Radioactivity in a body in space may constitute a charging mechanism through both the escape of the emitted charged primaries from the radioactive nuclei and the escape of the secondary electrons excited by a primary in its passage through the surface. The amount of ordinary radioactivity material in bodies is insignificant for charging effects (Whipple 1981). However, Yanagita (1977) has suggested that the dust grains formed in nova and supernova may have significant radioactive levels, particularly Ni^{22} or Al^{26} which are β emitters. The charging due to β emission varies with the dimension of the grain and hence larger grains tend to be positively charged. It is also a fact that satellites sometimes carry quantities of radioactive materials in connection with certain types of experiments, or as a power source. Though such sources are usually well shielded, these may constitute possible charging mechanisms for spacecraft.

2.2.4.4 Impact ionization

When a sufficiently high energetic neutral atom or ion strikes a dust grain surface, either the incident neutral atom or atoms on the grain surface are ionized with subsequent escape of ions and/or electrons. This phenomenon (known as impact ionization) can thus lead to the charging of the dust grains. The effect is more important when the neutral density is very high or when the dust particle or neutral velocity is such that impact ionization can occur.

2.3 Non-isolated Dust Grains

The different dust grain charging processes, which we have discussed up to now, are valid for small isolated dust grains ($r_d \ll \lambda_D \ll a$). It is obvious that as the dust grain number density n_d increases, the intergrain distance may drop below the shielding distance and the grains start to interact electrostatically. For such a case we have to consider non-isolated dust grains, instead of isolated ones. Therefore, in this section we consider a dusty plasma consisting of electrons, ions and non-isolated negatively charged dust grains, and discuss non-isolated dust grain charge and associated electrostatic dust cloud potential.

2.3.1 Dust grain charge

We first start with the charge neutrality condition

$$\frac{n_e}{n_i} = 1 - Z_d \frac{n_d}{n_i}. \tag{2.3.1}$$

We note that when $Z_d n_d/n_i$ is much smaller than one, the dust particles can be considered as isolated and when $Z_d n_d/n_i$ is comparable to one the dust particles can be considered as non-isolated. Therefore, equation (2.3.1) clearly indicates that as n_d increases, Z_d decreases more rapidly in the non-isolated case than in an isolated case. This allows us to draw a physical interpretation: for a non-isolated case an increase in the dust particle number density means that the dust grains together have a large appetite for the electrons, but the number of available electrons per dust grain decreases. This conclusion might have a significant influence on the transition of a dusty plasma from a strongly coupled regime to a weakly coupled regime as the Coulomb coupling parameter (Γ_c) is directly proportional to Z_d^2.

We can also arrive at the same conclusion from the expressions of electron and ion currents given in equations (2.2.6) and (2.2.7). For negatively charged dust grains, I_e (equation (2.2.7)) and I_i (equation (2.2.6)) are (Barnes *et al* 1992)

$$I_e = -4\pi r_d^2 n_e e \left(\frac{k_B T_e}{2\pi m_e}\right)^{1/2} \exp\left(\frac{e\phi_d}{k_B T_e}\right) \tag{2.3.2}$$

and

$$I_i = 4\pi r_d^2 n_i e \left(\frac{k_B T_i}{2\pi m_i}\right)^{1/2} \left(1 - \frac{e\phi_d}{k_B T_i}\right). \tag{2.3.3}$$

It is obvious that $I_i \ll |I_e|$ (since $m_e \ll m_i$) and the dust grain surface becomes negatively charged. This increases the ion current and decreases the electron current until $I_e + I_i = 0$. Using equations (2.3.1)–(2.3.3) in $I_e + I_i = 0$, we have

$$\left(\frac{T_i m_e}{T_e m_i}\right)^{1/2}\left(1 - \frac{e\phi_d}{k_B T_i}\right)\exp\left(-\frac{e\phi_d}{k_B T_e}\right) = 1 - Z_d\frac{n_d}{n_i} \qquad (2.3.4)$$

where Z_d and ϕ_d can be related as

$$\phi_d = -\frac{Z_d e}{r_d}. \qquad (2.3.5)$$

It is clear from equations (2.3.4) and (2.3.5) that for isolated dust grains ($Z_d n_d/n_i \ll 1$), ϕ_d and Z_d depend only on the dust particle radius while for non-isolated dust grains ($Z_d n_d/n_i$ is comparable to one), ϕ_d and Z_d do not only depend on the dust grain radius, but also on the dust particle number density n_d. Now, substituting Z_d (obtained from equation (2.3.5)) into equation (2.3.4) and taking $T_e = T_i = T$ we have

$$1 - \frac{e\phi_d}{k_B T} - \left(\frac{m_i}{m_e}\right)^{1/2}\left(1 + P\frac{e\phi_d}{k_B T}\right)\exp\left(\frac{e\phi_d}{k_B T}\right) = 0 \qquad (2.3.6)$$

where $P = 4\pi n_d r_d \lambda_{D0}^2$ and $\lambda_{D0} = (k_B T/4\pi n_i e^2)^{1/2}$. We can now numerically solve equation (2.3.6) and can easily calculate ϕ_d and Z_d. Figure 2.4 shows the variation of $e\phi_d/k_B T$ with $\log P$. When n_i, T and r_d are assumed to be constant, figure 2.4 shows the effect of n_d on ϕ_d (or on $Z_d = -(r_d/e)\phi_d$). It is obvious from figure 2.4 that when we gradually increase n_d (i.e. we gradually decrease the intergrain spacing) and when it exceeds a critical value (i.e. the intergrain spacing becomes smaller than a critical value), the value of $-e\phi_d/k_B T$ starts to decrease, i.e. the average dust grain charge Z_d starts to decrease. When n_d, T and r_d are assumed to be constant, figure 2.4 represents the effect of n_i or n_e (since $n_i \propto n_e$ for a constant n_d) on ϕ_d (or on Z_d) and shows that as we increase the ambient plasma density (n_i or n_e), the value of $-e\phi/k_B T$ increases, i.e. Z_d increases. Furthermore, by plotting curves for different values of r_d one can show that the critical value of n_d/n_i for which Z_d starts to decrease is lower for the dust grains of larger radii. As an example, in a plasma with a temperature of the order of 10^4 K, the charge (Z_d) on a 1 μm dust grain starts to be affected by n_d/n_i when its value is larger than 3×10^{-4}, while the charge (Z_d) on a 0.1 μm dust grain starts to be affected by n_d/n_i when its value is larger than 3×10^{-2}.

2.3.2 Dust cloud potential

We consider a finite dust cloud immersed in a plasma and follow the model of Havnes *et al* (1987) to calculate the dust cloud potential in space plasmas. However, this model may also be applicable for laboratory plasmas in which the temperatures of the plasma particles (electrons and ions) are not affected by the

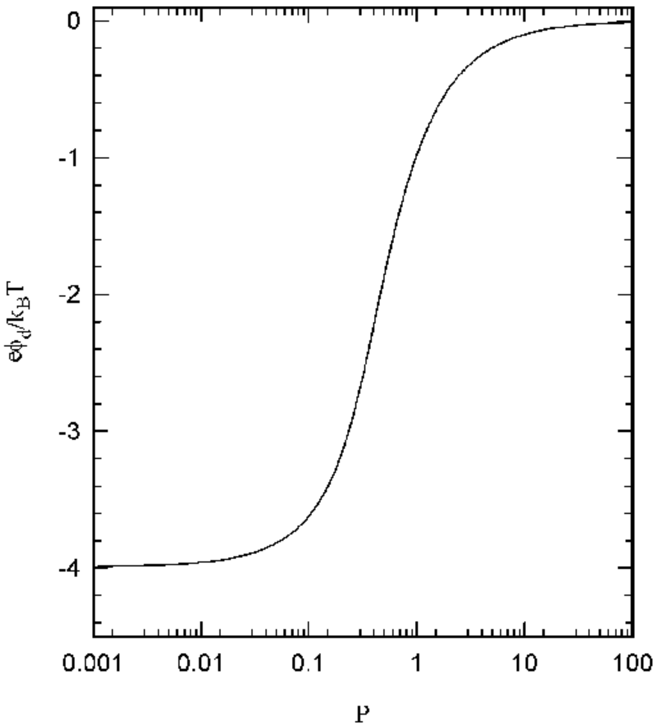

Figure 2.4. The variation of $e\phi_d/k_BT$ with log P: solution of equation (2.3.6).

dust cloud and the source of the plasma particles are at infinite distance from the dust cloud. If ϕ_c is the dust cloud potential measured with respect to the plasma potential ϕ_p, we can express n_e, n_i, I_e and I_i as

$$n_e = n_0 \exp\left(\frac{e\phi_c}{k_BT_e}\right) \tag{2.3.7}$$

$$n_i = n_0 \exp\left(-\frac{e\phi_c}{k_BT_i}\right) \tag{2.3.8}$$

$$I_e = -4\pi r_d^2 n_e e \left(\frac{k_BT_e}{2\pi m_e}\right)^{1/2} \exp\left(\frac{e\phi_f}{k_BT_e}\right) \tag{2.3.9}$$

and

$$I_i = 4\pi r_d^2 n_i e \left(\frac{k_BT_i}{2\pi m_i}\right)^{1/2} \left(1 - \frac{e\phi_f}{k_BT_i}\right) \tag{2.3.10}$$

where n_0 is the plasma (electron or ion) number density at $\phi_c = 0$ (i.e. at a distance far from the dust cloud) and $\phi_f = \phi_d - \phi_c$ is the floating potential of the dust particle in the cloud. Substituting equations (2.3.7) and (2.3.8) into the quasi-neutrality condition ($n_i = n_e + Z_d n_d$) and using $Z_d = -r_d\phi_f/e$, we obtain

$$\exp\left(\frac{e\phi_c}{k_B T_e}\right) - \exp\left(-\frac{e\phi_c}{k_B T_i}\right) - 4\pi r_d \lambda_{De}^2 n_d \left(\frac{e\phi_f}{k_B T_e}\right) = 0. \tag{2.3.11}$$

On the other hand, substituting equations (2.3.7)–(2.3.10) into $I_e + I_i = 0$, we obtain

$$\left(\frac{T_i m_e}{T_e m_i}\right)^{1/2} \left(1 - \frac{e\phi_f}{k_B T_i}\right) \exp\left(-\frac{e\phi_f}{k_B T_e}\right) = \exp\left[\frac{e\phi_c}{k_B}\left(\frac{1}{T_e} + \frac{1}{T_i}\right)\right]. \tag{2.3.12}$$

We can now numerically solve equations (2.3.11) and (2.3.12) and obtain the two unknowns, namely the potential of the dust cloud (ϕ_c) and the floating potential of the dust particle in the cloud (ϕ_f).

2.4 Grain Charging in Laboratory

We have discussed the dust grain charge and associated potential in both isolated and non-isolated cases. These discussions are mainly based on theoretical investigations. In this section we confine ourselves to some laboratory experiments for the measurement of the dust grain charge in both isolated and non-isolated cases.

2.4.1 Isolated dust grains

To investigate the charging of isolated dust grains in a plasma, Walch *et al* (1994) devised an experimental set-up as shown in figure 2.5. The experimental set-up mainly consists of four parts, namely DP machine, dust dropper, Faraday cup and electrometer. The DP machine consists of two identical aluminium cylinders (30 cm diameter and 30 cm long) which are joined end to end (shown in figure 2.5). The vacuum is produced by a 15 cm diameter diffusion pump with a base pressure of 6×10^{-7} Torr. There are diagnostic ports on the end flanges and pairs of vertical and horizontal ports. The filaments (three strings of 0.1 mm tungsten wires, each containing 10 filaments, placed inside each of the two cylinders) are operated at approximately 17 A and 45 V. The positive end of the filament string may be biased up to -125 V. The dust particles are dropped by agitating a thin metal disc with a small central hole. The disc is agitated by an electromagnet mounted above a small rare-earth permanent magnet (5 mm diameter and 2 mm long) cemented to the disc. The dust grain material selected for this experiment is silicon carbide. This material has the advantage of being available in a variety of sizes and does not have tendency to form clumps. The uniformity in size is improved by using screen mesh sieves. Relatively large grains (30–125 μm) are used in order to give a large signal-to-noise ratio. The dust grain charge is detected and measured by a sensitive electrometer attached to a Faraday cup on the bottom. The Faraday cup is made of copper and is approximately 8 mm in diameter. It

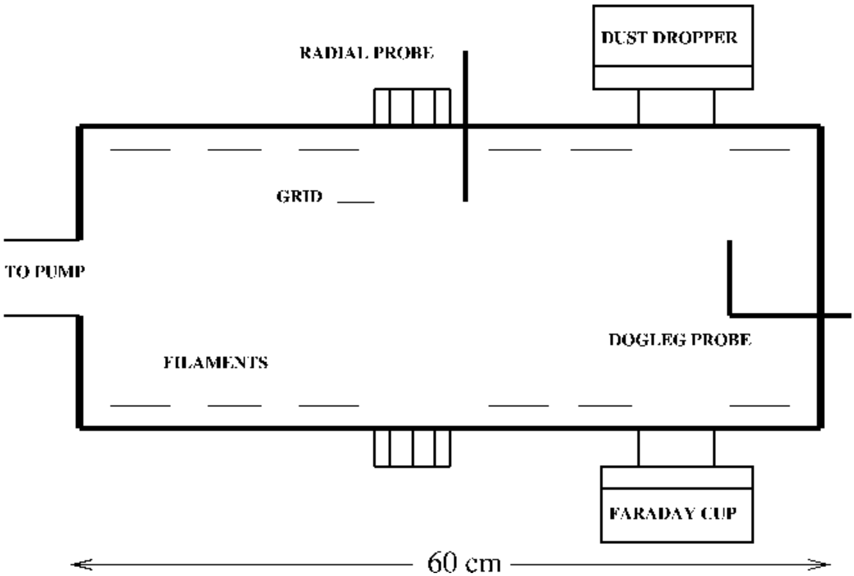

Figure 2.5. Schematic illustration of the DP machine showing the location of the Langmuir probes, the dust dropper and the Faraday cup (after Walch *et al* 1994).

is electrostatically shielded and a 6 mm hole in the shield immediately above the cup allows entry of the dust grain. The electrometer is an integrator followed by two bandpass amplifiers. The charge falling into the cup is transferred to a 200 pF feedback capacitor by an operational amplifier to generate a step-wise increase in the output voltage of the first stage. The voltage is returned to zero by 200 MΩ feedback resistor which gives 40 ms decay constant.

The grain charge is determined by the floating potential. The net current $I_{\rm net}$ is

$$I_{\rm net} = I_{\rm e} + I_{\rm i} + I_{\rm f} + I_{\rm s} \tag{2.4.1}$$

where $I_{\rm e}$ ($I_{\rm i}$) is the incident current of the plasma electrons (ions), $I_{\rm f}$ is the current of fast electrons emitted from the filaments and $I_{\rm s}$ is the current of secondary electrons emitted from the dust grain due to the fast electron bombardment. It is assumed that photoelectric emission is negligible, because there is little ultraviolet radiation in the blackbody spectrum of the filament emission. It is physically obvious that each current depends upon the potential of the dust grain as well as on the operating parameters of the experiment. There are two operating regimes, namely the vacuum regime and the plasma regime. The vacuum regime is without the argon gas, i.e. without the plasma ($I_{\rm e} = 0$ and $I_{\rm i} = 0$). The plasma regime is with the argon gas, i.e. with the plasma ($I_{\rm e} \neq 0$ and $I_{\rm i} \neq 0$).

When there is no plasma ($I_{\rm e} = I_{\rm i} = 0$) and no secondary emission ($I_{\rm s} = 0$), the dust grains, which should be negatively charged by filament-emitted electron

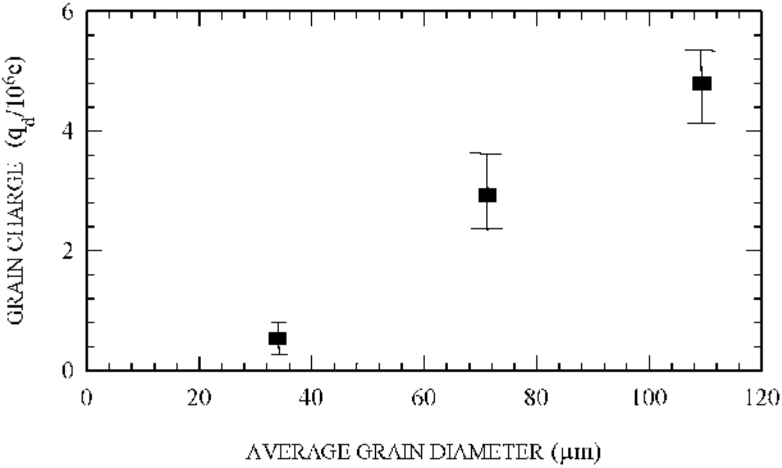

Figure 2.6. The grain charge as a function of the average grain size at a filament bias of −25 (after Walch *et al* 1994). These data are for 30–35 μm, 62–74 μm and 95–125 μm.

current I_f, retard further electrons from the filaments. This occurs when the dust grain potential is of the order of the potential on the most negative end of the filament string. The secondary emission can be neglected when the energy of the primary electrons is so low that the secondary emission coefficient is small. The dust grain charging time is shorter than the time of flight through the plasma. Walch *et al* (1994) used 0–125 μm SiC grains and a filament bias of −100 V and showed that the grain charge is nearly independent of the filament emission for emission currents from 0.25 A to 2 A. It has also been shown by this experiment that the grain charge begins to decrease when the voltage on the negative end of the filament string exceeds 70 V. This indicates that the secondary emission from SiC grains becomes important for incident electron energies above 70 eV. The charging data shown in figure 2.6 are for grains with sizes in the range 30–35 μm, 62–74 μm and 90–125 μm.

These data are taken for a bias voltage of −25 V where the secondary emission is unimportant. The charge on the grains increases with size but deviates from linear scaling. To explain the reason for this deviation, more data corresponding to the different sizes are needed. When 1×10^{-4} Torr of argon is added, the plasma is generated in the chamber. The plasma parameters are determined from Langmuir probe data. Figure 2.7 shows the probe current–voltage characteristic curve. Typical operating parameters of the DP machine for the plasma regime are: filament voltage, 45 V; filament current, 17 A; filament emission current, 1 A; filament bias voltage, −25 V; argon pressure, 1×10^{-4} Torr; electron temperature, 2.8 eV; electron density, 6.6×10^8 cm^{-3}; plasma Debye length, 0.48 cm; plasma potential, 6.8 V; floating potential, −9.0 V.

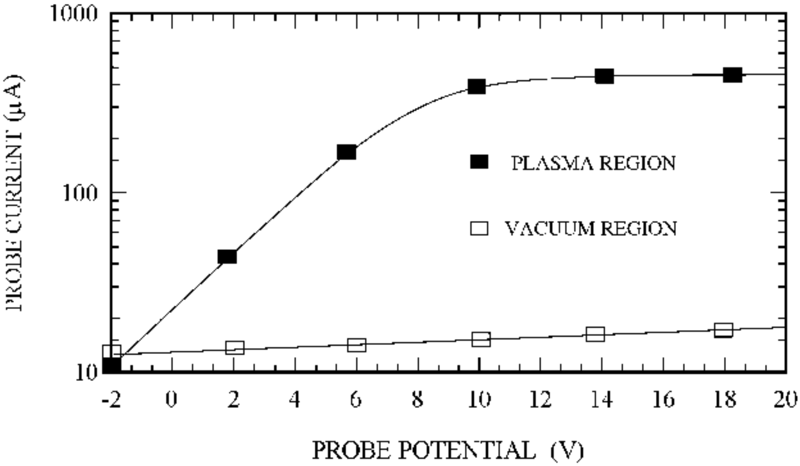

Figure 2.7. Langmuir probe trace for vacuum and plasma regimes (after Walch *et al* 1994).

2.4.2 Non-isolated dust grains

Barkan *et al* (1994) devised an experiment for the investigation of the charging of micron-size, non-isolated dust grains in a plasma. They utilize a Q-machine (as schematically shown in figure 1.8) in which a fully ionized magnetized ($B \leq 4 \times 10^3$ G) potassium plasma column of $\sim$4 cm diameter and $\sim$80 cm long is produced by the surface ionization of potassium atoms from an atomic beam oven on a hot ($\sim$2500 K) tantalum plate. The basic constituents of the ambient plasma are K^+ ions and electrons with approximately equal temperatures $k_B T_e = k_B T_i = 0.2$ eV and densities in the range $\sim 10^6$–10^{10} cm^{-3}. To dispense dust particles into the plasma, the plasma column is surrounded over a portion of its length by a dust dispenser which mainly consists of a rotating metal cylinder and a stationary screen.

The dust grains were hydrated aluminium silicate of various sizes and shapes. The screen limits the dispensed grain sizes to $<$100 μm. The samples of the dust grains were collected from within the vacuum chamber and an analysis was made of photographs taken with an electron microscope to determine their size distribution. These photographs showed that 90% of the grains had sizes in the 1–15 μm range with an average grain size $r_d \simeq 5$ μm. The dust density n_d was estimated as $\sim 5 \times 10^4$ cm^{-3}.

The main diagnostic tool of the dusty plasma was a Langmuir probe, movable along the axis of the plasma column and consisting of a tantalum disc $\sim$5 mm in diameter, oriented normally to the magnetic field. The Langmuir probe enables us to determine how the negative charge in the plasma is divided between free electrons and negatively charged dust grains. Figure 2.8 shows Langmuir probe characteristics obtained under identical conditions except for the

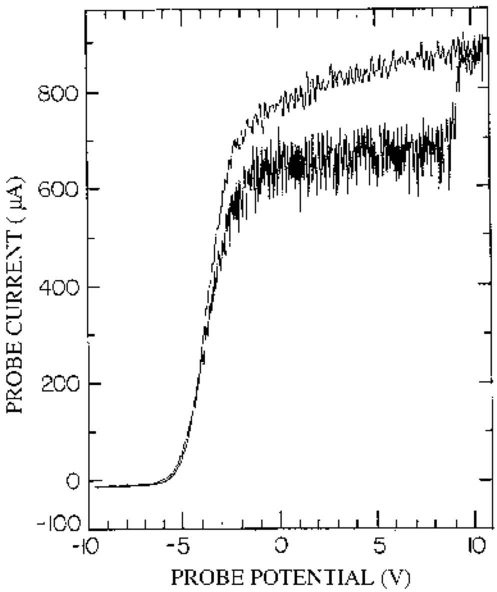

Figure 2.8. Langmuir probe characteristics obtained under identical conditions, except for the absence (upper plot) or the presence (lower plot) of kaolin dust (after Barkan *et al* 1994).

absence (upper curve) or the presence (lower curve) of dust. Here it is shown that the electron saturation current I_e measured with dust is smaller than that (I_e^0) measured without dust. This is due to the fact that the electrons attached to dust grains are of extremely low mobility and are not collected by the probe. The ratio $\eta = (I_e/I_e^0)/(I_i/I_i^0)$ is then a measure of the fraction of negative charge present as free electrons in the dusty plasma, i.e. $\eta = n_e/n_i$, where I_i/I_i^0 (the ratio of the ion probe current with dust to that without dust) takes into account the attenuation of the plasma by the dust cloud.

The plasma density n_e was computed using the relation $I_e = en_e V_{Te} A$, where A is the collecting area of the probe. The quantity $Z_d n_d = n_i(1 - \eta)$ (obtained from the condition of the charge neutrality) can be obtained from the measurements of η and n_i. As n_i is known, the experimental procedure consists of measuring η as a function of the plasma number density n_e, while holding n_d, r_d and T fixed. The experimental measurements for the variation of $Z_d n_d$ (i.e. of Z_d for constant n_d) with n_i shows that (keeping n_d constant) as the electron plasma density (n_e) decreases, the average charge on a dust grain does not remain constant but decreases with decreasing n_e. This effect arises when the intergrain distance d ($\simeq n_d^{-1/3}$) is comparable to or smaller than the dusty plasma Debye radius λ_D. This means that the experimental results agree with the theoretical prediction: for non-isolated (relatively closely packed) dust grains, Z_{d} decreases with increasing dust grain number density (i.e. with decreasing the intergrain spacing), but increases with ambient plasma number density (de Angelis and Forlani 1998).

2.5 Grain Charge Evolution

The time evolution of the charge on a dust grain immersed in a plasma is determined by the charging equation

$$\frac{\mathrm{d}q_{\mathrm{d}}}{\mathrm{d}t} = I_{+} + I_{-} \tag{2.5.1}$$

where I_{+} (I_{-}) is the positive (negative) current which charges the dust grain. The quantity as well as the properties of the currents I_{+} and I_{-} completely depend on the charging processes under consideration. To understand how the dust grain charge evolves with time, we consider an isolated dust grain immersed in a plasma and determine the charging time (the time characterizing the evolution of the dust grain charge to its equilibrium value after some perturbation). As depending on the environment surrounded by the dust grain (i.e. on charging processes) a dust grain can be either positively or negatively charged, we consider both these situations in the next two sections.

2.5.1 Negatively charged grains

We consider a simple situation where the dust grain is charged only by the collection of the primary plasma particles (electrons and ions) and where the OLM theory is valid. The dust grain immersed in such a plasma will be charged up according to a dynamical equation

$$\frac{\mathrm{d}Z_{\mathrm{d}}}{\mathrm{d}t} = -\frac{I_{\mathrm{e}} + I_{\mathrm{i}}}{e} \tag{2.5.2}$$

where I_{e} and I_{i} are given by equations (2.3.2) and (2.3.3), respectively. Substituting equations (2.3.2) and (2.3.3), $n_{\mathrm{e}} = n_{\mathrm{i}} = n_0$ and $\phi_{\mathrm{d}} = -Z_{\mathrm{d}}e/r_{\mathrm{d}}$ into equation (2.5.2) and introducing a normalized variable defined by $y_{\mathrm{n}} = Z_{\mathrm{d}}e^2/r_{\mathrm{d}}k_{\mathrm{B}}T_{\mathrm{e}}$, we have

$$\frac{\mathrm{d}y_{\mathrm{n}}}{\mathrm{d}t} = -\alpha_{\mathrm{n}}\left[1 + y_{\mathrm{n}}\frac{T_{\mathrm{e}}}{T_{\mathrm{i}}} - \frac{V_{\mathrm{Te}}}{V_{\mathrm{Ti}}}\exp(-y_{\mathrm{n}})\right] \tag{2.5.3}$$

where $\alpha_{\mathrm{n}} = \sqrt{8\pi}r_{\mathrm{d}}n_0e^2V_{\mathrm{Ti}}/k_{\mathrm{B}}T_{\mathrm{e}}$. We first discuss an equilibrium solution of equation (2.5.3). Substituting $y_{\mathrm{n}} = y_0 + y_1$, where y_0 (y_1) is the equilibrium (perturbed) part of y_{n}, into equation (2.5.3) we have for the equilibrium state ($\mathrm{d}y_0/\mathrm{d}t = 0$)

$$1 + y_0\frac{T_{\mathrm{e}}}{T_{\mathrm{i}}} - \frac{V_{\mathrm{Te}}}{V_{\mathrm{Ti}}}\exp(-y_0) = 0. \tag{2.5.4}$$

We can numerically solve equation (2.5.4) for y_0 and can easily show that as we increase T_i/T_e (from 0.001 to 0.1), y_0 increases (from 0.7 to 2.5). On the other hand, substituting $y_n = y_0 + y_1$ into equation (2.5.3), we can express the linearized equation for y_1 as

$$\frac{dy_1}{dt} = -\alpha_n y_1 \left[\frac{T_e}{T_i} + \frac{V_{Te}}{V_{Ti}} \exp(-y_0) \right]. \tag{2.5.5}$$

Assuming $y_1 \propto \exp(-t/\tau_c)$, where τ_c is the charging time, we can express the charging time τ_c ($= -y_1/(dy_1/dt)$) as

$$\tau_c = \frac{1}{\alpha_n [T_e/T_i + (V_{Te}/V_{Ti}) \exp(-y_0)]}. \tag{2.5.6}$$

It is obvious that the charging time τ_c is a complicated function of T_i or T_e, but it is inversely proportional to the plasma density and the dust particle radius. We can also numerically show that for $r_d = 0.1$ nm, $n_0 = 5 \times 10^9$ cm^3, $T_e = 3 \times 10^4$ K and $T_i = 0.1 T_e$, the charging time τ_c is of the order of 7 μs.

2.5.2 Positively charged grains

To find the charging time for a positively charged dust grain, we consider a situation where the dust grain is charged by the photoemission of the electrons (in the presence of UV radiation) and the collection of the ions. We also assume that there are no free ions in the dusty plasma, i.e. all the ions are attached onto the dust grain surface. The dust grain immersed in such a plasma will be charged up according to a dynamical equation

$$\frac{dZ_d}{dt} = \frac{I_e + I_p}{e}. \tag{2.5.7}$$

Using equations (2.2.6) and (2.2.28) and $\phi_d = Z_d e / r_d$ the electron collection current I_e and the photoemission current I_p are

$$I_e = -\pi r_d^2 e n_e \left(\frac{8 k_B T_e}{\pi m_e} \right)^{1/2} \left(1 + \frac{Z_d e^2}{r_d k_B T_e} \right) \tag{2.5.8}$$

and

$$I_p = \pi r_d^2 e J_p Y_p \exp\left(-\frac{Z_d e^2}{r_d k_B T_p} \right). \tag{2.5.9}$$

Substituting equations (2.5.8) and (2.4.9) into equation (2.5.7) and introducing a normalized variable defined by $z_p = Z_d e^2 / r_d k_B T_p$, we have

$$\frac{dz_p}{dt} = -\alpha_p \left[1 + z_p \frac{T_p}{T_e} - \alpha_0 \exp(-z_p) \right] \tag{2.5.10}$$

where $\alpha_{\rm p} = \sqrt{8\pi} r_{\rm d} n_{\rm e} e^2 V_{\rm Te}/k_{\rm B} T_{\rm p}$ and $\alpha_0 = J_{\rm p} Y_{\rm p} \sqrt{\pi}/(\sqrt{8} n_{\rm e} V_{\rm Te})$. As we did in the case of negatively charged dust grains, we first discuss the equilibrium solution of equation (2.5.10). Substituting $z_{\rm p} = z_0 + z_1$, where z_0 (z_1) is the equilibrium (perturbed) part of $z_{\rm p}$, into equation (2.5.10) we have for the equilibrium state ($\mathrm{d}z_0/\mathrm{d}t = 0$)

$$1 + z_0 \frac{T_{\rm p}}{T_{\rm e}} - \alpha_0 \exp(-z_0) = 0. \tag{2.5.11}$$

One can numerically solve equation (2.5.11) for z_0. However, if we take $T_{\rm e} \simeq T_{\rm p} \simeq 2$ eV, $J_{\rm p} \simeq 4 \times 10^{18}$ photons cm^{-2}, $Y_{\rm p} = 0.5$ and $n_{\rm e} \simeq 10^9$ cm^{-3}, we have $z_0 \simeq 2.22$. On the other hand, substituting $z_{\rm p} = z_0 + z_1$ into equation (2.5.10), we can express the linearized equation for z_1 as

$$\frac{\mathrm{d}z_1}{\mathrm{d}t} = -\alpha_{\rm p} z_1 \left[\frac{T_{\rm p}}{T_{\rm e}} + \alpha_0 \exp(-z_0) \right]. \tag{2.5.12}$$

Assuming $z_1 \propto \exp(-t/\tau_{\rm c})$, we can express the charging time $\tau_{\rm c}$ as

$$\tau_{\rm c} = \frac{1}{\alpha_{\rm p}[T_{\rm p}/T_{\rm e} + a_0 \exp(-z_0)]}. \tag{2.5.13}$$

It is now obvious that the charging time $\tau_{\rm c}$ is a complicated function of $T_{\rm p}$ or $T_{\rm e}$ and $n_{\rm e}$, but that it is inversely proportional to the dust particle radius. It can be numerically shown that for $r_{\rm d} = 0.1$ μm, $T_{\rm e} \simeq T_{\rm p} \simeq 2 \times 10^4$ K, $J_{\rm p} = 4 \times 10^{18}$ photons cm^{-2}, $Y_{\rm p} = 0.5$ and $n_{\rm e} = 10^9$ cm^{-3} the charging time $\tau_{\rm c}$ is of the order of 0.1 μs.

2.6 Consequences of Charging Processes

We have discussed different possible charging processes that cause the dust grain charge to vary with space and time. The consequences of these dust grain charging processes do not only significantly modify some basic plasma properties, but also introduce new phenomena and interesting aspects of plasma physics. We now discuss some of these consequences of dust grain charging processes.

2.6.1 Debye shielding

We have already discussed the Debye shielding in a dusty plasma where the dust particle charge has been assumed to be constant (section 1.2.2). We now discuss the effects of the dust grain charge fluctuation on the shielding distance or the thickness of the plasma cloud in a dusty plasma. As before, the electrons and the ions are assumed to be in local thermodynamic equilibrium and their number densities $n_{\rm e}$ and $n_{\rm i}$ obey the Boltzmann distribution given by equations (1.2.3) and (1.2.4). Poisson's equation for charge fluctuating stationary dust grains becomes

$$\nabla^2 \phi_{\rm s} = 4\pi(e n_{\rm e} - e n_{\rm i} - q_{\rm d0} n_{\rm d} - q_{\rm d1} n_{\rm d}) \tag{2.6.1}$$

where the dust particle number density n_d is assumed to be the same both inside and outside of the cloud, i.e. $en_{e0} = q_{\mathrm{d}0}n_\mathrm{d} + en_{\mathrm{i}0}$, $q_{\mathrm{d}0}$ ($q_{\mathrm{d}1}$) is the constant (perturbed) part of the dust grain charge q_d. The dust grain charge q_d may fluctuate around an equilibrium value since the OLM electron and ion currents (I_e and I_i) are affected when the dust grain collects electrons and ions at random intervals and in a random sequence. If ϕ_d ($= q_\mathrm{d}/r_\mathrm{d}$) is the dust grain surface potential measured with respect to the plasma potential ϕ_p, from equations (2.2.6) and (2.2.7) the OLM electron and ion currents (for $q_\mathrm{d} < 0$) are

$$I_\mathrm{e} = -4\pi r_\mathrm{d}^2 n_\mathrm{e}(\phi_\mathrm{s})e\left(\frac{k_\mathrm{B}T_\mathrm{e}}{2\pi m_\mathrm{e}}\right)^{1/2}\exp\left(\frac{eq_\mathrm{d}}{k_\mathrm{B}T_\mathrm{e}r_\mathrm{d}}\right) \tag{2.6.2}$$

and

$$I_\mathrm{i} = 4\pi r_\mathrm{d}^2 n_\mathrm{i}(\phi_\mathrm{s})e\left(\frac{k_\mathrm{B}T_\mathrm{i}}{2\pi m_\mathrm{i}}\right)^{1/2}\left(1 - \frac{eq_\mathrm{d}}{k_\mathrm{B}T_\mathrm{i}r_\mathrm{d}}\right). \tag{2.6.3}$$

Inserting $q_\mathrm{d} = q_{\mathrm{d}0} + q_{\mathrm{d}1}$, where $q_{\mathrm{d}1} \ll q_{\mathrm{d}0}$, and substituting equations (2.6.2) and (2.6.3) into $I_\mathrm{e} + I_\mathrm{i} = 0$, we have (Stenflo and Shukla 2000)

$$q_{\mathrm{d}1} = -\frac{\nu_1}{\nu_2} r_\mathrm{d}\phi_\mathrm{s}, \tag{2.6.4}$$

where

$$\nu_1 = \frac{r_\mathrm{d}}{\sqrt{2\pi}}\left[\frac{\omega_\mathrm{pe}}{\lambda_\mathrm{De}}\exp\left(\frac{eq_{\mathrm{d}0}}{k_\mathrm{B}T_\mathrm{e}r_\mathrm{d}}\right) + \frac{\omega_\mathrm{pi}}{\lambda_\mathrm{Di}}\left(1 - \frac{q_{\mathrm{d}0}}{k_\mathrm{B}T_\mathrm{i}r_\mathrm{d}}\right)\right] \tag{2.6.5}$$

and

$$\nu_2 = \frac{r_\mathrm{d}}{\sqrt{2\pi}}\left[\frac{\omega_\mathrm{pe}}{\lambda_\mathrm{De}}\exp\left(\frac{eq_{\mathrm{d}0}}{k_\mathrm{B}T_\mathrm{e}r_\mathrm{d}}\right) + \frac{\omega_\mathrm{pi}}{\lambda_\mathrm{Di}}\right]. \tag{2.6.6}$$

In obtaining equations (2.6.5) and (2.6.6) we have further assumed that $|e\phi_\mathrm{s}/k_\mathrm{B}T_\mathrm{e}| \ll 1$, $|e\phi_\mathrm{s}/k_\mathrm{B}T_\mathrm{i}| \ll 1$, $|q_{\mathrm{d}1}e/k_\mathrm{B}T_\mathrm{e}r_\mathrm{d}| \ll 1$ and $|q_{\mathrm{d}1}e/k_\mathrm{B}T_\mathrm{i}r_\mathrm{d}| \ll 1$. It should be noted that the first two approximations may not be valid near $r = 0$. However, this region, where the potential ϕ_s falls very rapidly, does not have much contribution to the thickness of the cloud (called a sheath). Substituting equations (1.2.3), (1.2.4) and (2.6.4) into equation (2.6.1) we have

$$\nabla^2\phi_\mathrm{s} = \left(\frac{1}{\lambda_\mathrm{De}^2} + \frac{1}{\lambda_\mathrm{Di}^2} + \frac{1}{\lambda_\mathrm{Dg}^2}\right)\phi_\mathrm{s} \tag{2.6.7}$$

where $\lambda_\mathrm{Dg}^{-2} = \nu_2/4\pi n_{\mathrm{d}0}r_\mathrm{d}\nu_1$. Assuming $\phi_\mathrm{s} = \phi_{\mathrm{s}0}\exp(-r/\lambda_\mathrm{Dc})$, we obtain from equation (2.6.7)

$$\lambda_\mathrm{Dc} = \frac{\lambda_\mathrm{Di}}{\sqrt{1 + (\lambda_\mathrm{Di}/\lambda_\mathrm{De})^2 + (\lambda_\mathrm{Dg}/\lambda_\mathrm{Di})^2}} \tag{2.6.8}$$

which is a measure of the shielding distance or the thickness of the sheath in a dusty plasma with the charge fluctuating dust grains. The term $(\lambda_{\rm Dg}/\lambda_{\rm Di})^2$ represents the effect of the dust grain charge fluctuation. For a dusty plasma with negatively charged dust particles we have $n_{e0} \ll n_{i0}$ and $T_e \geq T_i$, i.e. $\lambda_{\rm De} \gg \lambda_{\rm Di}$. Thus, equation (2.6.8) reduces to

$$\lambda_{\rm Dc} \simeq \frac{\lambda_{\rm Di}}{\sqrt{1 + (\lambda_{\rm Dg}/\lambda_{\rm Di})^2}}. \tag{2.6.9}$$

Equation (2.6.9) clearly explains how the Debye length is modified by the dust grain charge fluctuation. It is obvious that when the dust grain radius is very small, i.e. when $\lambda_{\rm Dg} \ll \lambda_{\rm Di}$, one can neglect the effect of this dust grain charge fluctuation. However, when $\lambda_{\rm Dg}$ is comparable to $\lambda_{\rm Di}$, one should take into account the effect of dust grain charge fluctuations.

2.6.2 Electrostatic sheath

We have discussed the properties of the electrostatic sheath in a dusty plasma with constant charged dust particles (section 1.5). We now wish to explain the effect of the dust grain charge fluctuation on some basic properties of such an electrostatic sheath. We consider almost the same dusty plasma model as we considered in section 1.5. The only difference is that instead of a constant dust grain charge we will consider here a fluctuating dust grain charge. Thus, as before the electron number density n_e is given by equation (1.2.3) and the ion number density n_i is given by (1.6.5). Using equations (1.2.3), (1.6.5) and $q_{d0}n_{d0} = en_{e0} - en_{i0}$ we can express Poisson's equation in terms of normalized variables as

$$\frac{d^2\psi_s}{d\xi^2} = \delta\left(1 + \frac{2\psi_s}{M^2}\right)^{-1/2} - \exp(-\psi_s) - (\delta - 1)\frac{Q_d}{Q_{d0}} \tag{2.6.10}$$

where $Q_d = eq_d/k_B T_e r_d$ and $Q_{d0} = eq_{d0}/k_B T_e r_d$. We note that for constant charged dust particles, $Q_d/Q_{d0} = 1$ and equation (2.6.10) is identical with equation (1.6.5). But for the present case the charge Q_d is not constant and is determined from the condition $I_e + I_i = 0$, where I_e is given by equation (2.6.2) and I_i is

$$I_i = \pi r_d^2 e n_i v_i \left(1 - \frac{2eq_d}{r_d m_i v_i^2}\right). \tag{2.6.11}$$

Using equations (1.2.3), (1.2.4), (2.6.2) and (2.6.11) we can express the condition $I_e + I_i = 0$ in the form

$$\left(\frac{\pi m_e}{8m_i}\right)^{1/2} \delta M(M^2 - 2Q'_d)e^{-Q'_d} = M^2 + 2\psi_s \tag{2.6.12}$$

where $Q'_{\mathrm{d}} = Q_{\mathrm{d}} - \psi_{\mathrm{s}}$. Now, following Ma and Yu (1995) we can reduce equations (2.6.10) and (2.6.12) to an 'energy integral'

$$\frac{1}{2}\left(\frac{\mathrm{d}\psi_{\mathrm{s}}}{\mathrm{d}\xi}\right)^2 + V(\psi_{\mathrm{s}}, Q'_{\mathrm{d}}) = 0 \qquad (2.6.13)$$

where the Sagdeev potential $V(\psi_{\mathrm{s}}, Q'_{\mathrm{d}})$ is

$$V(\psi_{\mathrm{s}}, Q'_{\mathrm{d}}) \simeq 1 + \delta M^2 - \exp(-\psi_{\mathrm{s}}) - \delta M^2\left(1 + \frac{2\psi_{\mathrm{s}}}{M^2}\right)^{1/2} + V_{\mathrm{d}} \qquad (2.6.14)$$

in which

$$V_{\mathrm{d}} = \left(\frac{\delta - 1}{2Q_{\mathrm{d0}}}\right)\left[\psi_{\mathrm{s}}^2 + \delta M\left(\frac{\pi m_{\mathrm{e}}}{8m_{\mathrm{i}}}\right)^{1/2}[A_{\mathrm{s}}(Q'_{\mathrm{d}}) - A_{\mathrm{s}}(Q_{\mathrm{d0}})]\right] \qquad (2.6.15)$$

and $A_{\mathrm{s}}(z) = [(M^2 - 2z)(1+z) - 2]\exp(-z)$. It may be noted that in order to derive equation (2.6.13) we have used the appropriate boundary conditions, namely $\psi_{\mathrm{s}} = \mathrm{d}\psi_{\mathrm{s}}/\mathrm{d}\xi = 0$ at $\xi = 0$. Equation (2.6.14) clearly indicates how the Sagdeev potential is modified by the dust grain charge variation. The part $V_{\mathrm{d}}(\psi_{\mathrm{s}}, Q'_{\mathrm{d}})$ is due to the effect of the dust grain charge variation. The nature of ψ_{s} in the plasma sheath can, therefore, be studied either by an analysis of the Sagdeev potential $V(\psi_{\mathrm{s}}, Q'_{\mathrm{d}})$ or by a numerical solution of equation (2.6.13). To examine the nature of ψ_{s} in a dusty plasma with charge fluctuating dust grains, we analyse $V(\psi_{\mathrm{s}}, Q'_{\mathrm{d}})$ for the small-amplitude limit ($|\psi_{\mathrm{s}}| \ll 1$) as we did in section 1.5 (of chapter 1). For $|\psi_{\mathrm{s}}| \ll 1$ we can expand $V(\psi_{\mathrm{s}}, Q'_{\mathrm{d}})$ in a Taylor series

$$V(\psi_{\mathrm{s}}, Q'_{\mathrm{d}}) = \frac{1}{2}\left[-1 + \frac{\delta}{M^2} + \left(\frac{\mathrm{d}^2 V_{\mathrm{d}}}{\mathrm{d}\psi_{\mathrm{s}}^2}\right)_{\psi_{\mathrm{s}}=0}\right]\psi_{\mathrm{s}}^2 + \cdots. \qquad (2.6.16)$$

It is clear that a solution of equation (2.6.13) will exist if

$$\left[\frac{\delta}{M^2} + \left(\frac{\mathrm{d}^2 V_{\mathrm{d}}}{\mathrm{d}\psi_{\mathrm{s}}^2}\right)_{\psi_{\mathrm{s}}=0}\right] < 1. \qquad (2.6.17)$$

This is the modified Bohm criterion in a dusty plasma with charge fluctuating dust grains. It is clear that for constant dust grain charge ($\psi_{\mathrm{s}} = 0$ and $Q_{\mathrm{d}} = Q_{\mathrm{d0}}$), $V_{\mathrm{d}}(\psi_{\mathrm{s}}, Q'_{\mathrm{d}}) = 0$ and the Bohm criterion becomes $M > \sqrt{\delta}$. However, when the effect of the dust grain charge fluctuation is included, the Bohm criterion becomes $M > M_{\mathrm{c}}$, where M_{c} is (Ma and Yu 1995)

$$M_{\mathrm{c}}^2 = \frac{-\delta + 2Q_{\mathrm{d0}} + \sqrt{(3\delta - 2Q_{\mathrm{d0}})^2 + 8(\delta - 1)[2 - (3\delta - 2)/Q_{\mathrm{d0}}]}}{2[1 - (\delta - 1)/Q_{\mathrm{d0}}]}.$$

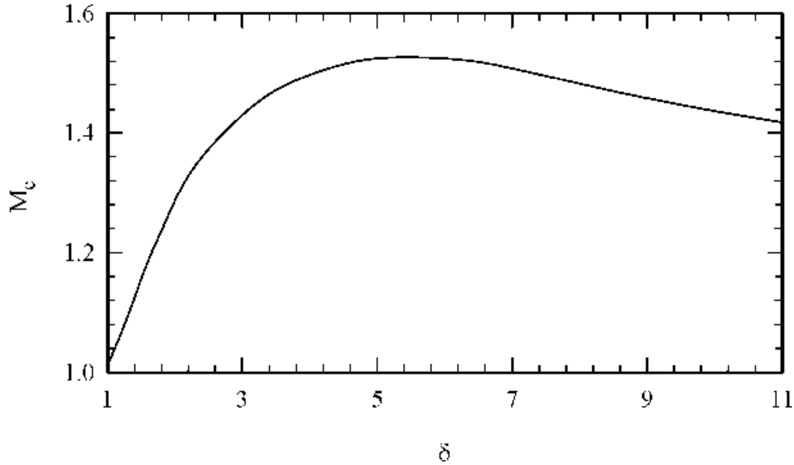

Figure 2.9. The variation of the critical Mach number M_c with δ.

This clearly explains how the effect of the dust grain charge fluctuation modifies the Bohm criterion or the critical Mach number M_c. Since δ is a function of n_{d0}, the Bohm criterion or the critical Mach number is significantly modified by the dust particle number density as well by the dust grain charge at $x = 0$. A plot of M_c versus δ, as shown in figure 2.9, indicates that M_c increases with δ for values within a smaller range. This means that a larger accelerating field is required for pushing the ions towards the wall. Figure 2.9 also shows that M_c decreases with δ for its values within a higher range. This means that for higher values of δ the electrons become virtually depleted, so that the dust grains are less negative and M_c can be smaller.

2.6.3 Coagulation of dust grains

It is well known that in the secondary emission the current–energy curve can have multiple roots. This fact led Meyer-Vernet (1982) to propose that dust grains with identical electrical properties, embedded in the same plasma but having different charging histories, could achieve opposite potentials. This idea was further developed by Horányi and Goertz (1990). The variation of the normalized grain surface potential ($e\phi_d/k_B T$) as a function of the plasma temperature ($T_e = T_i = T$) for different values of the secondary yield parameter (δ_m) is shown in figure 2.10. As an illustration, we consider grains of different sizes immersed in a plasma and assume that they all have the same $\delta_m = 8$. We suppose that the temperature of the plasma is gradually increased. The potentials of all the grains will follow the $\delta_m = 8$ curve. At a lower plasma temperature $T < T_1$, the grain surface potential is negative because the flux of the secondary electron emission is smaller than that of the primary electrons. At a higher temperature $T > T_2$,

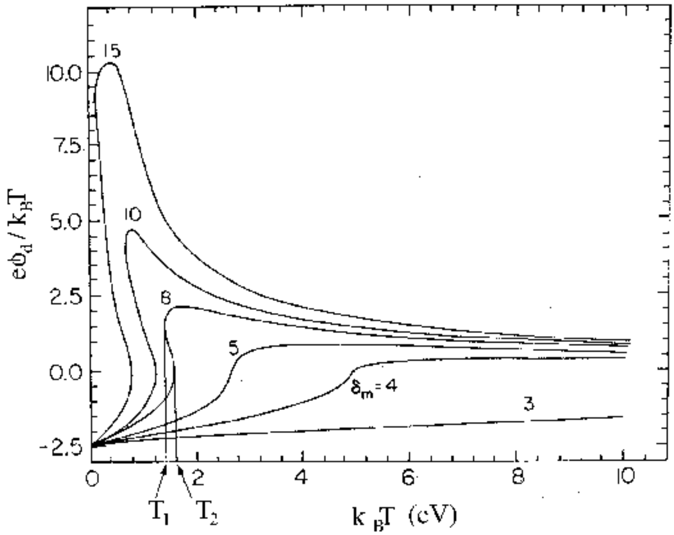

Figure 2.10. The equilibrium surface potential $e\phi_d/k_BT$ as a function of the plasma temperature for different values of the secondary yield parameter δ_m (after Goertz 1989).

its surface potential becomes positive because the flux of the secondary electron emission exceeds the flux of the primary electrons. However, the grain surface potential (i.e. the grain charge) will not change instantaneously but will evolve according to $\partial q_d/\partial t$ = net current. Using this charging equation, we have shown in section 2.5 that the charging time τ_c is inversely proportional to the dust grain radius r_d. This means that the larger dust grains respond more rapidly and acquire a positive charge more quickly than the smaller grains. Once the temperature increases beyond T_2, the grains clearly have to make a transition to the upper part of the curve, thereby changing the potential from a negative value to a positive value. Since the larger dust grains acquire the necessary positive charge to make this transition faster than the smaller grains, there will be oppositely charged grains in the plasma for a certain period of time. Horányi and Goertz (1990) have studied the implication of this effect for the grain coagulation and have found that the attractive Coulomb force between the positively charged larger dust grains and the negatively charged smaller dust grains enhances the coagulation rate. Of course, such a coagulation can occur only during transient heating events, when the ambient plasma is temporarily heated, or when the dust grains move through a spatially confined hot plasma region.

We have already shown in section 2.2.2 that due to the secondary electron emission, different-sized grains of opposite polarity—negatively charged large grains and positively charged small grains—may exist in a warm plasma even in the absence of changes in its environment (Chow *et al* 1993). This is due to the fact that the excited secondary electrons have shorter distances to travel to reach the surface of the smaller dust grains.

Chow *et al* (1993) have also calculated the equilibrium potential for insulating grains immersed in both Maxwellian and generalized Lorentzian plasmas. Due to the size effect on the secondary emission they have found that insulating grains with diameters 0.01 μm and 1 μm have opposite polarity (with smaller ones being positive) when the plasma temperature is in the range 25–48 eV for a Maxwellian plasma and in the range 7–17 eV for a Lorentzian plasma ($\kappa = 2$). These values may be in the range of the inferred values of $k_B T_e$ in different regions of planetary ring systems, comets, the interplanetary medium, supernova remnants, etc (Goertz 1989, Mendis and Horányi 1991, Mendis and Rosenberg 1994). Therefore, the existence of different-sized grains of opposite polarity (negatively charged large grains and positively charged small grains) is possible, i.e. enhanced coagulation may also take place in all of these environments.

It has been shown by Feuerbacher *et al* (1973) that the photoemission may cause the dust grains to acquire opposite charges in the same plasma and radiative environment, even if they have the same size, provided that they have wildly different photoemission yields. This also can lead to an enhanced dust coagulation in certain regions of interstellar space.

2.6.4 Disruption of dust grains

Coagulation is not the only physical effect of grain charging. The exactly opposite effect, namely physical disruption of the dust grains, could also occur if the grains acquire a very high potential. This is a consequence of the electrostatic repulsion of like surface charges, which produces electrostatic tension in the body. If the electrostatic tension exceeds the tensile strength of the body across any section, the body will break up across that section. Opik (1956) showed that electrostatic disruption will occur across a section if the electrostatic energy density ($\phi_g^2/8\pi r_d^2$) exceeds the tensile strength F_t, i.e.

$$F_t < \frac{\phi_g^2}{8\pi r_d^2}. \tag{2.6.18}$$

We can express this in a way that the electrostatic disruption will occur if the grain radius is less than a critical value r_d^c, i.e.

$$r_d < r_d^c = 6.65 F_t^{-1/2} |\phi_g| \tag{2.6.19}$$

where ϕ_g is in volts, F_t is in dyn cm^{-2} and r_d^c (or r_d) is in microns. It is clear from equation (2.6.19) that as the size of the dust grains (i.e. r_d) decreases, the value of F_t required to prevent grain disruption increases rapidly. This also implies that as a dust grain begins to disrupt electrostatically, the process continues until smaller fragments for which $r_d > r_d^c$ appear. If this were so, it also provides an insurmountable obstacle for the growth of the dust grain in a plasma. What the dust grain enables to circumvent this runaway disruption is the electric field emission of the electrons from small grains (Mendis 1991). This is because as the grain radius decreases, the surface electric field increases to reach such a value (typically $\simeq 10^7$ V cm^{-1}) that rapid electron emission occurs from negatively charged dust grains and the value of the grain potential decreases to a value that is no longer given by the plasma environment but rather by the size alone, e.g. $\phi_g \simeq 900 r_d$ (Mendis and Rosenberg 1994). Substituting $\phi_g \simeq 900 r_d$ into equation (2.6.19) we find that when $F_t > 3.6 \times 10^7$ dyn/cm^2, the electric field emission limitation of the grain potential will prevent electrostatic disruption of the grains, regardless of their size. Consequently, materials such as iron ($F_t \simeq 2 \times 10^{10}$ dyn cm^{-2}) and tektites ($F_t \simeq 7 \times 10^{10}$ dyn cm^{-2}) are stabilized by this process against electrostatic disruption no matter how small the size is. On the other hand, very fragile grains such as cometary grains ($F_t \simeq 10^6$ dyn cm^{-2}) of very small radii ($\simeq$Å) will be stable only if $\phi_d \leq 0.15$ eV. It is important to note that the electric field emission effect will enable the growth of the dust grain to take place in the above environments only if the grains are negatively charged. This means that if there is sufficient UV radiation to make the grain charge positive due to the photoemission, the growth of the dust grains will not proceed even in a low-temperature plasma.

2.6.5 Disruption of bacteria

Recently, Mendis *et al* (2000) have modelled an electro-physical mechanism for the electrostatic disruption of a bacterium in the discharge plasma (Laroussi *et al* 1999). They have shown that the electrostatic disruption of the bacterium takes place when the bacterium has acquired a sufficient electrostatic charge for which the outward electrostatic stress exceeds its tensile strength. It also appears in their model that surface roughness or irregularity would render it more sensitive to electrostatic disruption. To illustrate this model, we idealize the bacterium to be a sphere of radius R_b, with a hemispherical irregularity (a 'pimple') of radius $r_b \ll R_b$. We also assume the outer membrane to have a thickness Δ_b ($\ll r_b$, R_b) and to have a uniform surface potential ϕ_b. Since the electrostatic disruption will take place across a section with minimum radius of curvature because of the larger electric fields there (Hill and Mendis 1981b), in this case the condition for the electrostatic disruption is that the component of the total electric force along the axis joining the centres of the larger spheres and small hemisphere exceeds the total tensile force on the membrane along this axis, i.e.

$$\int_0^{r_b} \left(\frac{\phi_b^2}{8\pi r_b^2} \right) 2\pi\rho \, d\rho > \boldsymbol{F}_t \cdot 2\pi \boldsymbol{r}_b \Delta_b \qquad (2.6.20)$$

where ρ is the cylindrical coordinate normal to this axis, F_t is the tensile strength of the membrane and $\phi_b^2/8\pi$ is the electrostatic tension normal to the surface of the bacterium. If we express F_t in dyn cm^{-2}, ϕ_b in volts, and r_b, R_b and Δ_b in μm, equation (2.6.20) leads to the condition

$$|\phi_b| \geq 0.2(r_b \Delta_b F_t)^{1/2}. \tag{2.6.21}$$

We note that if the bacterium had been idealized as a perfect sphere, the condition for disruption across the middle (into two hemispheres) is obtained from equation (2.6.21) by replacing r_b by R_b. So, it is easier to disrupt or tear the membrane by breaking off the 'pimple' than by breaking it into more or less equal pieces.

To have some numerical appreciations of the analytical results, let us take $R_b = 1$ μm, $\Delta_b = 0.008$ μm (Madigan *et al* 1997) and $r_b = 0.02$ μm. The actual measured value of the tensile strength F_t of the outer membrane is not available. However, since Gram-negative bacteria can maintain turgor pressure of 1–5 atm and the purpose of the strong murein layer appears to withstand such pressures (Madigan *et al* 1997), it seems that the tensile strength of the membranes (both inner and outer) could not exceed the above values. We, therefore, assume that $F_t = (1\text{–}5) \times 10^6$ dyn cm^{-2}. If we assume the higher value, i.e. $F_t = 5 \times 10^6$ dyn cm^{-2}, we obtain $|\phi_b| \geq 6$ V as the condition for the electrostatic disruption of the membrane by rupturing the pimple. The condition to break it in half (obtained by replacing r_b by R_b in equation (2.6.21)) is $|\phi_b| \geq 40$ V. If we use the smaller value of F_t ($\sim 10^6$ dyn cm^{-2}) the corresponding conditions are, respectively, $|\phi_b| \geq 3$ V and $|\phi_b| \geq 18$ V.

On the other hand, in a glow discharge plasma experiment of Laroussi *et al* (1999), the plasma electron temperature $k_B T_e = 1\text{–}5$ eV. If we assume that both electrons and ions (largely He^+) are Maxwellian with $T_e = T_i$ (although T_e is significantly larger than T_i in this case), and solve the standard transcendental equation for the equilibrium potential obtained by equating the orbit-limited electron and ion currents to the bacterium immersed in the plasma, we obtain (Mendis *et al* 2000) $|\phi_b| \simeq 15$ V if $k_B T_e = 5$ eV. In such discharges, the plasmas (particularly, the electrons) are not expected to be Maxwellian, having thicker tails at higher energies and are better fit by generalized Lorentzian κ-distribution (Rosenberg and Mendis 1992). If we assume this to be the case with $\kappa = 2$, we get $|\phi_b| \simeq 20$ V. We, therefore, see that the potential expected to be achieved by the *E. coli* bacteria in a glow discharge plasma could be sufficient to break the outer membrane in half if its tensile strength is low ($F_t \simeq 10^6$ dyn cm^{-2}). If the tensile strength is higher ($F_t \simeq 5 \times 10^6$ dyn cm^{-2}), the surface potential achieved is insufficient to break this membrane in half, but would be sufficient to tear it if it had a surface roughness on the scale of a few percent (Mendis *et al* 2000).

2.6.6 Levitation of dust grains

The electrostatic charging of the dust grains can also lead to the levitation of the fine dust lying on large surfaces. In this case, the charge q_d acquired by the dust grain is proportional to its projected surface area (Mendis and Rosenberg

1994) and so q_d = surface area $\times$ surface charge density $= (1/4)(r_\mathrm{d}/\lambda_\mathrm{D})(r_\mathrm{d}\phi_\mathrm{d})$. Typically $r_\mathrm{d}/\lambda_\mathrm{D} \ll 1$ and hence the dust grain charge in a plasma medium is much smaller than that in free space. Mendis *et al* (1982) considered the charging of the bare cometary nucleus by the solar wind plasma and the solar UV radiation at large heliocentric distances. They showed that while the subsolar point of the cometary surface acquires a positive potential of the order of 15 V due to the dominance of the photoemission, the nightside could acquire a negative potential of the order of -1 kV (where the solar wind speed is considered to be of the order of 600 km s^{-1}). Consequently, submicron-sized dust grains could overcome the gravitational attraction of the nucleus and levitate on the nightside of the comet, even when they had a deficit of just one electron charge.

Chapter 3

Dynamics of Dust Grains

3.1 Introduction

The dynamics of charged dust grains in space attracted the main stream of interest of space physicists about 20 years ago, when Voyager 1 and 2 passed Saturn and sent back pictures of mysterious dark spokes sweeping around the B ring (Smith *et al* 1981, 1982). It was then independently proposed by Hill and Mendis (1981a) and Goertz and Morfill (1983) that the spokes might be charged dust and sculptured by electrostatic forces. The dynamical patterns of charged dust particles in interplanetary space observed by Voyager 1 and 2 also seem to account for the combined effects of electromagnetic and gravitational forces acting on the dust particles. On the other hand, in laboratory plasmas, dust particles, which are subjected to various forces, often accumulate near the plasma boundaries (walls) and cause contamination to substrates and wafers (Selwyn 1993). It is, therefore, crucial to understand the behaviour of macroscopic particles under the action of various forces (such as gravitational force, electric force, ion drag force, neutral drag force, thermophoretic force, etc) in order to control the dust transport. Thus, in this chapter, we confine ourselves to the study of different forces acting on charged dust particles and their dynamics in both space and laboratory dusty plasmas. The forces that are relevant to dust grain crystallization are discussed in chapter 8.

3.2 Forces on Dust Grains

There are a number of forces, such as electromagnetic force, gravitational force, ion and neutral drag forces, thermophoretic force, radiation pressure force, etc that may act on charged dust grains and may govern their dynamics in the plasma. The basic equation governing the dynamics of a charged dust grain of mass m_d and velocity $\boldsymbol{v}_\mathrm{d}$ is

$$m_\mathrm{d}\frac{\mathrm{d}\boldsymbol{v}_\mathrm{d}}{\mathrm{d}t} = \boldsymbol{F}_\mathrm{EL} + \boldsymbol{F}_\mathrm{G} + \boldsymbol{F}_\mathrm{D} + \boldsymbol{F}_\mathrm{T} + \boldsymbol{F}_\mathrm{P} \tag{3.2.1}$$

where $\boldsymbol{F}_{\mathrm{EL}}$ is the electromagnetic force associated with the combined effects of the electric and magnetic fields, $\boldsymbol{F}_{\mathrm{G}}$ is the gravitational force associated with the attraction between the dust particles themselves (if they are massive enough) or between the dust particle and the massive planet or satellite, $\boldsymbol{F}_{\mathrm{D}}$ is the drag force associated with the dragging of plasma particles or neutrals, which in fact arises from the relative motion between the plasma and the dust, or between the neutral and the dust, $\boldsymbol{F}_{\mathrm{T}}$ is the thermophoretic force associated with the temperature gradient of the neutral gas and $\boldsymbol{F}_{\mathrm{P}}$ is the radiation pressure force.

3.2.1 Electromagnetic force

The electromagnetic force $\boldsymbol{F}_{\mathrm{EL}}$ acting on a moving charged dust particle of charge q_{d} is the sum of the electric force

$$\boldsymbol{F}_{\mathrm{E}} = q_{\mathrm{d}}\boldsymbol{E} \tag{3.2.2}$$

and the Lorentz force

$$\boldsymbol{F}_{\mathrm{L}} = \frac{q_{\mathrm{d}}}{c}\boldsymbol{v}_{\mathrm{d}} \times \boldsymbol{B} \tag{3.2.3}$$

where $\boldsymbol{E}$ is the electric field and $\boldsymbol{B}$ is the magnetic field. That is, we have

$$\boldsymbol{F}_{\mathrm{EL}} = \boldsymbol{F}_{\mathrm{E}} + \boldsymbol{F}_{\mathrm{L}} = q_{\mathrm{d}}\left(\boldsymbol{E} + \frac{1}{c}\boldsymbol{v}_{\mathrm{d}} \times \boldsymbol{B}\right). \tag{3.2.4}$$

We consider this force first in space dusty plasmas and later in laboratory dusty plasmas.

We consider a magnetized planet in which the magnetic field $\boldsymbol{B}$ can be further simplified by assuming that it is the field of a magnetic dipole of moment $\boldsymbol{M}$ located at its (planet's) centre of gravity and oriented along its rotation axis. Thus, we can express $\boldsymbol{B}(r)$ as

$$\boldsymbol{B}(r) = 3\boldsymbol{r}(\boldsymbol{M}\boldsymbol{r})r^{-5} - \boldsymbol{M}r^{-3} \tag{3.2.5}$$

where $\boldsymbol{r}$ is the distance from the centre of gravity of the planet. Within the equatorial plane, equation (3.2.5) becomes

$$\boldsymbol{B}(r) = -\boldsymbol{M}r^{-3} \tag{3.2.6}$$

and

$$|\boldsymbol{B}(r)| = B_0 L^{-3} \tag{3.2.7}$$

where B_0 is the magnitude of the magnetic field at the planet surface and L ($= r/R_{\mathrm{p}}$, where R_{p} is the planet radius) is the magnetic shell parameter. We assume that the planet is a uniformly magnetized sphere. The induction $\boldsymbol{B}(r)$ and the field strength $\boldsymbol{H}(r)$ are equal at any point outside the planet, but are different inside the planet due to the magnetization. Therefore, inside the planet we can express $\boldsymbol{B}(r)$ and $\boldsymbol{H}(r)$ as

$$\boldsymbol{B}(r \leq R_{\mathrm{p}}) = 2\boldsymbol{M}R_{\mathrm{p}}^{-3} \tag{3.2.8}$$

Table 3.1. Typical magnetic field parameters of Earth, Saturn and Jupiter.

Parameter	Earth	Saturn	Jupiter
M (G cm^3)	8×10^{25}	4.4×10^{28}	1.6×10^{30}
B_0 (G)	0.5	0.2	4.2
R_p (cm)	6.38×10^8	6.03×10^9	7.14×10^9

and

$$\boldsymbol{H}(r \leq R_p) = -\boldsymbol{M} R_p^{-3}. \tag{3.2.9}$$

The magnetic field parameters of different planets, namely Earth, Saturn and Jupiter are given in table 3.1. The electric field $\boldsymbol{E}$ near a rotating magnetized sphere can be evaluated in a simple way by assuming that the plasma is of sufficiently high conductivity (i.e. $\sigma_{con} \rightarrow \infty$, where σ_{con} is the plasma conductivity) and co-rotates rigidly with the angular rotation frequency Ω_{pl} of the magnetized planet. The medium would be at rest in a moving frame moving at the velocity $\boldsymbol{V}_{pl} = \boldsymbol{\Omega}_{pl} \times \boldsymbol{r}$ with respect to the fixed point of observation. Thus, we can express Ohm's law in the form

$$\boldsymbol{j} = \sigma_{con}\left(\boldsymbol{E} + \frac{1}{c}\boldsymbol{V}_{pl} \times \boldsymbol{B}\right) \tag{3.2.10}$$

where $\boldsymbol{j}$ is the current density observed in the fixed frame (transformation of the value $\boldsymbol{j}$ itself results in corrections of the order V_{pl}^2/c^2 that are neglected). The assumption that the current density $\boldsymbol{j}$ is finite at $\sigma_{con} \rightarrow \infty$ allows us to express the electric field as

$$\boldsymbol{E} = -\frac{1}{c}[(\boldsymbol{\Omega}_{pl} \times \boldsymbol{r}) \times \boldsymbol{B}]. \tag{3.2.11}$$

The force $\boldsymbol{F}_{EL}$ acting on a dust particle orbiting the planet at an angular velocity $\boldsymbol{\omega}_d$ (i.e. with the velocity $\boldsymbol{v}_d = \boldsymbol{\omega}_d \times \boldsymbol{r}$) is (Bliokh *et al* 1995)

$$\boldsymbol{F}_{EL} = \frac{q_d}{c}\{[(\boldsymbol{\omega}_d - \boldsymbol{\Omega}_{pl}) \times \boldsymbol{r}] \times \boldsymbol{B}\}. \tag{3.2.12}$$

We consider the force $\boldsymbol{F}_{EL}$ acting on a dust particle within the equatorial plane, where $\boldsymbol{F}_{EL}$ is radially oriented and $B = B_0/L^3$. Thus, within the equatorial plane, we have $F_{EL} = (q_d B_0 r/L^3 c)(\omega_d - \Omega_{pl})$. This means that the Lorentz force is zero at the synchronous orbit where $\omega_d = \Omega_{pl}$. It is important to note here that equation (3.2.12) is valid for a highly conducting plasma around the planet. However, it is also possible to analyse the unipolar induction $\boldsymbol{E}$ without considering this assumption.

We now consider electric forces in a laboratory dusty plasma in which the magnetic force is almost insignificant. We particularly concentrate on the electric force that a conducting (i.e. equipotential) dust particle in a plasma in the presence of a non-zero macroscopic field (i.e. a pre-sheath field of a glow discharge) experiences. To calculate such an electric force acting on a dust particle, we start with the linearized Poisson equation (1.2.6) that can be expressed in spherical coordinates with an azimuthal symmetry as

$$\frac{1}{r^2}\frac{\partial}{\partial r}\left(r^2\frac{\partial\phi_{\rm s}}{\partial r}\right)+\frac{1}{r^2\sin\theta}\frac{\partial}{\partial\theta}\left(\sin\theta\frac{\partial\phi_{\rm s}}{\partial\theta}\right)=k_{\rm D}^2\phi_{\rm s} \tag{3.2.13}$$

where $k_{\rm D}^2 = \lambda_{\rm De}^{-2} + \lambda_{\rm Di}^{-2}$. The boundary condition far from the particle is now a constant field condition, which in spherical coordinates takes the form

$$\phi_{\rm s}(r,\theta)|_{r\to\infty} = -E_0 r\cos\theta \tag{3.2.14}$$

where E_0 is the constant electric field strength. The surface of a conducting dust particle is at a uniform potential $\phi_{\rm d}$. Thus, the boundary condition at the particle surface is

$$\phi_{\rm s}(r,\theta)|_{r\to r_{\rm d}} = \phi_{\rm d}. \tag{3.2.15}$$

Also, all the components of $\nabla\phi_{\rm s}$ tangential to the surface of the dust grain, which is assumed to be a conductor, vanish, i.e.

$$(\nabla\phi_{\rm s})_\theta|_{r\to r_{\rm d}} = 0. \tag{3.2.16}$$

Introducing the variable transformations $\xi = k_{\rm D}r$ and $\mu = \cos\theta$ we can express equation (3.2.13) in the form

$$\frac{1}{\xi^2}\frac{\partial}{\partial\xi}\left(\xi^2\frac{\partial\phi_{\rm s}}{\partial\xi}\right)+\frac{1}{\xi^2}\frac{\partial}{\partial\mu}\left[(1-\mu^2)\frac{\partial\phi_{\rm s}}{\partial\mu}\right]=\phi_{\rm s}. \tag{3.2.17}$$

Substituting

$$\phi_{\rm s}(\xi,\mu) = Y(\xi)Z(\mu) \tag{3.2.18}$$

into equation (3.2.17), we can separate the latter into two ordinary differential equations, namely

$$\xi^2\frac{{\rm d}^2Y}{{\rm d}\xi^2}+2\xi\frac{dY}{d\xi}-[\xi^2+n(n+1)]Y=0 \tag{3.2.19}$$

and

$$(1-\mu^2)\frac{{\rm d}^2Z}{{\rm d}\mu^2}-2\mu\frac{{\rm d}Z}{{\rm d}\mu}+n(n+1)Z=0 \tag{3.2.20}$$

where $n = 0, 1, 2, \ldots$. It is obvious that the modified spherical Bessel functions and Legendre functions are the solutions of equations (3.2.19) and (3.2.20), respectively. Therefore, substituting these two solutions into equation (3.2.18) we have (Daugherty *et al* 1993)

$$\phi_{\rm s}(\xi,\mu) = \phi_\infty + A_0\left(\frac{1}{\xi}\right)\exp(-\xi) + A_1\mu\left(\frac{1}{\xi}+\frac{1}{\xi^2}\right)\exp(-\xi)+\cdots \tag{3.2.21}$$

where ϕ_∞, A_0 and A_1 are constants. The latter can be determined by the boundary conditions given in equations (3.2.14)–(3.2.16), i.e. equation (3.2.14) determines $\phi_\infty = -E_0 r\cos\theta$, equation (3.2.15) determines $A_0 = \phi_{\rm d} k_{\rm D} r_{\rm d}\exp(k_{\rm D} r_{\rm d})$ and equation (3.2.16) determines $A_1 = [E_0 k_{\rm D}^2 r_{\rm d}^3/(1 + k_{\rm D} r_{\rm d})]\exp(k_{\rm D} r_{\rm d})$. All other higher-order terms vanish for a constant field boundary condition, i.e. terms with $\cos^2\theta$ and higher are not needed to match a constant field condition. Therefore, the solution of equation (3.2.13) for the perturbed potential profile is

$$\begin{aligned}\phi_{\rm s}(r,\theta) = &-E_0 r\cos\theta + \phi_{\rm d}\frac{r_{\rm d}}{r}\exp[-k_{\rm D}(r - r_{\rm d})]\\ &+ \frac{E_0 k_{\rm D}^2 r_{\rm d}^3}{1 + k_{\rm D} r_{\rm d}}\cos\theta\left(\frac{1}{k_{\rm D} r} + \frac{1}{k_{\rm D}^2 r^2}\right)\exp[-k_{\rm D}(r - r_{\rm d})]. \qquad (3.2.22)\end{aligned}$$

It is obvious from equation (3.2.22) that the electric potential $\phi_{\rm s}(r,\theta)$ consists of three separate potential fields. The first term is the potential due to the constant applied field E_0. The second term is the spherically symmetric Debye–Hückel potential. The last term is the polarization response of the plasma, and it depends on $\cos\theta$ and represents the characteristics of a dipole distribution of the dust grain charge.

The electrostatic force associated with this potential field may be calculated by the application of the electrostatic stress tensor (Daugherty *et al* 1993). The electrostatic force $\boldsymbol{F}_{\rm E}$ on the spherical dust grain is given by

$$\boldsymbol{F}_{\rm E} = \frac{1}{4\pi}\oint_{\rm surface}\left[\boldsymbol{E}_{\rm s}(\boldsymbol{E}_{\rm s}\cdot\hat{\boldsymbol{n}}) - \frac{1}{2}E_{\rm s}^2\hat{\boldsymbol{n}}\right]{\rm d}A \qquad (3.2.23)$$

where $E_{\rm s}^2$ is the square of the magnitude of the surface electric field vector. We have considered the dust grain as a conducting sphere, i.e. the electric field is normal to its surface. Therefore, for spherical symmetry we can simplify equation (3.2.23) as

$$F_{{\rm E}z} = \frac{1}{4}r_{\rm d}^2\int_0^\pi\left[\left(\frac{\partial\phi_{\rm s}}{\partial r}\right)_{r=r_{\rm d}}\right]^2\cos\theta\sin\theta\,{\rm d}\theta. \qquad (3.2.24)$$

Note that the constant electric field $\boldsymbol{E}_0$ is along the z-direction. Substituting equation (3.2.22) into equation (3.2.24) and then performing the integration we have

$$F_{{\rm E}z} = r_{\rm d}\phi_{\rm d}E_0(1 + k_{\rm d} r_{\rm d})\left[1 + \frac{k_{\rm D}^2 r_{\rm d}^2}{3(1 + k_{\rm D} r_{\rm d})}\right]. \qquad (3.2.25)$$

Equation (3.2.25) can be further simplified by calculating $\phi_{\rm d}$ in terms of the dust grain charge

$$q_{\rm d} = 2\pi r_{\rm d}^2\int_0^\pi\sigma_{\rm q}(\theta)\sin\theta\,{\rm d}\theta \qquad (3.2.26)$$

where the surface charge density $\sigma_{\mathrm{q}}(\theta)$ is given by

$$\sigma_q(\theta) = -\frac{1}{4\pi}\left(\frac{\partial\phi_{\mathrm{s}}}{\partial r}\right)_{r=r_{\mathrm{d}}}. \tag{3.2.27}$$

Using equations (3.2.22), (3.2.26) and (3.2.27) we can express q_{d} as

$$q_{\mathrm{d}} = r_{\mathrm{d}}\phi_{\mathrm{d}}(1 + k_{\mathrm{d}}r_{\mathrm{d}}). \tag{3.2.28}$$

Substituting ϕ_{d} (obtained from (3.2.28)) into equation (2.3.25) we finally obtain

$$F_{\mathrm{E}z} = q_{\mathrm{d}}E_0\left[1 + \frac{k_{\mathrm{D}}^2 r_{\mathrm{d}}^2}{3(1 + k_{\mathrm{D}}r_{\mathrm{d}})}\right]. \tag{3.2.29}$$

Equation (3.2.29) implies that for most of the dusty plasma in which $k_{\mathrm{D}}r_{\mathrm{d}} \ll 1$, we have $F_{\mathrm{E}z} \simeq q_{\mathrm{d}}E_0$. It also implies an intersecting result that the plasma does not shield the dust particle from the bulk electric field and thereby the electrostatic force is reduced. This prediction was first made by Daugherty *et al* (1993) by their analytical calculations of electrostatic forces acting on small particles in a uniform plasma in the presence of a constant electric field E_0. However, there are some situations where the electric field may be associated with a non-uniform plasma density and where the deformation of the sheath may occur due to the density gradient.

Hamaguchi and Farouki (1994) have investigated the electrostatic force acting on a dust particle in a plasma in the presence of a density gradient and an externally applied constant electric field E_0. They have shown that another force, which is proportional to the density gradient (or the Debye-length gradient) should be added in order to account for the deformation of the sheath. They derived a first-order correction to the Debye–Hückel potential associated with the density or Debye-length gradient by expanding the linearized Debye length around the position of the dust grain. They have expressed the total force acting on a dust particle as

$$F_{\mathrm{E}z} = q_{\mathrm{d}}E_0 - \frac{q_{\mathrm{d}}^2}{2(\lambda_{\mathrm{D}} + r_{\mathrm{d}})^2}\left(\frac{\mathrm{d}\lambda_{\mathrm{D}}}{\mathrm{d}z}\right) \tag{3.2.30}$$

where $\lambda_{\mathrm{D}} = 1/k_{\mathrm{D}}$. The total force is clearly the superposition of two separate forces. The first term is the electric force which is due to the constant applied dc electric field E_0 and is unaffected by the sheath, as predicted by Daugherty *et al* (1993). The second term is another force known as polarization force which is due to the gradient in the density.

3.2.2 Gravitational force

The gravitational force $\boldsymbol{F}_{\mathrm{G}}$ acting on a dust particle is in general a combination (resultant) of three forces, namely (i) the force of attraction acting on a dust grain by the nearby planet: $\boldsymbol{F}_{\mathrm{Gp}} = Gm_{\mathrm{d}}M_{\mathrm{p}}\boldsymbol{r}/r^3$, where $G = 6.672\times10^{-8}$ dyn cm^2 g^{-2} is the gravitational constant and $\boldsymbol{r}$ is the distance of the grain from the gravity centre of the nearby planet of the mass M_{p}, (ii) the force of attraction between the dust grains themselves: $\boldsymbol{F}_{\mathrm{Gd}} = Gm_{\mathrm{d}}M_{\mathrm{d}}\boldsymbol{r}/r^3$, where $\boldsymbol{r}$ is the distance of the first grain of mass m_{d} from the gravity centre of the second grain of mass M_{d} (this force is, in fact, grain–grain interaction through the gravitational fields produced by themselves and is known as the self-gravitational force) and (iii) the force of attraction acting on a dust grain by a nearby satellite (in some spacial situation): $\boldsymbol{F}_{\mathrm{Gs}} = Gm_{\mathrm{d}}M_{\mathrm{s}}\boldsymbol{r}/r^3$, where $\boldsymbol{r}$ is the distance of the grain from the gravity centre of the nearby satellite of the mass M_{s}. Therefore, the total gravitational force $\boldsymbol{F}_{\mathrm{G}}$ acting on a dust grain is

$$\boldsymbol{F}_{\mathrm{G}} = \boldsymbol{F}_{\mathrm{Gp}} + \boldsymbol{F}_{\mathrm{Gd}} + \boldsymbol{F}_{\mathrm{Gs}}. \tag{3.2.31}$$

This representation for the gravitational force is valid when it is spherically symmetric, but not valid when it deviates from spherical symmetry, such as oblate geometry or non-uniformity of the planet itself that gives rise to multipole moments in the gravitational field. We define different forces $\boldsymbol{F}_{\mathrm{Gp}}$, $\boldsymbol{F}_{\mathrm{Gd}}$ and $\boldsymbol{F}_{\mathrm{Gs}}$ in a very simple way, but in practice each of these forces may be affected by others.

The motion of large celestial bodies is typically governed by the gravitational force, while trajectories of charged micro-particles (i.e. electrons and ions) are mostly controlled by electromagnetic fields. This is certainly true, but the situation is different with electrically charged macroscopic particles of micron or submicron size for which the electromagnetic and gravitational forces are equipotent. This is why the dynamics of dust particles under the combined effects of the gravitational and electromagnetic forces is referred to as gravito-electrodynamics (Mendis *et al* 1982, Goertz 1989). However, we can roughly say that the dust grains with $r_{\mathrm{d}} > 1$ μm are dominated by the gravitational force, while those with $r_{\mathrm{d}} < 1$ μm are dominated by the electromagnetic force (Howard *et al* 1999, 2000).

3.2.3 Drag forces

The drag force is defined as the time rate of the momentum transfer from the dust particles to the plasma components (particularly, to the ions and neutrals, since collisions between the electrons and the dust particles can be neglected) or from the plasma components (mainly from the ions and neutrals) to the dust particles. Therefore, in a dusty plasma there are basically two types of drag forces, namely the ion drag force that is due to the momentum exchange between positive ions and dust particles, and the neutral drag force that is due to the momentum exchange between the dust particles and neutrals during their collisions. These two important drag forces may be described as follows.

3.2.3.1 Ion drag force

The ion drag force is discussed by a number of authors (e.g. Nitter 1996, Boeuf and Punset 1999). The ions can transfer their momentum to a dust particle in three possible ways, namely (i) direct ion impacts, i.e. the collection of ions, (ii) electrostatic Coulomb collisions and (iii) ion fluid flow (collective) effects which modify or distort the shape of the Debye sheath around the dust particle. The ion drag force associated with the collection of positive ions by their direct impacts will be referred to as the 'collection drag force' ($\boldsymbol{F}_{\mathrm{di}}^{\mathrm{coll}}$). The ion drag force associated with the electrostatic Coulomb interaction will be termed as 'Coulomb drag force' ($\boldsymbol{F}_{\mathrm{di}}^{\mathrm{coul}}$). The force associated with the effect of the ion fluid flow will be termed as 'ion flow drag force' ($\boldsymbol{F}_{\mathrm{di}}^{\mathrm{flow}}$). Therefore, the total ion drag force $\boldsymbol{F}_{\mathrm{di}}$ can be expressed as

$$\boldsymbol{F}_{\mathrm{di}} = \boldsymbol{F}_{\mathrm{di}}^{\mathrm{coll}} + \boldsymbol{F}_{\mathrm{di}}^{\mathrm{coul}} + \boldsymbol{F}_{\mathrm{di}}^{\mathrm{flow}}. \tag{3.2.32}$$

The ion flow drag force $\boldsymbol{F}_{\mathrm{di}}^{\mathrm{flow}}$, which is much more difficult to calculate, will be neglected since it has a minor effect on the total ion drag force (Northrop and Birmingham 1990). However, two other drag forces, $\boldsymbol{F}_{\mathrm{di}}^{\mathrm{coll}}$ and $\boldsymbol{F}_{\mathrm{di}}^{\mathrm{coul}}$, may be calculated in the following fashion.

We consider a dusty plasma with static dust particles and positive ions. The ion drag forces $\boldsymbol{F}_{\mathrm{di}}^{\mathrm{coll,coul}}$ can be expressed as

$$\boldsymbol{F}_{\mathrm{di}}^{\mathrm{coll,coul}} = n_{\mathrm{i}} m_{\mathrm{i}} \sigma^{\mathrm{coll,coul}} V_{\mathrm{it}} \boldsymbol{v}_{\mathrm{i}} \tag{3.2.33}$$

where σ^{coll} (σ^{coul}) is the momentum collision cross section corresponding to the collection of ions by direct ion impacts (electrostatic Coulomb collisions) and $V_{\mathrm{it}} = (v_{\mathrm{i}}^2 + 8k_B T_{\mathrm{i}}/\pi m_{\mathrm{i}})^{1/2}$ is the total ion speed (a combination of directed and thermal speeds).

The collection cross section σ^{coll} has already been expressed in terms of the dust grain surface potential ϕ_{d} and the ion kinetic energy ($m_{\mathrm{i}} v_{\mathrm{i}}^2/2$) by equation (2.2.5). That is

$$\sigma^{\mathrm{coll}} = \pi r_{\mathrm{d}}^2 \left(1 - \frac{2e\phi_{\mathrm{d}}}{m_{\mathrm{i}} v_{\mathrm{i}}^2}\right). \tag{3.2.34}$$

We have assumed here that the momentum transfer cross section for the collection drag is equal to the cross section used for the ion charging current. Therefore, the collection force $F_{\mathrm{di}}^{\mathrm{coll}}$ can finally be expressed as

$$\boldsymbol{F}_{\mathrm{di}}^{\mathrm{coll}} = \pi r_{\mathrm{d}}^2 n_{\mathrm{i}} m_{\mathrm{i}} V_{\mathrm{it}} \boldsymbol{v}_{\mathrm{i}} \left(1 - \frac{2e\phi_{\mathrm{d}}}{m_{\mathrm{i}} v_{\mathrm{i}}^2}\right). \tag{3.2.35}$$

To obtain the expression for the Coulomb drag force, we now calculate σ^{coul}. The laws of the conservation of energy and the angular momentum allow us to express the momentum transfer cross section for the Coulomb drag ($\sigma^{\rm coul}$) as (Bittencourt 1986, Nitter 1996)

$$\sigma^{\rm coul} = 4\pi b_0^2 \int_{b_{\rm c}}^{\lambda_{\rm De}} \frac{b\,{\rm d}b}{b_0^2 + b^2} \tag{3.2.36}$$

where b is the impact parameter,

$$b_0 = r_{\rm d} \frac{e\phi_{\rm d}}{m_{\rm i} v_{\rm i}^2} \tag{3.2.37}$$

is the impact radius corresponding to a 90° deflection and

$$b_{\rm c} = r_{\rm d} \left(1 - \frac{2e\phi_{\rm d}}{m_{\rm i} v_{\rm i}^2}\right)^{1/2} \tag{3.2.38}$$

is the direct collision impact parameter. Note that the direct collision impact parameter $b_{\rm c}$ is used in order to exclude the collected ions from the calculation of the Coulomb drag force $\boldsymbol{F}_{\rm di}^{\rm coul}$. If we choose the upper integration limit of the integral in equation (3.2.36) at infinity, it diverges. Therefore, it is common to introduce a cut-off for this upper integration limit at $\lambda_{\rm De}$ (Nitter 1996). The electron Debye length $\lambda_{\rm De}$ is the appropriate cut-off (or shielding length) in this case, because the ions, having a drift speed that is large compared with the ion thermal speed, are unable to form the sheath around the dust particle. Thus, the Debye sheath consists only of a deficiency of electrons, with thickness given approximately by $\lambda_{\rm De}$. The integration of equation (3.2.36) yields

$$\sigma^{\rm coul} = 2\pi b_0^2 \ln\left(\frac{b_0^2 + \lambda_{\rm De}^2}{b_0^2 + b_{\rm c}^2}\right). \tag{3.2.39}$$

The Coulomb ion drag forces $\boldsymbol{F}_{\rm di}^{\rm coul}$ is thus given by

$$\boldsymbol{F}_{\rm di}^{\rm coul} = 2\pi b_0^2 n_{\rm i} m_{\rm i} V_{\rm it} \boldsymbol{v}_{\rm i} \ln\left(\frac{b_0^2 + \lambda_{\rm De}^2}{b_0^2 + b_{\rm c}^2}\right). \tag{3.2.40}$$

3.2.3.2 *Neutral drag force*

The neutral drag force may be defined as the rate of momentum exchange between dust particles and neutrals during their collisions. To estimate the neutral drag force, there are two regimes to be considered. These are the hydrodynamic regime, where the Knudsen number is much smaller than unity, i.e. $K_{\rm n}$ (= neutral mean free path/dust particle radius) $\ll$ 1, and a kinetic regime in which the Knudsen number is much larger than unity, i.e. $K_{\rm n} \gg 1$. In the hydrodynamic (high-pressure) regime, the drag force can be estimated from Stokes' law and is found to be proportional to the speed (v_d) and the radius (r_d) of the dust particle. It is shown that for a typical low-pressure (i.e. less than one 1 Torr), the neutral mean free path is longer than a few 100 μm while the dust particle radius is less than a few μm. Thus, to estimate the neutral drag force $\boldsymbol{F}_\mathrm{dn}$ in plasma processing conditions, we must consider the kinetic regime. The method of deriving the neutral drag force is almost the same as that we used in deriving the ion drag force. The only difference is that the collision cross section is constant (the hard-sphere cross section) for the present case. The neutral drag force $\boldsymbol{F}_\mathrm{dn}$ for a Maxwellian distribution of the neutral gas molecules is (Baines *et al* 1965)

$$\boldsymbol{F}_\mathrm{dn} = -\sqrt{2\pi} r_\mathrm{d}^2 m_\mathrm{n} n_\mathrm{n} V_\mathrm{Tn} H(s)(\boldsymbol{v}_\mathrm{d} - \boldsymbol{v}_\mathrm{n}) \tag{3.2.41}$$

where $\boldsymbol{v}_\mathrm{n}$ is the velocity of the neutral fluid. The function $H(s)$ is

$$H(s) = \frac{1}{s}\left[\left(s + \frac{1}{2s}\right)\exp(-s^2) + \sqrt{\pi}\left((s^2 + 1 - \frac{1}{4s^2}\right)\mathrm{erf}(s)\right] \tag{3.2.42}$$

where $s = |\boldsymbol{v}_\mathrm{d} - \boldsymbol{v}_\mathrm{n}|/\sqrt{2}V_\mathrm{Tn}$. We note that equation (3.2.41) represents the neutral drag force for specular collisions in which the neutrals colliding with the dust particle have their velocity components normal to the dust particle surface reversed after collisions. However, in most practical situations collisions are not specular because the neutrals are first absorbed at the surface and are then re-emitted from the latter. We can also define perfect diffuse reflections in which the neutrals are absorbed and re-emitted by the surface of the dust particle with a semi-isotropic Maxwellian distribution at the dust particle temperature T_d. The neutral drag force for the perfect diffuse reflection can be obtained just by replacing the function $H(s)$ in equation (3.2.41) by $H(s)+\pi/3$ (Boeuf and Punset 1999).

When the relative speed $|\boldsymbol{v}_\mathrm{d} - \boldsymbol{v}_\mathrm{n}|$ is very small in comparison with the neutral thermal speed V_Tn, i.e. $s \ll 1$, we can easily expand the function $H(s)$, and thus can approximate the neutral drag force $\boldsymbol{F}_\mathrm{dn}$ as a simple expression (the so-called Epstein expression (Epstein 1924)) as

$$\boldsymbol{F}_\mathrm{dn} = -\tfrac{8}{3}\sqrt{2\pi} r_\mathrm{d}^2 m_\mathrm{n} n_\mathrm{n} V_\mathrm{Tn}(\boldsymbol{v}_\mathrm{d} - \boldsymbol{v}_\mathrm{n}) \tag{3.2.43}$$

for the specular reflection, and as

$$\boldsymbol{F}_\mathrm{dn} = -\frac{8}{3}\sqrt{2\pi} r_\mathrm{d}^2 m_\mathrm{n} n_\mathrm{n} V_\mathrm{Tn}\left(1 + \frac{\pi}{8}\right)(\boldsymbol{v}_\mathrm{d} - \boldsymbol{v}_\mathrm{n}) \tag{3.2.44}$$

for the perfect diffuse reflection. When the relative speed $|\boldsymbol{v}_\mathrm{d} - \boldsymbol{v}_\mathrm{n}|$ is very high in comparison with the neutral thermal speed V_Tn, i.e. $s \gg 1$, the approximated expression for the neutral drag force is same for both the specular and prefect diffuse reflections and is

$$\boldsymbol{F}_\mathrm{dn} = -\pi r_\mathrm{d}^2 m_\mathrm{n} n_\mathrm{n} |\boldsymbol{v}_\mathrm{d} - \boldsymbol{v}_\mathrm{n}|(\boldsymbol{v}_\mathrm{d} - \boldsymbol{v}_\mathrm{n}). \tag{3.2.45}$$

It is important to point out that in a realistic laboratory dusty plasma situation we have $s \ll 1$, and the Epstein limit is a good approximation for calculating the neutral drag force. Draine and Salpeter (1979) have considered the specular reflection and derived an approximate expression for the neutral drag force

$$\boldsymbol{F}_{\mathrm{dn}} = -\frac{8}{3}\sqrt{2\pi} r_{\mathrm{d}}^2 m_{\mathrm{n}} n_{\mathrm{n}} V_{\mathrm{Tn}} \left(1 + \frac{9\pi}{64} s^2\right)^{1/2} (\boldsymbol{v}_{\mathrm{d}} - \boldsymbol{v}_{\mathrm{n}}) \tag{3.2.46}$$

which is accurate to within 1% for all velocities and exact in the limits $s \to 0$ and $s \to \infty$. The specular and perfect diffuse reflections that we have considered are just two extreme assumptions for collisions between dust particles and neutrals. To account for the intermediate situation, one can use the accommodation coefficient α_{ac}, which measures the probability of a perfect diffuse reflection and depends on the surface properties of the dust particle. Knudsen (1991) first introduced the accommodation coefficient to take into account the fact that absorbed neutrals do not necessarily reach thermal equilibrium with the particle surface before they are absorbed. Using the accommodation coefficient α_{ac}, the neutral drag force $\boldsymbol{F}_{\mathrm{dn}}$ in the Epstein limit ($s \ll 1$) becomes (Perrin *et al* 1994, Boeuf and Punset 1999)

$$\boldsymbol{F}_{\mathrm{dn}} = -\frac{8}{3}\sqrt{2\pi} r_{\mathrm{d}}^2 m_{\mathrm{n}} n_{\mathrm{n}} V_{\mathrm{Tn}} \left(1 + \alpha_{\mathrm{ac}} \frac{\pi}{8}\right) (\boldsymbol{v}_{\mathrm{d}} - \boldsymbol{v}_{\mathrm{n}}). \tag{3.2.47}$$

Note that the accommodation coefficient α_{ac} would be zero for specular reflection and unity for perfect diffuse reflection.

3.2.4 Thermophoretic force

We consider a dust particle that resides in a neutral gas with a temperature gradient ∇T_{n}. The molecules on the hot side of the particle have higher thermal speeds than those on the cold side. This means that a net momentum transfer from the gas to the dust particle occurs (since the momentum transfer rate from the gas to the dust particle depends upon the speed of the molecules). The rate of this net momentum transfer is known as the thermophoretic force $\boldsymbol{F}_{\mathrm{T}}$. Its magnitude is directly proportional to the temperature gradient and its direction is in the direction of the heat flux, i.e. in the direction opposite to the neutral gas temperature gradient.

Talbot *et al* (1980), who assumed that the non-uniform velocity distribution of the unperturbed neutral gas in the vicinity of the dust particle can be represented in the Chapman–Enskog form and that the particle is small enough to influence this distribution function, have analytically derived the expression for the thermophoretic force. Daugherty and Graves (1995) have also physically explained this force in order to understand a particulate transport model for a glow discharge. The thermophoretic force $\boldsymbol{F}_{\mathrm{T}}$ acting on a dust particle for a non-uniform (unperturbed) gas velocity distribution of the Chapman–Enskog form is given by (Talbot *et al* 1980, Daugherty and Graves 1995)

$$\boldsymbol{F}_{\mathrm{T}} = -\frac{8\sqrt{2\pi}}{15}\frac{r_{\mathrm{d}}^2}{V_{\mathrm{Tn}}}\left[1 + \frac{5\pi}{32}(1 - \alpha_{\mathrm{ac}})\right] k_{\mathrm{n}}^{\mathrm{con}} \nabla T_{\mathrm{n}} \tag{3.2.48}$$

where $k_{\mathrm{n}}^{\mathrm{con}}$ is the translational thermal conductivity of the neutral gas. Talbot *et al* (1980) have suggested that for gas and dust having temperatures less than 500 K, the accommodation coefficient α_{ac} can be close to unity. As in most space and laboratory dusty plasmas the neutral temperature is below/around the room temperature, we can set $\alpha_{\mathrm{ac}} = 1$. On the other hand, using the Chapman–Enskog expression for the thermal conductivity we can express $k_{\mathrm{n}}^{\mathrm{con}}$ as (Daugherty and Graves 1995)

$$k_{\mathrm{n}}^{\mathrm{con}} = \frac{75}{64\sqrt{\pi}}\frac{k_B V_{\mathrm{Tn}}}{\sigma_{\mathrm{LJ}}^2 \Omega_{\mathrm{LJ}}^\star} \tag{3.2.49}$$

where σ_{LJ} is the Lennard-Jones collision diameter of the gas and $\Omega_{\mathrm{LJ}}^\star$ is a collision integral for scattering in a Lennard-Jones potential. The asterisk indicates that the collision integral has been reduced by its value for hard-sphere scattering. The integral $\Omega_{\mathrm{LJ}}^\star$ is a weak function of the temperature, and its value is close to unity for most mono-polar gases near room temperature (Daugherty and Graves 1995). Therefore, substituting equation (3.2.49) into equation (3.2.48) the thermophoretic force $\boldsymbol{F}_{\mathrm{T}}$ can be simplified as

$$\boldsymbol{F}_{\mathrm{T}} \simeq -\frac{5}{4\sqrt{2}}\left(\frac{r_{\mathrm{d}}}{\sigma_{\mathrm{LJ}}}\right)^2 k_B \nabla T_{\mathrm{n}}. \tag{3.2.50}$$

Now if we can consider ∇T_{n} in equation (3.2.50) to be an independent variable, the thermophoretic force $\boldsymbol{F}_{\mathrm{T}}$ is independent of the neutral pressure and the mass of the neutral gas. However, this is only true if the neutral pressure is so high that the number of the neutral mean free path between the dust particle and the system boundaries is much larger than one (Daugherty and Graves 1995). Of course, if the pressure approaches zero, the thermophoretic force must eventually approach zero because at sufficiently low pressure collisions between the neutrals and the dust particles cease. However, if the mean free path is of the order of the system size, a thermophoretic force can still exist, although the velocity distribution will no longer take the Chapman–Enskog form. This effect has been considered by Havnes *et al* (1994) who found that the thermophoretic force is reduced by a factor $\sim$2 within one mean free path of the wall.

We have discussed the thermophoretic force associated with the neutral temperature gradient. It is conceivable that temperature gradients in the ion and electron fluids could result in an additional contribution to the thermophoretic force. This possibility has been addressed by several authors (e.g. Chen and Tao 1992, Daugherty and Graves 1995). It is reasonable that the thermophoretic force from neutrals in equation (3.2.46) scales as hard-sphere cross section $\sim r_{\mathrm{d}}^2$, and we might expect the thermophoretic force to scale as the screened

Coulomb cross section $\sim\lambda_D^2$. At first glance it might seem that the thermophoretic force associated with the ion and electron temperature gradients dominates that associated with neutral temperature gradient because $r_d \ll \lambda_D$, and the thermophoretic force is apparently independent of the gas density and the mass of the colliding species. However, in a weakly ionized gas ion–neutral and electron–neutral collisions are usually much more important than ion-ion or electron–electron self-collisions, and this leads to a different functional form of the thermal conductivity for these species. The thermal conductivity $k_{e,i}^{con}$ of the electrons and ions has the general functionality given by (Daugherty and Graves 1995)

$$k_{e,i}^{con} \simeq \frac{n_{e,i} k_B V_{Te,i}^2}{\nu_{e,i}} \tag{3.2.51}$$

where the subscript e (i) represents the corresponding quantity for the electron (ion) and ν_e (ν_i) is the collision frequency of the electrons (ions). As the dominant part of ν_e (ν_i) is usually due to collisions of electrons (ions) with the neutrals, from equation (1.2.14) we have $\nu_{e,i} \simeq \nu_{en,in} = n_n \sigma_{e,i}^n V_{Te,i}$. This reduces the ion or electron thermal conductivity $k_{e,i}^{con}$ to the form

$$k_{e,i}^{con} \simeq \frac{n_{e,i}}{n_n} \frac{k_B V_{Te,i}}{\sigma_{e,i}^n}. \tag{3.2.52}$$

Since in partially ionized dusty plasmas $n_{e,i}/n_n$ is seldom larger than 10^{-6} and $V_{Te,i}$ cancels out when equation (3.2.52) is substituted into the thermophoretic force, it appears that the ion and electron thermophoretic forces will not be particularly important unless the temperature gradients are very large. However, in a high-density plasma (e.g. electron cyclotron resonances (ECR), inductively coupled plasma (ICP), helicon plasma, etc) the ratio $n_{e,i}/n_n$ may be as large as 0.1, and in this case one must consider ion and electron thermophoretic forces more seriously.

3.2.5 Radiation pressure force

We know that dust particles (particularly in space) are immersed in an environment of electromagnetic waves/radiation emitted from various sources and are therefore continuously irradiated. Thus, an irradiated dust particle intercepts a fraction of the radiation energy E_R and associated momentum $P_R = E_R/c$. To estimate the force, i.e. the rate of the momentum transfer to a dust particle, we consider the electromagnetic radiation as a beam of photons, each of which has energy $E_R^{(1)} = \hbar\omega_R$ and momentum $P_R^{(1)} = E_R^{(1)}/c$, where ω_R is the radiation angular frequency. The intensity of the electromagnetic radiation is then characterized by the photon energy flux (photon energy distributed per unit area per unit time) $I_0 = N_{ph}\hbar\omega_R c$, where N_{ph} is the photon number density. Thus, the radiation pressure force $\boldsymbol{F}_\mathrm{R}$ acting on a dust particle of radius r_d is given by

$$\boldsymbol{F}_\mathrm{R} = \frac{\pi r_\mathrm{d}^2}{c} I_0 \hat{\boldsymbol{e}}_\mathrm{r} \tag{3.2.53}$$

where $\hat{\boldsymbol{e}}_\mathrm{r}$ is a unit vector along the incident wavevector $\boldsymbol{k}$. If the radiation source is so far away that it can be considered as a point source, $\boldsymbol{F}_\mathrm{R}$ is directed along the radiation vector connecting it with the dust particle.

We now discuss the validity of equation (3.2.53). It is only valid for the particles that can absorb all the radiation incident on their surfaces, and whose radii are much larger than the radiation wavelength (ray optical approximation). We also did not account for the fact that the particle can be heated by the absorbed power and can hence emit electromagnetic radiation. To take into account the effects of scattering/reflection and re-emission from the dust particle, we should replace I_0 in equation (3.2.53) by $I_0(\theta, \varphi) - I_\mathrm{sc}(\theta, \varphi) - I_\mathrm{em}(\theta, \varphi)$, where $I_\mathrm{sc}(\theta, \varphi)$ and $I_\mathrm{em}(\theta, \varphi)$ are the scattered and emitted photon energy fluxes, respectively, with θ (φ) being the polar (scattering) angle. That is, we can rewrite equation (3.2.53) in a more general form as (Bliokh *et al* 1995)

$$F_\mathrm{R}(\theta, \varphi) = \frac{A_\mathrm{s}}{c}[I_0(\theta, \varphi) - I_\mathrm{sc}(\theta, \varphi) - I_\mathrm{em}(\theta, \varphi)] \tag{3.2.54}$$

where $\boldsymbol{F}_\mathrm{R}$ is replaced by its angular density function $F_\mathrm{R}(\theta, \varphi)$ and A_s is the area which is πr_d^2 for a spherical dust grain (we have used A_s instead of πr_d^2 because particles may not always be spherical). To evaluate the total pressure force, it is necessary to estimate its radial and tangential components by integrating equation (3.2.54) over the polar (θ) and azimuthal (φ) angles.

We know that both $I_\mathrm{sc}(\theta, \varphi)$ and $I_\mathrm{em}(\theta, \varphi)$ are proportional to I_0. Thus, we can take into account all the re-emitted modes through a single factor $\gamma(\theta, \varphi)$ and can express equation (3.2.54) in a simple form as

$$F_\mathrm{R}(\theta, \varphi) = \frac{A_\mathrm{s}\gamma(\theta, \varphi)}{c} I_0. \tag{3.2.55}$$

We note that within the ray optical approximation, $\gamma = 1$ in the case of total absorption of the incident power and $\gamma = 2$ in the case of total reflection (Bliokh *et al* 1995). The product $A_\mathrm{s}\gamma(\theta, \varphi)$ is the effective cross-sectional area that may greatly exceed the geometrical area of the dust particle, especially if its size is comparable to the radiation wavelength. When the dust particle is spherically symmetric, i.e. the factor γ is independent of φ, upon integrating over θ and φ we can find that the net radiation pressure force will have only a radial component along the direction of incidence. On the other hand, for a dust particle of an irregular geometry a tangential force component will be also present. However, a tangential force can appear in the radiation field even for a spherical particle if it moves with respect to the radiation source at a velocity $\boldsymbol{u}$ that is not purely radial. This tangential component decelerates the moving particle. This effect is known as the 'Poynting–Robertson effect'.

We can explain this effect clearly by considering scattering and emission of the radiation in a frame of reference moving with the particle, i.e. moving with the dust velocity $\boldsymbol{v}_\mathrm{d}$. To make equation (3.2.53), which we have derived for a particle at rest, valid for this moving frame, we should take into account the Doppler and aberration effects. Because of the Doppler effect the frequency of the radiation incident of the particle will be $\omega_\mathrm{R}(1 - u_\mathrm{r}/c)$, where u_r is the radial component of $\boldsymbol{u}$ and the photon momentum $P_\mathrm{R}^{(1)} = \hbar\omega_\mathrm{R}(1 - u_\mathrm{r}/c)$ will be changed in magnitude. On the other hand, owing to the aberration the wave will propagate at an angle $\Delta\theta = u_\theta/c$, where u_θ is the tangential component of $\boldsymbol{u}$. As a result, the axial symmetry with respect to the radial direction will be violated and a tangential force component will develop. These two considerations allow us to rewrite equation (3.2.54) as (Bliokh *et al* 1995)

$$\boldsymbol{F}_\mathrm{R} = \frac{A_\mathrm{s}\gamma}{c} I_0 \left[\left(1 - \frac{u_\mathrm{r}}{c}\right)\hat{\boldsymbol{e}}_\mathrm{r} - \frac{u_\theta}{c}\hat{\boldsymbol{e}}_\theta\right] \tag{3.2.56}$$

where $\hat{\boldsymbol{e}}_\theta$ is the tangential unit vector, $\hat{\boldsymbol{e}}_\theta \perp \hat{\boldsymbol{e}}_\mathrm{r}$. Due to the tangential component of the radiation pressure force, a particle orbiting around the attraction centre, which at the same time is the radiation source (e.g. the Sun), is continuously slowed down. Because of this decelerating force, known as the 'radiation drag force', the particle loses a part of its energy and its orbital radius decreases. Consequently, the particle moves closer to the radiation source.

Now an important question may arise: will the radiation pressure force be significantly changed if an electric charge q_d possibly carried by the dust grain is taken into consideration? Let us present an answer to this question. The force acting on a charged dust particle in an electric field is $q_\mathrm{d}\boldsymbol{E}_0 \exp(-\mathrm{i}\omega_\mathrm{R}t + \mathrm{i}\boldsymbol{k}\cdot\boldsymbol{r})$, where $\boldsymbol{E}_0$ is the amplitude of the electric field vector. It produces periodic oscillations of the dust grain which thus becomes a source of electromagnetic radiation of the same frequency ω_R. The power radiated by the vibrating particle comes from the primary electromagnetic wave. The dust particle thus receives some power along with a fraction of the wave momentum by which equation (3.2.53) is affected. This effect can be included by using an effective cross-sectional area σ_ef instead of the geometric cross-sectional area πr_d^2. The effective cross-sectional area σ_ef corresponds to that fraction of the wave power which is transformed into the radiation scattered by the charge q_d and can be estimated by using the Thomson scattering formula as

$$\sigma_\mathrm{ef} = \frac{8\pi}{3}\left(\frac{q_\mathrm{d}^2}{m_\mathrm{d}c^2}\right)^2. \tag{3.2.57}$$

It is seen that the effective (charge dependent) cross section σ_ef involves the grain radius only implicitly through $q_\mathrm{d} \simeq r_\mathrm{d}\phi_\mathrm{d}$ and $m_\mathrm{d} = (4\pi/3)r_\mathrm{d}^3\rho_\mathrm{d}$, where ρ_d is the mass density of the dust material, and can be written as $\sigma_\mathrm{ef} \simeq (9/16\pi^2)\phi_\mathrm{d}^4/r_\mathrm{d}^2\rho_\mathrm{d}^2c^4$. This implies that the effective cross section σ_ef is inversely proportional to r_d^2, whereas the geometric cross section is directly proportional to

$r_{\rm d}^2$. The ratio of the effective cross section $\sigma_{\rm ef}$ to the geometric cross section ($\pi r_{\rm d}^2$) can be approximated as

$$\frac{\sigma_{\rm ef}}{\pi r_{\rm d}^2} \simeq 4.4 \times 10^{-39} \frac{\phi_{\rm d}^4[{\rm V}]}{r_{\rm d}^4[\mu{\rm m}]\rho_{\rm d}^2[{\rm g\ cm}^{-3}]}. \tag{3.2.58}$$

It is obvious from equation (3.2.58) that $\sigma_{\rm ef} \ll \pi r_{\rm d}^2$ for any reasonable values of $r_{\rm d}$, $\rho_{\rm d}$ and $\phi_{\rm d}$. Thus, we can finally conclude that the effect of the dust grain charge on the radiation pressure force acting on an isolated dust grain is negligible.

3.3 Particle Dynamics in Space

The dynamics of a charged dust particle in space plasmas, particularly in planetary magnetospheres, was first considered by Mendis and Axford (1974) more than 25 years ago. A special interest in investigating the dynamics of a charged dust particle in space has been significantly accelerated by mysterious dark spokes in Saturn's B ring and spatial distributions of dust grains near Jupiter and Saturn observed by Voyager 1 and 2 (Smith *et al* 1981, 1982). The dynamics of such charged dust particles is governed by the combined effects of different forces that we discussed in the previous section. A number of review articles (e.g. Goertz 1989, Mendis and Rosenberg 1994) have provided significant information on particle trajectories in planetary magnetospheres. However, most of the information on particle trajectories are based on negatively charged particles in prograde (co-rotating) equatorial orbits or insignificant perturbations transverse to the equatorial plane. Therefore, in this section, based on a recent work of Howard *et al* (1999, 2000) we provide a more general picture of the dust particle dynamics in planetary magnetospheres, which is valid for both negatively and positively charged dust grains in both prograde and retrograde orbits about an axisymmetric planet like Saturn or Jupiter.

We consider a dust grain of mass $m_{\rm d}$ and charge $q_{\rm d}$ orbiting about an axisymmetric planet of mass $M_{\rm p}$, radius $R_{\rm p}$ and angular frequency $\Omega_{\rm pl}$. To study the dynamics of such a particle, we start with the inertial frame Hamiltonian (Howard *et al* 1999) in cylindrical coordinates (ρ, φ, z)

$$H = \frac{1}{2m_{\rm d}}(p_\rho^2 + p_z^2) + \frac{1}{2m_{\rm d}\rho^2}\left(p_\varphi - \frac{q_{\rm d}}{c}\Psi\right)^2 + U + \frac{q_{\rm d}\Omega_{\rm pl}}{c}\Psi \tag{3.3.1}$$

where $p_\varphi = m_{\rm d}\rho^2\omega_{\rm d} + q_{\rm d}\Psi/c$ is the conserved angular momentum (with $\omega_{\rm d} = \partial\varphi/\partial t$ being the orbital angular frequency of the dust particle), $\Psi(\rho, z) = \rho A_\varphi$ is the magnetic stream function which is $M\rho^2/r^3$ (with the dipole strength $M = B_0 R_{\rm p}^3$) for a centered dipole, and $U(\rho, z)$ is the gravitational potential which is $-\mu m_{\rm d}/r$ (with $\mu = GM_{\rm p}$ and $r = \sqrt{\rho^2 + z^2}$) for the Keplerian gravity. Thus, for a centered dipole and Keplerian gravity, we can express H as

$$H = \frac{1}{2m_{\rm d}}(p_\rho^2 + p_z^2) + U_{\rm ef}(\rho, z) \tag{3.3.2}$$

with the effective potential

$$U_{\rm ef}(\rho, z) = \frac{1}{2m_{\rm d}\rho^2}\left(p_\varphi - \frac{\gamma_{\rm df}\rho^2}{r^3}\right)^2 - \frac{\mu m_{\rm d}}{r} + \frac{\gamma_{\rm df}\Omega_{\rm pl}\rho^2}{r^3} \tag{3.3.3}$$

where p_φ can be rewritten as $p_\varphi = m_{\rm d}\rho^2\omega_{\rm d} + \rho^2\gamma_{\rm df}/r^3$ and $\gamma_{\rm df} = q_{\rm d}M/c$ measures the relative strength of the dipole field. Measuring ρ and r in units of the planetary radius $R_{\rm p}$, we can express the effective potential in the form

$$U_{\rm ef}(\rho, z) = m_{\rm d}R_{\rm p}^2\left[\frac{1}{2\rho^2}\left(p_\varphi - \frac{\rho^2\omega_{\rm cd}}{r^3}\right)^2 - \frac{\Omega_{\rm k}^2}{r} + \frac{\rho^2\Omega_{\rm pl}\omega_{\rm cd}}{r^3}\right] \tag{3.3.4}$$

where $p_\varphi = \rho^2\omega_{\rm d} + \rho^2\omega_{\rm cd}/r^3$ is the scaled angular momentum, $\omega_{\rm cd} = q_{\rm d}B_0/m_{\rm d}c$ and $\Omega_{\rm k} = (\mu/R_{\rm p}^3)^{1/2}$ are the dust gyro and Kepler frequencies, both evaluated at a point on the planetary equator.

We analyse equilibrium states which are given by

$$\left[\frac{\partial U_{\rm ef}}{\partial\rho}\right] = \left[\frac{\partial U_{\rm ef}}{\partial z}\right] = 0. \tag{3.3.5}$$

The equilibrium states described by equations (3.3.4) and (3.3.5) are valid for both equatorial ($z = 0$, i.e. $r = \rho$) and non-equatorial ($z \neq 0$, i.e. $r = \sqrt{\rho^2 + z^2}$) planes. However, for a better understanding, we consider first a simple situation, i.e. equatorial equilibria ($z = 0$) and then a more general situation, i.e. non-equatorial equilibria ($z \neq 0$).

3.3.1 Equatorial equilibria ($z = 0$)

For equatorial equilibria ($z = 0$, i.e. $r = \rho$) the radial part of equation (3.3.5) yields a quadratic equation in $\omega_{\rm d}$ (Howard *et al* 1999)

$$\rho^3\omega_{\rm d}^2 - \omega_{\rm cd}\omega_{\rm d} - (\Omega_{\rm k}^2 - \omega_{\rm cd}\Omega_{\rm pl}) = 0. \tag{3.3.6}$$

The solutions of the quadratic equation (3.3.6) are

$$2\rho^3\omega_{\rm d1,2} = \omega_{\rm cd} \pm \sqrt{\omega_{\rm cd}^2 + 4\rho^3(\Omega_{\rm k}^2 - \omega_{\rm cd}\Omega_{\rm pl})}. \tag{3.3.7}$$

Equation (3.3.7) indicates that the consideration of a positively charged dust particle, i.e. $\omega_{\rm cd} > 0$ corresponds to three regimes, namely (i) Keplerian regime: $\Omega_{\rm k}^2 > \omega_{\rm cd}\Omega_{\rm pl}$ which corresponds to $\omega_{\rm d1} > 0$ and $\omega_{\rm d2} < 0$, (ii) transition regime: $\Omega_{\rm k}^2 = \omega_{\rm cd}\Omega_{\rm pl}$ which corresponds to $\omega_{\rm d1} = \omega_{\rm cd}/\rho^3$ and $\omega_{\rm d2} = 0$, and (iii) magnetic regime: $\Omega_{\rm k}^2 < \omega_{\rm cd}\Omega_{\rm pl}$ which corresponds to $\omega_{d1,d2} > 0$. The branch $\omega_{\rm d2}$ may be referred to as semi-retrograde, since it is retrograde only for large $q_{\rm d}/m_{\rm d}$. It is seen that in a magnetic regime there is cutoff when

$\omega_{\rm cd}^2 = 4\rho^3(\omega_{\rm cd}\Omega_{\rm pl} - \Omega_{\rm k}^2)$ which is itself a quadratic in $\omega_{\rm cd}$. It can be easily shown that this inner quadratic has real roots only for $\rho > (\Omega_{\rm k}/\Omega_{\rm pl})^{2/3}$. Equation (3.3.7) also implies that for a negatively charged dust particle ($\omega_{\rm cd} < 0$), we can consider only one situation, namely $\omega_{\rm d1} > 0$, $\omega_{\rm d2} < 0$. Obviously there is no cutoff: a pair of prograde–retrograde orbits exist everywhere on the equatorial plane. Figure 3.1 shows the orbital frequencies (normalized by the Kepler frequency) $\omega_{\rm d1,2}/\Omega_{\rm k}$ as a function of $\omega_{\rm cd}/\Omega_{\rm k}$ for (*a*) $\rho = 1.5$ and (*b*) $\rho = 2.0$ for both positively and negatively changed dust particles. The asymptotes are shown as dashed lines. We note that as $\rho = 1.882 = \rho_{\rm s}$ corresponds to the synchronous radius in the case of Saturn, figure 3.1(*a*) represents orbital frequencies inside the synchronous radius ($\rho < \rho_{\rm s}$) and figure 3.1(*b*) represents orbital frequencies outside the synchronous radius ($\rho > \rho_{\rm s}$). It may also be noted here that when $\omega_{\rm cd} \to 0$, $\omega_{\rm d1,2} \to \pm\Omega_{\rm k}/\rho^{3/2}$ (the local Kepler frequency) and when $\rho < \rho_{\rm s}$ and $q_{\rm d}/m_{\rm d}$ lies within the limit of large positive values, $\omega_{\rm d1} \to \omega_{\rm cd}/\rho^3$ (the local gyrofrequency), $\omega_{\rm d2} \to \Omega_{\rm pl}$. On the other hand, when $\rho < \rho_{\rm s}$ and $q_{\rm d}/m_{\rm d}$ lies within the limit of large negative values, $\omega_{\rm d1} \to \Omega_{\rm pl}$, $\omega_{\rm d2} \to -\omega_{\rm cd}/\rho^3$.

3.3.2 Non-equatorial equilibria ($z \neq 0$)

The simultaneous solutions of equation (3.3.5) for $z \neq 0$ are given by (Howard *et al* 2000)

$$r^5\omega_{\rm d}^2 + \omega_{\rm cd}(\omega_{\rm d} - \Omega_{\rm pl})(2r^2 - 3\rho^2) = \Omega_{\rm k}^2 r^2 \tag{3.3.8}$$

and

$$3\omega_{\rm cd}(\omega_{\rm d} - \Omega_{\rm pl})\rho^2 + \Omega_{\rm k}^2 r^2 = 0. \tag{3.3.9}$$

It follows immediately from equation (3.3.9) that the orbital frequency $\omega_{\rm d} \neq \Omega_{\rm pl}$, i.e. non-equatorial synchronous orbits are not possible. We also see from equation (3.3.9) that for a positively charged dust grain $\omega_{\rm d} < \Omega_{\rm pl}$, whereas for a negatively charged grain $\omega_{\rm d} > \Omega_{\rm pl}$. The latter also holds for equatorial orbits.

We know that for a spherical dust grain of a uniform material density $\rho_{\rm d} \simeq 1$ g cm^{-3}, radius $r_{\rm d}$ (in microns) and a surface potential $\phi_{\rm d}$ (in volts) $q_{\rm d}/m_{\rm d} \simeq (10^6/4\pi)\phi_{\rm d}/r_{\rm d}^2$ esu g^{-1}. Typical values of $\phi_{\rm d}$ for Jupiter and Saturn lie in the range -20 V $< \phi_{\rm d} <$ 10 V (Howard *et al* 1999, 2000). For a given planet and an equilibrium radial position r_0, the stability of the dust particle orbit depends on $q_{\rm d}/m_{\rm d}$ alone, conveniently measured by the parameter $\hat{\Phi} = \phi_{\rm d}/r_{\rm d}^2 = (4\pi c/10^6 B_0)\omega_{\rm cd}$, which we shall express as a pure number. We now analyse whether a stable equilibrium orbit exists for some $\hat{\Phi}$, i.e. for some $\omega_{\rm cd}$ for a specific location (ρ_0, z_0). We first eliminate $\omega_{\rm cd}$ between equations (3.3.8) and (3.3.9) and obtain

$$\omega_{\rm d}^2 = \frac{2}{3}\frac{\Omega_{\rm k}^2}{\rho_0^2 r_0}. \tag{3.3.10}$$

It is seen that both signs of $\omega_{\rm d}$ are possible. The requisite value of $\hat{\Phi}(\omega_{\rm cd})$ (if it

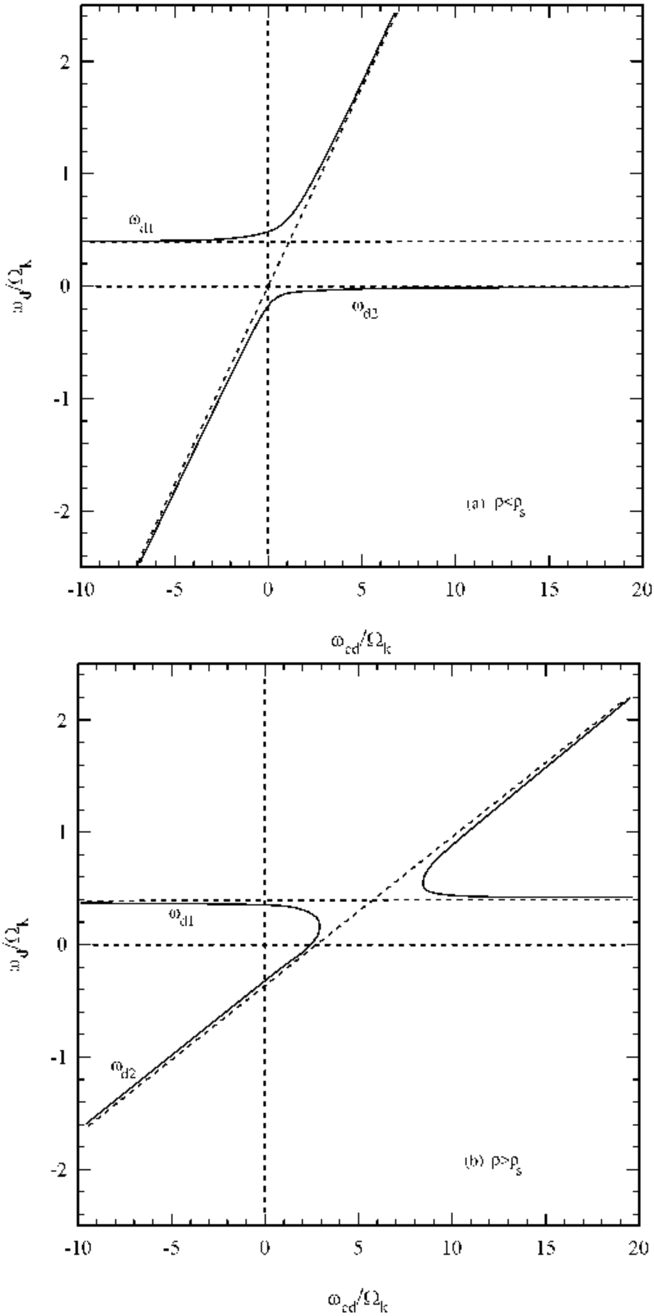

Figure 3.1. The orbital frequencies (normalized by the Kepler frequency) $\omega_{d1,2}/\Omega_k$ as a function of ω_{cd}/Ω_k for (*a*) $\rho = 1.5$ and (*b*) $\rho = 2.0$ (after Howard *et al* 1999).

exists) is then determined from

$$\omega_{\mathrm{cd}} = \frac{\omega_{\mathrm{d}}^2 r_0^3}{2(\Omega_{\mathrm{pl}} - \omega_{\mathrm{d}})}. \tag{3.3.11}$$

It is obvious that when dust particles are positively charged, equation (3.3.11) is automatically satisfied for negative (retrograde) ω_{d} but demands $\omega_{\mathrm{d}} < \Omega_{\mathrm{pl}}$ for positive (prograde) ω_{d}. On the other hand, when dust particles are negatively charged, this will be only satisfied if $\omega_{\mathrm{d}} > \Omega_{\mathrm{pl}} > 0$, which excludes retrograde orbits. There are no retrograde non-equatorial equilibria for negative charge, but either sense is possible for positive charge (Howard *et al* 2000). We now take the point of view that r_0 and ω_{cd} are specified and seek conditions for an equilibrium somewhere on the sphere $r = r_0$. We can express equation (3.3.11) as a quadratic in ω_{d} and find its solution as

$$r_0^3 \omega_{\mathrm{d}} = -\omega_{\mathrm{cd}} \pm \sqrt{\omega_{\mathrm{cd}}^2 + 2r_0^3 \Omega_{\mathrm{pl}} \omega_{\mathrm{cd}}} \tag{3.3.12}$$

which is subjected to the constraint $\rho < r$. Thus, equation (3.3.10) implies $\omega_{\mathrm{d}}^2 \geq \omega_\star^2 = 2\Omega_{\mathrm{k}}^2/3r_0^2$, with corresponding ω_{cd} given by equation (3.3.11), which yields ($\omega_\star > 0$)

$$\frac{\Omega_{\mathrm{k}}^2}{3(\Omega_{\mathrm{pl}} + \omega_\star)} \leq \omega_{\mathrm{cd}} \leq \frac{\Omega_{\mathrm{k}}^2}{3(\Omega_{\mathrm{pl}} - \omega_\star)}. \tag{3.3.13}$$

The numerical solutions of equation (3.3.12) for $r_0 = 2$ are shown in figure 3.2. This shows that for $\omega_{\mathrm{cd}} > 0$ and $|\omega_{\mathrm{d}}| > \omega_\star$ there is a prograde/retrograde pair, but for $-2r_0^3\Omega < \omega_{\mathrm{cd}} < 0$ there are no equilibria. It also shows that if $\omega_{\mathrm{cd}} < -2r_0^3\Omega_{\mathrm{pl}}$, there are two possible prograde equilibria. Since $\omega_\star < \Omega_{\mathrm{pl}}$ there are no constraints in $q_{\mathrm{d}}/m_{\mathrm{d}}$. However, for large $q_{\mathrm{d}}/m_{\mathrm{d}}$ there are two asymptotic limits: $\omega_{\mathrm{d}} \simeq \Omega_{\mathrm{pl}}$ and $\omega_{\mathrm{d}} \simeq -\Omega_{\mathrm{pl}} - 2\omega_{\mathrm{cd}}/r_0^3$.

3.4 Particle Dynamics in Laboratory

The dynamics of a dust particle in a laboratory plasma, particularly in the plasma sheath boundary of a gas discharge under a time varying background gas pressure, is an extremely complex problem due to both the nature of the plasma sheath and the charging currents that reach the dust grain surface. However, a number of approximations and simplifications may make possible a treatment of such a complicated problem. Recently, Winske and Jones (1994), Elskens *et al* (1997) and Resendes and Shukla (2001) have investigated the dynamics of a dust particle in the plasma sheath boundary by using a fluid (so-called continuum) model which primarily involves calculating the electron and ion densities, the electric field and the dust grain charge under different approximations and simplifications. To provide some basic understanding of the dust particle dynamics in the plasma sheath, here we will briefly summarize the work of Resendes and Shukla (2001).

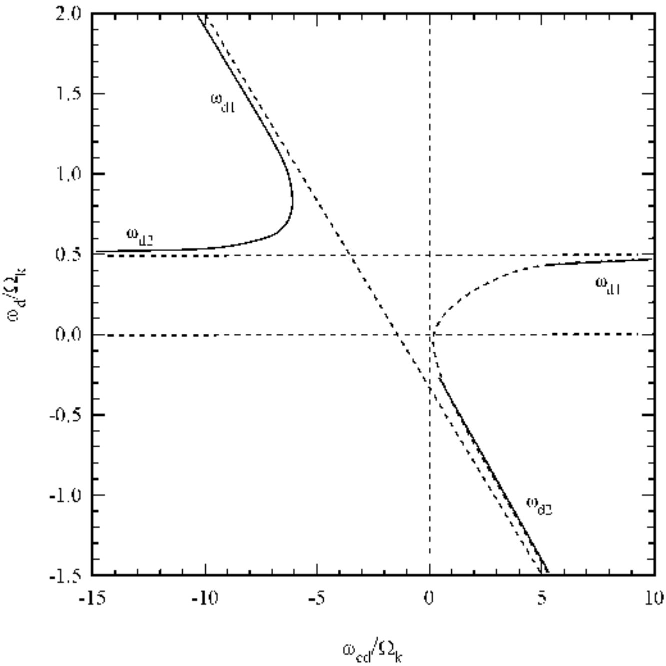

Figure 3.2. The orbital frequencies (normalized by the Kepler frequency) $\omega_{d1,2}/\Omega_k$ as a function of ω_{cd}/Ω_k for $r = 2$. Equilibria do not exist on the dashed part of the right-hand curve ($q_d < 0$) (after Howard *et al* 2000).

We consider a simple one-dimensional problem. The dynamics of a dust particle under the force F_d is governed by

$$\frac{dx}{dt} = v_d \tag{3.4.1}$$

and

$$\frac{dv_d}{dt} = \frac{F_d}{m_d}. \tag{3.4.2}$$

To estimate F_d we consider the most significant three forces, namely the electric force F_E, the Coulomb ion drag force F_{di}^{coul} and the neutral drag force F_{dn}, but neglect all other forces that are insignificant in the plasma sheath. Thus, the force F_d acting on the dust particle is given by

$$F_d = F_E + F_{di}^{coul} + F_{dn} \tag{3.4.3}$$

where F_E, F_{di}^{coul} and F_{dn} are given by equations (3.2.2), (3.2.40) and (3.2.43), respectively. For $b_0 \gg b_c$, $v_d \gg v_n$ and the one-dimensional case they can be expressed as

$$F_{\mathrm{E}} = q_{\mathrm{d}} E \tag{3.4.4}$$

$$F_{\mathrm{di}}^{\mathrm{coul}} = 2\pi n_{\mathrm{i}} m_{\mathrm{i}} V_{\mathrm{it}} v_{\mathrm{i}} b_0^2 \ln\left(1 + \frac{\lambda_{\mathrm{De}}^2}{b_0^2}\right) \tag{3.4.5}$$

and

$$F_{\mathrm{dn}} = -\tfrac{8}{3}\sqrt{2\pi} r_{\mathrm{d}}^2 m_{\mathrm{n}} n_{\mathrm{n}} V_{\mathrm{Tn}} v_{\mathrm{d}} \tag{3.4.6}$$

where b_0 is given by equation (3.2.37) and can be expressed in terms of the dust particle charge as $b_0 = eq_{\mathrm{d}}/mv_{\mathrm{i}}^2$. The charge q_{d} of a dust particle in a laboratory plasma environment (particularly in the plasma sheath boundary) is not constant but varies with space. To estimate q_{d} we consider only the orbit-limited charging currents that are due to the collection of primary plasma particles (electrons and ions). As the ions are much heavier than the electrons, initially the ion current is much smaller than the electron current, and the grain becomes negatively charged (i.e. $q_{\mathrm{d}} < 0$). This increases the ion current I_{i} and decreases the electron current I_{e} until $I_{\mathrm{e}} + I_{\mathrm{i}} = 0$, where I_{e} and I_{i} are given by equations (2.6.2) and (2.6.11). Thus, the dust grain charge q_{d} (< 0) can be determined from $I_{\mathrm{e}} + I_{\mathrm{i}} = 0$, yielding

$$\frac{n_{\mathrm{e}}}{n_{\mathrm{i}}}\left(\frac{T_{\mathrm{e}} m_{\mathrm{i}}}{T_{\mathrm{i}} m_{\mathrm{e}}}\right)^{1/2} \exp\left(\frac{eq_{\mathrm{d}}}{r_{\mathrm{d}} k_B T_{\mathrm{e}}}\right) = \left(1 + \frac{\pi}{8}\frac{v_{\mathrm{i}}^2}{V_{Ti}^2}\right)^{1/2}\left(1 - \frac{2eq_{\mathrm{d}}}{r_{\mathrm{d}} m_{\mathrm{i}} V_{\mathrm{it}}^2}\right) \tag{3.4.7}$$

where we have taken the ion speed as its total speed V_{it} (a combination of directed and thermal speeds). It is clear from equations (3.4.1)–(3.4.7) that in order to solve equations (3.4.1) and (3.4.2) we still need to know four other variables, namely n_{e}, n_{i}, v_{i} and E.

To estimate these variables we consider a simple one-dimensional, time-independent glow discharge model (Winske and Jones 1994, Resendes and Shukla 2001) which employs the usual diffusion approximation to solve numerically the electron and ion continuity equations, the electron momentum equation and Poisson's equation, which are, respectively,

$$\frac{\mathrm{d}J_{\mathrm{e}}}{\mathrm{d}x} = n_{\mathrm{e}}\nu_{\mathrm{i}} \tag{3.4.8}$$

$$\frac{\mathrm{d}J_{\mathrm{i}}}{\mathrm{d}x} = n_{\mathrm{e}}\nu_{\mathrm{i}} \tag{3.4.9}$$

$$\frac{\mathrm{d}n_{\mathrm{e}}}{\mathrm{d}x} = -\frac{1}{D_{\mathrm{e}}}(J_{\mathrm{e}} + n_{\mathrm{e}}\mu_{\mathrm{e}} E) \tag{3.4.10}$$

and

$$\frac{\mathrm{d}E}{\mathrm{d}x} = 4\pi e(n_{\mathrm{i}} - n_{\mathrm{e}}) \tag{3.4.11}$$

where $J_{\mathrm{e}} = n_{\mathrm{e}} v_{\mathrm{e}}$ and $J_{\mathrm{i}} \simeq n_{\mathrm{i}}\mu_{\mathrm{i}} E$ are electron and ion fluxes, respectively, $\nu_{\mathrm{i}} = n_{\mathrm{n}} K_{\mathrm{i}} \exp(-E_{\mathrm{i}}/k_B T_{\mathrm{e}})$, μ_{e} ($= 6\times 10^7$ cm^2/statV s) and μ_{i} ($= 6\times 10^5$ cm^2/statV s)

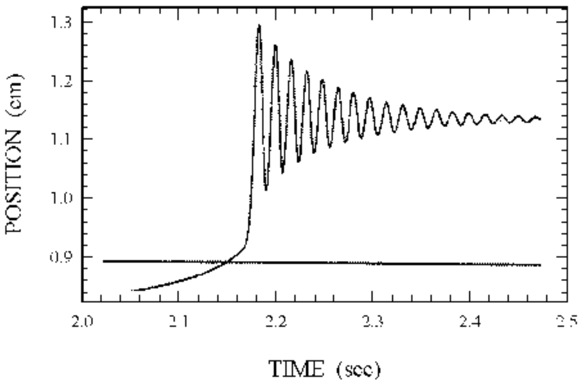

Figure 3.3. The position x of a dust particle as a function of time t: large-amplitude self-excited oscillations resulting from a neutral gas pressure between 100 and 10 mTorr (after Resendes and Shukla 2001).

are the electron and ion mobilities, respectively, D_e ($= 10^6$ cm^2/s^{-1}) is the electron diffusion coefficient (ion diffusion has been neglected, i.e. $D_i = 0$), E_i ($=$ 24 eV) is the activation energy and K_i ($= 9 \times 10^{-6}$ cm^3 s^{-1}) is the frequency factor. The electron, ion and neutral thermal energies are, respectively $k_B T_e = 2$ eV, $k_B T_i = 0.05$ eV and $k_B T_n = 0.025$. The parametric values that we have chosen here are for argon discharges (Winske and Jones 1994).

Now using appropriate boundary conditions and numerical values of different parameters depending on the plasma system considered, one can numerically solve equations (3.4.8)–(3.4.11) in order to obtain n_i, n_e, v_i and E and equations (3.4.1) and (3.4.2) (with equations (3.4.3)–(3.4.7)) in order to study the dynamics of a dust particle in the plasma sheath. Resendes and Shukla (2001) have used the boundary conditions, namely $J_e = -1.3 \times 10^{15}$ statA/(cm^2 statC), $J_i = -1.131 \times 10^{16}$ statA/(cm^2 statC), $E = 0.001$ statV cm^{-1} and $n_e = 10^{10}$ cm^{-3} at $x = 0.5$, and have solved equations (3.4.8)–(3.4.11) by using the fourth order Runge–Kutta method in order to obtain n_e, n_i, v_i and E for different values of the neutral gas pressure in between 10 mTorr ($n_n = 3.33 \times 10^{14}$ cm^{-3}) and 1000 mTorr ($n_n = 3.33 \times 10^{16}$ cm^{-3}). Then they have solved equation (3.4.7) in order to obtain the corresponding dust grain charge q_d for $r_d = 0.1$ μm. Using these numerical values of n_i, v_i and q_d they have finally solved equations (3.4.1) and (3.4.2) and obtained the position x of the dust particle as a function of time t as shown in figure 3.3. It is evident that large-amplitude oscillations are excited by the ion flow force in the sheath. Furthermore, Elskens *et al* (1997) have studied the nonlinear dynamics of a charged dust grain in an unbounded plasma subject to an external field and electron and ion charging currents. It has been found that dissipation of the charging process forbids periodic behaviour and ensures the existence of attractors.

Chapter 4

Linear Waves

4.1 Introduction

The charged particles in a plasma move randomly, interact with each other through their own electromagnetic forces, and also respond to perturbations that are applied externally. Therefore, a great variety of collective wave phenomena arises due to the coherent motions of an ensemble of plasma particles. It is well known (Ichimaru 1973, Chen 1974, Alexandrov *et al* 1984) that an electron–ion plasma supports both longitudinal and transverse waves. Examples of longitudinal waves in an unmagnetized plasma are Langmuir and ion-acoustic waves which are accompanied with density and potential fluctuations. On the other hand, transverse waves in an unmagnetized plasma are purely electromagnetic and they do not accompany density fluctuations. The presence of an external magnetic field in a plasma provides the possibility of a great variety of longitudinal and transverse waves.

When neutral dust grains are added in an electron–ion plasma, they are charged due to a variety of processes, as described in chapter 2. The presence of charged dust grains can modify or even dominate the wave propagation (Rao *et al* 1990, Shukla and Silin 1992, Verheest 2000, Shukla 2001). The modification of the wave phenomena occurs owing to the inhomogeneity associated with the random distribution of the charged particulates and the departure from the conventional quasi-neutrality condition in an electron–ion plasma due to the presence of charged dust grains, as well as due to the consideration of the dust particle dynamics. The quasi-neutrality condition at the equilibrium in a dusty plasma with singly charged ions is (cf equation (1.1.1))

$$en_{i0} - en_{e0} + q_{d0}n_{d0} = 0. \tag{4.1.1}$$

Using

$$q_{d0}n_{d0} = r_d\phi_d n_{d0} \equiv 4\pi n_{d0} r_d \lambda_{De}^2 n_{e0} e \frac{e\phi_d}{k_B T_e} \tag{4.1.2}$$

we obtain from equation (4.1.1)

$$\frac{n_{i0}}{n_{e0}} \equiv \delta = 1 - P_{de}\frac{e\phi_d}{k_B T_e} \tag{4.1.3}$$

where $P_{de} = 4\pi n_{d0} r_d \lambda_{De}^2$ is a dust parameter. Equation (4.1.3) shows that δ is larger (smaller) than one for negatively (positively) charged dust grains for which $\phi_d < 0$ ($\phi_d > 0$). In most of the laboratory dusty plasmas, we have $P_{de}e|\phi_d|/k_B T_e \leq 1$. However, when most of the electrons from the background plasma stick onto the dust grain surface, we have from equation (4.1.1)

$$n_{i0} \approx P_{di} n_{i0} \frac{e|\phi_d|}{k_B T_i} \tag{4.1.4}$$

for $n_{e0} \ll n_{i0}$, where $P_{di} = 4\pi n_{d0} r_d \lambda_{Di}^2$. On the other hand, when the dust grains are positively charged and most of the ions from the background plasma stick onto the dust grain surface, we have from equation (4.1.3)

$$n_{e0} \approx P_{de} n_{e0} \frac{e|\phi_d|}{k_B T_e} \tag{4.1.5}$$

for $n_{i0} \ll n_{e0}$. Equations (4.1.4) and (4.1.5) exhibit new types of quasi-neutrality conditions in negative dust–ion and positive dust–electron plasmas, respectively.

In this chapter, we discuss the properties of low-frequency longitudinal and transverse waves in dusty plasmas which are either unmagnetized or magnetized. The *weakly coupled dusty plasma model* used here is valid if the grain radius r_d as well as the average intergrain spacing a are much smaller than the dusty plasma Debye radius λ_D and the thermal ion gyroradius ρ_{Ti} (if the ambient magnetic field is present). We also assume that there is a sufficient number of dust grains within the dusty plasma Debye sphere so that grains can participate in collective interactions.

4.2 Acoustic Modes

There are two types of acoustic modes in uniform, unmagnetized, collisionless dusty plasmas with a weak Coulomb coupling between the charged dust grains. These are the dust acoustic (DA) and dust ion-acoustic (DIA) waves. In the following, we describe the underlying physics as well as the mathematical details of these wave modes.

4.2.1 Dust acoustic waves

The DA waves have been theoretically predicted by Rao *et al* (1990) in a multi-component collisionless dusty plasma whose constituents are the electrons, ions and negatively charged dust grains. The phase velocity of the DA waves is much smaller than the electron and ion thermal speeds. Accordingly, the inertialess electrons and ions establish equilibrium in the DA wave potential ϕ. Here the pressure gradient is balanced by the electric force, leading to Boltzmann electron and ion number density perturbations n_{j1}, which are, respectively,

$$n_{\mathrm{e}1} \approx n_{\mathrm{e}0} \frac{e\phi}{k_{\mathrm{B}} T_{\mathrm{e}}} \tag{4.2.1}$$

and

$$n_{\mathrm{i}1} \approx -n_{\mathrm{i}0} \frac{e\phi}{k_{\mathrm{B}} T_{\mathrm{i}}}. \tag{4.2.2}$$

The dust inertia is very important for the DA waves. Accordingly, the dust number density perturbation is obtained from the dust continuity equation

$$\frac{\partial n_{\mathrm{d}1}}{\partial t} + n_{\mathrm{d}0} \nabla \cdot \boldsymbol{v}_{\mathrm{d}} = 0 \tag{4.2.3}$$

and the dust momentum equation

$$\frac{\partial \boldsymbol{v}_{\mathrm{d}}}{\partial t} = -\frac{q_{\mathrm{d}0}}{m_{\mathrm{d}}} \nabla \phi - \frac{3 k_{\mathrm{B}} T_{\mathrm{d}}}{m_{\mathrm{d}} n_{\mathrm{d}0}} \nabla n_{\mathrm{d}1} \tag{4.2.4}$$

where $n_{\mathrm{d}1}$ and $\boldsymbol{v}_{\mathrm{d}}$ are the dust number density perturbation and the dust fluid velocity, respectively. Equations (4.2.1)–(4.2.4) are closed by Poisson's equation

$$\nabla^2 \phi = 4\pi (e n_{\mathrm{e}1} - q_{\mathrm{d}0} n_{\mathrm{d}1} - e n_{\mathrm{i}1}) \tag{4.2.5}$$

where, for convenience, the dust charge $q_{\mathrm{d}0}$ is assumed to be constant. The effect of dust charge fluctuations will be considered in section 4.3.

Let us now derive the dispersion relation for the DA waves. For this purpose we combine equations (4.2.3) and (4.2.4) and obtain

$$\left(\frac{\partial^2}{\partial t^2} - 3 V_{\mathrm{Td}}^2 \nabla^2 \right) n_{\mathrm{d}1} = \frac{n_{\mathrm{d}0} q_{\mathrm{d}0}}{m_{\mathrm{d}}} \nabla^2 \phi. \tag{4.2.6}$$

Substituting equations (4.2.1) and (4.2.2) into equation (4.2.5) we have

$$\nabla^2 \phi = k_{\mathrm{D}}^2 \phi - 4\pi q_{\mathrm{d}0} n_{\mathrm{d}1}. \tag{4.2.7}$$

Assuming $n_{\mathrm{d}1} = \hat{n}_{\mathrm{d}1} \exp(-\mathrm{i}\omega t + \mathrm{i}\boldsymbol{k} \cdot \boldsymbol{r})$ and $\phi = \hat{\phi} \exp(-\mathrm{i}\omega t + \mathrm{i}\boldsymbol{k} \cdot \boldsymbol{r})$, where ω and $\boldsymbol{k}$ are the frequency and the wavevector, respectively, we Fourier transform equations (4.2.6) and (4.2.7) (i.e. set $\partial/\partial t = -\mathrm{i}\omega$ and $\nabla = \mathrm{i}\boldsymbol{k}$) and combine the resultant equations to obtain the dispersion relation for the DA waves

$$1 + \frac{k_{\mathrm{D}}^2}{k^2} - \frac{\omega_{\mathrm{pd}}^2}{\omega^2 - 3k^2 V_{\mathrm{Td}}^2} = 0 \tag{4.2.8}$$

which gives

$$\omega^2 = 3k^2 V_{\mathrm{Td}}^2 + \frac{k^2 C_{\mathrm{D}}^2}{1 + k^2 \lambda_{\mathrm{D}}^2} \tag{4.2.9}$$

where $C_{\mathrm{D}} = \omega_{\mathrm{pd}} \lambda_{\mathrm{D}}$ is the DA speed. Since $\omega \gg kV_{\mathrm{Td}}$, we deduce from equation (4.2.9) the DA wave frequency (Rao *et al* 1990)

$$\omega = \frac{kC_{\mathrm{D}}}{(1 + k^2 \lambda_{\mathrm{D}}^2)^{1/2}} \tag{4.2.10}$$

which in the long-wavelength limit (namely $k^2 \lambda_{\mathrm{D}}^2 \ll 1$) reduces to

$$\omega = kZ_{\mathrm{d0}} \left(\frac{n_{\mathrm{d0}}}{n_{\mathrm{i0}}} \right)^{1/2} \left(\frac{k_{\mathrm{B}} T_{\mathrm{i}}}{m_{\mathrm{d}}} \right)^{1/2} \left[1 + \frac{T_{\mathrm{i}}}{T_{\mathrm{e}}} \left(1 - \frac{Z_{\mathrm{d0}} n_{\mathrm{d0}}}{n_{\mathrm{i0}}} \right) \right]^{-1/2} \tag{4.2.11}$$

when the dust grains are charged negatively. Equation (4.2.11) reveals that the restoring force in the DA waves comes from the pressures of the inertialess electrons and ions, while the dust mass provides the inertia to support the waves. The frequency of the DA waves is much smaller than the dust plasma frequency. Using equation (4.2.11), the DA wave phase velocity ($V_{\mathrm{p}} = \omega/k$) can be estimated if one knows the plasma and dust parameters. The DA waves have been spectacularly observed in several laboratory experiments (e.g. Barkan *et al* 1995a, Pieper and Goree 1996). Since the observed DA wave frequencies are of the order of 10–20 Hz, video images of the DA wavefronts are possible and they can be seen with the naked eye.

4.2.2 Dust ion-acoustic waves

The DIA waves were predicted by Shukla and Silin (1992). The phase velocity of the DIA waves is much smaller (larger) than the electron thermal speed (ion and dust thermal speeds). Here the electron number density perturbation associated with the DIA waves is given by equation (4.2.1), while the ion number density perturbation n_{i1} is determined from the ion continuity equation

$$\frac{\partial n_{\mathrm{i1}}}{\partial t} + n_{\mathrm{i0}} \nabla \cdot \boldsymbol{v}_{\mathrm{i}} = 0 \tag{4.2.12}$$

and the ion momentum equation

$$\frac{\partial \boldsymbol{v}_{\mathrm{i}}}{\partial t} = -\frac{e}{m_{\mathrm{i}}} \nabla \phi - \frac{3k_{\mathrm{B}} T_{\mathrm{i}}}{m_{\mathrm{i}} n_{\mathrm{i0}}} \nabla n_{\mathrm{i1}} \tag{4.2.13}$$

where $\boldsymbol{v}_{\mathrm{i}}$ is the ion fluid velocity. Combining equations (4.2.12) and (4.2.13) we obtain

$$\left(\frac{\partial^2}{\partial t^2} - 3V_{\mathrm{Ti}}^2 \nabla^2 \right) n_{\mathrm{i1}} = \frac{n_{\mathrm{i0}} e}{m_{\mathrm{i}}} \nabla^2 \phi. \tag{4.2.14}$$

Equation (4.2.6) for the dust number density perturbation remains intact for the DIA waves as well. However, for stationary dust grains, we have $n_{d1} \approx 0$ and the DIA waves appear on a time scale much shorter than the dust plasma period $(= 2\pi/\omega_{pd})$.

Assuming $\omega \gg kV_{Ti}, kV_{Td}$, we combine equations (4.2.1), (4.2.5), (4.2.6) and (4.2.14) and Fourier transform the resultant equation in order to obtain the DIA wave dispersion relation (Shukla and Silin 1992)

$$1 + \frac{k_{De}^2}{k^2} - \frac{\omega_{pi}^2 + \omega_{pd}^2}{\omega^2} = 0. \tag{4.2.15}$$

Because of the large mass of the dust grains, the ion plasma frequency ω_{pi} is much larger than the dust plasma frequency ω_{pd}. Hence, equation (4.2.15) yields (Shukla and Silin 1992)

$$\omega^2 = \frac{k^2 C_S^2}{1 + k^2 \lambda_{De}^2} \tag{4.2.16}$$

where $C_S = \omega_{pi}\lambda_{De} = (n_{i0}/n_{e0})^{1/2} c_s$ and $c_s = (k_B T_e/m_i)^{1/2}$. In the long-wavelength limit (namely $k^2\lambda_{De}^2 \ll 1$) equation (4.2.16) reduces to

$$\omega = k \left(\frac{n_{i0}}{n_{e0}}\right)^{1/2} c_s. \tag{4.2.17}$$

Equation (4.2.17) shows that the phase velocity ($V_p = \omega/k$) of the DIA waves in a dusty plasma is larger than c_s because $n_{i0} > n_{e0}$ for negatively charged dust grains. The increase in the phase velocity is attributed to the electron density depletion in the background plasma, so that the electron Debye radius becomes larger. As a result, there appears a stronger space charge electric field which is responsible for the enhanced phase velocity of the DIA waves. The latter are subjected to insignificant electron and ion Landau damping because of the conditions $kV_{Ti} \ll \omega \ll kV_{Te}$. The DIA waves have also been observed in laboratory experiments (Barkan *et al* 1996, Nakamura *et al* 1999). Typical frequencies of the DIA waves for laboratory plasma parameters are tens of kHz.

4.2.3 Effects of boundaries and collisions

Dusty plasmas in laboratory devices are of finite extent and they also contain a large fraction of neutral atoms. Thus, the effects associated with device boundaries and collisions can modify the dispersion properties of the DA and DIA waves, which are shown below for the case when the dust charge fluctuations are ignored.

In the presence of low-frequency (in comparison with the electron–neutral and electron–dust collision frequencies) electrostatic waves, the dynamics of the electrons, ions and dust grains is governed by (Shukla and Rosenberg 1999), respectively,

$$\frac{\partial n_{e1}}{\partial t} + \frac{n_{e0} V_{Te}^2}{\nu_{en}} \nabla^2 \left(\frac{e\phi}{k_B T_e} - \frac{n_{e1}}{n_{e0}} \right) = 0 \tag{4.2.18}$$

$$\left(\frac{\partial}{\partial t} + \nu_{in} \right) \frac{\partial n_{i1}}{\partial t} - n_{i0} V_{Ti}^2 \nabla^2 \left(\frac{e\phi}{k_B T_i} + \frac{n_{i1}}{n_{i0}} \right) = 0 \tag{4.2.19}$$

and

$$\left(\frac{\partial}{\partial t} + \nu_{dn} \right) \frac{\partial n_{d1}}{\partial t} - \frac{n_{d0} q_{d0}}{m_d} \nabla^2 \phi = 0 \tag{4.2.20}$$

and Poisson's equation (4.2.5). The wave phase velocity is assumed to be much larger than V_{Td} and the adiabatic indices for the electron and ion fluids are assumed to be one. Furthermore, in cylindrical coordinates (r, θ, z) the Laplacian operator is defined as

$$\nabla^2 \phi = \nabla_\perp^2 \phi + \frac{\partial^2 \phi}{\partial z^2} \equiv \frac{1}{r} \frac{\partial}{\partial r} \left(r \frac{\partial \phi}{\partial r} \right) + \frac{1}{r^2} \frac{\partial^2 \phi}{\partial \theta^2} + \frac{\partial^2 \phi}{\partial z^2}. \tag{4.2.21}$$

Assuming $n_{j1} = \hat{n}_{j1}(r, \theta, z) \exp(-\mathrm{i}\omega t)$ and $\phi = \hat{\phi}(r, \theta, z) \exp(-\mathrm{i}\omega t)$, we study effects of the plasma boundary and collisions on the DA and DIA waves. For both cases, we assume $V_{Te}^2 |\nabla^2| \gg \nu_{en} |\omega|$, so that from equation (4.2.18) one obtains the Boltzmann electron number density perturbation, given by equation (4.2.1).

4.2.3.1 DA waves

To study the DA waves, we take equation (4.2.1) and assume that the ion number density perturbation is given by equation (4.2.2), which is deduced from equation (4.2.19) for $|\omega(\omega + \mathrm{i}\nu_{in})| \ll V_{Ti}^2 |\nabla^2|$. Then, substituting equations (4.2.1), (4.2.2) and

$$\hat{n}_{d1} = -\frac{n_{d0} q_{d0}}{m_d \omega (\omega + \mathrm{i}\nu_{dn})} \nabla^2 \hat{\phi} \tag{4.2.22}$$

into equation (4.2.5) and assuming that $\hat{\phi}$ is proportional to $\exp(\mathrm{i}k_z z + \mathrm{i}l\theta)$, we obtain

$$\frac{1}{r} \frac{\partial}{\partial r} \left(r \frac{\partial \hat{\phi}}{\partial r} \right) - \frac{l^2}{r^2} \hat{\phi} + \beta_{da} \hat{\phi} = 0 \tag{4.2.23}$$

where we have introduced

$$\beta_{da} = -k_z^2 + \frac{k_D^2 \omega (\omega + \mathrm{i}\nu_{dn})}{\omega_{pd}^2 - \omega (\omega + \mathrm{i}\nu_{dn})}. \tag{4.2.24}$$

Equation (4.2.23) is the lth-order Bessel equation, the solution of which is

$$\hat{\phi}(r) = \hat{\phi}_0 J_l \left(\sqrt{\beta_{da}} r \right) \tag{4.2.25}$$

where J_l is the lth-order Bessel function. On the surface of the cylindrical wave guide with the radius R, we must have $J_l(\sqrt{\beta_{\mathrm{da}}}R) = 0$. Thus, if γ_l is a root of J_0, then $\sqrt{\beta_{\mathrm{da}}}R = \gamma_l$ gives (Shukla and Rosenberg 1999)

$$k_z^2\lambda_{\mathrm{D}}^2 + \frac{\gamma_l^2\lambda_{\mathrm{D}}^2}{R^2} = \frac{\omega(\omega + \mathrm{i}\nu_{\mathrm{dn}})}{\omega_{\mathrm{pd}}^2 - \omega(\omega + \mathrm{i}\nu_{\mathrm{dn}})} \tag{4.2.26}$$

which is the desired dispersion relation of the DA waves in a collisional dusty plasma wave guide. We note that $J_0(\sqrt{\beta_{\mathrm{da}}}r)$ has many zeros. The first few zeros of $J_0(\sqrt{\beta_{\mathrm{da}}}r)$ are $\gamma_1 = 2.4$, $\gamma_2 = 5.5$, $\gamma_3 = 8.7$, $\gamma_4 = 11.8$.

The spatial damping rate k_{i} of the DA waves is deduced by letting $k_z = k_{\mathrm{r}} + \mathrm{i}k_{\mathrm{i}}$ in equation (4.2.26), where the subscripts r and i stand for the real and imaginary parts, respectively. We obtain

$$k_{\mathrm{i}} = \frac{\omega_{\mathrm{pd}}^2\nu_{\mathrm{dn}}\omega}{2k_{\mathrm{r}}\lambda_{\mathrm{D}}^2[(\omega_{\mathrm{pd}}^2 - \omega^2)^2 + \nu_{\mathrm{dn}}^2\omega^2]} \tag{4.2.27}$$

and

$$k_{\mathrm{r}}^2\lambda_{\mathrm{D}}^2 = k_{\mathrm{i}}^2\lambda_{\mathrm{D}}^2 - \frac{\gamma_l^2\lambda_{\mathrm{D}}^2}{R^2} + \frac{\omega^2\omega_{\mathrm{pd}}^2 - \omega^2(\omega^2 + \nu_{\mathrm{dn}}^2)}{(\omega_{\mathrm{pd}}^2 - \omega^2)^2 + \nu_{\mathrm{dn}}^2\omega^2}. \tag{4.2.28}$$

On the other hand, the temporal damping rate is obtained from

$$\omega(\omega + \mathrm{i}\nu_{\mathrm{dn}}) = \frac{\omega_{\mathrm{pd}}^2 P_{\mathrm{a}}}{1 + P_{\mathrm{a}}} \tag{4.2.29}$$

where $P_{\mathrm{a}} = k_z^2\lambda_{\mathrm{D}}^2 + \gamma_l^2\lambda_{\mathrm{D}}^2/R^2$. Equation (4.2.29) gives the following expressions for the real and imaginary parts of the frequency ($\omega = \omega_{\mathrm{r}} + \mathrm{i}\omega_{\mathrm{i}}$)

$$\omega_{\mathrm{r}}^2 = \frac{\omega_{\mathrm{pd}}^2 P_{\mathrm{a}}}{1 + P_{\mathrm{a}}} - \frac{\nu_{\mathrm{dn}}^2}{4} \tag{4.2.30}$$

and

$$\omega_{\mathrm{i}} = -\frac{\nu_{\mathrm{dn}}}{2}. \tag{4.2.31}$$

We note from equation (4.2.30) that ω_{r} can be close to zero for finite k_z. This occurs at

$$k_z^2\lambda_{\mathrm{D}}^2 = \frac{\nu_{\mathrm{dn}}^2}{4\omega_{\mathrm{pd}}^2} - \frac{\gamma_l^2\lambda_{\mathrm{D}}^2}{R^2} \tag{4.2.32}$$

for $P_{\mathrm{a}} \ll 1$.

4.2.3.2 DIA waves

We consider the DIA waves for which $|\omega(\omega + i\nu_{in})| \gg V_{Ti}^2|\nabla^2|$. This approximation reduces equation (4.2.19) to

$$\hat{n}_{i1} = -\frac{n_{i0}e}{m_i\omega(\omega + i\nu_{in})}\nabla^2\hat{\phi}. \tag{4.2.33}$$

Since the DIA wave frequency is much larger than the dust plasma frequency, the dust grains are considered immobile. Hence a combination of equations (4.2.1), (4.2.5) and (4.2.33) gives an equation similar to equation (4.2.23) except that β_{da} is replaced by

$$\beta_{di} = -k_z^2 + \frac{k_{De}^2\omega(\omega + i\nu_{in})}{\omega_{pi}^2 - \omega(\omega + i\nu_{in})}. \tag{4.2.34}$$

The dispersion relation of the DIA waves in a bounded collisional dusty plasma is of the form (Shukla and Rosenberg 1999)

$$k_z^2\lambda_{De}^2 + \frac{\gamma_l^2\lambda_{De}^2}{R^2} = \frac{\omega(\omega + i\nu_{in})}{\omega_{pi}^2 - \omega(\omega + i\nu_{in})}. \tag{4.2.35}$$

The expressions for k_r and k_i for the DIA waves are similar to equations (4.2.27) and (4.2.28) except that here we have to replace ω_{pd} by ω_{pi}, ν_{dn} by ν_{in}, and λ_D by λ_{De}. Similar replacements, along with $P_a \to k_z^2\lambda_{De}^2 + \gamma_l^2\lambda_{De}^2/R^2$, have to be made in equations (4.2.30) and (4.2.31) in order to obtain the real and imaginary parts of the DIA wave frequencies for real k_z.

The above results demonstrate that the finite cylindrical boundary leads to an effective wavenumber given by $(k_z^2 + k_\perp^2)^{1/2}$, where the effective radial wavenumber $k_\perp = \gamma_l/R$ is quantized. We observe that in the absence of collisions, ω_r is finite even for $k_z = 0$, because of the finite radial boundary which essentially results in a minimum effective $k_\perp$. Collisional effects cause the spatio-temporal damping of DA and DIA waves.

4.3 Kinetic Theory

We now develop a unified kinetic theory for longitudinal waves, taking into account dust charge fluctuations in unbounded, collisionless, unmagnetized dusty plasmas. We will then have the possibility of studying Landau damping of the DA, DIA and Langmuir waves.

4.3.1 General formulation

In the presence of waves, the distribution functions of the electrons and ions would change. Accordingly, electron and ion currents reaching the dust grain surface would assume oscillatory forms. The dust grain charge would then be perturbed

(Varma *et al* 1993, Melandsø *et al* 1993, Tsytovich and Havnes 1993, Jana *et al* 1993). In the following, we derive a general dispersion relation for electrostatic waves taking into account the dust charge perturbations. For negatively charged dust grains, the oscillating currents that reach the dust grain surface are of the form

$$\delta I_{-} = \sum_{j=\mathrm{e,i}} q_j \int v[\sigma_j^{\mathrm{d}}(v, q_{\mathrm{d1}}) f_{j0} + \sigma_j^{\mathrm{d}}(v, q_{\mathrm{d0}}) f_{j1}(\boldsymbol{r}, \boldsymbol{v}, t)]\,\mathrm{d}^3 v \tag{4.3.1}$$

where the subscripts 0 and 1 stand for the unperturbed and perturbed quantities, respectively. The effective collision cross section $\sigma_j^{\mathrm{d}}(v_j, q_{\mathrm{d0}})$ reads

$$\sigma_j^{\mathrm{d}}(v_j, q_{\mathrm{d0}}) = \pi r_{\mathrm{d}}^2 \left(1 - \frac{2q_j q_{\mathrm{d0}}}{C m_j v_j^2}\right) \tag{4.3.2}$$

while the unperturbed and perturbed distribution functions are denoted by f_{j0} and f_{j1}, respectively. It can be shown that

$$\begin{aligned}\delta I_{-} &= \nu_{\mathrm{ch}} q_{\mathrm{d1}} - e \int_{v_{\mathrm{m}}}^{\infty} v \sigma_{\mathrm{e}}^{\mathrm{d}}(v, q_{\mathrm{d0}}) f_{\mathrm{e1}}(\boldsymbol{r}, \boldsymbol{v}, t)\,\mathrm{d}^3 v \\ &\quad + e \int_0^{\infty} v \sigma_{\mathrm{i}}^{\mathrm{d}}(v, q_{\mathrm{d0}}) f_{\mathrm{i1}}(\boldsymbol{r}, \boldsymbol{v}, t)\,\mathrm{d}^3 v \equiv \nu_{\mathrm{ch}} q_{\mathrm{d1}} + I_{\mathrm{e1}} + I_{\mathrm{i1}}\end{aligned} \tag{4.3.3}$$

where the charge relaxation rate ν_{ch}, originating from the variations in the effective collision cross section due to charge perturbations at the grain surface as experienced by the unperturbed particles, can be written as (Jana *et al* 1993)

$$\nu_{\mathrm{ch}} = \frac{e|I_{\mathrm{e0}}|}{C}\left[\frac{1}{k_{\mathrm{B}} T_{\mathrm{e}}} + \frac{1}{k_{\mathrm{B}} T_{\mathrm{i}} - (e q_{\mathrm{d0}}/C)}\right]. \tag{4.3.4}$$

The perturbed distribution function f_{j1} in the presence of electrostatic waves is determined from the Boltzmann equation

$$\frac{\partial f_{j1}}{\partial t} + \boldsymbol{v} \cdot \nabla f_{j1} - \frac{q_j}{m_j} \nabla\phi \cdot \nabla_{\boldsymbol{v}} f_{j0} = \left(\frac{\partial F_j}{\partial t}\right)_{\mathrm{coll}} \tag{4.3.5}$$

where $F_j = f_{j0} + f_{j1}$. The right-hand side of equation (4.3.5) represents a collision operator describing the rate of electron and ion captures. On the other hand, the perturbed dust distribution function f_{d1} is generally obtained from the Vlasov equation

$$\left(\frac{\partial}{\partial t} + \boldsymbol{v} \cdot \nabla\right) f_{\mathrm{d1}} - \frac{q_{\mathrm{d0}}}{m_{\mathrm{d}}} \nabla\phi \cdot \nabla_{\boldsymbol{v}} f_{\mathrm{d0}} = 0 \tag{4.3.6}$$

if we neglect collisions between the charged dust grains and the other plasma species (namely electrons and ions) and the neutrals.

The variation of the dust charge q_{d1} is calculated from (Shukla 1996)

$$\frac{\partial q_{d1}}{\partial t} + \nu_{ch} q_{d1} = I_{e1} + I_{i1} \tag{4.3.7}$$

which is a new dynamical equation in our dusty plasma containing electrostatic waves. The equations are closed by Poisson's equation

$$\nabla^2 \phi = 4\pi (e n_{e1} - e n_{i1} - q_{d0} n_{d1} - n_{d0} q_{d1}) \tag{4.3.8}$$

which includes the dust charge perturbation q_{d1}. Here the number density perturbation is

$$n_{s1} = \int f_{s1}\, d^3 v. \tag{4.3.9}$$

Now assuming that the first-order distribution function and the wave potential vary as $\exp(\mathrm{i}\boldsymbol{k} \cdot \boldsymbol{r} - \mathrm{i}\omega t)$, we Fourier transform equations (4.3.5)–(4.3.8) and combine them. The resultant equation is of the form

$$\epsilon(\omega, \boldsymbol{k})\phi = 0 \tag{4.3.10}$$

where the dielectric constant is given by

$$\epsilon(\omega, \boldsymbol{k}) = 1 + \left(\sum_{s=e,i,d} \chi_s \right) + \chi_{qe} + \chi_{qi}. \tag{4.3.11}$$

The plasma dielectric susceptibility for the one-dimensional wave propagation is denoted by

$$\chi_s = \frac{\omega_{ps}^2}{k^2} \frac{1}{n_{s0}} \int \frac{\frac{\partial f_{s0}}{\partial v_x}}{V_p - v_x}\, d^3 v. \tag{4.3.12}$$

The electron and ion susceptibilities χ_{qe} and χ_{qi}, which are associated with dust charge fluctuations caused by electrostatic waves, are (Ma and Yu 1994a, b)

$$\chi_{qe} = \frac{\mathrm{i}\omega_{pe}^2}{k^2(\omega + \mathrm{i}\nu_{ch})} \frac{n_{d0}}{n_{e0}} \int_{v_m}^{\infty} \frac{\frac{\partial f_{e0}}{\partial v_x}}{V_p - v_x} v \sigma_e^d(v, q_{d0})\, d^3 v \tag{4.3.13}$$

and

$$\chi_{qi} = \frac{\mathrm{i}}{\omega + \mathrm{i}\nu_{ch}} \left(\frac{\nu_3}{k^2 \lambda_{De}^2} - \nu_4 \frac{\omega_{pi}^2}{\omega^2} \right) \tag{4.3.14}$$

where the coefficients

$$\nu_3 = \frac{|I_{e0}| n_{d0}}{e n_{e0}} \tag{4.3.15}$$

and

$$\nu_4 = -\frac{\omega^2}{k^2} \frac{n_{d0}}{n_{i0}} \int_0^{\infty} \frac{\frac{\partial f_{i0}}{\partial v_x}}{V_p - v_x} v \sigma_i^d(v, q_{d0})\, d^3 v \tag{4.3.16}$$

originate from the coupling of the dust charge fluctuations with the electron and ion number density perturbations, respectively. For unperturbed Maxwellian distribution functions, namely $f_{s0} = n_{s0}(m_s/2\pi k_B T_s)^{3/2} \exp(-v_s^2/2V_{Ts}^2)$, we can write

$$\chi_s = \frac{k_{Ds}^2}{k^2} W\left(\frac{\omega}{kV_{Ts}}\right) \tag{4.3.17}$$

where $k_{Ds} = \omega_{ps}/V_{Ts}$ and the function $W(\zeta)$ is defined as (Ichimaru 1973)

$$W(\zeta) = \frac{1}{\sqrt{2\pi}} \int_{-\infty}^{\infty} \frac{x}{x - \zeta - \mathrm{i}\eta} \exp\left(-\frac{x^2}{2}\right). \tag{4.3.18}$$

For $|\zeta| \ll 1$ we have

$$W(\zeta) = \mathrm{i}\sqrt{\frac{\pi}{2}}\zeta \exp(-\zeta^2) + 1 - \zeta^2 + \frac{\zeta^4}{3} \tag{4.3.19}$$

whereas in the opposite limit, namely $\zeta \gg 1$, $W(\zeta)$ takes the form

$$W(\zeta) = \mathrm{i}\sqrt{\frac{\pi}{2}}\zeta \exp\left(-\frac{\zeta^2}{2}\right) - \frac{1}{\zeta^2} - \frac{3}{\zeta^4}. \tag{4.3.20}$$

We now present explicit expressions for the dielectric susceptibilities in the following three cases.

4.3.1.1 DA waves

To express the dielectric susceptibilities for the DA waves, we use the approximations $kV_{Td} \ll \omega \ll kV_{Te}, kV_{Ti}$. Thus for the DA waves, we have

$$\epsilon_{da} = 1 + \chi_e + \chi_i - \frac{\omega_{pd}^2}{\omega^2}\left(1 + \frac{3k^2V_{Td}^2}{\omega^2}\right) + \chi_q = 0 \tag{4.3.21}$$

where

$$\chi_e \approx \frac{1}{k^2\lambda_{De}^2}\left(1 + \mathrm{i}\sqrt{\frac{\pi}{2}}\frac{\omega}{kV_{te}}\right) \tag{4.3.22}$$

$$\chi_i = \frac{1}{k^2\lambda_{Di}^2} + \mathrm{i}\chi_{im} \tag{4.3.23}$$

$$\chi_{im} = \sqrt{\frac{\pi}{2}}\frac{\omega}{k^2\lambda_{Di}^2 kV_{Ti}} \exp\left(-\frac{\omega^2}{2k^2V_{Ti}^2}\right) \tag{4.3.24}$$

and

$$\chi_q = \frac{k_q^2 \nu_1}{k^2(\nu_1 - \mathrm{i}\omega)} \tag{4.3.25}$$

where $k_q^2 = 4\pi n_{d0} r_d \nu_2/\nu_1$ and $\nu_1 \equiv \nu_{ch}$.

4.3.1.2 DIA waves

The limits $kV_{\mathrm{Ti}}, \omega_{\mathrm{pd}} \ll \omega \ll kV_{\mathrm{Te}}$ correspond to the DIA waves for which we have

$$\epsilon_{\mathrm{ia}} = 1 + \chi_{\mathrm{e}} + \chi_{\mathrm{ia}} + \frac{\mathrm{i}}{\omega + \mathrm{i}\nu_{\mathrm{ch}}}\left(\frac{\nu_3}{k^2\lambda_{\mathrm{De}}^2} - \nu_4\frac{\omega_{\mathrm{pi}}^2}{\omega^2}\right) = 0 \tag{4.3.26}$$

where

$$\chi_{\mathrm{ia}} \approx -\frac{\omega_{\mathrm{pi}}^2}{\omega^2}\left(1 + \frac{3k^2V_{\mathrm{Ti}}^2}{\omega^2}\right) + \mathrm{i}\chi_{\mathrm{im}} \tag{4.3.27}$$

and

$$\nu_4 \equiv \frac{16}{3}\pi r_{\mathrm{d}}^2 n_{\mathrm{d0}}\left(\frac{k_{\mathrm{B}}T_{\mathrm{i}}}{2\pi m_{\mathrm{i}}}\right)^{1/2}\left(1 - \frac{eq_{\mathrm{d0}}}{2Ck_{\mathrm{B}}T_{\mathrm{i}}}\right). \tag{4.3.28}$$

4.3.1.3 Langmuir waves

The limit $\omega \gg kV_{\mathrm{Te}}, \omega_{\mathrm{pi}}$ corresponds to the Langmuir waves for which we have

$$\epsilon_{\mathrm{L}} = 1 + \chi_{\mathrm{eL}} - \mathrm{i}\frac{\nu_5\omega_{\mathrm{pe}}^2}{(\omega + \mathrm{i}\nu_{\mathrm{ch}})\omega^2} = 0 \tag{4.3.29}$$

where

$$\chi_{\mathrm{eL}} \approx -\frac{\omega_{\mathrm{pe}}^2}{\omega^2}\left(1 + \frac{3k^2V_{\mathrm{Te}}^2}{\omega^2}\right) + \mathrm{i}\chi_{\mathrm{BG}} \tag{4.3.30}$$

$$\chi_{\mathrm{BG}} = \sqrt{\frac{\pi}{2}}\frac{\omega}{k^2\lambda_{\mathrm{De}}^2 kV_{\mathrm{Te}}}\exp\left(-\frac{\omega^2}{2k^2V_{\mathrm{Te}}^2}\right) \tag{4.3.31}$$

and

$$\nu_5 = \frac{16}{3}\pi r_{\mathrm{d}}^2 n_{\mathrm{d0}}\left(\frac{k_{\mathrm{B}}T_{\mathrm{e}}}{2\pi m_{\mathrm{e}}}\right)^{1/2}\left(1 - \frac{eq_{\mathrm{d0}}}{2Ck_{\mathrm{B}}T_{\mathrm{e}}}\right)\exp\left(\frac{eq_{\mathrm{d0}}}{Ck_{\mathrm{B}}T_{\mathrm{e}}}\right). \tag{4.3.32}$$

4.3.2 Results without Landau damping

We first neglect the effect of Landau damping and discuss the properties of the above-mentioned three electrostatic modes (namely the DA, DIA and Langmuir waves) in the presence of dust charge fluctuations.

4.3.2.1 DA waves

The dispersion relation (4.3.21) can be written in the form

$$1 + \frac{k_{\mathrm{D}}^2}{k^2} - \frac{\omega_{\mathrm{pd}}^2}{\omega^2 - 3k^2V_{\mathrm{Td}}^2} + \frac{k_{\mathrm{q}}^2\nu_1}{k^2(\nu_1 - \mathrm{i}\omega)} = 0 \tag{4.3.33}$$

which for $|\omega| \ll \nu_1$ gives

$$\omega^2 \approx 3k^2V_{\mathrm{Td}}^2 + \frac{k^2C_{\mathrm{D}}^2}{1+k^2\lambda_{\mathrm{D}}^2+k_{\mathrm{q}}^2\lambda_{\mathrm{D}}^2}\left[1 - \frac{\mathrm{i}\omega}{\nu_1(1+k^2\lambda_{\mathrm{D}}^2+k_{\mathrm{q}}^2\lambda_{\mathrm{D}}^2)}\right]. \tag{4.3.34}$$

Now letting $\omega = \omega_{\mathrm{r}} + \mathrm{i}\omega_{\mathrm{i}}$ in equation (4.3.34), where $\omega_{\mathrm{i}} \ll \omega_{\mathrm{r}}$, we easily obtain the real and imaginary parts of the frequency. For $kV_{\mathrm{Td}} \ll \omega_{\mathrm{r}}$, we have

$$\omega_{\mathrm{r}} \approx \frac{kC_{\mathrm{D}}}{(1+k^2\lambda_{\mathrm{D}}^2+k_{\mathrm{q}}^2\lambda_{\mathrm{D}}^2)^{1/2}} \tag{4.3.35}$$

and

$$\omega_{\mathrm{i}} \approx -\frac{k^2C_{\mathrm{D}}^2}{2\nu_1(1+k^2\lambda_{\mathrm{D}}^2+k_{\mathrm{q}}^2\lambda_{\mathrm{D}}^2)^2}. \tag{4.3.36}$$

Equation (4.3.35) shows that for $k^2\lambda_{\mathrm{D}}^2 \ll 1$ the real part of the DA wave frequency is somewhat reduced by a factor $(1 + k_{\mathrm{q}}^2\lambda_{\mathrm{D}}^2)^{1/2}$ when one considers dust charge fluctuations. The latter also introduce a collisionless temporal damping whose rate is given by equation (4.3.36).

The spatial damping rate of the DA waves with a real frequency can be obtained by letting $k = k_{\mathrm{r}} + \mathrm{i}k_{\mathrm{i}}$ in equation (4.3.33). For $kV_{\mathrm{Td}} \ll |\omega| \ll \nu_1$ and $k^2\lambda_{\mathrm{D}}^2 \ll 1$ we obtain

$$k_{\mathrm{r}}^2 = k_{\mathrm{i}}^2 + \left[1 + \frac{k_{\mathrm{q}}^2\lambda_{\mathrm{D}}^2\nu_1^2}{\nu_1^2+\omega^2}\right]\frac{\omega^2}{C_{\mathrm{D}}^2} \tag{4.3.37}$$

and

$$k_{\mathrm{i}} = \frac{k_{\mathrm{q}}^2\lambda_{\mathrm{D}}^2\nu_1\omega^3}{2k_{\mathrm{r}}C_{\mathrm{D}}^2(\nu_1^2+\omega^2)}. \tag{4.3.38}$$

4.3.2.2 DIA waves

We consider the effects of dust charge fluctuations on the DIA waves. The dispersion relation for the DIA waves, given by equation (4.3.26), can be expressed as

$$(\omega^2 - \omega_{ss}^2)(\omega + \mathrm{i}\nu_{\mathrm{ch}}) = -\mathrm{i}\omega^2\left(\frac{\nu_3}{1+k^2\lambda_{\mathrm{De}}^2} - \nu_4\frac{\omega_{ss}^2}{\omega^2}\right) \tag{4.3.39}$$

where $\omega_{ss} = kC_{\mathrm{S}}/(1+k^2\lambda_{\mathrm{De}}^2)^{1/2}$. Equation (4.3.39) predicts the damping of the DIA waves. For $|\omega| \ll \nu_{\mathrm{ch}}$ and $k^2\lambda_{\mathrm{De}}^2 \ll 1$ we obtain from equation (4.3.39)

$$\omega^2 = k^2C_{\mathrm{S}}^2\frac{\nu_{\mathrm{ch}}+\nu_4}{\nu_{\mathrm{ch}}+\nu_3}. \tag{4.3.40}$$

4.3.2.3 Langmuir waves

We consider the Langmuir waves which are deduced from equation (4.3.29). The dispersion relation has the form

$$(\omega^2 - \omega_{\mathrm{BG}}^2)(\omega + \mathrm{i}\nu_{\mathrm{ch}}) = \mathrm{i}\nu_5\omega_{\mathrm{pe}}^2 \tag{4.3.41}$$

where $\omega_{\mathrm{BG}} = (\omega_{\mathrm{pe}}^2 + 3k^2V_{\mathrm{Te}}^2)^{1/2}$ is the Bohm–Gross frequency. Equation (4.3.41) yields the frequency and the damping rate of the modified Langmuir waves.

4.3.3 Landau damping rates

We consider Landau damping rates of various wave modes by ignoring dust charge fluctuations. The Landau damping rates of the DA, DIA and Langmuir waves can be obtained by letting $\omega = \omega_{\mathrm{r}} + \mathrm{i}\omega_{\mathrm{i}}$ in the appropriate dispersion relations of section 4.3.2, and by employing the formula

$$\omega_{\mathrm{i}} = -\left[\frac{\mathrm{Im}\,\epsilon}{(\partial\epsilon_{\mathrm{r}}/\partial\omega)}\right]_{\omega=\omega_{\mathrm{r}}}. \tag{4.3.42}$$

The Landau damping rates of the DA, DIA and Langmuir waves can therefore be expressed as follows

(i) DA waves: $[\omega_{\mathrm{r}} = kC_{\mathrm{D}}/(1 + k^2\lambda_{\mathrm{D}}^2)^{1/2}]$

$$\omega_{\mathrm{i}} \approx -\sqrt{\frac{\pi}{8}}\frac{kC_{\mathrm{D}}}{(1 + k^2\lambda_{\mathrm{D}}^2)^2}\frac{\lambda_{\mathrm{D}}^2}{\lambda_{\mathrm{Di}}^2}\left[\frac{n_{\mathrm{e0}}T_{\mathrm{i}}}{n_{\mathrm{i0}}T_{\mathrm{e}}}\frac{C_{\mathrm{D}}}{V_{\mathrm{Te}}}\exp(-s_{\mathrm{e}}) + \frac{C_{\mathrm{D}}}{V_{\mathrm{Ti}}}\exp(-s_{\mathrm{i}})\right] \tag{4.3.43}$$

where we have denoted $s_{\mathrm{e,i}} = C_{\mathrm{D}}^2/2V_{\mathrm{Te,Ti}}^2(1 + k^2\lambda_{\mathrm{D}}^2)$.

(ii) DIA waves: $[\omega_{\mathrm{r}} = \sqrt{3}kV_{\mathrm{Ti}} + kC_{\mathrm{S}}/(1 + k^2\lambda_{\mathrm{De}}^2)^{1/2}]$

$$\omega_{\mathrm{i}} = -\sqrt{\frac{\pi}{8}}\frac{kC_{\mathrm{S}}}{(1 + k^2\lambda_{\mathrm{De}}^2)^2}\left[\left(\frac{n_{\mathrm{i0}}m_{\mathrm{e}}}{n_{\mathrm{e0}}m_{\mathrm{i}}}\right)^{1/2} + \left(\frac{n_{\mathrm{i0}}T_{\mathrm{e}}}{n_{\mathrm{e0}}T_{\mathrm{i}}}\right)^{3/2}\exp\left(-s_{\mathrm{ip}} - \frac{3}{2}\right)\right] \tag{4.3.44}$$

where $s_{\mathrm{ip}} = n_{\mathrm{i0}}T_{\mathrm{e}}/2n_{\mathrm{e0}}T_{\mathrm{i}}(1 + k^2\lambda_{\mathrm{De}}^2)$.

(iii) Langmuir waves: $[\omega_{\mathrm{r}} = (\omega_{\mathrm{pe}}^2 + 3k^2V_{\mathrm{Te}}^2)^{1/2}]$

$$\omega_{\mathrm{i}} = -\sqrt{\frac{\pi}{8}}\omega_{\mathrm{pe}}\frac{(1 + 3k^2\lambda_{\mathrm{De}}^2)^2}{k^3\lambda_{\mathrm{De}}^3}\exp\left(-s_l - \frac{3}{2}\right) \tag{4.3.45}$$

where $s_l = 1/2k^2\lambda_{\mathrm{De}}^2$. We note that in deriving equations (4.3.43) and (4.3.44), we have neglected the contribution of the dust Landau damping rate since $C_{\mathrm{D}}, C_s \gg V_{\mathrm{Td}}$. We suggest that laboratory experiments should be conducted to verify the results in equations (4.3.43) and (4.3.44).

4.3.4 Role of dust size distributions

The dust particles in cosmic and laboratory dusty plasmas may not be mono-sized. Specifically, in planetary rings, comets and interstellar space conditions, the dust grains have the size distributions such that grain sizes have a non-zero minimum radius r_1 and a finite maximum radius r_2. Thus, it is necessary to examine the influence of the dust grain size distributions on the plasma and wave properties.

When all grain sizes r_d are much smaller than the Debye radius λ_D, we can express the mass and charge of a dust particle as

$$m_d(r) = \frac{4}{3}\pi\rho_d r_d^3 \sim r_d^3 \tag{4.3.46}$$

and

$$q_d(r_d) = r_d\phi_d \sim r_d \tag{4.3.47}$$

where the dust material mass density ρ_d ($= 1$ g cm^{-3}) is assumed to be constant and equal for all grains.

The effects of the dust size distributions can be studied by assuming that the dust distribution is given by either a power law (Brattli *et al* 1997)

$$n_d(r_d)\,dr_d = N_1 r_d^{-s}\,dr_d \tag{4.3.48}$$

or by a normal distribution (Meuris 1997)

$$n_d(r_d)\,dr_d = \frac{N_2}{\sqrt{\pi}r_w\,\mathrm{erf}(r_\epsilon/r_w)}\exp\left[\frac{(r_d - \langle r_d\rangle)^2}{r_w^2}\right]dr_d \tag{4.3.49}$$

for $r_1 \le r_d \le r_2$. Outside the limits in dust sizes, r_1 and r_2, we use $n_d = 0$. Here N_1, N_2 and s are constants, r_w is the width of the normal distribution, and r_ϵ is the domain $[\langle r_d\rangle - r_\epsilon, \langle r_d\rangle + r_\epsilon]$ in which the particle sizes can be found. Assuming $r_\epsilon/r_w > 2$ one can approximate $\mathrm{erf}(r_\epsilon/r_w)$ by one. The average dust grain radius is defined as

$$\langle r_d\rangle = \frac{\int_{r_1}^{r_2} n_d(r_d)r_d\,dr_d}{N_2} \tag{4.3.50}$$

where

$$N_2 = \int_{r_1}^{r_2} n_d(r_d)\,dr_d \tag{4.3.51}$$

represents the total number density of the dust grains.

The density distribution of the power law form, given by equation (4.3.48), is widely accepted in cosmic plasmas (Meuris 1997). For the F ring of Saturn the dust size distributions appear to have the exponent $s \sim 4.6$, while for the G ring $s = 7$ and $s = 6$ have been obtained. For cometary environments, we recall a value of $s = 3.4$, while in the interstellar space one finds that $s = 3.5$. A realistic power law can be modelled if we assume that there are more grains of smaller size than larger ones.

The dust size distributions affect the equilibrium quasi-neutrality condition (Havnes *et al* 1990)

$$e(n_{e0} - n_{i0}) - \int_{r_1}^{r_2} q_{d0}(r_d) n_{d0}(r_d)\, dr_d = 0. \tag{4.3.52}$$

The dust plasma frequency is redefined as

$$\omega_{pd}^2 = 4\pi \int_{r_1}^{r_2} \frac{n_d(r_d) q_d^2(r_d)}{m_d(r_d)}\, dr_d. \tag{4.3.53}$$

In the presence of electrostatic waves, the dust dielectric susceptibility with the dust size distributions reads (Havnes *et al* 1996)

$$\chi_d = \frac{4\pi}{k^2} \int_{r_1}^{r_2} \frac{q_{d0}^2(r_d)}{m_d(r_d)}\, dr_d \int \frac{\boldsymbol{k} \cdot \frac{\partial f_{d0}}{\partial \boldsymbol{v}}}{\omega - \boldsymbol{k} \cdot \boldsymbol{v}}\, d^3v. \tag{4.3.54}$$

Meuris (1997) has shown that the dust plasma frequency increases for both power and normal laws of the dust size distributions. The increased dust plasma frequency will somewhat increase the phase velocity of the DA waves.

4.4 Other Effects

There are some other effects, such as thickness of dust layers, strong dust correlations, etc that may significantly modify the dispersion properties of the DA waves. Therefore, in the following, we discuss the properties of the DA waves in weakly coupled non-uniform thin plasma layers as well as in strongly coupled dusty plasmas.

4.4.1 Thin dust layers

We now consider the propagation of the DA waves in a lattice of thin dusty plasma layers which are non-uniform along the x-axis. Accordingly, at equilibrium we have the charge neutrality condition

$$en_{i0}(x) = en_{e0}(x) - q_{d0} n_{d0}(x). \tag{4.4.1}$$

Let us assume that small amplitude DA waves with the electrostatic potential $\hat{\phi}(x) \exp(ik_z z - i\omega t)$ propagate along the z-axis in an unmagnetized dusty plasma. Then the governing equations are Fourier transformed in time and along the z direction in order to obtain (Stenflo *et al* 2000) the DA wave equation for $|\omega| < \nu_1$

$$\frac{\partial}{\partial x}\left[\left(1 - \frac{\omega_{pd}^2}{\omega^2}\right)\frac{\partial \hat{\phi}}{\partial x}\right] - k_z^2\left(1 - \frac{\omega_{pd}^2}{\omega^2}\right)\hat{\phi} - k_p^2 \hat{\phi} = 0 \tag{4.4.2}$$

where $\omega_{pd} = [4\pi q_{d0}^2 n_{d0}(x)/m_d]^{1/2}$ and $k_p^2 = k_D^2 + k_q^2$.

We now consider a plasma that contains thin dust layers at $x = x_n$ ($n = 1, 2, 3, \ldots$), so that $n_{\mathrm{d}0} = 0$ in the regions between the layers, whereas $n_{\mathrm{d}0}(x)$ is so large within the layers that the total number of dust particles in each layer ($\int n_{\mathrm{d}0}\,\mathrm{d}x$ integrated over the width Δd ($\Delta d \ll 1/k_z$) of the layer) remains finite when the layer width approaches zero. Denoting the potential in an arbitrary region $x_n < x < x_{n+1}$ by ϕ_n, we have to solve the equation

$$\nabla^2 \phi_n - k_{\mathrm{p}}^2 \phi_n = 0 \tag{4.4.3}$$

which has the solution

$$\phi_n = [\phi_{n+} \exp(K_z x) + \phi_{n-} \exp(-K_z x)] \exp(\mathrm{i} k_z z) \tag{4.4.4}$$

where $K_z = (k_z^2 + k_{\mathrm{p}}^2)^{1/2}$ and ϕ_{n+} and ϕ_{n-} are constants which have to be determined from the boundary conditions

$$\phi_n \equiv \phi(x_n + 0) = \phi(x_n - 0) \tag{4.4.5}$$

and

$$\frac{\partial \phi(x_n + 0)}{\partial x} - \frac{\partial \phi(x_n - 0)}{\partial x} = -\left(\frac{k_z^2}{\omega^2} \int \omega_{\mathrm{pd}}^2 dx - \int k_{\mathrm{p}}^2 \,\mathrm{d}x \right) \phi_n . \tag{4.4.6}$$

For the particular case of a lattice with identical layers (where the distance between the layers is equal to l) we can put $\phi_n \equiv \phi_{n+1} \equiv \phi_{n-1}$. It then turns out that a simple and exact dispersion relation is obtained from equations (4.4.4)–(4.4.6). It is (Stenflo and Shukla 2000)

$$\omega^2 = \frac{k_z^2 \int \omega_{\mathrm{pd}}^2 \,\mathrm{d}x}{2K_z \tanh(K_z l/2) + \int k_{\mathrm{p}}^2 \,\mathrm{d}x} . \tag{4.4.7}$$

Thus we have found the frequency of the DA wave that propagates in the z direction (with the wavenumber k_z) in a system of dusty plasma layers. A single layer corresponds to the limit $l \to \infty$, in which equation (4.4.7) reduces to (Stenflo *et al* 2000)

$$\omega^2 = \frac{k_z^2 \int \omega_{\mathrm{pd}}^2 \,\mathrm{d}x}{2K_z + \int k_{\mathrm{p}}^2 \,\mathrm{d}x} . \tag{4.4.8}$$

On the other hand, in the opposite limit, namely $l \to 0$, we have

$$\omega^2 = \frac{k_z^2 \int \omega_{\mathrm{pd}}^2 \,\mathrm{d}x}{\int k_{\mathrm{p}}^2 \,\mathrm{d}x} \tag{4.4.9}$$

which describes the DA wave propagation in the z direction. Equation (4.4.8) shows that the frequency of the DA waves on a thin slab of a dusty plasma does not depend on the structural details of the density profile.

4.4.2 Dust correlations

We have discussed up to now various aspects of electrostatic plasma waves in a weakly coupled dusty plasma regime. The weak coupling assumption is sometimes justified because when the coupling parameter Γ_c for the dust grain is large, the corresponding coupling parameter for electrons and ions can still be small due to their higher temperatures and smaller electric charges. There are two approaches to consider the effects of dust correlations, which are described below.

4.4.2.1 Generalized hydrodynamic model

Kaw and Sen (1998) adopted the generalized hydrodynamic (GH) model which provides a simple physical picture of the effects of strong dust correlations through the introduction of viscoelastic coefficients. This phenomenological model is generally valid over a large range of the coupling parameter, all the way from the weakly coupled gaseous phase ($\Gamma_c \ll 1$) to the strongly coupled liquid state ($\Gamma_c \gg 1$) and may even be used in the supercooled regime (beyond the critical Γ_c for dust crystallization) as long as the plasma retains its fluid character. The linearized GH equations comprise the dust continuity equation (4.2.3) and the dust momentum equation (Kaw and Sen 1998)

$$\left(1+\tau_m\frac{\partial}{\partial t}\right)\left[m_d n_{d0}\left(\frac{\partial \boldsymbol{v}_d}{\partial t}+\nu_{dn}\boldsymbol{v}_d\right)-q_{d0}n_{d0}\left(\boldsymbol{E}+\frac{1}{c}\boldsymbol{v}_d\times\boldsymbol{B}\right)+\nabla P_d\right]$$
$$=\eta_s\nabla\cdot\nabla\boldsymbol{v}_d+\left(\xi_b+\frac{\eta_s}{3}\right)\nabla(\nabla\cdot\boldsymbol{v}_d) \qquad (4.4.10)$$

where

$$\tau_m=\frac{\xi_b+\frac{4}{3}\eta_s}{n_{d0}k_B T_d(1-\gamma_d\mu_d)+\frac{4}{15}U(\Gamma_c)} \qquad (4.4.11)$$

is the viscoelastic relaxation time that removes a certain rigidity inherent in the Navier–Stokes equation with regard to the temporal response, or relaxation of the internal energy against the viscous motion of the dust fluid. Furthermore, η_s and ξ_b are the coefficients for the shear viscosity and the bulk viscosity, respectively, γ_d is the adiabatic index,

$$\mu_d=\frac{1}{k_B T_d}\left(\frac{\partial P_d}{\partial n_d}\right)_{T_d}=1+\frac{U(\Gamma_c)}{3}+\frac{\Gamma_c}{9}\frac{\partial U(\gamma_c)}{\partial \Gamma_c} \qquad (4.4.12)$$

is the compressibility and $U(\Gamma_c)=E_c/n_{d0}k_B T_d$ is the so-called excess internal energy or the normalized correlation energy. The quantity $U(\Gamma_c)$ is usually calculated from simulations or from statistical schemes and expressed in terms of an analytically fitted formula. Typically, for weakly coupled plasmas ($\Gamma_c < 1$), we have $U(\Gamma_c) \approx (\sqrt{3}/15)\Gamma_c^{3/2}$. In the range $1 \le \Gamma_c \le 200$, Slattery *et al* (1980) have given the relation $U(\Gamma_c)=-0.89\Gamma_c+0.95\Gamma_c^{1/4}+0.19\Gamma_c^{-1/4}-0.81$, where we omit a small correction term due to finite number of particles. The dependence of the other transport coefficients, e.g. η_s, ξ_b, on Γ_c are somewhat more complex and are available as tabulated results derived from molecular dynamics simulations and a variety of statistical schemes (Ichimaru *et al* 1987). Finally, we note that the plasma equations are closed by the full set of Maxwell and Poisson equations for the field quantities, and the equilibrium quasi-neutrality condition (4.1.1).

We consider the properties of the DA waves in an unmagnetized plasma with strongly coupled dust grains and weakly coupled electrons and ions. Assuming that the perturbed quantities are proportional to $\exp(-\mathrm{i}\omega t+\mathrm{i}\boldsymbol{k}\cdot\boldsymbol{r})$, we obtain (Kaw and Sen 1998) from the dust continuity equation (4.2.3) and equation (4.4.10)

$$\hat{n}_{\mathrm{d1}} = \frac{n_{\mathrm{d0}} q_{\mathrm{d0}} k^2}{m_{\mathrm{d}}(\omega^2 + \mathrm{i}\omega\eta^* - \gamma_{\mathrm{d}}\mu_{\mathrm{d}} k^2 V_{\mathrm{Td}}^2)}\hat{\phi} \tag{4.4.13}$$

where $\eta^* = \nu_{\mathrm{dn}} + \eta_{\mathrm{d}}(\omega, \boldsymbol{k})$ and

$$\eta_{\mathrm{d}}(\omega, \boldsymbol{k}) = \frac{(\xi_{\mathrm{b}} + 4\eta_{\mathrm{s}}/3)k^2}{m_{\mathrm{d}} n_{\mathrm{d0}}(1 - \mathrm{i}\omega\tau_{\mathrm{m}})}. \tag{4.4.14}$$

Now inserting equations (4.2.1), (4.2.2), (4.3.7) and (4.4.13) into (4.3.8) and Fourier transforming, we obtain the dispersion relation for low-frequency (in comparison with ν_{ch}) DA waves when dust grains are strongly correlated. The result is

$$1 + \frac{k_{\mathrm{D}}^2}{k^2} - \frac{\omega_{\mathrm{pd}}^2}{\omega^2 + \mathrm{i}\omega\eta^* - \gamma_{\mathrm{d}}\mu_{\mathrm{d}} k^2 V_{\mathrm{Td}}^2} + \frac{k_{\mathrm{q}}^2 \nu_1}{k^2(\nu_1 - \mathrm{i}\omega)} = 0. \tag{4.4.15}$$

For $\sqrt{\gamma_{\mathrm{d}}\mu_{\mathrm{d}}} k V_{\mathrm{Td}}, \nu_{\mathrm{dn}} \ll |\omega| \ll \nu_1, \tau_{\mathrm{m}}^{-1}$, we obtain from equation (4.4.15)

$$\omega^2 = k^2 \left[\gamma_{\mathrm{d}}\mu_{\mathrm{d}} V_{\mathrm{Td}}^2 + \frac{C_{\mathrm{D}}^2}{1 + k^2\lambda_{\mathrm{D}}^2 + k_{\mathrm{q}}^2\lambda_{\mathrm{D}}^2} \right] - \mathrm{i}\omega\eta_* k^2 \tag{4.4.16}$$

where we have denoted $\eta_* = (\xi_{\mathrm{b}} + 4\eta_{\mathrm{s}}/3)/m_{\mathrm{d}} n_{\mathrm{d0}}$. For $\mu_{\mathrm{d}} = \eta_* = 0$ equation (4.4.16) describes the usual undamped DA waves in a weakly correlated plasma. In the presence of dust correlations ($\mu_{\mathrm{d}} \neq 0$ and $\eta_* \neq 0$), Kaw and Sen (1998) found that the DA wave changes its phase velocity through the μ_{d} term, and got an additional dispersive correction through the η_* term. The modified DA waves are subjected to a damping whose rate is proportional to $\eta_* k^2$. Furthermore, for $|\omega| \gg \tau_{\mathrm{m}}^{-1}$, ν_{dn}, we obtain from equation (4.4.15)

$$\omega^2 \approx k^2 \left[\gamma_{\mathrm{d}}\mu_{\mathrm{d}} V_{\mathrm{Td}}^2 + \frac{C_{\mathrm{D}}^2}{1 + k^2\lambda_{\mathrm{D}}^2 + k_{\mathrm{q}}^2\lambda_{\mathrm{D}}^2} + \frac{\eta_*}{\tau_{\mathrm{m}}} \right] \tag{4.4.17}$$

which exhibits the modification of the DA waves.

4.4.2.2 *Quasi-localized charge approximation*

Rosenberg and Kalman (1997) have also examined the properties of the DA waves including strong coupling of dust grains in an unmagnetized dusty plasma. They employed the quasi-localized charge approximation (QLCA) which has been developed and used to determine the dielectric response function and plasmon dispersion for various strongly coupled systems. The QLCA describes the motions of the system around the average configuration represented through the equilibrium correlation function. The model resembles that of a disordered system in which the particles occupy randomly distributed sites and undergo small-amplitude oscillations around them. Assuming that the weakly coupled Boltzmann electrons and ions provide a polarizable background and that the dust grains interact with each other via the Debye–Hückel potential (also referred to as the Yukawa potential), the longitudinal dielectric response function for the DA waves is found to be (Rosenberg and Kalman 1997)

$$\epsilon_{\mathrm{L}}(\omega, \boldsymbol{k}) = 1 - \frac{k^2}{(k^2 + k_{\mathrm{D}}^2)} \frac{\omega_{\mathrm{pd}}^2}{[\omega^2 - \omega_{\mathrm{pd}}^2 D(\boldsymbol{k})]} \tag{4.4.18}$$

where in the small-k limit, we have

$$D(\boldsymbol{k}) = \frac{1}{V} \sum_{\boldsymbol{q}} \left(\frac{[\boldsymbol{k} \cdot (\boldsymbol{k} - \boldsymbol{q})]^2}{k^2[(\boldsymbol{k} - \boldsymbol{q})^2 + k_{\mathrm{D}}^2]} - \frac{(\boldsymbol{k} \cdot \boldsymbol{q})^2}{k^2[q^2 + k_{\mathrm{D}}^2]} \right) g(\boldsymbol{q}) \tag{4.4.19}$$

in which $g(\boldsymbol{q})$ is the Fourier transform of the pair correlation function $g(\boldsymbol{r})$. Using $\epsilon(\omega, \boldsymbol{k}) = 0$ we obtain for the DA wave frequency

$$\omega(\boldsymbol{k}) = \omega_{\mathrm{pd}} \left[\frac{k^2}{k^2 + k_{\mathrm{D}}^2} + D(k, \Gamma_{\mathrm{c}}) \right]^{1/2}. \tag{4.4.20}$$

In the regime $k^2\lambda_{\mathrm{D}}^2 \ll 1$, equation (4.4.20) gives

$$\omega \approx k C_{\mathrm{D}}[1 + f_s(\kappa, \Gamma_{\mathrm{c}})\kappa^2]^{1/2} \tag{4.4.21}$$

which shows that the effect of strong coupling is to reduce the DA wave phase velocity, since $f_s \approx -(4/45)(0.9 + 0.5\kappa^2)$ when $\kappa = k_{\mathrm{D}}a \leq 1$ and $\Gamma_{\mathrm{c}} \gg 1$. The decrease in the phase speed with κ may be related to an increase in the compressibility of the dust fluid as the range of the intergrain potential decreases. In the regime $ka > \kappa$ (i.e. $k\lambda_{\mathrm{D}} \gg 1$) we obtain from equation (4.4.20)

$$\omega \approx \omega_{\mathrm{pd}}(1 + f_s\kappa^2 k^2 \lambda_{\mathrm{D}}^2)^{1/2} \tag{4.4.22}$$

which shows that the effective dust plasma frequency is reduced due to a decrease in the effective dust charge with stronger screening.

Figure 4.1. One-dimensional line of equally sized dust grains are separated by an equal distance.

4.5 Dust Lattice Waves

Recent research has predicted the appearance of both longitudinal and transverse dust lattice (DL) waves (Melandsø 1996; Farokhi *et al* 1999, Wang *et al* 2001) in a strongly coupled dusty plasma system, analogous to those in solid-state physics (Kittel 1956). However, in a dusty plasma each dust grain interacts with its neighbour due to the short-range Debye–Hückel interaction (as well as with other dust grains due to long range interactions) involving a potential U_{ij} which depends on the dust charge, the separation between dust grains and the Debye radius λ_{D}. Using an appropriate expression for U_{ij}, Melandsø (1996) developed a theory for linear and nonlinear longitudinal DL (LDL) waves, taking into account only the interaction between the nearest dust grains. In the following, we present Melandsø's LDL wave dispersion relation and its improved version when the nearest-neighbour approximation is relaxed.

4.5.1 Longitudinal DL waves

We study a simple one-dimensional line of equal dust grains equally spaced, as shown in figure 4.1. We give a slight displacement to the dust grains which are connected by a set of springs. The dust grain interacts with its neighbour via the Debye–Hückel potential

$$U_{ij} = \frac{q_{\mathrm{d}i}q_{\mathrm{d}j}}{|\boldsymbol{r}_i - \boldsymbol{r}_j|}\exp\left(-\frac{|\boldsymbol{r}_i - \boldsymbol{r}_j|}{\lambda_{\mathrm{D}}}\right) \tag{4.5.1}$$

where $q_{\mathrm{d}i,\mathrm{d}j}$ and $\boldsymbol{r}_{i,j}$ are the charge and position of a dust particle. In the case of longitudinal motions in the arrangement of a one-dimensional horizontal dust chain, their oscillations are governed by the equation of motion

$$m_{\mathrm{d}}\left(\frac{\partial^2 x_j}{\partial t^2} + \nu_{\mathrm{dn}}\frac{\partial x_j}{\partial t}\right) = -\sum_i \frac{\partial U_{ij}}{\partial x}. \tag{4.5.2}$$

Accounting for the relevant near-neighbour interactions, i.e. $i = j - 1$ and $j + 1$, we have for the right-hand side of equation (4.5.2)

$$q_{\mathrm{d}0}\left(\frac{\partial E}{\partial x}\right)_{x=a}(2\delta x_j - \delta x_{j-1} - \delta x_{j+1}) \tag{4.5.3}$$

where we have assumed a constant charge q_{d0} on every grain. The electric field is given by (Ishihara 1998)

$$E(x) = \frac{q_{d0}}{x^2}\left(1 + \frac{x}{\lambda_D}\right)\exp\left(-\frac{x}{\lambda_D}\right). \tag{4.5.4}$$

We note that $(\partial E/\partial x)_{x=a}$ is evaluated at the inter-particulate distance $a = |x_j - x_{j-1}| = |x_{j+1} - x_j|$. In the case of vertical (z direction) vibrations of a dust particle, the equation of motion would contain a force term (Ishihara 1998)

$$\frac{q_{d0}E(a)}{a}(2\delta z_j - \delta z_{j-1} - \delta z_{j+1}) \tag{4.5.5}$$

instead of equation (4.5.3). Now assuming $\delta x_j = \delta x_0 \exp[-i(\omega t - jka)]$, we obtain from equations (4.5.2)–(4.5.4) the dispersion relation for LDL waves (Melandsø 1996)

$$\omega^2 + i\omega\nu_{dn} = \frac{2q_{d0}^2}{m_d a^3}\left(1 + \frac{a}{\lambda_D} + \frac{a^2}{2\lambda_D^2}\right)\exp\left(-\frac{a}{\lambda_D}\right)\sin^2\left(\frac{ka}{2}\right). \tag{4.5.6}$$

4.5.2 An improved model

Farokhi *et al* (1999) have refined the result of Melandsø (1996) by including short- and long-range interactions between dust grains in one space dimension. Accordingly, calculations have been carried out for the one-dimensional lattice with the cyclic boundary condition imposed on the chain of dust grains. We consider a multi-component dusty plasma in which negatively charged massive dust grains are considered as discrete particles. The number densities of weakly coupled electrons and ions follow the Boltzmann distributions, given by equations (4.2.1) and (4.2.2). The normalized potential $\varphi = e\phi/k_B T$ in the linear limit ($\varphi \ll 1$) satisfies the Schrödinger equation

$$\nabla^2\varphi + \left[-k_D^2 + \sum_n r_{dn}\delta(\boldsymbol{r} - \boldsymbol{r}_n)\right]\varphi = 0 \tag{4.5.7}$$

where r_{dn} is the radius of dust grains which are assumed to be spherical conductors. For small dust grains, when the grain radius is smaller than the dust grain separation (namely $r_{dn} \ll a$), the location of a dust grain can be described by the Dirac δ-function. Equation (4.5.7) is often used in solid-state physics for the description of the lattice waves in the one-dimensional approximation.

Equation (4.5.7) determines the real potential φ and the condition of the periodicity (for the ideal lattice) cannot contain an exponential factor (Bloch coefficient), as occurs in solid-state physics. The one-dimensional form of equation (4.5.7) is

$$\frac{\partial^2\varphi(z)}{\partial z^2} - k_D^2\varphi(z) + \sum_n b_n\delta(z - z_n)\varphi(z) = 0 \tag{4.5.8}$$

where $b_n = r_{\mathrm{dn}} N_0/S$ is the size of the dust grain averaged over the area S perpendicular to the linear lattice and N_0 is the number of dust grains embraced by the area S. In the region $z_n < z < z_{n+1}$, equation (4.5.8) has the solution

$$\varphi(z) = A_n \sinh[k_{\mathrm{D}}(z - z_n)] + B_n \cosh[k_{\mathrm{D}}(z - z_n)] \tag{4.5.9}$$

while in the region $z_{n-1} < z < z_n$ the solution of equation (4.5.8) reads

$$\varphi(z) = A_{n-1} \sinh[k_{\mathrm{D}}(z - z_{n-1})] + B_{n-1} \cosh[k_{\mathrm{D}}(z - z_{n-1})] \tag{4.5.10}$$

with $B_n = \varphi(z_n) = \varphi_n$, where φ_n is the known potential of the nth grain. The solution of equation (4.5.8) and its derivative must satisfy the following boundary conditions at $z = z_n$

$$\varphi(z)|_{z_n+0} = \varphi|_{z_n-0} \tag{4.5.11}$$

and

$$\left.\frac{\partial \varphi}{\partial z}\right|_{z_n+0} - \left.\frac{\partial \varphi}{\partial z}\right|_{z_n-0} = -b_n \varphi_n. \tag{4.5.12}$$

From equations (4.5.9)–(4.5.12) one can easily obtain the coefficients A_{n-1} and A_n. We have

$$A_{n-1} = \varphi_n \sinh^{-1}[k_{\mathrm{D}}(z_n - z_{n-1})] - \varphi_{n-1} \coth[k_{\mathrm{D}}(z_n - z_{n-1})] \tag{4.5.13}$$

and

$$A_n = \varphi_n \coth[k_{\mathrm{D}}(z_n - z_{n-1})] - \frac{b_n}{k_{\mathrm{D}}} - \varphi_{n-1} \sinh^{-1}[k_{\mathrm{D}}(z_n - z_{n-1})]. \tag{4.5.14}$$

By the replacement $n \to n + 1$, equation (4.5.13) should give equation (4.5.14). This condition gives (Farokhi *et al* 1999)

$$\begin{aligned} \varphi_n \left\{ \tanh\left[\frac{k_{\mathrm{D}}}{2}(z_n - z_{n-1})\right] + \tanh\left[\frac{k_{\mathrm{D}}}{2}(z_{n+1} - z_n)\right] - \frac{b_n}{k_{\mathrm{D}}} \right\} \\ = \frac{(\varphi_{n-1} - \varphi_n)}{\sinh[k_{\mathrm{D}}(z_n - z_{n-1})]} + \frac{(\varphi_{n+1} - \varphi_n)}{\sinh[k_{\mathrm{D}}(z_{n+1} - z_n)]} \end{aligned} \tag{4.5.15}$$

and the solution (4.5.9) in the region $z_n < z < z_{n+1}$ will have the form

$$\varphi(z) = \frac{\{\varphi_n \sinh[k_{\mathrm{D}}(z_{n+1} - z)] + \varphi_{n+1} \sinh[k_{\mathrm{D}}(z - z_n)]\}}{\sinh[k_{\mathrm{D}}(z_{n+1} - z_n)]}. \tag{4.5.16}$$

Under the condition specified by equation (4.5.15), the solution (4.5.10) in the region $z_{n-1} < z < z_n$ has an analogous form, which can be found from equation (4.5.16) by the replacement $n \to n - 1$.

For a lattice with identical grains (they have the same surface potentials, $\varphi_0 = \varphi_1 = \cdots = \varphi_n =$ constant and $b_0 = b_1 = \cdots = b_n =$ constant), it follows from equation (4.5.15) that distances between the grains are equal and one obtains (Farokhi *et al* 1999)

$$\tan\left(\frac{k_{\mathrm{D}}a}{2}\right) = \frac{b_0}{2k_{\mathrm{D}}} \tag{4.5.17}$$

where $a = |z_{n+1} - z_n|$ is the separation between two consecutive grains. On the other hand, if the dust grains are separated with an equal distance and the relation (4.5.17) is satisfied, then the potentials of dust grains are the same. A relation which is identical with equation (4.5.17) is well known in solid-state physics (Kittel 1956). Consequently, the parameters of a dusty plasma have to satisfy a definite relation (equation (4.5.17)) for the formation of an ideal lattice.

Let us assume that dust particles execute small oscillations about their equilibrium position. The dust grains are assumed to have the same potential φ_0 (and the charge Q_0) with a uniform separation distance a. During the oscillations, distances between the grains change, and according to equation (4.5.15), the grain's potential would change as well. However, on a timescale of the DL wave appearance, we assume the dust particles to maintain their equilibrium potential (and the charge).

The potential given by equation (4.5.16) can then be expressed in the form

$$\varphi(z) = \varphi_0 \frac{\cosh\left[\frac{k_{\mathrm{D}}}{2}(z_{n+1} + z_n - 2z)\right]}{\cosh\left[\frac{k_{\mathrm{D}}}{2}(z_{n+1} - z_n)\right]} \tag{4.5.18}$$

for $z_n < z < z_{n+1}$. The expression (4.5.18) gives the total electrostatic energy of the interaction for the dust grain system, namely

$$u = \sum_n Q_n \varphi(z_n) = Q_0\varphi_0 \sum_n \frac{\cosh\left[\frac{k_{\mathrm{D}}}{2}(z_{n+1} + z_{n-1} - 2z_n)\right]}{\cosh\left[\frac{k_{\mathrm{D}}}{2}(z_{n+1} - z_{n-1})\right]}. \tag{4.5.19}$$

From the sum in equation (4.5.19) we have excluded the interaction of the charge with its own field. The grains execute small oscillations, $z_n = z_{n0} + \xi_n$, about their equilibrium positions z_{n0}. From equation (4.5.19) it is easy to construct the equation of motion for the nth dust grain. As usual, we seek a wave-train solution of the form $\xi_n = A_n \exp(-\mathrm{i}\omega t + \mathrm{i}kna)$. For $k_{\mathrm{D}}\xi \ll 1$ we obtain after some straightforward algebra (Farokhi *et al* 1999, 2000)

$$\omega = \pm Q_0 \left[\frac{2k_{\mathrm{D}}^2}{m_{\mathrm{d}} r_{\mathrm{d}} \cosh(k_{\mathrm{D}}a)}\right]^{1/2} \sin\left(\frac{ka}{2}\right). \tag{4.5.20}$$

Equation (4.5.20) determines the frequency of the DL waves in an infinite chain of dust grains, ignoring the periodic boundary conditions. On the other hand, if our system contains $N + 1$ dust particles, the periodic boundary condition gives the following N different frequencies for the first Brillouin zone

$$\omega = \pm Q_0 \left[\frac{2k_{\mathrm{D}}^2}{m_{\mathrm{d}} r_{\mathrm{d}} \cosh(k_{\mathrm{D}} a)} \right]^{1/2} \sin\left(\frac{\pi m}{N}\right) \tag{4.5.21}$$

for $m = 1, 2, 3, \ldots, N/2$. According to equation (4.5.21) the maximum frequency is given by

$$\omega_{\mathrm{m}} = \pm Q_0 \left[\frac{2k_{\mathrm{D}}^2}{m_{\mathrm{d}} r_{\mathrm{d}} \cosh(k_{\mathrm{D}} a)} \right]^{1/2} . \tag{4.5.22}$$

Expressions (4.5.20) and (4.5.22) differ from the expression found by Melandsø (1996), where the expression for the frequency includes also the polynomial dependence on the parameter $k_{\mathrm{D}} a$. For $k_{\mathrm{D}} a \ll 1$ equation (4.5.20) gives

$$\omega = \pm Q_0 \left(\frac{2k_{\mathrm{D}}^2}{m_{\mathrm{d}} r_{\mathrm{d}}} \right)^{1/2} \sin\left(\frac{ka}{2}\right) . \tag{4.5.23}$$

4.6 Waves in Uniform Magnetoplasmas

It is well known that the presence of an external magnetic field significantly modifies the dispersion properties of both the electrostatic and electromagnetic waves in an electron–ion plasma. Thus, we focus our attention on low-frequency (in comparison with the electron gyrofrequency) electrostatic and electromagnetic waves in a weakly coupled dusty magnetoplasma.

4.6.1 Electrostatic waves

The dispersion properties of electrostatic plasma waves in a dusty plasma are obtained by Fourier analysing the Vlasov and Poisson equations that are supplemented by the dust charging equation. However, the latter is rather complex when an external magnetic field $B_0 \hat{z}$ is present. Thus, to avoid the mathematical complexities, we neglect the effects of dust charge fluctuations without losing any physical insight. The dusty plasma wave response in the electrostatic wave potential ϕ is then deduced from

$$\epsilon(\omega, \boldsymbol{k}) = 1 + \sum_{s=\mathrm{e,i,d}} \chi_s = 0 \tag{4.6.1}$$

where the dielectric susceptibility χ_s reads (Stenflo 1981)

$$\chi_s = \frac{\omega_{\mathrm{p}s}^2}{k^2 V_{\mathrm{T}s}^2} \left(1 - \omega \sum_{n=-\infty}^{\infty} \Gamma_n \int_{\infty}^{\infty} \frac{F_z \, \mathrm{d}v_z}{\omega - k_z v_z - n\omega_{\mathrm{c}s}} \right). \tag{4.6.2}$$

Here $\Gamma_n = I_n(b_s)\exp(-b_s)$, I_n is the modified Bessel function of order n, $b_s = k_\perp^2 V_{\mathrm{T}s}^2/\omega_{\mathrm{c}s}^2 \equiv k_\perp^2 \rho_{\mathrm{T}s}^2$, $\omega_{\mathrm{c}s} = |q_s|B_0/m_s c$ is the gyrofrequency of the species s and $F_z = (2\pi V_{\mathrm{T}s}^2)^{-1/2}\exp(-v_z^2/2V_{\mathrm{T}s}^2)$. The components of the wavevector $\boldsymbol{k}$ along and across the z direction are denoted by k_z and $k_\perp$, respectively. To explain how the external magnetic field modifies different low-frequency modes, we consider a number of limiting cases. These are as follows.

(i) We first consider waves which satisfy the approximations $\omega_{\mathrm{cd}}, kV_{\mathrm{Td}}, kV_{\mathrm{Ti}} \ll \omega \ll k_z V_{\mathrm{Te}}, \omega_{\mathrm{ce}} k_z/k_\perp, kV_{\mathrm{T}j}/\omega_{\mathrm{c}j} \ll 1$ and $Z_{\mathrm{d}} m_{\mathrm{i}} \ll m_{\mathrm{d}}$. Thus, we have

$$\chi_{\mathrm{e}} \approx \frac{1}{k^2\lambda_{\mathrm{De}}^2} \tag{4.6.3}$$

$$\chi_{\mathrm{i}} \approx -\frac{\omega_{\mathrm{pi}}^2 k_\perp^2}{(\omega^2-\omega_{\mathrm{ci}}^2)k^2} - \frac{\omega_{\mathrm{pi}}^2 k_z^2}{\omega^2 k^2} \tag{4.6.4}$$

and

$$\chi_{\mathrm{d}} \approx -\frac{\omega_{\mathrm{pd}}^2}{\omega^2}. \tag{4.6.5}$$

Since the dust plasma frequency ω_{pd} is much smaller than the ion plasma frequency ω_{pi}, we obtain from $1+\chi_{\mathrm{e}}+\chi_{\mathrm{i}} = 0$ the frequency of the electrostatic ion cyclotron (EIC) waves as

$$\omega \approx \omega_{\mathrm{ci}}\left(1+\frac{n_{\mathrm{i0}}}{n_{\mathrm{e0}}}\frac{k_\perp^2 c_s^2}{\omega_{\mathrm{ci}}^2}\right)^{1/2} \tag{4.6.6}$$

where $k^2\lambda_{\mathrm{De}}^2 \ll 1$ and $k_z \ll |\boldsymbol{k}_\perp|$ have been assumed. Equation (4.6.6) reveals that the phase velocity of the usual EIC waves in an electron–ion plasma is increased in the presence of a dust component.

(ii) We now consider the limit $\omega \ll \omega_{\mathrm{ci}}$, simplify equation (4.6.4) and substitute that expression together with equations (4.6.3) and (4.6.5) into $1+\sum_s \chi_s = 0$ to obtain the frequency of the modified DIA waves

$$\omega = \frac{k\lambda_{\mathrm{De}}}{(1+k^2\lambda_{\mathrm{De}}^2+k_\perp^2\rho_s^2)^{1/2}}\left(\omega_{\mathrm{pi}}^2\frac{k_z^2}{k^2}+\omega_{\mathrm{pd}}^2\right)^{1/2} \tag{4.6.7}$$

where $\rho_s = \lambda_{\mathrm{De}}\omega_{\mathrm{pi}}/\omega_{\mathrm{ci}} \equiv C_{\mathrm{S}}/\omega_{\mathrm{ci}}$. Equation (4.6.7) shows that for $k_z/k \gg \omega_{\mathrm{pd}}/\omega_{\mathrm{pi}}$ and $k_\perp\rho_s \gg k\lambda_{\mathrm{De}}$, we have

$$\omega \approx \frac{k_z C_{\mathrm{S}}}{(1+k_\perp^2\rho_s^2)^{1/2}} \tag{4.6.8}$$

which is the frequency of the DIA waves in an external magnetic field. On the other hand, in the opposite limit $k_z/k \ll \omega_{\mathrm{pd}}/\omega_{\mathrm{pi}}$, equation (4.6.7) gives

$$\omega = \frac{k\lambda_{\mathrm{De}}\omega_{\mathrm{pd}}}{(1+k^2\lambda_{\mathrm{De}}^2+k_\perp^2\rho_s^2)^{1/2}} \tag{4.6.9}$$

which is the frequency of a DA-like wave.

(iii) We focus on the limits $kV_{Tj}, \omega_{cd} \ll \omega \ll \omega_{ci}, \omega_{ce}k_z/k_\perp$ for which we have

$$\chi_j \approx \frac{\omega_{pj}^2 k_\perp^2}{\omega_{cj}^2 k^2} - \frac{\omega_{pj}^2 k_z^2}{\omega^2 k^2} \tag{4.6.10}$$

and χ_d is given by equation (4.6.5). Hence from $1 + \sum_s \chi_s = 0$ we obtain

$$\omega = \left[\omega_{pe}^2(1+\delta_i)\frac{k_z^2}{k^2} + \omega_{pd}^2\right]^{1/2}\left(1 + \frac{\omega_{pi}^2}{\omega_{ci}^2}\frac{k_\perp^2}{k^2}\right)^{-1/2} \tag{4.6.11}$$

where $\delta_i = m_e n_{i0}/m_i n_{e0}$. Since $(\omega_{pi}/\omega_{ci})k_\perp/k \gg 1$, equation (4.6.11) for $\omega_{pe}(1+\delta_i)^{1/2}k_z/k \gg \omega_{pd}$ and $\delta_i \ll 1$ gives the frequency of finite-frequency convective cells in a dusty plasma, namely

$$\omega \approx \left(\frac{n_{e0}m_i}{n_{i0}m_e}\right)^{1/2}\frac{k_z}{k_\perp}\omega_{ci}. \tag{4.6.12}$$

On the other hand, for $\omega_{pd} \gg \omega_{pe}(1+\delta_i)^{1/2}k_z/k \equiv \Omega_p$ and $(\omega_{pi}/\omega_{ci})k_\perp/k \gg 1$, we have from equation (4.6.11)

$$\omega \approx \frac{\omega_{pd}}{\omega_{pi}}\left(1 + \frac{\Omega_p^2}{\omega_{pd}^2}\right)^{1/2}\frac{k}{k_\perp}\omega_{ci}. \tag{4.6.13}$$

(iv) Next we consider the modified lower-hybrid waves and use the approximations $kV_{Tj}, \omega_{cd}, \omega_{ci} \ll \omega \ll \omega_{ce}$. Thus using $1 + \sum_s \chi_s = 0$, equation (4.6.10) and $\chi_{i,d} = -\omega_{pi,pd}^2/\omega^2$ we have (Shukla 1992)

$$\omega = \frac{\omega_{pi}}{(1+\delta_e)^{1/2}}\left(1 + \frac{m_i n_{e0} k_z^2}{m_e n_{i0} k_\perp^2}\right)^{1/2} \tag{4.6.14}$$

where $\delta_e = \omega_{pe}^2 k_\perp^2/\omega_{ce}^2 k^2$. For $\delta_e \gg 1$ and $k_z \ll k_\perp$ equation (4.6.14) gives

$$\omega = \left(\frac{n_{i0}}{n_{e0}}\right)^{1/2}(\omega_{ce}\omega_{ci})^{1/2}\left(1 + \frac{m_i n_{e0} k_z^2}{m_e n_{i0} k_\perp^2}\right)^{1/2}. \tag{4.6.15}$$

The various cases discussed above are valid for static dust grains. We now include the dynamics of magnetized dust grains and discuss the possibility of extremely low-frequency electrostatic dust cyclotron (EDC) waves for which we use the assumptions $\omega/k_z \ll V_{Te}$, $V_{Td} \ll |\omega - \omega_{cd}|/k_z$, $k_\perp/k_z \ll \omega_{ce}/\omega$ and $\rho_{Te} \ll k_\perp^{-1} \ll \rho_{Ti}$. The dielectric constant for the EDC waves is of the form

$$\epsilon(\omega, \boldsymbol{k}) = 1 + \frac{k_D^2}{k^2} + \frac{k_{Dd}^2}{k^2}\left[1 - \Lambda_0(b_d) - \frac{2\omega^2\Lambda_1(b_d)}{\omega^2 - \omega_{cd}^2}\right] \tag{4.6.16}$$

where $k_{Dd} = \omega_{pd}/V_{Td}$ is the dust Debye wavenumber and $\rho_{Ts} = V_{Ts}/\omega_{cs}$ is the thermal gyroradius of species s. Assuming that the EDC wave frequency is close to ω_{cd}, we obtain from $\epsilon(\omega, \boldsymbol{k}) = 0$ the frequency of long-wavelength (namely $b_d \ll 1$) EDC waves

$$\omega \approx \omega_{cd} \left(1 + \frac{k_\perp^2 C_D^2}{\omega_{cd}^2}\right)^{1/2}. \tag{4.6.17}$$

4.6.2 Electromagnetic waves

There also exists a number of different low-frequency (in comparison with ω_{ci}) electromagnetic waves in a homogeneous dusty magnetoplasma. The dispersion properties of such electromagnetic modes are discussed as follows.

4.6.2.1 *Circularly polarized waves*

We consider the propagation of low-frequency, right-hand circularly polarized electromagnetic waves parallel to the external magnetic field $B_0\hat{\boldsymbol{z}}$. The wave electric field is denoted by $\boldsymbol{E} = E_\perp(\hat{\boldsymbol{x}} + \mathrm{i}\hat{\boldsymbol{y}})\exp(-\mathrm{i}\omega t + \mathrm{i}k_z z)$. The dispersion relation for $\omega \ll \omega_{ce}$, $|\omega - \omega_{cs}| \gg k_z V_{Ts}$ and $k^2\rho_{Ts}^2 \ll 1$ is (Shukla 1992)

$$\frac{k_z^2 c^2}{\omega^2} = 1 + \frac{\omega_{pe}^2}{\omega\omega_{ce}} - \frac{\omega_{pi}^2}{\omega(\omega_{ci} + \omega)} + \frac{\omega_{pd}^2}{\omega(\omega_{cd} - \omega)}. \tag{4.6.18}$$

When the wave frequency is much smaller than the dust gyrofrequency, equation (4.6.18) reduces to

$$\frac{k_z^2 c^2}{\omega^2} = 1 + \frac{n_{e0}\omega_{pi}^2}{n_{i0}\omega\omega_{ci}} - \frac{\omega_{pi}^2}{\omega\omega_{ci}} + \frac{\omega_{pi}^2}{\omega_{ci}^2} + \frac{Z_{d0}n_{d0}\omega_{pi}^2}{n_{i0}\omega\omega_{ci}} + \frac{\omega_{pd}^2}{\omega_{cd}^2} \tag{4.6.19}$$

which yields the modified Alfvén wave frequency

$$\omega = \frac{k_z V_A}{[1 + (V_A^2/c^2) + n_{d0}m_d/n_{i0}m_i]^{1/2}} \tag{4.6.20}$$

where $V_A = B_0/(4\pi n_{i0}m_i)^{1/2} \equiv \omega_{ci}/\omega_{pi}$ is the Alfvén speed. On the other hand, for $\omega_{cd} \ll \omega \ll \omega_{ci}$, equation (4.6.18) gives

$$\frac{k_z^2 c^2 + \omega_{pd}^2}{\omega^2} = 1 - \frac{Z_{d0}n_{d0}}{n_{i0}}\frac{\omega_{pi}^2}{\omega\omega_{ci}} + \frac{\omega_{pi}^2}{\omega_{ci}^2}. \tag{4.6.21}$$

The solution of equation (4.6.21) is

$$\omega = \tfrac{1}{2}\omega_d \pm \tfrac{1}{2}(\omega_D^2 + 4\omega_a^2)^{1/2} \tag{4.6.22}$$

where $\omega_d = Z_{d0}n_{d0}\omega_{ci}/n_{i0}(1 + V_A^2/c^2)$ and $\omega_a^2 = (k_z^2 + \omega_{pd}^2/c^2)V_A^2/(1 + V_A^2/c^2)$. Equation (4.6.22) exhibits new circularly polarized electromagnetic waves associated with charged dust grains.

4.6.2.2 Mixed modes: dynamic dust

The properties of mixed modes are described by the magnetohydrodynamic (MHD) equations of dusty plasmas for the case in which the dust inertia plays an important role (Shukla and Rahman 1996, Birk *et al* 1996). The dynamics of low-frequency (in comparison with the ion gyrofrequency) electromagnetic waves in our dusty plasma is governed by the dust continuity equation

$$\frac{\partial n_\mathrm{d}}{\partial t} + \nabla \cdot (n_\mathrm{d}\boldsymbol{v}_\mathrm{d}) = 0 \tag{4.6.23}$$

the inertial dust momentum equation

$$m_\mathrm{d}n_\mathrm{d}\left(\frac{\partial}{\partial t} + \boldsymbol{v}_\mathrm{d}\cdot\nabla\right)\boldsymbol{v}_\mathrm{d} = -Z_{\mathrm{d}0}n_\mathrm{d}e\left(\boldsymbol{E} + \frac{1}{c}\boldsymbol{v}_\mathrm{d}\times\boldsymbol{B}\right) - \nabla p_\mathrm{d} \tag{4.6.24}$$

the inertialess ion momentum equation

$$0 = n_\mathrm{i}e\left(\boldsymbol{E} + \frac{1}{c}\boldsymbol{v}_\mathrm{i}\times\boldsymbol{B}\right) - \nabla p_\mathrm{i} \tag{4.6.25}$$

the inertialess electron momentum equation

$$0 = -n_\mathrm{e}e\left(\boldsymbol{E} + \frac{1}{c}\boldsymbol{v}_\mathrm{e}\times\boldsymbol{B}\right) - \nabla p_\mathrm{e} \tag{4.6.26}$$

Faraday's law

$$\frac{\partial \boldsymbol{B}}{\partial t} = -c\nabla\times\boldsymbol{E} \tag{4.6.27}$$

Ampère's law

$$\nabla\times\boldsymbol{B} = \frac{4\pi e}{c}(n_\mathrm{i}\boldsymbol{v}_\mathrm{i} - n_\mathrm{e}\boldsymbol{v}_\mathrm{e} - Z_{\mathrm{d}0}n_\mathrm{d}\boldsymbol{v}_\mathrm{d}) \equiv \frac{4\pi}{c}\boldsymbol{J} \tag{4.6.28}$$

together with $\nabla\cdot\boldsymbol{B} = 0$ and the electron and ion continuity equations. Here $p_s = n_s k_\mathrm{B} T_s$ is the pressure and $\boldsymbol{E}$ and $\boldsymbol{B}$ are the electric and magnetic fields, respectively. Furthermore, in equation (4.6.28) we have neglected the displacement current as we are concerned with electromagnetic waves whose phase velocity is much smaller than the speed of light. We have also assumed $Z_{\mathrm{d}0}/m_\mathrm{d}$ to be uniform. Adding equations (4.6.24)–(4.6.26) and making use of equation (4.6.28) we obtain

$$m_\mathrm{d}n_\mathrm{d}\left(\frac{\partial}{\partial t} + \boldsymbol{v}_\mathrm{d}\cdot\nabla\right)\boldsymbol{v}_\mathrm{d} = -\nabla\left(P + \frac{B^2}{8\pi}\right) + \frac{1}{4\pi}(\boldsymbol{B}\cdot\nabla)\boldsymbol{B} \tag{4.6.29}$$

where $P = \sum_s p_s \equiv n_\mathrm{d}k_\mathrm{B}(T_\mathrm{d} + Z_{\mathrm{d}0}T_\mathrm{i}) + n_\mathrm{e}k_\mathrm{B}(T_\mathrm{e} + T_\mathrm{i})$. Eliminating $\boldsymbol{E}$ from equations (4.6.24) and (4.6.27) we have

$$\frac{\partial \boldsymbol{B}}{\partial t} = \nabla\times(\boldsymbol{v}_\mathrm{d}\times\boldsymbol{B}) + \frac{ck_\mathrm{B}}{Z_{\mathrm{d}0}en_\mathrm{d}^2}\nabla n_\mathrm{d}\times\nabla T_\mathrm{d} + \frac{m_\mathrm{d}}{Z_{\mathrm{d}0}e}\nabla\times\left[\left(\frac{\partial}{\partial t} + \boldsymbol{v}_\mathrm{d}\cdot\nabla\right)\boldsymbol{v}_\mathrm{d}\right]. \tag{4.6.30}$$

Equations (4.6.23), (4.6.29) and (4.6.30) are the desired MHD equations for a dusty magnetoplasma in which the dust inertia dominates. They govern the dynamics of various low-frequency electromagnetic waves in a magnetized dusty plasma. In order to study these waves, we Fourier transform equations (4.6.23), (4.6.29) and (4.6.30) by letting $n_{\rm d} = n_{\rm d0} + n_{\rm d1}$ and $\boldsymbol{B} = B_0\hat{z} + \boldsymbol{B}_1$, where $n_{\rm d1} \ll n_{\rm d0}$, $\boldsymbol{B}_1 \ll B_0\hat{z}$ and $n_{\rm e0}(T_{\rm e} + T_{\rm i}) \ll n_{\rm d0}(T_{\rm d} + Z_{\rm d0}T_{\rm i})$. Combining Fourier-transformed equations (4.6.23), (4.6.29) and (4.6.30), we obtain the dispersion relation (Shukla and Rahman 1996)

$$(\omega^2 - \omega_{\rm DA}^2)D_{\rm m}(\omega, \boldsymbol{k}) = \frac{\omega_{\rm DA}^2}{\omega_{\rm cd}^2}\omega^2 k^2 V_{\rm A}^2(\omega^2 - k^2 V_{\rm da}^2) \tag{4.6.31}$$

where $\omega_{\rm DA} = k_z V_{\rm DA}$ is the dust-Alfvén frequency

$$D_{\rm m}(\omega, \boldsymbol{k}) = \omega^4 - \omega^2 k^2 (V_{\rm DA}^2 + V_{\rm da}^2) + \omega_{\rm DA}^2 k^2 V_{\rm da}^2 \tag{4.6.32}$$

$V_{\rm DA} = B_0/(4\pi n_{\rm d0} m_{\rm d})^{1/2}$ is the dust Alfvén speed and $V_{\rm da} = [(Z_{\rm d0}k_{\rm B}T_{\rm i} + k_{\rm B}T_{\rm d})/m_{\rm d}]^{1/2}$ is the modified DA speed. We note that the dust-Alfvén and DA speeds are inversely proportional to $m_{\rm d}^{1/2}$, indicating that the dust inertia plays a major role in the wave dynamics. Equation (4.6.31), which exhibits a linear coupling between various dusty plasma modes, is a sixth-order polynomial in ω and can be readily analysed numerically. However, some interesting analytical results follow in several limiting cases, which are presented below.

(i) Perpendicular propagation ($k_z = 0$)

We first consider flute perturbations ($k_z = 0$) for which equation (4.6.31) gives (Rao 1993)

$$\omega = k_\perp (V_{\rm DA}^2 + V_{\rm da}^2)^{1/2} \tag{4.6.33}$$

which is the frequency of the dust-magnetosonic waves.

(ii) Parallel propagation ($k_\perp = 0$)

For the wave propagation along the external magnetic field lines, we obtain from equation (4.6.31)

$$k_z^2 V_{\rm DA}^2 = \frac{\omega^2 \omega_{\rm cd}}{(\omega_{\rm cd} \mp \omega)} \tag{4.6.34}$$

which is the dispersion relation for coupled dust cyclotron and dust-Alfvén waves. For $\omega \ll \omega_{\rm cd}$ equation (4.6.34) gives the dispersive dust-Alfvén wave frequency

$$\omega \approx k_z V_{\rm DA}\left(1 \pm \frac{k_z V_{\rm DA}}{2\omega_{\rm cd}}\right). \tag{4.6.35}$$

On the other hand, in the limit $\omega \gg \omega_{\rm cd}$, equation (4.6.34) reduces to

$$\omega \approx \frac{k_z^2 V_{\rm DA}^2}{\omega_{\rm cd}} \equiv \frac{k_z^2 c^2 \omega_{\rm cd}}{\omega_{\rm pd}^2} \tag{4.6.36}$$

which is the dust whistler frequency.

(iii) Oblique propagation

We use the approximations $k_z/k \ll 1$ and $\omega/k_\perp \ll V_{\rm da} \ll V_{\rm DA}$ in equation (4.6.31) and obtain the dispersion relation for the shear dust Alfvén waves as

$$\omega \approx k_z V_{\rm DA}(1 + k_\perp^2 \rho_{\rm a}^2)^{1/2} \tag{4.6.37}$$

where $\rho_{\rm a} = V_{\rm da}/\omega_{\rm cd}$. Furthermore, for $\omega \ll k_z V_{\rm DA}$ and $V_{\rm da} \ll V_{\rm DA}$, equation (4.6.31) yields

$$(\omega^2 - k_z^2 V_{\rm da}^2) = \frac{\omega^2}{\omega_{\rm cd}^2}(\omega^2 - k^2 V_{\rm da}^2) \tag{4.6.38}$$

which exhibits a coupling between the modified DA and dust cyclotron waves. When $\omega \sim k_z V_{\rm da}$, we have from equation (4.6.38)

$$\omega \approx \frac{k_z V_{\rm da}}{(1 + k_\perp^2 \rho_{\rm a}^2)^{1/2}} \tag{4.6.39}$$

which is the frequency of the dispersive DA waves in a magnetized dusty plasma.

4.7 Waves in Non-uniform Magnetoplasmas

It is well established that all plasma systems, especially dusty plasma systems, always contain some region of inhomogeneity capable of causing drift motions and associated waves in a magnetized dusty plasma. Thus, we consider here a non-uniform dusty magnetoplasma containing *immobile dust grains* and the equilibrium density gradient $\partial n_{s0}/\partial x$ (unperturbed plasma number densities $n_{s0}(x)$ are assumed to be inhomogeneous along the x-axis) and study the dispersion properties of low-frequency (in comparison with $\omega_{\rm ci}$), long-wavelength (in comparison with the ion gyroradius) electrostatic and electromagnetic waves. The external magnetic field $\hat{z}B_0$ is along the z-axis. The quasi-neutrality condition at equilibrium is given by equation (4.4.1). In the electric field ($\boldsymbol{E}_\perp = -\nabla_\perp\phi$) of low-frequency waves, the perpendicular components of the electron and ion fluid velocities are (Weiland 2000)

$$\boldsymbol{v}_{\rm e\perp} \approx \frac{c}{B_0}\hat{z} \times \nabla_\perp\phi - \frac{ck_{\rm B}T_{\rm e}}{eB_0 n_{\rm e0}}\hat{z} \times \nabla_\perp n_{\rm e1} \tag{4.7.1}$$

and

$$\boldsymbol{v}_{i\perp} \approx \frac{c}{B_0}\hat{z} \times \nabla_\perp \phi + \frac{ck_B T_i}{eB_0 n_{i0}}\hat{z} \times \nabla n_{i1} - \frac{c}{B_0 \omega_{ci}}\left(\frac{\partial}{\partial t} + \boldsymbol{u}_{i*} \cdot \nabla\right)\nabla_\perp \phi \quad (4.7.2)$$

where $\boldsymbol{u}_{i*} = (ck_B T_i/eB_0 n_{i0})\hat{z} \times \nabla n_{i0}(x)$ is the unperturbed ion diamagnetic drift velocity.

4.7.1 Electrostatic waves

We first consider propagation of coupled convective cells and dust drift-acoustic waves. Accordingly, we substitute equation (4.7.1) into the electron continuity equation and obtain

$$\frac{\partial n_{e1}}{\partial t} + \frac{c}{B_0}\hat{z} \times \nabla \phi \cdot \nabla n_{e0} + n_{e0}\frac{\partial v_{ez}}{\partial z} = 0 \quad (4.7.3)$$

where the parallel (to $\hat{z}$) component of the electron fluid velocity v_{ez} is determined by

$$\frac{\partial v_{ez}}{\partial t} = \frac{e}{m_e}\frac{\partial}{\partial z}\left(\phi - \frac{k_B T_e}{en_{e0}}\frac{\partial n_{e1}}{\partial z}\right). \quad (4.7.4)$$

Next, we substitute equations (4.7.1) and (4.7.2) into the charge conservation equation

$$\nabla \cdot (en_{i0}\boldsymbol{v}_i - en_{e0}\boldsymbol{v}_e) = 0 \quad (4.7.5)$$

by imposing the quasi-neutrality approximation ($n_{e1} \approx n_{i1}$), which is valid for a dense plasma in which $\omega_{pi} \gg \omega_{ci}$. We obtain

$$\frac{\partial \nabla_\perp^2 \phi}{\partial t} + \frac{\omega_{ci}^2}{\omega_{pi}^2}\frac{4\pi c}{B_0}\hat{z} \times \nabla(q_{d0}n_{d0}) \cdot \nabla \phi - \frac{B_0 \omega_{ci}}{c}\frac{\partial}{\partial z}\left(v_{iz} - \frac{n_{e0}}{n_{i0}}v_{ez}\right) = 0 \quad (4.7.6)$$

where the parallel component of the ion fluid velocity perturbation v_{iz} is determined from

$$\frac{\partial v_{iz}}{\partial t} = -\frac{e}{m_i}\frac{\partial}{\partial z}\left(\phi + \frac{3k_B T_i n_{i1}}{en_{i0}}\right). \quad (4.7.7)$$

Equations (4.7.3)–(4.7.7) are the desired equations for studying coupled convective cells and dust drift-ion acoustic waves in a dusty magnetoplasma. We now consider two limiting cases.

(i) $|\partial/\partial t| \gg V_{Te}|\partial/\partial z|$

Using $|\partial/\partial t| \gg V_{Te}\partial/\partial z$ and ignoring the parallel ion dynamics, we have from equations (4.7.4) and (4.7.6)

$$\frac{\partial v_{ez}}{\partial t} = \frac{e}{m_e}\frac{\partial \phi}{\partial z} \quad (4.7.8)$$

and

$$\frac{\partial \nabla_\perp^2 \phi}{\partial t} + \frac{\omega_{\rm ci}^2}{\omega_{\rm pi}^2} \frac{4\pi c}{B_0} \hat{z} \times \nabla(q_{\rm d0} n_{\rm d0}) \cdot \nabla\phi + \frac{n_{\rm e0} B_0 \omega_{\rm ci}}{n_{\rm i0} c} \frac{\partial v_{\rm ez}}{\partial z} = 0. \tag{4.7.9}$$

Assuming that $v_{\rm ez}$ and ϕ are proportional to $\exp(-{\rm i}\omega t + {\rm i}\boldsymbol{k}\cdot\boldsymbol{r})$, we obtain from equations (4.7.8) and (4.7.9) the linear dispersion relation (Mamun and Shukla 2000) for coupled modified convective cells and the Shukla–Varma (SV) mode (Shukla and Varma 1993)

$$\omega = \omega_{\rm sv} \pm \tfrac{1}{2}(\omega_{\rm sv}^2 + 4\omega_{\rm cc}^2)^{1/2} \tag{4.7.10}$$

where

$$\omega_{\rm sv} = -\frac{4\pi c \omega_{\rm ci}^2 k_y \partial(q_{\rm d0} n_{\rm d0})/\partial x}{B_0 k_\perp^2 \omega_{\rm pi}^2} \tag{4.7.11}$$

is the SV frequency (Shukla and Varma 1993) and

$$\omega_{\rm cc} = \left(\frac{n_{\rm e0}}{n_{\rm i0}}\right)^{1/2} (\omega_{\rm ce}\omega_{\rm ci})^{1/2} \frac{k_z}{k_\perp} \tag{4.7.12}$$

is the modified convective cell frequency (Okuda and Dawson 1973). We note that in a uniform plasma, the SV mode disappears.

(ii) $|\partial/\partial t| \ll V_{\rm Te}|\partial/\partial z|$

We consider coupled drift-DIA waves in the approximation $|\partial/\partial t| \ll V_{\rm Te}|\partial/\partial z|$. Here the inertialess electrons rapidly thermalize along the $\hat{z}$ direction and the corresponding electron number density perturbation is given by the Boltzmann relation

$$n_{\rm e1} \approx n_{\rm e0}(x) \frac{e\phi}{k_{\rm B} T_{\rm e}} \tag{4.7.13}$$

which follows from equation (4.7.4). Invoking the quasi-neutrality approximation $n_{\rm i1} = n_{\rm e1}$, we can substitute equation (4.7.13) into the ion continuity equation to obtain

$$\frac{\partial}{\partial t}(\phi - \rho_s^2 \nabla_\perp^2 \phi) - \rho_s^2 \omega_{\rm ci} \hat{z} \times \nabla \ln n_{\rm i0} \cdot \nabla\phi + \frac{n_{\rm i0} k_{\rm B} T_{\rm e}}{n_{\rm e0} e} \frac{\partial v_{\rm iz}}{\partial z} = 0. \tag{4.7.14}$$

By using equation (4.7.13) we can write equation (4.7.7) as

$$\frac{\partial v_{\rm iz}}{\partial t} = -\left(1 + 3\frac{n_{\rm e0} T_{\rm i}}{n_{\rm i0} T_{\rm e}}\right) \frac{e}{m_{\rm i}} \frac{\partial \phi}{\partial z}. \tag{4.7.15}$$

Fourier transforming equations (4.7.14) and (4.7.15) and combining them, we obtain the dispersion relation (Shukla *et al* 1991)

$$\omega = \frac{\omega_*}{2(1 + k_y^2 \rho_s^2)} \pm \frac{1}{2} \left[\frac{\omega_*^2}{(1 + k_y^2 \rho_s^2)^2} + 4\frac{k_z^2 C_{ss}^2}{1 + k_y^2 \rho_s^2} \right]^{1/2} \tag{4.7.16}$$

where $\omega_* = -(ck_B T_e/eB_0 n_{e0})k_y \partial n_{i0}/\partial x$ is the modified drift wave frequency and $C_{ss} = C_S(1 + 3n_{e0}T_i/n_{i0}T_e)^{1/2}$. When $\omega_* \gg k_z C_{ss}$ equation (4.7.16) yields

$$\omega = \frac{\omega_*}{1 + k_\perp^2 \rho_s^2} \tag{4.7.17}$$

which is the frequency of the dispersive dust drift waves.

4.7.2 Electromagnetic waves

To study electromagnetic waves that may exist in a non-uniform dusty magnetoplasma, we first consider different types of mixed modes (mixture of electrostatic and electromagnetic waves) and then a purely electromagnetic mode, namely a non-ducted dust whistler.

4.7.2.1 Mixed modes: static dust

We consider a low-β ($\beta = 8\pi n_0 k_B T/B_0^2 \ll 1$) plasma in which the parallel component of the electron fluid velocity is determined by equation (4.6.28), yielding

$$v_{ez} \approx \frac{c}{4\pi n_{e0} e} \nabla_\perp^2 A_z \tag{4.7.18}$$

where A_z is the parallel component of the vector potential. In obtaining equation (4.7.18) we set $\boldsymbol{B} = \nabla A_z \times \hat{z}$ and neglected the parallel components of the ion and dust current densities as well as the compressional magnetic field perturbation. Thus, the DIA and magnetosonic waves are decoupled in our low-β dusty plasma system. Substituting equations (4.7.1) and (4.7.18) into the electron continuity equation and letting $n_j = n_{j0}(x) + n_{j1}$, where $n_{j1} \ll n_{j0}$, we obtain

$$\frac{\partial n_{e1}}{\partial t} - \frac{c}{B_0} \hat{z} \times \nabla n_{e0} \cdot \nabla \phi + \frac{c}{4\pi e} \frac{\partial \nabla_\perp^2 A_z}{\partial z} = 0. \tag{4.7.19}$$

On the other hand, substitution of the ion fluid velocity (4.7.2) into the ion continuity equation yields

$$\frac{\partial n_{i1}}{\partial t} - \frac{c}{B_0} \hat{z} \times \nabla_\perp n_{i0} \cdot \nabla_\perp \phi - \frac{c n_{i0}}{B_0 \omega_{ci}} \left(\frac{\partial}{\partial t} + \boldsymbol{u}_{i*} \cdot \nabla_\perp \right) \nabla_\perp^2 \phi = 0. \tag{4.7.20}$$

Subtracting equation (4.7.20) from equation (4.7.19) and making use of Poisson's equation (namely $\nabla^2 \phi = 4\pi e(n_{e1} - n_{i1})$ for stationary dust grains), we obtain the modified ion vorticity equation

$$\left(\frac{\partial}{\partial t} + u_{i0} \frac{\partial}{\partial y} \right) \nabla_\perp^2 \phi + \frac{V_A^2}{c^2} \frac{\partial \nabla^2 \phi}{\partial t} + \omega_{ci} \delta_d \kappa_d \frac{\partial \phi}{\partial y} + \frac{V_A^2}{c} \frac{\partial \nabla_\perp^2 A_z}{\partial z} = 0 \tag{4.7.21}$$

where $u_{i0} = (ck_B T_i/eB_0 n_{i0}) \partial n_{i0}/\partial x$ is the y component of the unperturbed ion diamagnetic drift velocity, $\delta_d = q_{d0} n_{d0}/e n_{i0}$ and $\kappa_d = \partial \ln[(q_{d0} n_{d0}(x)]/\partial x$.

By using equations (4.7.1) and (4.7.18), the parallel component of the electron momentum equation can be written as

$$\left(\frac{\partial}{\partial t} + u_{e0}\frac{\partial}{\partial y}\right) A_z - \lambda_e^2 \frac{\partial \nabla_\perp^2 A_z}{\partial t} + c\frac{\partial}{\partial z}\left(\phi - \frac{k_B T_e}{e}\frac{n_{e1}}{n_{e0}}\right) = 0 \qquad (4.7.22)$$

where $u_{e0} = -(ck_B T_e/eB_0 n_{e0})\partial n_{e0}(x)/\partial x$ is the y component of the unperturbed electron diamagnetic drift velocity and $\lambda_e = c/\omega_{pe}$ is the electron skin depth.

Equations (4.7.19), (4.7.21) and (4.7.22) are the desired equations for the coupled drift-Alfvén–Shukla–Varma modes in a non-uniform dusty magnetoplasma. The dispersion relation can be derived by supposing that n_{e1}, ϕ and A_z are proportional to $\exp(-i\omega t + ik_y y + ik_z z)$. Accordingly, in the local approximation, when the wavelength is much smaller than the scalelength of the density gradient, we can Fourier transform equations (4.7.19), (4.7.21) and (4.7.22) and combine them to obtain the general dispersion relation (Pokhotelov *et al* 1999)

$$(\omega^2 - \omega\omega_m - \omega_{IA}^2 k_y^2 \rho_s^2)(\omega - \omega_{i*} - \omega_{sv}) = \omega_{IA}^2(\omega - \omega_{e*}) \qquad (4.7.23)$$

where

$$\omega_m = \frac{\omega_{e*}}{(1 + k_y^2\lambda_e^2)} \qquad (4.7.24)$$

is the magnetic drift wave frequency

$$\omega_{j*} = k_y u_{j0} \qquad (4.7.25)$$

is the drift wave frequency and

$$\omega_{IA} = \frac{k_z V_A}{(1 + k_y^2\lambda_e^2)^{1/2}} \qquad (4.7.26)$$

is the frequency of the inertial Alfvén waves. In deriving equation (4.7.23) we have assumed $(k^2/k_y^2)\omega_{ci}^2/\omega_{pi}^2 \ll 1$, where $k^2 = k_y^2 + k_z^2$. We now examine equation (4.7.23) in various limiting cases.

(i) $\omega_{j*} = 0$

For a homogeneous dusty plasma (namely $\omega_{j*} = 0$), equation (4.7.23) correctly reproduces the frequency of the dispersive Alfvén waves (Shukla and Stenflo 1999). When the parallel phase velocity (ω/k_z) of the dispersive Alfvén waves is much smaller than the electron thermal speed V_{Te}, we can neglect the parallel electron inertial effect (namely $k_y^2\lambda_e^2 \ll 1$) and obtain from (4.7.23)

$$\omega = k_z V_A(1 + k_y^2\rho_s^2)^{1/2} \qquad (4.7.27)$$

which is the frequency of the dispersive kinetic Alfvén waves in an intermediate-β ($m_e/m_i \ll \beta \ll 1$) plasma. On the other hand, for $\omega/k_z \gg V_{Te}$, we can neglect the parallel electron pressure gradient term (or the $k_y^2\rho_s^2$ term in comparison with unity), and obtain from equation (4.7.23)

$$\omega = \frac{k_z V_A}{(1 + k_y^2\lambda_e^2)^{1/2}} \tag{4.7.28}$$

which is the frequency of the dispersive inertial Alfvén waves in a very low-β plasma ($\beta \ll m_e/m_i$).

(ii) $\omega \gg \omega_m, \omega_{j*}$

We observe from equation (4.7.23) that for $\omega \gg \omega_m, \omega_{j*}$ the dispersive Alfvén waves are linearly coupled with the SV mode, $\omega = \omega_{sv}$. Specifically, in a cold ($T_j \rightarrow 0$) dusty plasma with $\omega/k_z \gg V_{Te}$ and $\omega \gg \omega_{i*}$, we obtain from equation (4.7.23)

$$\omega^2 - \omega\omega_{sv} - \frac{k_z^2 V_A^2}{1 + k_y^2\lambda_e^2} = 0 \tag{4.7.29}$$

which clearly shows that the coupling between the SV mode and the inertial Alfvén wave arises due to the parallel electron motion in the wave electric and magnetic fields.

Furthermore, in the limit $k_y\rho_s \rightarrow 0$ (or vanishing parallel electron pressure gradient force) and $\omega_{i*} = 0$, we obtain from equation (4.7.23)

$$[(1 + k_y^2\lambda_e^2)\omega - \omega_{e*}](\omega - \omega_{sv})\omega = k_z^2 V_A^2(\omega - \omega_{e*}) \tag{4.7.30}$$

which shows that the magnetostatic drift mode ($\omega = \omega_m$), the SV mode ($\omega = \omega_{sv}$), the inertial Alfvén wave ($\omega = \omega_{IA}$), and the electron drift mode ($\omega = \omega_{e*}$) are linearly coupled.

(iii) $k_z v_{ez} = 0$

When the parallel electron motion is completely neglected (namely $k_z v_{ez} = 0$), we see from equation (4.7.23) that the flute-like magnetostatic mode ($\omega = \omega_m$) and the modified SV mode ($\omega = \omega_{i*} + \omega_{sv}$) appear as independent normal modes of a non-uniform dusty magnetoplasma containing warm ions.

(iv) $k_y^2\lambda_e^2 \ll 1$

When the perpendicular wavelength is much larger than λ_e, we obtain from equation (4.7.23) for $\omega \gg \omega_{i*}$

$$(\omega^2 - \omega\omega_{sv} - k_z^2 V_A^2)(\omega - \omega_{e*}) = k_y^2\rho_s^2 k_z^2 V_A^2(\omega - \omega_{sv}) \tag{4.7.31}$$

which exhibits a coupling between the drift-kinetic Alfvén waves and the SV mode due to the finite Larmor radius correction of the ions at the electron temperature in a dusty plasma. Equation (4.7.31) resembles

$$(\omega^2 - \omega\omega_{i*} - k_z^2 V_A^2)(\omega - \omega_{e*}) = k_y^2 \rho_s^2 k_z^2 V_A^2 (\omega - \omega_{i*}) \tag{4.7.32}$$

which is the dispersion relation (Weiland 2000) of the coupled drift-kinetic Alfvén waves in a warm electron–ion magnetoplasma without charged dust grains.

4.7.2.2 Non-ducted dust whistlers

We have already shown in section 4.6 (e.g. equation (4.6.36)) that a whistler-like ducted mode (guided along the external magnetic field lines) can exist in a uniform dusty magnetoplasma. The ducted mode is referred to as the dust whistler because its frequency ($\omega = k_z^2 c^2 \omega_{cd}/\omega_{pd}^2$), which is much smaller than the ion gyrofrequency, is proportional (inversely proportional) to ω_{cd} (ω_{pd}^2). Since the group velocity of the dust whistlers increases with frequency, similar to the electron whistlers (Chen 1974) which have frequencies much smaller (much larger) than the electron (ion) gyrofrequency, low-frequency components shall travel slower than the higher-frequency components. Consequently, the dust whistlers would have the descending tone while observed at a location far away from the source region where the dust whistlers are excited. The dispersion characteristics of the dust whistlers can be employed for inferring the dust number density and dust charges in the source region.

We now consider the propagation of non-ducted (guided obliquely to the external magnetic field lines) dust whistlers in a dusty magnetoplasma containing equilibrium density and magnetic field inhomogeneities (Shukla 1999). We show that the plasma and magnetic field inhomogeneities cause spatio-temporal dampings of dust whistlers which are characterized by $kV_{Tj}, \omega_{cd} \ll \omega \ll \omega_{ci}, kc$. We suppose that in our non-uniform dusty plasma there exist an external magnetic field $\hat{z}B_0(x)$ and the density $n_{i0}(x) = n_{e0}(x) + Z_{d0}n_{d0}(x)$. In the presence of electromagnetic fields, the fluid velocities of the electrons, ions and dust grains are, respectively

$$\boldsymbol{v}_{e\perp} \approx \frac{c}{B_0}\boldsymbol{E}_\perp \times \hat{\boldsymbol{z}} \tag{4.7.33}$$

$$\boldsymbol{v}_{i\perp} \approx \frac{c}{B_0}\boldsymbol{E}_\perp \times \hat{\boldsymbol{z}} + \frac{c}{B_0\omega_{ci}}\frac{\partial \boldsymbol{E}_\perp}{\partial t} \tag{4.7.34}$$

$$\frac{\partial v_{ez}}{\partial t} = -\frac{e}{m_e}E_z \tag{4.7.35}$$

$$\frac{\partial v_{iz}}{\partial t} = \frac{e}{m_i}E_z \tag{4.7.36}$$

and

$$\frac{\partial \boldsymbol{v}_d}{\partial t} = -\frac{Z_{d0}e}{m_d}\boldsymbol{E} \tag{4.7.37}$$

where $\boldsymbol{E} = \boldsymbol{E}_\perp + E_z\hat{z}$ is the wave electric field, the subscript $\perp$ and z denote the components transverse and parallel to $\hat{z}$ and $\omega_{\text{ci}} = eB_0(x)/m_\text{i}c$.

The linear propagation of non-ducted dust whistlers is governed by Faraday's and Ampère's laws, which are, respectively, given by equations (4.6.27) and (4.6.28). Taking the curl of equation (4.6.27) and eliminating $\nabla \times \boldsymbol{B}$ by means of equation (4.6.28), we obtain by using equations (4.7.33)–(4.7.37)

$$c^2\nabla \times \nabla \times \boldsymbol{E} = -\frac{\omega_{\text{pd}}^2}{\omega_{\text{cd}}}\frac{\partial \boldsymbol{E}_\perp}{\partial t} \times \hat{z} - \frac{\omega_{\text{pi}}^2}{\omega_{\text{ci}}}\frac{\partial \boldsymbol{E}_\perp}{\partial t} - \omega_\text{p}^2 E_z\hat{z} - \omega_{\text{pd}}^2\boldsymbol{E} \tag{4.7.38}$$

where $\omega_\text{p} = (\omega_{\text{pe}}^2 + \omega_{\text{pi}}^2)^{1/2}$. We note that the first term on the right-hand side of equation (4.7.38) comes from the finite $\boldsymbol{E} \times \boldsymbol{B}_0$ current, whereas the second and fourth terms are, respectively, associated with the ion polarization drift and the dust acceleration by the wave electric field. The $\omega_\text{p}^2 E_z$ term in equation (4.7.38) represents the contribution of the parallel electron and ion currents. In the absence of the dust grains, the first and the fourth terms in the right-hand side of equation (4.7.38) would vanish. Assuming that the wave electric field is proportional to $\exp(-\text{i}\omega t)$, we obtain from equation (4.7.38)

$$\left(\nabla^2 - \frac{1}{\lambda_\text{d}^2}\right)\boldsymbol{E} - \nabla\nabla \cdot \boldsymbol{E} - \frac{\omega^2}{V_\text{A}^2}\boldsymbol{E}_\perp - \frac{\omega_\text{p}^2}{c^2}E_z\hat{z} + \text{i}\frac{\omega_{\text{pd}}^2\omega}{\omega_{\text{cd}}c^2}\boldsymbol{E}_\perp \times \hat{z} = 0 \tag{4.7.39}$$

where $\lambda_\text{d}(x) = c/\omega_{\text{pd}}(x)$ is the collisionless skin depth of the dust grains and $V_\text{A}(x) = B_0(x)/[4\pi n_{\text{i}0}(x)m_\text{i}]^{1/2}$.

Let us now focus on non-ducted dust whistlers by assuming that the parallel component of the wave electric field E_z is much smaller than the E_x and E_y components. Using $\omega^2 \ll k^2V_\text{A}^2$ and $\omega_{\text{pd}}^2 \ll k^2c^2$, and considering propagation of the dust whistlers in the x–z plane, we obtain from equation (4.7.39)

$$\frac{\partial^2 E_x}{\partial z^2} + \text{i}\frac{\omega_{\text{pd}}^2\omega}{\omega_{\text{cd}}c^2}E_y = 0 \tag{4.7.40}$$

and

$$\left(\frac{\partial^2}{\partial x^2} + \frac{\partial^2}{\partial z^2}\right)E_y - \text{i}\frac{\omega_{\text{pd}}^2\omega}{\omega_{\text{cd}}c^2}E_x = 0. \tag{4.7.41}$$

The dispersion relation of non-ducted dust whistlers in a uniform plasma is obtained from equations (4.7.40) and (4.7.41) by assuming that the x and y components (namely E_x and E_y) of the electric field vector $\boldsymbol{E}_\perp$ are proportional to $\exp(\text{i}k_x x + \text{i}k_z z)$. We have

$$\omega = \frac{k_z(k_z^2 + k_x^2)^{1/2}c^2\omega_{\text{cd}}}{\omega_{\text{pd}}^2} \tag{4.7.42}$$

which yields the magnetic field-aligned dust whistler wave frequency when $k_x = 0$. Physically, the dust whistlers are associated with the oscillating non-zero $\boldsymbol{E} \times \boldsymbol{B}_0$ plasma current when the dust grains are present.

However, in a non-uniform dusty plasma the electric field components E_x and E_y may vary as $E_x(x)\exp(\mathrm{i}k_z z)$ and $E_y(x)\exp(\mathrm{i}k_z z)$. Furthermore, for our purposes, the equilibrium density $n_{\mathrm{d}0}(x)$ and magnetic field B_0 have typical profiles of the form $n_0(1 + x/L_n)$ and $B_0(1 + x/L_{\mathrm{B}})$, where L_n and L_{B} are the scale sizes of the density and magnetic field inhomogeneities, respectively. Thus, equations (4.7.40) and (4.7.41) can be combined to yield

$$\frac{\partial^2 E_x}{\partial x^2} + \lambda_1 E_x + \lambda_2 x E_x + \lambda_3 x^2 E_x = 0 \tag{4.7.43}$$

where $\lambda_1 = k_z^2(\omega^2 - \omega_{\mathrm{w}}^2)/\omega_{\mathrm{w}}^2$, $\lambda_2 = 2\omega^2 k_z^2(k_n - k_{\mathrm{b}})/\omega_{\mathrm{w}}^2$, $\lambda_3 = (\omega^2 k_z^2/\omega_{\mathrm{w}}^2)(k_n^2 - k_{\mathrm{b}}^2 - 4k_n k_{\mathrm{b}})$, $k_n = \partial \ln n_{\mathrm{d}0}/\partial x \equiv L_n^{-1}$, and $k_{\mathrm{b}} = \partial \ln B_0/\partial x \equiv L_{\mathrm{B}}^{-1}$. The frequency of the ducted dust whistler is defined as $\omega_{\mathrm{w}} = k_z^2 c^2 \omega_{\mathrm{cd}}/\omega_{\mathrm{pd}}^2$, where ω_{cd} and ω_{pd} are the values of the dust gyro and dust plasma frequencies at $x = 0$. We have assumed that $|x| \ll |L_n|, |L_{\mathrm{B}}|$. It is seen that for $\lambda_3 < 0$ the solution of equation (4.7.43) is bounded and is (for large $|x|$)

$$E_x = E_0 \exp\left[-\frac{\sqrt{|\lambda_3|}}{2}(x - x_0)^2\right] \tag{4.7.44}$$

where $x_0 = \lambda_2/2|\lambda_3|$. The dust whistlers would not propagate and are damped. On the other hand, for $\lambda_3 > 0$, equation (4.7.43) has for large $|x|$ the solution

$$E_x = E_0 \exp\left[-\frac{\sqrt{\lambda_3}}{2}(x + x_0)^2\right] \tag{4.7.45}$$

which indicates that non-localized non-ducted whistlers would carry energy outwards and are damped.

We now consider the propagation of non-ducted dust whistlers in the presence of a uniform external magnetic field and a parabolic density profile of the form $n_{\mathrm{d}0} = n_{\mathrm{d}0}(1 - x^2/L_n^2)$. Here equation (4.7.43) for $x^2 \ll L_n^2$ is replaced by a parabolic cylinder equation

$$\frac{\partial^2 E_x}{\partial x^2} + \lambda_1 E_x - \lambda_4 x^2 E_x = 0 \tag{4.7.46}$$

where $\lambda_4 = \omega^2 k_z^2 k_n^2/2\omega_{\mathrm{w}}^2$. The eigenfunction solutions of equation (4.7.46) with outgoing wave boundary conditions are

$$E_x = H_n(\sqrt{\sigma}x)\exp(-\sigma x^2/2) \tag{4.7.47}$$

where $\sigma = \sqrt{\lambda_4}$, H_n are the Hermite polynomials and $n = 0, 1, 2$. We note that the eigenfunction decays exponentially with x^2, so that the width of the mode can be approximated by $2/\lambda_4^{1/4}$.

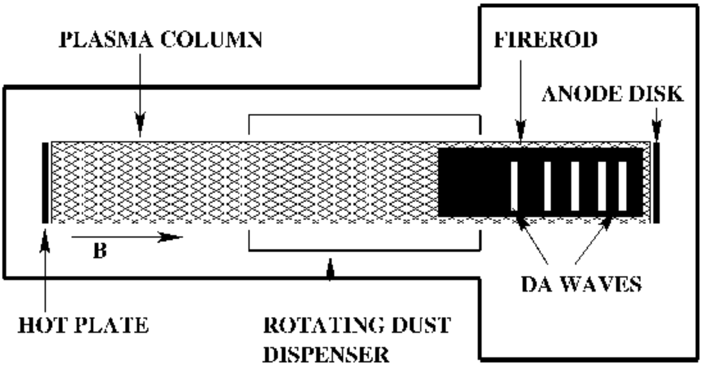

Figure 4.2. Schematic illustration of the experimental set-up for producing a confined dusty plasma where the DA waves are observed (after Thompson *et al* 1999).

4.8 Experimental Observations

We have described different types of waves/modes that are theoretically found to exist in unmagnetized and magnetized dusty plasmas. Recently, some of these waves, namely the DA waves, the DIA waves and the DL waves have also been observed in laboratory experiments (Barkan *et al* 1995a, 1996, D'Angelo *et al* 1996, Pieper and Goree 1996, Morfill *et al* 1997, Homann *et al* 1997, Thompson *et al* 1999, Thomas and Watson 2000). This section is concerned with the excitation of these waves in laboratory experiments.

4.8.1 Dust acoustic waves

The low-frequency DA waves have been observed (Barkan *et al* 1995a, Thompson *et al* 1999) by using the experimental set-up schematically shown in figure 4.2. The potassium plasma column of a Q-machine was surrounded over its end portion ($\sim$30 cm in length) by a rotating dust dispenser that continually recycled the dust particles (kaolin). The average grain size was around 5 μm (approximately 90% of the dust grains had sizes in between 1 and 15 μm). The lifetime of the dust grain in the plasma column was around 0.1 s. The DA waves with periods comparable to or longer than 0.1 s could not evidently be studied in this device. So a suitable modification was made by using an anode double layer (shown in figure 4.2) to trap and confine the negatively charged dust grains in the Q-machine for much longer times. A neutral gas (generally nitrogen at a pressure of 60–80 mTorr was introduced into the device and a bias voltage ($\sim$200 V) was applied to a small anode disc (of $\sim$1.6 cm diameter) located near the far end of the plasma column. This produces a cylindrical double layer (fire-rod) within which the space potential is $\sim$55 V that is above the space potential of the surrounding K^+-electron plasma. Thus, negatively charged dust grains can

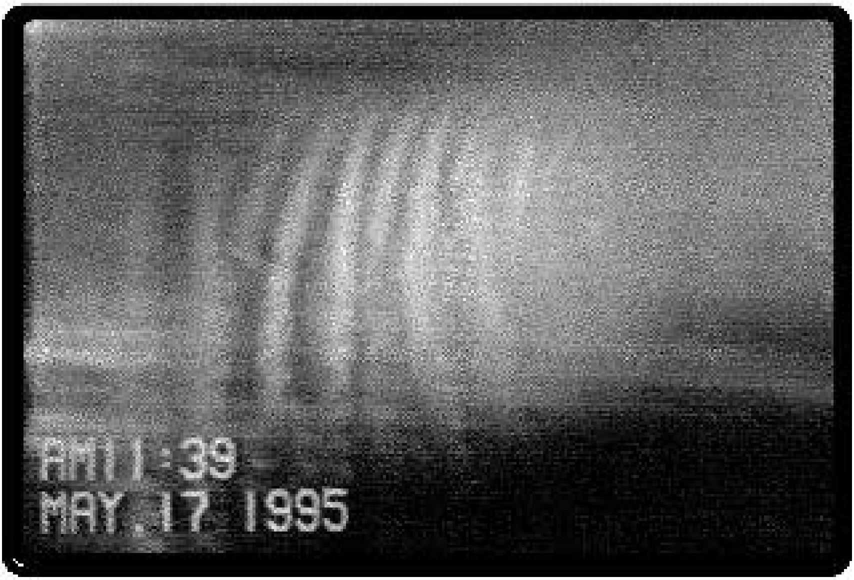

Figure 4.3. A typical single-frame image of a DA wave pattern recorded in the video camera (after Thompson *et al* 1999).

be indefinitely trapped within the fire-rod, provided their mass is not too large. Not only at the edges of the fire-rod but also within it there exists an electric field which (on axis) is directed away from the disc electrode and has an average magnitude of $\simeq$1 V cm^{-1}. Under these conditions, the DA waves are observed through a side port, within the dust-loaded fire-rod. The waves appear as soon as the kaolin dust is introduced into the fire-rod. The observations were made by using a simple flashlight and a video camera. A typical wave pattern with a wavelength of $\sim$0.6 cm is shown in figure 4.3.

The speed with which the pattern moved from right to left away from the disc electrode towards the Q-machine hot plate was measured from a succession of such pictures. A characteristic plot of the position of some given wave feature versus time of arrival yields a propagation speed of $\sim$9 cm s^{-1} (Barkan *et al* 1995a). The frequency of the wave with a wavelength of 0.6 cm and a speed of 9 cm s^{-1} turns out to be 15 Hz. The other parameters used for this experiment (Barkan *et al* 1995a) are $n_{\rm d}/n_{\rm e} \simeq 10^{-4}$, $Z_{\rm d} \simeq 4 \times 10^4$ and $m_{\rm d} \simeq 10^{-9}$ g. For the parameters of Barkan *et al* (1995a) one finds that equation (4.2.11) yields a DA wave frequency (Rao *et al* 1990) which is in perfect agreement with the experimentally observed value.

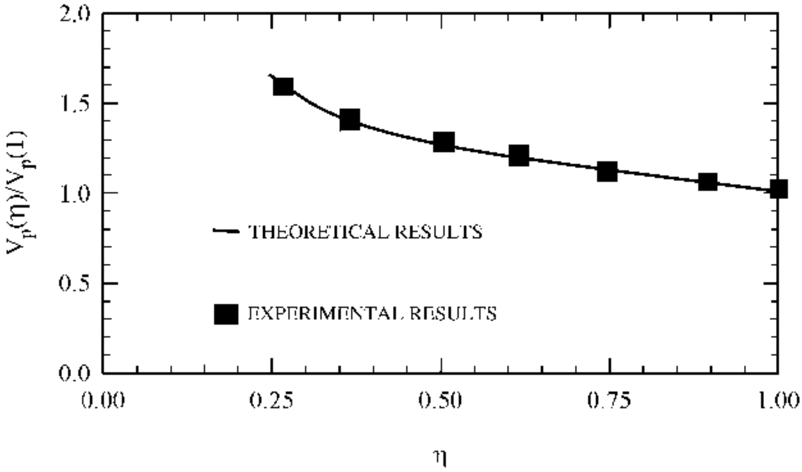

Figure 4.4. The variation of the quantity $V_p(\eta)/V_p(1)$ with η (after Barkan *et al* 1996), where $\eta = n_{e0}/n_{i0}$. The theoretical results (based on fluid model) correspond to $v_0 = c_s$, where v_0 (c_s) is the plasma drift (ion-acoustic) speed.

4.8.2 Dust ion-acoustic waves

DIA waves have been experimentally excited (Barkan *et al* 1996, Merlino *et al* 1998) by means of a grid inserted into the plasma column produced in a Q-machine as shown in figure 1.8. A fully ionized, magnetized ($B_0 \leq 4.0 \times 10^3$ G) potassium plasma column of a Q-machine was surrounded over its end portion ($\sim$30 cm in length) by a rotating dust dispenser that continually recycled the dust particles (kaolin). The grid was placed perpendicular to the magnetic field and approximately 3 cm upstream from the dust dispenser.

The grid was biased at several volts negative with respect to the space charge potential and a tone-burst sinusoidal voltage signal of frequency 20–80 kHz and amplitude 4–5 V peak to peak was applied to it. This produced near the grid a density perturbation which then travelled down the column, into the region of the dust dispenser, as the DIA waves. By means of an axially moveable Langmuir probe (a disc of 1 cm in diameter) the phase and amplitude measurements could be performed at various axial locations and the wave phase speed V_p, the wavelength λ and the attenuation length λ_a were determined with ($\eta < 1$) and without ($\eta = 1$) the dust. The quantity $V_p(\eta)/V_p(1)$ is plotted as a function of η in figure 4.4. The other parameters for this experiment (Barkan *et al* 1996) are $n_i \simeq n_e \simeq 10^6$ cm^{-3}, $T_e \simeq T_i \simeq 2320$ K, $r_d \simeq 5$ μm and $m_d \simeq 10^{-9}$ g. As the wavelength corresponding to these plasma parameters (the number density and the temperature) is $\sim$0.3 cm, the launcher grid had to have the rather unusual feature of an inter-wire spacing of $\sim$0.5 cm in order to obtain an appropriate density modulation by the applied sinusoidal voltage. A further condition that

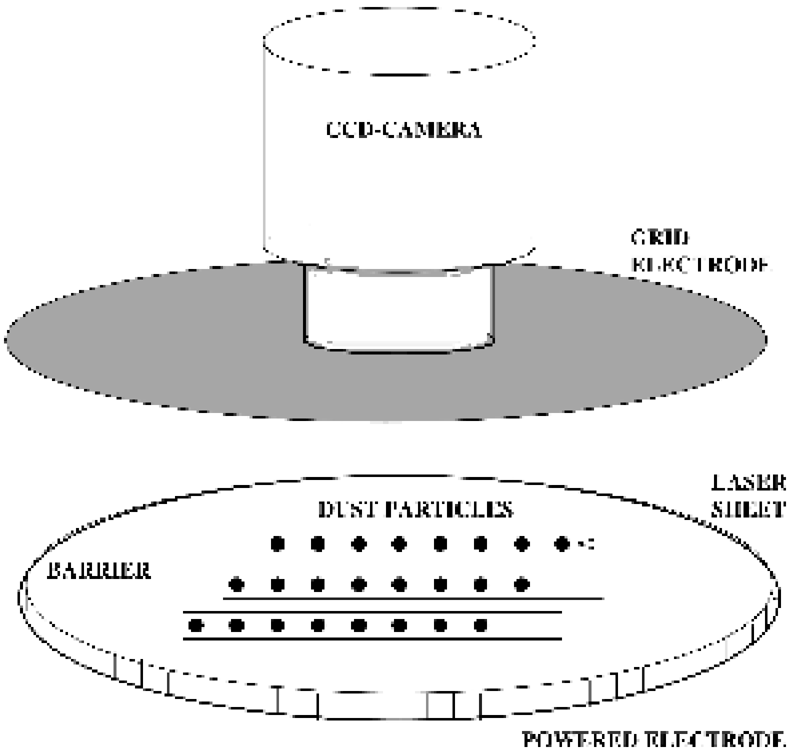

Figure 4.5. The experimental set-up for the observation of laser excited DL waves (after Homann *et al* 1997).

the ion gyroradius is comparable to or larger than the grid wire spacing required that the magnetic field is not much above 1000 G at which the gyroradius of 0.2 eV K^+ ions is $\sim$0.3 cm. It is obvious from figure 4.4 that (i) the DIA wave is indeed a normal mode in a dusty plasma and (ii) the phase speed of the DIA wave increases when $\eta < 1$. The experimental observations of enhanced phase speed and reduced damping of the DIA waves are consistent with the theoretical prediction of Shukla and Silin (1992).

4.8.3 Dust lattice waves

DL waves have been experimentally observed by Morfill *et al* (1997) and Homann *et al* (1997). The experimental arrangements of the latter are shown in figure 4.5. The dust particles are trapped in the lower sheath of a parallel plate. The upper electrode is grounded and the lower one is powered at a frequency of 13.56 MHz and a rf power of 7 W. To arrange the dust grains in a linear chain, a rectangular barrier of 4 mm height and $x = 90$ mm $\times$ $y = 20$ mm inner spacing is put

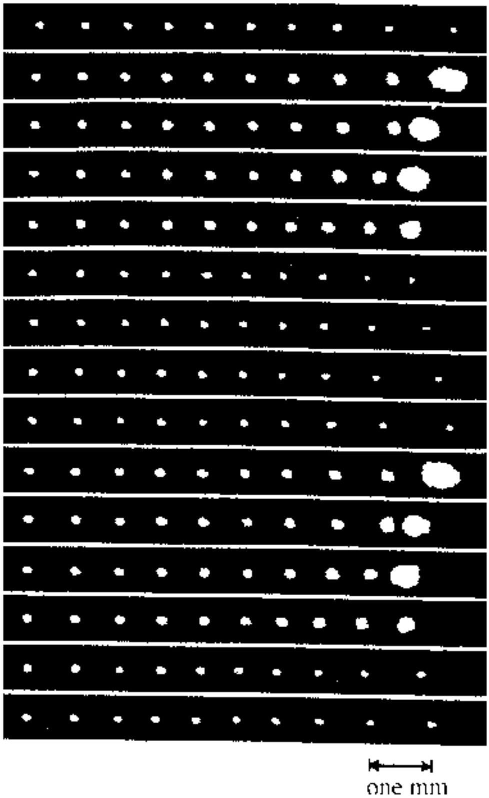

Figure 4.6. The sequences of 15 snapshots for a linear chain arrangement of 10 particles.

on the lower electrode (as shown in figure 4.5). In this experiment a dozen of mono-disperse spherical melamine formaldehyde plastic particles of radius $r_{\rm d} = (4.75 \pm 0.15)$ μm and mass density $\rho_{\rm d} = 1.514$ g cm^{-3} are inserted into the plasma chamber. These particles arrange in a linear chain with an interparticle distance of $a = 930$ μm at a gas pressure of 22 Pa. The particles are illuminated by a horizontally expanded thin laser sheet for observation. The whole arrangement is viewed in scattered light from the top with a video camera. The beam (20 mW, 690 nm) of a laser diode is focused on the first particle. The laser's radiation pressure pushes the first particle, thus exciting the chain. Although the focus diameter is larger than the particle diameter, the particle must be close to the inner focus to be moved by the laser. The other particles are in the defocused region and are, therefore, almost unaffected by the beam. The laser diode is switched on and off by a transistor–transistor–logic (TTL) signal. The switching frequency of the TTL signal used in the experiment of Homann *et al* (1997) was varied between 0.4 and 3 Hz with a constant duty cycle of 50%.

The mechanism of the excitation is mainly attributed to the radiation pressure. Homann *et al* (1997) used a 20 mW laser for which the radiation pressure force is of the order of or smaller than the gravitational force and electrostatic field force, but much larger than all other related forces (e.g. thermophoretic force). Because of the narrow width of the potential well in the y direction (due to the barrier) and z direction due to the balance of the gravitational force and the electrostatic field force, the dust particles can only move in the x direction. An impression of their oscillatory motion, whose dispersion relation (equation (4.5.6)) can be described by that of the LDL waves, is shown in figure 4.6. It shows a series of video images at the frequency of 1.3 Hz and at a pressure of 22 Pa. The time-step between each video image is 100 ms. It is clearly seen that only the first particle (the rightmost particle which is seen by the bright spot of scattered light) is pushed by the exciting laser. It should be noted that the exciting laser was on for images 2–5 and 10–13 and was off in the other images.

Chapter 5

Instabilities

5.1 Introduction

We have discussed in chapter 4 the properties of electrostatic and electromagnetic waves in dusty plasmas near thermodynamical equilibrium. The normal wave modes represent stable elementary excitations. The collective modes suffer a certain amount of collisional and non-collisional (Landau and dust charge fluctuation induced) damping.

However, most dusty plasmas in space and laboratories are far from thermodynamic equilibrium. A non-equilibrium plasma is characterized by the presence of unstable collective modes whose amplitudes grow exponentially. There are several mechanisms by which the plasma waves can be driven at non-thermal levels when free energy sources are available in our dusty plasma system. For example, dusty plasmas can be subjected to the influence of external force fields which create flows of particles, momentum and energy. Furthermore, the spatial variation of the physical quantities, such as the pressure, the intensity of the dc electric and magnetic fields, the plasma flow velocity and the dust grain charge, are involved in laboratory and space plasmas. The energies of laser/radar beams and radio-frequency waves can also be coupled to normal modes of dusty plasmas.

There are new classes of instabilities associated with the ion drag force, ionization, dust charge gradient, etc in dusty plasmas, besides the usual Buneman, Kelvin–Helmholtz, Rayleigh–Taylor, pressure gradient and parametric (stimulated scattering) instabilities. The studies of instabilities are of great importance because they are helpful for understanding the origin of enhanced fluctuations as well as of dust voids and nonlinear dust oscillations in space and laboratory dusty plasmas. This chapter is devoted to linear and nonlinear mechanisms that cause instabilities of numerous electrostatic modes in dusty plasmas.

5.2 Streaming Instabilities

As shown in many textbooks (e.g. Ichimaru 1973, Chen 1974, Alexandrov *et al* 1984) the dispersion relations for electrostatic waves in the presence of free energy sources can be derived by Fourier analysing the Vlasov–Poisson system of equations or the hydrodynamic equations that are supplemented by Poisson's equation. The hydrodynamic as well as kinetic instabilities (Havnes 1988) of low-frequency electrostatic waves in a multi-component dusty plasma can be studied from the dispersion relation that includes an equilibrium drift of the plasma particles. The general dispersion relation of electrostatic waves in a dusty plasma (without dust charge fluctuation) is

$$1 + \sum_{s=\mathrm{e,i,d}} \chi_s = 0 \tag{5.2.1}$$

where χ_s is the dielectric susceptibility. The expression for the latter in the presence of streaming plasma particles in unmagnetized and magnetized plasmas will be discussed and analysed below.

5.2.1 Unmagnetized plasmas

The dielectric susceptibility χ_s for an unmagnetized collisional plasma has the form (Rosenberg 1996)

$$\chi_s = \frac{1}{k^2\lambda_{\mathrm{D}s}^2} \frac{[1 + \xi_s Z(\xi_s)]}{[1 + \mathrm{i}(\nu_{\mathrm{sn}}/\sqrt{2}\mathrm{k}\mathrm{V}_{\mathrm{Ts}})\mathrm{Z}(\xi_{\mathrm{s}})]} \tag{5.2.2}$$

where $\xi_s = (\omega - kV_{s0}\cos\theta + \mathrm{i}\nu_{s\mathrm{n}})/\sqrt{2}kV_{\mathrm{T}s}$, θ is the angle between the wavevector $\boldsymbol{k}$ and the equilibrium streaming velocity $\boldsymbol{V}_{s0}$ of the particle species s, and $Z(\xi_s)$ is the plasma dispersion function of Fried and Conte (1961). The collision frequency $\nu_{s\mathrm{n}}$ of each species is assumed to be primarily due to their collisions with stationary neutrals. The streaming of charged particles in a dusty plasma can be set up by a constant electric field $\boldsymbol{E}_0$. At equilibrium, when the electric force is balanced by a collisional drag force, we have $\boldsymbol{V}_{\mathrm{e}0} = -e\boldsymbol{E}_0/m_{\mathrm{e}}\nu_{\mathrm{en}}$ and $\boldsymbol{V}_{\mathrm{i}0} = e\boldsymbol{E}_0/m_{\mathrm{i}}\nu_{\mathrm{in}}$ for the electron and ion streaming velocities, respectively. We now consider several interesting cases for instabilities in dusty plasmas.

5.2.1.1 Hydrodynamic instability

We first focus on hydrodynamic instability in a dusty plasma. The resonance interaction between a dust mode and a streaming plasma component produces a two-stream or Buneman-type hydrodynamic instability. We consider that the ions are streaming against the dust grains. Assuming $\xi_{\mathrm{e}} \ll 1$, $\xi_{\mathrm{i,d}} \gg 1$, $\nu_{\mathrm{in}}, \nu_{\mathrm{dn}}, kV_{\mathrm{Td}} \ll \omega \ll \nu_{\mathrm{en}} \ll kV_{\mathrm{Te}}$ and $|\omega - kV_{\mathrm{i}0}\cos\theta| \gg kV_{\mathrm{Ti}}$, we obtain from equations (5.2.1) and (5.2.2)

$$1+\frac{1}{k^2\lambda_{\mathrm{De}}^2}-\frac{\omega_{\mathrm{pi}}^2}{(\omega-kV_{\mathrm{i0}}\cos\theta)^2}-\frac{\omega_{\mathrm{pd}}^2}{\omega^2}=0. \tag{5.2.3}$$

Letting $\omega = kV_{\mathrm{i0}}\cos\theta+\Omega$ in equation (5.2.3) and assuming

$$\Omega \ll kV_{\mathrm{i0}}\cos\theta \simeq \omega_{\mathrm{de}}=\frac{k\lambda_{\mathrm{De}}\omega_{\mathrm{pd}}}{(1+k^2\lambda_{\mathrm{De}}^2)^{1/2}}\equiv\frac{kC_{\mathrm{De}}}{(1+k^2\lambda_{\mathrm{De}}^2)^{1/2}} \tag{5.2.4}$$

we obtain

$$\Omega^3=\tfrac{1}{2}\omega_{\mathrm{di}}^2\omega_{\mathrm{de}} \tag{5.2.5}$$

where

$$\omega_{\mathrm{di}}=\frac{k\lambda_{\mathrm{De}}\omega_{\mathrm{pi}}}{(1+k^2\lambda_{\mathrm{De}}^2)^{1/2}}\equiv\frac{kC_{\mathrm{S}}}{(1+k^2\lambda_{\mathrm{De}}^2)^{1/2}}. \tag{5.2.6}$$

Equation (5.2.5) has the solution

$$\Omega=\frac{1}{2^{1/3}}\left(1+\mathrm{i}\frac{\sqrt{3}}{2}\right)\left(\frac{\omega_{\mathrm{di}}}{\omega_{\mathrm{de}}}\right)^{2/3}\omega_{\mathrm{de}} \tag{5.2.7}$$

which predicts an instability with the growth rate

$$\omega_{\mathrm{i}}=\frac{\sqrt{3}}{2^{4/3}}\left(\frac{\omega_{\mathrm{di}}}{\omega_{\mathrm{de}}}\right)^{2/3}\omega_{\mathrm{de}}. \tag{5.2.8}$$

5.2.1.2 Kinetic instability

To study kinetic instability involving wave–particle interactions, we consider the following situations.

(i) DIA waves

We consider the excitation of the DIA waves in the presence of streaming electrons and stationary dust grains. Assuming $\xi_{\mathrm{e}} \ll 1$, $\xi_{\mathrm{i,d}} \gg 1$, $\nu_{\mathrm{in}}, kV_{\mathrm{Ti}}, \nu_{\mathrm{dn}}, \omega_{\mathrm{pd}}, kV_{\mathrm{Td}} \ll \omega \ll \nu_{\mathrm{en}} \ll kV_{\mathrm{Te}}$, we obtain from equations (5.2.1) and (5.2.2)

$$1+\frac{1}{k^2\lambda_{\mathrm{De}}^2}\left[1+\mathrm{i}\sqrt{\frac{\pi}{2}}\frac{(\omega-kV_{\mathrm{e0}}\cos\theta)}{kV_{\mathrm{Te}}}\right]-\frac{\omega_{\mathrm{pi}}^2}{\omega^2}=0. \tag{5.2.9}$$

Letting $\omega=\omega_{\mathrm{r}}+\mathrm{i}\omega_{\mathrm{i}}$ into equation (5.2.9), where $\omega_{\mathrm{i}} \ll \omega_{\mathrm{r}}=\omega_{\mathrm{di}}$, we obtain the growth rate of the DIA waves

$$\omega_{\mathrm{i}}=\sqrt{\frac{\pi}{8}}\frac{1}{k^2\lambda_{\mathrm{De}}^2}\frac{|kV_{\mathrm{e0}}\cos\theta-\omega_{\mathrm{di}}|}{kV_{\mathrm{Te}}}\frac{\omega_{\mathrm{di}}^3}{\omega_{\mathrm{pi}}^2} \tag{5.2.10}$$

for

$$V_{\mathrm{e0}}\cos\theta>\frac{C_{\mathrm{S}}}{(1+k^2\lambda_{\mathrm{De}}^2)^{1/2}}. \tag{5.2.11}$$

(ii) DA waves

We now consider the instability of the DA waves in the presence of streaming ions. For $\xi_{e,i} \ll 1$, $\xi_{\rm d} \gg 1$ and $\nu_{\rm dn}, kV_{\rm Td} \ll \omega \ll \nu_{\rm en} \ll kV_{\rm Te}$, equations (5.2.1) and (5.2.2) yield (Rosenberg 1993)

$$1 + \frac{1}{k^2\lambda_{\rm D}^2} + {\rm i}\frac{1}{k^2\lambda_{\rm Di}^2}\sqrt{\frac{\pi}{2}}\frac{\omega - kV_{\rm i0}\cos\theta}{kV_{\rm Ti}} - \frac{\omega_{\rm pd}^2}{\omega^2} = 0. \qquad (5.2.12)$$

As before, letting $\omega = \omega_{\rm r} + {\rm i}\omega_{\rm i}$ into equation (5.2.12), where $\omega_{\rm i} \ll \omega_{\rm r} = kC_{\rm D}/(1+k^2\lambda_{\rm D}^2)^{1/2} \equiv \omega_{\rm da}$, we notice that there exists an oscillatory instability of the DA waves when

$$V_{\rm i0}\cos\theta > \frac{\omega_{\rm da}}{k} = \frac{C_{\rm D}}{(1+k^2\lambda_{\rm D}^2)^{1/2}}. \qquad (5.2.13)$$

The growth rate of that instability is

$$\omega_{\rm i} \approx \sqrt{\frac{\pi}{8}}\frac{1}{k^2\lambda_{\rm Di}^2}\frac{|kV_{\rm i0}\cos\theta - \omega_{\rm da}|}{kV_{\rm Ti}}\frac{\omega_{\rm da}^3}{\omega_{\rm pd}^2}. \qquad (5.2.14)$$

(iii) Collisional effects

We finally consider the ion–dust two-stream regime in a collisional dusty plasma with streaming ions and non-streaming electrons and dust grains (namely $V_{\rm e0,d0} = 0$). Assuming $\xi_{\rm e} \ll 1$, $\xi_{\rm i,d} \gg 1$, $\nu_{\rm in}| \ll |\omega - kV_{\rm i0}\cos\theta|$ and $\nu_{\rm dn}, kV_{\rm Td} \ll \omega \ll \nu_{\rm en} \ll kV_{\rm Te}$, we obtain from equations (5.1.1) and (5.1.2)

$$1 - \frac{\omega_{\rm pi}^2}{A_{\rm e}(\omega - kV_{\rm i0}\cos\theta)^2}\left[1 - \frac{{\rm i}\nu_{\rm in}}{(\omega - kV_{\rm i0}\cos\theta)}\right] - \frac{\omega_{\rm pd}^2}{A_{\rm e}\omega^2} = 0 \qquad (5.2.15)$$

where $A_{\rm e} = 1 + (k\lambda_{\rm De})^{-2}$. For $|\omega| \ll \nu_{\rm in}$, $kV_{\rm i0}\cos\theta \sim \omega_{\rm pi}/\sqrt{A_{\rm e}}$, equation (5.2.15) has an approximate solution (Rosenberg 1996, Winske and Rosenberg 1998)

$$\omega \approx \frac{(1+{\rm i})\omega_{\rm pd}}{\sqrt{2}}\left(\frac{\omega_{\rm pi}}{\nu_{\rm in}}\right)^{1/2}\frac{1}{A_{\rm e}^{3/4}} \qquad (5.2.16)$$

which yields an oscillatory dissipative instability whose growth rate is $(\omega_{\rm pd}/\sqrt{2}A_{\rm e}^{3/4})(\omega_{\rm pi}/\nu_{\rm in})^{1/2}$.

5.2.2 Magnetized plasmas

We now discuss the instabilities of electrostatic waves in a dusty plasma embedded in a uniform external magnetic field $\hat{z}B_0$. In the presence of a dc electric field $\boldsymbol{E}_0 = -\hat{\boldsymbol{x}}E_0$ (as shown in figure 5.1), the plasma particles in a weakly collisional plasma ($\nu_{s{\rm n}} \ll \omega_{{\rm c}s}$) would have a cross-field ($\boldsymbol{E}_0 \times \boldsymbol{B}_0$) drift velocity

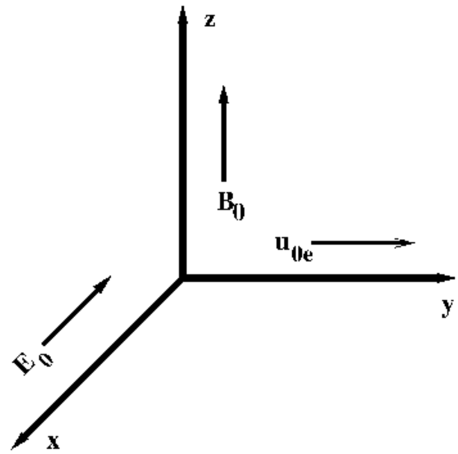

Figure 5.1. The $\boldsymbol{E}_0 \times \boldsymbol{B}_0$ plasma particle drift.

$\boldsymbol{u}_0 = \hat{\boldsymbol{y}} c E_0/B_0 (\equiv \hat{\boldsymbol{y}} u_0)$ in the y direction. On the other hand, in a magnetoplasma with $\nu_{\mathrm{en}} \ll \omega_{\mathrm{ce}}$ and $\nu_{\mathrm{in}} \gg \omega_{\mathrm{ci}}$ (Rosenberg and Shukla 2000) the magnetized electrons have an $\boldsymbol{E}_0 \times \boldsymbol{B}_0$ drift, while the unmagnetized ions would have a drift $\boldsymbol{u}_{\mathrm{i}0} = -\hat{\boldsymbol{x}} e E_0/m_{\mathrm{i}}\nu_{\mathrm{in}}$. The presence of some other external sources (e.g. magnetic field aligned electron and ion currents) may cause the charged particles to drift (with a speed v_{s0}) along the z-axis as well. The unperturbed plasma particle distribution function in a plasma with $\nu_{s\mathrm{n}} \ll \omega_{\mathrm{c}s}$ can be modelled as

$$f_{s0} = n_{s0} \left(\frac{m_s}{2\pi k_{\mathrm{B}} T_s}\right)^{3/2} \exp\left(-\frac{m_s[v_x^2 + (v_y - u_0)^2 + (v_z - v_{s0})^2]}{2k_{\mathrm{B}} T_s}\right). \tag{5.2.17}$$

The dispersion relation for electrostatic waves in a magnetized dusty plasma with the distribution function (5.2.17) is also given by equation (5.2.1), but here we have to replace the electron and ion susceptibilities by (Schmidt and Gary 1973)

$$\chi_{j=\mathrm{e,i}} = \frac{1}{k^2\lambda_{\mathrm{D}j}^2} \frac{\left[1 + \sum_{n=-\infty}^{\infty} \xi_{jn} Z(\xi_{jn}) \Gamma_n(b_j)\right]}{\left[1 + \mathrm{i}\sum_{n=-\infty}^{\infty} (\nu_{jn}/\sqrt{2} k_z V_{\mathrm{T}j}) Z(\xi_{jn}) \Gamma_n(b_j)\right]} \tag{5.2.18}$$

and the dust susceptibility by

$$\chi_{\mathrm{d}} = \frac{1}{k^2\lambda_{\mathrm{Dd}}^2} \frac{\left[1 + \sum_{n=-\infty}^{\infty} \xi_{\mathrm{d}} Z(\xi_{\mathrm{d}})\right]}{\left[1 + \mathrm{i}\sum_{n=-\infty}^{\infty} (\nu_{\mathrm{dn}}/\sqrt{2} k_z V_{\mathrm{Td}}) Z(\xi_{\mathrm{d}})\right]} \tag{5.2.19}$$

for $\omega \gg \omega_{\mathrm{cd}}$ and $b_{\mathrm{d}} \ll 1$. We have denoted

$$\xi_{jn} = \frac{\omega - k_y u_0 - k_z v_{j0} + \mathrm{i}\nu_{jn} - n\omega_{\mathrm{c}j}}{\sqrt{2} k_z V_{\mathrm{T}j}}$$

and

$$\xi_d = \frac{\omega - k_y u_0 - k_z v_{d0} + i\nu_{dn}}{\sqrt{2} k V_{Td}}.$$

We now consider a collisionless dusty magnetoplasma without the dc electric field and focus on both hydrodynamic and kinetic instabilities.

5.2.2.1 Hydrodynamic instability

We first consider the ion–dust two-stream instability of long-wavelength (namely $b_s \ll 1$) modes. Assuming $\xi_e \ll 1, \xi_{i,d} \ll 1, \omega_{cd}, kV_{Td}, k_z v_{d0} \ll \omega \ll \nu_{en} \ll k_z V_{Te}$, and $\nu_{in}, k_z V_{Ti} \ll |\omega - k_z v_{i0}| \ll \omega_{ci}$, we can reduce equations (5.2.1), (5.2.18) and (5.2.19) to the form

$$1 - \frac{\omega_{pi}^2 k_z^2}{A_b(\omega - k_z v_{i0})^2 k^2} - \frac{\omega_{pd}^2}{A_b \omega^2} = 0 \tag{5.2.20}$$

where $A_b = 1 + (k\lambda_{De})^{-2} + \omega_{pi}^2 k_\perp^2/\omega_{ci}^2 k^2$. For $k_z v_{i0} \gg \omega$ equation (5.2.20) gives

$$\omega_r \simeq \omega_i \simeq \left(\frac{\omega_{pi} k_z}{\omega_{pd} k}\right)^{1/3} \frac{\omega_{pd}}{A_b^{1/2}} \tag{5.2.21}$$

with the maximum growth rate at $k_z v_{i0} \simeq \omega_{pi} k_z / k A_b^{1/2}$.

5.2.2.2 Kinetic instability

To study kinetic instability in a dusty magnetoplasma, we consider two types of electrostatic modes, namely electrostatic ion-cyclotron (EIC) waves and electrostatic dust cyclotron (EDC) waves.

(i) EIC waves

We consider kinetic instability of EIC waves ($\omega \sim \omega_{ci}$) in a collisionless dusty plasma in the presence of an equilibrium electron flow along $\hat{z}$. For $\xi_e \ll 1, b_e \ll 1, |\omega - k_z v_{e0}| \ll k_z V_{Te}, |\omega - n\omega_{ci}| \gg k_z V_{Ti}$, and $\nu_{dn}, kV_{Td} \ll \omega \ll \nu_{en} \ll k_z V_{Te}$, the various dielectric susceptibilities are of the form (Chow and Rosenberg 1995)

$$\chi_e \approx 1 + \frac{1}{k^2 \lambda_{De}^2}\left[1 + i\sqrt{\frac{\pi}{2}} \frac{(\omega - k_z v_{e0})}{k_z V_{Te}}\right] \tag{5.2.22}$$

$$\chi_i \approx \frac{1}{k^2 \lambda_{Di}^2}\left\{1 - \Gamma_1(b_i)\frac{\omega}{\omega - \omega_{ci}} - \frac{1 - \Gamma_0(b_i)}{b_i} + i\sqrt{\frac{\pi}{2}} \frac{\omega}{k_z V_{Ti}} \Gamma_0(b_i) \exp\left[-\left(\frac{\omega - \omega_{ci}}{\sqrt{2} k_z V_{Ti}}\right)^2\right]\right\} \tag{5.2.23}$$

and $\chi_d \approx -\omega_{pd}^2/\omega^2$. When $\omega \simeq \omega_{ci} \gg \omega_{pd}$, the dust contribution to the dispersion relation is small, namely $\chi_d \ll \chi_i$. The dust influences the instability only via the quasi-neutrality condition, but not through its dynamics. Hence using equations (5.2.1), (5.2.22) and (5.2.23) and letting $\omega = \omega_r + i\omega_i$, we obtain

$$\omega_r \approx \omega_{ci}(1+\delta_s)^{1/2} \tag{5.2.24}$$

and the growth rate (Chow and Rosenberg 1995)

$$\omega_i \approx \sqrt{\frac{\pi}{8}}\frac{(\omega_r-\omega_{ci})^2}{\Gamma_1(b_i)\omega_{ci}}\left\{\frac{n_{e0}T_i}{n_{i0}T_e}\frac{k_z v_{e0}-\omega_r}{k_z V_{Te}} - \Gamma_1(b_i)\frac{\omega_r}{k_z V_{Ti}}\exp\left[-\left(\frac{\omega_r-\omega_{ci}}{\sqrt{2}k_z V_{Ti}}\right)^2\right]\right\} \tag{5.2.25}$$

where we have denoted

$$\delta_s = \frac{\Gamma_1(b_i)}{1-\Gamma_1(b_i)-b_i^{-1}[1-\Gamma_0(b_i)]+n_{e0}T_i(1+k^2\lambda_{De}^2)/n_{i0}T_e}.$$

Equation (5.2.25) admits an oscillatory instability of the EIC waves when $k_z v_{e0} > \omega_r \gg \omega_i$. For $b_i \ll 1$ and $k^2\lambda_{De}^2 \ll 1$ we have $\delta_s \approx k_\perp^2 C_S^2/\omega_{ci}^2$ and $\omega_r \approx \omega_{ci}(1+k_\perp^2 C_S^2/\omega_{ci}^2)^{1/2}$. The corresponding growth rate is

$$\omega_i \approx \sqrt{\frac{\pi}{8}}\frac{1}{k_\perp^2\lambda_{De}^2}\frac{|k_z v_{e0}-\omega_r|}{k_z V_{Te}}\frac{(\omega_r^2-\omega_{ci}^2)^2}{\omega_r\omega_{pi}^2} \tag{5.2.26}$$

which far exceeds the ion cyclotron damping rate, given by the second term in the curly bracket in the right-hand side of equation (5.2.25).

(ii) EDC waves

The kinetic instability of EDC waves (D'Angelo 1990) with $\xi_e \ll 1$, $\omega \ll \nu_{en} \ll k_z V_{Te}$, $\nu_{in} \ll kV_{Ti}$, $|\omega-\omega_{cd}| \gg kV_{Td}$ and $\rho_{Te} \ll k_\perp^{-1} \ll \rho_{Ti}$ in the presence of the streaming ions can be investigated by means of the dispersion relation

$$1+\frac{1}{k^2\lambda_D^2}+\frac{1}{k^2\lambda_{Dd}^2}\left[1-\Gamma_0(b_d)-\frac{2\omega^2\Gamma_1(b_d)}{(\omega^2-\omega_{cd}^2)}\right]+i\sqrt{\frac{\pi}{2}}\frac{1}{k^2\lambda_{Di}^2}\frac{\omega-k_z v_{i0}}{kV_{Ti}}=0. \tag{5.2.27}$$

Letting $\omega = \omega_r + i\omega_i$ into equation (5.2.27), where $\omega_i \ll \omega_r$, we obtain

$$\omega_r = \frac{\omega_{cd}}{(1-\Xi)^{1/2}} \tag{5.2.28}$$

and the growth rate

$$\omega_i \approx \sqrt{\frac{\pi}{32}}\frac{|k_z v_{i0}-\omega_r|}{kV_{Ti}}\frac{\lambda_{Dd}^2}{\lambda_{Di}^2}\frac{(\omega_r^2-\omega_{cd}^2)^2}{\omega_{cd}^2\omega_r\Gamma_1(b_d)} \tag{5.2.29}$$

where

$$\Xi = 1 - \frac{\lambda_{\mathrm{D}}^2}{\lambda_{\mathrm{Dd}}^2} \frac{2\Gamma_1(b_{\mathrm{d}})}{(1 + k^2\lambda_{\mathrm{D}}^2 + \lambda_{\mathrm{D}}^2[1 - \Gamma_0(b_{\mathrm{d}})]/\lambda_{\mathrm{Dd}}^2)}. \tag{5.2.30}$$

Equation (5.2.29) exhibits that the EDC waves would grow if $k_z v_{\mathrm{i0}} > \omega_{\mathrm{r}}$. For $b_{\mathrm{d}} \ll 1$ and $k^2\lambda_{\mathrm{D}}^2 \ll 1$ the growth rate is

$$\omega_{\mathrm{i}} \approx \sqrt{\frac{\pi}{8}} \frac{1}{k_\perp^2 \lambda_{\mathrm{Di}}^2} \frac{|k_z v_{\mathrm{i0}} - \omega_{\mathrm{r}}|}{k V_{\mathrm{Ti}}} \frac{(\omega_{\mathrm{r}}^2 - \omega_{\mathrm{cd}}^2)^2}{\omega_{\mathrm{pd}}^2 \omega_{\mathrm{r}}} \tag{5.2.31}$$

with $\omega_{\mathrm{r}} = \omega_{\mathrm{cd}}(1 + k_\perp^2 C_{\mathrm{D}}^2/\omega_{\mathrm{cd}}^2)^{1/2}$.

5.2.3 Boundary effects

We have discussed instabilities of numerous electrostatic waves in an infinite plasma. However, for laboratory dusty plasmas those instabilities have to be reconsidered in a longitudinally bounded dusty plasma system. Accordingly, we discuss an example of the ion beam instability in a collisionless unmagnetized bounded dusty plasma (Rosenberg and Shukla 1998). We assume that the streaming ions, which comprise an ion beam, flow from a grounded grid at $z = 0$ in the dusty plasma to a target at $z = L$. The grid and the target have infinite extent in the x and y directions. In the steady state, the zeroth-order drifts in the z direction are $V_{\mathrm{i0}} \equiv U_0 \gg V_{\mathrm{Ti}}$ and $V_{\mathrm{e0}} = V_{\mathrm{d0}} = 0$.

The one-dimensional DIA wave behaviour is governed by the continuity and momentum equations for the ion and dust fluids, supplemented by a Boltzmann distribution (equation (4.2.1)) for the electrons and Poisson's equation for the wave potential ϕ. From the linearized equations for the DIA waves, we easily obtain the dispersion relation by assuming that the density perturbations and the wave potential vary as $\exp(-\mathrm{i}\omega t + \mathrm{i}kz)$. The result for an unbounded plasma is

$$k^2 \left[1 + \frac{k_{\mathrm{De}}^2}{k^2} - \frac{\omega_{\mathrm{pi}}^2}{(\omega - kU_0)^2} - \frac{\omega_{\mathrm{pd}}^2}{\omega^2}\right] = 0. \tag{5.2.32}$$

We consider the effect of longitudinal boundaries on the instability analysis (Iizuka *et al* 1985). Two roots of equation (5.2.32) for $\omega \ll kU_0$ are

$$k_{1,2} \approx \pm \frac{\omega_{\mathrm{pi}}}{U_0} \left(\frac{1 - \frac{U_0^2}{C_{\mathrm{S}}^2}}{1 - \frac{\omega_{\mathrm{pd}}^2}{\omega^2}} \right)^{1/2} \left[1 \pm \frac{\left(1 - \frac{\omega_{\mathrm{pd}}^2}{\omega^2}\right)^{1/2}}{\left(1 - \frac{U_0^3}{C_{\mathrm{S}}^3}\right)} \frac{\omega}{\omega_{\mathrm{pi}}} \right]. \tag{5.2.33}$$

It is straightforward to obtain a dispersion relation for a bounded dusty plasma in the frequency domain $\omega_{\mathrm{pi}} \gg \omega \simeq (\omega_{\mathrm{pd}}^2 \omega_{\mathrm{pi}})^{1/3} > \omega_{\mathrm{pd}}$. The procedure (Iizuka *et al* 1985) involves using the other two roots of equation (5.2.32), which come from the spatial derivative $\partial^2\phi/\partial z^2$, expressing the perturbations in the system using these four roots and using the following boundary conditions on the potential perturbation and the perturbed ion density and velocity: $\phi(z=0)=\phi(z=L)=0$ (the potential perturbations are assumed to be zero at the end electrodes) and $n_{i1}(z=0)=v_i(z=0)=0$ (since the unperturbed ion beam is injected at the grid). This yields (Rosenberg and Shukla 1998)

$$\sin\vartheta+\frac{\omega_{pd}^2}{2\omega^2}\vartheta\cos\vartheta+i\frac{\omega}{\omega_{pi}}\frac{X}{\vartheta}\left[X^2\frac{\sin\vartheta}{\vartheta}+2(\cos\vartheta-1)\right]=0 \qquad (5.2.34)$$

where $\vartheta^2=X^2-D^2$, $X=\omega_{pi}L/U_0$ and $D=k_{De}L$. We note that $\vartheta^2>0$ requires $n_{i0}T_e/n_{e0}T_i>U_0^2/V_{Ti}^2$ in the dusty plasma.

We consider the solutions of equation (5.2.34) in two regimes; one corresponding to an ion–dust Buneman-type instability driven by the ion beam in which case the dust dynamics are retained, and the other corresponding to the Pierce instability of the ion beam. Now retaining the dust dynamics, we find that equation (5.2.34) admits a strongly unstable solution when $\vartheta\approx\pi(2m-1)$, where $m=1,2,3,\ldots$. At $\vartheta=(2m-1)\pi=S\pi$ equation (5.2.34) gives (Rosenberg and Shukla 1998)

$$\frac{\omega_{pd}^2}{\omega^2}+i\frac{\omega}{\omega_{pi}}\left[\frac{8}{S\pi}\left(1+\frac{k_{De}^2L^2}{S^2\pi^2}\right)^{1/2}\right]\approx 0. \qquad (5.2.35)$$

An unstable root of equation (5.2.35) is

$$\frac{\omega}{\omega_{pd}}=\frac{(\sqrt{3}+i)}{2\left(1+\frac{k_{De}^2L^2}{S^2\pi^2}\right)^{1/6}}\left(\frac{S\pi}{8}\right)^{1/3}\left(\frac{\omega_{pi}}{\omega_{pd}}\right)^{1/3}. \qquad (5.2.36)$$

We can also define a characteristic current associated with this ion–dust Buneman instability when $\vartheta=S\pi$. Since from the latter condition we have $\omega_{pi}^2=k_{De}^2U_0^2+S^2\pi^2/L^2$, the ion beam current $I_i=en_{i0}U_0\pi R_b^2$ is given by

$$I_i\sim R_b^2\frac{m_i}{4e}\frac{S^2\pi^2}{L^2}U_0^3\left(1+\frac{k_{De}^2L^2}{S^2\pi^2}\right) \qquad (5.2.37)$$

where R_b is the beam radius. We note that for $m=1$ at $\vartheta=\pi$, the ion beam current is smaller than the characteristic current for the usual Buneman instability of the electron beam in a bounded electron beam plasma system. This is due to $V_{Te}\gg U_0\gg V_{Ti}$ for the ion beam case, whereas for the electron beam case we have $U_0\gg V_{Te}$.

An aperiodic instability of the ion beam can be obtained from equation (5.2.34) by neglecting the dust dynamics, i.e. in the limit $m_d\to\infty$.

This gives a purely imaginary solution

$$\frac{\omega}{\omega_{\mathrm{pi}}} \approx \mathrm{i}\frac{\vartheta^2}{X}\frac{\sin\vartheta}{[X^2\sin\vartheta + 2\vartheta(\cos\vartheta - 1)]} \tag{5.2.38}$$

which corresponds to a Pierce instability of the ion beam including screening by the electrons. Thus, for large L and $\vartheta \neq S\pi$, we obtain

$$\omega \simeq \mathrm{i}\frac{U_0}{L}\left(1 - \frac{U_0^2}{C_\mathrm{S}^2}\right). \tag{5.2.39}$$

Let us now consider a possible application of the present results for designing a dusty plasma diode system to study the physics of bounded beam–plasma systems. To investigate longitudinal boundary effects on the ion–dust Buneman instability, the system should have $\vartheta \sim \pi(2m-1)$, where m is low. Since

$$\vartheta^2 = \left(\frac{C_\mathrm{S}^2}{U_0^2} - 1\right)k_{\mathrm{De}}^2 L^2 \equiv \left(\frac{n_{\mathrm{i}0}T_\mathrm{e}}{n_{\mathrm{e}0}T_\mathrm{i}}\frac{V_{\mathrm{Ti}}^2}{U_0^2} - 1\right)\frac{L^2}{\lambda_{\mathrm{De}}^2} \tag{5.2.40}$$

one would require that the first term in parentheses in equation (5.2.40) is much smaller than 1 when $L \gg \lambda_{\mathrm{De}}$. For example, using $n_{\mathrm{e}0} \simeq 10^8$ cm^{-3} and $k_\mathrm{B}T_\mathrm{e} \simeq 3$ eV we obtain $\lambda_{\mathrm{De}} \simeq 0.1$ cm. Then, if $n_{\mathrm{i}0}/n_{\mathrm{e}0} \simeq 1.01$, $U_0/V_{\mathrm{Ti}} \simeq 3$ and $T_\mathrm{e}/T_\mathrm{i} \simeq 9$, the $m = 2$ mode might be observed if $L \simeq 9$ cm. We also note that in this case the growth rate of the Pierce instability, as given by equation (5.2.39), would be significantly reduced. However, the ion–dust Buneman instability persists in the large-L regime where the effects of longitudinal boundaries can be neglected. Thus, the interplay between that instability and the Pierce instability of the ion beam might be investigated in that regime. As an example, let us consider a N_2 plasma with $n_{\mathrm{i}0} \simeq 4 \times 10^8$ cm^{-3}, $n_{\mathrm{d}0}/n_{\mathrm{i}0} \simeq 4 \times 10^{-4}$, $m_\mathrm{d}/m_\mathrm{i} \simeq 10^{10}$ (corresponding to dust with a radius $r_\mathrm{d} \simeq 0.5$ μm) and $Z_\mathrm{d} \simeq 1.3 \times 10^3$ (assuming $k_\mathrm{B}T_\mathrm{e} \simeq 2$ eV). The growth rate of the ion–dust Buneman instability for these parameters is $(\omega_{\mathrm{pi}}\omega_{\mathrm{pd}}^2)^{1/3} \simeq 16 \times 10^3$ s^{-1}. If the ions stream with a speed $U_0 \simeq 2 \times 10^5$ cm s^{-1} (corresponding to $U_0/V_{\mathrm{Ti}} \simeq 3$ for $k_\mathrm{B}T_\mathrm{i} \simeq 0.1$ eV), the growth rate ($\simeq U_0/L$) of the Pierce instability of the ion beam would be of the same order as the growth rate of the ion–dust Buneman instability for $L \simeq 25$ cm.

5.3 Ion Drag Force Induced Instabilities

Radio-frequency capacitively coupled argon and silane discharges are often employed for generating dust particles (Prabhuram and Goree 1996, Melzer *et al* 1998, Samsonov and Goree 1999). The dust particles in these discharges grow from molecule size to a few hundred nanometres in diameter. The particles usually fill the entire plasma volume, although dust-free regions, or so-called 'dust voids', have been observed in silane and other dust-laden plasmas. Furthermore, in a partially ionized dusty plasma, ionization of neutral atoms plays a crucial role. Accordingly, studies of instabilities in the presence of the ion drag force and ionization is of practical interest in processing plasmas.

As mentioned in chapter 3, the ion drag force arises from the ion orbital motion around negatively charged dust particles as well as from the momentum transfer from all the ions which are collected by the dust grains. The instability may arise due to the ion fluid compression by the ion drag force. The latter, which is proportional to the square of the particle radius, dominates over the electrostatic force when the dust grains have sufficiently large sizes. Here we consider instabilities of electrostatic waves whose frequency is much smaller than ν_{en} and whose wavelength is much shorter than $V_{\mathrm{Te}}/\nu_{\mathrm{en}}$. The electron number density in such a situation is given by equation (4.2.1). The dynamics of the ions and negatively charged dust grains in the presence of ionization and ion drag force is governed by a set of equations (D'Angelo 1997, 1998, Shukla and Morfill 1999) comprising the ion continuity equation

$$\frac{\partial n_{\mathrm{i}}}{\partial t} + \nabla \cdot (n_{\mathrm{i}} \boldsymbol{v}_{\mathrm{i}}) = -Q_{\mathrm{L}} + Q_{\mathrm{i}} \tag{5.3.1}$$

the ion momentum equation

$$m_{\mathrm{i}} \left(\frac{\partial}{\partial t} + \boldsymbol{v}_{\mathrm{i}} \cdot \nabla + \nu_{\mathrm{in}} + \frac{Q_{\mathrm{i}}}{n_{\mathrm{i}}} - \mu_{\mathrm{i}} \nabla^2 \right) \boldsymbol{v}_{\mathrm{i}} = -e \nabla \phi - \frac{\gamma_{\mathrm{i}} k_{\mathrm{B}} T_{\mathrm{i}}}{n_{\mathrm{i}0}} \nabla n_{\mathrm{i}} \tag{5.3.2}$$

the dust continuity equation (4.2.3), the dust momentum equation

$$m_{\mathrm{d}} \left(\frac{\partial}{\partial t} + \boldsymbol{v}_{\mathrm{d}} \cdot \nabla + \nu_{\mathrm{dn}} \right) \boldsymbol{v}_{\mathrm{d}} = Z_{\mathrm{d}0} e \nabla \phi + m_{\mathrm{d}} \boldsymbol{g} + \boldsymbol{F}_{\mathrm{di}} \tag{5.3.3}$$

and the quasi-neutrality condition $n_{\mathrm{i}} = n_{\mathrm{e}} + Z_{\mathrm{d}0} n_{\mathrm{d}}$. Here $Q_{\mathrm{L}} = \nu_l n_{\mathrm{i}}$, ν_l is the ion loss rate occurring both to the walls of the plasma container and to the dust grains within the plasma, Q_{i} ($= \sigma_{\mathrm{i}0} n_n \psi_{\mathrm{i}}$, where $\sigma_{\mathrm{i}0}$ is the ionization cross section and ψ_{i} is the flux of ionizing electrons) accounts for the creation of new ions through ionization of the neutral atoms by fast electrons and μ_{i} is the coefficient of the kinematic ion viscosity. For simplicity, dust charge fluctuations have been ignored and the neutrals are assumed to be immobile.

We assume that the ion drag force $\boldsymbol{F}_{\mathrm{di}}$ arising form the ion orbital motion around the dust grains dominates over that arising from the momentum transfer from all the ions that are collected by the dust grains. This is justified as long as the collection impact parameter is much smaller than the orbital impact parameter and the Coulomb logarithm far exceeds 1. Thus, the orbital motion related ion drag force acting on the dust grains takes the form

$$\boldsymbol{F}_{\mathrm{di}} = n_{\mathrm{i}} m_{\mathrm{i}} V_{\mathrm{it}} \boldsymbol{v}_{\mathrm{i}} 4\pi b_{\pi/2}^2 \Lambda(V_{\mathrm{it}}) \tag{5.3.4}$$

where $V_{\mathrm{it}} = (v_{\mathrm{i}}^2 + 8V_{\mathrm{Ti}}^2/\pi)^{1/2}$, $b_{\pi/2}^2 = Z_{\mathrm{d}0}^2 e^4 / m_{\mathrm{i}}^2 V_{\mathrm{it}}^4$ is the orbital impact parameter and $\Lambda(V_{\mathrm{it}}) = \ln[(\lambda_{\mathrm{De}}^2 + b_{\pi/2}^2)/(b_{\mathrm{c}}^2 + b_{\pi/2}^2)]^{1/2}$ is the Coulomb logarithm integrated over the interval from the collection impact parameter $b_c = r_d(1 + 2Z_{d0}e^2/r_d m_i V_{it}^2)$ to the electron Debye radius λ_{De}. Clearly, the ion drag force depends on the ion velocity as well as on the dust grain charge. In the absence of equilibrium dust streaming and the dc electric field, the dust grains are held under the combined influence of the gravity force and the equilibrium ion drag force involving unperturbed ion flow towards the dust grain surface.

We now study the instability of an equilibrium dusty plasma against electrostatic waves. Thus, the densities, fluid velocities as well as the ionization and the ion drag force are perturbed. Accordingly, we let $n_s = n_{s0} + n_{s1}$ and $\sigma_{i0} = \sigma_0 + (d\sigma_{i0}/d\phi)_0\phi$, where $n_{s1} \ll n_{s0}$ and σ_0 represents some value of the ionization cross section slightly above the threshold, when the ion flow and unperturbed dust plasma densities are uniform. In zeroth order, we have $\nu_l n_{i0} = \sigma_0 n_{n0}\psi_i$. Now substituting the perturbed electron number density (e.g. equation (4.2.1)) into the perturbed quasi-neutrality condition, we have

$$n_{i1} = n_{e0}\frac{e\phi}{k_B T_e} + Z_{d0}n_{d1}. \tag{5.3.5}$$

The linearized equations (5.3.1) and (5.3.2) are written as, respectively

$$\left(\frac{\partial}{\partial t} + \boldsymbol{v}_{i0}\cdot\nabla + \nu_l\right)n_{i1} + n_{i0}\nabla\cdot\boldsymbol{v}_i = A_d\phi \tag{5.3.6}$$

and

$$\left(\frac{\partial}{\partial t} + \boldsymbol{v}_{i0}\cdot\nabla + \nu_{in} + \frac{Q_{i0}}{n_{i0}} - \mu_i\nabla^2\right)\boldsymbol{v}_i = -\frac{e}{m_i}\nabla\left(\phi + \frac{\gamma_i k_B T_i}{e}\frac{n_{i1}}{n_{i0}}\right) \tag{5.3.7}$$

where $\boldsymbol{v}_{i0}$ is the unperturbed ion streaming velocity, $A_d = (d\sigma_{i0}/d\phi)_0 n_{n0}\psi_i$ and $Q_{i0} = \sigma_0 n_{n0}\psi_i \equiv \nu_l n_{i0}$. On the other hand, from equations (4.2.3) and (5.3.3) one obtains

$$\left(\frac{\partial}{\partial t} + \nu_{dn}\right)\frac{\partial n_{d1}}{\partial t} = -\frac{n_{d0}Z_{d0}e}{m_d}\nabla^2\phi - \frac{8\sqrt{2\pi}n_{d0}n_{i0}m_i V_{Ti}b_{id}^2\Lambda_0}{m_d}\nabla\cdot\boldsymbol{v}_i \tag{5.3.8}$$

where $b_{id}^2 \approx \pi^2 Z_{d0}^2 e^4/64k_B^2 T_i^2(1+p_i)^{3/2}$, $p_i = \pi v_{i0}^2/8V_{Ti}^2$, $\Lambda_0 = \Lambda(V_{it0})$ and $V_{it0} = (v_{i0}^2 + 8V_{Ti}^2/\pi)^{1/2}$. We now derive the dispersion relations for the DIA and DA waves in a collisional dusty plasma by using equations (5.3.5)–(5.3.8).

5.3.1 DIA waves

To study the DIA waves, we assume $|(\partial/\partial t) + \boldsymbol{v}_{i0}\cdot\nabla - \mu_i\nabla^2| \ll \nu_{in} + \nu_l \equiv \nu_{il}$. Thus, equation (5.3.7) gives

$$\boldsymbol{v}_i \approx -\frac{e}{m_i\nu_{il}}\nabla\left(\phi + \frac{\gamma_i k_B T_i}{e}\frac{n_{i1}}{n_{i0}}\right). \tag{5.3.9}$$

Now substituting $\boldsymbol{v}_{\rm i}$ from equation (5.3.9) into equation (5.3.6), we have

$$\left(\frac{\partial}{\partial t} + \boldsymbol{v}_{\rm i0} \cdot \nabla + \nu_l - D_{\rm i}\nabla^2\right) n_{\rm i1} = n_{\rm i0}\left(\frac{e}{m_{\rm i}\nu_{{\rm i}l}}\nabla^2 + \frac{A_{\rm d}}{n_{\rm i0}}\right)\phi \tag{5.3.10}$$

where $D_{\rm i} = \gamma_{\rm i} V_{\rm Ti}^2/\nu_{{\rm i}l}$. Eliminating $\boldsymbol{v}_{\rm i}$ from equations (5.3.8) and (5.3.9) we obtain

$$\left(\frac{\partial}{\partial t} + \nu_{\rm dn}\right)\frac{\partial n_{\rm d1}}{\partial t} = -\frac{n_{\rm d0}Z_{\rm d0}e}{m_{\rm d}}\nabla^2\phi + \frac{n_{\rm d0}e\alpha_{\rm i}}{m_{\rm d}}\nabla^2\left(\phi + \frac{\gamma_{\rm i}k_{\rm B}T_{\rm i}}{e}\frac{n_{\rm i1}}{n_{\rm i0}}\right) \tag{5.3.11}$$

where $\alpha_{\rm i} = \sqrt{\pi/2}Z_{\rm d0}^2\Lambda_0\omega_{\rm pi}/64\nu_{{\rm i}l}\Delta(1 + p_{\rm i})^{3/2}$ and $\Delta = n_{\rm i0}\lambda_{\rm Di}^3$. Equations (5.3.5), (5.3.10) and (5.3.11) are the desired equations for studying the instability of low-frequency DIA waves in a collisional dusty plasma including ionization and the orbital ion drag force.

Let us now Fourier transform equations (5.3.10) and (5.3.11), combine the resultant expressions and use equation (5.3.5) to obtain the dispersion relation for the DIA waves (Shukla and Morfill 1999)

$$\begin{aligned}[][\omega(\omega + {\rm i}\nu_{\rm dn}) - k^2C_{\rm i}^2](\omega - \boldsymbol{k}\cdot\boldsymbol{v}_{\rm i0} + {\rm i}\Gamma_{\rm i} + {\rm i}\nu_l + {\rm i}\Omega_s - {\rm i}\omega_{\rm I})&\\ = k^2C_{\rm De}^2(\omega - \boldsymbol{k}\cdot\boldsymbol{v}_{\rm i0} + {\rm i}\Gamma_{\rm i} + {\rm i}\nu_l)\left(1 - \frac{\alpha_{\rm i}\tau_{\rm i}}{Z_{\rm d0}}\right)&\end{aligned} \tag{5.3.12}$$

where $C_{\rm i}^2 = Z_{\rm d0}n_{\rm d0}\gamma_{\rm i}k_{\rm B}T_{\rm i}\alpha_{\rm i}/n_{\rm i0}m_{\rm d}$, $\Gamma_{\rm i} = D_{\rm i}k^2$, $\Omega_s = k^2C_{\rm S}^2/\nu_{{\rm i}l}$, $\omega_{\rm I} = \nu_l I_\sigma$, $I_\sigma = (n_{\rm e0}k_{\rm B}T_{\rm e}/n_{\rm i0}e\sigma_0)(d\sigma_{\rm i0}/d\phi)_0$, $C_{\rm De} = \omega_{\rm pd}\lambda_{\rm De}$ and $\tau_{\rm i} = 1 + n_{\rm e0}\gamma_{\rm i}T_{\rm i}/n_{\rm i0}T_{\rm e}$. Two comments are in order.

(i) When the electrostatic and ion drag forces exactly balance each other, i.e. when $Z_{\rm d0} = \alpha_{\rm i}\tau_{\rm i}$, equation (5.3.12) yields $\omega = -{\rm i}(\nu_{\rm dn}/2) \pm (k^2C_{\rm i}^2 - \nu_{\rm dn}^2/4)^{1/2}$ and $\omega = \boldsymbol{k}\cdot\boldsymbol{v}_{\rm i0} - {\rm i}(\Gamma_{\rm i} + \nu_l + \Omega_s) + {\rm i}\omega_{\rm I}$. The latter predicts an ionization instability if $\omega_{\rm I} > \Gamma_{\rm i} + \nu_l + \Omega_s$.

(ii) When we assume $|\omega - \boldsymbol{k}\cdot\boldsymbol{v}_{\rm i0} + {\rm i}\nu_l + {\rm i}\Gamma_{\rm i}| \gg \Omega_s, \omega_{\rm I}$ and $|\omega| \gg \nu_{\rm dn}, kC_{\rm i}$, equation (5.3.12) gives a purely growing ($\omega = {\rm i}\omega_{\rm i}$) instability provided that $\alpha_{\rm i}\tau_{\rm i} > Z_{\rm d0}$. The latter indicates that the origin of the instability is the ion orbital drag force which causes the ion fluid compression that is out of phase with the dust fluid perturbation. Thus, energy stored in the ion flow is coupled to low-frequency density perturbations which temporally grow. We note that the ion drag force driven instability occurs when

$$Z_{\rm d0} > \frac{64\nu_{{\rm i}l}\Delta(1 + p_{\rm i})^{3/2}}{\omega_{\rm pi}\Lambda_0\tau_{\rm i}}. \tag{5.3.13}$$

Since $Z_{\rm d0}$ is proportional to the dust radius, the latter is a decisive parameter for the onset of the instability due to the ion drag force. The interplay between ionization and the ion drag drivers can be studied by numerically analysing equation (5.3.12).

5.3.2 DA waves

We now consider the effect of the ion drag force on the DA waves by neglecting the ionization process completely. We assume that in low phase velocity (in comparison with the ion thermal speed) DA waves the ion number density perturbation is given by equation (4.2.2). Hence equations (5.3.5) and (5.3.8) take the form

$$\left(\frac{n_{\rm i0}}{k_{\rm B}T_{\rm i}} + \frac{n_{\rm e0}}{k_{\rm B}T_{\rm e}}\right) e\phi + Z_{\rm d0}n_{\rm d1} = 0 \tag{5.3.14}$$

and

$$\begin{aligned}\left(\frac{\partial}{\partial t} + \nu_{\rm dn}\right)\frac{\partial n_{\rm d1}}{\partial t} = & -\frac{n_{\rm d0}Z_{\rm d0}e}{m_{\rm d}}\nabla^2\phi \\ & -\frac{8\sqrt{2\pi}n_{\rm d0}n_{\rm i0}m_{\rm i}V_{\rm Ti}b_{\rm id}^2\Lambda_0 e}{m_{\rm d}k_{\rm B}T_{\rm i}}\left(\frac{\partial}{\partial t} + \boldsymbol{v}_{\rm i0}\cdot\nabla\right)\phi\end{aligned} \tag{5.3.15}$$

where we have used the ion continuity equation to eliminate the compressibility $\nabla \cdot \boldsymbol{v}_{\rm i}$. Equations (5.3.14) and (5.3.15) are the desired equations for the DA waves in the presence of dust–neutral collisions and the ion drag force. Thus, combining equations (5.3.14) and (5.3.15) and Fourier transforming the resultant equation, we have

$$\omega(\omega + {\rm i}\nu_{\rm dn}) - k^2C_{\rm D}^2 - {\rm i}\omega\omega_{\rm id} = 0 \tag{5.3.16}$$

where $\omega_{\rm id} = \sqrt{\pi/2}\omega_{\rm pi}Z_{\rm d0}^3 n_{\rm d0}k_{\rm B}T_{\rm e}\Lambda_0/64\Delta(1 + p_{\rm i})^{3/2}(n_{\rm i0}k_{\rm B}T_{\rm e} + n_{\rm e0}k_{\rm B}T_{\rm i})$. Equation (5.3.16) admits a purely growing instability for $\omega \gg \boldsymbol{k}\cdot\boldsymbol{v}_{\rm i0}$, $\omega_{\rm id} \gg \nu_{\rm dn}$ and $\omega_{\rm id}^2 > 4k^2C_{\rm D}^2$. The growth rate of that instability is roughly $\omega_{\rm id}/2$. Again, the dust radius is a crucial parameter for the onset of the ion drag force induced instability. However, in order to have a complete picture of the latter we should numerically solve equation (5.3.16).

5.4 Dust Charge Gradient Induced Instabilities

There exist a dc electric field and an equilibrium dust charge gradient in the plasma sheath. The dust charge gradient strongly depends on the distance from the electrode (see figure 5.2). A non-uniform dusty plasma can be destabilized due to the combined effects of a dc electric field and an equilibrium dust charge gradient.

5.4.1 Equilibrium properties

We first discuss the equilibrium properties of our dusty plasma and show how an equilibrium dust charge gradient is maintained by an equilibrium dust flow that is created by a dc electric field. The instability of that equilibrium is then investigated against electrostatic perturbations.

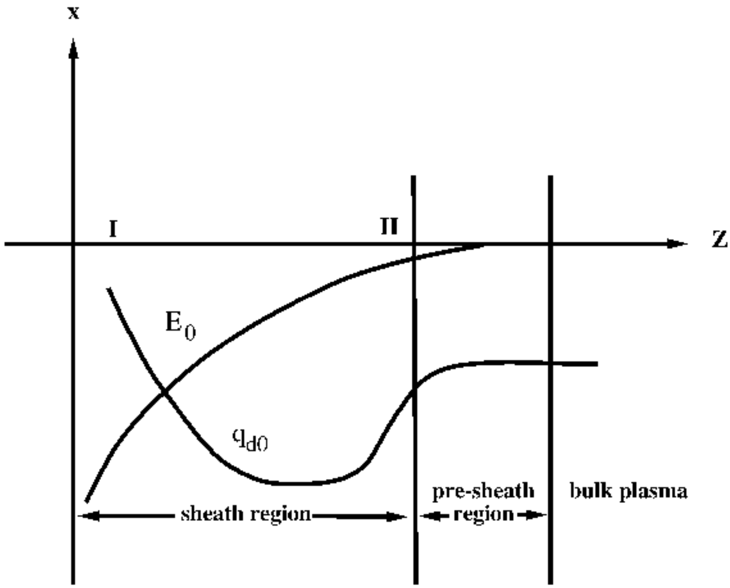

Figure 5.2. Typical profiles of the equilibrium electric field ($\boldsymbol{E}_0$) and the dust charge (q_{d0}) in the plasma sheath (after Ivlev *et al* 2000a).

Let us consider a non-uniform, unmagnetized dusty plasma in the presence of a homogeneous dc electric field $\boldsymbol{E}_0 = -\hat{z}E_{0z}$ and an equilibrium dust charge gradient $\partial q_{d0}/\partial z$. Adopting a fluid treatment for an ensemble of dust grains, we obtain in the steady state (Shukla 2000b)

$$n_{d0}u_0 = \text{constant} \tag{5.4.1}$$

$$u_0 u_0' + \frac{q_{d0}}{m_d}\phi_0' + g_z = 0 \tag{5.4.2}$$

$$u_0 q_{d0}' = I_{e0} + I_{i0} \equiv I_0 \tag{5.4.3}$$

and

$$e(n_{i0} - n_{e0}) + q_{d0}n_{d0} = 0 \tag{5.4.4}$$

where u_0 is the component of the equilibrium dust fluid velocity along the z-axis, $u_0' = \partial u_0/\partial z$, $\phi_0' = \partial\phi_0/\partial z \equiv -E_{0z}$ and $m_d g_z$ is the z component of the gravity force. For negatively charged dust grains, the unperturbed OLM currents in the presence of the dc potential ϕ_0 are

$$I_{e0} = -4\pi r_d^2 e n_{e0} \exp\left(\frac{e\phi_0}{k_B T_e}\right)\frac{V_{Te}}{\sqrt{2\pi}} \exp\left(\frac{e q_{d0}}{r_d k_B T_e}\right) \tag{5.4.5}$$

and

$$I_{i0} = 4\pi r_d^2 e n_{i0} \exp\left(-\frac{e\phi_0}{k_B T_i}\right)\frac{V_{Ti}}{\sqrt{2\pi}}\left(1 - \frac{e q_{d0}}{r_d k_B T_i}\right). \tag{5.4.6}$$

Equations (5.4.1)–(5.4.4) reveal that in the absence of the equilibrium dust fluid velocity, we have $q_{d0}E_{0z} = m_d g_z$ and $I_{e0} + I_{i0} = 0$. The latter determines the equilibrium charge on the dust grain surface, while the former dictates that a balance between the sheath electric and gravity forces is responsible for the levitation of the dust grains. On the other hand, in the presence of a uniform dust flow there appears a dust charge gradient $q'_{d0} = I_0/u_0$, which can be expressed as

$$q'_{d0} = -4\pi r_d^2 e\alpha_0 \left[N_e \exp\left(\frac{eq_{d0}}{r_d k_B T_e}\right) - N_i \frac{V_{Ti}}{V_{Te}} \left(1 - \frac{eq_{d0}}{r_d k_B T_i}\right)\right] \tag{5.4.7}$$

where $N_e = n_{e0}\exp(e\phi_0/k_B T_e)$, $N_i = n_{i0}\exp(-e\phi_0/k_B T_i)$ and $\alpha_0 = V_{Te}/\sqrt{2\pi}u_0$.

5.4.2 DA waves

To study the instability of our equilibrium state against the DA waves, we let $n_d = n_{d0} + n_{d1}$, $\boldsymbol{v}_d = u_0\hat{\boldsymbol{z}} + \boldsymbol{u}_1$, $\phi = \phi_0(z) + \phi_1$ and $q_d = q_{d0}(z) + q_1$, where n_{d0} and u_0 are uniform and n_1, $\boldsymbol{u}_1$, ϕ_1 and q_1 are small perturbations of their equilibrium values. Hence we obtain from the dust continuity and dust momentum equations (Shukla 2000b)

$$\frac{dn_{d1}}{dt} + n_{d0}\nabla\cdot\boldsymbol{u}_1 = 0 \tag{5.4.8}$$

and

$$\frac{d\boldsymbol{u}_1}{dt} + \frac{q_{d0}}{m_d}\nabla\phi_1 + \frac{\phi'_0}{m_d}q_1 = 0. \tag{5.4.9}$$

The Poisson equation takes the form

$$\nabla^2\phi_1 = k_D^2\phi_1 - 4\pi(q_{d0}n_{d1} + n_{d0}q_1) \tag{5.4.10}$$

while the dust grain charging equation reads

$$\frac{dq_1}{dt} + \nu_1 q_1 + q'_{d0}u_{1z} = -\nu_2 r_d\phi_1 \tag{5.4.11}$$

where $d/dt = (\partial/\partial t) + u_0(\partial/\partial z)$. Note that equations (5.4.9) and (5.4.11) contain the terms $\phi'_0 q_1/m_d$ and $q'_{d0}u_{1z}$, which are associated with perturbed electrostatic forces involving the unperturbed sheath electric field and the advection of the equilibrium dust charge gradient by the dust fluid velocity u_{1z}, respectively. These two forces are responsible for the novel absolute instabilities, as described below.

The dispersion relation can be obtained by combining (5.4.8)–(5.4.11) and Fourier transforming the resultant equation by supposing that the perturbed quantities are proportional to $\exp(-i\omega t + iky)$. Accordingly, for $k^2/k_D^2 \ll 1$ we obtain (Shukla 2000b)

$$1 - \frac{\omega_D^2}{\omega^2} + \left(1 + \frac{\Omega_D^2}{\omega^2}\right)\frac{k_q^2\lambda_D^2\nu_1}{\nu_1 - i(\omega + \Omega)} = 0 \tag{5.4.12}$$

where $\Omega_D^2 = q_{d0}k_Q\phi_0'/m_d$, $k_Q = q_{d0}'/q_{d0}$ and $\Omega = \Omega_D^2/\omega$. The local dispersion relation (5.4.12) is valid when the scalelength of the dust charge inhomogeneity is much larger than the wavelength $2\pi/k$. Supposing that the wave frequency is much smaller than ν_1, which is typically the case in low-temperature laboratory dusty plasma discharges, we obtain from equation (5.4.12)

$$(\omega^2 - \omega_D^2)\left(\nu_1 - \mathrm{i}\frac{\Omega_D^2}{\omega}\right) + (\omega^2 + \Omega_D^2)k_q^2\lambda_D^2\nu_1 = 0. \tag{5.4.13}$$

We now extract some useful results that follow from equation (5.4.13).

(i) We first assume that there is no dc electric field and dust charge gradient. Thus, substituting $\Omega_D = 0$ into equation (5.4.13) we have the modified DA wave frequency $\omega = \omega_D/(1 + k_q^2\lambda_D^2)^{1/2} \equiv \Omega_0$.

(ii) We next consider $\Omega_D \neq 0$. Substituting $\omega \approx \omega_D + \mathrm{i}\gamma_q$ into equation (5.4.13), where $\gamma_q < \omega_D, |\Omega_D|$, we obtain the growth rate

$$\gamma_q = \frac{(\omega_D^2 + \Omega_D^2)\Omega_D^2 k_q^2\lambda_D^2\nu_1}{2(\nu_1^2\omega_D^2 + \Omega_D^4)} \tag{5.4.14}$$

if $\Omega_D^2 > 0$. The latter is fulfilled if $E_{0z}q_{d0}' < 0$. Clearly, the dc electric field and the dust charge gradient must oppose each other for the dusty plasma to become unstable. Physically, the instability arises because the dc sheath electric field does work on the dust grains to create dust charge fluctuations which cannot keep in phase with the potential of the electrostatic disturbance in a non-uniform dusty plasma with a dust charge gradient. Thus, free energy stored in the latter is coupled to unstable DA waves when the dc electric field (in association with the dust charge fluctuation) produces a charge imbalance in the dusty plasma. As an illustration, we mention that in laboratory experiments (Nunomura *et al* 1999) we typically have $n_{e0} \simeq n_{i0} \simeq 10^8$ cm^{-3}, $k_BT_e \simeq 10k_BT_i \simeq 1$ eV, $r_d \simeq 1$–10 μm and $\lambda_D \simeq 10^2$–10^3 μm. Accordingly, for $k_q^2\lambda_D^2 \simeq 1$, $\nu_1 \simeq 10^3$ s^{-1}, $\omega_D \simeq 60$ s^{-1} and $\Omega_D = 10$ s^{-1} the growth time (γ_q^{-1}) is a fraction of a second.

(iii) We now consider the regime $\Omega_D \ll |\omega| \ll \omega_D, |\Omega_D^2|/\nu_1$. Here equation (5.4.13) reduces to

$$\omega^3 = -\mathrm{i}\frac{\omega_D^2\Omega_D^2}{k_q^2\lambda_D^2\nu_1} \tag{5.4.15}$$

which predicts a reactive instability. The growth rate of that instability is roughly $(\omega_D^2|\Omega_D^2|/k_q^2\lambda_D^2\nu_1)^{1/3}$.

(iv) We finally examine whether there also exists convective amplification/attenuation of waves having a real frequency. For this purpose, we let

$k = k_\mathrm{r} + \mathrm{i}k_\mathrm{i}$ in equation (5.4.12) and obtain the real (k_r) and imaginary (k_i) parts of the wavenumber. We have

$$k_\mathrm{r}^2 = k_\mathrm{i}^2 + \frac{\omega^2}{C_\mathrm{D}^2}\left[1 + \frac{(\omega^2 + \Omega_\mathrm{D}^2)\nu_1^2 k_\mathrm{q}^2 \lambda_\mathrm{D}^2}{\nu_1^2\omega^2 + (\omega^2 + \Omega_\mathrm{D}^2)^2}\right] \tag{5.4.16}$$

and

$$k_\mathrm{i} = \frac{\omega\nu_1}{k_\mathrm{r}C_\mathrm{D}^2}\frac{(\omega^2 + \Omega_\mathrm{D}^2)^2}{\omega_\mathrm{pd}^2}\frac{k_\mathrm{q}^2\lambda_\mathrm{D}^2}{\nu_1^2\omega^2 + (\omega^2 + \Omega_\mathrm{D}^2)^2}. \tag{5.4.17}$$

It turns out that equation (5.4.17) does not admit a convective instability, but one encounters only a spatial attenuation of the waves.

5.4.3 Transverse DL waves

We now discuss the dispersion properties of the transverse DL (TDL) waves on the one-dimensional dust particle chain in a strongly coupled Yukawa (or the Debye–Hückel) system by incorporating the dust charge gradient effect. We consider the vibration of the one-dimensional horizontal chain of dust particles of equal mass m_d separated by the distance a. When the nth dust particle is vertically displaced from its equilibrium position, it experiences forces due to intergrain interactions through a Debye-screened Coulomb force and through a direct interaction with a vertically varying sheath electric field E_0. The balance of these forces in the linear approximation with respect to a small vertical displacement δz_n of the nth particle at the equilibrium $z_n = z_0$ gives the equation of motion for vertical oscillations (Miswa *et al* 2001)

$$\frac{\partial^2\delta z_n}{\partial t^2} + \nu_\mathrm{dn}\frac{\partial\delta z_n}{\partial t} = -\omega_\gamma^2\delta z_n + \Omega_\mathrm{t}^2(2\delta z_n - \delta z_{n-1} - \delta z_{n+1}) + \frac{E_0\delta q_n}{m_\mathrm{d}} \tag{5.4.18}$$

where $\omega_\gamma^2 = \gamma_\mathrm{r}/m_\mathrm{d}$, γ_r is the restoring force coefficient for a single particle oscillating in an electrostatic potential well

$$\Omega_\mathrm{t}^2 = \frac{q_\mathrm{d0}^2}{m_\mathrm{d}a^3}\left(1 + \frac{a}{\lambda_\mathrm{D}}\right)\exp\left(-\frac{a}{\lambda_\mathrm{D}}\right) \tag{5.4.19}$$

is the quantity related to the screened interparticle potential, q_d0 is the equilibrium charge of the dust particle levitated at the equilibrium position z_0 and δq_n is the charge deviation from q_d0 associated with the inhomogeneous q_d0 variation in the vertical direction and the delayed charging due to the finite charging time when the dust particle oscillates through the sheath. The last term in the right-hand side of equation (5.4.18) represents the perturbed electric force acting on a dust particle due to the charge variation. The force becomes positive or negative depending on the signs of δq_n and E_0 around the equilibrium, which may lead to damping (or growth) of the TDL waves. The time variation of δq_n is modelled by the equation (Ivlev *et al* 2000a, Miswa *et al* 2001)

$$\frac{\partial \delta q_n}{\delta t} = -\nu_c \delta q_n + \nu_c \left(\frac{\partial q_{d0}}{\partial z}\right)_{z=z_0} \delta z_n \tag{5.4.20}$$

where ν_c is the typical charging frequency for the dust particle. Equation (5.4.20) shows that when the charging time τ_c is sufficiently large, we have $\delta q_n = (\partial q_{d0}/\partial z)_{z=z_0}\delta z_n$, which indicates that the charge takes a value determined by the instantaneous vertical position. On the other hand, if ν_c tends to zero, δq_n tends to zero and the charge retains its original value. For a typical TDL wave with finite $\nu_c/\omega \ll 1$, one may assume that δz_n and δq_n oscillate as $\exp(-\mathrm{i}\omega t + \mathrm{i}kna)$. Hence from equations (5.4.18) and (5.4.20) we obtain the modified TDL wave dispersion relation (Miswa *et al* 2001)

$$\omega^2 + \mathrm{i}\nu_* \omega = \omega_{\gamma *}^2 - \Omega_t^2[2 - \exp(\mathrm{i}ka) - \exp(-\mathrm{i}ka)] \tag{5.4.21}$$

where $\nu_* = \nu_{dn} - \Omega_*$, $\Omega_* = -(E_0/m_d\nu_c)(\partial q_{d0}/\partial z)_{z=z_0}$, $\omega_{\gamma *}^2 = \gamma_*/m_d$ and $\gamma_* = \gamma_r - E_0(\partial q_{d0}/\partial z)_{z=z_0}$. It is evident from equation (5.4.21) that the imaginary part of k arises from not only due to the neutral drag force, but also from the delayed charging effect Ω_*. The latter has little effect on the real part of k. However, the imaginary part of k is found to be influenced by the delayed charging effect. Miswa *et al* (2001) found that if Ω_* takes a large positive value to yield the condition $\nu_* < 0$, one may have instability of the TDL waves. Furthermore, in the absence of the dust charge gradient and the dc electric field, equation (5.4.21) takes the form

$$\omega^2 + \mathrm{i}\nu_{dn}\omega = \omega_\gamma^2 - 4\Omega_t^2 \sin^2\left(\frac{ka}{2}\right) \tag{5.4.22}$$

which yields $\omega = \pm\omega_\gamma$ for $k = 0$.

5.5 Drift Wave Instabilities

It is well known that free energy stored in equilibrium density, temperature and velocity gradients can be coupled to electrostatic and electromagnetic waves in a magnetized electron–ion plasma (Ichimaru 1973, Weiland 2000). Here we discuss instabilities of electrostatic waves in a non-uniform dusty plasma in a uniform magnetic field $\hat{z}B_0$.

5.5.1 Universal instability

The presence of an equilibrium dust charge gradient $(\partial q_{d0}/\partial x)$ can produce instability of low-frequency ($\ll \omega_{ci}$) electrostatic drift waves in a non-uniform magnetized plasma which also contains a density gradient $\partial n_{e0}/\partial x$ along the x-axis. Since the drift wave frequency is typically much larger than the dust plasma and dust gyro-frequencies, the dust grains can be considered immobile. The electron number density perturbation in this case is (Ichimaru 1973, Weiland 2000)

$$n_{e1} = \frac{k^2}{4\pi e}\chi_e\phi \equiv n_{e0}\left(1 + i\sqrt{\frac{\pi}{2}}\frac{\omega + \omega_{e*}}{k_z V_{Te}}\right)\frac{e\phi}{k_B T_e} \tag{5.5.1}$$

where the electron susceptibility χ_e has been deduced from the general susceptibility (Miyamoto 1980, Stenflo 1981)

$$\chi_j \approx \frac{1}{k^2\lambda_{Dj}^2}\left\{1 - \sum_{n=-\infty}^{\infty}\Gamma_n(b_j)\left[\omega + \omega_{j*}\left(1 + \frac{n\omega}{b_j\omega_{cj}}\right)\right]\Re_j\right\} \tag{5.5.2}$$

in the limits $b_e \ll 1$, $\omega \ll \omega_{ce}$ and $|\omega + \omega_{j*}| \ll k_z V_{Te}$. Here we have denoted $\omega_{j*} = (k_y c k_B T_j/eB_0 n_{j0})(\partial n_{j0}/\partial x) \equiv k_y c k_B T_e/eB_0 L_j$, $\Re_j = \int_{\infty}^{\infty} F_z\, dv_z/(\omega - k_z v_z - n\omega_{cj})$ and $F_z = (2\pi V_{Tj}^2)^{-1/2}\exp(-v_z^2/2V_{Tj}^2)$. The ion density perturbation is given by

$$n_{i1} = -\frac{k^2}{4\pi e}\chi_i\phi \equiv -n_{i0}\left(\frac{T_e}{T_i}\frac{\omega_{i*}}{\omega} + \frac{k_\perp^2 c_s^2}{\omega_{ci}^2}\right)\frac{e\phi}{k_B T_e} \tag{5.5.3}$$

where the ion susceptibility has been obtained from equation (5.5.2) by assuming $b_i \ll 1$ and $k_z V_{Ti} \ll \omega \ll \omega_{ci}$. By invoking the quasi-neutrality condition, namely $n_{e1} = n_{i1}$, we then obtain from equations (5.5.1) and (5.5.3)

$$1 + i\sqrt{\frac{\pi}{2}}\frac{\omega + \omega_{e*}}{k_z V_{Te}} + \frac{n_{i0}T_e}{n_{e0}T_i}\frac{\omega_{i*}}{\omega} + k_\perp^2\rho_s^2 = 0 \tag{5.5.4}$$

which is the dispersion relation for the drift waves in a dusty plasma. Letting $\omega = \omega_r + i\omega_i$ in equation (5.5.4) and assuming $k_\perp^2\rho_s^2 \ll 1$ we obtain the real part of the dust drift wave frequency (Shukla *et al* 1991)

$$\omega_r = -\frac{n_{i0}T_e}{n_{e0}T_i}\omega_{i*} \tag{5.5.5}$$

and the growth/damping rate (Benkadda *et al* 1995)

$$\omega_i = \sqrt{\frac{\pi}{2}}\omega_r\frac{k_y c k_B T_e}{e^2 B_0 n_{e0} k_z V_{Te}}\frac{\partial(n_{d0}q_{d0})}{\partial x} \tag{5.5.6}$$

where we have used the relation

$$\omega_{e*} - \frac{n_{i0}T_e}{n_{e0}T_i}\omega_{i*} = \frac{k_y c k_B T_e}{e^2 B_0 n_{e0}}\frac{\partial(n_{d0}q_{d0})}{\partial x}. \tag{5.5.7}$$

Equation (5.5.6) reveals that long-wavelength (in comparison with ρ_s) drift waves are universally unstable in a dusty plasma with $\partial(n_{d0}q_{d0})/\partial x > 0$. The instability is caused by the wave–electron interaction in a magnetoplasma containing either density or charge gradient.

5.5.2 Velocity shear instability

We next discuss the parallel velocity shear instability (PVSI) in a non-uniform dusty magnetoplasma. The PVSI is a fluid instability that occurs in a plasma in which the ions flow parallel to $\hat{z}B_0$ with a flow velocity $\hat{z}v_{i0}(x)$ that varies in a direction perpendicular to $\hat{z}B_0$. This instability was first analysed by D'Angelo (1965) for an electron–ion plasma. In the presence of stationary charged dust grains, the growth rate of the PVSI instability is modified (D'Angelo and Song 1990), as observed experimentally by Luo *et al* (2001).

To study the PVSI instability of low-frequency ($\ll \omega_{ci}$) electrostatic waves in a collisional dusty plasma, we derive the relevant dispersion relation. Accordingly, we substitute equation (4.7.2) into the ion continuity and parallel component of the ion momentum equations, which are, respectively

$$\left(\frac{\partial}{\partial t} + v_{i0}\frac{\partial}{\partial z}\right) n_{i1} - \frac{n_{i0}c}{B_0\omega_{ci}}\left(\frac{\partial}{\partial t} + v_{i0}\frac{\partial}{\partial z} + \nu_{in}\right)\nabla_\perp^2\phi$$
$$- \frac{c}{B_0}\hat{z}\times\nabla n_{i0}\cdot\nabla\phi + n_{i0}\frac{\partial v_{iz}}{\partial z} = 0 \tag{5.5.8}$$

and

$$\left(\frac{\partial}{\partial t} + v_{i0}\frac{\partial}{\partial z} + \nu_{in}\right) v_{iz} = \frac{c}{B_0}\hat{z}\times\nabla v_{i0}\cdot\nabla\phi - \frac{e}{m_i}\frac{\partial\phi}{\partial z} - \frac{3k_B T_i}{m_i n_{i0}}\frac{\partial n_{i1}}{\partial z}. \tag{5.5.9}$$

Equations (5.5.8) and (5.5.9) are closed by means of the quasi-neutrality condition $n_{i1} = n_{e1} \approx n_{e0}e\phi/k_B T_e$ (where the Boltzmann electron density perturbation is used). Now assuming that the perturbations vary as $\exp(-i\omega t + ik_y y + ik_z z)$, we obtain from equations (5.5.8) and (5.5.9) the local dispersion relation for $\omega \gg k_z v_{i0}$ and $k_y^2\rho_s^2 \ll 1$

$$\omega(\omega + i\nu_{in}) + \frac{n_{i0}T_e}{n_{e0}T_i}\omega\omega_{i*} - \frac{n_{i0}}{n_{e0}}k_z^2 c_s^2\left(1 + \frac{3T_i}{T_e} - \frac{S_i k_y}{k_z}\right) = 0 \tag{5.5.10}$$

where $S_i = V'_{i0}/\omega_{ci}$ and $V'_{i0} = \partial v_{i0}/\partial x$. Equation (5.5.10) is the dispersion relation for the coupled drift and DIA waves in the presence of the parallel ion velocity gradient. For $|\omega| \gg \nu_{in}, (n_{i0}T_e/n_{e0}T_i)\omega_{i*}$ equation (5.5.10) admits an instability if

$$S_i > \frac{k_z}{k_y}\left(1 + \frac{3T_i}{T_e}\right). \tag{5.5.11}$$

On the other hand, for $(n_{i0}T_e/n_{e0}T_i)\omega_{i*} \ll |\omega| \ll \nu_{in}$ we obtain from equation (5.5.10)

$$\omega = i\frac{k_z^2 C_S^2}{\nu_{in}}\left[\frac{S_i k_y}{k_z} - \left(1 + \frac{3T_i}{T_e}\right)\right] \tag{5.5.12}$$

which predicts a resistive instability if equation (5.5.11) is satisfied.

5.5.3 Self-gravitational instability

In self-gravitating astrophysical objects massive charged dust grains experience both electromagnetic and gravitational forces, while the electrons and ions experience the electromagnetic force only because their masses are much smaller than those of the dust grains. Thus, knowledge of the instabilities in a non-uniform, self-gravitating cosmic dusty magnetoplasma is essential for the understanding of the collapse of astrophysical objects and the formation of stars. We discuss here the Jeans instability in a self-gravitating non-uniform dusty plasma.

In the steady state without equilibrium plasma flows, the gravitational force $-m_\mathrm{d}n_{\mathrm{d}0}\nabla\Psi_0$ acting on the dust grains is balanced by the gradient of the sum of the plasma and magnetic field pressures. Hence we have

$$-m_\mathrm{d}n_{\mathrm{d}0}\nabla\Psi_0 = \nabla\left(P + \frac{B_0^2}{8\pi}\right) \tag{5.5.13}$$

where Ψ_0 is the unperturbed gravitational potential, determined by

$$\nabla^2\Psi_0 = 4\pi G m_\mathrm{d} n_{\mathrm{d}0} \tag{5.5.14}$$

and G is the gravitational constant.

The appropriate electron and ion susceptibilities are obtained from equation (5.5.2) because the effect of the perturbed self-gravitational force acting on the electrons and ions is insignificant, unlike that acting on the massive charged dust grains. The dielectric susceptibility of the latter in the presence of electrostatic as well as Lorentz and gravitational forces is obtained as follows. We start with the dust momentum equation

$$\left(\frac{\partial}{\partial t} + \nu_\mathrm{dn}\right)\boldsymbol{v}_\mathrm{d} = \frac{q_{\mathrm{d}0}}{m_\mathrm{d}}\nabla\phi - \nabla\psi_1 + \omega_\mathrm{cd}\boldsymbol{v}_\mathrm{d}\times\hat{z} \tag{5.5.15}$$

and Poisson's equation that relates the perturbed gravitational potential ψ_1 and the dust mass density $m_\mathrm{d}n_{\mathrm{d}1}$

$$\nabla^2\psi_1 = 4\pi G m_\mathrm{d} n_{\mathrm{d}1}. \tag{5.5.16}$$

Combining equations (5.5.15) and (5.5.16) with the linearized dust continuity equation (4.2.3) and Fourier transforming the resultant equation, we obtain for the dust number density perturbation

$$n_{\mathrm{d}1} = -\frac{k^2}{4\pi q_{\mathrm{d}0}}\chi_\mathrm{d}\phi \tag{5.5.17}$$

where the dust susceptibility is (Salimullah and Shukla 1999)

$$\chi_\mathrm{d} = -\frac{\omega_\mathrm{pd}^2[k_\perp^2\omega^2/(\omega^2-\omega_\mathrm{cd}^2) + k_z^2]}{k^2\omega^2 + k_\perp^2\omega_\mathrm{J}^2\omega^2/(\omega^2-\omega_\mathrm{cd}^2) + k_z^2\omega_\mathrm{J}^2} \tag{5.5.18}$$

and $\omega_{\rm J} = (4\pi G m_{\rm d} n_{\rm d0})^{1/2}$ is Jean's frequency. In deriving equation (5.5.17) we have assumed $\omega \gg \nu_{\rm dn}$, $\omega_{\rm cd}/k_y L_{\rm d}, k V_{\rm Td}$, where $L_{\rm d}^{-1} = \partial \ln n_{\rm d0}/\partial x$. In the absence of the external magnetic field, equation (5.5.18) reduces to

$$\chi_{\rm d} = -\frac{\omega_{\rm pd}^2}{\omega^2 + \omega_{\rm J}^2}. \tag{5.5.19}$$

The dispersion properties of electrostatic modes in a self-gravitating magnetized dusty plasma are deduced from equation (5.2.1) by inserting the appropriate plasma particle susceptibilities. We now discuss several low-frequency regimes where self-gravitation of charged dust grains may play an important role.

5.5.3.1 Uniform unmagnetized dusty plasmas

In a uniform unmagnetized dusty plasma, one encounters the Jeans swindle for the equilibrium state. That means that the latter is unspecified. Accepting this fact, we consider the dispersion properties of the DA waves ($\omega \ll k V_{\rm Te}, k V_{\rm Ti}$) in a self-gravitating dusty plasma. Here we can use (5.5.19) and take $\chi_{\rm e} = 1/k^2\lambda_{\rm De}^2$ and $\chi_{\rm i} = 1/k^2\lambda_{\rm Di}^2$ to obtain (Pandey *et al* 1994, Avinash and Shukla 1994)

$$\omega^2 = -\omega_{\rm J}^2 + \frac{k^2 C_{\rm D}^2}{1 + k^2\lambda_{\rm D}^2} \tag{5.5.20}$$

which shows that the Jeans instability does not occur in the domain $\lambda_{\rm D} \ll k^{-1} \leq C_{\rm D}/\omega_{\rm J}$.

5.5.3.2 Non-uniform dusty magnetoplasmas

We now study the influence of the external magnetic field on the Jeans instability in a non-uniform dusty magnetoplasma. We focus on the frequency domain $\omega_{\rm cd} \ll \omega \ll \omega_{\rm ci}$ for which the electrons and ions are magnetized, but the dust grains are unmagnetized. Accordingly, we can use equation (5.5.19) for the dust susceptibility, but introduce two different kinds of responses for the electrons and ions.

(i) We first consider long-wavelength ($k_\perp^2 \rho_{{\rm T}s}^2 \ll 1$) flute-like perturbations. Thus, using

$$\chi_j = \frac{\omega_{\rm pj}^2}{k_\perp^2}\left(\frac{m_j c k_y}{L_j q_j B_0 \omega} + \frac{k_\perp^2}{\omega_{\rm cj}^2}\right) \tag{5.5.21}$$

and equation (5.5.19) we obtain (Salimullah and Shukla 1999)

$$1 + \frac{\omega_{\rm pi}^2}{\omega_{\rm ci}^2} - \frac{\omega_{\rm pi}^2}{\omega_{\rm ci}\omega}\frac{k_y K_{\rm qn}}{k_\perp^2} - \frac{\omega_{\rm pd}^2}{\omega^2 + \omega_{\rm J}^2} = 0 \tag{5.5.22}$$

where $K_{\rm qn} = (en_{\rm i0})^{-1}\partial(q_{\rm d0}n_{\rm d0})/\partial x$. Equation (5.5.22) can be rewritten as

$$(\omega^2 + \omega_{\rm J}^2)(\omega - \omega_{\rm sv}) - \omega_{\rm DH}^2\omega = 0 \tag{5.5.23}$$

which exhibits a coupling between the Jeans and Shukla–Varma modes. We have denoted $\omega_{\rm DH} = \omega_{\rm pd}\omega_{\rm ci}/\omega_{\rm pi}$ and assumed $\omega_{\rm pi} \gg \omega_{\rm ci}$. The effects of the external magnetic field as well as of the density and dust charge inhomogeneities can be deduced by numerically analysing equation (5.5.23). However, for $\omega \gg \omega_{\rm sv}$ the latter yields $\omega^2 = -\omega_{\rm J}^2 + \omega_{\rm DH}^2$, which shows that the magnetic field stabilizes the purely growing Jeans instability.

(ii) We next consider the effects of finite k_z on waves in a warm dusty plasma. Considering the frequency regime $kV_{\rm Ti}, k_zC_{\rm S}, \omega_{\rm cd} \ll \omega \ll k_zV_{\rm Te}, \omega_{\rm ci}$, we use the appropriate electron and ion susceptibilities (e.g. those given in equations (5.5.1) and (5.5.3)) along with equation (5.5.19) to obtain (Salimullah and Shukla 1999)

$$(\omega^2 + \omega_{\rm J}^2)(\omega - \omega_{\rm d*}) - \omega_{s\rm e}^2\omega = 0 \tag{5.5.24}$$

which exhibits a coupling between the Jeans and dust drift modes. Here we have denoted $\omega_{\rm d*} = (n_{\rm i0}T_{\rm e}/n_{\rm e0}T_{\rm i})\omega_{\rm i*}/(1 + k_y^2\rho_s^2)$ and $\omega_{s\rm e} = k\lambda_{\rm De}\omega_{\rm pd}/(1 + k_y^2\rho_s^2)^{1/2}$. The effects of the external magnetic field and the ion density gradient can be found by numerically analysing equation (5.5.24). Finally, we mention that inclusion of dust–neutral collisions in the above analysis yields a new resistive Jeans instability, as discussed by Shukla and Verheest (1999).

5.6 Parametric Instabilities

We have described numerous instabilities in the presence of streaming of plasma particles, ion drag force, as well as dust charge, plasma number density and ion flow gradients, etc. We now wish to discuss a few examples of the parametric instabilities in the presence of large-amplitude electromagnetic (EM) waves in an unmagnetized dusty plasma.

5.6.1 Modulational interactions

We consider the nonlinear interaction between large-amplitude EM waves and the DA waves in a dusty plasma. The nonlinear equation for coherent EM waves in the presence of DA waves is obtained from

$$\nabla \times \boldsymbol{B} = \frac{4\pi}{c}\boldsymbol{J} + \frac{1}{c}\frac{\partial \boldsymbol{E}}{\partial t} \tag{5.6.1}$$

with $\boldsymbol{B} = \nabla \times \boldsymbol{A}$, $\boldsymbol{E} = -\partial \boldsymbol{A}/\partial t$ and $\boldsymbol{J} = -e(n_{\rm e0} + n_{\rm e1})\boldsymbol{v}_{\rm e}$, where $n_{\rm e1}$ is the electron number density perturbation associated with the DA waves and the electron quiver velocity in the presence of the EM vector potential $\boldsymbol{A}$ is determined from

$$\frac{\partial \boldsymbol{v}_{\mathrm{e}}}{\partial t} + \nu_{\mathrm{e}}\boldsymbol{v}_{\mathrm{e}} = \frac{e}{m_{\mathrm{e}}c}\frac{\partial \boldsymbol{A}}{\partial t} \tag{5.6.2}$$

where ν_{e} is the effective electron collision frequency. Combining equations (5.6.1) and (5.6.2) we obtain

$$\left[\left(\frac{\partial}{\partial t} + \nu_{\mathrm{e}}\right)\frac{\partial}{\partial t} - c^2\nabla^2 + \omega_{\mathrm{pe}}^2\right]\boldsymbol{A} = -\omega_{\mathrm{pe}}^2\frac{n_{\mathrm{e}1}}{n_{\mathrm{e}0}}\boldsymbol{A}. \tag{5.6.3}$$

The right-hand side of equation (5.6.3) arises due to the nonlinear coupling between the EM pump and the DA waves.

Assuming that the frequency of the DA waves is much smaller than the electron–neutral and electron–dust collision frequencies and that their wavelengths are smaller than $V_{\mathrm{Te}}/\nu_{\mathrm{e}}$, we obtain from the inertialess electron equation of motion

$$\frac{n_{\mathrm{e}1}}{n_{\mathrm{e}0}} = \frac{e\phi_s}{k_{\mathrm{B}}T_{\mathrm{e}}} - \frac{T_{\mathrm{e}1}}{T_{\mathrm{e}}} - \frac{e^2|\boldsymbol{A}|^2}{2m_{\mathrm{e}}k_{\mathrm{B}}T_{\mathrm{e}}c^2} \tag{5.6.4}$$

where ϕ_s is the ambipolar potential of the DA waves, $T_{\mathrm{e}1}$ is a small temperature fluctuation ($\ll T_{\mathrm{e}}$) and the third term in the right-hand side of equation (5.6.4) represents the ponderomotive potential of the EM waves whose frequency is much larger than ν_{e}. The ponderomotive force comes from the averaging of the terms $m_{\mathrm{e}}\boldsymbol{v}_{\mathrm{e}} \cdot \nabla\boldsymbol{v}_{\mathrm{e}} + (e/c)\boldsymbol{v}_{\mathrm{e}} \times \boldsymbol{B}$ over one period of the EM waves.

The electron temperature perturbation is determined from

$$\frac{3k_{\mathrm{B}}}{2}\frac{\partial T_{\mathrm{e}1}}{\partial t} - \frac{\chi_0 k_{\mathrm{B}}}{n_{\mathrm{e}0}}\nabla^2 T_{\mathrm{e}1} - \frac{k_{\mathrm{B}}T_{\mathrm{e}}}{n_{\mathrm{e}0}}\frac{\partial n_{\mathrm{e}1}}{\partial t} = m_{\mathrm{e}}\nu_{\mathrm{e}}|\boldsymbol{v}_{\mathrm{e}}|^2 \tag{5.6.5}$$

where $\chi_0 = 3.2n_{\mathrm{e}0}V_{\mathrm{Te}}^2/\nu_{\mathrm{e}}$ is the electron thermal conductivity and $|\boldsymbol{v}_{\mathrm{e}}|^2 = (e/m_{\mathrm{e}}c)^2|\boldsymbol{A}|^2$ is the squared electron quiver velocity. The right-hand side of equation (5.6.5) represents the electron Joule heating (Stenflo 1985) caused by electron collisions in the EM fields.

To illustrate the physics of the parametric processes, we consider a weakly coupled dusty plasma composed of the electrons and positively charged dust grains. The dust number density perturbation is then obtained by combining the continuity and momentum equations, yielding

$$\frac{\partial^2 n_{\mathrm{d}1}}{\partial t^2} + \nu_{\mathrm{dn}}\frac{\partial n_{\mathrm{d}1}}{\partial t} = -\frac{n_{\mathrm{d}0}Z_{\mathrm{d}0}e}{m_{\mathrm{d}}}\nabla^2\phi_s \tag{5.6.6}$$

where the contribution of the EM ponderomotive force on the dust grains, which is insignificant, has been neglected. By invoking the quasi-neutrality condition, namely $Z_{d0}n_{d1} = n_{e1}$, we can combine equations (5.6.4)–(5.6.6) to obtain (Shukla and Stenflo 2001a)

$$\left[\left(\frac{\partial}{\partial t} - \frac{2\chi_0}{3n_{e0}}\nabla^2\right)\left(\frac{\partial^2}{\partial t^2} + \nu_{dn}\frac{\partial}{\partial t} - C_{De}^2\nabla^2\right) - \frac{2}{3}C_{De}^2\nabla^2\frac{\partial}{\partial t}\right]\frac{n_{e1}}{n_{e0}}$$
$$= \frac{C_{De}^2\omega_{pe}^2}{8\pi n_{e0}k_B T_e c^2}\left(\frac{\partial}{\partial t} - \frac{2\chi_0}{3n_e}\nabla^2 + \frac{4}{3}\nu_e\right)\nabla^2|\boldsymbol{A}|^2 \tag{5.6.7}$$

which is the DA wave equation in the presence of the radiation pressure and the thermal nonlinearity produced by the differential Joule heating of electrons in the presence of EM waves. Here $C_{De} = \omega_{pd}\lambda_{De}$ is the DA speed in a positive dust–electron plasma (Shukla 2000a, c).

We consider the parametric excitation of the DA waves by EM waves. Let us suppose that an EM pump, $\boldsymbol{A}_0 \exp(-i\omega_0 t + i\boldsymbol{k}_0 \cdot \boldsymbol{r})$ + complex conjugate, interacting with low-frequency (ω ($\ll \omega_0$), $\boldsymbol{k}$) DA waves generates EM sidebands $\boldsymbol{A}_\pm \exp(-i\omega_\pm t + i\boldsymbol{k}_\pm \cdot \boldsymbol{r})$, where $\omega_\pm = \omega \pm \omega_0$ and $\boldsymbol{k}_\pm = \boldsymbol{k} \pm \boldsymbol{k}_0$ are the frequencies and wavenumbers for the EM sidebands. Hence we obtain from (5.6.3) and (5.6.7) after Fourier transformation and matching the phasors

$$D_\pm \boldsymbol{A}_\pm = \omega_{pe}^2 N \boldsymbol{A}_{0\pm} \tag{5.6.8}$$

and

$$[(\omega + i\omega_\chi)\epsilon_l - \tfrac{2}{3}\omega\omega_d^2]N$$
$$= \frac{\omega_{de}^2\omega_{pe}^2}{8\pi n_{e0}k_B T_e c^2}\left(\omega + i\omega_\chi + i\frac{4}{3}\nu_e\right)(\boldsymbol{A}_{0-}\cdot\boldsymbol{A}_+ + \boldsymbol{A}_{0+}\cdot\boldsymbol{A}_-) \tag{5.6.9}$$

where $D_\pm = \omega_\pm(\omega_\pm + i\nu_e) - \omega_{pe}^2 - k_\pm^2 c^2$, $\epsilon_l = \omega(\omega + i\nu_{dn}) - \omega_{de}^2$, $\omega_{de} = kC_{De}$, $\omega_\chi = 2k^2\chi_e/3n_{e0}$, $N = \hat{n}_{e1}/n_{e0}$, $n_{e1} = \hat{n}_{e1}\exp(-i\omega t + i\boldsymbol{k}\cdot\boldsymbol{r})$, $\boldsymbol{A}_{0+} = \boldsymbol{A}_0$, $\boldsymbol{A}_{0-} = \boldsymbol{A}_0^*$ and the asterisk denotes the complex conjugate. From equations (5.6.8) and (5.6.9) we readily obtain the nonlinear dispersion relation (Shukla and Stenflo 2001)

$$(\omega + i\omega_\chi)\epsilon_l - \frac{2}{3}\omega\omega_{de}^2 = \left(\omega + i\omega_\chi + i\frac{4\nu_e}{3}\right)\omega_{de}^2\omega_{pe}^4\frac{W_0}{c^2}\sum_\pm \epsilon_\pm^{-1} \tag{5.6.10}$$

where $W_0 = |\boldsymbol{A}_0|^2/8\pi n_{e0}k_B T_e$. Note that $\epsilon_\pm \approx \pm 2\omega_0(\omega + i\Gamma_e - \boldsymbol{k}\cdot\boldsymbol{v}_g \mp \delta_e)$, where $\boldsymbol{v}_g \approx \boldsymbol{k}c^2/\omega_0$ is the group velocity of the pump, $\omega_0 = (k_0^2c^2 + \omega_{pe}^2)^{1/2}$ is the pump wave frequency, $\Gamma_e = \nu_e\omega_{pe}^2/2\omega_0$ is the collisional damping rate of the EM waves and $\delta_e = k^2c^2/2\omega_0$ is the frequency shift caused by the nonlinear interaction of the EM waves with the DA waves. The pump and sidebands are assumed to be coplanar.

Let us focus on the modulational instabilities for which $\epsilon_\pm \approx 0$. Thus equation (5.6.10) takes the form

$$[(\omega + \mathrm{i}\Gamma_\mathrm{e} - \boldsymbol{k}\cdot\boldsymbol{v}_\mathrm{g})^2 - \delta_\mathrm{e}^2]\{(\omega + \mathrm{i}\omega_\chi)[(\omega(\omega + \mathrm{i}\nu_\mathrm{dn}) - \omega_\mathrm{de}^2] - \tfrac{2}{3}\omega\omega_\mathrm{de}^2\}$$
$$= \left(\omega + \mathrm{i}\omega_\chi + \mathrm{i}\frac{4\nu_\mathrm{e}}{3}\right)\delta_\mathrm{e}\frac{\omega_\mathrm{pe}^4\omega_\mathrm{de}^2}{\omega_0 c^2}W_0. \tag{5.6.11}$$

We analyse equation (5.6.11) in two limiting cases.

(i) For ω_χ, $\nu_\mathrm{dn}\omega_\mathrm{de} \ll \omega \ll \nu_\mathrm{e}$, Γ_e and $\boldsymbol{k}\cdot\boldsymbol{v}_\mathrm{g} = 0$ we have from equation (5.6.11)

$$\omega^3 = -\mathrm{i}\frac{4\nu_\mathrm{e}\delta_\mathrm{e}}{3(\Gamma_\mathrm{e}^2 + \delta_\mathrm{e}^2)}\frac{\omega_\mathrm{pe}^4\omega_\mathrm{de}^2}{\omega_0 c^2}W_0 \equiv (\mathrm{i}\Omega_\mathrm{b})^3 \tag{5.6.12}$$

which predicts an instability whose increment is

$$\gamma \approx \left(\frac{\nu_\mathrm{e}\delta_\mathrm{e}}{\Gamma_\mathrm{e}^2 + \delta_\mathrm{e}^2}\right)^{1/3}\left(\frac{\omega_\mathrm{pe}^2\omega_\mathrm{de}}{\omega_0 c}\right)^{2/3}(\omega_0 W_0)^{1/3}. \tag{5.6.13}$$

(ii) For $|\omega - \boldsymbol{k}\cdot\boldsymbol{v}_\mathrm{g}| \ll \Gamma_\mathrm{e}$, $|\omega| \gg \omega_\chi$ and $|\omega + \mathrm{i}\omega_\chi| \ll \nu_\mathrm{e}$, we have from equation (5.6.11)

$$\omega(\omega^2 + \mathrm{i}\nu_\mathrm{dn}\omega - \tfrac{5}{3}\omega_\mathrm{de}^2) = (\mathrm{i}\Omega_\mathrm{b})^3. \tag{5.6.14}$$

Considering the limit $|\omega(\omega + \mathrm{i}\nu_\mathrm{dn})| \ll \omega_\mathrm{de}^2$ we deduce from equation (5.6.14)

$$\omega = \mathrm{i}\frac{3\Omega_\mathrm{b}^3}{5\omega_\mathrm{de}^2} \tag{5.6.15}$$

which depicts a purely growing mode.

5.6.2 Nonlinear particle oscillations

Several experimental observations reveal the presence of nonlinear dust particle oscillations in the sheath of low-pressure rf discharges (Nunomura *et al* 1999, Ivlev *et al* 2000b). It turns out that the dynamics of dust particles in a non-uniform medium containing rf waves is governed by a driven nonlinear (cubic) Klein–Gordon equation which admits a variety of patterns via modulational instabilities (Vanossi *et al* 2000). To study the latter, we start with the Klein–Gordon lattice equation for a dust particle

$$\frac{\partial^2 x_n}{\partial t^2} + \nu_\mathrm{dn}\frac{\partial x_n}{\partial t} + \omega_0^2 x_n = \Omega_\mathrm{t}^2\Delta_n x_n + \lambda x_n^3 + \mathcal{E}_\mathrm{rf}\cos(\omega t) \tag{5.6.16}$$

where ω_0 is the natural frequency of the oscillators, λ is the coefficient of the nonlinearity and $\mathcal{E}_\mathrm{rf} = \omega v_\mathrm{rf}$, $v_\mathrm{rf}(= q_\mathrm{d}E_\mathrm{rf}/m_\mathrm{d}\omega)$ is the quiver speed of the dust particle in the rf field $E_{\mathrm{rf}}\cos(\omega t)$. The nearest-neighbour coupling is $\Delta_n x_n = 2x_n - x_{n+1} - x_{n-1}$. The origin of the nonlinear term λx_n^3 in a dusty plasma sheath is not yet fully understood, although Ivlev *et al* (2000b) suggest that it could be associated with the change in the electrostatic energy of the particles. However, in the presence of dust charge fluctuations we may deduce the parameter $\lambda = (E_0/m_{\mathrm{d}})(\partial^3 q_{\mathrm{d}0}/\partial x_n^3)_{x_n=x_0}$, by assuming $(\partial^2 q_{\mathrm{d}0}/\partial x^2)_{x_n=x_0} = 0$, and thereby ignoring the quadratic term. The properties of equation (5.6.16) have been rigorously analysed in textbooks (e.g. Landau and Lifshitz 1960, Nayfeh and Mook 1979). We now seek a solution of equation (5.6.16) in the form $x_n = x_{n0}\cos(\omega t + \delta_{\mathrm{c}})$ within the rotating frame approximation. The amplitude x_{n0} and phase δ_{c} of the spatially homogeneous solution satisfy

$$x_{n0}^2[\nu_{\mathrm{dn}}^2\omega^2 + (\omega^2 - \omega_0^2 + \tfrac{3}{4}\lambda x_{n0}^2)^2] = \mathcal{E}_{\mathrm{rf}}^2 \tag{5.6.17}$$

which admits two classes of solutions (Vanossi *et al* 2000) for the amplitude x_{n0} of the response to a driving amplitude $\mathcal{E}_{\mathrm{rf}}$. The solutions depend on the values of ω/ω_0, $\nu_{\mathrm{dn}}/\omega_0$ and λ.

Let us analyse the modulational stability of the homogenous solution against spatial perturbations of the form $x_n = y + z_n$. Assuming periodic boundary conditions, we may expand $z_n = \sum_k \exp(\mathrm{i}kn)\xi_k(t)$, where the mode amplitude $\xi_k(t)$ is governed by (Vanossi *et al* 2000)

$$\frac{\partial^2\xi_k}{\partial t^2} + \nu_{\mathrm{dn}}\frac{\partial\xi_k}{\partial t} + \omega_k^2\xi_k = \frac{3}{2}\lambda x_{n0}^2[1 + \cos(2\omega t + 2\delta_{\mathrm{c}})]\xi_k \tag{5.6.18}$$

where $\omega_k^2 = \omega_0^2 + 4\Omega_{\mathrm{t}}^2\sin^2(k/2)$ denotes the linear dispersion relation of the system. The transformation $\xi_k(t) = \xi_k(\omega t + \delta_{\mathrm{c}})\exp[-(\nu_{\mathrm{dn}}/2\omega)(\omega t + \delta_{\mathrm{c}})] \equiv \xi_k(\tau)\exp[-(\nu_{\mathrm{dn}}/2\omega)\tau]$ reduces equation (5.6.18) to a standard Mathieu equation

$$\frac{\mathrm{d}^2\xi_k}{\mathrm{d}\tau^2} + a_{\mathrm{c}}\xi_k - 2b_{\mathrm{c}}\cos(2\tau)\xi_k = 0 \tag{5.6.19}$$

where

$$a_{\mathrm{c}} = \frac{1}{4\omega^2}(4\omega_k^2 - 6\lambda x_{n0}^2 - \nu_{\mathrm{dn}}^2) \qquad \text{and} \qquad b_{\mathrm{c}} = \frac{3\lambda x_{n0}^2}{4\omega^2}. \tag{5.6.20}$$

It is well known that equation (5.6.19) exhibits parametric resonances when $\sqrt{a_{\mathrm{c}}} = j$, where $j = 1, 2, 3\ldots$. The width of the resonance depends on the ratio $b_{\mathrm{c}}/a_{\mathrm{c}}$. The extent of the primary resonance $a_{\mathrm{c}} \simeq 1$ can easily be estimated to be $(a_{\mathrm{c}} - 1)^2 < b_{\mathrm{c}}^2$. However, in the presence of the damping ν_{dn} the resonance condition for equation (5.6.18) becomes

$$b_{\mathrm{c}}^2 > \frac{\nu_{\mathrm{dn}}^2}{\omega^2} + (a_{\mathrm{c}} - 1)^2. \tag{5.6.21}$$

Vanossi *et al* (2000) have presented a stability diagram showing the stability boundaries between the possible patterns in the $(\mathcal{E}_{\mathrm{rf}}, k)$ plane. The modulational instability arises in a very narrow region. The effect of the damping is to pinch off the instability region at a finite driving $\mathcal{E}_{\mathrm{rf}} > 0$. Numerical simulations of the two-dimensional version of (5.6.16) have allowed Vanossi *et al* (2000) to follow the full nonlinear development of the modulational instability and saturation leading to a variety of mesoscopic patterns of intrinsic local modes. The patterns consist of localized regions of large-amplitude coherent oscillations residing on a background that oscillates at the frequency ω of the rf driver. The appearance of spatially periodic structures can be connected to a perturbation of the translational symmetry of thermodynamic states in equilibrium.

5.7 Laboratory Studies

We have theoretically studied different types of possible instabilities that may be excited in unmagnetized and magnetized dusty plasmas. Recently, some of these instabilities, namely the DA instability, the current-driven DIA instability and the current-driven DIC instability have been observed in laboratory experiments (Barkan *et al* 1995a, 1995b, Barkan *et al* 1996, Merlino *et al* 1998, Molotkov *et al* 1999, Fortov *et al* 2000). In this section, we summarize the observations of some important instabilities in current carrying laboratory discharges.

5.7.1 DA wave instability

The confinement of a dusty plasma and the excitation of the DA waves in a Q-machine have already been discussed in section 4.9 (e.g. figure 4.2). The DA waves are spontaneously excited probably due to the ion–dust streaming instability (Rosenberg 1993). The speed with which the pattern of such DA waves moved from the right to the left away from the disc electrode towards the Q-machine's hot plate was measured from a succession of pictures of such waves. A characteristic plot of the position of some given wave feature versus time of arrival is shown in figure 5.3, which yields a propagation speed of $\sim$9 cm s^{-1}. On the other hand, from experimentally observed parameters, such as the fire-rod electric field E_0 (which is directed outwards from the disc electrode) having an average value of 1 V/cm and the corresponding ion mobility $\mu_{\mathrm{m}} \simeq 2 \times 10^5$ cm^2 V^{-1} s^{-1}, one can easily calculate the value of the ion drift velocity $V_{\mathrm{Di}} = \mu_{\mathrm{m}} E_0 \simeq 2 \times 10^5$ cm s^{-1}. A comparison between the values of the DA wave phase velocity $V_p \simeq 9$ cm s^{-1} and the ion drift velocity $V_{\mathrm{Di}} \simeq 2 \times 10^5$ cm s^{-1} clearly indicates that the condition ($V_{\mathrm{p}} < V_{\mathrm{Di}}$) for the onset of the DA streaming instability is well satisfied in the experiment of Barkan *et al* (1995a).

5.7.2 DIA wave instability

The excitation of the DIA waves by means of a grid inserted into the plasma column produced in the Q-machine has been described in section 4.9 (e.g. figure 4.4). It has been observed that the presence of a sufficient amount of

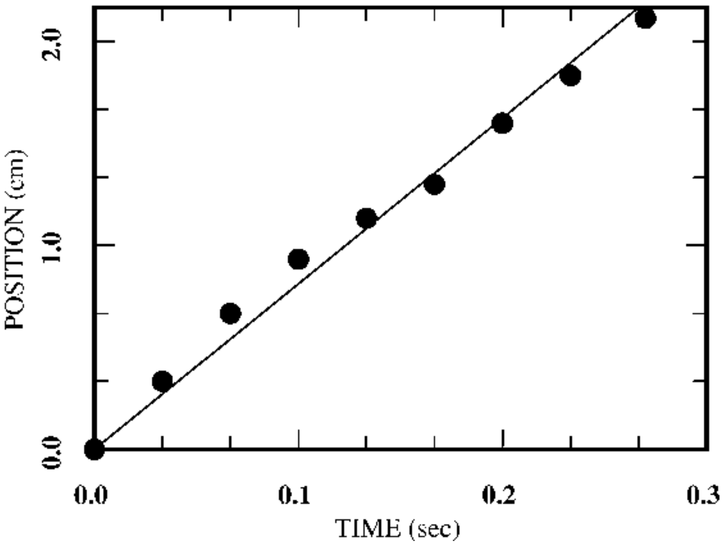

Figure 5.3. The position versus time of arrival of a given wave feature. A propagation speed of $\sim$9 cm s^{-1} is inferred (after Barkan *et al* 1995a).

negatively charged dust particles reduces the spatial damping of the excited DIA waves. A similar effect was experimentally observed when the DIA waves were excited in the plasma by an electron drift relative to the ions (Barkan *et al* 1996, Merlino *et al* 1998). The cold end plate of the Q-machine (shown in figure 4.4) was biased at a constant voltage of +20 V to draw an electron current through the entire cross section of the plasma column. It is well known that in a normal Q-machine plasma, this configuration does not lead to a clear excitation of an ion-acoustic instability, but rather low-frequency (few kHz) potential relaxation oscillations are produced. However, when a sufficient number of dust particles was introduced into the plasma column, the potential relaxation oscillations were quenched while somewhat higher-frequency (3–5 kHz) DIA oscillations were generated. The frequency of these DIA oscillations depends on the dust parameter $Z_d n_d/n_i$ that was varied by changing the rotation rate of the dust dispenser. The variation of the frequency of the current-driven DIA waves as a function of $Z_d n_d/n_i$ is shown in figure 5.4. The increase in the frequency with $Z_d n_d/n_i$ is presumably due to the increase in the phase velocity as $Z_d n_d/n_i$ is increased, since the wavelength is fixed by the boundary conditions. The solid line corresponds to the theoretically derived dispersion relation for the DIA waves, namely $\omega = k(k_B T/m_i)^{1/2}[1 + (1 - Z_d n_d/n_i)^{-1}]^{1/2}$, where we have taken $T = T_e = T_i$. The normalization frequency f_0 is the frequency of the DA waves at $Z_d n_d = 0$ and is equal to 2.8 kHz (Barkan *et al* 1996, Merlino *et al* 1998). The reasonable agreement obtained between the theoretical prediction (Shukla and

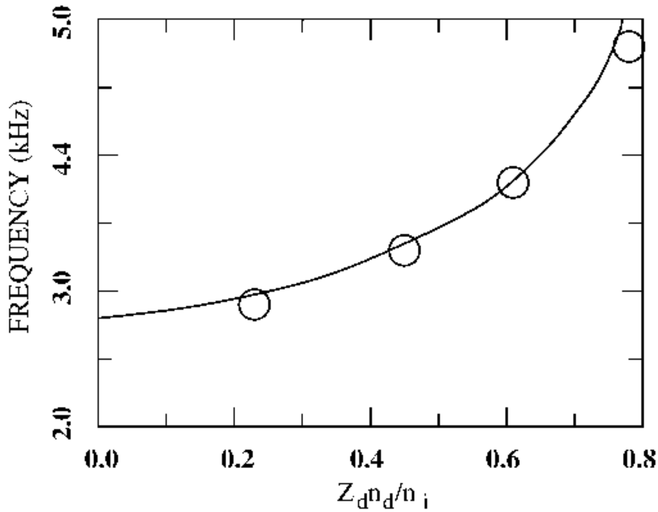

Figure 5.4. The variation of the frequency of the current-driven DIA waves as a function of $Z_d n_d / n_i$. The open circles correspond to laboratory measurements (after Merlino *et al* 1998), whereas the solid line corresponds to the theoretically derived dispersion relation (Shukla and Silin 1992) for the DIA waves.

Silin 1992) and the experimental results supports the identification of the source of the oscillations.

5.7.3 EIC instability

The EIC instability is produced by drawing an electron current along the axis of the plasma column to a 5 mm diameter disc located near the end of the dust dispenser far away from the hot plate of the DPD machine shown in figure 1.8. A disc bias (0.5–1 V) above the space potential produces an electron drift sufficient to excite electrostatic waves with a frequency slightly above the ion gyrofrequency, which propagate radially outwards from the current channel with a wavevector that is nearly perpendicular to the magnetic field. To study the effect of the dust on the instability, the wave amplitude A_0 without the dust particle was measured, and without introducing any other changes in the plasma conditions the dust dispenser was turned on and the wave amplitude A_d and the corresponding $Z_d n_d / n_i$ were measured in the presence of the dust particles (Barkan *et al* 1995b, Merlino *et al* 1998). The ratio A_d / A_0 could then be used as an indication of the effect of the dust. This procedure was repeated for various dust dispenser rotation rates. The results of these measurements are shown in figure 5.5. It appears that as more and more electrons attach onto the dust grains, i.e. $Z_d n_d$ increases, it becomes increasingly easier to excite the EIC waves in the sense that for a given

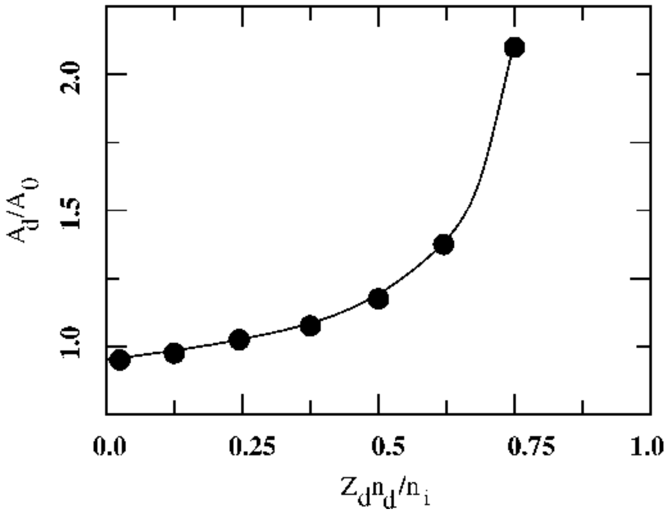

Figure 5.5. The variation of A_d/A_0 (the ratio of the EIC wave amplitude with the dust particles to that without the dust particles) as a function of $Z_d n_d/n_i$ (after Merlino *et al* 1998).

value of the electron drift speed along the magnetic field, the wave amplitude is higher when the dust particles are present. By determining the minimum disc bias (i.e. the critical electron drift for the excitation of the EIC waves) without and with the dust particles, this experiment also verified the theoretical prediction of Chow and Rosenberg (1995) that the presence of negatively charged dust particles reduces the critical electron drift for the excitation of the EIC waves.

Chapter 6

Elongated Dust Grains

6.1 Introduction

Elongated charged dust grains are ubiquitous in cosmic (Spitzer 1977, Harwit 1988) and laboratory plasmas (Chu and I 1994, Mohideen *et al* 1998, Rahman *et al* 2001). The formation of elongated charged dust grains is attributed to the coagulation of particulates in partially or fully ionized gases. Elongated charged grains can acquire rotational and spinning motions due to their interaction with photons and particles of the surrounding gas or due to the presence of an oscillating electric field in a plasma (Tskhakaya and Shukla 2001). In astrophysical objects the angular frequency of the dust grain rotation can reach a rather large value, namely between tens of kHz to MHz for thermal dust grains and hundreds and thousands of MHz for super-thermal grains (Spitzer 1977, Harwit 1988). Furthermore, recent laboratory experiments use cylindrical macroscopic grains in studies of ordered structures (Molotkov *et al* 2000) and levitation of micro-rods in the collisional sheath of an rf plasma (Annaratone *et al* 2001).

In this chapter, we discuss the electrodynamics (Tskhakaya *et al* 2001) and dispersion properties of a dusty magnetoplasma whose constituents are electrons, ions and *finite-sized elongated dust grains*. Specifically, we develop expressions for the charge and current densities for elongated dust grains by including the effects of the dust dipole moment and the dust grain rotation. The forces acting on the dust grains as well as the corresponding dust kinetic equation and the equations of motion are deduced. The dispersion relations for both electromagnetic and electrostatic waves are obtained and analysed. The rotational dust grain energy can be coupled to the various dusty plasma modes. Also described are some mechanisms which are responsible for bouncing, vibrational (quivering) and rotational motions of charged dust grains in a dusty plasma.

6.2 Dust Charge and Current Densities

Let us consider a multi-component dusty plasma in an external magnetic field $\hat{z}B_0$. The dusty plasma constituents are electrons, ions and negatively charged non-spherical rotating dust grains. To construct the electrodynamics of elongated charged dust grains in a magnetized dusty plasma, we have to obtain appropriate expressions for the charge and current densities of dust grains through a dust grain distribution function, taking into account the size of the dust grains. For our purposes, we assume that the charged dust grains form a system of discrete parts (Landau and Lifshitz 1971). The charge microdensity of the grains is represented as

$$\rho_{\mathrm{m}} = \sum_i \left[\sum_j \mathrm{d}q_i\,(\boldsymbol{r}_j)\delta(\boldsymbol{r} - \boldsymbol{r}_j) \right] \tag{6.2.1}$$

where the first summation over i is taken over different grains, while the second over j is taken over different parts of the ith grain, as shown in figure 6.1. Here $\mathrm{d}q_i\,(\boldsymbol{r}_j)$ is the charge of the jth part of the ith grain and $\delta(\boldsymbol{r} - \boldsymbol{r}_j)$ is the usual Dirac delta function. If there is a continuous charge distribution onto the grain, the summation over j can be changed by an integral over the grain's volume and the density of the charge onto the dust grain can be written as

$$\rho_{\mathrm{m}} = \sum_i \int_{V_i(\boldsymbol{R}_i)} \bar{\rho}_i(\boldsymbol{r}' - \boldsymbol{R}_i, \boldsymbol{R}_i)\delta(\boldsymbol{r} - \boldsymbol{r}') \tag{6.2.2}$$

where $\boldsymbol{R}_i$ is the radius vector of the centre of mass of the grain and the integral is taken over the volume $V_i(\boldsymbol{R}_i)$ of the grain. In equation (6.2.2) we introduced the density of the charge distribution onto the grain as

$$\mathrm{d}q_i(\boldsymbol{r}) = \frac{\mathrm{d}q_i(\boldsymbol{r})}{\mathrm{d}\boldsymbol{r}}\,\mathrm{d}\boldsymbol{r} \equiv \bar{\rho}_i(\boldsymbol{r} - \boldsymbol{R}_i, \boldsymbol{R}_i)\,\mathrm{d}\boldsymbol{r}. \tag{6.2.3}$$

For a point grain charge, we have

$$\bar{\rho}_i(\boldsymbol{r} - \boldsymbol{R}_i, \boldsymbol{R}_i) = q_i\delta(\boldsymbol{r} - \boldsymbol{R}_i) \tag{6.2.4}$$

which leads to the usual expression for the charge microdensity of the grain

$$\rho_{\mathrm{m}} = \sum_i q_i\delta(\boldsymbol{r} - \boldsymbol{R}_i) \tag{6.2.5}$$

where q_i is the total charge of the ith grain.

To present a statistical description of the dust grain gas, we have to introduce the probability density D for the grain's gas state (Landau and Lifshitz 1971, Klimontovich 1982). If all grains are identical, we have

$$D = D(\boldsymbol{R}_1, \boldsymbol{v}_1, \boldsymbol{\Omega}_1, \theta_1, \psi_1, \varphi_1; \boldsymbol{R}_2, \boldsymbol{v}_2, \Omega_2, \theta_2, \psi_2, \varphi_2; \ldots, t) \tag{6.2.6}$$

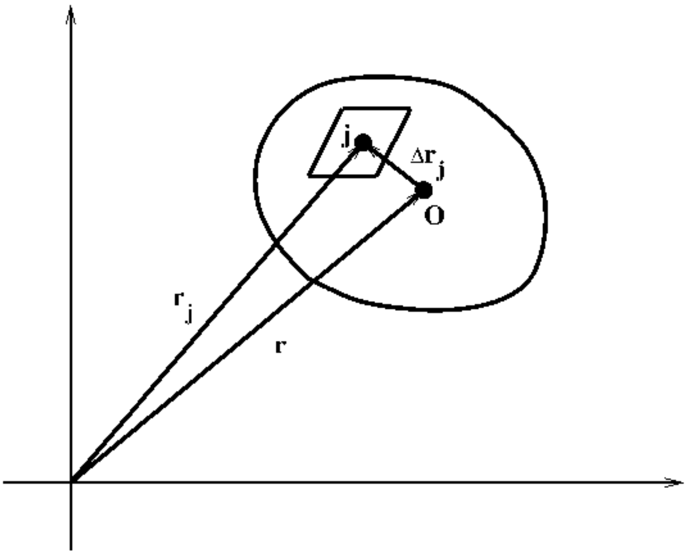

Figure 6.1. A schematic representation of the jth part of an elongated grain.

where $\boldsymbol{v}_i$ is the velocity of the centre of mass, $\boldsymbol{\Omega}_i$ is the angular velocity of the ith grain and θ_i, ψ_i and φ_i (Euler angles) describe the orientation of the elongated grains. The average charge density of the grain in this case can be expressed as

$$\rho(\boldsymbol{r},t) = \int \mathrm{d}\Gamma_1, \mathrm{d}\Gamma_2, \ldots, \mathrm{d}\Gamma_N D\rho_{\mathrm{m}} \tag{6.2.7}$$

where N is the total number of the grains and $\mathrm{d}\Gamma_i = \mathrm{d}\boldsymbol{R}_i\,\mathrm{d}\boldsymbol{v}_i\,\mathrm{d}\boldsymbol{\Omega}_i\,\mathrm{d}\theta_i\,\mathrm{d}\psi_i\,\mathrm{d}\varphi_i$. Now introducing the one-particle distribution function for the dust grains

$$f_{\mathrm{d}}(\boldsymbol{R}_1, \boldsymbol{v}_1, \boldsymbol{\Omega}_1, \theta_1, \psi_1, \varphi_1, t) = N \int \mathrm{d}\Gamma_2, \mathrm{d}\Gamma_3, \ldots \mathrm{d}\Gamma_N D \tag{6.2.8}$$

we can write the charge density of the grains in the following form

$$\rho(\boldsymbol{r},t) = \int \mathrm{d}\Gamma_1 \int_{V_1} \bar{\rho}_1(\boldsymbol{r}'')\delta(\boldsymbol{r} - \boldsymbol{R}_1 - \boldsymbol{r}'') f_{\mathrm{d}}(\boldsymbol{R}_1, \boldsymbol{v}_1, \boldsymbol{\Omega}_1, \theta_1, \psi_1, \varphi_1, t)\,\mathrm{d}\boldsymbol{r}''. \tag{6.2.9}$$

To avoid more complexity, let us omit the subscript 1 and consider one-dimensional dust grain rotation so that the angular velocity is along the external magnetic field direction, namely $\boldsymbol{\Omega} = (0, 0, \Omega)$. Accordingly, equation (6.2.9) can be represented as

$$\rho(\boldsymbol{r},t) = \int d\Gamma \hat{\rho}(\boldsymbol{r} - \boldsymbol{R}, \varphi) f_{\mathrm{d}}(\boldsymbol{R}, \boldsymbol{v}, \Omega, \varphi, t) \tag{6.2.10}$$

where the integrand

$$\hat{\rho}(\boldsymbol{r}-\boldsymbol{R},\varphi)=\int_V \mathrm{d}\boldsymbol{r}'\,\bar{\rho}(\boldsymbol{r}')\delta(\boldsymbol{r}-\boldsymbol{R}-\boldsymbol{r}') \tag{6.2.11}$$

describing the charge distribution onto a single grain depends on the shape of the grain and the azimuthal orientation of the grain's elongation axis. Outside of the grain's volume, we have $\hat{\rho}=0$. For identical grains, we can partly determine the dependence of $\hat{\rho}$ on the azimuthal angle φ. Every given direction of the grain's elongation axis, determined by the angle φ, can be considered as a final position of the turning of the axis (and simultaneously of the whole grain) from the direction with $\varphi=0$. This allows us to write

$$\hat{\rho}(\boldsymbol{r}-\boldsymbol{R},\varphi)=\hat{\rho}[\overset{\leftrightarrow}{\boldsymbol{F}}(\varphi)(\boldsymbol{r}-\boldsymbol{R}),0]\equiv\hat{\rho}[\overset{\leftrightarrow}{\boldsymbol{F}}(\varphi)(\boldsymbol{r}-\boldsymbol{R})] \tag{6.2.12}$$

where $\overset{\leftrightarrow}{\boldsymbol{F}}(\varphi)$ is the tensor of turning by the angle φ, namely

$$\overset{\leftrightarrow}{\boldsymbol{F}}=F_{ij}(\varphi)=\begin{pmatrix}\cos\varphi & -\sin\varphi\\ \sin\varphi & \cos\varphi\end{pmatrix}. \tag{6.2.13}$$

In the dipole approximation, when the dust grain size r_d is much smaller than the scalelength of the plasma inhomogeneity λ_in, namely

$$r_\mathrm{d}\ll\lambda_\mathrm{in} \tag{6.2.14}$$

we substitute equation (6.2.12) into equation (6.2.10) and expand the distribution function f_d around the point $\boldsymbol{r}$ and obtain for the grain's charge density

$$\rho_\mathrm{d}(\boldsymbol{r},t)=\int(q-\boldsymbol{d}\cdot\nabla)f_\mathrm{d}(\boldsymbol{r},\boldsymbol{v},\Omega,\varphi,t)\,\mathrm{d}\Lambda \tag{6.2.15}$$

where $\mathrm{d}\Lambda=\mathrm{d}\boldsymbol{v}\,\mathrm{d}\Omega\,\mathrm{d}\varphi$,

$$q=\int\mathrm{d}\boldsymbol{r}\,\hat{\rho}(\boldsymbol{r}) \tag{6.2.16}$$

and

$$\boldsymbol{d}=\overset{\leftrightarrow}{\boldsymbol{F}}{}^{-1}(\varphi)\int\mathrm{d}\boldsymbol{r}\,\boldsymbol{r}\hat{\rho}(\boldsymbol{r}) \tag{6.2.17}$$

are the total charge and the dipole moment of the dust grain, respectively, and $\overset{\leftrightarrow}{\boldsymbol{F}}{}^{-1}$ is the inverse of the tensor $\overset{\leftrightarrow}{\boldsymbol{F}}(\varphi)$. An analogous calculation leads to the following expression for the dust current density (Tskhakaya *et al* 2001)

$$\boldsymbol{J}_\mathrm{d}(\boldsymbol{r},t)=\int\mathrm{d}\Lambda\,[\boldsymbol{v}(q-\boldsymbol{d}\cdot\nabla)+\boldsymbol{\Omega}\times\boldsymbol{d}]f_\mathrm{d}(\boldsymbol{r},\boldsymbol{v},\Omega,\varphi,t). \tag{6.2.18}$$

The first term in the right-hand side of equation (6.2.18) describes the transfer of the charge (6.2.15) and the second term describes the current arising from the dust grain rotation.

6.3 Grain Kinetic Equation

To construct a kinetic equation for the elongated dust grains, we should have a complete knowledge of the forces that act on the dust grains in the presence of electromagnetic fields. Supposing that charged dust grains constitute a discrete system of particles, we have for the Lagrangian (Tskhakaya *et al* 2001)

$$\mathcal{L} = \sum_i \frac{\Delta m_i u_i^2}{2} + \frac{1}{c}\sum_i \Delta q_i [\boldsymbol{v}_i \cdot \boldsymbol{A}(\boldsymbol{r}_i, t)] - \sum_i \Delta q_i \phi(\boldsymbol{r}_i, t) \tag{6.3.1}$$

where Δm_i and Δq_i are the mass and the charge of the ith grain, respectively, $\boldsymbol{r}_i$ and $\boldsymbol{u}_i$ are its position and velocity. Separating the motions of the centre of mass and the rotation around it, we can write $\boldsymbol{u}_i = \boldsymbol{v} + \boldsymbol{\Omega} \times \boldsymbol{\Delta r}_i$ and $\boldsymbol{r}_i = \boldsymbol{r} + \Delta \boldsymbol{r}_i$, where $\boldsymbol{v}$ and $\boldsymbol{r}_i$ are the velocity and position of the centre of mass, $\Delta \boldsymbol{r}_i$ is the coordinate of the ith part of the grain relative to the centre of mass and $\boldsymbol{\Omega}$ is the angular velocity of the dust grain. The dipole approximation (namely equation (6.2.14)) allows us to expand the potentials as

$$\boldsymbol{A}(\boldsymbol{r}_i, t) = \boldsymbol{A}(\boldsymbol{r}_i, t) + (\Delta \boldsymbol{r}_i \cdot \nabla)\boldsymbol{A}(\boldsymbol{r}_i, t) + \tfrac{1}{2}(\Delta \boldsymbol{r}_i \cdot \nabla)^2 \boldsymbol{A}(\boldsymbol{r}_i, t) + \cdots \tag{6.3.2}$$

and

$$\phi(\boldsymbol{r}_i, t) = \phi(\boldsymbol{r}_i, t) + (\Delta \boldsymbol{r}_i \cdot \nabla)\phi(\boldsymbol{r}, t) + \tfrac{1}{2}(\Delta \boldsymbol{r}_i \cdot \nabla)^2 \phi(\boldsymbol{r}, t) + \cdots. \tag{6.3.3}$$

Accordingly, the Lagrangian (6.3.1) becomes

$$\begin{aligned}\mathcal{L} = {} & \frac{m_{\mathrm{d}} \boldsymbol{v}^2}{2} + \frac{1}{2} I_{\alpha\beta}\Omega_\alpha \Omega_\beta + \frac{q}{c}\boldsymbol{v} \cdot \boldsymbol{A}(\boldsymbol{r}_i, t) - q\phi(\boldsymbol{r}_i, t) + \boldsymbol{m} \cdot \boldsymbol{B} \\ & + \left[\boldsymbol{d} + \frac{1}{2}\sum_i \Delta q_i \Delta \boldsymbol{r}_i (\Delta \boldsymbol{r}_i \cdot \nabla)\right] \cdot \left(\boldsymbol{E} + \frac{\boldsymbol{v}}{c} \times \boldsymbol{B}\right)\end{aligned} \tag{6.3.4}$$

where $m_{\mathrm{d}} = \sum_i \Delta m_i$ and $q = \sum_i \Delta q_i$ are the total mass and the charge of the grain, respectively, $I_{\alpha,\beta} = \sum_i \Delta m_i [(\Delta \boldsymbol{r}_i)^2 \delta_{\alpha\beta} - (\Delta \boldsymbol{r}_i)_\alpha \cdot (\Delta \boldsymbol{r}_i)_\beta]$ is the tensor of the moment of inertia, $\boldsymbol{d} = \sum_i \Delta q_i \Delta \boldsymbol{r}_i$ is the dipole moment of the elongated grain and $\boldsymbol{m} = (1/2c)\sum_i \Delta q_i (\Delta \boldsymbol{r}_i \times \boldsymbol{U}_i)$ is the magnetic moment of the grain. Here $\boldsymbol{U}_i = \boldsymbol{\Omega} \times \Delta \boldsymbol{r}_i$ is the rotational velocity. The electric and magnetic fields are $\boldsymbol{E} = -\nabla\phi - c^{-1}\partial \boldsymbol{A}(\boldsymbol{r}_i, t)/\partial t$ and $\boldsymbol{B} = \nabla \times \boldsymbol{A}(\boldsymbol{r}_i, t)$, respectively. In deriving (6.3.4), we used the relation

$$\frac{\mathrm{d}\boldsymbol{d}}{\mathrm{d}t} = \boldsymbol{\Omega} \times \boldsymbol{d}. \tag{6.3.5}$$

Note that in the presence of the gravitational field $\boldsymbol{g}$, we must add the term $m_{\mathrm{d}}\boldsymbol{g} \cdot \boldsymbol{r}_i$ in the right-hand side of equation (6.3.4). We neglect the second term (which is associated with the multi-dipole effect) in the square bracket of equation (6.3.4) and obtain the equations of motion for the elongated dust grains as

$$\frac{\mathrm{d}\boldsymbol{p}}{\mathrm{d}t} = (q + \boldsymbol{d} \cdot \nabla)\left(\boldsymbol{E} + \frac{1}{c}\boldsymbol{v} \times \boldsymbol{B}\right) + \frac{1}{c}(\boldsymbol{\Omega} \times \boldsymbol{d}) \times \boldsymbol{B} + (\boldsymbol{m} \times \nabla) \times \boldsymbol{B} \tag{6.3.6}$$

and

$$\frac{\mathrm{d}M_\alpha}{\mathrm{d}t} = -\frac{1}{2}S_{\alpha\beta}\left[\frac{\partial B_\beta}{\partial t} + (\boldsymbol{v}\cdot\nabla)B_\beta\right] + \left[\boldsymbol{d}\times\left(\boldsymbol{E} + \frac{1}{c}\boldsymbol{v}\times\boldsymbol{B}\right)\right]_\alpha + (\boldsymbol{m}\times\boldsymbol{B})_\alpha \tag{6.3.7}$$

where $\boldsymbol{p} = m_\mathrm{d}\boldsymbol{v}$, $S_{\alpha\beta} = c^{-1}\sum_i \Delta q_i[(\Delta\boldsymbol{r}_i)^2\delta_{\alpha\beta} - (\Delta\boldsymbol{r}_i)_\alpha(\Delta\boldsymbol{r}_i)_\beta]$ and $M_\alpha = I_{\alpha\beta}\Omega_\beta$ is the angular momentum of the grain. The kinetic equation for the elongated dust grains can now be written as

$$\frac{\partial f_\mathrm{d}}{\partial t} + \boldsymbol{v}\cdot\frac{\partial f_\mathrm{d}}{\partial \boldsymbol{r}} + \boldsymbol{\Omega}\cdot\frac{\partial f_\mathrm{d}}{\partial \boldsymbol{\varphi}} + \frac{\mathrm{d}\boldsymbol{p}}{\mathrm{d}t}\cdot\frac{\partial f_\mathrm{d}}{\partial \boldsymbol{p}} + \frac{\mathrm{d}\boldsymbol{M}}{\mathrm{d}t}\cdot\frac{\partial f_\mathrm{d}}{\partial \boldsymbol{M}} = 0. \tag{6.3.8}$$

It can be easily shown from equations (6.3.8), (6.2.15) and (6.2.18) that the dust grain charge and current densities satisfy the continuity equation

$$\frac{\partial \rho_\mathrm{d}}{\partial t} + \nabla\cdot\boldsymbol{J}_\mathrm{d} = 0. \tag{6.3.9}$$

We can, therefore, construct the kinetics and electrodynamics of a dusty plasma with elongated and rotating dust grains by means of the expressions for ρ_d and $\boldsymbol{J}_\mathrm{d}$.

6.4 Dielectric Permittivity

We assume that the dust grain size is much smaller than the grain gyroradius and that the dust grain thermal speed is smaller than the characteristic speed of our problem. Under these conditions along with equation (6.2.14), the equations of motion (6.3.6) and (6.3.7) can be simplified. We consider the one-dimensional case of dust grain rotation so that $\boldsymbol{M} = (0, 0, M)$, where $M = I\Omega$ and I is the z component of the principal moment of inertia. The kinetic equation (6.3.8) for the dust grain then takes the form

$$\frac{\partial f_\mathrm{d}}{\partial t} + \boldsymbol{v}\cdot\frac{\partial f_\mathrm{d}}{\partial \boldsymbol{r}} + \Omega\frac{\partial f_\mathrm{d}}{\partial \varphi} + (\boldsymbol{d}\times\boldsymbol{E})_z\frac{\partial f_\mathrm{d}}{\partial M} + q\left(\boldsymbol{E} + \frac{1}{c}\boldsymbol{v}\times\boldsymbol{B}\right)\cdot\frac{\partial f_\mathrm{d}}{\partial \boldsymbol{p}} = 0. \tag{6.4.1}$$

The well known kinetic equations for the electrons and ions are

$$\frac{\partial f_j}{\partial t} + \boldsymbol{v}\cdot\frac{\partial f_j}{\partial \boldsymbol{r}} + q_j\left(\boldsymbol{E} + \frac{1}{c}\boldsymbol{v}\times\boldsymbol{B}\right)\cdot\frac{\partial f_j}{\partial \boldsymbol{p}} = 0. \tag{6.4.2}$$

Now assuming that the wave electric and magnetic field perturbations are small, we can express the perturbed distribution function as $\delta f_s = f_s - f_{s0} \ll f_{s0}$. The equilibrium distribution functions are of the form (Landau and Lifshitz 1989)

$$f_{\mathrm{d}0} = \frac{n_{\mathrm{d}0}}{2\pi(2\pi m_\mathrm{d}k_\mathrm{B}T_\mathrm{d})^{3/2}}\frac{1}{(2\pi Ik_\mathrm{B}T_\mathrm{d})^{1/2}} \times \exp[-(p^2/2m_\mathrm{d}k_\mathrm{B}T_\mathrm{d}) - (M - M_0)^2/2Ik_\mathrm{B}T_\mathrm{d}] \tag{6.4.3}$$

and

$$f_{j0} = \frac{n_{j0}}{(2\pi m_j k_B T_j)^{3/2}} \exp[-(p^2/2m_j k_B T_j)]. \tag{6.4.4}$$

We assumed that the dust grains rotate with a preferred angular velocity Ω_0 so that $M_0 = I\Omega_0$. The components of the dust dipole moment are

$$d_x = d\cos\varphi, \qquad d_y = d\sin\varphi. \tag{6.4.5}$$

Thus, the perturbed dust grain distribution function is represented as

$$\delta f_d = \sum_{n=-\infty}^{\infty} \delta f_n \exp(\mathrm{i}n\varphi). \tag{6.4.6}$$

6.4.1 Unmagnetized dusty plasmas

We first consider an unmagnetized dusty plasma ($B_0 = 0$) and assume that all perturbed quantities are proportional to $\exp(-\mathrm{i}\omega t + \mathrm{i}\boldsymbol{k}\cdot\boldsymbol{r})$. We linearize (6.4.1) and (6.4.2) and substitute them into the Poisson–Maxwell equations and obtain the dielectric tensor for the dusty plasma following the standard method. The result is (Alexandrov *et al* 1984)

$$\epsilon_{ij}(\omega,\boldsymbol{k}) = \frac{k_i k_j}{k^2}\epsilon^{\mathrm{l}}(\omega,\boldsymbol{k}) + \left(\delta_{ij} - \frac{k_i k_j}{k^2}\right)\epsilon^{\mathrm{t}}(\omega,\boldsymbol{k}) + \left(\delta_{ij} - \frac{\Omega_i\Omega_j}{\Omega^2}\right)\epsilon^{\mathrm{d}}(\omega,\boldsymbol{k}) \tag{6.4.7}$$

where $\epsilon^{\mathrm{l}}(\omega,\boldsymbol{k})$ and $\epsilon^{\mathrm{t}}(\omega,\boldsymbol{k})$ are the usual longitudinal and transverse dielectric permittivities, respectively. They are given by

$$\epsilon^{\mathrm{l}}(\omega,\boldsymbol{k}) = 1 + \sum_s \frac{\omega_{ps}^2}{k^2 V_{Ts}^2}\left[1 - J_+\left(\frac{\omega}{kV_{Ts}}\right)\right] \tag{6.4.8}$$

and

$$\epsilon^{\mathrm{t}}(\omega,\boldsymbol{k}) = 1 - \sum_s \frac{\omega_{ps}^2}{\omega^2} J_+\left(\frac{\omega}{kV_{Ts}}\right). \tag{6.4.9}$$

The function $J_+(x)$ is

$$J_+(x) = \frac{x}{\sqrt{2\pi}}\int_{-\infty}^{\infty} \mathrm{d}z\, \frac{\exp(-z^2/2)}{x - z}. \tag{6.4.10}$$

The asymptotic forms of equation (6.4.10) are

$$J_+(x) \approx 1 + \frac{1}{x^2} + \cdots - \mathrm{i}\sqrt{\frac{\pi}{2}}\, x \exp\left(-\frac{x^2}{2}\right) \tag{6.4.11}$$

for $|x| \gg 1$, $|\mathrm{Re}\, x| \gg |\mathrm{Im}\, x|$, $\mathrm{Im}\, x < 0$ and

$$J_+(x) \approx -\mathrm{i}\sqrt{\frac{\pi}{2}}\, x \tag{6.4.12}$$

for $|x| \ll 1$. The influence of the dust grain rotation is described by $\epsilon^{\mathrm{d}}(\omega, \boldsymbol{k})$, which is

$$\epsilon^{\mathrm{d}}(\omega, \boldsymbol{k}) = -\frac{\Omega_{\mathrm{r}}^2}{\omega^2}\frac{k^2}{K^2}\frac{\omega}{\omega - \Omega_0} J_+\left(\frac{\omega - \Omega_0}{K V_{\mathrm{Td}}}\right) + \frac{\Omega_{\mathrm{r}}^2}{K^2 V_{\mathrm{Td}}^2}\left(\frac{\kappa^2}{K^2} + \frac{k^2}{K^2}\frac{\Omega_0}{\omega}\right)\left[1 - J_+\left(\frac{\omega - \Omega_0}{K V_{\mathrm{Td}}}\right)\right] \tag{6.4.13}$$

where $\Omega_{\mathrm{r}} = (4\pi d^2 n_{\mathrm{d}0}/4I)^{1/2}$, $K = (k^2 + \kappa^2)^{1/2}$ and $\kappa = (m_{\mathrm{d}}/I)^{1/2}$.

6.4.2 Magnetized dusty plasmas

We now consider a magnetized dusty plasma ($B_0 \neq 0$). Here equations (6.4.1) and (6.4.2) for the dust grains read

$$\frac{\partial \delta f_n}{\partial t} + \boldsymbol{v} \cdot \frac{\partial \delta f_n}{\partial \boldsymbol{r}} + \mathrm{i} n \Omega \delta f_n - \omega_{\mathrm{cd}}\frac{\partial \delta f_n}{\partial \psi_{\mathrm{a}}} = -q\boldsymbol{E} \cdot \frac{\partial f_{\mathrm{d}0}}{\partial \boldsymbol{p}}\Delta(n) - \frac{\mathrm{i}}{2}\frac{\partial f_{\mathrm{d}0}}{\partial M} d[(E_x - \mathrm{i}E_y)\Delta(n-1) - (E_x + \mathrm{i}E_y)\Delta(n+1)] \tag{6.4.14}$$

while for the electrons and ions we have

$$\frac{\partial \delta f_j}{\partial t} + \boldsymbol{v} \cdot \frac{\partial \delta f_j}{\partial \boldsymbol{r}} - \omega_{cj}\frac{\partial \delta f_j}{\partial \psi_{\mathrm{a}}} = -q_j \boldsymbol{E} \cdot \frac{\partial f_{j0}}{\partial \boldsymbol{p}} \tag{6.4.15}$$

where $\omega_{\mathrm{cd}} = qB_0/m_{\mathrm{d}}c$, $\omega_{\mathrm{c}j} = q_j B_0/m_j c$ and $\Delta(n) = 1$ for $n = 0$ and 0 for $n \neq 0$. The symbol ψ_{a} is the azimuthal angle in the momentum space, $p_x = p_\perp \cos\psi_{\mathrm{a}}$ and $p_y = p_\perp \sin\psi_{\mathrm{a}}$. According to equation (6.4.14) only $n = 0, \pm 1$ give a contribution in the summation of equation (6.4.6).

Assuming that the perturbed quantities are proportional to $\exp(-\mathrm{i}\omega t + \mathrm{i}\boldsymbol{k}\cdot\boldsymbol{r})$, we obtain the following solutions of equations (6.4.14) and (6.4.15)

$$\delta f_0 = \frac{q_{\mathrm{d}}\boldsymbol{E}}{\omega_{\mathrm{cd}}} \cdot \int_{\pm\infty}^{\psi_{\mathrm{a}}} \mathrm{d}\psi' \frac{\partial f_{\mathrm{d}0}}{\partial \boldsymbol{p}} \exp\left\{-\int_{\psi'}^{\psi_{\mathrm{a}}}\left[\frac{\Omega_{\mathrm{R}}(\psi'')}{\omega_{\mathrm{cd}}}\right]\mathrm{d}\psi''\right\} \tag{6.4.16}$$

$$\delta f_{\pm 1} = \pm\frac{\mathrm{i}}{2}\frac{dE_{\mp}}{\omega_{\mathrm{cd}}} \int_{\pm\infty}^{\psi_{\mathrm{a}}} \mathrm{d}\psi' \frac{\partial f_{\mathrm{d}0}}{\partial M} \exp\left\{-\int_{\psi'}^{\psi_{\mathrm{a}}}\left[\frac{\Omega_{\mathrm{R}}(\psi'') \mp \Omega}{\omega_{\mathrm{cd}}}\right]\mathrm{d}\psi''\right\} \tag{6.4.17}$$

and

$$\delta f_j = \frac{q_j \boldsymbol{E}\cdot}{\omega_{c\alpha}} \int_{\pm\infty}^{\psi_{\mathrm{a}}} \mathrm{d}\psi' \frac{\partial f_{j0}}{\partial \boldsymbol{p}} \exp\left\{-\int_{\psi'}^{\psi_{\mathrm{a}}}\left[\frac{\Omega_{\mathrm{R}}(\psi'')}{\omega_{cj}}\right]\mathrm{d}\psi''\right\} \tag{6.4.18}$$

where $\Omega_{\mathrm{R}}(\psi'') = \omega - \boldsymbol{k} \cdot \boldsymbol{v}(\psi'')$ and $E_{\mp} = E_x \mp \mathrm{i}E_y$. Substituting equations (6.4.16)–(6.4.18) into equation (6.2.18) as well as the linearized version of equation (6.4.2) into the expression for the electron and ion current densities, namely

$$\boldsymbol{J}_j = q_j \int \mathrm{d}\boldsymbol{p}\, \boldsymbol{v} \delta f_j \tag{6.4.19}$$

we obtain for the total current density

$$J_i = \left[\sigma^{\mathrm{r}}_{ij}(\omega, \boldsymbol{k}) + \sum_{s=\mathrm{e,i,d}} \sigma^{s}_{ij}(\omega, \boldsymbol{k})\right] E_j \tag{6.4.20}$$

where the first term in the right-hand side of equation (6.4.20) is connected with the rotation of the dust grain, while the second term represents the contributions of the electrons and ions including the centre of mass motion of the grains. We have denoted

$$\sigma^{\mathrm{r}}_{ij}(\omega, \boldsymbol{k}) = \begin{pmatrix} \sigma^{\mathrm{r}}_{xx} & \sigma^{\mathrm{r}}_{xy} & 0 \\ -\sigma^{\mathrm{r}}_{xy} & \sigma^{\mathrm{r}}_{yy} & 0 \\ 0 & 0 & 0 \end{pmatrix} \tag{6.4.21}$$

where (Tskhakaya *et al* 2001)

$$\sigma^{\mathrm{r}}_{xx} = \sigma^{\mathrm{r}}_{yy} = \mathrm{i}\frac{n_{\mathrm{d}0} d^2}{4I} \frac{1}{K V_{\mathrm{Td}}} \sum_{n=-\infty}^{\infty} \Gamma_n(b_{\mathrm{d}})(\Phi^n_- + \Phi^n_+) \tag{6.4.22}$$

$$\sigma^{\mathrm{r}}_{xy} = \frac{n_{\mathrm{d}0} d^2}{4I} \frac{1}{K V_{\mathrm{Td}}} \sum_{n=-\infty}^{\infty} \Gamma_n(b_{\mathrm{d}})(\Phi^n_- - \Phi^n_+) \tag{6.4.23}$$

with

$$\begin{aligned} \Phi^n_{\pm} = {} & \frac{k_z^2}{K^2} \frac{K V_{\mathrm{Td}}}{\omega \pm \Omega_0 - n\omega_{\mathrm{cd}}} J_+\left(\frac{\omega \pm \Omega_0 - n\omega_{\mathrm{cd}}}{K V_{\mathrm{Td}}}\right) \\ & - \left(\frac{\kappa^2}{K^2} \frac{\omega - n\omega_{\mathrm{cd}}}{K V_{\mathrm{Td}}} \mp \frac{k_z^2}{K^2} \frac{\Omega_0}{K V_{\mathrm{Td}}}\right) \left[1 + J_+\left(\frac{\omega \pm \Omega_0 - n\omega_{\mathrm{cd}}}{K V_{\mathrm{Td}}}\right)\right]. \end{aligned} \tag{6.4.24}$$

For the tensor $\sigma^{s}_{ij}(\omega, \boldsymbol{k})$, we have

$$\begin{aligned} \sigma_{ij}(\omega, \boldsymbol{k}) = {} & \frac{q_s^2}{\omega_{\mathrm{c}s}} \int \mathrm{d}\boldsymbol{p}\, v_i(\psi_{\mathrm{a}}) \int_{\pm\infty}^{\psi_{\mathrm{a}}} \mathrm{d}\psi' \left(\frac{\partial f_{s0}}{\partial p_j}\right)_{\psi'} \\ & \times \exp\left\{\mathrm{i} \int_{\psi'}^{\psi_{\mathrm{a}}} \left[\frac{\Omega_{\mathrm{R}}(\psi'')}{\omega_{\mathrm{c}s}}\right] \mathrm{d}\psi''\right\}. \end{aligned} \tag{6.4.25}$$

We now carry out straightforward calculations and obtain the expressions for the different elements of the tensor of the dielectric permittivity (Alexandrov *et al* 1984). We have

$$\epsilon_{ij}(\omega, \boldsymbol{k}) = \hat{\epsilon}_{ij}(\omega, \boldsymbol{k}) + \epsilon^{\mathrm{r}}_{ij}(\omega, \boldsymbol{k}) \tag{6.4.26}$$

where

$$\hat{\epsilon}_{xx} = 1 - \sum_s \sum_n \frac{n^2 \omega_{ps}^2}{\omega(\omega - n\omega_{cs})} \frac{\Gamma_n(b_s)}{b_s} J_+(\xi_n) \tag{6.4.27}$$

$$\hat{\epsilon}_{yy} = \hat{\epsilon}_{xx} + 2 \sum_s \sum_n \frac{\omega_{ps}^2 b_s}{\omega(\omega - n\omega_{cs})} \Gamma_n'(b_s) J_+(\xi_n) \tag{6.4.28}$$

$$\hat{\epsilon}_{xy} = -\hat{\epsilon}_{yx} = -\mathrm{i} \sum_s \sum_n \frac{n^2 \omega_{ps}^2}{\omega(\omega - n\omega_{cs})} \Gamma_n'(b_s) J_+(\xi_n) \tag{6.4.29}$$

$$\hat{\epsilon}_{xz} = \hat{\epsilon}_{zx} = \sum_s \sum_n \frac{n\omega_{ps}^2 k_\perp}{\omega\omega_{cs} k_z} \frac{\Gamma_n(b_s)}{b_s} [1 - J_+(\xi_n)] \tag{6.4.30}$$

$$\hat{\epsilon}_{yz} = -\hat{\epsilon}_{zy} = -\mathrm{i} \sum_s \sum_n \frac{\omega_{ps}^2 k_\perp}{\omega\omega_{cs} k_z} \Gamma_n'(b_s)[1 - J_+(\xi_n)] \tag{6.4.31}$$

$$\hat{\epsilon}_{zz} = 1 + \sum_s \sum_n \frac{\omega_{ps}^2(\omega - n\omega_{cs})}{\omega k_z^2 V_{Ts}^2} \Gamma_n(b_s)[1 - J_+(\xi_n)] \tag{6.4.32}$$

and

$$\epsilon_{ij}^{\mathrm{r}}(\omega, \boldsymbol{k}) = \frac{4\pi\mathrm{i}}{\omega} \sigma_{ij}^{\mathrm{r}}(\omega, \boldsymbol{k}) \tag{6.4.33}$$

with $\xi_n = (\omega - n\omega_{cs})/k_z V_{Ts}$ and $\boldsymbol{k} \equiv (k_\perp, 0, k_z)$.

We consider a cold gas of dust grains. Assuming $b_d \ll 1$ and $|\omega \pm \Omega_0| \gg K V_{Td}$, we have for the rotational part of the dielectric tensor (Tskhakaya *et al* 2001)

$$\epsilon_{ij}^{\mathrm{r}} = \begin{pmatrix} \epsilon_\perp^{\mathrm{r}} & \mathrm{i}g^{\mathrm{r}} & 0 \\ -\mathrm{i}g^{\mathrm{r}} & \epsilon_\perp^{\mathrm{r}} & 0 \\ 0 & 0 & 0 \end{pmatrix} \tag{6.4.34}$$

where

$$\epsilon_\perp^{\mathrm{r}} = -\frac{\Omega_{\mathrm{r}}^2}{(\omega - \Omega_0)^2} - \frac{\Omega_{\mathrm{r}}^2}{(\omega + \Omega_0)^2} \tag{6.4.35}$$

and

$$g^{\mathrm{r}} = \frac{\Omega_{\mathrm{r}}^2}{(\omega - \Omega_0)^2} - \frac{\Omega_{\mathrm{r}}^2}{(\omega + \Omega_0)^2}. \tag{6.4.36}$$

The dispersion relation for a magnetized dusty plasma can be obtained by inserting equation (6.4.20) into the Maxwell equations.

6.5 Dispersion Properties of the Waves

We now consider the properties of numerous waves in dusty plasmas without and with an external magnetic field.

6.5.1 Unmagnetized dusty plasmas

Let us consider the frequency regimes $kV_{\mathrm{Td}} \ll \omega \ll kV_{\mathrm{Ti}}, kV_{\mathrm{Te}}$ and $\omega \pm \Omega_0 \gg KV_{\mathrm{Td}}$. Without loss of generality, we may assume that the wavevector $\boldsymbol{k}$ lies in the (x, z) plane, i.e. $\boldsymbol{k} = (k_\perp, 0, k_z)$. In such a situation, the general dispersion relation is of the form (Alexandrov *et al* 1984)

$$\left| k^2\delta_{ij} - k_i k_j - \frac{\omega^2}{c^2}\epsilon_{ij}(\omega, \boldsymbol{k}) \right| = 0. \tag{6.5.1}$$

We now discuss two specific examples for wave phenomena associated with the elongated and rotating dust grains.

6.5.1.1 *Transverse waves*

We assume that the transverse waves under consideration are polarized along the y-axis so that $\boldsymbol{E} = (0, E, 0)$. Thus, equation (6.5.1) gives

$$\frac{k^2c^2 + \omega_{\mathrm{pd}}^2}{\omega^2} = 1 - \frac{2\Omega_{\mathrm{r}}^2}{(\omega - \Omega_0)^2}. \tag{6.5.2}$$

For $\Omega_0 = 0$ the influence of the dust grain rotation disappears. However, for waves with frequencies close to Ω_0 ($\omega_{\mathrm{pd}} \approx \Omega_{\mathrm{r}}$), we obtain

$$\omega = \Omega_0 \left[1 \pm \mathrm{i}\frac{\sqrt{2}\Omega_{\mathrm{r}}}{(k^2c^2 + \omega_{\mathrm{pd}}^2)^{1/2}} \right]. \tag{6.5.3}$$

Equation (6.5.3) reveals that the ordinary transverse waves become unstable. The growth rate is given by $\sqrt{2}\Omega_0\Omega_{\mathrm{r}}/(k^2c^2 + \omega_{\mathrm{pd}}^2)^{1/2}$, which strongly depends upon Ω_{r} (which is a function of the dipole moment as well as the moment of inertia of the dust grains) and the dust rotation frequency Ω_0. It is worth noting that in the plasma without the dust grains, the low-frequency transverse oscillations decay aperiodically due to their collisionless absorption by the electrons.

6.5.1.2 *Longitudinal waves*

Equation (6.5.1) also admits low-frequency ($|\omega| \ll kc, kV_{\mathrm{Te}}, kV_{\mathrm{Ti}}, |\omega - \Omega_0| \gg KV_{\mathrm{Td}}$) longitudinal waves. We consider two cases.

(i) DA waves

The modified dispersion relation for the DA waves (Rao *et al* 1990), which is deduced from equation (6.5.1) by using the appropriate susceptibilities, reads (Mahmoodi *et al* 2000)

$$1 + \frac{1}{k^2\lambda_{\mathrm{D}}^2} - \frac{\omega_{\mathrm{pd}}^2}{\omega^2} - \frac{k_\perp^2}{k^2}\left[\frac{\Omega_{\mathrm{r}}^2}{(\omega - \Omega_0)^2} + \frac{\Omega_{\mathrm{r}}^2}{(\omega + \Omega_0)^2} \right] = 0. \tag{6.5.4}$$

Equation (6.5.4) is formally similar to the dispersion relation which has been discussed in the literature (Mikhailovskii 1974, Alexandrov *et al* 1984) in connection with the two-stream instability. It follows from equation (6.5.4) that the dust grain rotation gives a contribution only for waves with $k_\perp \neq 0$. When there is no grain rotation, i.e. $\Omega_0 = 0$, from equation (6.5.4) we have

$$\omega = \left(\omega_{\mathrm{pd}}^2 + \frac{k_\perp^2}{k^2}\Omega_{\mathrm{r}}^2\right)^{1/2}\left(1 + \frac{1}{k^2\lambda_{\mathrm{D}}^2}\right)^{-1/2}. \tag{6.5.5}$$

However, in the presence of the dust grain rotation, equation (6.5.4) admits complex solutions for any rotation frequency Ω_0, satisfying the condition

$$\Omega_0^2 < \omega_{\mathrm{pd}}^2\left(1 + \frac{1}{k^2\lambda_{\mathrm{D}}^2}\right)^{-1}\left[1 + \left(\frac{k_\perp^2}{k^2}\frac{\Omega_{\mathrm{r}}^2}{\omega_{\mathrm{pd}}^2}\right)^{1/3}\right]^3. \tag{6.5.6}$$

The equality of Ω_0 in the right-hand side of equation (6.5.6) defines the boundary of the stability of the DA wave. Letting $\omega \simeq \Omega_0 + \mathrm{i}\omega_i$, where $\omega_i \ll \Omega_0$, we obtain from equation (6.5.4) the growth rate for $\omega_{\mathrm{pd}}^2 + k_\perp^2\Omega_{\mathrm{r}}^2/k^2 \approx \Omega_0^2(1 + 1/k^2\lambda_{\mathrm{D}}^2)$

$$\omega_i = \frac{3^{1/2}}{2^{4/3}}\left(\frac{k_\perp^2}{k^2}\frac{\Omega_{\mathrm{r}}^2}{\omega_{\mathrm{pd}}^2}\right)^{1/3}\Omega_0. \tag{6.5.7}$$

Equation (6.5.7) exhibits that the growth rate of the instability is directly proportional to $\Omega_{\mathrm{r}}^{2/3}\Omega_0$.

(ii) DIA waves

We now focus on the DIA waves (Shukla and Silin 1992) whose phase velocity ($V_{\mathrm{p}} = \omega/k$) satisfies $V_{\mathrm{Td}}, V_{\mathrm{Ti}} \ll V_{\mathrm{p}} \ll V_{\mathrm{Te}}$. Assuming $\omega \ll kc$ and $|\omega - \Omega_0| \gg KV_{\mathrm{Td}}$, we have

$$\epsilon^{\mathrm{l}}(\omega, \boldsymbol{k}) = 1 + \frac{1}{k^2\lambda_{\mathrm{De}}^2} - \frac{\omega_{\mathrm{p}}^2}{\omega^2} \tag{6.5.8}$$

$$\epsilon^{\mathrm{t}}(\omega, \boldsymbol{k}) = 1 + \mathrm{i}\sqrt{\frac{\pi}{2}}\frac{\omega_{\mathrm{pe}}^2}{\omega^2}\frac{\omega}{kV_{\mathrm{Te}}} - \frac{\omega_{\mathrm{p}}^2}{\omega^2} \tag{6.5.9}$$

and

$$\epsilon^{\mathrm{r}}(\omega, \boldsymbol{k}) = -\frac{\Omega_{\mathrm{r}}^2}{(\omega - \Omega_0)^2} - \frac{\Omega_{\mathrm{r}}^2}{(\omega + \Omega_0)^2} \tag{6.5.10}$$

where $\omega_{\mathrm{p}} = (\omega_{\mathrm{pi}}^2 + \omega_{\mathrm{pd}}^2)^{1/2}$. Neglecting the electron Landau damping term in equation (6.5.9), which holds for $|\omega| \ll \omega_{\mathrm{p}}^2 kV_{\mathrm{Te}}/\omega_{\mathrm{pe}}^2$, we obtain from equations (6.5.1) and (6.5.8)–(6.5.10) the modified dispersion relation for the DIA waves. We have

$$1+\frac{1}{k^2\lambda_{\mathrm{De}}^2}-\frac{\omega_{\mathrm{p}}^2}{\omega^2}-\frac{2k_\perp^2}{k^2}\frac{\Omega_{\mathrm{r}}^2(\omega^2+\Omega_0^2)}{(\omega^2-\Omega_0^2)^2}=0. \tag{6.5.11}$$

When we neglect the effect of the dust grain rotation (i.e. $\Omega_0 = 0$), we obtain from equation (6.5.11)

$$\omega=(\Omega_{ss}^2+\Omega_n^2)^{1/2} \tag{6.5.12}$$

where $\Omega_{ss} = kC_{\mathrm{S}}(1+\omega_{\mathrm{pd}}^2/\omega_{\mathrm{pi}}^2)^{1/2}/(1+k^2\lambda_{\mathrm{De}}^2)^{1/2}$ and $\Omega_n = \sqrt{2}k_\perp\lambda_{\mathrm{De}}\Omega_{\mathrm{r}}/(1+k^2\lambda_{\mathrm{De}}^2)^{1/2}$. Furthermore, it can be readily shown that in the presence of the dust grain rotation (namely $\Omega_0 \neq 0$), equation (6.5.11) admits complex solutions, for any rotation frequency Ω_0 satisfying the condition

$$\Omega_0^2<\Omega_{ss}^2\left[1+\left(\frac{k_\perp^2}{k^2}\frac{\Omega_{\mathrm{r}}^2}{\omega_{\mathrm{p}}^2}\right)^{1/3}\right]^3. \tag{6.5.13}$$

The equality of Ω_0 in the right-hand side of equation (6.5.13) defines the boundary of the stability of the DIA waves. We focus on the resonant interaction between the latter and the elongated, rotating dust grains. Thus, letting $\omega \simeq \Omega_{ss} + \mathrm{i}\omega_i$ and $\Omega_{ss} \approx \Omega_0$, where $\omega_i \ll \Omega_0$, we obtain from equation (6.5.11) the maximum growth rate

$$\omega_i=\frac{\sqrt{3}}{2^{4/3}}\left(\frac{k_\perp^2}{k^2}\frac{\Omega_{\mathrm{r}}^2}{\omega_{\mathrm{p}}^2}\right)^{1/3}\Omega_0. \tag{6.5.14}$$

The above analyses reveal that free energy of elongated, rotating dust grains is coupled to the DA and DIA waves when the frequencies of the latter are equal to the dust grain rotation frequency. However, the instabilities occur only when the wavevector lies in the plane of the dust grain rotation. In this case, there is a coupling between the longitudinal electric field and the charges that are placed on the dust grain surface, which also rotate together with the dust grains.

6.5.2 Cold magnetized dusty plasmas

We now generalize our investigation to a cold uniform magnetized dusty plasma and derive dispersion relations for a number of wave branches that may exist in such a dusty plasma. Thus, using appropriate approximations, which are valid for a cold dusty plasma, namely

$$k_\perp V_{\mathrm{T}s} \ll \omega_{\mathrm{c}s}, \qquad k_z V_{\mathrm{T}s} \ll \omega \qquad \text{and} \qquad |\omega \pm n\omega_{\mathrm{c}s}| \gg k_z V_{\mathrm{T}s} \tag{6.5.15}$$

we obtain

$$\epsilon_{xx}=\epsilon_{yy}=\epsilon_\perp=1-\sum_s\frac{\omega_{\mathrm{p}s}^2}{\omega^2-\omega_{\mathrm{c}s}^2}-\frac{\Omega_{\mathrm{r}}^2}{(\omega-\Omega_0)^2}-\frac{\Omega_{\mathrm{r}}^2}{(\omega+\Omega_0)^2} \tag{6.5.16}$$

$$\epsilon_{xy} = -\epsilon_{yx} = \mathrm{i}g_{s\mathrm{r}} = -\mathrm{i}\sum_s \frac{\omega_{\mathrm{p}s}^2 \omega_{\mathrm{c}s}}{\omega(\omega^2 - \omega_{\mathrm{c}s}^2)} + \mathrm{i}\frac{\Omega_\mathrm{r}^2}{(\omega - \Omega_0)^2} - \mathrm{i}\frac{\Omega_\mathrm{r}^2}{(\omega + \Omega_0)^2} \tag{6.5.17}$$

$$\epsilon_{zz} = \epsilon_\parallel = 1 - \sum_s \frac{\omega_{\mathrm{p}s}^2}{\omega^2} \tag{6.5.18}$$

and

$$\epsilon_{xz} = \epsilon_{zx} = \epsilon_{yz} = \epsilon_{zy} = 0. \tag{6.5.19}$$

The components of the electric field are given by the set of equations

$$\left(k_z^2 - \frac{\omega^2}{c^2}\epsilon_\perp\right) E_x - \mathrm{i}\frac{\omega^2}{c^2} g_{s\mathrm{r}} E_y - k_\perp k_z E_z = 0 \tag{6.5.20}$$

$$\frac{\omega^2}{c^2} g_{s\mathrm{r}} E_x + \left(k^2 - \frac{\omega^2}{c^2}\epsilon_\perp\right) E_y = 0 \tag{6.5.21}$$

and

$$-k_\perp k_z E_x + (k_\perp^2 - \frac{\omega^2}{c^2}\epsilon_\parallel) E_z = 0. \tag{6.5.22}$$

We note that for $k_\perp = 0$ (i.e. $\boldsymbol{k} = \hat{z}k_z$) and $E_z \neq 0$ we have $\epsilon_\parallel = 0$, which exhibits that there is no influence of the dust grain rotation on the longitudinal waves. Obviously, the dust grain rotation can act on the waves only when the electric field is situated in the plane of rotation. The energy exchange between the dust grain rotation and such a wave is most efficient when the frequency of rotation is close to the wave frequency.

6.5.2.1 *Transverse waves*

We now focus on circularly polarized electromagnetic waves propagating along $\hat{z}$. The corresponding dispersion relation is (Tskhakaya *et al* 2001)

$$\frac{k_z^2 c^2}{\omega^2} = 1 - \sum_s \frac{\omega_{\mathrm{p}s}^2}{\omega(\omega \mp \omega_{\mathrm{c}s})} - \frac{2\Omega_\mathrm{r}^2}{(\omega \pm \Omega_0)^2} \tag{6.5.23}$$

where the $\pm$ in the denominators corresponds to the left/right-hand circularly polarized waves. By replacing Ω_0 by $-\Omega_0$, the dust grain rotation direction can be manipulated in order to coincide with the direction of the wave polarization. The dispersion relation (6.5.23) is then written as

$$\frac{k_z^2 c^2}{\omega^2} = \epsilon(\omega) - \frac{2\Omega_\mathrm{r}^2}{(\omega - \Omega_0)^2} \tag{6.5.24}$$

where

$$\epsilon(\omega) = 1 - \sum_s \frac{\omega_{\mathrm{p}s}^2}{\omega(\omega + \omega_{\mathrm{c}s})}. \tag{6.5.25}$$

Introducing a small frequency shift Δ_0 around Ω_0, we let $\omega = \Omega_0 + \Delta_0$, where $\Delta_0 \ll \Omega_0$ and express equation (6.5.24) as

$$\frac{k_z^2 c^2}{\Omega_0^2} - \epsilon(\Omega_0) + \Delta_0 \frac{\partial}{\partial \Omega_0}\left[\frac{k_z^2 c^2}{\Omega_0^2} - \epsilon(\Omega_0)\right] = -\frac{2\Omega_r^2}{\Delta_0^2}. \tag{6.5.26}$$

If Ω_0 is far away from the characteristic frequency ω_0 of a magnetized dusty plasma, which satisfies

$$H(\omega_0) = \frac{k_z^2 c^2}{\omega^2} - \epsilon(\omega_0) = 0 \tag{6.5.27}$$

so that the condition

$$|H(\Omega_0)/\Omega_0 \partial H(\Omega_0)/\partial \Omega_0| \gg \Delta_0/\Omega_0 \tag{6.5.28}$$

is fulfilled (this case is referred to as a non-resonant case), we obtain

$$\Delta_0 = \pm \mathrm{i}\sqrt{2}\frac{\Omega_r}{k_z c}\Omega_0\left[1 + \frac{\Omega_0^2}{k_z^2 c^2}\epsilon(\Omega_0)\right] \tag{6.5.29}$$

where we have assumed that $\Omega_0^2 \ll k_z^2 c^2$. Equation (6.5.29) depicts a new type of unstable transverse wave whose frequency is close to the rotation frequency Ω_0. In the resonance case, when the inequality in equation (6.5.28) is reversed, Ω_0 is close to some characteristic frequency of the magnetized dusty plasma, namely

$$H(\Omega_0) = 0 \tag{6.5.30}$$

we obtain for the frequency shift

$$\Delta_0 = \left[-\frac{2\Omega_r^2}{\Omega_0^3 \partial H(\Omega_0)/\partial \Omega_0}\right]^{1/3} \Omega_0 \begin{pmatrix} 1 \\ -\frac{1 \pm \mathrm{i}\sqrt{3}}{2} \end{pmatrix}. \tag{6.5.31}$$

Equation (6.5.31) exhibits an unstable root with a substantial growth rate, which is proportional to $\Omega_r^{2/3}$.

We now discuss the dispersion properties of electromagnetic waves for the resonance case. As Ω_0 is small in most of the astrophysical and terrestrial environments, we consider the low-frequency regimes of the plasma oscillations. For $|\omega_{cd}|, \omega_{ci} \ll \omega \ll |\omega_{ce}|$ we have

$$H(\omega) = \frac{k_z^2 c^2}{\omega^2} - \frac{\omega_{pe}^2}{\omega |\omega_{ce}|}. \tag{6.5.32}$$

Letting $\omega = \Omega_0 + \mathrm{i}\omega_i$, where $\Omega_0 \simeq \omega_0 = k_z^2 c^2 |\omega_{ce}|/\omega_{pe}^2$ (the electron whistler waves), we obtain for the growth rate

$$\omega_i \simeq \Omega_0 \left[2\frac{\Omega_r^2}{k^2 c^2}\right]^{1/3}. \tag{6.5.33}$$

In the frequency regime $|\omega_{\rm cd}| \ll \omega \ll \omega_{\rm ci}$, we have

$$H(\omega) = \frac{k_z^2 c^2}{\omega^2} - \frac{\omega_{\rm pd}^2}{\omega|\omega_{\rm cd}|}. \tag{6.5.34}$$

In deriving equation (6.5.34) we have used the quasi-neutrality condition at equilibrium, namely

$$en_{\rm e0} + |q|n_{\rm d0} = en_{\rm i0}. \tag{6.5.35}$$

Letting $\omega = \Omega_0 + {\rm i}\omega_i$, where $\Omega_0 \simeq \omega_0 = k_z^2 c^2|\omega_{\rm cd}|/\omega_{\rm pd}^2$ (the dust whistler waves), we obtain for the growth rate

$$\omega_i \simeq \left(2\frac{\Omega_{\rm r}^2}{k_z^2 c^2}\right)^{1/3} \Omega_0. \tag{6.5.36}$$

On the other hand, for $\omega \sim \omega_{\rm cd}$ we have

$$H(\omega) = \frac{k_z^2 c^2}{\omega^2} - \frac{\omega_{\rm pd}^2}{\omega(|\omega_{\rm cd}| - \omega)}. \tag{6.5.37}$$

As before, setting $\omega = \Omega_0 + {\rm i}\omega_i$, where $\Omega_0 = \omega_0 = |\omega_{\rm cd}|(1 - \omega_{\rm pd}^2/k_z^2 c^2)$ (the EDC waves), we obtain for the growth rate

$$\omega_i \simeq \left(2\frac{\Omega_{\rm r}^2}{k_z^2 c^2}\frac{\omega_{\rm pd}^2}{k_z^2 c^2}\right)^{1/3} |\omega_{\rm cd}|. \tag{6.5.38}$$

Considering the EIC waves in the frequency range $\omega \simeq \omega_{\rm ci}$, we obtain the growth rate

$$\omega_i \simeq \left(2\frac{\Omega_{\rm r}^2}{k_z^2 c^2}\frac{\omega_{\rm pi}^2}{k_z^2 c^2}\right)^{1/3} \omega_{\rm ci}. \tag{6.5.39}$$

6.5.2.2 Longitudinal waves

We now consider the longitudinal waves for which the dispersion relation has the form (Tshkhakaya *et al* 2001)

$$\frac{k_\perp^2}{k^2}\epsilon_{xx}(\omega, \boldsymbol{k}) + \frac{k_z^2}{k^2}\epsilon_{zz}(\omega, \boldsymbol{k}) = 0 \tag{6.5.40}$$

where the components ϵ_{xx} and ϵ_{zz} for the cold plasma are defined by equations (6.5.16) and (6.5.18). Substituting the latter into equation (6.5.40), we obtain

$$1 - \frac{k_\perp^2}{k^2}\sum_s \frac{\omega_{\rm ps}^2}{\omega^2 - \omega_{\rm cs}^2} - \frac{k_z^2}{k^2}\sum_s \frac{\omega_{\rm ps}^2}{\omega^2} = \frac{k_\perp^2}{k^2}\left[\frac{\Omega_{\rm r}^2}{(\omega - \Omega_0)^2} + \frac{\Omega_{\rm r}^2}{(\omega + \Omega_0)^2}\right]. \tag{6.5.41}$$

The growth rate of longitudinal waves, defined by equation (6.5.41), can be obtained by using the same procedure as presented before for deducing equations (6.5.29) and (6.5.31). Thus, letting $\omega = \Omega_0 + \mathrm{i}\omega_i$ in equation (6.5.41) we have for the lower-hybrid waves ($\omega_{\mathrm{ci}} \ll \omega \ll |\omega_{\mathrm{ce}}|$ and $k_z \ll k_\perp$)

$$\Omega_0 = \omega_0 = \frac{\omega_{\mathrm{pi}}\omega_{\mathrm{ce}}}{\sqrt{\omega_{\mathrm{pe}}^2 + \omega_{\mathrm{ce}}^2}} \tag{6.5.42}$$

and the growth rate

$$\omega_i = \left(\frac{1}{2}\frac{\Omega_{\mathrm{r}}^2}{\omega_{\mathrm{pi}}^2}\right)^{1/3} \Omega_0. \tag{6.5.43}$$

6.5.3 Warm magnetized dusty plasmas

We have studied the dispersion properties of different transverse and longitudinal waves by considering a cold magnetized dusty plasma, i.e. by neglecting the thermal motion of plasma particles. As the thermal motion of the plasma particles can significantly modify the existing modes/instabilities as well as introduce some new modes/instabilities, in this section we consider a warm magnetized dusty plasma and briefly describe the transverse and longitudinal waves.

6.5.3.1 Transverse waves

We first consider the influence of the thermal motion of the electrons and assume

$$k_z V_{\mathrm{Td}}, k_z V_{\mathrm{Ti}} \ll \omega \ll k_z V_{\mathrm{Te}}. \tag{6.5.44}$$

We also assume that the wavelengths of the waves under consideration are larger than the Larmor radii, namely $k_\perp^2 V_{\mathrm{T}s}^2, k_z^2 V_{\mathrm{T}s}^2 \ll \omega_{\mathrm{c}s}^2$. Thus, the components of the dielectric permittivity tensor for $\omega \ll \omega_{\mathrm{ci}}$ are expressed as

$$\epsilon_{xx} = \epsilon_{yy} = 1 + \frac{c^2}{V_{\mathrm{A}}^2} - \frac{\omega_{\mathrm{pd}}^2}{\omega^2 - \omega_{\mathrm{cd}}^2} - \frac{\Omega_{\mathrm{r}}^2}{(\omega - \Omega_0)^2} - \frac{\Omega_{\mathrm{r}}^2}{(\omega + \Omega_0)^2} \tag{6.5.45}$$

$$\epsilon_{xy} = -\epsilon_{yx} = -\mathrm{i}\frac{\omega_{\mathrm{pd}}^2}{\omega^2 - \omega_{\mathrm{cd}}^2}\frac{\omega}{\omega_{\mathrm{cd}}} + \mathrm{i}\frac{\Omega_{\mathrm{r}}^2}{(\omega - \Omega_0)^2} - \mathrm{i}\frac{\Omega_{\mathrm{r}}^2}{(\omega + \Omega_0)^2} \tag{6.5.46}$$

$$\epsilon_{zz} = 1 - \frac{\omega_{\mathrm{pi}}^2}{\omega^2} - \frac{\omega_{\mathrm{pd}}^2}{\omega^2} + \frac{\omega_{\mathrm{pe}}^2}{k_z^2 V_{\mathrm{Te}}^2} \tag{6.5.47}$$

where we have made use of equation (6.5.35) and ignored the Landau damping on the electrons. Here the general dispersion relation (6.4.7) separates into two equations

$$\epsilon_{zz}(\omega, k_z) = 0 \tag{6.5.48}$$

which is not influenced by the rotation of the grain and

$$H(\omega) = \frac{k_z^2 c^2}{\omega^2} - \frac{c^2}{V_A^2} + \frac{\omega_{pd}^2}{\omega_{cd}(\omega \pm \omega_{cd})} = -\frac{2\Omega_r^2}{(\omega \mp \Omega_0)^2} \tag{6.5.49}$$

which is affected by the dust grain rotation. Assuming $\omega \ll |\omega_{cd}|$, letting $\omega = \Omega_0 + i\omega_i$, where $\Omega_0 = k_z V_A$ and using equation (6.5.31), we obtain for the growth rate

$$\omega_i \simeq \left(\frac{\Omega_r^2}{k_z^2 c^2}\right)^{1/3} k_z V_A. \tag{6.5.50}$$

6.5.3.2 Longitudinal waves

We now consider the frequency regime $k_z V_{Td}, k_z V_{Ti} \ll \omega \ll k_z V_{Te}$. Here we obtain from equations (6.5.40) and (6.5.47) the dispersion relation

$$\begin{aligned} 1 + \frac{1}{k^2 \lambda_{De}^2} - \frac{k_\perp^2}{k^2}\left(\frac{\omega_{pi}^2}{\omega^2 - \omega_{ci}^2} + \frac{\omega_{pd}^2}{\omega^2 - \omega_{cd}^2}\right) - \frac{k_z^2}{k^2}\frac{\omega_{pi}^2}{\omega^2} \\ = \frac{k_\perp^2}{k^2}\left[\frac{\Omega_r^2}{(\omega - \Omega_0)^2} + \frac{\Omega_r^2}{(\omega + \Omega_0)^2}\right]. \end{aligned} \tag{6.5.51}$$

Equation (6.5.51) can be analysed in the following limiting cases.

(i) EIC waves

We now consider EIC waves with $\omega_{cd} \ll \omega \simeq \Omega_{ci}$ and $k_z \ll k_\perp$. As before, setting $\omega \simeq \Omega_0 + i\omega_i$, we obtain the growth rate from equation (6.5.51)

$$\omega_i \simeq \left(\frac{\Omega_r^2}{2\omega_{pi}^2}\frac{k_\perp^4 C_s^4}{\Omega_0^4}\right)^{1/3} \Omega_0 \tag{6.5.52}$$

where $\Omega_0 = \omega_0 = (\omega_{ci}^2 + k_\perp^2 C_s^2)^{1/2}$.

(ii) Modified DIA waves

Next, we consider the modified DIA (MDIA) waves, which are characterized by $\omega_{pd}, \omega_{cd} \ll \omega \ll \omega_{ci}$, for which equation (6.5.51) gives

$$1 + k^2\lambda_{De}^2 + k_\perp^2 \rho_s^2 - \frac{k_z^2 C_S^2}{\omega^2} = k_\perp^2 \lambda_{De}^2 \left[\frac{\Omega_r^2}{(\omega - \Omega_0)^2} + \frac{\Omega_r^2}{(\omega + \Omega_0)^2}\right]. \tag{6.5.53}$$

Equation (6.5.53) admits an instability of the MDIA waves with the frequency $\Omega_0 = \omega_0 = k_z C_S/(1 + k^2\lambda_{De}^2 + k_\perp^2 \rho_s^2)^{1/2}$ and the growth rate

$$\omega_i \simeq \left(\frac{k_\perp^2}{2k^2} \frac{\Omega_r^2}{\omega_{pi}^2} \right)^{1/3} \Omega_0. \tag{6.5.54}$$

(iii) Modified DA or DC waves

We finally consider the coupled DA–DC waves in a dust–electron plasma (without the ions) with positive dust grains. Thus, for $kV_{Td} \ll \omega \ll k_z V_{Te}$, we have

$$1 + \frac{1}{k^2\lambda_{De}^2} - \frac{k_\perp^2}{k^2} \frac{\omega_{pd}^2}{\omega^2 - \omega_{cd}^2} - \frac{k_z^2}{k^2} \frac{\omega_{pd}^2}{\omega^2} = \frac{k_\perp^2}{k^2} \left[\frac{\Omega_r^2}{(\omega - \Omega_0)^2} + \frac{\Omega_r^2}{(\omega + \Omega_0)^2} \right]. \tag{6.5.55}$$

For $\omega \ll \omega_{cd}$ equation (6.5.55) admits an instability of short-wavelength modified DA waves with the frequency $\Omega_0 = \omega_0 = kC_{De}/(1 + k^2\lambda_{De}^2 + k_\perp^2 \rho_{sd}^2)^{1/2}$ and the growth rate

$$\omega_i \simeq \left(\frac{1}{2} \frac{k_\perp^2}{k_z^2} \frac{\Omega_r^2}{\omega_{pd}^2} \right)^{1/3} \Omega_0 \tag{6.5.56}$$

where $\rho_{sd} = C_{De}/\omega_{cd}$. On the other hand, for $\omega \sim |\omega_{cd}|$, $k_\perp \gg k_z$ and $k^2\lambda_{De}^2 \ll 1$ we have an instability of the DC waves with frequency $\Omega_0 = \omega_0 = (\omega_{cd}^2 + k^2 C_{De}^2)^{1/2}$ and growth rate

$$\omega_i \simeq \left(\frac{1}{2} k_\perp^4 \lambda_{De}^4 \frac{\Omega_r^2}{\Omega_0^2} \frac{\omega_{pd}^2}{\Omega_0^2} \right)^{1/3} \Omega_0. \tag{6.5.57}$$

The above instability analyses of modified DA/DC waves can be generalized to a three-component warm dusty magnetoplasma composed of electrons, ions and negative dust grains. Here, we may add in equation (6.5.55) a more general ion susceptibility that is given by equation (4.6.2).

6.5.4 Scattering cross section

An important question which one would like to ask is: What are the consequences of non-thermal fluctuations involving elongated and rotating dust grains? To answer this question, we note that the cross section of the scattering of transverse electromagnetic waves in a plasma has sharp maxima near the natural plasma frequencies. Since the thermal motion of the dust particles can typically be neglected, the scattering would occur on the electrons and ions only and the form of the scattering line will be determined by their contribution to the spectral distribution of fluctuations. Therefore, for the dependence of the cross section on the frequency, we have

$$\mathrm{d}\sigma \approx \delta[\mathrm{Re}\,\epsilon^1(\omega, \boldsymbol{k})] \frac{\mathrm{d}\omega}{\omega}. \tag{6.5.58}$$

The cross section, given by equation (6.5.58), has a sharp maximum at $\omega \simeq \Omega_0$. When the dust grain rotation frequency Ω_0 approaches a critical value, defined by any normal mode of our dusty plasma, the fluctuations of longitudinal/transverse waves sharply increase and the scattering cross section must also sharply increase. Hence the presence of non-thermal fluctuations can be used for diagnostic purposes. For example, coherent or incoherent scattering of star light and/or electromagnetic waves off non-thermal fluctuations in cosmic plasmas may yield valuable information regarding the light polarization, the dust number density and the dust charge in situ, as well as other plasma parameters including the external magnetic field strength. The existence of a preferred frequency of the dust grain rotation can also be found by means of the scattering of transverse electromagnetic waves off enhanced low-frequency fluctuations in a dusty plasma. The usual Mie and Debye scattering theories (Guerra and Mendonça 2000) have to be reconsidered to account for collective interactions that are dependent on elongated and rotating dust grains in plasmas.

6.6 Grain Vibration and Rotation

Studies of the levitation and dynamics of charged dust grains are of significant interest in space and laboratory environments. Recent laboratory experiments (Rahman *et al* 2001) have conclusively demonstrated different types of motions of charged dust clouds near negatively biased electrodes in low-temperature dusty plasma discharges. The dust grains in a dusty plasma sheath are levitated due to the balance between the gravity and electrostatic forces and the dust cloud is usually located away from the electrode at a distance several times larger than the Debye length. The dust grains execute bouncing motions which are repeatedly away and towards the electrodes. The dust grains also perform transverse quivering across the sheath electric field. Here we discuss a theory (Tskhakaya and Shukla 2001) for the bouncing, vibrational (or quivering) and rotational motions of elongated dust grains in the presence of electric fields in a plasma without and with an external magnetic field.

To describe the dynamics of a single charged dust grain in electromagnetic fields, it is more convenient to start with equations (6.3.6) and (6.3.7) and separate the motions of the centre of mass and the rotation around it. Thus, we can write $\boldsymbol{v}_i = \boldsymbol{V} + \boldsymbol{\Omega} \times \boldsymbol{\Delta r}_i$ and $\boldsymbol{r}_i = \boldsymbol{r} + \Delta \boldsymbol{r}_i$, where $\boldsymbol{V}$ and $\boldsymbol{r}$ are the velocity and position of the centre of mass and $\Delta \boldsymbol{r}_i$ is the coordinate of the ith part of the grain relative to the centre of mass.

The equations of motion for charged dust grains can be readily deduced from equations (6.3.6) and (6.3.7), which are generalized to include a gravity force $m_\mathrm{d}\boldsymbol{g}$. We have

$$\frac{\mathrm{d}\boldsymbol{p}}{\mathrm{d}t} = (q+\boldsymbol{d}\cdot\nabla)\left(\boldsymbol{E} + \frac{1}{c}\boldsymbol{V}\times\boldsymbol{B}\right) + \frac{1}{c}(\boldsymbol{\Omega}\times\boldsymbol{d})\times\boldsymbol{B} + (\boldsymbol{m}\times\nabla)\times\boldsymbol{B} + m_\mathrm{d}\boldsymbol{g} \quad (6.6.1)$$

and

$$\frac{\mathrm{d}M_\alpha}{\mathrm{d}t} = -\frac{q}{2m_\mathrm{d}c} I_{\alpha\beta}\left[\frac{\partial B_\alpha}{\partial t} + (\boldsymbol{V}\cdot\nabla)B_\alpha\right] + \left[\boldsymbol{d}\times\left(\boldsymbol{E}+\frac{1}{c}\boldsymbol{V}\times\boldsymbol{B}\right)\right]_\alpha + (\boldsymbol{m}\times\boldsymbol{B})_\alpha \tag{6.6.2}$$

where $\boldsymbol{p} = m_\mathrm{d}\boldsymbol{V}$ is the momentum and $M_\alpha = I_{\alpha\beta}\Omega_\beta$ is the angular momentum of the grain. We now consider the dust particle motions in three interesting cases.

6.6.1 Bouncing motion

We first consider a simple situation in which the effect of the magnetic field can be neglected. Thus, the equation of motion (6.6.1) for $r_\mathrm{d}/\lambda_\mathrm{in} \ll 1$ has the form

$$m_\mathrm{d}\frac{\mathrm{d}V_z}{\mathrm{d}t} = -\frac{\partial U_\mathrm{b}}{\partial z} \tag{6.6.3}$$

where (Tskhakaya and Shukla 2001)

$$U_\mathrm{b} = q\varphi + d_z\frac{\partial\varphi}{\partial z} + m_\mathrm{d}g_z z \tag{6.6.4}$$

is the effective potential energy and the electric field $E_z = -\partial\varphi/\partial z$ is aligned along the z-axis. The z component of the gravity is denoted by g_z. Since in most of the low-temperature laboratory dusty plasma discharges, the charge of the dust grains is negative, we have $q < 0$. For negatively biased electrodes, the potential $\varphi(< 0)$ tends monotonically to zero away from the electrode. In the plasma sheath, whose thickness is of the order of several Debye lengths λ_D, the increase of the potential φ is rather sharp. Beyond this region, i.e. in the pre-sheath, the effective potential φ changes smoothly. Thus, between the electrode and the unperturbed plasma, the effective potential energy U_b has the shape of a well with a minimum at the point ($z = z_0$) where $m_\mathrm{d}g_z \approx -q\partial\varphi/\partial z$. Hence the grains trapped in the potential well execute bouncing motions between the electrode and the unperturbed plasma. On the other hand, for the description of rotational motions of dust clouds, it is necessary to account for the transverse inhomogeneity (parallel to the electrode) of the electric field.

6.6.2 Vibrational motion

We consider the quivering motion of the grains in the presence of a homogeneous electric field $\boldsymbol{E} = \hat{z}E$, as depicted in figure 6.2. In the absence of the magnetic field, neglecting small terms that are of order $r_\mathrm{d}/\lambda_\mathrm{in}$, we obtain for the angular momentum (Tskhakaya and Shukla 2001)

$$\frac{\mathrm{d}\boldsymbol{M}}{\mathrm{d}t} = \boldsymbol{d}\times\boldsymbol{E}. \tag{6.6.5}$$

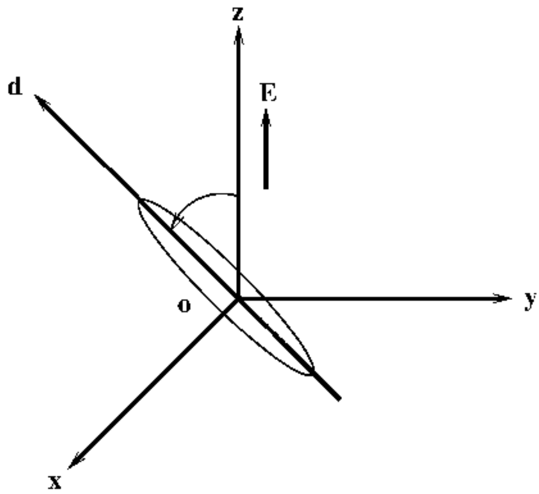

Figure 6.2. The orientation of a rotating elongated grain in a homogeneous electric field.

Assuming that the angular velocity $\mathbf{\Omega} = (0, \Omega, 0)$ is directed along the y-axis, we obtain

$$I\frac{\mathrm{d}\Omega}{\mathrm{d}t} = -dE\sin\psi \tag{6.6.6}$$

where ψ is the angle between the dipole moment and the z-axis, I is the y component of the principal moment of the dust grain inertia and the x component of the dipole moment is $d_x = d\sin\psi$. Subsequently, we have from equation (6.6.6)

$$\frac{\mathrm{d}^2\psi}{\mathrm{d}t^2} = -\Omega_0^2\sin\psi \tag{6.6.7}$$

where $\Omega_0 = (dE/I)^{1/2}$ is a characteristic frequency of the grain vibration (or quivering). Equation (6.6.7) is subjected to the initial conditions $\psi = \psi_0$ and $\mathrm{d}\psi/\mathrm{d}t = 0$ at $t = 0$. It describes the motion in the potential well $U_v = -\cos\psi$, where $-\psi_0 \le \psi \le \psi_0$. The solution of equation (6.6.7) is

$$\Omega_0 t = F\left[\arcsin\left(\frac{\sin(\psi/2)}{\sin(\psi_0/2)}\right), \sin(\psi_0/2)\right] - F\left[\frac{\pi}{2}, \sin(\psi_0/2)\right] \tag{6.6.8}$$

where F is the elliptic integral of the second kind (Gradsteyn and Ryzhik 2000). Equation (6.6.7) exhibits vibrational (or quivering) motions across the direction of the electric field with a non-constant angular velocity

$$\Omega = \frac{\mathrm{d}\psi}{\mathrm{d}t} = \pm\sqrt{2(\cos\psi - \cos\psi_0)}. \tag{6.6.9}$$

It turns out that Ω varies in the range $0 \leq \Omega \leq 2\Omega_0 \sin(\psi_0/2)$. The period of a single swing is

$$T = \frac{4}{\sqrt{2}\Omega_0} \int_0^{\psi_0} \frac{\mathrm{d}\psi}{\sqrt{\cos\psi - \cos\psi_0}} \equiv \frac{4}{\Omega_0} F\left[\frac{\pi}{2}, \sin(\psi_0/2)\right]. \tag{6.6.10}$$

The averaged angular velocity is then $\langle\Omega\rangle = (4/T)\psi_0$. An order of magnitude estimate for the characteristic angular velocity for the grain quivering is

$$\Omega_0 \sim 10^4 \sqrt{14.4(Z_\mathrm{d}/m_\mathrm{d} n_\mathrm{d}) E(\mathrm{V\ cm}^{-1})}. \tag{6.6.11}$$

In obtaining equation (6.6.11) we have assumed that the dust grain size is approximately 1 μm. It follows from equation (6.6.11) that the grain vibration frequency can reach a value of 100 kHz and more for a moderate electric field strength of a few mV cm^{-1}.

6.6.3 Rotational and vibrational motions

We consider the dust particle dynamics in the presence of a constant ambient magnetic field $\boldsymbol{B} = (0, 0, B_0)$. We assume that the dust magnetic moment is along the direction of the ambient magnetic field and neglect the grain precision. We also consider circularly polarized electromagnetic fields and choose $E_x = E\cos(\omega t)$ and $E_y = E\sin(\omega t)$, where ω is the wave frequency. The x and y components of the dipole moment are $d_x = d\cos\phi$ and $d_y = d\sin\phi$, respectively. These assumptions allow us to express equation (6.6.2) for the dust grain rotating around the z-axis. Thus, we have (Tskhakaya and Shukla 2001)

$$I_z \frac{\mathrm{d}\Omega}{\mathrm{d}t} = -dE\sin(\phi - \omega t) \tag{6.6.12}$$

which can be put in the form

$$\frac{\mathrm{d}^2\phi}{\mathrm{d}t^2} = -\Omega_{0z}^2 \sin(\phi - \omega t) \tag{6.6.13}$$

where $\Omega_{0z} = (dE/I_z)^{1/2}$ and I_z is the z component of the principal moment of the dust grain inertia. The angular velocity is now defined by $\Omega = \mathrm{d}\phi/\mathrm{d}t$. We solve (6.6.13) by introducing the initial conditions $\phi = \phi_0$ and $\mathrm{d}\phi/\mathrm{d}t = 0$, as before. Accordingly, integrating equation (6.6.13) we obtain

$$\frac{1}{2\Omega_{0z}^2}\left(\frac{\partial\Phi}{\partial t}\right)^2 - \cos\Phi = \frac{1}{2}\frac{\omega^2}{\Omega_{0z}^2} - \cos\phi_0 \equiv \mathcal{E} \tag{6.6.14}$$

where

$$\Phi = \phi - \omega t. \tag{6.6.15}$$

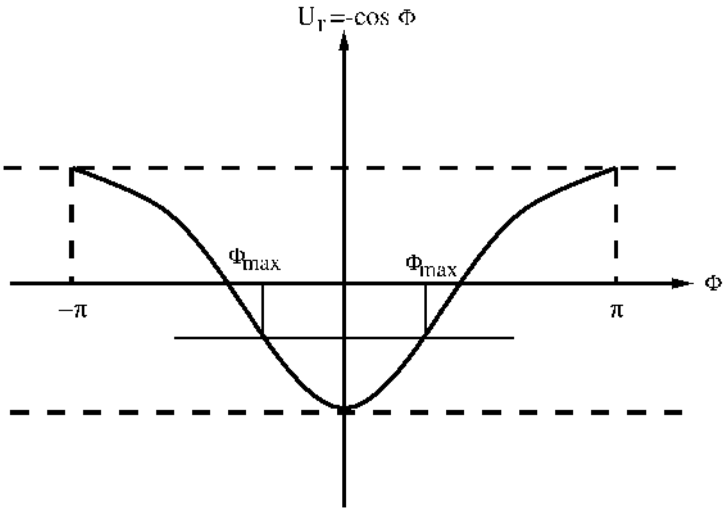

Figure 6.3. A schematic representation of the potential $U_{\mathrm{r}} = -\cos\Phi$ versus Φ.

If the effective energy $\mathcal{E}$ lies between -1 and 1, Φ satisfies $-\Phi_{\max} < \Phi < \Phi_{\max}$, as shown in figure 6.3. Here $\Phi_{\max}$ is defined by $\sin(\Phi_{\max}/2) = \sqrt{\sin^2(\phi_0/2) + \omega^2/4\Omega_{0z}^2}$. A typical solution of equation (6.6.14) is

$$\begin{aligned}\Omega_{0z}t = {} & F\left[\arcsin\left(\frac{\sin(\phi_0/2)}{\sin(\Phi_{\max}/2)}\right), \sin(\Phi_{\max}/2)\right] \\ & - F\left[\arcsin\left(\frac{\sin(\Phi/2)}{\sin(\Phi_{\max}/2)}\right), \sin(\Phi_{\max}/2)\right]. \end{aligned} \tag{6.6.16}$$

Equation (6.6.16) exhibits that in a system of reference rotating with the electric field, the dust grain now vibrates (quivers) with a frequency which roughly equals Ω_{0z}. The vibrational (or quivering) period is

$$T = \frac{4}{\Omega_{0z}} F\left[\frac{\pi}{2}, \sin(\Phi_{\max}/2)\right]. \tag{6.6.17}$$

The dust grain rotates with the frequency of the electromagnetic field and at the same time it also vibrates (quivers) across the electric field direction. The angular velocity is $\Omega = \omega + \mathrm{d}\Phi/\mathrm{d}t$. It follows that the average angular velocity of the dust grain is $\langle\Omega\rangle = \omega$, where the angular bracket denotes the averaging over the vibrational (quivering) period, given by equation (6.6.17). We note that when the effective energy $\mathcal{E}$ is approximately unity, we have no quivering. When $t \to \infty$, the angular velocity of the dust grain exactly matches the electromagnetic field frequency, namely $\Omega = \omega$.

For a large effective energy $\mathcal{E}$, namely $\omega^2/\Omega_{0z}^2 \gg 1$, we have again the rotation and vibration of the dust grains. The angular velocity of such motions is

$$\Omega = \frac{\Omega_{0z}^2}{\omega}[\cos\phi_0 - \cos(\omega t - \phi_0)] \tag{6.6.18}$$

while the averaged value of Ω turns out to be

$$\langle\Omega\rangle = \frac{\Omega_{0z}^2}{\omega}\cos\phi_0. \tag{6.6.19}$$

The above model describes the trapping of elongated dust clouds in a plasma sheath that contains homogeneous and oscillating electric fields. The model depicts that the dust grains bounce back and forth from a negatively biased electrode and that they also quiver simultaneously across the electric field direction. Physically, the present complex motions of dust clouds arise due to the combined effects of the sheath electric field and the dipole moment of the dust grain; both of which produce a potential well that can trap and confine the dust particles. The rotation of elongated dust grains can also be set by circularly polarized electromagnetic fields (namely helicons/whistlers or rf waves).

A charged dust particle placed in a plasma sheath may also admit spinning motion. The sheared ion flow velocity in the sheath can induce self-rotation of a particle, resulting in the formation of a magnetic dipole moment. The presence of an external magnetic field can cause the spinning dust particle to precess around the magnetic field direction, in addition to performing the gyro motion. For the laboratory dust experimental conditions (Sato *et al* 2000, 2001) the spinning frequency is of the order of 10 Hz, while the precession is much slower. Ishihara and Sato (2001) have presented a model for the dust grain spinning in the presence of an ion flow in a magnetic field. Clearly, more experimental and rigorous theoretical studies are needed to explore the underlying physics of rotation and spinning of elongated dust grains as well as their alignment (Mendonça *et al* 2001), which should also play a very significant role for determining the light polarization in astrophysical objects.

Chapter 7

Nonlinear Structures

7.1 Introduction

We have studied in chapters 4–6 the properties of numerous waves and instabilities by assuming a harmonic wave solution that is proportional to $\exp(-i\omega t + i\boldsymbol{k} \cdot \boldsymbol{r})$. This means that we have dealt with a wide variety of small-amplitude waves which are driven by linear and nonlinear mechanisms. There are numerous processes via which unstable modes can saturate and attain large amplitudes. When the amplitudes of the waves are sufficiently large, nonlinearities cannot be ignored. The nonlinearities come from the harmonic generation involving fluid advection, the nonlinear Lorentz force, trapping of particles in the wave potential, ponderomotive force, etc. The nonlinearities in plasmas contribute to the localization of waves, leading to different types of interesting coherent structures (namely solitary structures, shock waves, vortices, etc) which are important from both theoretical and experimental points of view.

A solitary structure is a hump or dip shaped nonlinear wave of permanent profile (to distinguish it from a soliton, we note that a soliton is a special type of solitary waves which preserve their shape and speed after interactions). It arises because of the balance between the effects of the nonlinearity and the dispersion (when the effect of dissipation is negligible in comparison with those of the nonlinearity and dispersion). However, when the dissipative effect is comparable to or more dominant than the dispersive effect, one encounters shock waves. The small but finite amplitude solitary waves (known as the KdV solitons) are governed by a Korteweg–de Vries (KdV) type equation, while the shock waves are described by a KdV–Burgers type equation. On the other hand, when the convective derivative is in the form of a vector product (for a two-dimensional case), one may obtain highly nonlinear waves in the form of vortices which are governed by the Navier–Stokes (NS) equation (Hasegawa 1985) or the Charney–Hasegawa–Mima equation (Charney 1947, Hasegawa and Mima 1978).

The nonlinear structures, which represent the plasma states far from thermodynamic equilibrium, are either spontaneously created in laboratory and space plasmas on account of free energy sources or externally launched in laboratory plasmas under controlled conditions. The presence of charged dust grains introduces new features to the nonlinear structures, which are otherwise absent in the usual electron–ion plasma. This chapter is concerned with some theories for numerous nonlinear structures (solitary waves, double layers, shock waves, vortices, etc) in dusty plasmas. We also present experimental observations of some of these nonlinear structures (e.g. DIA shocks).

7.2 Solitary Waves

To study the properties of non-envelope solitons associated with a specific wave mode, we have to account for the harmonic generation within a multi-fluid description and the modification of the distribution functions (due to trapped particles) within a kinetic description. In an unmagnetized dusty plasma, we can have solitary and shock waves (Rao *et al* 1990, Bharuthram and Shukla 1992a, Rao and Shukla 1994, Melandsø and Shukla 1995, Popel *et al* 1996, Mamun *et al* 1996a, Mamun 1999) as well as double layers associated with DA, DIA and DL waves. We have already shown in section 1.6 (of chapter 1) that the presence of immobile negatively charged dust particles can modify the Bohm criterion for the dusty plasma sheath. The modified Bohm criterion is $M > \sqrt{n_{\mathrm{i}0}/n_{\mathrm{e}0}}$ (where M = ion-acoustic solitary wave speed/ion-acoustic speed). This means that if we replace the Mach number M by an effective Mach number $M_* = M/\sqrt{n_{\mathrm{i}0}/n_{\mathrm{e}0}}$, the nonlinear properties of the DIA waves turn out to be the same (Bharuthram and Shukla 1992a) as those of the ion-acoustic waves in an electron–ion plasma (Sagdeev 1966, Washimi and Taniuti 1966). However, there are new features for the DA solitary (DAS) waves (Rao *et al* 1990) whose dynamics is governed by the nonlinear Boltzmann electron and ion distributions as well as the nonlinear dust continuity and dust momentum equations. These are described below.

The dynamics of low phase velocity (namely $V_{\mathrm{Td}} \ll V_{\mathrm{p}} \ll V_{\mathrm{Te}}, V_{\mathrm{Ti}}$) one-dimensional DAS waves is governed by (Rao *et al* 1990)

$$\frac{\partial n_{\mathrm{d}}}{\partial t} + \frac{\partial}{\partial z}(n_{\mathrm{d}} u_{\mathrm{d}}) = 0 \tag{7.2.1}$$

$$\frac{\partial u_{\mathrm{d}}}{\partial t} + u_{\mathrm{d}} \frac{\partial u_{\mathrm{d}}}{\partial z} = \frac{\partial \varphi}{\partial z} \tag{7.2.2}$$

and

$$\frac{\partial^2 \varphi}{\partial z^2} = n_{\mathrm{d}} + \mu_{\mathrm{e}} n_{\mathrm{e}} - \mu_{\mathrm{i}} n_{\mathrm{i}} \tag{7.2.3}$$

where n_s is the particle number density normalized by n_{s0}, u_{d} is the dust fluid velocity normalized by $C_{\mathrm{d}} = (Z_{\mathrm{d}0} k_{\mathrm{B}} T_{\mathrm{i}}/m_{\mathrm{d}})^{1/2}$ and φ is the electrostatic wave potential normalized by $k_{\mathrm{B}} T_{\mathrm{i}}/e$. The time and space variables are in units of the dust plasma period $\omega_{\mathrm{pd}}{}^{-1}$ and the Debye length $\lambda_{\mathrm{Dm}} = (k_{\mathrm{B}} T_{\mathrm{i}}/4\pi Z_{\mathrm{d}0} n_{\mathrm{d}0} e^2)^{1/2}$, respectively. Here we have denoted $\mu_{\mathrm{e}} = n_{\mathrm{e}0}/Z_{\mathrm{d}0} n_{\mathrm{d}0} = 1/(\delta - 1)$, $\mu_{\mathrm{i}} =$

$n_{i0}/Z_{d0}n_{d0} = \delta/(\delta - 1)$, $\sigma_i = T_i/T_e$ and $\delta = n_{i0}/n_{e0}$. The normalized electron and ion number densities are, respectively

$$n_e = \exp(\sigma_i \varphi) \tag{7.2.4}$$

and

$$n_i = \exp(-\varphi). \tag{7.2.5}$$

Equations (7.2.1)–(7.2.5) are analysed for two cases. First we study small but finite amplitude DAS waves for which we use the reductive perturbation method (Washimi and Taniuti 1966) and later we focus on arbitrary amplitude DAS waves for which we employ the Sagdeev potential approach (Sagdeev 1966).

7.2.1 Small-amplitude DAS waves

To study the dynamics of small but finite amplitude DAS waves, we derive the KdV equation from equations (7.2.1)–(7.2.5) by employing the reductive perturbation technique (Washimi and Taniuti 1966) and the stretched coordinates $\zeta = \epsilon^{1/2}(z - v_0 t)$ and $\tau = \epsilon^{3/2} t$, where ϵ is a smallness parameter measuring the weakness of the amplitude or dispersion and v_0 is the soliton speed (normalized by C_d). We can then expand the variables n_d, u_d and φ about the unperturbed states in power series of ϵ as

$$n_d = 1 + \epsilon n_d^{(1)} + \epsilon^2 n_d^{(2)} + \cdots \tag{7.2.6a}$$

$$u_d = \epsilon u_d^{(1)} + \epsilon^2 u_d^{(2)} + \cdots \tag{7.2.6b}$$

$$\varphi = \epsilon \varphi^{(1)} + \epsilon^2 \varphi^{(2)} + \cdots \tag{7.2.6c}$$

and develop equations in various powers of ϵ. To lowest order in ϵ, equations (7.2.1)–(7.2.6) give $n_d^{(1)} = -\varphi^{(1)}/v_0^2$, $u_d^{(1)} = -\varphi^{(1)}/v_0$ and $v_0 = 1/\sqrt{\mu_i + \sigma_i \mu_e}$. To next higher order in ϵ, we obtain a set of equations

$$\frac{\partial n_d^{(1)}}{\partial \tau} - v_0 \frac{\partial n_d^{(2)}}{\partial \zeta} + \frac{\partial u_d^{(2)}}{\partial \zeta} + \frac{\partial}{\partial \zeta}[n_d^{(1)} u_d^{(1)}] = 0 \tag{7.2.7}$$

$$\frac{\partial u_d^{(1)}}{\partial \tau} - v_0 \frac{\partial u_d^{(2)}}{\partial \zeta} - \frac{\partial \varphi^{(2)}}{\partial \zeta} + u_d^{(1)} \frac{\partial u_d^{(1)}}{\partial \zeta} = 0 \tag{7.2.8}$$

and

$$\frac{\partial^2 \varphi^{(1)}}{\partial \zeta^2} - \frac{1}{v_0^2}\varphi^{(2)} - n_d^{(2)} + \frac{1}{2}(\mu_i - \sigma_i^2 \mu_e)[\varphi^{(1)}]^2 = 0. \tag{7.2.9}$$

Combining equations (7.2.7)–(7.2.9) we readily obtain

$$\frac{\partial \varphi^{(1)}}{\partial \tau} + a_s \varphi^{(1)} \frac{\partial \varphi^{(1)}}{\partial \zeta} + b_s \frac{\partial^3 \varphi^{(1)}}{\partial \zeta^3} = 0 \tag{7.2.10}$$

which is the KdV equation with the coefficients (Mamun 1999)

$$a_s = \frac{v_0^3}{2}\left(\mu_\mathrm{i} - \sigma_\mathrm{i}^2\mu_\mathrm{e} - \frac{3}{v_0^4}\right) \tag{7.2.11a}$$

and

$$b_s = \frac{v_0^3}{2}. \tag{7.2.11b}$$

The stationary solution of the KdV equation (7.2.10) is obtained by transforming the independent variables ζ and τ to $\eta = \zeta - u_0\tau$ and $\tau = \tau$, where u_0 is a constant speed normalized by C_d, and imposing the appropriate boundary conditions for localized perturbations, namely $\varphi \to 0$, $\mathrm{d}\varphi^{(1)}/\mathrm{d}\eta \to 0$, $\mathrm{d}^2\varphi^{(1)}/\mathrm{d}\eta^2 \to 0$ at $\eta \to \pm\infty$. Accordingly, the stationary solution of equation (7.2.10) is of the form (Washimi and Taniuti 1966)

$$\varphi^{(1)} = \varphi_\mathrm{m}^{(1)}\,\mathrm{sech}^2[(\zeta - u_0\tau)/\Delta_s] \tag{7.2.12}$$

where the amplitude $\varphi_\mathrm{m}^{(1)}$ and the width Δ_s are given by $\varphi_\mathrm{m}^{(1)} = 3u_0/a_s$ and $\Delta_s = \sqrt{4b_s/u_0}$, respectively. As $u_0 > 0$, equation (7.2.12) reveals that (i) small-amplitude solitary waves with $\varphi > 0$ exist if $a_s > 0$ and (ii) small-amplitude solitary waves with $\varphi < 0$ exists if $a_s < 0$. Expressing a_s as

$$a_s = -\frac{v_0^3}{(\delta - 1)^2}[\delta^2 + (3\delta + \sigma_\mathrm{i})\sigma_\mathrm{i} + \frac{1}{2}\delta(1 + \sigma_\mathrm{i}^2)]. \tag{7.2.13}$$

we observe that a_s is always negative for all possible values of σ_i and δ. This means that in our dusty plasma system we have only DAS waves with $\varphi < 0$. Furthermore, as u_0 increases, the amplitude of the DAS waves increases but their width decreases.

7.2.2 Arbitrary-amplitude DAS waves

To study time-independent arbitrary-amplitude DAS waves (Rao *et al* 1990), we make all the dependent variables depend only on a single variable $\xi = z - Mt$ (where ξ is normalized by λ_Dm and M is the Mach number = solitary wave speed/C_d), use the steady-state condition, impose the appropriate boundary conditions (namely $n_\mathrm{d} \to 1$, $u_\mathrm{d} \to 0$, $\varphi \to 0$ and $\mathrm{d}\varphi/\mathrm{d}\xi \to 0$ at $\xi \to \pm\infty$) and reduce equations (7.2.1)–(7.2.5) to the form (Mamun 1999)

$$\frac{1}{2}\left(\frac{\mathrm{d}\varphi}{\mathrm{d}\xi}\right)^2 + V(\varphi) = 0 \tag{7.2.14}$$

where the Sagdeev potential $V(\varphi)$ for our purposes reads

$$V(\varphi) = \mu_\mathrm{i}[1 - \exp(-\varphi)] + \frac{\mu_\mathrm{e}}{\sigma_\mathrm{i}}[1 - \exp(\sigma_\mathrm{i}\varphi)] + M^2\left[1 - \left(1 + \frac{2\varphi}{M^2}\right)^{1/2}\right]. \tag{7.2.15}$$

It is obvious from equation (7.2.15) that $V(\varphi) = \mathrm{d}V(\varphi)/\mathrm{d}\varphi = 0$ at $\varphi = 0$. Therefore, solitary wave solutions of equation (7.2.14) exist if (i) $(\mathrm{d}^2V/\mathrm{d}\varphi^2)_{\varphi=0} < 0$ so that the fixed point at the origin is unstable and (ii) $(\mathrm{d}^3V/\mathrm{d}\varphi^3)_{\varphi=0} > (<)0$ for solitary waves with $\varphi > (<)0$. The nature of these solitary waves, whose amplitude tends to zero as the Mach number M tends to its critical value, can be found by expanding the Sagdeev potential $V(\varphi)$ to third order in a Taylor series in φ. The critical Mach number is that which corresponds to the vanishing of the quadratic term. At the same time, if the cubic term is negative, there is a potential well on the negative side and if the cubic term is positive, there is a potential well on the positive side. Therefore, by expanding the Sagdeev potential $V(\varphi)$ around the origin, the critical Mach number at which the second derivative changes sign can be found as

$$M_\mathrm{c} = \sqrt{\frac{\delta - 1}{\delta + \sigma_\mathrm{i}}}. \tag{7.2.16}$$

At this critical value of M the cubic term of $V(\varphi)$ can be expressed as

$$-\frac{1}{3(\delta - 1)^2}\left[\delta^2 + (3\delta + \sigma_\mathrm{i})\sigma_\mathrm{i} + \frac{1}{2}\delta(1 + \sigma_\mathrm{i}^2)\right] \tag{7.2.17}$$

which reveals that the cubic term is always (for any values of σ_i and δ) negative, i.e. only solitary waves with $\varphi < 0$ can exist. In other words, arbitrary-amplitude DAS waves with $\varphi > 0$ are not allowed within our model. Figure 7.1 depicts the variation of the critical Mach number M_c against $n_{\mathrm{e}0}/n_{\mathrm{i}0}$ $(= 1/\delta)$ for different values of σ_i. The figure shows that the critical Mach number increases with σ_i and δ. It is of interest to examine whether or not there exists an upper limit of M for which DAS waves with $\varphi < 0$ exist. This upper limit of M can be found by the condition $V(\varphi_\mathrm{c}) \geq 0$, where $\varphi_\mathrm{c} = -M^2/2$ is the minimum value of φ for which the dust number density n_d is real. Thus, the upper limit of M is that maximum value of M for which $S_\mathrm{m} \geq 0$, where $S_\mathrm{m} = \mu_\mathrm{i} + \mu_\mathrm{e}/\sigma_\mathrm{i} + M^2 - \mu_\mathrm{i}\exp(M^2/2) - (\mu_\mathrm{e}/\sigma_\mathrm{i})\exp(-\sigma_\mathrm{i}M^2/2)$. Figure 7.2 shows the variation of S_m against M for different values of $n_{\mathrm{e}0}/n_{\mathrm{i}0}$ $(= 1/\delta)$. We notice that as we increase δ, the upper limit of M increases.

We have also numerically analysed the Sagdeev potential $V(\varphi)$ and have found the minimum and maximum values of M for which the DAS waves exist. These are incorporated in figures 7.3 and 7.4 which show that for $\sigma_\mathrm{i} = 0.05$ and $\delta = 10$, there exists a potential well only in the negative φ-axis, i.e. there exist solitary waves with $\varphi < 0$ for $0.95 < M < 1.52$. The results in figure 7.1 agree with those in figure 7.3, whereas the results in figure 7.2 agree with those in figure 7.4. Theses plots also agree with our analytical results in that our dusty plasma may support only the DAS waves with $\varphi < 0$.

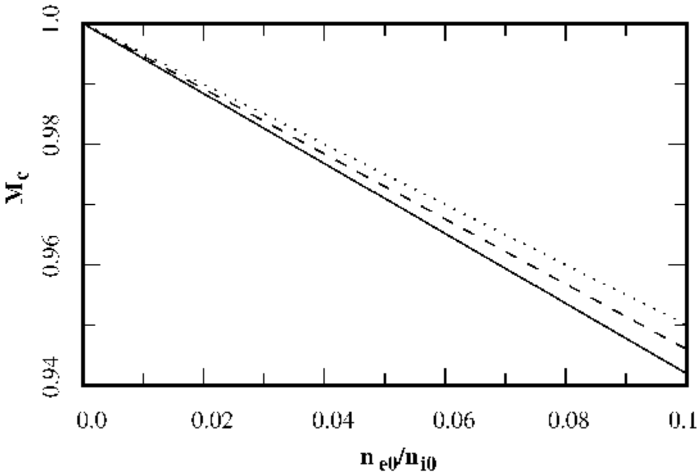

Figure 7.1. Variation of the critical Mach number M_c against n_{e0}/n_{i0} for $\sigma_i = 0.01$ (solid curve), $\sigma_i = 0.05$ (dashed curve) and $\sigma_i = 0.1$ (dotted curve).

7.2.3 Effect of the dust fluid temperature

The properties of the DAS waves that we have described in the preceeding sections are valid for a cold dust fluid. To include the effect of the finite dust fluid temperature (Singh and Rao 1997, Mendoza-Briceño *et al* 2000), we use the modified dust momentum equation

$$\frac{\partial u_d}{\partial t} + u_d \frac{\partial u_d}{\partial z} = \frac{\partial \varphi}{\partial z} - \frac{\sigma_d}{n_d}\frac{\partial P_d}{\partial z} \tag{7.2.18}$$

supplemented by the energy equation

$$\frac{\partial P_d}{\partial t} + u_d \frac{\partial P_d}{\partial z} + 3P_d \frac{\partial u_d}{\partial z} = 0 \tag{7.2.19}$$

and equations (7.2.1), (7.2.3)–(7.2.5). Here P_d is the dust fluid pressure normalized by $n_{d0}k_B T_d$ and $\sigma_d = T_d/Z_d T_i$. To obtain a solitary wave solution, we make all the dependent variables depend on a single independent variable $\xi = z - Mt$. Thus, in the steady-state, equations (7.2.1), (7.2.18) and (7.2.3) (after substituting equations (7.2.4) and (7.2.5)) are written as

$$-M\frac{\partial n_d}{\partial \xi} + \frac{\partial}{\partial \xi}(n_d u_d) = 0 \tag{7.2.20}$$

$$-M\frac{\partial u_d}{\partial \xi} + u_d \frac{\partial u_d}{\partial \xi} + \frac{\sigma_d}{n_d}\frac{\partial P_d}{\partial \xi} = \frac{\partial \varphi}{\partial \xi} \tag{7.2.21}$$

$$-M\frac{\partial P_d}{\partial \xi} + u_d \frac{\partial P_d}{\partial \xi} + 3P_d \frac{\partial u_d}{\partial \xi} = 0 \tag{7.2.22}$$

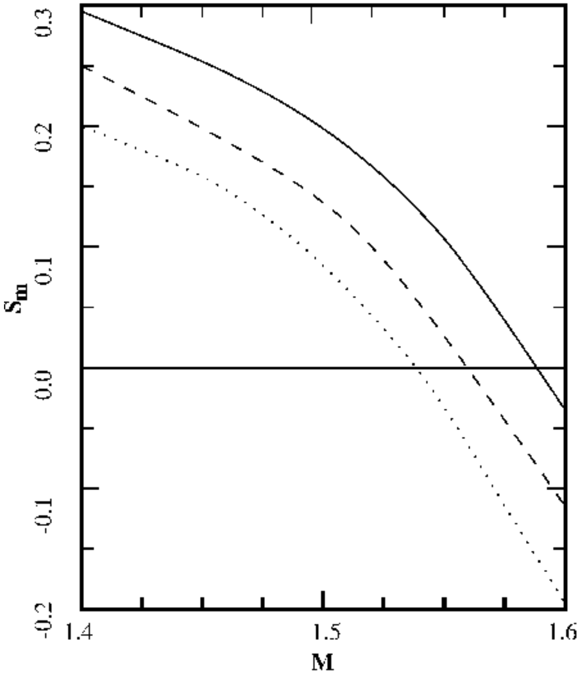

Figure 7.2. Variation of S_m against M for $\sigma_i = 0.05$, $n_{e0}/n_{i0} = 0$ (solid curve), $n_{e0}/n_{i0} = 0.05$ (dashed curve) and $n_{e0}/n_{i0} = 0$ (dotted curve). The upper limit of M is that value for which $S_m = 0$.

and

$$\frac{\partial^2 \varphi}{\partial \xi^2} = n_d + \mu_e \exp(\sigma_i \varphi) - \mu_i \exp(-\varphi). \tag{7.2.23}$$

Integrating equations (7.2.20) and (7.2.22) and imposing the appropriate boundary conditions for localized perturbations, namely $\varphi \to 0$, $u_d \to 0$, $P_d \to 1$ and $n_d \to 1$ at $\xi \to \pm\infty$, we obtain

$$n_d = \frac{M}{M - u_d} \tag{7.2.24}$$

and

$$P_d = n_d^3. \tag{7.2.25}$$

If we substitute equation (7.2.24) into equation (7.2.21) and multiply the resultant equation by 2, we obtain

$$2M\frac{\partial u_d}{\partial \xi} - 2u_d\frac{\partial u_d}{\partial \xi} - 2\sigma_d\frac{\partial P_d}{\partial \xi} + 2\frac{\sigma_d}{M}u_d\frac{\partial P_d}{\partial \xi} = -2\frac{\partial \varphi}{\partial \xi}. \tag{7.2.26}$$

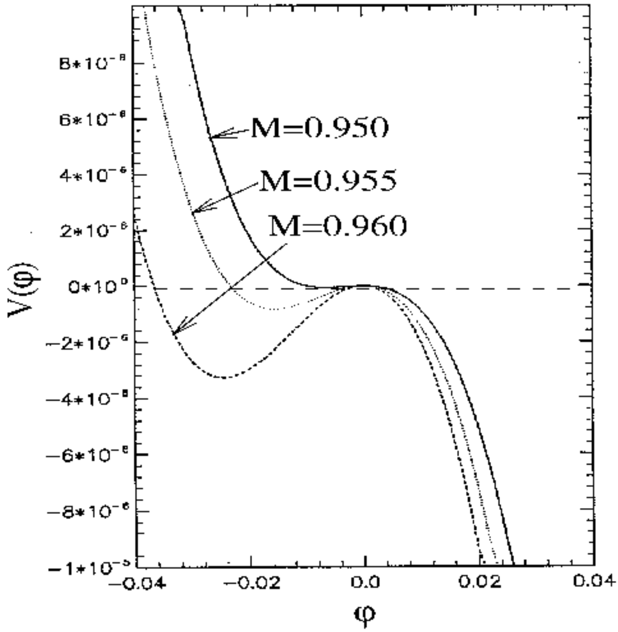

Figure 7.3. The behaviour of the Sagdeev potential $V(\varphi)$ for $\sigma_\mathrm{i} = 0.05$ and $\delta = 10$. We see that the DAS waves with $\varphi < 0$ exist when the Mach number M exceeds 0.95 (after Mamun 1999).

Multiplying equation (7.2.22) by σ_d/M we can write

$$\sigma_\mathrm{d}\frac{\partial P_\mathrm{d}}{\partial \xi} - \frac{\sigma_\mathrm{d}}{M}u_\mathrm{d}\frac{\partial P_\mathrm{d}}{\partial \xi} - 3\frac{\sigma_\mathrm{d}}{M}P_\mathrm{d}\frac{\partial u_\mathrm{d}}{\partial \xi} = 0. \tag{7.2.27}$$

Subtracting equation (7.2.26) from equation (7.2.27) we obtain

$$3\sigma_\mathrm{d}\frac{\partial P_\mathrm{d}}{\partial \xi} - 3\frac{\sigma_\mathrm{d}}{M}\frac{\partial}{\partial \xi}(P_\mathrm{d}u_\mathrm{d}) - 2M\frac{\partial u_\mathrm{d}}{\partial \xi} + 2u_\mathrm{d}\frac{\partial u_\mathrm{d}}{\partial \xi} - 2\frac{\partial \varphi}{\partial \xi} = 0. \tag{7.2.28}$$

The integration of equation (7.2.28) yields

$$3\frac{\sigma_\mathrm{d}}{M}P_\mathrm{d}u_\mathrm{d} - 3\sigma_\mathrm{d}(P_\mathrm{d} - 1) + 2Mu_\mathrm{d} - u_\mathrm{d}^2 + 2\varphi = 0 \tag{7.2.29}$$

where we have again imposed the appropriate boundary conditions for localized perturbations. Substituting u_d and P_d (which is obtained from equations (7.2.24) and (7.2.25), respectively) into equation (7.2.29) we obtain

$$3\sigma_\mathrm{d}n_\mathrm{d}^4 - (3\sigma_\mathrm{d} + M^2 + 2\varphi)n_\mathrm{d}^2 + M^2 = 0 \tag{7.2.30}$$

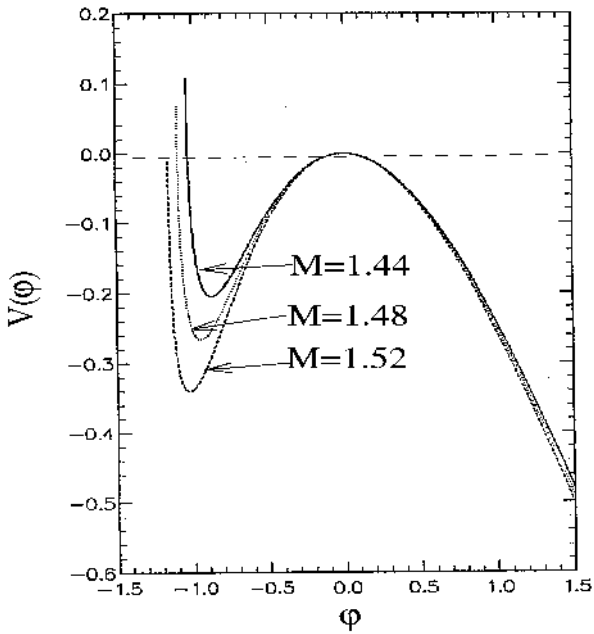

Figure 7.4. The behaviour of the Sagdeev potential $V(\varphi)$ for $\sigma_{\rm i} = 0.05$ and $\delta = 10$. We see that the DAS waves no longer exist when the Mach number M exceeds 1.52 (after Mamun 1999).

which possesses the solution (Mendoza-Briceño *et al* 2000)

$$n_{\rm d} = \frac{\sigma_1}{\sqrt{2}\sigma_0}\left[1 + \frac{2\varphi}{M^2\sigma_1^2} - \sqrt{\left(1 + \frac{2\varphi}{M^2\sigma_1^2}\right)^2 - 4\frac{\sigma_0^2}{\sigma_1^4}}\right]^{1/2} \tag{7.2.31}$$

where $\sigma_0 = \sqrt{3\sigma_{\rm d}/M^2}$ and $\sigma_1 = \sqrt{1+\sigma_0^2}$. Substituting $n_{\rm d}$ (obtained from equation (7.2.31)) into equation (7.2.23) we have

$$\frac{{\rm d}^2\varphi}{{\rm d}\xi^2} = \mu_{\rm e}\exp(\sigma_{\rm i}\varphi) - \mu_{\rm i}\exp(-\varphi) + \frac{\sigma_1}{\sqrt{2}\sigma_0}\left[1 + \frac{2\varphi}{M^2\sigma_1^2} - \sqrt{\left(1 + \frac{\varphi}{M^2\sigma_1^2}\right)^2 - 4\frac{\sigma_0^2}{\sigma_1^4}}\right]^{1/2}. \tag{7.2.32}$$

The qualitative nature of the solutions of equation (7.2.32) is most easily seen by rewriting equation (7.2.32) in the form of an energy integral

$$\frac{1}{2}\left(\frac{\mathrm{d}\varphi}{\mathrm{d}\xi}\right)^2 + V(\varphi, M, \sigma_\mathrm{d}, \sigma_\mathrm{i}, \delta) = 0 \tag{7.2.33}$$

where the Sagdeev potential $V(\varphi, M, \sigma_\mathrm{d}, \sigma_\mathrm{i}, \delta)$ is

$$\begin{aligned} V(\varphi, M, \sigma_\mathrm{d}, \sigma_\mathrm{i}, \delta) = &-\left(\frac{\mu_\mathrm{e}}{\sigma_\mathrm{i}}\right)\exp(\sigma_\mathrm{i}\varphi) - \mu_\mathrm{i}\exp(-\varphi) \\ &- M^2\sqrt{\sigma_0}[\mathrm{e}^{\theta/2} + \tfrac{1}{3}\mathrm{e}^{-3\theta/2}] + C_1 \end{aligned} \tag{7.2.34}$$

with

$$\theta = \cosh^{-1}\left[\frac{\sigma_1^2}{2\sigma_0}\left(1 + \frac{2\varphi}{M^2\sigma_1^2}\right)\right] \tag{7.2.35}$$

and C_1 is an integration constant which we choose such that $V(\varphi, M, \sigma_\mathrm{d}, \sigma_\mathrm{i}, \delta) = 0$ at $\varphi = 0$. It is important to note here that we cannot consider the limit $\sigma_\mathrm{d} \to 0$ in the Sagdeev potential $V(\varphi, M, \sigma_\mathrm{d}, \sigma_\mathrm{i}, \delta)$ in its present form. To consider the limit $\sigma_\mathrm{d} \to 0$, we express θ as

$$\theta = \ln\left[\frac{\sigma_1^2}{2\sigma_0}\left(1 + \frac{2\varphi}{M^2\sigma_1^2}\right) + \sqrt{\frac{\sigma_1^4}{4\sigma_0^2}\left(1 + \frac{2\varphi}{M^2\sigma_1^2}\right)^2 - 1}\,\right]. \tag{7.2.36}$$

We note that in our study the condition for the ion density to be real requires $|1 + 2\varphi/M^2\sigma_1^2| \geq 2\sigma_0/\sigma_1^2$.

One can now examine how the dust fluid temperature σ_d modifies the properties of arbitrary-amplitude DAS waves by analysing the Sagdeev potential $V(\varphi, M, \sigma_\mathrm{d}, \sigma_\mathrm{i}, \delta)$, as we described in the previous section. We can also examine the effect of the dust fluid temperature on the DAS waves by direct numerical solitary wave solutions of equation (7.2.33) for different values of σ_d, as shown in figure 7.5. It is obvious from figure 7.5 that as we increase the dust fluid temperature, the amplitude of the solitary wave decreases, but the width increases.

7.2.4 Effect of the trapped ion distribution

It is well known (Schamel 1972, 1986) that the electron and ion distribution functions can be significantly modified in the presence of large-amplitude waves that are excited by the two-stream instability (Winske *et al* 1995). Accordingly, the electron and ion number densities depart from the Boltzmann distributions when phase space vortex distributions appear in a plasma. For the DA waves, the ion trapping in the wave potential is of interest. To study the effects of

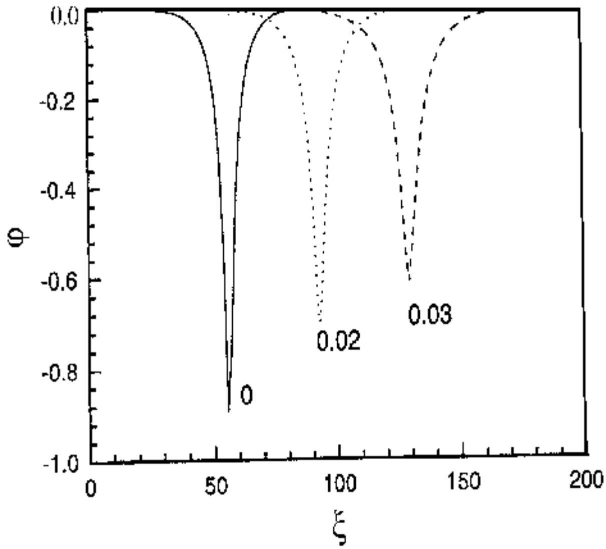

Figure 7.5. Potential profiles for $\sigma_i = 0.2$, $\delta = 10$, $M = 1.455$ and $\sigma_d = 0$ (solid curve), $\sigma_d = 0.02$ (dotted curve) and $\sigma_d = 0.03$ (dashed curve).

non-isothermal ions on the DAS waves, we consider the trapped or vortex-like (Schamel 1972, Schamel *et al* 2001) ion distribution $f_i = f_{if} + f_{it}$, where

$$f_{if} = \frac{1}{\sqrt{2\pi}} \exp\left[-\frac{1}{2}(v_i^2 + 2\varphi)\right] \tag{7.2.37}$$

for $|v_i| > \sqrt{-2\varphi}$ and

$$f_{it} = \frac{1}{\sqrt{2\pi}} \exp\left[-\frac{1}{2}\sigma_{it}(v_i^2 + 2\varphi)\right] \tag{7.2.38}$$

for $|v_i| \leq \sqrt{-2\varphi}$. We note that the ion distribution function, as prescribed above, is continuous in velocity space and satisfies the regularity requirements for an admissible BGK solution (Schamel 1972). Here the ion velocity v_i in equations (7.2.37) and (7.2.38) is normalized by the ion thermal velocity V_{Ti} and σ_{it} ($= T_i/T_{it}$), which is the ratio of the free ion temperature T_i to the trapped ion temperature T_{it}, is a parameter determining the number of trapped ions. Integrating the ion distributions over the velocity space we readily obtain the ion number density n_i as (Schamel 1986)

$$n_i = I(-\varphi) + \frac{1}{\sqrt{\sigma_{it}}} \exp(-\sigma_{it}\varphi) \operatorname{erf}(\sqrt{-\sigma_{it}\varphi}) \tag{7.2.39}$$

for $\sigma_{it} > 0$ and

$$n_i = I(-\varphi) + \frac{1}{\sqrt{\pi|\sigma_{it}|}} W_D(\sqrt{\sigma_{it}\varphi}) \tag{7.2.40}$$

for $\sigma_{\mathrm{it}} < 0$, where

$$I(z_0) = [1 - \mathrm{erf}(\sqrt{z_0})]\exp(z_0), \tag{7.2.41a}$$

$$\mathrm{erf}(z_0) = \frac{2}{\sqrt{\pi}}\int_0^{z_0} \exp(-y^2)\,\mathrm{d}y \tag{7.2.41b}$$

and

$$W_{\mathrm{D}}(z_0) = \exp(-z_0^2)\int_0^{z_0} \exp(y^2)\,\mathrm{d}y. \tag{7.2.41c}$$

If we expand n_{i} in the small-amplitude limit (namely $\varphi \ll 1$) and keep terms up to φ^2, it is found that n_{i} is the same for both $\sigma_{\mathrm{it}} < 0$ and $\sigma_{\mathrm{it}} > 0$. It is expressed as

$$n_{\mathrm{i}} = 1 - \varphi - \frac{4(1-\sigma_{\mathrm{it}})}{3\sqrt{\pi}}(-\varphi)^{3/2} + \frac{1}{2}\varphi^2. \tag{7.2.42}$$

We now follow the reductive perturbation technique of Schamel (1975) and construct a weakly nonlinear theory for the DAS waves by introducing the stretched coordinates $\zeta = \epsilon^{1/4}(z - v_0 t)$ and $\tau = \epsilon^{3/4}t$. We can then expand the variables n_{d}, u_{d} and φ about the unperturbed states in a power series of ϵ as

$$n_{\mathrm{d}} = \epsilon n_{\mathrm{d}}^{(1)} + \epsilon^{3/2} n_{\mathrm{d}}^{(2)} + \cdots \tag{7.2.43a}$$

$$u_{\mathrm{d}} = \epsilon u_{\mathrm{d}}^{(1)} + \epsilon^{3/2} u_{\mathrm{d}}^{(2)} + \cdots \tag{7.2.43b}$$

$$\varphi = \epsilon \varphi^{(1)} + \epsilon^{3/2}\varphi^{(2)} + \cdots \tag{7.2.43c}$$

and develop equations in various powers of ϵ by using equations (7.2.1)–(7.2.4), (7.2.42) and (7.2.43). Following the same mathematical steps as we used in section 7.2.1, one can finally obtain (Mamun *et al* 1996b, Mamun 1998)

$$\frac{\partial \varphi^{(1)}}{\partial \tau} + a_{\mathrm{t}}\sqrt{-\varphi^{(1)}}\frac{\partial \varphi^{(1)}}{\partial \zeta} + b_s\frac{\partial^3 \varphi^{(1)}}{\partial \zeta^3} = 0 \tag{7.2.44}$$

where

$$a_{\mathrm{t}} = \frac{v_0^3\delta(1-\sigma_{\mathrm{it}})}{\sqrt{\pi}(\delta - 1)}. \tag{7.2.45}$$

Equation (7.2.44) is the modified KdV equation exhibiting a stronger nonlinearity, smaller width and larger propagation speed of the DAS waves.

The stationary soliton-like solution of the modified KdV equation (7.2.44) can be obtained by transforming the space variable ζ to $\eta = \zeta - u_0\tau$ and by imposing the appropriate boundary conditions, namely $\varphi \to 0$, $\mathrm{d}\varphi^{(1)}/\mathrm{d}\eta \to 0$, $\mathrm{d}^2\varphi^{(1)}/\mathrm{d}\eta^2 \to 0$ at $\eta \to \pm\infty$. Thus, the steady-state solution of equation (7.2.44) can be expressed as

$$\varphi^{(1)} = -\varphi_{\mathrm{m}}^{(1)}\,\mathrm{sech}^4[(\zeta - u_0\tau)/\Delta_{\mathrm{t}}] \tag{7.2.46}$$

where the amplitude $\varphi_{\mathrm{m}}^{(1)}$ and the width Δ_{t} are given by $\varphi_{\mathrm{m}}^{(1)} = (15u_0/8a_{\mathrm{t}})^2$ and $\Delta_{\mathrm{t}} = \sqrt{16b_s/u_0}$, respectively. As $u_0 > 0$ and $\delta > 1$, equation (7.2.46) reveals that there exist solitary waves with $\varphi < 0$ only. It is also observed that as u_0 increases, the amplitude increases while the width decreases, and that as $|\sigma_{\rm it}|$ increases the amplitude decreases for $\sigma_{\rm it} < 0$ (a vortex-like excavated trapped ion distribution (Schamel 1972)) and increases for $\sigma_{\rm it} > 0$.

7.2.5 Effect of dust charge fluctuations

We now investigate the effect of the dust grain charge fluctuation (Rao and Shukla 1994) on the arbitrary-amplitude DAS waves discussed in section 7.2.2. We use equations (7.2.1), (7.2.4) and (7.2.5) along with equations (7.2.2) and (7.2.3) (with a minor modification which includes the dust grain charge as another variable). Thus, we start with

$$\frac{\partial u_{\rm d}}{\partial t} + u_{\rm d}\frac{\partial u_{\rm d}}{\partial z} = Z_{\rm d}\frac{\partial \varphi}{\partial z} \tag{7.2.47}$$

and

$$\frac{\partial^2 \varphi}{\partial z^2} = Z_{\rm d} n_{\rm d} + \mu_{\rm e} n_{\rm e} - \mu_{\rm i} n_{\rm i} \tag{7.2.48}$$

where $Z_{\rm d}$ is normalized by its equilibrium value $Z_{\rm d0}$. Equations (7.2.1), (7.2.4), (7.2.5), (7.2.47) and (7.2.48) are completed by the charging equation (2.5.2), which can be expressed in terms of the normalized variables as

$$\frac{\partial Z_{\rm d}}{\partial t} + u_{\rm d}\frac{\partial Z_{\rm d}}{\partial z} = -(I_{\rm e} + I_{\rm i}) \tag{7.2.49}$$

where the normalized electron and ion currents $I_{\rm e}$ and $I_{\rm i}$ are

$$I_{\rm e} = -\sqrt{\frac{1}{2\pi}}\frac{V_{\rm Te}}{\omega_{\rm pd}} 4\pi r_{\rm d}^2 n_{\rm d0} \mu_{\rm e} n_{\rm e} \exp(-\sigma_{\rm i} S_{\rm d} Z_{\rm d}) \tag{7.2.50}$$

and

$$I_{\rm i} = \sqrt{\frac{1}{2\pi}}\frac{V_{\rm Ti}}{\omega_{\rm pd}} 4\pi r_{\rm d}^2 n_{\rm d0} \mu_{\rm i} n_{\rm i} (1 + S_{\rm d} Z_{\rm d}) \tag{7.2.51}$$

where $S_{\rm d} = Z_{\rm d0} e^2 / r_{\rm d} k_{\rm B} T_{\rm i}$. Using the current balance equation ($I_{\rm e} + I_{\rm i} = 0$) as well as substituting $n_{\rm e}$ and $n_{\rm i}$ we have

$$(1 + S_{\rm d} Z_{\rm d})\frac{\delta V_{\rm Ti}}{V_{\rm Te}} = \exp[-\sigma_{\rm i} S_{\rm d} Z_{\rm d} + (1 + \sigma_{\rm i})\varphi] \tag{7.2.52}$$

which can be simplified to

$$\varphi = \frac{1}{1 + \sigma_{\rm i}}\left[\sigma_{\rm i} S_{\rm d} Z_{\rm d} + \ln\left(\frac{\delta V_{\rm Ti}}{V_{T_{\rm e}}}\right) + \ln(1 + S_{\rm d} Z_{\rm d})\right]. \tag{7.2.53}$$

To reduce equations (7.2.1), (7.2.4), (7.2.5), (7.2.47) and (7.2.48) into a single equation, we introduce a dimensionless function (Ma and Liu 1997)

$$\Psi = -\int_0^{\varphi} Z_{\rm d} {\rm d}\varphi \tag{7.2.54}$$

which, after using equation (7.2.53), can be expressed as

$$\Psi = -\frac{\varphi}{S_\mathrm{d}} - (Z_\mathrm{d} - 1) - \frac{\sigma_\mathrm{i} S_\mathrm{d}}{2(1+\sigma_\mathrm{i})}(Z_\mathrm{d}^2 - 1). \tag{7.2.55}$$

To study arbitrary amplitude time-independent DAS waves, we make all the dependent variables depend only on a single variable $\xi = z - Mt$, use the steady-state condition and impose the appropriate boundary conditions for localized perturbations. Hence from equations (7.2.1), (7.2.47) and (7.2.54) we obtain

$$n_\mathrm{d} = \left(1 - \frac{2\Psi}{M^2}\right)^{-1/2}. \tag{7.2.56}$$

Substituting equations (7.2.4), (7.2.5) and (7.2.56) into equation (7.2.48) and integrating the resultant equation we obtain the 'energy integral'

$$\frac{1}{2}\left(\frac{\mathrm{d}\varphi}{\mathrm{d}\xi}\right)^2 + V(\varphi, Z_\mathrm{d}) = 0 \tag{7.2.57}$$

where the Sagdeev potential $V(\varphi, Z_\mathrm{d})$ is of the form

$$V(\varphi, Z_\mathrm{d}) = \mu_\mathrm{i}[1 - \exp(-\varphi)] + \frac{\mu_\mathrm{e}}{\sigma_\mathrm{i}}[1 - \exp(\sigma_\mathrm{i}\varphi)] + M^2\left[\left(1 - \frac{2\Psi}{M^2}\right)^{1/2} - 1\right]. \tag{7.2.58}$$

It is obvious from equation (7.2.58) that the effect of dust grain charge fluctuations is contained in Ψ. Now analysing the Sagdeev potential $V(\varphi, Z_\mathrm{d})$ (as we have done in section 7.2.2), one can easily investigate the properties of the DAS waves accounting for dust charge fluctuations. We can also directly solve equation (7.2.57) numerically and examine the structures of the DAS profiles (as shown in figure 7.6) that may exist in a dusty plasma with fluctuating charges on the dust grain surface.

7.2.6 Cylindrical and spherical DAS waves

The studies of the DAS waves that we have presented up to now are restricted to a planar one-dimensional geometry. However, in laboratory devices one may encounter multi-dimensional DAS structures. Here we are concerned with the propagation of radially ingoing DAS structures in non-planar cylindrical and spherical geometries. The dynamics of low phase velocity nonlinear DAS waves in cylindrical and spherical geometries are governed by

$$\frac{\partial n_\mathrm{d}}{\partial t} + \frac{1}{r^\nu}\frac{\partial}{\partial r}(r^\nu n_\mathrm{d} u_\mathrm{d}) = 0 \tag{7.2.59}$$

$$\frac{\partial u_\mathrm{d}}{\partial t} + u_\mathrm{d}\frac{\partial u_\mathrm{d}}{\partial r} = \frac{\partial \varphi}{\partial r} \tag{7.2.60}$$

$$\frac{1}{r^\nu}\frac{\partial}{\partial r}\left(r^\nu \frac{\partial \varphi}{\partial r}\right) = n_\mathrm{d} + \mu_\mathrm{e}\exp(\sigma_\mathrm{i}\varphi) - \mu_\mathrm{i}\exp(-\varphi) \tag{7.2.61}$$

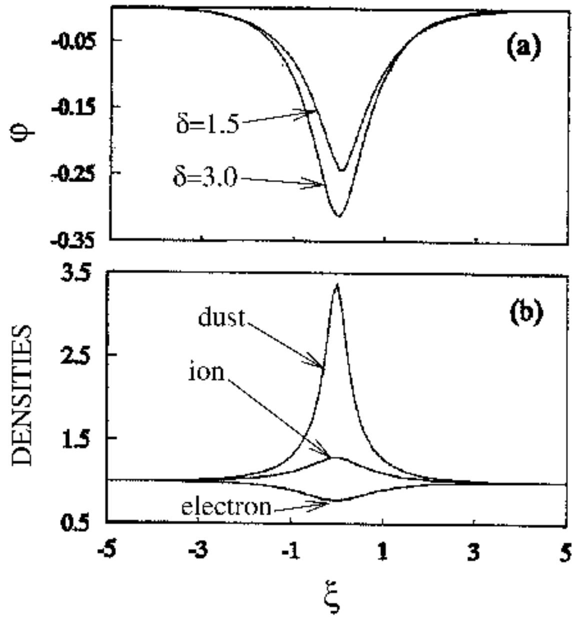

Figure 7.6. Solitary wave solutions of equation (7.2.57) with $\sigma_\mathrm{i} = 1$ and $M = S_\mathrm{d}^{-1/2}$: (*a*) potential profiles for $\delta = 3$ and $\delta = 1.5$, and (*b*) electron, ion and dust density profiles for $\delta = 3$ (after Ma and Liu 1997).

where $\nu = 1, 2$ for cylindrical and spherical geometries, respectively. The space variable r is normalized by the Debye radius λ_{Dm}.

To investigate ingoing solutions of equations (7.2.59)–(7.2.61), we introduce the stretched coordinates $\zeta = -\epsilon^{1/2}(r + v_0 t)$ and $\tau = \epsilon^{3/2} t$ and use the expansion of n_d, u_d and φ, as given in equation (7.2.6). Following the same procedure as applied in section 7.2.1, we can readily derive

$$\frac{\partial \varphi^{(1)}}{\partial \tau} + \frac{\nu}{2\tau}\varphi^{(1)} + a_s \varphi^{(1)} \frac{\partial \varphi^{(1)}}{\partial \zeta} + b_s \frac{\partial^3 \varphi^{(1)}}{\partial \zeta^3} = 0 \tag{7.2.62}$$

which is a modified KdV equation with the coefficients a_s and b_s given by equation (7.2.11). It is obvious that in equation (7.2.62) the second term, namely $(\nu/2\tau)\varphi^{(1)}$, is due to the effect of the cylindrical or spherical geometry (Maxon and Viecelli 1974). One can numerically solve equation (7.2.62) by using a two-level finite difference approximation method (Maxon and Viecelli 1974) and can study the effects of cylindrical and spherical geometries on time-dependent DAS waves.

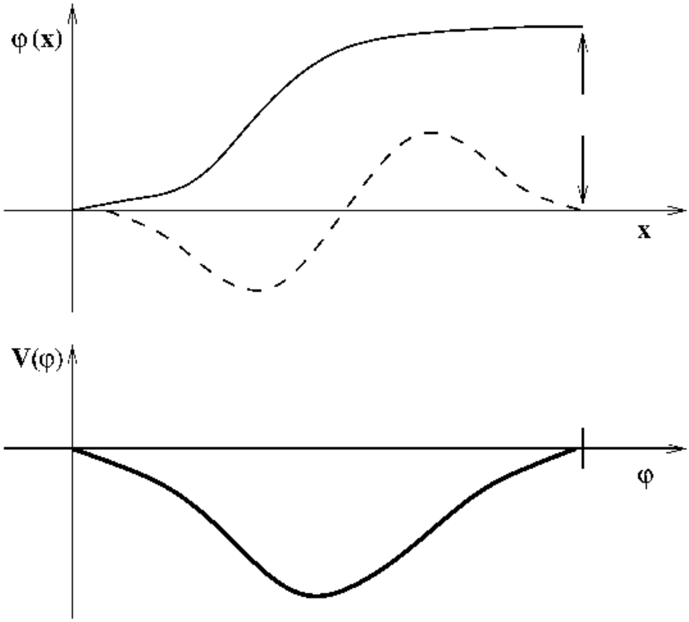

Figure 7.7. The electric and classical potentials (φ and $V(\varphi)$) of a double layer. The dotted line represents the total charge density (after Schamel 1986).

7.2.7 Double layers

A double layer is defined as a monotonic transition of the electric potential connecting smoothly two differently biased plasmas. This is achieved by a bipolar charge distribution, as shown in figure 7.7 where the electric and classical potentials (φ and $V(\varphi)$) are displayed together with the charge density. According to Poisson's equation, a positively charged layer gives rise to a region of negative curvature of the potential and vice versa, and hence two oppositely charged layers are needed to buildup the double-layer structure (Schamel 1986). In order for the latter to appear, we must account for the trapped particle effect. The reason is that if only streaming (i.e. non-reflected) particles were present, the spatial constancy of the electron and ion currents would imply that the required charge neutrality cannot hold simultaneously on both sides of the double-layer structure. Due to the different acceleration of electrons and ions in the double layer, their densities are affected. We assume that in the double layer the electrons follow the Boltzmann response (7.2.4), while the non-thermal ions obey equation (7.2.42). Thus, the structure of a small-amplitude dust double layer is deduced from

$$\frac{\partial^2\varphi}{\partial\xi^2} = \lambda_1\varphi + \frac{4}{3}b_{\rm ti}(-\varphi)^{3/2} - \lambda_2\varphi^2 \qquad (7.2.63)$$

which is obtained from equations (7.2.3), (7.2.4), (7.2.42) and $n_{\mathrm{d}} = (1 + 2\varphi/M^2)^{-1/2}$. We have denoted $\lambda_1 = -M^{-2} + \mu_{\mathrm{e}}\sigma_{\mathrm{i}} + \mu_{\mathrm{i}}$, $b_{\mathrm{ti}} = \mu_{\mathrm{i}}(1 - \sigma_{\mathrm{i}})/\sqrt{\pi}$ and $\lambda_2 = (3/2M^4) + (\mu_{\mathrm{e}}\sigma_{\mathrm{i}}^2 - \mu_{\mathrm{i}})/2$. Introducing $-\varphi = \psi$, multiplying equation (7.2.63) by $\partial\psi/\partial x$ and integrating once, we obtain

$$\frac{1}{2}\left(\frac{\partial\psi}{\partial\xi}\right)^2 + U_{s\mathrm{d}}(\psi, M, \alpha) = 0 \tag{7.2.64}$$

where the classical potential is

$$U_{s\mathrm{d}}(\psi, M, \alpha) = -\frac{\lambda_1}{2}\psi^2 + \frac{2}{5}b_{\mathrm{ti}}\psi^{5/2} + \frac{\lambda_2}{3}\psi^3. \tag{7.2.65}$$

The dust double layers must satisfy two conditions, namely $U_{s\mathrm{d}}(\psi_{\mathrm{m}}, M, \alpha) = 0$ and $(\partial U_{s\mathrm{d}}/\partial\psi)_{\psi=\psi_{\mathrm{m}}} = 0$, which express the vanishing of the electric field and the charge density on the high potential side. Accordingly, we obtain from equation (7.2.65)

$$\lambda_1 - \frac{4}{5}b_{\mathrm{ti}}\psi_{\mathrm{m}}^{1/2} - \frac{2}{3}\lambda_2\psi_{\mathrm{m}} = 0 \tag{7.2.66}$$

and

$$\lambda_1 - b_{\mathrm{ti}}\psi_{\mathrm{m}}^{1/2} - \lambda_2\psi_{\mathrm{m}} = 0 \tag{7.2.67}$$

which can be solved for λ_1 and b_{ti}, resulting in

$$\lambda_1 = -\frac{2}{3}\lambda_2\psi_{\mathrm{m}} \tag{7.2.68}$$

and

$$b_{\mathrm{ti}} = -\frac{5}{3}\lambda_2\psi_{\mathrm{m}}^{1/2}. \tag{7.2.69}$$

Subsequently, we can express equation (7.2.64) as

$$\left(\frac{\partial\psi}{\partial\xi}\right)^2 + \frac{2}{3}\lambda_2\psi^2(\sqrt{\psi} - \sqrt{\psi_{\mathrm{m}}})^2 = 0 \tag{7.2.70}$$

which admits a double-layer solution (Kim 1983)

$$\psi(\xi) = \frac{1}{4}\psi_{\mathrm{m}}\left[1 + \tanh\left(\frac{\xi}{\lambda_{\mathrm{dl}}}\right)\right]^2 \tag{7.2.71}$$

where the width of the dust double layers is

$$\lambda_{\mathrm{dl}} = \left(\frac{\lambda_2}{24}\psi_{\mathrm{m}}\right)^{-1/2}. \tag{7.2.72}$$

We observe that the dust double layers require $\lambda_2 > 0$, which yields $M^4(\mu_{\mathrm{e}}\sigma_{\mathrm{i}}^2 - \mu_{\mathrm{i}}) + 1.5 > 0$.

7.2.8 Dust lattice solitary waves

The linear propagation of the dust lattice waves has been studied in section 4.5. We consider here the nonlinear propagation of small but finite amplitude DL waves for which we can express the potential energy u (given by equation (4.5.19)) in the form (Farokhi *et al* 1999)

$$u = \frac{Q_0\Phi_0}{\cosh(k_\mathrm{D}a)} \frac{\left[1 + \frac{k_\mathrm{D}^2}{4}(\xi_{n+1} + \xi_{n-1} - 2\xi_n)^2 + \frac{k_\mathrm{D}^4}{384}(\xi_{n+1} + \xi_{n-1} - 2\xi_n)^4\right]}{\left[1 + \frac{k_\mathrm{D}}{2}\tanh(k_\mathrm{D}a)(\xi_{n+1} - \xi_{n-1})\right]}. \tag{7.2.73}$$

Using equation (7.2.73) the nonlinear equation (4.5.2) can be written as

$$\frac{\partial^2\xi_n}{\partial t^2} = \frac{Q_0\Phi_0 k_\mathrm{D}^2}{m_\mathrm{d}\cosh(k_\mathrm{D}a)} \frac{\left[(\xi_{n+1} + \xi_{n-1} - 2\xi_n) + \frac{k_\mathrm{D}^2}{48}(\xi_{n+1} + \xi_{n-1} - 2\xi_n)^3\right]}{\left[1 + \frac{k_\mathrm{D}}{2}\tanh(k_\mathrm{D}a)(\xi_{n+1} - \xi_{n-1})\right]} \tag{7.2.74}$$

where dust–neutral collisions have been neglected. To simplify the nonlinear equation (7.2.74), we only include weak nonlinearities. We also consider the long-wavelength approximation ($k_\mathrm{D}a \ll 1$), where the wave dispersion is small and equation (7.2.74) can be approximated by the differential equations for a continuum. Thus, we introduce the Taylor expansions of ξ_{n+1} and ξ_{n-1} as $\xi_n + (\partial\xi/\partial z)_n a + 0.5(\partial^2\xi/\partial z^2)_n a^2 + \cdots$ and $\xi_n - (\partial\xi/\partial z)_n a + 0.5(\partial^2\xi/\partial z^2)_n a^2 + \cdots$, respectively. Inserting these expansions in equation (7.2.74), we obtain (Farokhi *et al* 1999)

$$\frac{\partial^2\xi}{\partial t^2} - v_0^2\left[\frac{\partial^2\xi}{\partial z^2} + \frac{a^2}{12}\frac{\partial^4\xi}{\partial z^4} - \frac{k_\mathrm{D}a}{2}\tanh(k_\mathrm{D}a)\frac{\partial}{\partial z}\left(\frac{\partial\xi}{\partial z}\right)^2\right] = 0. \tag{7.2.75}$$

Here

$$v_0 = \left[\frac{Q_0\Phi_0 k_\mathrm{D}^2 a^2}{m_\mathrm{d}\cosh(k_\mathrm{D}a)}\right]^{1/2} \tag{7.2.76}$$

is the phase velocity for $k_\mathrm{D}a \ll 1$, where the Debye shielding around each dust particle has been neglected. Equation (7.2.75) includes the DL waves propagating in both positive and negative z directions with phase velocities close to v_0 and $-v_0$, respectively. For the waves with phase velocities close to v_0, equation (7.2.75) takes the form

$$\left(\frac{\partial}{\partial t} + v_0\frac{\partial}{\partial z}\right)\xi + v_0\left[\frac{a^2}{12}\frac{\partial^3\xi}{\partial z^3} - \frac{k_\mathrm{D}a}{2}\tanh(k_\mathrm{D}a)\left(\frac{\partial\xi}{\partial z}\right)^2\right] = 0. \tag{7.2.77}$$

Equation (7.2.77) is now transformed to a wave-frame moving with a relative speed v_0 in a new frame ($z' = z - v_0 t$ and $\tau = t$). It is then differentiated with respect to z', yielding the KdV equation

$$\frac{\partial u}{\partial \tau} + a_l u \frac{\partial u}{\partial z'} + b_l \frac{\partial^3 u}{\partial z'^3} = 0 \tag{7.2.78}$$

where $u = \partial\xi/\partial z'$, $a_l = -v_0 k_D a\ \tanh(k_D a)$ and $b_l = v_0 a^2/12$. The steady-state solution of equation (7.2.78) is exactly similar to equation (7.2.12), i.e.

$$u = u_m \operatorname{sech}^2[(\zeta - u_0 t)/\Delta_l] \tag{7.2.79}$$

where the amplitude u_m and the width Δ_l are given by $3u_0/a_l$ and $\sqrt{4b_l/u_0}$, respectively. As $u_0 > 0$ and $a_l < 0$, equation (7.2.79) predicts the existence of small but finite amplitude DL solitary waves with $u < 0$.

7.3 Shock Waves

We have discussed solitary structures which arise only when the dissipative effects are negligible in comparison with the dispersive effect. However, in practice there are some dusty plasmas in which the dissipative effects may be comparable or even dominant over the dispersive effect. In such a circumstance, the nonlinear dusty plasma waves (particularly the DA and DIA waves) may appear in the form of shock structures instead of solitary structures. In this section, we study the properties of the DA and DIA shock waves that may form in a dusty plasma.

7.3.1 DA shock waves

The nonlinear propagation of the DA waves in a strongly coupled dissipative dusty plasma can be investigated by means of the generalized hydrodynamic (GH) equations, namely equations (7.2.1), (7.2.3)–(7.2.5) and (Shukla and Mamun 2001)

$$(1 + \tau_m D_t)\left[n_d \left(D_t u_d + \nu_{dn} u_d - \frac{\partial \varphi}{\partial z}\right)\right] = \eta_d \frac{\partial^2 u_d}{\partial z^2} \tag{7.3.1}$$

where $D_t = (\partial/\partial t) + u_d \partial/\partial z$, ν_{dn} is normalized by the dust plasma frequency ω_{pd}, the viscoelastic relaxation time τ_m is normalized by the dust plasma period ω_{pd}^{-1} and $\eta_d = (\tau_d/m_d n_{d0} \lambda_{Dm}^2)[\eta_b + (4/3)\zeta_b]$ is the normalized longitudinal viscosity coefficient. The transport coefficients of the shear and bulk viscosities are given in chapter 4.

To derive a dynamical equation for the DA shock waves from our basic equations (7.2.1), (7.2.3)–(7.2.5) and (7.3.1), we employ the reductive perturbation technique. Thus, as before, we introduce the stretched coordinates $\xi = \epsilon^{1/2}(z - u_0 t)$ and $\tau = \epsilon^{3/2} t$ and use the expansion of n_d, u_d and φ given by equations (7.2.6). Substituting the latter into equations (7.2.1), (7.2.3)–(7.2.5) and

(7.3.1), we obtain from the equations of the lowest order in ϵ, $u_{\rm d}^{(1)} = -\varphi^{(1)}/v_0$, $n_{\rm d}^{(1)} = -\varphi^{(1)}/v_0^2$ and $v_0 = (\sigma_{\rm i}\mu_{\rm e} + \mu_{\rm i})^{-1/2}$. To next order in ϵ, we have

$$\frac{\partial n_{\rm d}^{(1)}}{\partial \tau} - v_0 \frac{\partial n_{\rm d}^{(2)}}{\partial \xi} + \frac{\partial}{\partial \xi}[n_{\rm d}^{(1)} u_{\rm d}^{(1)}] + \frac{\partial u_{\rm d}^{(2)}}{\partial \xi} = 0 \tag{7.3.2}$$

$$(1 + \nu_{\rm dn}\tau_{\rm m})\frac{\partial u_{\rm d}^{(1)}}{\partial \tau} - u_0 \frac{\partial u_{\rm d}^{(2)}}{\partial \xi} - \frac{\partial \varphi^{(2)}}{\partial \xi} + (1 - \nu_{\rm dn}\tau_{\rm m}) u_{\rm d}^{(1)} \frac{\partial u_{\rm d}^{(1)}}{\partial \xi} - \eta_{\rm d0}\frac{\partial^2 u_{\rm d}^{(1)}}{\partial \xi^2} = 0 \tag{7.3.3}$$

and

$$\frac{\partial^2 \varphi^{(1)}}{\partial \xi^2} - \frac{1}{u_0^2}\varphi^{(2)} - n_{\rm d}^{(2)} = \frac{1}{2}(\sigma_{\rm i}^2\mu_{\rm e} - \mu_{\rm i})[\varphi^{(1)}]^2 \tag{7.3.4}$$

where we have assumed $\eta_{\rm d} \sim \epsilon^{1/2}\eta_{\rm d0}$. By eliminating $n_{\rm d}^{(2)}$, $u_{\rm d}^{(2)}$ and $\varphi^{(2)}$ from equations (7.3.2)–(7.3.4) we readily obtain the KdV–Burgers equation

$$A_{\rm d}^{-1}\frac{\partial \varphi^{(1)}}{\partial \tau} + \varphi^{(1)}\frac{\partial \varphi^{(1)}}{\partial \xi} + \beta_{\rm d}\frac{\partial^3 \varphi^{(1)}}{\partial \xi^3} = \mu_{\rm da}\frac{\partial^2 \varphi^{(1)}}{\partial \xi^2} \tag{7.3.5}$$

where $A_{\rm d} = (v_0^3 a_{\rm d}/2)(1 + \nu_{\rm dn}\tau_{\rm m}/2)^{-1}$, $\mu_{\rm da} = \eta_{\rm d0}/a_{\rm d}v_0^3$, $\beta_{\rm d} = 1/a_{\rm d}$ and $a_{\rm d} = [(\nu_{\rm dn}\tau_{\rm m} - 3)/v_0^4 + \mu_{\rm i} - \mu_{\rm e}\sigma_{\rm i}^2]$. As $\nu_{\rm dn} > 0$, $\tau_{\rm m} > 0$, $\eta_{\rm d0} > 0$, and $v_0 = (\sigma_{\rm i}\mu_{\rm e} + \mu_{\rm i})^{-1/2} > 0$, the sign of the coefficients $A_{\rm d}$, $\beta_{\rm d}$ and $\mu_{\rm da}$ are determined by the sign of $a_{\rm d}$, which can be expressed as $a_{\rm d} = (\nu_{\rm dn}\tau_{\rm m} - 3)(\mu_{\rm i} + \sigma_{\rm i}\mu_{\rm e})^2 - \sigma_{\rm i}^2\mu_{\rm e} + \mu_{\rm i} = \mu_{\rm e}[(\nu_{\rm dn}\tau_{\rm m} - 3)\sigma_{\rm i}^2\mu_{\rm e} - \sigma_{\rm i}^2] + \mu_{\rm i}^2(\nu_{\rm dn}\tau_{\rm m} - 3 + Z_{\rm d}n_{\rm d0}/n_{\rm i0}) + 2(\nu_{\rm dn}\tau_{\rm m} - 3)\mu_{\rm e}\mu_{\rm i}\sigma_{\rm i}$. It is obvious that for a strongly coupled dusty plasma with a significant background of neutrals, we have $\nu_{\rm dn}\tau_{\rm m} \gg 1$, i.e. $a_{\rm d} > 0$, which corresponds to $A_{\rm d} > 0$, $\mu_{\rm da} > 0$ and $\beta_{\rm d} > 0$, whereas for a weakly coupled or a collisionless dusty plasma ($\nu_{\rm dn}\tau_{\rm m} \to 0$), we have $a_{\rm d} < 0$, which corresponds to $A_{\rm d} < 0$, $\mu_{\rm da} < 0$ and $\beta_{\rm d} < 0$.

7.3.2 DIA shock waves

We present here an analytical model for the one-dimensional DIA shocks in an unmagnetized dusty plasma. The governing nonlinear equations for the DIA shocks in terms of normalized variables are (Shukla 2000d)

$$\frac{\partial n_{\rm i}}{\partial t} + \frac{\partial (n_{\rm i}u_{\rm i})}{\partial z} = 0 \tag{7.3.6}$$

$$\frac{\partial u_{\rm i}}{\partial t} + u_{\rm i}\frac{\partial u_{\rm i}}{\partial z} = -\frac{\partial \Phi}{\partial z} - 3\sigma_{\rm i}n_{\rm i}\frac{\partial n_{\rm i}}{\partial z} + \eta_{\rm i}\frac{\partial^2 u_{\rm i}}{\partial z^2} \tag{7.3.7}$$

and

$$\delta\frac{\partial^2 \Phi}{\partial z^2} = \exp(\Phi) - \delta n_{\rm i} + (\delta - 1) \tag{7.3.8}$$

where u_{i} is the ion fluid speed normalized by the ion-acoustic speed c_s, Φ is the electrostatic wave potential normalized by $k_{\mathrm{B}}T_{\mathrm{e}}/e$ and $\eta_{\mathrm{i}} = \delta\mu_{\mathrm{d}}/\omega_{\mathrm{pi}}\lambda_{\mathrm{De}}^2$ (in which μ_{d} is the kinematic viscosity). Here the time and space variables are in units of the ion plasma period $\omega_{\mathrm{pi}}{}^{-1}$ and the electron Debye length $\lambda_{\mathrm{De}}/\sqrt{\delta}$, respectively.

To derive a dynamical equation for the DIA shock waves, we expand

$$n_{\mathrm{i}} = 1 + \epsilon n_{\mathrm{i}}^{(1)} + \epsilon^2 n_{\mathrm{i}}^{(2)} + \cdots \tag{7.3.9a}$$

$$u_{\mathrm{i}} = \epsilon u_{\mathrm{i}}^{(1)} + \epsilon^2 u_{\mathrm{i}}^{(2)} + \cdots \tag{7.3.9b}$$

and

$$\Phi = \epsilon\Phi^{(1)} + \epsilon^2\Phi^{(2)} + \cdots \tag{7.3.9c}$$

and introduce the stretched variables $\xi = \epsilon^{1/2}(z - v_0 t)$ and $\tau = \epsilon^{3/2}t$. Now substituting equations (7.3.9) into (7.3.6)–(7.3.8), we obtain from the lowest order in ϵ, $\Phi^{(1)} = \delta n_{\mathrm{i}}^{(1)}$, $u_{\mathrm{i}}^{(1)} = v_0 n_{\mathrm{i}}^{(1)}$ and $v_0 = (\delta + 3\sigma_{\mathrm{i}})^{1/2}$. To next order in ϵ, we have

$$\frac{\partial n_{\mathrm{i}}^{(1)}}{\partial\tau} - v_0\frac{\partial n_{\mathrm{i}}^{(2)}}{\partial\xi} + \frac{\partial}{\partial\xi}[n_{\mathrm{i}}^{(1)}u_{\mathrm{i}}^{(1)}] + \frac{\partial u_{\mathrm{i}}^{(2)}}{\partial\xi} = 0 \tag{7.3.10}$$

$$\begin{aligned}\frac{\partial u_{\mathrm{i}}^{(1)}}{\partial\tau} &- v_0\frac{\partial u_{\mathrm{i}}^{(2)}}{\partial\xi} + u_{\mathrm{i}}^{(1)}\frac{\partial u_{\mathrm{i}}^{(1)}}{\partial\xi}\\ &= -\frac{\partial\Phi^{(2)}}{\partial\xi} + \eta_{\mathrm{i}0}\frac{\partial^2 u_{\mathrm{i}}^{(1)}}{\partial\xi^2} - 3\sigma_{\mathrm{i}}n_{\mathrm{i}}^{(1)}\frac{\partial n_{\mathrm{i}}^{(1)}}{\partial\xi} - 3\sigma_{\mathrm{i}}\frac{\partial n_{\mathrm{i}}^{(2)}}{\partial\xi}\end{aligned} \tag{7.3.11}$$

and

$$\delta\frac{\partial^2\Phi^{(1)}}{\partial\xi^2} = \frac{1}{2}[\Phi^{(1)}]^2 + \Phi^{(2)} - n_{\mathrm{i}}^{(2)}\delta \tag{7.3.12}$$

where we have assumed $\eta_{\mathrm{i}} = \epsilon^{1/2}\eta_{\mathrm{i}0}$. Eliminating $n_{\mathrm{i}}^{(2)}$, $u_{\mathrm{i}}^{(2)}$ and $\Phi^{(2)}$ from (7.3.10)–(7.3.12) we readily obtain the desired KdV–Burgers equation

$$A_{\mathrm{i}}^{-1}\frac{\partial\Phi^{(1)}}{\partial\tau} + \Phi^{(1)}\frac{\partial\Phi^{(1)}}{\partial\xi} + \beta_{\mathrm{i}}\frac{\partial^3\Phi^{(1)}}{\partial\xi^3} - \mu_{\mathrm{i}}\frac{\partial^2\Phi^{(1)}}{\partial\xi^2} = 0 \tag{7.3.13}$$

where $A_{\mathrm{i}} = a_{\mathrm{i}}/2v_0$, $\beta_{\mathrm{i}} = \delta^2/a_{\mathrm{i}}$, $\mu_{\mathrm{i}} = v_0\eta_{\mathrm{i}0}/a_{\mathrm{i}}$ and $a_{\mathrm{i}} = (3\delta - \delta^2 + 12\sigma_{\mathrm{i}})/\delta$. As $v_0 > 0$ and $\eta_{\mathrm{i}0} > 0$, the sign of the coefficients A_{i}, β_{i} and μ_{i} are determined by the sign of a_{i}.

7.3.3 Solutions of the KdV–Burgers equation

We now discuss possible stationary solutions of the KdV–Burgers equation (7.3.5) or (7.3.13) which can be written in the form

$$A^{-1}\frac{\partial y}{\partial\tau} + y\frac{\partial y}{\partial\xi} + \beta\frac{\partial^3 y}{\partial\xi^3} = \mu\frac{\partial^2 y}{\partial\xi^2} \tag{7.3.14}$$

where $y = \Phi^{(1)}$ for the DIA shock waves, while $y = \phi^{(1)}$ for the DA shock waves. We first transform the space variables ξ to $\zeta = \xi - U_0\tau$, where U_0 is the normalized velocity of the shock waves and find a third-order ordinary differential equation for $y(\zeta)$. The latter can be integrated once, yielding

$$\beta\frac{\delta^2 y}{\partial\zeta^2} - \mu\frac{\partial y}{\partial\zeta} + \frac{1}{2}y^2 - \frac{U_0}{A}y = 0 \tag{7.3.15}$$

where we have imposed the appropriate boundary conditions, namely $y \to 0$, $\mathrm{d}y/\mathrm{d}\zeta \to 0$, $\mathrm{d}^2y/\mathrm{d}\zeta^2 \to 0$ at $\zeta \to \infty$. We can now easily show (Karpman 1975, Hasegawa 1975) that equation (7.3.15) describes a shock wave whose velocity (in the reference frame under consideration) U_0 is related to the extreme values $y(-\infty) - y(\infty) = Y$ by $U_0/A = Y/2$. Thus, in the rest frame the normalized velocity of the shock waves is $(1+AY/2)$. The nature of the structure of the shock waves depends on the relation between the dispersive and dissipative parameters β and μ.

We first consider a situation where the dissipative term is dominant over the dispersive term. In this case, we can express equation (7.3.15) as

$$\left(y - \frac{U_0}{A}\right)\frac{\mathrm{d}y}{\mathrm{d}\zeta} = \mu\frac{\mathrm{d}^2 y}{\mathrm{d}\zeta^2}. \tag{7.3.16}$$

Equation (7.3.16) can be easily integrated, using the condition that y is bounded as $\zeta \to \pm\infty$, to obtain (Karpman 1975)

$$y = \frac{U_0}{A}\left[1 - \tanh\left(\frac{U_0}{2A\mu}(\xi - U_0\tau)\right)\right]. \tag{7.3.17}$$

Equation (7.3.17) represents a monotonic shock solution with the shock speed, the shock height and the shock thickness given by U_0, U_0/A and $A\mu/U_0$, respectively. The shock solution appears because of the dissipative term, which is proportional to the viscosity coefficient.

We now discuss the effects of the dispersive term on the shock solution of equation (7.3.15). When μ is extremely small, the shock wave will have an oscillatory profile in which the first few oscillations at the wave front will be close to solitons (Karpman 1975) moving with velocity U_0. If μ is increased and it is larger than a certain critical value μ_c, the shock wave will have a monotonic behaviour. To determine the values of the dissipation coefficient μ corresponding to monotonic or oscillating shock profiles, we investigate the asymptotic behaviour of the solutions of equation (7.3.15) for $\zeta \to -\infty$. We first substitute $y(\zeta) = y_0 + y_1(\zeta)$, where $y_1 \ll y_0$, into equation (7.3.15) and then linearize it with respect to y_1 in order to obtain

$$\beta\frac{\delta^2 y_1}{\partial\zeta^2} - \mu\frac{\partial y_1}{\partial\zeta} + \frac{U_0}{A}y_1 = 0. \tag{7.3.18}$$

The solutions of equation (7.3.18) are proportional to $\exp(p_s x)$, where p_s is given by

$$p_s = \frac{\mu}{2\beta} \pm \left(\frac{\mu^2}{4\beta^2} - \frac{U_0}{A\beta}\right)^{1/2}. \tag{7.3.19}$$

It turns out that the shock wave has a monotonic profile for $\mu > \mu_c$ and an oscillatory profile for $\mu < \mu_c$, where $\mu_c = (4\beta U_0/A)^{1/2}$. Thus, for $\mu < \mu_c$, the stationary solution of equation (7.3.14) is (Karpman 1975)

$$y = y_0 + C \exp\left(\frac{\zeta'\mu}{2\beta}\right) \cos\left(\zeta'\sqrt{\frac{U_0}{A\beta}}\right) \tag{7.3.20}$$

where $\zeta' = \zeta - U_0\tau$ and C is a constant.

7.3.4 Experimental observations of DIA shock waves

Recently the DIA shock waves were experimentally excited in a dusty double plasma (DP) device by Nakamura *et al* (1999). Here we briefly illustrate the formation of these experimentally excited DIA shock waves by summarizing the experimental work of Nakamura *et al* (1999). The inner diameter of the dusty DP device is 40 cm and its length is 90 cm. The device is separated into a source and a target section by a fine mesh grid which is kept electrically floating. The chamber is evacuated down to 5×10^{-7} Torr with a turbo-molecular pump. The argon gas is bled into the chamber at a partial pressure of about 5×10^{-4} Torr. A dust dispersing set-up fitted at the target section consisted of a dust reservoir coupled to an ultrasonic vibrator. The dust reservoir consists of a fine stainless steel mesh (118 lines per cm) of 10 cm (width) $\times$16 cm (axial length) area at the bottom end and is placed horizontally closer to the anode wall. An ultrasonic vibrator is tuned at 27 kHz to vibrate the dust reservoir by using a signal generator and a power amplifier. Glass powder of average diameter 8.8 μm is used. The dust number density is easily controlled by adjusting the power of the signal applied to the vibrator and is measured from the extinction intensity of the laser light which passes through the dust column and is collected by a photodiode array. A maximum dust density of the order of 10^5 cm^{-3} is obtained in this set-up. The plasma parameters measured by a plane Langmuir probe of 6 mm diameter and a retarding potential analyser are as follows: $n_e = 10^8$–10^9 cm^{-3}, $T_e = (1$–$1.5) \times 10^4$ K, $T_i \simeq 0.1T_e$, $Z_d \simeq 10^5$ for $n_d < 10^3$ cm^{-3} and $Z_d \simeq 10^2$ for $n_d < 10^5$ cm^{-3}.

The shock waves are excited in the plasma by applying a ramp signal with an amplitude of 2 V and a rise time of approximate 10 μs. The Langmuir probe is biased above the plasma potential in order to detect the signal as fluctuations in the electron saturation currents. The oscillatory shock waves are first excited in the plasma without the dust and the dust density is then increased at smaller steps keeping the probe fixed at 12 cm measured from the grid. The corresponding time

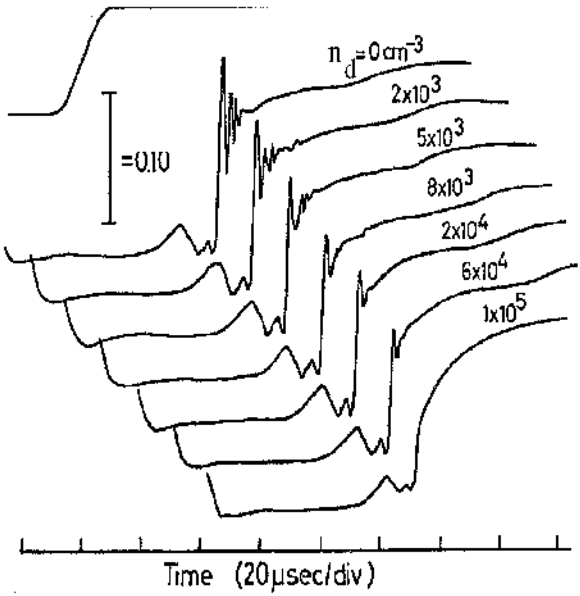

Figure 7.8. The variation of the plasma number density with time at a fixed probe position (12 cm) showing the transition of an oscillatory shock to a monotonic shock when the dust particle number density is increased (after Nakamura *et al* 1999).

normalized by the ion plasma period (ω_{pi}^{-1}) for the signal at 12 cm is about 150. A number of these signals are shown in figure 7.8.

It reveals that the oscillatory wave structure behind the shock becomes less in number with increasing the dust particle number density and finally completely disappears at a sufficiently high dust particle number density leaving only the laminar shock front. The shock speed also increases with increasing the dust particle number density. It is also noted that the particle density behind the shock remains constant, although the amplitude of the shock front (steepened part) seems to decrease when the dust particle number density is increased.

The effect of the dust particle number density on the ion acoustic compressional pulses has also been experimentally studied by Luo *et al* (1999, 2000) who observed a steepening of the ion-acoustic pulses as they propagated through a dusty plasma if the percentage of the negative charge in the plasma on the dust grains was about 75% or more.

7.4 Envelope Solitons

Envelope solitons in plasmas are formed due to the action of the ponderomotive force of high-frequency waves on plasma slow motions. Here we discuss the formation of a Langmuir wave envelope soliton in an unmagnetized dusty plasma without considering the dust charge fluctuation effect.

The nonlinear coupling between a large-amplitude Langmuir pump with non-resonant DA perturbations gives rise to an envelope of Langmuir waves which is governed by

$$\frac{\partial n_{\mathrm{el}}}{\partial t} + \nabla \cdot [(n_{\mathrm{e0}} + n_{\mathrm{e}s})\boldsymbol{v}_{\mathrm{l}}] = 0 \tag{7.4.1}$$

$$\frac{\partial \boldsymbol{v}_{\mathrm{l}}}{\partial t} = -\frac{e}{m_{\mathrm{e}}}\boldsymbol{E}_{\mathrm{l}} - \frac{3V_{\mathrm{Te}}^2}{n_{\mathrm{e0}}}\nabla n_{\mathrm{el}} \tag{7.4.2}$$

and

$$\nabla \cdot \boldsymbol{E}_{\mathrm{l}} = -4\pi e n_{\mathrm{el}} \tag{7.4.3}$$

where n_{el} and $n_{\mathrm{e}s}$ are small electron number density perturbations associated with Langmuir and DA waves, respectively and $\boldsymbol{E}_{\mathrm{l}}$ is the Langmuir wave electric field. Combining equations (7.4.1)–(7.4.3) we obtain the Langmuir wave equation in the presence of the DA perturbations

$$\frac{\partial^2 \boldsymbol{E}_{\mathrm{l}}}{\partial t^2} - 3V_{\mathrm{Te}}^2\nabla^2\boldsymbol{E}_{\mathrm{l}} + \omega_{\mathrm{pe}}^2\left(1 + \frac{n_{\mathrm{e}s}}{n_{\mathrm{e0}}}\right)\boldsymbol{E}_{\mathrm{l}} = 0. \tag{7.4.4}$$

We assume that the Langmuir wave electric field varies on the spatio-temporal scales of the DA perturbations. Thus, letting $\boldsymbol{E}_{\mathrm{l}} = \boldsymbol{E}(\boldsymbol{r}, \tau)\exp(-\mathrm{i}\omega_0 t + \mathrm{i}\boldsymbol{k}_0 \cdot \boldsymbol{r})$, where $\omega_0 = (\omega_{\mathrm{pe}}^2 + 3k_0^2V_{\mathrm{Te}}^2)^{1/2} \sim \omega_{\mathrm{pe}}$, in equation (7.4.4) we obtain the envelope equation

$$2\mathrm{i}\omega_0\left(\frac{\partial}{\partial \tau} + \boldsymbol{v}_{\mathrm{g0}} \cdot \nabla\right)\boldsymbol{E} + 3V_{\mathrm{Te}}^2\nabla^2\boldsymbol{E} - \omega_{\mathrm{pe}}^2\frac{n_{\mathrm{e}s}}{n_{\mathrm{e0}}}\boldsymbol{E} = 0 \tag{7.4.5}$$

where in the spirit of the slowly varying envelope approximation we have $\partial\boldsymbol{E}/\partial\tau \ll \omega_0$. The Langmuir wave group velocity is denoted by $\boldsymbol{v}_{\mathrm{g0}} = 3V_{\mathrm{Te}}^2\boldsymbol{k}_0/\omega_{\mathrm{pe}}$.

The electron number density perturbation $n_{\mathrm{e}s}$ associated with the DA perturbations is obtained by averaging the inertialess electron momentum equation over the Langmuir wave period ($= 2\pi/\omega_0$). The result is

$$\frac{m_{\mathrm{e}}}{4}\nabla|\boldsymbol{v}_{\mathrm{l}}|^2 \cong \frac{e^2}{4m_{\mathrm{e}}\omega_{\mathrm{pe}}^2}\nabla|\boldsymbol{E}|^2 = e\nabla\phi_s - \frac{k_{\mathrm{B}}T_{\mathrm{e}}}{n_{\mathrm{e0}}}\nabla n_{\mathrm{e}s} \tag{7.4.6}$$

where the left-hand side represents the Langmuir wave ponderomotive force. The latter is transmitted to the ions and dust grains through the DA wave potential ϕ_s. The ion and dust number density perturbations are determined from

$$0 = -e\nabla\phi_s - \frac{k_{\mathrm{B}}T_{\mathrm{i}}}{n_{\mathrm{i0}}}\nabla n_{\mathrm{i}s} \tag{7.4.7}$$

and

$$\frac{\partial^2 n_{\mathrm{d}s}}{\partial \tau^2} - \frac{q_{\mathrm{d0}} n_{\mathrm{d0}}}{m_{\mathrm{d}}} \nabla^2 \phi_s = 0. \tag{7.4.8}$$

For long-wavelength (in comparison with λ_{D}) DA perturbations, we can use the quasi-neutrality condition ($en_{\mathrm{i}s} = en_{\mathrm{e}s} - q_{\mathrm{d0}} n_{\mathrm{d}s}$) and equations (7.4.7) and (7.4.8) to obtain

$$\frac{\partial^2 n_{\mathrm{e}s}}{\partial \tau^2} + \frac{n_{\mathrm{i0}} e}{k_{\mathrm{B}} T_{\mathrm{i}}} \left(\frac{\partial^2}{\partial \tau^2} - C_{\mathrm{Di}}^2 \nabla^2 \right) \phi_s = 0. \tag{7.4.9}$$

Substituting for ϕ_s from equation (7.4.6) into equation (7.4.9) we have the driven DA wave equation

$$\left(\frac{\partial^2}{\partial \tau^2} - C_{\mathrm{DA}}^2 \nabla^2 \right) \frac{n_{\mathrm{e}s}}{n_{\mathrm{e0}}} = -\frac{1}{1+\delta_n} \left(\frac{\partial^2}{\partial \tau^2} - C_{\mathrm{Di}}^2 \nabla^2 \right) \frac{|\boldsymbol{E}|^2}{16\pi n_{\mathrm{e0}} k_{\mathrm{B}} T_{\mathrm{e}}} \tag{7.4.10}$$

where $C_{\mathrm{DA}}^2 = C_{\mathrm{Di}}^2/(1+\delta_n)$ and $\delta_n = n_{\mathrm{e0}} T_{\mathrm{i}}/n_{\mathrm{i0}} T_{\mathrm{e}}$. For $\delta_n \ll 1$ equation (7.4.10) gives

$$\frac{n_{\mathrm{e}s}}{n_{\mathrm{e0}}} = -\frac{|\boldsymbol{E}|^2}{16\pi n_{\mathrm{e0}} k_{\mathrm{B}} T_{\mathrm{e}}} \tag{7.4.11}$$

which shows the formation of an electron density cavity by the ponderomotive force of the Langmuir waves in a collisionless dusty plasma. Inserting equation (7.4.11) into equation (7.4.5) we obtain the cubic nonlinear Schrödinger equation

$$2\mathrm{i}\omega_0 \left(\frac{\partial}{\partial \tau} + \boldsymbol{v}_{\mathrm{g0}} \cdot \nabla \right) \boldsymbol{E} + 3V_{\mathrm{Te}}^2 \nabla^2 \boldsymbol{E} + \omega_{\mathrm{pe}}^2 |\boldsymbol{E}|^2 \boldsymbol{E} = 0 \tag{7.4.12}$$

where the Langmuir wave electric field is normalized by $(16\pi n_{\mathrm{e0}} k_{\mathrm{B}} T_{\mathrm{e}})^{1/2}$. Equation (7.4.12) exhibits collapse of Langmuir waves in a spherical symmetric situation (Zakharov 1972). However, in one-space dimension, the stationary solution of equation (7.4.12) can be obtained by introducing $\boldsymbol{E} = \hat{z}\mathcal{E}(z)\exp[\mathrm{i}\vartheta_1(\tau) + \mathrm{i}\vartheta_2(z)]$, where $\vartheta_1(\tau)$ and $\vartheta_2(z)$ are some constants. Hence, in the steady-state, equation (7.4.12) can be written as

$$3\lambda_{\mathrm{De}}^2 \frac{\partial^2 \mathcal{E}}{\partial z^2} - \lambda_1 \mathcal{E} + |\mathcal{E}|^2 \mathcal{E} = 0 \tag{7.4.13}$$

where $\lambda_1 = (2/\omega_{\mathrm{pe}})(\partial \vartheta_1/\partial \tau) + 24 k_{0z}^2 \lambda_{\mathrm{De}}^2$ is a nonlinear frequency shift and $\vartheta_2(z) = 2k_{0z} z$. A possible localized solution of equation (7.4.13) is

$$\mathcal{E} = \mathcal{E}_{\mathrm{m}} \operatorname{sech}\left(\frac{z}{L} \right) \tag{7.4.14}$$

where $\mathcal{E}_{\mathrm{m}}$ is the maximum normalized amplitude of the envelope soliton and $\lambda_1 = \mathcal{E}_{\mathrm{m}}^2$. The width of the envelope soliton is

$$L = \lambda_{\mathrm{De}} \left(\frac{6}{\mathcal{E}_{\mathrm{m}}} \right)^{1/2}. \tag{7.4.15}$$

The corresponding electron density depletion is

$$\frac{n_{es}}{n_{e0}} = -|\mathcal{E}_m|^2 \operatorname{sech}^2\left(\frac{z}{L}\right). \tag{7.4.16}$$

Thus, a Langmuir envelope soliton consists of a bell shaped electric field envelope that is trapped in a self-created density cavity in a dusty plasma.

7.5 Vortices

Coherent vortices appear in two-dimensional fluids and magnetized plasmas. In a simplest possible scenario, the vortex dynamics is governed by the NS equation which admits a monopolar vortex (Hasegawa 1985). However, in a magnetized dusty plasma we have the possibility of vortices comprising a dipolar (Bharuthram and Shukla 1992b), a tripolar, and a chain (Vranješ *et al* 2001). Here the vortices are associated with nonlinear dispersive waves that possess, at least, a two-dimensional character. When the velocity of the fluid (or plasma particles) motion associated with the dispersive waves become locally larger than the wave phase velocity because of the nonlinear effects, one encounters a curving of the wave front which lead to the formation of a two-dimensional travelling vortex structure. In this section, we discuss the properties of vortices in a non-uniform dusty magnetoplasma.

7.5.1 Electrostatic vortices

We have shown in chapter 4 the existence of a low-frequency (in comparison with the ion gyrofrequency) Shukla–Varma (SV) mode (Shukla and Varma 1993) that involves two-dimensional electron and ion motions in a non-uniform dusty magnetoplasma containing stationary dust grains. We now discuss possible vortex solutions involving nonlinear SV modes. In the presence of low-frequency (namely $\omega_{cd}, \omega_{\mathrm{pd}} \ll |\mathrm{d}/\mathrm{d}t| \ll \omega_{\mathrm{ci}}$) electrostatic waves, the electron and ion velocities in our collisionless cold dusty plasma are, respectively

$$\boldsymbol{v}_{\mathrm{e}} \approx \frac{c}{B_0}\hat{z} \times \nabla\phi \tag{7.5.1}$$

and

$$\boldsymbol{v}_{\mathrm{i}} \approx \frac{c}{B_0}\hat{z} \times \nabla\phi - \frac{c}{B_0\omega_{\mathrm{ci}}}\left(\frac{\partial}{\partial t} + \frac{c}{B_0}\hat{z} \times \nabla\phi \cdot \nabla\right)\nabla_{\perp}\phi \tag{7.5.2}$$

where the dynamics of the electrons and ions parallel to $\hat{z}B_0$ has been neglected. The last term in the right-hand side of equation (7.5.2) represents the nonlinear ion polarization drift (Hasegawa and Mima 1978). It comes from the advection term $(\boldsymbol{v}_{\mathrm{i}} \cdot \nabla \boldsymbol{v}_{\mathrm{i}})$ in the ion momentum equation. Substituting equations (7.5.1) and (7.5.2) into the electron and ion continuity equations, letting $n_j = n_{j0} + n_{j1}$, where $n_{j1} \ll n_{j0}$, and subtracting the ion continuity equation from that of the electrons, we obtain after using $n_{e1} = n_{i1}$

$$\left(\frac{\partial}{\partial t} + \frac{c}{B_0}\hat{z} \times \nabla\phi \cdot \nabla\right) \nabla_\perp^2 \phi + u_{sv}\frac{\partial \phi}{\partial y} = 0 \tag{7.5.3}$$

which governs the nonlinear dynamics of the SV modes. Here we have denoted $u_{sv} = \omega_{ci} K_{qn}$. In a uniform magnetoplasma, equation (7.5.3) takes the form

$$\left(\frac{\partial}{\partial t} + \frac{c}{B_0}\hat{z} \times \nabla\phi \cdot \nabla\right) \nabla_\perp^2 \phi = 0 \tag{7.5.4}$$

which is the NS equation governing the dynamics of two-dimensional convective cells in a collisionless plasma. Equation (7.5.4) admits dual cascading and a monopolar vortex (Hasegawa 1985). The presence of the inhomogeneous term (the third term) in the left-hand side of equation (7.5.3) provides the possibility of a stationary dipolar vortex structure, as discussed below.

We seek a solution of the generalized NS equation (7.5.3) in the stationary frame $\xi = y - ut$, where u is the translational speed of the vortex. Thus, equation (7.5.3) takes the form

$$u\frac{\partial}{\partial \xi}\nabla_\perp^2 \phi - u_{sv}\frac{\partial \phi}{\partial \xi} - \frac{c}{B_0}J(\phi, \nabla_\perp^2 \phi) = 0 \tag{7.5.5}$$

where the Jacobian is denoted by

$$J(\phi, \nabla_\perp^2 \phi) = \left(\frac{\partial \phi}{\partial x}\frac{\partial}{\partial \xi} - \frac{\partial \phi}{\partial \xi}\frac{\partial}{\partial x}\right) \nabla_\perp^2 \phi \tag{7.5.6}$$

with $\nabla_\perp^2 \phi = (\partial^2 \phi/\partial x^2) + (\partial^2 \phi/\partial \xi^2)$. Equation (7.5.5) is satisfied by the Ansatz

$$\nabla_\perp^2 \phi = C_1 \phi + C_2 x \tag{7.5.7}$$

provided that the constants C_1 and C_2 are related by $uC_1 - u_{sv} - (c/B_0)C_2 = 0$. The double vortex solution of equation (7.5.7) can be constructed following standard methods (Larichev and Reznik 1976). Accordingly, we divide the (r, θ) plane into outer ($r > R_v$) and inner ($r < R_v$) regions, where $r = (x^2 + \xi^2)^{1/2}$ and $\theta = \arctan(\xi/x)$ are the polar coordinates and R_v corresponds to the vortex radius. For localized solutions we must have $C_2 = 0$ in the outer region so that $C_1^o = u_{sv}/u \equiv k_0^2$. The outer region solution is

$$\phi^o(r, \theta) = \phi_0 K_1(k_0 r) \cos\theta \tag{7.5.8}$$

where ϕ_0 is a constant and K_1 is the modified Bessel function of the first kind. Thus a well-behaved outer solution is possible for $k_0^2 > 0$, which is satisfied for $u_{sv} > 0$. The inner region solution is

$$\phi^i = \left[\phi_i J_1(k_i r) + \frac{C_v}{k_i^2} r\right] \cos\theta \tag{7.5.9}$$

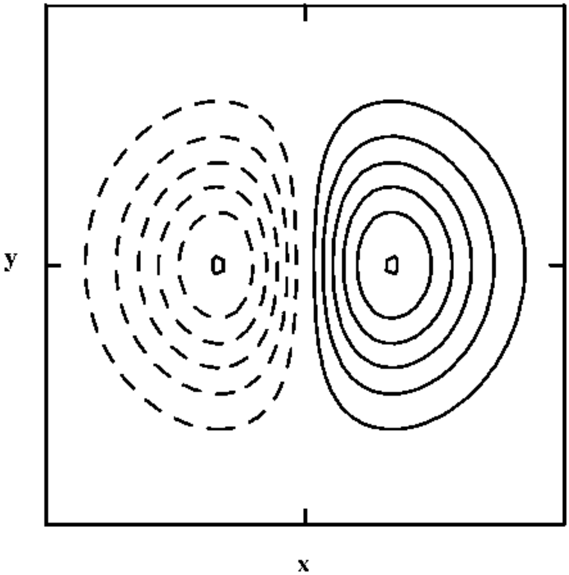

Figure 7.9. A typical dipolar vortex (courtesy of Dr J Vranješ, Institute of Physics, Belgrade).

where $\phi_{\rm i}$, $k_{\rm i} = -C_1^{\rm i}$ and $C_{\rm v} = uB_0(k_0^2 + k_{\rm i}^2)/c$ are constants and J_1 is the Bessel function of the first order. The superscripts o and i stand for the quantities in the outer and inner regions, respectively. The constants ϕ_0 and $\phi_{\rm i}$ are determined from the continuity of ϕ and $\nabla_\perp^2 \phi$ at the vortex interface $r = R_{\rm v}$. One finds that

$$\phi_0 = \frac{R_{\rm v} C_{\rm v}}{(k_0^2 + k_{\rm i}^2) K_1(k_0 R_{\rm v})} \tag{7.5.10a}$$

and

$$\phi_{\rm i} = -\frac{k_0^2 R_{\rm v} C_{\rm v}}{k_{\rm i}^2 (k_0^2 + k_{\rm i}^2) J_1(k_{\rm i} R_{\rm v})}. \tag{7.5.10b}$$

For a given value of $k_0 > 0$, the value of $k_{\rm i}$ is determined from

$$\frac{J_2(k_{\rm i} R_{\rm v})}{J_1(k_{\rm i} R_{\rm v})} = -\frac{k_{\rm i} K_2(k_0 R_{\rm v})}{k_0 K_1(k_0 R_{\rm v})} \tag{7.5.11}$$

which comes from the matching of $\nabla_\perp \phi$ at $r = R_{\rm v}$. Here J_2 and K_2 are the Bessel and modified Bessel functions of the second order. A typical double vortex profile is shown in figure 7.9

7.5.2 Electromagnetic vortices

We now discuss electromagnetic vortices (Pokhotelov *et al* 1999) that involve nonlinear low-frequency (in comparison with the ion gyrofrequency), long-wavelength (in comparison with the ion gyroradius) electromagnetic waves in a non-uniform dusty magnetoplasma containing a density inhomogeneity along the x-axis. The dust component is considered to be immobile. In the electromagnetic fields, the electron and ion fluid velocities in a warm dusty plasma are

$$\boldsymbol{v}_{\mathrm{e}} \approx \frac{c}{B_0}\hat{z} \times \nabla\phi - \frac{ck_{\mathrm{B}}T_{\mathrm{e}}}{eB_0 n_{\mathrm{e}}}\hat{z} \times \boldsymbol{\nabla} n_{\mathrm{e}} + v_{\mathrm{e}z}\left(\hat{z} + \frac{\nabla A_z \times \hat{z}}{B_0}\right) \tag{7.5.12}$$

and

$$\boldsymbol{v}_{\mathrm{i}} \approx \frac{c}{B_0}\hat{z} \times \nabla\phi + \frac{ck_{\mathrm{B}}T_{\mathrm{i}}}{eB_0 n_{\mathrm{i}}}\hat{z} \times \boldsymbol{\nabla} n_{\mathrm{i}} - \frac{c}{B_0\omega_{\mathrm{ci}}}\left(\frac{\partial}{\partial t} + \boldsymbol{v}_{\mathrm{i}} \cdot \nabla\right)\nabla_\perp\phi \tag{7.5.13}$$

where the parallel component of the electron fluid velocity is given by (cf equation (4.7.18))

$$v_{\mathrm{e}z} \approx \frac{c}{4\pi n_{\mathrm{e}} e}\boldsymbol{\nabla}_\perp^2 A_z \tag{7.5.14}$$

where we have ignored the ion motion parallel to $\hat{z}$ as well as neglected the compressional magnetic field perturbation. Thus, the DIA and magnetosonic waves are decoupled in our low-β ($\beta \ll 1$) dusty plasma system.

Substituting equation (7.5.12) into the electron continuity equation, letting $n_j = n_{j0}(x) + n_{j1}$, where $n_{j1} \ll n_{j0}$ and using equation (7.5.14) we obtain

$$\frac{\mathrm{d}n_{\mathrm{e}1}}{\mathrm{d}t} - \frac{c}{B_0}\frac{\partial n_{\mathrm{e}0}}{\partial x}\frac{\partial\phi}{\partial y} + \frac{c}{4\pi e}\frac{\mathrm{d}\boldsymbol{\nabla}_\perp^2 A_z}{\mathrm{d}z} = 0, \tag{7.5.15}$$

where $\mathrm{d}/\mathrm{d}t = (\partial/\partial t) + (c/B_0)\hat{z} \times \boldsymbol{\nabla}\phi \cdot \boldsymbol{\nabla}$ and $\mathrm{d}/\mathrm{d}z = (\partial/\partial z) + B_0^{-1}\boldsymbol{\nabla} A_z \times \hat{z} \cdot \boldsymbol{\nabla}$. We have assumed $\boldsymbol{v}_{EB} \cdot \nabla \gg v_{\mathrm{e}z}\partial/\partial z$, which implies that $(\omega_{\mathrm{pe}}^2/\omega_{ce})|\hat{z} \times \boldsymbol{\nabla}\phi \cdot \boldsymbol{\nabla}| \gg c\partial_z \boldsymbol{\nabla}_\perp^2 A_z$. On the other hand, substitution of the ion fluid velocity, given by equation (7.5.13) into the ion continuity equation yields

$$\begin{aligned} \frac{\mathrm{d}n_{i1}}{\mathrm{d}t} - \frac{c}{B_0}\frac{\partial n_{\mathrm{i}0}}{\partial x}\frac{\partial\phi}{\partial y} - \frac{cn_{\mathrm{i}0}}{B_0\omega_{\mathrm{ci}}}\left(\frac{\mathrm{d}}{\mathrm{d}t} + u_{\mathrm{i}*}\frac{\partial}{\partial y}\right)\boldsymbol{\nabla}_\perp^2\phi& \\ - \frac{c^2 k_{\mathrm{B}}T_{\mathrm{i}}}{eB_0^2\omega_{\mathrm{ci}}}\boldsymbol{\nabla}_\perp \cdot [(\hat{z} \times \boldsymbol{\nabla} n_{i1}) \cdot \boldsymbol{\nabla}\boldsymbol{\nabla}_\perp\phi] = 0& \end{aligned} \tag{7.5.16}$$

where $u_{\mathrm{i}*} = (ck_{\mathrm{B}}T_{\mathrm{i}}/eB_0 n_{\mathrm{i}0})\partial n_{\mathrm{i}0}/\partial x$ is the unperturbed ion diamagnetic drift speed. Subtracting equation (7.5.16) from equation (7.5.15) and assuming $n_{i1} = n_{\mathrm{e}1}$, we obtain the modified ion vorticity equation

$$\begin{aligned} \left(\frac{\mathrm{d}}{\mathrm{d}t} + u_{\mathrm{i}*}\partial_y\right)\boldsymbol{\nabla}_\perp^2\phi + \frac{V_{\mathrm{A}}^2}{c}\frac{\mathrm{d}\boldsymbol{\nabla}_\perp^2 A_z}{\mathrm{d}z} + u_{\mathrm{sv}}\frac{\partial\phi}{\partial y}& \\ + \frac{ck_{\mathrm{B}}T_{\mathrm{i}}}{eB_0 n_{\mathrm{i}0}}\boldsymbol{\nabla}_\perp \cdot [(\hat{z} \times \boldsymbol{\nabla} n_{\mathrm{e}1}) \cdot \boldsymbol{\nabla}\boldsymbol{\nabla}_\perp\phi] = 0.& \end{aligned} \tag{7.5.17}$$

By using equations (7.5.12) and (7.5.14), the parallel component of the electron momentum equation can be written as

$$\left(\frac{\partial}{\partial t} + u_{e*}\frac{\partial}{\partial y}\right) A_z - \lambda_e^2 \frac{d\nabla_\perp^2 A_z}{dt} + c\frac{d\phi}{dz} - \frac{ck_B T_e}{en_{e0}}\frac{dn_{e1}}{dz} = 0 \tag{7.5.18}$$

where $u_{e*} = -(ck_B T_e/eB_0 n_{e0})\partial n_{e0}/\partial x$ is the unperturbed electron diamagnetic drift speed.

Let us now seek stationary solutions (Pokhotelov *et al* 1999) of the nonlinear equations (7.5.15), (7.5.17) and (7.5.18) by assuming that all the field variables depend on x and $\eta = y + \alpha z - ut$, where α represents the angle between the wavefront normal and the (x, y) plane. Two cases are considered.

7.5.2.1 Warm plasma

In the stationary η-frame, equation (7.5.18) for $\lambda_e^2|\nabla_\perp^2| \ll 1$ can be written as

$$\hat{D}_A\left(\phi - \frac{k_B T_e}{en_{e0}} n_{e1} - \frac{u - u_{e*}}{\alpha c} A_z\right) = 0 \tag{7.5.19}$$

where $\hat{D}_A = (\partial/\partial\eta) + (1/\alpha B_0)[(\partial A_z/\partial\eta)(\partial/\partial x) - (\partial A_z/\partial x)(\partial/\partial\eta)]$. A solution of equation (7.5.19) is (Liu and Horton 1986)

$$n_{e1} = \frac{n_{e0}e}{k_B T_e}\phi - \frac{(u - u_{e*})n_{e0}e}{\alpha c k_B T_e} A_z. \tag{7.5.20}$$

Writing equation (7.5.15) in the stationary frame and making use of equation (7.5.20) it can be put in the form

$$\hat{D}_A\left[\lambda_{De}^2\nabla_\perp^2 A_z + \frac{u(u - u_{e*})}{\alpha^2 c^2} A_z - \frac{u - u_{e*}}{\alpha c}\phi\right] = 0. \tag{7.5.21}$$

A solution of equation (7.5.21) is

$$\lambda_{De}^2\nabla_\perp^2 A_z + \frac{u(u - u_{e*})}{\alpha^2 c^2} A_z - \frac{u - u_{e*}}{\alpha c}\phi = 0. \tag{7.5.22}$$

The modified ion vorticity equation (7.5.17) for cold ions can be expressed as

$$\hat{D}_\phi(\nabla_\perp^2\phi - k_0^2\phi) - \frac{V_A^2\alpha}{cu}\hat{D}_A\nabla_\perp^2 A_z = 0 \tag{7.5.23}$$

where $\hat{D}_\phi = (\partial/\partial\eta) - (c/uB_0)[(\partial\phi/\partial x)(\partial/\partial\eta) - (\partial\phi/\partial\eta)(\partial/\partial x)]$. Combining equations (7.5.22) and (7.5.23) we obtain

$$\hat{D}_\phi\left(\nabla_\perp^2\phi + \frac{p}{\rho_s^2}\phi + \frac{u - u_{e*}}{\alpha c\rho_s^2} A_z\right) = 0 \tag{7.5.24}$$

where $p = (C_S/u)[K_d\rho_s + (u_{e*} - u)/C_S]$. A typical solution of equation (7.5.24) is

$$\nabla_\perp^2\phi + \frac{p}{\rho_s^2}\phi + \frac{u-u_{e*}}{\alpha c\rho_s^2}A_z = C_3\left(\phi - \frac{uB_0}{c}x\right) \qquad (7.5.25)$$

where C_3 is an integration constant. Eliminating A_z from equations (7.5.22) and (7.5.25), we obtain a fourth-order inhomogeneous differential equation (Pokhotelov *et al* 1999)

$$\nabla^4\phi + F_1\nabla_\perp^2\phi + F_2\phi + C_3\frac{u^2(u-u_{e*})B_0}{\alpha^2c^3\lambda_{De}^2}x = 0 \qquad (7.5.26)$$

where $F_1 = (p/\rho_s^2) - C_3 + u(u - u_{e*})/\alpha^2c^2\lambda_{De}^2$ and $F_2 = [(u - u_{e*})^2/\alpha^2c^2\lambda_{De}^2\rho_s^2] + (p - C_3\rho_s^2)u(u - u_{e*})/\alpha^2c^2\lambda_{De}^2\rho_s^2$. We note that in the absence of charged dust we have $u_{sv} = 0$ and $F_2 = 0$ in the outer region when $C_3 = 0$. In such a situation, the outer region solution of equation (7.5.26) would have a a long tail (decaying as $1/r$) for $(u - u_{e*})(\alpha^2V_A^2 - u^2) > 0$ (Liu and Horton 1986). On the other hand, inclusion of a small fraction of dust grains would make F_2 finite in the outer region. Here we have the possibility of well-behaved solutions. In fact, equation (7.5.26) admits spatially bounded dipolar vortex solutions. In the outer region ($r > R_v$), we set $C_3 = 0$ and obtain the solution of equation (7.5.26) as (Liu and Horton 1986)

$$\phi^o = [Q_1K_1(s_1r) + Q_2K_1(s_2r)]\cos\theta \qquad (7.5.27)$$

where Q_1 and Q_2 are constants and $s_{1,2}^2 = -[-\alpha_1 \pm (\alpha_1^2 - 4\alpha_2)^{1/2}/2]$ for $\alpha_1 < 0$ and $\alpha_1^2 > 4\alpha_2 > 0$. Here, $\alpha_1 = (p/\rho_s^2) + u(u - u_{e*})/\alpha^2c^2\lambda_{De}^2$ and $\alpha_2 = [(u - u_{e*})^2 + u(u - u_{e*})p]/\alpha^2c^2\lambda_{De}^2\rho_s^2$. In the inner region ($r < R_v$), the solution reads

$$\phi^i = \left[Q_3J_1(s_3r) + Q_4I_1(s_4r) - \frac{C_3^i}{\lambda_{De}^2}\frac{u^2(u-u_{e*})B_0}{\alpha^2c^3F_2^i}r\right]\cos\theta \qquad (7.5.28)$$

where Q_3, Q_4, C_3^i and F_2^i are constants. We have defined $s_{3,4} = [(F_1^{i2} - 4F_2^i)^{1/2} \pm F_1^i]/2$ for $F_2^i < 0$. Thus, the presence of charged dust grains is responsible for the complete localization of the vortex solutions in the outer as well as in the inner regions of the vortex core.

7.5.2.2 *Cold plasma*

We now present the double vortex solution of equations (7.5.17) and (7.5.18) in the cold plasma approximation. Hence we set $T_j = 0$ and write equations (7.5.17) in the form of equation (7.5.23), while equation (7.5.18) in the stationary frame can be expressed as

$$\hat{D}_\phi\left[(1 - \lambda_e^2\nabla_\perp^2)A_z - \frac{\alpha c}{u}\phi\right] = 0. \qquad (7.5.29)$$

It is easy to verify that equation (7.5.29) is satisfied by

$$(1 - \lambda_e^2 \nabla_\perp^2) A_z - \frac{\alpha c}{u} \phi = 0. \tag{7.5.30}$$

By using equation (7.5.30) one can eliminate $\nabla_\perp^2 A_z$ from equation (7.5.23), obtaining

$$\hat{D}_\phi \left[\nabla_\perp^2 \phi - k_0^2 \phi + \frac{\alpha^2 V_A^2}{c^2 \lambda_e^2} \phi - \frac{\alpha V_A^2}{u c \lambda_e^2} A_z \right] = 0. \tag{7.5.31}$$

A typical solution of equation (7.5.31) is

$$\nabla_\perp^2 \phi + \beta_1 \phi - \beta_2 A_z = C_4 \left(\phi - \frac{u B_0}{c} x \right) \tag{7.5.32}$$

where $\beta_1 = (\alpha^2 V_A^2 / u^2 \lambda_e^2) - k_0^2$, $\beta_2 = \alpha V_A^2 / u c \lambda_e^2$ and C_4 is an integration constant. Eliminating A_z from equations (7.5.30) and (7.5.32) we obtain

$$\nabla_\perp^4 \phi + G_1 \nabla_\perp^2 \phi + G_2 \phi - \frac{C_4 u B_0}{\lambda_e^2 c} x = 0 \tag{7.5.33}$$

where $G_1 = \lambda_e^{-2}[(\alpha^2 V_A^2 / c^2) - 1] - k_0^2 - C_4$ and $G_2 = (C_4 - k_0^2)/\lambda_e^2$. Equation (7.5.33) is similar to equation (7.5.26) and its bounded solutions (similar to equations (7.5.27) and (7.5.28)) exist provided that $u^2(1 + k_0^2 \lambda_e^2) > \alpha^2 V_A^2$ and $u_{sv} > 0$. In the absence of dust, we have $G_2 = 0$ in the outer region ($C_4 = 0$), and the outer region solution of equation (7.5.33) for the dust-free case also has a long tail. The various constants appearing in the section 7.5.2 are contained in Liu and Horton (1986).

Chapter 8

Dust Crystals

8.1 Preamble

In his classic paper Wigner (1938) showed that upon cooling an electron gas can condense and form an ordered crystalline structure, the so-called 'Wigner crystal'. The formation of a Wigner crystal (as well as crystallization of a quantum electron fluid) has been investigated experimentally. The crystal structures were also observed in electrostatic vacuum traps or charged macroparticles and in Paul and Penning traps with Mg and Be ions that are cooled to very low temperatures ($\sim 10^{-3}$ K). A Coulomb crystal is also realized in colloidal suspensions. The colloidal crystals consist of almost mono-dispersive micron-sized particles suspended in an electrolyte where they become charged negatively, having electron charges as high as 10^3–10^4. The particles are screened by ions of both signs in the electrolyte. The Coulomb interaction between the particles renders the formation of a crystal structure energetically more favourable. A strong coupling between the particles takes place at distances less than the screening radius, which in colloidal suspensions is very small. This leads to the result that for crystallization rather high particle number density ($N_{\mathrm{p}} \sim 10^{12}$) is necessary. Consequently, colloidal crystals are usually opaque, hindering an experimental study of their bulk properties. The drawback of the colloidal crystals is that they have a long equilibrium relaxation time, amounting to several weeks.

Condensation or self-organization in a many-particle system occurs provided that the potential due to nearest neighbouring forces is (substantially) larger than the thermal energy of the particles. Assuming that Coulomb collisions are dominant in our plasma, we can express the coupling parameter as

$$\Gamma_j \simeq \frac{q_j^2 n_j^{1/3}}{k_{\mathrm{B}} T_j} \geq 1. \tag{8.1.1}$$

When we consider an electron–ion plasma with multiply charged ions, we have

(Morfill *et al* 1999a)

$$\Gamma_e \simeq \frac{e^2 n_e^{1/3}}{k_B T_e} \tag{8.1.2}$$

and

$$\Gamma_i \simeq \frac{Z_i^2 e^2 n_i^{1/3}}{k_B T_i}. \tag{8.1.3}$$

Now invoking the quasi-neutrality condition ($Z_i n_i = n_e$) and putting $T_e = T_i$, we obtain

$$\Gamma_i \simeq Z_i^{5/3} \Gamma_e \tag{8.1.4}$$

which indicates that the Coulomb coupling increases with the charge state of the ions. The electrons rearrange themselves around the ions to effectively shield the excess charge over the electron Debye radius λ_{De}. Subsequently, the Coulomb interaction potential in equation (8.1.1) has to be modified to include this shielding. We then obtain, instead of equation (8.1.3)

$$\Gamma_i \simeq \frac{Z_i^2 e^2 n_i^{1/3}}{k_B T_i} \exp(-\kappa_i) \tag{8.1.5}$$

where κ_i is the ratio of the inter-ion distance ($\simeq n_i^{-1/3}$) to the electron Debye radius, i.e.

$$\kappa_i = \frac{1}{n_i^{1/3} \lambda_{De}}. \tag{8.1.6}$$

The quasi-neutrality condition along with $\kappa_i \ll 1$ leads to a strong coupling condition (Morfill *et al* 1999a)

$$Z_i > 4\pi \frac{T_i}{T_e} \Gamma_i. \tag{8.1.7}$$

This means that to have a strongly coupled plasma ($\Gamma_i \leq 1$ and $T_i \simeq T_e$), the ions have to be at least fourfold ionized. Furthermore, for plasma condensation ($\Gamma_i > 172$ and $T_i \simeq T_e$), we should have $Z_i > 50$. This is impossible for an ideal electron–ion plasma. The fluctuation in Z_i introduces a corresponding fluctuation in the Coulomb potential between neighbouring ions, which is proportional to $Z_{i1} Z_{i2}$. This will increase the effective thermal energy of the ions and lower Γ_i. Hence, if the distribution of the charge state is too wide, plasma condensation will be prevented. However, the strong coupling condition is easier to satisfy if the plasma ions (or at least one of the plasma particle constituents, e.g. dust) are multiply charged. Thus, as we defined in equation (1.2.17), the shielding of a dust particle by the other plasma particles (electrons and ions) introduces another important parameter (the ratio between the inter-particle separation $a \simeq n_d^{-1/3}$ and the Debye radius λ_D) $\kappa_d \simeq 1/n_d^{1/3} \lambda_D$. Ikezi (1986) considered this screening effect and theoretically predicted the possibility of crystallization of a

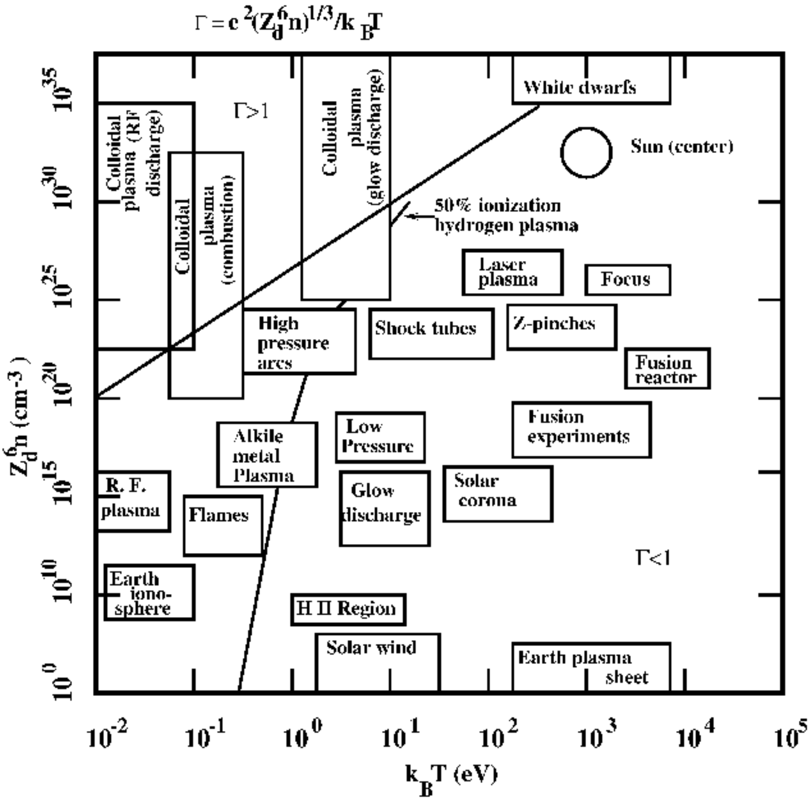

Figure 8.1. Parameter ranges for different kinds of plasmas in the universe. The solid line shows the $\Gamma = 1$ line, which marks the transition from strongly to weakly coupled plasmas (after Morfill *et al* 1999a).

dust subsystem in a non-equilibrium gas discharge plasma when the Coulomb coupling parameter

$$\Gamma_{\rm d} = \frac{Z_{\rm d}^2 e^2 n_{\rm d}^{1/3}}{k_{\rm B} T_{\rm d}} \exp(-\kappa_{\rm d}) \tag{8.1.8}$$

is larger than 172. It turns out that because of the large amount of dust grain charges (higher values of $Z_{\rm d}$) and lower dust temperature, it is more likely to have a significantly large $\Gamma_{\rm d}$ value in a dusty plasma in comparison with the $\Gamma_{\rm i}$ value in an electron–ion plasma. Figure 8.1 depicts the parameter regimes that are applicable to different kinds of weakly and strongly coupled plasmas in space and laboratories (Morfill *et al* 1999a).

About eight years after the publication of Ikezi's paper, the formation of dust crystals were finally observed experimentally in a high-frequency discharge near the lower electrode in the boundary of the near-cathode region (Chu and I 1994, Thomas *et al* 1994, Hayashi and Tachibana 1994, Melzer *et al* 1994). The dust crystals were also observed in the strata of a stationary glow discharge (Fortov *et al* 1997).

The Coulomb dust crystals consist of ordered arrangements of micron-sized dust grains (or rods) in low-temperature partially ionized plasmas. A dusty plasma crystal can have a varied crystal structure, with a lattice constant of the order of a fraction of a millimetre, which makes it possible to observe it under light illumination with the naked eye. The dusty plasma crystals possess many virtues, making them an indispensable diagnostic tool not only for the study of highly non-ideal plasmas, but also for the study of the fundamental properties of crystals. These include simplicity of dust crystal fabrication, observation and easy parameter control, their rapid equilibrium relaxation times and response times to external perturbations, etc. The dusty plasma crystals represent a bridge between atomic or molecular clusters and bulk materials and thus have the potential of elucidating fundamental aspects of micro- and macro-physical material properties. They open new perspectives for creating new materials which can be utilized for advanced schemes of radiation sources. The dusty plasma crystals can be used as macroscopic model systems for studying dislocations, phase transitions, annealing, wave propagation, etc. They also appear to be particularly suited as model systems for 'nanocrystals' with only a few lattice planes. The formation of dusty plasma crystals and their stability, growth, melting, etc may be of importance in plasma processing devices used in micro-electronics fabrications and integrated circuits where 'dust contaminants' inside the reactors play a crucial role in causing defects. The presence of smaller particulates in plasma technology can cause wafer contamination and break-down. Therefore, control of this contamination is of major importance for industry as well.

In this chapter, we discuss the formation of ordered structures of charged macroparticles of various sizes in rf and glow discharges. We study the influence of the discharge parameters on the possibility of the existence of quasi-crystalline structures of dust particles along with the conditions for their formation and destruction. We also consider some important questions related to different forms of potentials associated with the interactions between macroparticles, as well as to the generation of Mach cones in dusty plasmas.

8.2 Properties of Plasma Crystals

The properties of dusty plasma crystals have to be evaluated in relation to other crystal systems. In their review papers, Morfill *et al* (1997, 1999a) have highlighted common properties as well as differences, which are summarized below.

- Contrary to ion crystals, which are produced in traps or storage rings, dusty plasma crystals are easily produced in rf and dc plasma discharges as table-top experiments even at room temperature.

- Characteristic timescales for plasma crystal formation are of the order of one second. This very fast response (about a million times faster than that of colloidal suspensions) allows investigations of dynamical properties which were not accessible before.
- Plasma crystals consist of negatively charged microspheres, ions, and electrons. A Coulomb crystal in a plasma is usually formed around the plasma sheath boundary owing to the transport of particles to a balanced position by the resultant of the electrostatic force, ion drag force and gravity. In space-under microgravity conditions, larger three-dimensional systems can be formed and investigated in much weaker electric fields than those necessary for dust levitation on the ground. This unique situation allows the study of weak processes, namely surface tension, dipolar binding forces, shear effects etc, and controlled conditions for the investigation of critical phenomena. Gravity does not play a role for ion crystals, whereas for colloidal or surface crystals (e.g. Langmuir–Blodgett films) it is compensated by a suitable suspension medium, which may then lead to a heavy damping and a very long equilibration time.
- Plasma crystals are easy to control in laboratories. One can fabricate single hexagonal cells, linear chains, monolayer as well as flat multi-layer dust crystals with several thousand cells. Large fine particle crystals are also formed during the chemical reactions between silane and oxygen gases.
- The vertical positions of dusty plasma crystals in the electrostatic sheath can also be controlled, e.g. by using ultraviolet radiation. This may be quite important for testing the plasma crystal properties under conditions of variable ion flow. In rf discharges, the ions are accelerated towards the lower electrode in the sheath. At the edge of the main plasma this flow velocity is nearly thermal, but closer to the electrode it becomes highly super-thermal.
- Dusty plasma crystals are easily visualized using laser illumination and a CCD camera. In this way, a full three-dimensional monitoring is possible. The easy visualization, including direct storage and computer analysis, significantly enhances our diagnostic capacity with respect to the other crystal systems and makes a number of scientific investigations possible.
- Plasma crystals are easily manipulated by external electromagnetic forces. This opens up the possibility to perform active experiments serving carefully designed purposes.
- The variety of plasma crystals that can be produced is large. The plasma parameters (mass, density, temperature, gas pressure) play a role, as do the rf power input, microsphere size, shape, density and electrical properties.
- The propagation and damping of dust lattice waves (with the frequency of several Hz) is also possible in a plasma crystal, similar to the solid state ionic crystals.
- Compared with liquid colloid systems, strongly coupled dusty systems

have considerably less damping (about a factor of a million—depending on the neutral gas pressure). This allows the investigations of processes on timescales not previously accessible for experimental studies, in particular the investigation of critical phenomena, such as phase transitions.

- A Coulomb crystal in a particle plasma is, however, superior to others in a model of an atomic crystal because of the large lattice constant and strong interactions. The latter include new types of attractive forces (namely associated with wake fields) between like particles.

8.3 Potential of a Test Charge

A dust particle in a plasma usually acquires huge electric charges and interacts with other dust particles. The interaction potential between macroscopic dust particles depends on their own physical parameters and those of the ambient plasma. The question of the correct potential between dust particles is not purely fundamental and still remains open (Konopka *et al* 2000). The plasma flow anisotropies, dipole effects (Lapenta 1999) for larger dust particles and long-range attractive interactions due to wakefield (Nambu *et al* 1995, Shukla and Rao 1996) and shadowing effects (Tsytovich *et al* 1996, Lampe *et al* 2000) may play significant roles. To understand the behaviour of dusty plasmas in complicated situations, however, the results for simple and basic cases are indispensable. We now discuss various forms of the test charge potential in a dusty plasma.

Nearly four decades ago, Neufeld and Ritchie (1955) wrote an elegant paper dealing with the passage of charged particles through a plasma. They calculated the potential distributions of a test particle in an electron plasma with fixed ion background and pointed out their importance to the energy loss. Montgomery *et al* (1968) demonstrated that the far-field potential of a moving test charge in a uniform electron–ion plasma decreases as the inverse cube of the distance r from the test charge. On the other hand, the far-field potential in a collisional electron–ion plasma (Stenflo *et al* 1973) may decay as r^{-2}. The test charge potential calculation has been further extended by Chen *et al* (1973) by incorporating the ion dynamics. The latter allows the possibility of far-wake structures in rarefied plasma flows past charged bodies. The wakefield in an electron–ion plasma has also been found by Nambu and Akama (1985).

We consider the potential of a test particle in a homogeneous, isotropic dusty plasma. The electric potential of a test particle (with charge q_{t}) moving with a constant velocity $\boldsymbol{v}_0$ is (Krall and Trivelpiece 1973)

$$\phi(\boldsymbol{R}, t) = \frac{q_{\mathrm{t}}}{2\pi^2} \lim_{\epsilon \to 0} \int \mathrm{d}\boldsymbol{k} \, \frac{\exp(\mathrm{i}\boldsymbol{k} \cdot \boldsymbol{r} - \epsilon k)}{k^2 D(\boldsymbol{k}, -\boldsymbol{k} \cdot \boldsymbol{v}_0)} \tag{8.3.1}$$

where $\boldsymbol{r} = \boldsymbol{R} - \boldsymbol{v}_0 t$ and $D(\boldsymbol{k}, -\boldsymbol{k} \cdot \boldsymbol{v}_0)$ is the dielectric function of the dusty plasma. Following Montgomery *et al* (1968), the term $\lim_{\epsilon \to 0} \exp(-\epsilon k)$ has been included to ensure proper convergence of the integrals.

The calculation of the dielectric function for longitudinal disturbances in a dusty plasma has been carried out in chapter 4. The dielectric function is of the form

$$D(\boldsymbol{k}, -\boldsymbol{k}\cdot\boldsymbol{v}_0) = 1 + \chi_{\rm e} + \chi_{\rm i} + \chi_{\rm d} + \chi_{\rm q}. \tag{8.3.2}$$

We consider the parameter regimes $kV_{\rm Td} \ll |\boldsymbol{k}\cdot\boldsymbol{v}_0| \ll \nu_{\rm en,in} \ll kV_{\rm Te,Ti}$, and obtain the dielectric susceptibilities as

$$\chi_{\rm e} \approx \frac{k_{\rm De}^2}{k^2}\left[1 - {\rm i}\sqrt{\frac{\pi}{2}}\frac{\boldsymbol{k}\cdot\boldsymbol{v}_0}{kV_{\rm Te}}\left(1+\frac{\nu_{\rm en}}{kV_{\rm Te}}\right)\right] \tag{8.3.3}$$

$$\chi_{\rm i} \approx \frac{k_{\rm Di}^2}{k^2}\left[1 - {\rm i}\sqrt{\frac{\pi}{2}}\frac{\boldsymbol{k}\cdot\boldsymbol{v}_0}{kV_{\rm Ti}}\left(1+\frac{\nu_{\rm in}}{kV_{\rm Ti}}\right)\right] \tag{8.3.4}$$

$$\chi_{\rm d} = -\frac{\omega_{\rm pd}^2}{(-\boldsymbol{k}\cdot\boldsymbol{v}_0 + {\rm i}\nu_{\rm dn})^2} \tag{8.3.5}$$

and

$$\chi_{\rm q} = \frac{k_{\rm q}^2}{k^2}\frac{\nu_1}{(\nu_1 - {\rm i}\boldsymbol{k}\cdot\boldsymbol{v}_0)}. \tag{8.3.6}$$

Let us consider the case with $\omega_{\rm pd} \ll |\boldsymbol{k}\cdot\boldsymbol{v}_0| \ll \nu_1$, so that the dielectric function (8.3.2) takes the form

$$D(\boldsymbol{k}, -\boldsymbol{k}\cdot\boldsymbol{v}_0) \approx 1 + \frac{k_0^2}{k^2} - {\rm i}\sqrt{\frac{\pi}{2}}\sum_{j={\rm e,i}}\frac{\boldsymbol{k}\cdot\boldsymbol{v}_0 k_{{\rm D}j}^2}{k^3 V_{{\rm T}j}}\left(1+\frac{\nu_{j{\rm n}}}{kV_{{\rm T}j}}\right) - {\rm i}\frac{k_{\rm q}^2}{k^2}\frac{\boldsymbol{k}\cdot\boldsymbol{v}_0}{\nu_1} \tag{8.3.7}$$

where $k_0^2 = k_{\rm D}^2 + k_{\rm q}^2 \equiv 1/\lambda_0^2$. Since our test charge is supposed to move very slowly, namely $|\boldsymbol{v}_0| \ll V_{\rm Te,Ti}$, we have from equation (8.3.7)

$$\frac{1}{D(\boldsymbol{k}, -\boldsymbol{k}\cdot\boldsymbol{v}_0)} \approx \frac{k^2\lambda_0^2}{1+k^2\lambda_0^2} + {\rm i}\frac{k^4\lambda_0^4}{(1+k^2\lambda_0^2)^2} \times\left[\sqrt{\frac{\pi}{2}}\sum_{j={\rm e,i}}\frac{\boldsymbol{k}\cdot\boldsymbol{v}_0 k_{{\rm D}j}^2}{k^3 V_{{\rm T}j}}\left(1+\frac{\nu_{j{\rm n}}}{kV_{{\rm T}j}}\right) + \frac{k_{\rm q}^2}{k^2}\frac{\boldsymbol{k}\cdot\boldsymbol{v}_0}{\nu_1}\right]. \tag{8.3.8}$$

Substituting equation (8.3.8) into equation (8.3.1) and carrying out the integration in a straightforward manner, we readily obtain (Shukla and Stenflo 2001b)

$$\phi \approx \frac{q_{\rm t}}{r}\exp\left(-\frac{r}{\lambda_0}\right) + q_{\rm t}v_0\left(\frac{\alpha_2}{r^2}+\frac{\alpha_3}{r^3}+\frac{\alpha_4}{r^4}\right)\cos\gamma \tag{8.3.9}$$

where $\alpha_2 \approx \sum \nu_{j{\rm n}} k_{{\rm D}j}^2\lambda_0^4/V_{{\rm T}j}^2$, $\alpha_3 \approx \sum k_{{\rm D}j}^2\lambda_0^4/V_{{\rm T}j}$, $\alpha_4 \approx k_{\rm q}^2\lambda_0^4/\nu_1$, γ is the angle between $\boldsymbol{r}$ and $\boldsymbol{v}_0$ and $r = |\boldsymbol{R} - \boldsymbol{v}_0 t|$ is the distance between the test charge and the observer. The first term in the right-hand side of equation (8.3.9) is the usual Debye shielding term in which the dusty plasma Debye radius is reduced by a factor $1/(1 + k_q^2 \lambda_D^2)^{1/2}$ due to the consideration of the dust charge fluctuations. The third term in the right–hand side of equation (8.3.9) is the far-field potential of a moving test charge caused by Landau damping, while the second and fourth terms represent the far-field potentials associated with collisions (between neutrals and electrons/ions) and the dust charge perturbations, respectively. For large r ($\gg \lambda_0$), $\exp(-r/\lambda_0)$ can be so small that the first term is smaller than the last three terms in equation (8.3.9).

8.4 Attractive Forces

It is well known that two charged dust particles of similar sign repel each other because of their shielded Coulomb interaction at distances shorter than the dusty plasma Debye radius. This assertion holds as long as the dust grains move faster than the electron thermal speed in which case only the interaction between the grains should be taken into account. This leads to the Debye–Hückel potential energy

$$U_{\rm gg} = \frac{q_{\rm d1} q_{\rm d2}}{r} \exp\left(-\frac{r}{\lambda_{\rm D}}\right) \tag{8.4.1}$$

where $q_{\rm d1}$ and $q_{\rm d2}$ are the charges of two interacting grains. However, in practical experimental conditions, the grains in the plasma are moving so slowly that they always carry their Debye sphere due to the adiabatic condition. Such dust grains are referred to as dressed grains. The interaction potential between two dressed grains contains an attractive part at large distances. Further attraction mechanisms involve the wakefield arising from the coupling between the dust grains and acoustic modes, the asymmetric bombardment of a dust particle by plasma particles which produce shadowing of this dust particle by neighbouring ones, Coulomb scattering of charged plasma particles by charged dust particles, induced dipole moment created around an isolated dust grain, etc. Let us now describe some of these attractive forces.

8.4.1 Electrostatic energy between dressed grains

The electrostatic energy between two dressed grains should include four terms corresponding to that between two grains, two Debye spheres and a grain-Debye sphere (two cross terms). The relevant electrostatic energies are then the sum of $U_{\rm gg}$, $U_{\rm dd}$ and $U_{\rm gd}$. The sum of the electrostatic energies associated with the two Debye and grain-Debye spheres (namely $U_{\rm dd} + U_{\rm gd} \equiv U_{\rm sd}$) can be deduced from the expression (Wang 1999)

$$U_{\rm sd} = -\int_0^{-\infty}\int_0^{2\pi}\int_0^{\pi} \rho^2\,{\rm d}\rho\,\sin\theta\,{\rm d}\theta\,{\rm d}\varphi\,\frac{q_{\rm 1d}\exp(-\rho/r)}{4\pi\rho\lambda_{\rm D}^2}\frac{q_{\rm 2d}\exp(-\rho'/\lambda_{\rm D})}{\rho'} \tag{8.4.2}$$

where $\rho' = \sqrt{r^2 + \rho^2 - 2r\rho\cos\theta}$. Carrying out the integration in equation (8.4.2) we readily obtain

$$U_{\mathrm{sd}} = -\frac{q_{1\mathrm{d}}q_{2\mathrm{d}}}{2\lambda_{\mathrm{D}}}\exp\left(-\frac{r}{\lambda_{\mathrm{D}}}\right). \tag{8.4.3}$$

By adding equations (8.4.1) and (8.4.3) we obtain the total electrostatic energy (Resendes *et al* 1998, Wang 1999)

$$U_{\mathrm{T}} = \frac{q_{1\mathrm{d}}q_{2\mathrm{d}}}{r}\exp\left(-\frac{r}{\lambda_{\mathrm{D}}}\right)\left(1 - \frac{r}{2\lambda_{\mathrm{D}}}\right). \tag{8.4.4}$$

The potential U_{T} is much sharper than the Debye potential near the origin. It has a zero point at $r/\lambda_{\mathrm{D}} = 2$ and attains a minimum value $(-0.0087 q_{1\mathrm{d}}q_{2\mathrm{d}}/\lambda_{\mathrm{D}})$ at $r/\lambda_{\mathrm{D}} \approx 2.732$. Two dressed grains may attract each other when the intergrain distance is greater than $2.732\lambda_{\mathrm{D}}$.

8.4.2 Wake potentials

It has been shown theoretically by Nambu *et al* (1995) that collective interactions involving very low-frequency electrostatic waves in dusty plasmas can give rise to an oscillatory wake potential (Shukla and Rao 1996), which may cause grain attraction. The phonons in a dusty plasma are replaced by the DA and DIA oscillations. The resonance interaction between a test particle and these dusty plasma modes gives rise to an oscillatory wakefield. In the negative potential region of the wakefield, the ions are focused and they provide a possibility for attracting negatively charged dust grains in a linear chain. This proposed mechanism of the charged dust grain attraction is analogous to the Cooper pairing (de Gennes 1966) of electrons which are glued by phononic motions in superconductors.

To calculate the potential of a test charge including the wakefield effects, one should start from equation (8.3.1) by employing a general form of the plasma susceptibility χ_j, as given by equation (5.5.2). However, in order to illustrate the physics of the wakefield, we consider a collisionless dusty plasma.

8.4.2.1 Unmagnetized dusty plasmas

We consider two types of electrostatic responses in a collisionless dusty plasma by ignoring Landau damping. First, we assume the presence of ultra low-frequency DA waves for which the dielectric constant takes the form

$$D(\boldsymbol{k}, \omega) = 1 + \frac{1}{k^2\lambda_{\mathrm{D}}^2} - \frac{\omega_{\mathrm{pd}}^2}{\omega^2}. \tag{8.4.5}$$

Second, we consider the DIA waves for which the dielectric constant reads

$$D(\boldsymbol{k}, \omega) = 1 + \frac{1}{k^2\lambda_{\mathrm{De}}^2} - \frac{\omega_{\mathrm{pi}}^2}{(\omega - \boldsymbol{k}\cdot\boldsymbol{v}_{\mathrm{i0}})^2}. \tag{8.4.6}$$

The inverse of the dielectric response function associated with the DA waves, obtained from equation (8.4.5), is

$$\frac{1}{D(\boldsymbol{k},\omega)} = \frac{k^2\lambda_{\mathrm{D}}^2}{1+k^2\lambda_{\mathrm{D}}^2}\left(1+\frac{\omega_{\mathrm{da}}^2}{\omega^2-\omega_{\mathrm{da}}^2}\right) \tag{8.4.7}$$

where $\omega_{\mathrm{da}} = kC_{\mathrm{D}}/(1+k^2\lambda_{\mathrm{D}}^2)^{1/2}$ is the frequency of the DA waves. Similarly, from equation (8.4.6) we readily obtain

$$\frac{1}{D(\boldsymbol{k},\omega)} = \frac{k^2\lambda_{\mathrm{De}}^2}{1+k^2\lambda_{\mathrm{De}}^2}\left[1+\frac{\omega_{\mathrm{di}}^2}{(\omega-\boldsymbol{k}\cdot\boldsymbol{v}_{\mathrm{i}0})^2-\omega_{\mathrm{di}}^2}\right] \tag{8.4.8}$$

where $\omega_{\mathrm{di}} = kC_{\mathrm{S}}/(1+k^2\lambda_{\mathrm{De}}^2)^{1/2}$ is the frequency of the DA waves.

If we substitute equations (8.4.7) and (8.4.8) into equation (8.3.1), besides the well known Debye–Hückel screening potential of the dusty plasma, namely

$$\phi_{\mathrm{d}} = \frac{q_{\mathrm{t}}}{r}\exp\left(-\frac{r}{\lambda_{\mathrm{D}}}\right) \tag{8.4.9}$$

there appears an additional potential involving collective effects caused by the DA and DIA waves, namely

$$\phi_{\mathrm{c}} = \int \frac{q_{\mathrm{t}}}{2\pi^2k^2}F_{\mathrm{w}}(\boldsymbol{k},\omega)\exp(\mathrm{i}\boldsymbol{k}\cdot\boldsymbol{r})\delta(\omega-\boldsymbol{k}\cdot\boldsymbol{v}_0)\,\mathrm{d}\boldsymbol{k}\,\mathrm{d}\omega \tag{8.4.10}$$

where

$$F_{\mathrm{w}}(\boldsymbol{k},\omega) = \frac{k^2\lambda_{\mathrm{D}}^2\omega_{\mathrm{da}}^2}{(1+k^2\lambda_{\mathrm{D}}^2)(\omega^2-\omega_{\mathrm{da}}^2)} \tag{8.4.11}$$

for the DA waves and

$$F_{\mathrm{w}}(\boldsymbol{k},\omega) = \frac{k^2\lambda_{\mathrm{De}}^2\omega_{\mathrm{di}}^2}{(1+k^2\lambda_{\mathrm{De}}^2)[(\omega-\boldsymbol{k}\cdot\boldsymbol{v}_{\mathrm{i}0})^2-\omega_{\mathrm{di}}^2]} \tag{8.4.12}$$

for the DIA waves. It follows from equations (8.4.11) and (8.4.12) that the potential changes its sign due to the over screening-depending upon whether ω is larger or smaller than ω_{da} or ω_{di}. However, if ω is close to one of these frequencies, there appears a strong resonant interaction between the waves and the test particle. When the latter moves with a velocity slightly larger than the phase velocity of the DA or DIA waves, the potential behind the test particle oscillates as a wake. Thus, the formation of quasi-lattice structures is, in principle, possible because there are regions of attractive and repulsive forces between the particles of the same polarity.

The wake potential arises from the residues at the poles at $\omega = \pm\omega_{\mathrm{da}}, \pm\omega_{\mathrm{di}}$. Thus, following the standard procedure (Nambu and Akama 1985), we can integrate equation (8.4.10) and obtain the non-Coulombian part of the wake potential. For long-wavelength (in comparison with the Debye radius) DA waves with $k_\perp \rho \ll 1$ and $|z - vt| > \lambda_D$, where z and ρ are the cylindrical coordinates of the field point and $k_\perp$ is the wavenumber component perpendicular to the z axis, the wake potential for a near-field approximation is (Nambu *et al* 1995)

$$\phi_c(\rho = 0, z, t) \approx \frac{2q_t}{|z - vt|} \cos\left(\frac{|z - v_0 t|}{L_{da}}\right) \tag{8.4.13}$$

where $L_{da} = \lambda_D (v_0^2 - C_D^2)^{1/2} / C_D$ is the effective length. When we consider the DIA wave case with no ion streaming, we have to replace λ_D and C_D by λ_{De} and C_S respectively. However, in a plasma with streaming ions (namely $\boldsymbol{v}_{i0} = \hat{z} u_{i0}$) we have to use equation (8.4.12). For a static test charge we then obtain (Shukla and Rao 1996, Nambu *et al* 1997)

$$\phi_c(\boldsymbol{x}, t) = \frac{q_t}{2\pi^2 \lambda_{De}^2 M^2} \int \mathrm{d}\boldsymbol{k}_\perp \, \mathrm{d}k_z \, \frac{k^2}{1 + k^2} \frac{\exp\left(-\frac{\boldsymbol{k} \cdot \boldsymbol{x}}{\lambda_{De}}\right)}{(k_z^2 + k_+^2)(k_z^2 - k_-^2)} \tag{8.4.14}$$

where the wavevector is normalized by λ_{De}^{-1}, $M = u_{i0}/C_s$, $k^2 = k_z^2 + k_\perp^2$, and $k_\pm = \pm(1/2)(1 - M^{-2} + k_\perp^2) + [k_\perp^2 M^{-2} + (1 - M^{-2} + k_\perp^2)^2/4]^{1/2}$. The oscillating contribution to the collective potential in equation (8.4.14) arises from the residues at the poles at $k_z = \pm k_-$. The integration over angles in equation (8.4.14) can be carried out by using an expansion in spherical harmonics. The main contribution to the stationary wake potential is

$$\phi_c(\rho = 0, z) = \frac{q_t}{|z|} \frac{\cos(|z|/L_{di})}{1 - M^{-2}} \tag{8.4.15}$$

where $L_{di} = \lambda_{De} |M^2 - 1|^{1/2}$. It emerges from equations (8.4.13) and (8.4.15) that the wake potentials are attractive for $\cos(|z - v_0 t|/L_{da}) < 0$ and $\cos(|z|/L_{di}) < 0$ when the test charge is moving and stationary, respectively. For an effective attraction of stationary grains, the speed of the streaming ions should exceed C_S, which is usually the case in a plasma sheath. The attractive wake potential can dominate over the repulsive (the Debye–Hückel screening) potential because of the rapid decrease of the latter beyond the shielding cloud.

Physically, the force of attraction between two electrons (or negatively charged particulates) is attributed to the polarization of the medium caused by a test electron (negatively charged particulate) which attracts positive ions. The excess positive ions, in turn, attract a neighbouring electron (negatively charged particulate). Thus, the collective interactions involving phonons (DA and DIA waves) play an essential role in the Cooper pair mechanism in superconductivity as well as in dusty plasmas. Lampe *et al* (2000) have carried out computer simulations of the wake potential in a collisionless dusty plasma by using the kinetic ion response. A contour plot of the wake potential is shown in figure 8.2.

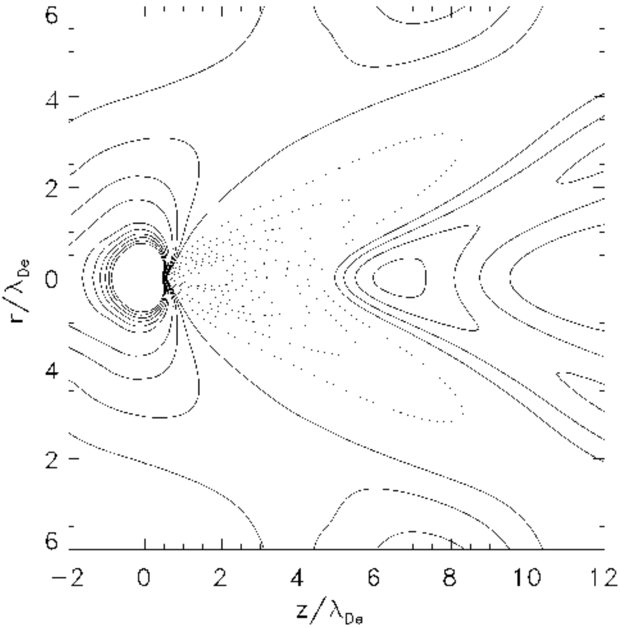

Figure 8.2. A contour plot of $\phi(r, z)$ for $M = 1.5$ and $T_e/T_i = 25$. The grain is at the centre of the left-most node. The solid curves indicate negative potential while the dashed curves indicate positive potential. The positive node just behind the grain is by far the stronger potential well (after Lampe *et al* 2000 and courtesy of G Joyce and M Lampe, NRL, Washington).

8.4.2.2 Magnetized dusty plasmas

Laboratory and astrophysical plasmas are usually held in a static magnetic field. Therefore, it is of practical interest to study the wake potential around a test particle in the presence of electrostatic waves in a dusty magnetoplasma.

Let us consider a dusty plasma embedded in an external magnetic field $\hat{z}B_0$. The dielectric constant of the dusty plasma in the presence of EIC waves with $kV_{Ti}, \omega_{pd}, \omega_{cd}, \omega_{pi}k_z/k \ll \omega \sim \omega_{ci} \ll k_z V_{Te}, \omega_{ce}$ is

$$D(\boldsymbol{k}, \omega) = 1 + \frac{1}{k^2\lambda_{De}^2} - \frac{\omega_{pi}^2}{\Omega^2 - \omega_{ci}^2}\frac{k_\perp^2}{k^2} \tag{8.4.16}$$

where $\Omega = \omega - \boldsymbol{k}\cdot\boldsymbol{v}_{i0}$. It can be readily shown that the reciprocal of the dielectric constant is of the form

$$\frac{1}{D(\boldsymbol{k}, \omega)} \approx \frac{k^2\lambda_{De}^2}{1 + k^2\lambda_{De}^2}\left(1 + \frac{\omega_{ds}^2}{\Omega^2 - \omega_{ci}^2 - \omega_{ds}^2}\right) \tag{8.4.17}$$

where $\omega_{ds} = k_\perp C_S/(1 + k^2\lambda_{De}^2)^{1/2}$. Now, substituting $1/D$ (obtained from equation (8.4.17)) into equation (8.3.1), we have $\phi = \phi_d + \phi_c$, where

$$\phi_d = \frac{q_t}{r}\exp\left(-\frac{r}{\lambda_{De}}\right) \tag{8.4.18}$$

is the wellknown Debye–Hückel screening potential and the potential involving the EIC waves is

$$\phi_c = \frac{q_t}{2\pi^2}\int \frac{\lambda_{De}^2}{(1 + k^2\lambda_{De}^2)}\frac{\omega_{ds}^2}{(\Omega^2 - \omega_{ic}^2)}\delta(\omega - \boldsymbol{k}\cdot\boldsymbol{v}_0)\exp[\mathrm{i}\boldsymbol{k}\cdot(\boldsymbol{r} - \boldsymbol{v}_0 t)]\,\mathrm{d}\boldsymbol{k}\,\mathrm{d}\omega \tag{8.4.19}$$

where $\omega_{ic}^2 = \omega_{ci}^2 + \omega_{ds}^2$. As mentioned earlier, the potential in equation (8.4.19) changes its sign due to the over-screening depending upon whether $|\omega - \boldsymbol{k}\cdot\boldsymbol{v}_{i0}|$ is larger or smaller than ω_{ic}. However, if ω is close to $\boldsymbol{k}\cdot\boldsymbol{v}_{i0} \pm \omega_{ic}$, there appears a strong resonant interaction between the EIC waves and the test particle. When the velocity of the latter or the ion streaming velocity is slightly larger than the phase velocity of the EIC waves, the potential behind the test particle oscillates as a wake. We now present the asymptotic behaviour of the wake potential in two limiting cases.

(i) We assume that the test particle speed is much larger than the ion streaming speed. Thus, the main contribution to the wakefield arises from the residues at the poles at $\omega = \pm\omega_{ic} \approx \omega_{ci} + k_\perp^2 C_S^2/2\omega_{ci}$. Accordingly, we can integrate equation (8.4.19) in a straightforward manner. For long-wavelength (in comparison with λ_{De} and ρ_s) EIC oscillations with $\xi = |z - v_z t| \gg \lambda_{De}, \rho_s$, we obtain the wake potential (Shukla and Salimullah 1996)

$$\phi_c \approx \frac{q_t}{\xi}\frac{\lambda_{De}^2}{\rho_s^2}\cos\left(\frac{\xi}{L_b}\right) \tag{8.4.20}$$

where $L_b = 2v_z/3\omega_{ci}$ is the effective attraction length and v_z is the z component of $\boldsymbol{v}_{i0}$. The maximum upper limit of the perpendicular wavelength is taken to be of the order of ρ_s. Equation (8.4.20) reveals that ϕ_c and L_b are a function of B_0.

(ii) When the test dust particulate is stationary, we have for the wake potential

$$\phi_c = \frac{q_t}{\pi}\frac{\lambda_{De}^2 C_S^2}{v_{iz}^2}\int \mathrm{d}k_z\,\mathrm{d}k_\perp\,\frac{k_\perp^3 J_0(k_\perp\rho)\exp(\mathrm{i}k_z z)}{(k_z^2 - k_0^2)} \tag{8.4.21}$$

where J_0 is the Bessel function of zeroth order, $k_0 = \omega_{ic}/v_{iz}$, v_{iz} is the magnetic field-aligned ion streaming velocity and $k^2\lambda_{De}^2 \ll 1$. We see from equation (8.4.21) that the contribution from the poles $k_z = \pm k_0$ provides the oscillatory non-Coulombian potential given by

$$\phi_c \approx \frac{q_t}{|z|}\frac{\lambda_{De}^2}{\rho_s^2}\cos\left(\frac{|z|}{L_s}\right) \tag{8.4.22}$$

where $L_s \approx 2v_{iz}/3\omega_{ci}$ is the scalelength of the attraction. To derive equation (8.4.22), we have assumed $k_\perp \sim \rho_s^{-1}$. Note that L_s is a function of both the strength of the external magnetic field and of the ion streaming speed.

8.4.3 Dipole–dipole interactions

The charged dust grains are levitated inside the electrode groove because the electrostatic force due to the vertical sheath electric field E_0 is balanced by gravity and ion-stream-induced drag forces. The dipole part of the sheath electric potential (e.g. the last term in the right-hand side of equation (3.2.22)) can produce an electric dipole moment on the particle charge distribution. The dipole moment $\boldsymbol{d}_m$ is the first moment of the charge density function

$$\rho_{dp}(r,\theta) = -\frac{k_D^2}{4\pi}\phi_{dp}(r,\theta) \tag{8.4.23}$$

which is caused by the polarization response of the plasma (Resendes 2000). The potential corresponding to a dipole distribution of charges is

$$\phi_{dp}(r,\theta) = E_0 \frac{k_D^2 r_d^3}{1+k_D r_d} \exp[-k_D(r-r_d)] \left(\frac{1}{k_D r} + \frac{1}{k_D^2 r^2}\right) \cos\theta. \tag{8.4.24}$$

It is obvious from the symmetry condition that $\boldsymbol{d}_m$ must point in the same direction as the sheath electric field. This means that the x and y components of $\boldsymbol{d}_m$ are identically zero. Hence, the z component of the dipole moment is

$$d_{mz} = \int_{vol} z\rho_{dp}(r,\theta)\,dV \equiv 2\pi \int_0^{2\pi}\int_0^{\infty} r^3 \rho_{dp}(r,\theta)\cos\theta\sin\theta\,dr \tag{8.4.25}$$

where $z = r\cos\theta$ is used. Now substituting $\rho_{dp}(r,\theta)$ (obtained from equation (8.4.23)) into equation (8.4.25), and performing the integration, we have (Daugherty *et al* 1993)

$$d_{mz} = r_d^3 E_0 \left[1 + \frac{k_D^2 r_d^2}{3(1+k_D r_d)}\right] \equiv r_d^3 E_{eff} \tag{8.4.26}$$

which indicates that the enhanced electric field E_{eff} is caused by the polarization of the plasma in response to the sheath electric field. For $k_D r_d \ll 1$, the dipole moment simplifies to

$$d_{mz} = r_d^3 E_0 \tag{8.4.27}$$

which is the dipole moment induced in a conducting sphere in vacuum by a uniform field E_0. The polarizability ($= d_{mz}/E_0$) of the particle with its screening cloud is proportional to the volume of the dust particle.

We now calculate the interaction between two particles carrying both charge and a dipole moment. We suppose that two given distributions of charge $\rho_1(\boldsymbol{s})$ and $\rho_2(\boldsymbol{s}')$, which are centered around $\boldsymbol{r}$ and $\boldsymbol{r}'$, respectively, interact through the potential (Lee *et al* 1997)

$$\begin{aligned}\Psi_{\mathrm{md}}(\boldsymbol{r}-\boldsymbol{r}') = {} & \int_{\boldsymbol{s}}\int_{\boldsymbol{s}'} \rho_1(\boldsymbol{s}) V_{\mathrm{c}}(\boldsymbol{s}-\boldsymbol{s}')\rho(\boldsymbol{s}') \\ & \equiv Q_1 Q_2 V_{\mathrm{c}}(\boldsymbol{r}-\boldsymbol{r}') + (Q_1 \boldsymbol{d}_{\mathrm{m}1} - Q_2 \boldsymbol{d}_{\mathrm{m}2}) \cdot \nabla_{\boldsymbol{r}} V_{\mathrm{c}}(\boldsymbol{r}-\boldsymbol{r}') \\ & \quad - (\boldsymbol{d}_{\mathrm{m}1} \cdot \nabla_{\boldsymbol{r}})(\boldsymbol{d}_{\mathrm{m}2} \cdot \nabla_{\boldsymbol{r}}) V_{\mathrm{c}}(\boldsymbol{r}-\boldsymbol{r}') \end{aligned} \tag{8.4.28}$$

where $V_{\mathrm{c}}(r) = r^{-1}\exp(-k_{\mathrm{D}} r)$ represents the monopole potential and $V_{\mathrm{c}}(\boldsymbol{s}-\boldsymbol{s}')$ has been expanded around $\boldsymbol{r}-\boldsymbol{r}'$ to $O(\boldsymbol{s}-\boldsymbol{r})$ and $O(\boldsymbol{s}'-\boldsymbol{r}')$. We have here denoted

$$Q_1 = \int_{\boldsymbol{s}} \rho_1(\boldsymbol{s}) \qquad Q_2 = \int_{\boldsymbol{s}'} \rho_2(\boldsymbol{s}')$$

$$\boldsymbol{d}_{\mathrm{m}1} = \int_{\boldsymbol{s}} (\boldsymbol{s}-\boldsymbol{r})\rho_1(\boldsymbol{s}) \qquad \text{and} \qquad \boldsymbol{d}_{\mathrm{m}2} = \int_{\boldsymbol{s}'} (\boldsymbol{s}'-\boldsymbol{r}')\rho_2(\boldsymbol{s}').$$

Equation (8.4.28) shows that the dipoles enter the picture via interactions of monopole–dipole and dipole–dipole type. When all the particles have the same charge (namely $Q_1 = Q_2 \equiv Q$) and the same dipole moment (namely $\boldsymbol{d}_{\mathrm{m}1} = \boldsymbol{d}_{\mathrm{m}2} = \hat{z} d_{\mathrm{m}z}$), the monopole–dipole interactions cancel exactly. Let us now focus on such a case. To avoid the mathematical complexity, we also ignore the finite dust size effects, which is justified since the ratio of particle size to lattice spacing is much less than unity. Accordingly, equation (8.4.28) takes the form (Lee *et al* 1997)

$$\Psi_{\mathrm{md}} = Q^2 V_{\mathrm{c}}(\boldsymbol{r}-\boldsymbol{r}') - d_{\mathrm{m}z}^2 \frac{\partial^2}{\partial z^2} V_{\mathrm{c}}(\boldsymbol{r}-\boldsymbol{r}'). \tag{8.4.29}$$

The energy of our system including the monopole and dipole–dipole interactions at $\boldsymbol{r}' = 0$ is then

$$U_{\mathrm{m-dd}}(r) = U_{\mathrm{m}}(r) - d_{\mathrm{m}z}^2 \left[z^2 \left(\frac{k_{\mathrm{D}}^2}{r^3} + \frac{3k_{\mathrm{D}}}{r^4} + \frac{3}{r^5} \right) - \frac{k_{\mathrm{D}}}{r^2} - \frac{1}{r^3} \right] \exp(-k_{\mathrm{D}} r) \tag{8.4.30}$$

where $U_{\mathrm{m}}(r) = (Q^2/r)\exp(-k_{\mathrm{D}} r)$ is the monopole contribution and the second term in the right-hand side of equation (8.4.30) represents the dipole–dipole interaction. When the grains are vertically aligned along the dipole (z) axis, we then have

$$U_{\mathrm{va}}(z) = \left[\frac{Q^2 - k_{\mathrm{D}}^2 d_{\mathrm{m}z}^2}{z} - 2d_{\mathrm{m}z}^2 \left(\frac{k_{\mathrm{D}}}{z^2} + \frac{1}{z^3} \right) \right] \exp(-k_{\mathrm{D}} z). \tag{8.4.31}$$

An examination of equations (8.4.30) reveals that dipole–dipole interactions cause dust attraction between two nearest neighbours in the z direction and repulsion

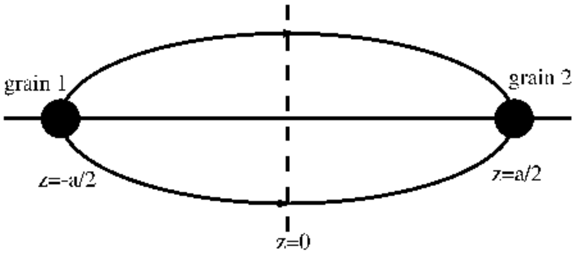

Figure 8.3. The trajectories of ions which intersect both grain 1 and grain 2 (after Lampe *et al* 2000).

in the x–y plane. For $k_{\mathrm{D}}r > 1$, which is true when the interparticle distance is larger than λ_{D}, the leading terms (which are proportional to $z^2k_{\mathrm{D}}^2/r^3$ and $(3z^2k_{\mathrm{D}} - k_{\mathrm{D}}r^2)/r^4$) come from screening. That is, the effect of the dipole–dipole interaction is enhanced by screening. The attractive dipole–dipole force between aligned dipoles plays a very important role (Mohideen *et al* 1998) in intergrain coupling of dielectric grains whose radius is larger than 50 μm.

8.4.4 Shadowing force

There is a continuous bombardment of the ions and electrons onto the dust grain surface. The ions that are absorbed by a grain impart their momentum to the grain. For a single isolated grain in a non-streaming plasma, the ion flow to the grain is spherically symmetric and thus there is on average no net momentum transfer from the ions to the grains. But if there are two isolated grains, and if the ion trajectories are collisionless, some of the ions flowing to grain 2 from the direction of grain 1 will be intercepted by grain 1 and never reach grain 2. As a result, the remaining ions that do reach grain 2 impart a net momentum directed toward grain 1. This represents an effective attractive force between two isolated grains in a plasma due to the shadow of a grain (Tsytovich *et al* 1996). The shadowing effect was used by Lesage (1782) at the end of the 18th century to explain the gravitational attraction, since the net force resulting from this effect goes as r^{-2}.

The calculation of the shadowing force in a dusty plasma is rather complicated because ion trajectories that intercept two grains are strongly curved by Coulomb interaction with the grains (Lampe *et al* 2000). We consider two grains located at $z = \pm a/2$ (as shown in figure 8.3). All such trajectories must cross the $z = 0$ plane with $\rho \leq r_{\mathrm{d}}(1 - 2e\phi_s/m_{\mathrm{i}}v_{\mathrm{i}}^2)^{1/2}$. To estimate the shadowing force, we assume that the angular momentum about grain 1 is conserved when the ion is to the left of the midplane $z = 0$ (i.e. $-a/2 \geq z \leq 0$), and the angular momentum about the grain 2 is conserved when the ion is to the right of the midplane $z = 0$ (i.e. $0 \geq z \leq a/2$). This is a very good approximation when

$a > \lambda_D$ (Tsytovich *et al* 1996, Lampe *et al* 2000). The ions (known as 'shadow ions') which are missing from the otherwise isotropic flux on grain 2 are attracted towards grain 2, and thus gain momentum during the part of their trajectories from the midplane ($z = 0$) to the grain 2 ($z = a/2$), but since the total momentum of these ions and grain 2 is conserved, this portion of the ion momentum is in fact extracted from grain 2 and then returned to the grain 2 at impact. This means that the shadowing force on grain 2 is equal to the negative of the momentum flux carried across the midplane by ions whose trajectories intersect both the grains. Using the assumption mentioned above, the condition for an ion trajectory to intersect the grain 1 and subsequently the grain 2 can be expressed as (Lampe *et al* 2000)

$$\left[1+\left(\frac{a}{2\rho}\right)^2 \tan^2\theta + \left(\frac{a}{\rho}\right)\tan\theta\cos\varphi\right] \leq \left(\frac{r_{\rm d}}{\rho}\right)^2\left(1-\frac{2e\phi_s}{m_{\rm i}v_{\rm i}^2}\right) \tag{8.4.32}$$

where θ is restricted by $0 < \theta < \pi/2$, ρ is the radial position of a point in the midplane ($z = 0$) and $(v_{\rm i}, \theta, \varphi)$ are spherical coordinates (aligned along z) for the velocity of an ion located at $(\rho, z = 0)$. We can write the rate of momentum transfer, i.e. the shadowing force $F_{\rm shadow}$ acting on grain 2 as an integral over the volume of the phase space which satisfies condition (8.4.32). That is, we have (Lampe *et al* 2000)

$$\begin{aligned} F_{\rm shadow} = &-n_{\rm i}\left(\frac{m_{\rm i}}{2\pi k_{\rm B}T_{\rm i}}\right)^{3/2}\int_0^\infty {\rm d}v\, v^2 \exp\left(-\frac{m_{\rm i}v^2}{2k_{\rm B}T_{\rm i}}\right) \\ &\times \int {\rm d}\rho\, 2\pi\rho \int {\rm d}\theta\, \sin\theta m_{\rm i}v^2\cos^2\theta \int {\rm d}\varphi \end{aligned} \tag{8.4.33}$$

where the integrals over ρ, θ and φ are restricted to the regions which satisfy the condition (8.4.32). This quadruple integral can be carried out analytically by considering only the approximation $\theta \ll 1$, so that $\sin\theta \simeq \theta$, $\tan\theta \simeq \theta$ and $\cos\theta \simeq 1$. Using this approximation in equations (8.4.32) and (8.4.33) we have

$$\begin{aligned} F_{\rm shadow} = &-\frac{2m_{\rm i}n_{\rm i}}{\sqrt{\pi}}\left(\frac{m_{\rm i}}{2k_{\rm B}T_{\rm i}}\right)^{3/2}\int_0^\infty {\rm d}v\, v^4 \exp\left(-\frac{m_{\rm i}v^2}{2k_{\rm B}T_{\rm i}}\right) \\ &\times \int_0^{r_{\rm d}\sqrt{1-2e\phi_s/m_{\rm i}v^2}} {\rm d}\rho\, \rho \int_0^{(2r_{\rm d}/a)\sqrt{1-2e\phi_s/m_{\rm i}v^2-\rho^2/r_{\rm d}^2}} {\rm d}\theta\, \theta \int {\rm d}\varphi \end{aligned} \tag{8.4.34}$$

where the integral over φ is limited to the region which satisfies the condition

$$\cos\varphi \leq \frac{r_{\rm d}^2}{\rho\theta a}\left(1-\frac{2e\phi_s}{m_{\rm i}v^2}-\frac{\rho^2}{r_{\rm d}^2}-\frac{\theta^2a^2}{4r_{\rm d}^2}\right). \tag{8.4.35}$$

Now performing all the integrations in equation (8.4.34), we can finally express the shadowing force as (Lampe *et al* 2000)

$$
\begin{aligned}
F_{\text{shadow}} &= -\frac{3\pi}{2}\frac{n_\mathrm{i} k_\mathrm{B} T_\mathrm{i} r_\mathrm{d}^4}{a^2}\left[\left(\frac{e\phi_s}{k_\mathrm{B}T_\mathrm{i}}\right)^2 - \frac{e\phi_s}{k_\mathrm{B}T_\mathrm{i}} + \frac{3}{8}\right] \\
&\simeq -\frac{3}{8}\frac{r_\mathrm{d}^2}{\lambda_{\mathrm{Di}}^2}\frac{Z_\mathrm{d}^2 e^2}{a^2}. \qquad (8.4.36)
\end{aligned}
$$

We note that this is an inverse square force, just like the bare Coulomb force. It is obvious from equation (8.4.36) that the magnitude of the shadowing force is always smaller than the bare Coulomb force by a factor $3r_\mathrm{d}^2/8\lambda_{\mathrm{Di}}^2 \ll 1$. Thus, the attractive shadowing force between two isolated grains could dominate only at large distances, $a \gg \lambda_{\mathrm{Di}}$, where the repulsive electrostatic force is strongly shielded and much weaker than the bare Coulomb force. Furthermore, statistical shadowing from many dust grains in a plasma can substantially reduce the shadowing force.

8.4.5 Experimental verification

Several experiments (Takahashi *et al* 1998, Melzer *et al* 1999, Konopka *et al* 2000, Samsonov *et al* 2001) have been conducted to study short-range repulsive and long-range attractive interactions between charged dust grains. Konopka *et al* (2000) experimentally studied head-on collisions (and the corresponding interaction potential) of two melamine/formaldehyde microspheres (8.9 ± 0.1 μm diameter) in the sheath region of an rf argon discharge at a pressure of 2.7 Pa. The interaction of microspheres with the background plasma leads to particle charging and their levitation in the sheath above the lower electrode where the electric field compensates gravity. To confine the particles horizontally a copper ring with an inner diameter of 40 mm and a height of 2 mm was placed on the rf electrode. It introduced a horizontal confining potential above the lower electrodes, that pushed the particles towards the centre. The particles were illuminated by a thin horizontal laser sheet, and their trajectories were recorded from the top using a high-speed camera. The tip of a Langmuir probe was used to manipulate the particle positions. By analysing the particle trajectories during head-on collisions, Konopka *et al* (2000) showed that the interaction parallel to the sheath boundary can be described by a screened Coulomb potential. The horizontal part of the interaction potential has also been determined for several plasma conditions. There was no evidence for any attractive or dipole part in the experimentally observed interaction potential. Single-particle oscillations have been used to calculate the structure of the particle confining potential (parabolic over an extended region around the experiment axis at the height of the levitated particle) as well as an effective dust charge and a screening length for the particle interaction. Furthermore, Samsonov *et al* (2001) have carried out experimental studies of long-range attractive and repulsive forces between the negatively charged particles of a monolayer plasma crystal and a negatively biased wire. It has been reported that the particles close to the wire were repelled from it electrostatically, while the far particles were attracted due to the drag of the ion flow deflected toward the wire. The ion drag force prevails far from the wire, whereas the electrostatic force is stronger close to the wire.

On the other hand, Takahashi *et al* (1998) and Melzer *et al* (1999) have experimentally confirmed the theoretical prediction of wakefields (Nambu *et al* 1995, 1997, Shukla and Rao 1996) and the associated attractive force between the negatively charged dust particles that form dust crystals and dust molecules. Specifically, Takahashi *et al* (1998) have presented an elegant method for optical manipulations of negatively charged grains in a simple hexagonal crystal. In the optical manipulation technique, the particles are moved by the radiation pressure of laser light. Such a method has also been utilized for trapping and accelerating particles in liquids and gases as well as for cell operations in biophysical fields. Takahashi *et al* (1998) created an rf plasma by supplying currents (at 13.56 MHz) to the electrode. The plasma chamber was filled with methane gas diluted by argon gas at a pressure of 87 Pa. Nanometre-sized carbon powder was put into the methane plasma as seeds for particles. The deposition of hydrogenated amorphous carbon increased the diameter of the seeds up to a few micrometres. Spherical particles of 5.4 μm diameter appear after 30 min growth at an rf power of 2 W. The equilibrium position of the particles was near the plasma–sheath boundary. When the particles were illuminated by an Ar ion laser light (whose wavelength was 488 nm), images of simple hexagonal Coulomb crystals were observed by a video camera that captured the scattered light. The average interparticle distance was 380 μm. The plasma density, the electron temperature, the ion temperature, the particle density and the particle diameter were 10^9 cm^{-3}, 3 eV, 0.03 eV, 10^5 cm^{-3} and 5.4 μm, respectively, where the ordered simple hexagonal structure is formed. The particle charge calculated from the plasma parameters is 6300 electrons.

To manipulate the particles, a semiconductor laser (whose power density is larger than that of the Ar ion laser) of a wavelength of 690 nm was used. When the semiconductor laser light was passed through the transparent particles, the top particles in vertical rows in dust crystals were moved by the radiation pressure along the direction of the light propagation. The particles were then trapped by the force of radiation pressure from the Gaussian beam as optical tweezers. The beam was not different from the one used to move particles. Pushing and trapping of particles showed that the upper particles could cause an attractive force on the lower ones and the lower ones could not cause a force on the upper ones. If there are particles in ion flows of the pre-sheath or sheath region, it is reasonable to suggest that the dust attraction in the experiment could be due to the wake potential (Nambu *et al* 1995, 1997, Shukla and Rao 1996) involving ion flow.

8.5 Formation of Dust Crystals

Let us now discuss the formation of dust crystals under different environments. Most dusty plasma crystal experiments employ rf plasmas and most researchers use experimental set-ups comparable to the so-called GEC (Gaseous Electronics Conference) rf reference cell with some modification (Thomas *et al* 1994) for diagnostics and dust control. However, dc glow discharges (e.g. Chu and I 1994, Fortov *et al* 1997, 1999) have also been used to fabricate dusty plasma crystals.

8.5.1 Thomas *et al*'s experiment

Thomas *et al* (1994) conducted a pioneering experiment to investigate the structure of a cloud of charged dust particles in a weakly ionized plasma. A low-power argon discharge at 2.05 ± 0.05 mbar was formed by applying a 13.56 MHz signal to the lower electrode of a parallel-plate reactor. A schematic drawing of the experimental set-up (with the optical detection system for the investigation of a single layer of particles parallel to the electrodes) is shown in figure 8.4. The individual particles are observed by scattered light. The illumination is provided by a He–Ne laser. The light reflected by the particles is recorded with a CCD–camera through the upper electrode. The particles are mono-dispersive 7 μm diameter spheres made of melamine/formaldehyde. The particles injected into the RF plasma charge up negatively and are suspended electrostatically against the downward force of gravity in the sheath–plasma boundary above the lower electrode. A monolayer of particles would occupy a plane defined by

$$-q_{\mathrm{d}}\frac{\partial \phi_s}{\partial z} = m_{\mathrm{d}} g_z \tag{8.5.1}$$

where ϕ_s is the sheath equipotential associated with the negative dc self-bias on the lower electrode. A multi-layer crystal is subject to the interactions between the layer particles in the lower layers supporting the upper ones. Thus, gravity severely restricts the vertical extent of plasma crystals.

A typical view of the dust crystal from the top is shown in figure 8.5. The structure is clearly very regular and hexagonal, typical for two-dimensional rather than three-dimensional systems. Based on frame-by-frame measurements of the mean particle velocity, the particle kinetic temperature was found to be 310 K, which is close to room temperature. The coupling parameter was estimated to be 3×10^4, taking some typical values for $k_{\mathrm{B}}T_{\mathrm{e}} = 2 \pm 1$ eV, $n_{i0} \sim 10^9$ cm^{-3} and $q_{\mathrm{d}} = (1.2 \pm 0.4) \times 10^4 e$. The crystals form easily at these parameters because the large charge ensures strong inter-particle Coulomb forces, while the neutral gas cools the particles to a low temperature. When the rf power was increased, Thomas *et al* (1994) found that particles moved more violently and many of them appeared to have no equilibrium positions, so the dust clouds qualitatively appeared to be liquid-like.

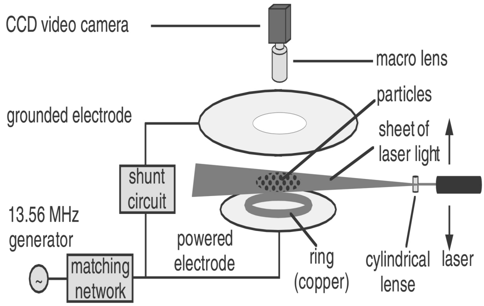

Figure 8.4. A schematic diagram of the experimental set-up for producing dusty plasma crystals (after Morfill *et al* 1997 and courtesy of Professor G Morfill's group, MPE, Garching).

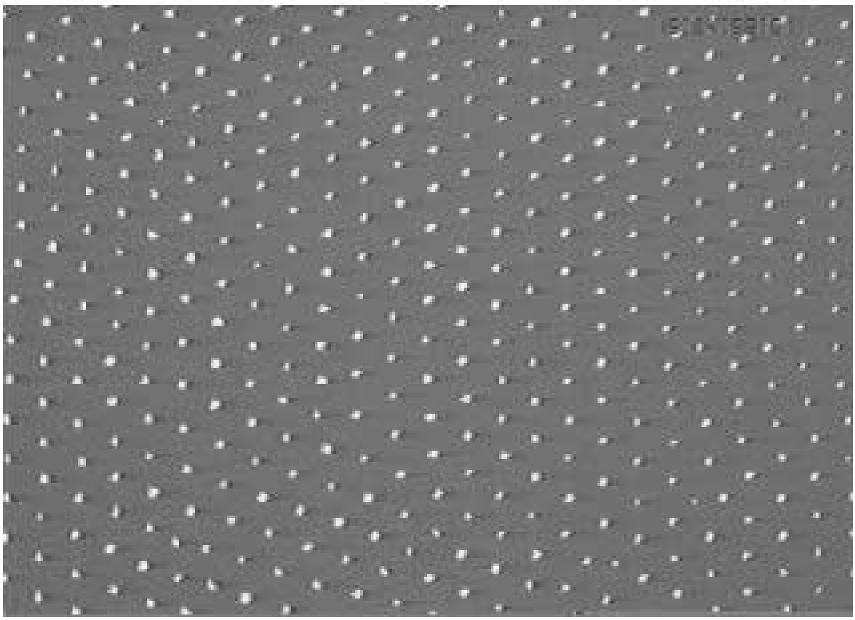

Figure 8.5. A CCD image of a horizontal lattice plane of a dusty plasma crystal (after Morfill *et al* 1997 and courtesy of Professor G Morfill's group, MPE, Garching).

8.5.2 Chu *et al*'s experiments

Chu *et al* (1994) conducted a series of studies on the synthesis of fine silicon oxide (SiO_2) particles in a glow discharge through the chemical reactions between silane and oxygen gases. They found that fine particles can be suspended in the plasma and demonstrated the first observations of Coulomb solid (particles are not mono-dispersive and they are thereby not in a crystal form) and low-frequency dust density waves. Later, Chu and I (1994) designed a cylindrical annular rf dusty plasma trap to generate micrometre SiO_2 particles through gas phase reaction and aggregation by introducing oxygen and silane gases into the lower-pressure rf argon discharge (shown in figure 1.10). A cylindrical system provided a better symmetry and particle trapping and allowed the observation of three-dimensional crystals with fcc, bcc, hcp and hexagonal cylinder structures, as well as chain-like structures normal to the sheath. The formation of crystals with different structures is observed in the groove region at low rf power and 200 mTorr argon pressure. Figure 8.6 shows the pictures of crystals of various shapes. In the solid phase, Chu and I (1994) observed dust crystals with coexisting domains with different orientations and crystals structures. In their system, Chu and I (1994) found fcc, bcc and hcp structures for particles with diameter smaller than 5 μm, but the hexagonal cylindrical crystal usually is the only stable structure for diameter larger than 9 μm. The hexagonal cylindrical crystal is not a stable structure for the isotropic Yukawa-type interaction. The dipole interaction introduced by the ion flow and attractive force due to the DA waves (Rao *et al* 1990, D'Angelo 1995) induced by the ion flow have been proposed to explain the symmetry breaking process. The-chain like structure of the hexagonal cylinder probably comes from the gravity-induced polarization of the screening cloud which introduces dipole interactions.

8.5.3 Molotkov *et al* 's experiment

We have presented experimental observation of plasma crystals that are made up of spherical dust grains. We have seen that as the discharge parameters change, namely the gas pressure decreases or the power increases, the point defects and dislocation emerge and finally the crystals melt. However, it is well known that colloidal solutions, which have much in common with strongly coupled dusty plasmas, show a much broader spectrum of the possible states in the case of strongly asymmetric needle-shaped or cylindrical grains. In this case, liquid phase and several liquid-crystal and crystal phases with different degrees of orientational and positional ordering can be observed. Molotkov *et al* (2000) carried out experimental studies of the formation of ordered structures in a subsystem of 300 μm long cylindrical nylon grains with a mass density of 1.1 g cm^{-3} and diameter of 15 and 7.5 μm in the striations of a dc discharge plasma containing an admixture of neon and hydrogen.

A glow discharge was excited in a cylindrical, vertically positioned glass tube with cold electrodes. The cylindrical grains were placed inside a container positioned at the upper end of the discharge tube. The container was shaken, and the grains fell into the discharge; a portion of them was trapped near the head of one of the striations, where a strong electric field balanced the gravity and the ion drag forces. Evidently, the levitation of dust grains can occur only in the region where the electric force acting on the grain increases towards the cathode.

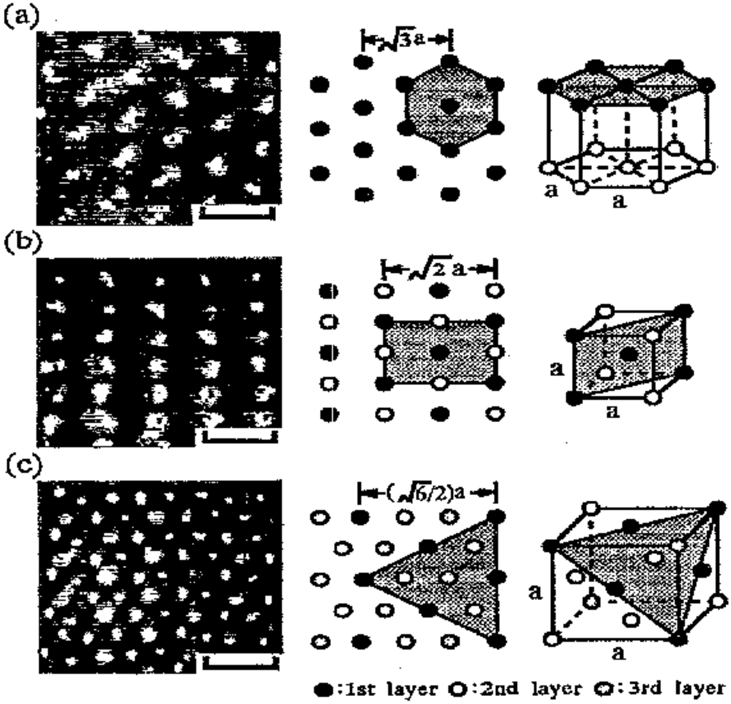

Figure 8.6. Micrographs and sketches of the different crystal structures: (*a*) hexagonal, (*b*) bcc and (*c*) fcc. The central column corresponds to the structures in the micrographs. The graded areas in the sketches are normal to the optical axis. The bars correspond to 0.2 mm (after Chu and I 1994).

Figure 8.7 is the image of the ordered structure of the heavier cylindrical grains (15 μm in diameter) at high gas pressure (0.9 Torr). All the particles lie in the plane perpendicular to the discharge axis and are oriented in a certain direction. At small pressures ($\sim$0.1 Torr), in the lower part of the structures, Molotkov *et al* (2000) observed oscillations with a wavelength of $\sim$1 mm and a frequency of 20–50 Hz. It was noted that for elongated cylindrical grains with $l/2r_\mathrm{d} \gg 1$, the charge-to-mass ratio is larger than for a spherical grain with the same mass, where l is the length of the grain. The charge of a cylindrical grain is (Molotkov *et al* 2000)

$$q_\mathrm{d} = C_l \phi_\mathrm{d} \tag{8.5.2}$$

where

$$C_l = \frac{l}{2} \ln\left(\frac{l}{r_\mathrm{d}}\right). \tag{8.5.3}$$

For a floating surface potential $\phi_\mathrm{d} = 30$ V, $l = 300\ \mu$m, $2r_\mathrm{d} = 15\ \mu$m, we have $q_\mathrm{d} = 7.7 \times 10^5 e$. Then, in order to balance the gravity acting on a nylon grain

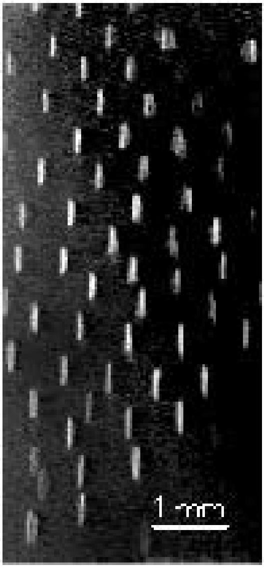

Figure 8.7. The image of the horizontal section of a structure formed from nylon grains of 30 μm in length and 15 μm in diameter. The discharge is excited in a 1:1 neon–hydrogen mixture, the pressure is 0.9 Torr and discharge current is 3.8 mA (after Molotkov *et al* 2000 and courtesy of Professor V Molotkov, RAS, Moscow).

of the given size ($m_{\mathrm{d}}g_z = 5.7 \times 10^{-10}$ N), the electric field required for the dust grain levitation is roughly 30 V cm^{-1}. For a spherical grain, the required field is 1.3 times greater than that for an elongated ($l/2r_{\mathrm{d}} = 20$) grain of the same mass.

The interaction energy of two grains positioned in parallel can be obtained by integrating the elementary interaction energy over the lengths of both grains. For the experimentally observed mutual position of two grains, this energy is about 10^5 eV, which is much larger than the kinetic energy of the dust grains ($\sim$0.3 eV). The importance of the ion flow force for the alignment of cylindrical dust grains has been discussed by Mendonça *et al* (2001).

8.5.4 Phase transitions

The phase transitions of a plasma crystal to its liquid and gas phases are important and modern topics in physics of dusty plasmas and is briefly explained. The melting of plasma crystals can be limited in two different ways (Thomas and Morfill 1996, Morfill *et al* 1999a).

(1) By increasing the rf power to the plasma: This increases the plasma number density and therefore decrease the Debye length λ_{D}. Accordingly, the particles come closer together. Observations show that the diameter of

the dust cloud shrinks (the number of particles remains constant) and the mobility of the particle increases. This could be due to the change in the electric potential distribution between the electrodes or the increase of the ion flow to the electrodes due to the increase of the dc self-bias, or both.

(2) By decreasing the neutral gas pressure: This, in turn, leads to an adjustment of the plasma parameters and correspondingly the experimental parameters that determine the value of Γ_d. The pressure variation provides an easy way to control the plasma conditions through the melting phase transitions.

The melting experiment, as conducted by Thomas and Morfill (1996), starts from the well-established crystalline state at 0.42 mbar pressure. Transitions are followed by continuous lowering of the gas pressure. Both structural and dynamical properties of the plasma crystal are determined. By analysing translational and bond orientational correlation functions, random and systematic particle motions, self-diffusion, viscosity and interaction cross sections, the following states have been identified during the melting transition.

- **Crystalline**: This is characterized by a hexagonal horizontal lattice structure and a vertical alignment.
- **Flow and floe:** This is characterized by the coexistence of islands of ordered crystalline structure (floes) and systematic directed particle motion (flows). Translational and orientational order have decreased significantly.
- **Vibrational:** This is characterized by a return to a more orientationally ordered structure and diminishing flow regions. Vibrational amplitudes, thermal energy and vertical migration of particles increase. The translational order continues to decrease.
- **Disordered:** This is characterized by collisions, complete vertical and horizontal migration. At this stage there is no discernible translational or orientational order: the thermal energy increases to approximately 200 times the room temperature, and the Coulomb coupling parameter is of the order of unity or less.

The lattice structure of a crystal is usually characterized by two quantities—the 'pair correlation function', which describes the translational order from one lattice plane to the next, etc and the 'bond correlation function', which describes the orientational order of the crystalline structure around a given origin. The pair correlation function for the crystalline, liquid and disordered states usually shows many sharp peaks corresponding to the various lattice plane locations in a hexagonal lattice and demonstrates the long-range order in the system. The bond correlation function tests the sixfold symmetry in bond angles to the nearest neighbours (for a hexagonal lattice).

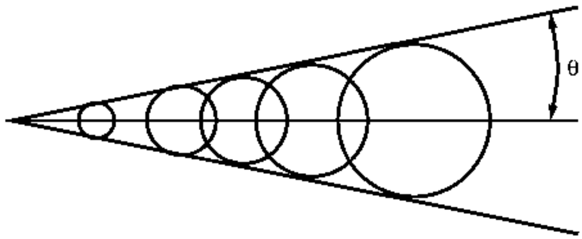

Figure 8.8. A sketch of a Mach cone produced by a supersonic disturbance moving to the left. The cones are a superposition of spherical (or circular in two dimensions) waves generated by the moving disturbance. The semivertex angle θ is the angle between the cone axis and the wave front (after Samsonov *et al* 2000).

8.6 Mach Cones

It is well known that an object moving with supersonic speed in a dispersive medium creates a pressure disturbance that is not felt upstream from the object. The cone that confines the disturbance is called a Mach cone. The latter is well known in gas dynamics. They are produced, for example, by bullets and supersonic jet planes. If the perturbing object moves straight at a constant velocity U, it creates expanding waves that are circular in two dimensions and spherical in three dimensions. The superposition of these waves forms a cone, which is displayed in figure 8.8. The Mach angle θ, defined as a semivertex angle of the cone, is determined by the geometry as

$$\theta = \sin^{-1}\left(\frac{1}{M}\right) \tag{8.6.1}$$

where $M = U/C_{\mathrm{A}}$ is the Mach number of the supersonic object and C_{A} is the acoustic (sound) speed in the undisturbed medium.

Mach cones are also known to occur in solid matter (Cheng *et al* 1994). In an elastic medium surrounding a fluid-filled borehole, spontaneously launched surface waves propagating along the fluid–solid boundary excite P and S waves propagating into the bulk solid. The interference between P and S waves forms Mach cones. The wavefront of the surface wave acts as the supersonic object as its speed is typically higher than the P and S waves.

Ship waves have an appearance similar to Mach cones. The latter are also known as the 'Kelvin wedge' that forms behind a ship in deep water. Here a moving point-like disturbance generates either gravity or capillary waves on the fluid surface. These deep water strongly dispersive surface waves (Crapper 1984) are responsible for multiple Mach cone structures.

Besides the above-mentioned Mach cones on human scales, Mach cones also occur on astronomical scales (e.g. the Earth's magnetotail formed by interaction with the solar wind) and microscopic scales (e.g. Cherenkov radiation created by rapidly moving elementary charge). Furthermore, in their classic papers, Havnes *et al* (1995, 1996b) theoretically predicted the existence of super DA Mach cones in dusty plasmas that are relevant to planetary rings. For example, they pointed out that the possibility of Mach cone formation behind a boulder that streams in the bath of small dust grains in planetary rings and interstellar space. In order for the Mach cone to arise, the relative speed (V_B) between a boulder and the small dust grain orbital speed should be larger than the DA speed C_D. The circular V-shaped wake front will be formed behind the boulder with an opening angle 2μ, where

$$\mu = \sin^{-1}\left(\frac{C_D}{|V_B|}\right). \tag{8.6.2}$$

Measurements of the half-opening angle will, therefore, provide additional information on dusty plasma conditions since the DA velocity can be determined when the relative velocity V_B is known. Havnes *et al* (1996b) suggested that this method can also be applied under laboratory conditions if a suitable controlling disturbance can be made.

Recently, the phenomenon of multiple Mach cones, which are due to the super DA particle motion through the dust crystal, are found to occur in a strongly coupled dusty plasma. Samsonov *et al* (1999, 2000) conducted experiments to observe Mach cones in two-dimensional Coulomb crystals. In the rf plasma discharge of Samsonov *et al* (1999) an electron–ion plasma was created by applying a 13.56 MHz rf voltage to a horizontal Al electrode 230 mm in diameter. A grounded upper ring and a vacuum vessel served as the other electrode. The plasma was weakly ionized krypton at 0.05 mbar. Approximately 10 000 polymer spheres of diameter 8.9 ± 0.1 μm and density 1.51 g cm^{-3} were introduced in the plasma above the electrode. The rf input power of 50 W produced self-bias potential ($= -245$ V) that was sufficient to levitate the negatively charged dust grains at $z = 6.5$ mm above the lower electrode in the sheath. In the radial direction, a gentle ambipolar electric field trapped the particles in a disc approximately 40 mm in diameter. The disc is termed as a two-dimensional 'lattice layer', with a particle spacing 256 μm, and very little particle motion.

Mach cones in the lattice layer were produced by a charge (another microsphere, or possibly an agglomeration of several microspheres) moving parallel to the crystal plane with nearly constant speed U_c (a few cm s^{-1} perturbed the positions of the dust grains), creating a wake in the lattice that could be imaged with a digital camera. Observations revealed multiple V-shaped Mach cones, which are exhibited in figure 8.9. Dubin (2000) presented a linear theory for multiple structures in the wake that are qualitatively similar to those observed in experiments. Specifically, Dubin suggested that the multiple wake structures are a consequence of the strongly dispersive nature of compressional phonons in a two-dimensional lattice. For the Debye–Hückel interaction potential, the excited

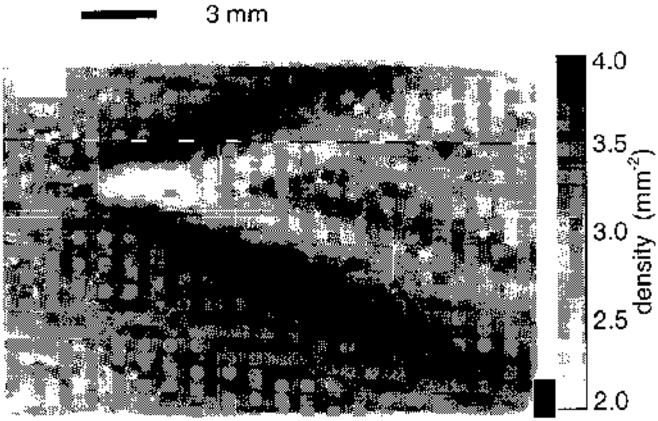

Figure 8.9. Experimentally observed multiple Mach cones (after Samsonov *et al* 1999 and courtesy of D Samsonov, MPE, Garching).

waves have the dispersion relation (Dubin 2000)

$$\omega^2(k) = \frac{2\pi n_{\mathrm{D}} q_{\mathrm{d}0}^2}{m_{\mathrm{d}}} \frac{k}{(1 + k^2\lambda_{\mathrm{D}}^2)^{1/2}} \tag{8.6.3}$$

which satisfy the Mach condition $\omega/k = C_{\mathrm{p}} = U_{\mathrm{c}} \sin\theta_{\mathrm{c}}$. Here n_{D} is the density per unit area of the dust. For $k^2\lambda_{\mathrm{D}}^2 \gg 1$ equation (8.6.3) takes the form $\omega^2 = (2\pi n_{\mathrm{D}} q_{\mathrm{d}0}^2/m_{\mathrm{d}})k$, which is identical to that for deep water surface gravity waves with $2\pi n_{\mathrm{D}} q_{\mathrm{d}0}^2/m_{\mathrm{d}}$ taking the role of gravity. However, equation (8.6.3) exhibits that the phonon phase speed strongly depends on the wavevector $\boldsymbol{k}$, namely $V_{\mathrm{p}} = V_{\mathrm{p}}(k)$. Hence different excited waves would travel at different propagation angle $\theta_{\mathrm{c}}(\boldsymbol{k})$. Phase mixing of the various excited dispersive waves causes constructive and destructive interference. As a result, along a line defined by some opening angle ψ_{c}, there are specific wavenumbers $\boldsymbol{k} = \boldsymbol{k}_0(\psi_{\mathrm{c}})$ that are dominant. In general, the propagation angle θ_{c} for these wavenumbers is not equal to ψ_{c}. These wavenumbers form the observed multiple wakes. The long-wavelength features of the wake in a two dimensional Coulomb crystal should resemble the Kelvin wedge behind a moving ship in deep water.

8.7 Particle Dynamics: Microgravity Experiment

The parabolic flight campaigns and sounding rocket experiments as well as dc glow discharges and UV-induced dusty plasmas provide the possibility of investigating the dynamics and trajectories of dust particles under microgravity conditions. The results of parabolic flights (short-time μg-flights of 25 s each) are summarized by Thomas *et al* (2001). The experiments use a symmetrically

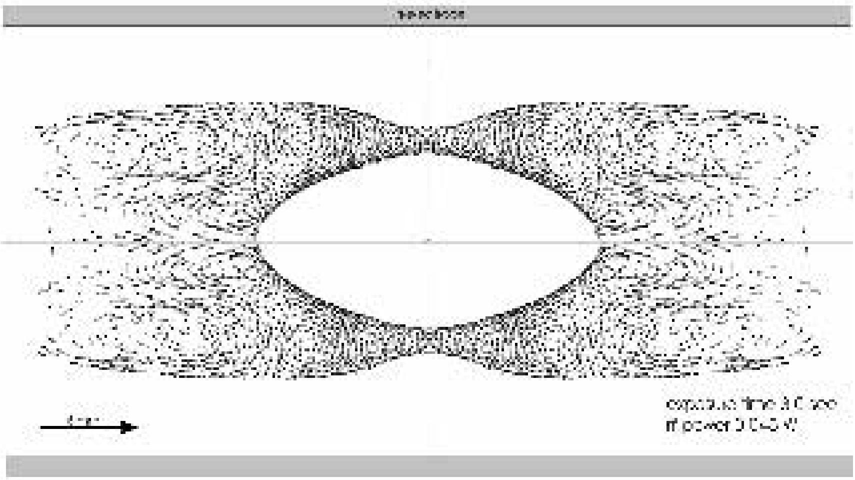

Figure 8.10. The particle trajectories grey-coded from the beginning of the trajectory to its end from the TEXUS 35 microgravity experiment (after Thomas *et al* 2001 and courtesy of Dr H Thomas, MPE, Garching).

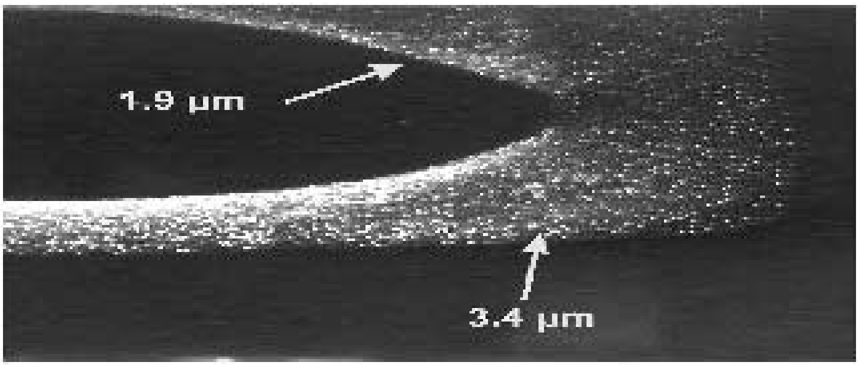

Figure 8.11. The original image of the distribution of the particles of different sizes (3.4 and 1.9 μm) in the plasma chamber (after Thomas *et al* 2001 and courtesy of Dr H Thomas, MPE, Garching).

driven rf discharge containing inert gases (argon, krypton and xenon). Particles of four different sizes (1.2, 1.9, 3.4 and 6.9 μm) were injected into the plasma through a specially designed dispenser incorporated in each of the electrodes. They are charged in a few tens of microseconds and then interact with each other and with the global electric field. A typical distribution of particles is shown in figure 8.10, which shows the particle motion between the two rf electrodes.

The centre of the system is particle free (Morfill *et al* 1999b). In the absence of gravity, charged dust microspheres are usually embedded in the main plasma, where the major bulk forces are the electric force ($q_d\boldsymbol{E}_0$), the thermophoretic force ($\boldsymbol{F}_T$), the ion drag force ($\boldsymbol{F}_{di}$), as well as the neutral density gradient ($\boldsymbol{F}_{gr}$) and drag ($\boldsymbol{F}_{dn}$) forces. The forces $\boldsymbol{F}_T$ and $\boldsymbol{F}_{di}$ are directed outwards, while $q_d\boldsymbol{E}_0$ and F_{gr} are directed into the main plasma. The frictional force slows the particles down. The ratio between the outward and inward forces determine the position of the particulates. For particles in the micron size range, it is possible, under microgravity conditions, to adjust the system largely force free provided that $\boldsymbol{F}_T$ and $\boldsymbol{F}_{di}$ are held small. For the conditions of figure 8.10, the outward force far exceeds the inward force, and consequently, there appears a void in the centre (Morfill *et al* 1999b). The void seems to be created by the thermophoretic force rather than by the ion drag force; the latter is at least one order of magnitude smaller than $\boldsymbol{F}_T$ under microgravity conditions. The behaviour of a mixture of particles of two different sizes was investigated during the parabolic flights. Under microgravity conditions, particle clouds of two different particle sizes become separated vertically due to their different charge-to-mass ratios. Only for those cases where the charge-to-mass ratio is identical for particles of different sizes, it is possible to obtain levitation at the same height. Under microgravity the mass of the particles no longer matters but the size of the particles still has to be taken into consideration, because the electric force acting on the microparticles depends on their size (namely $q_d\boldsymbol{E}_0 \propto r_d$). It is obvious that the different particle sizes separate. The smaller particles are found closer to the centre of the discharge, the larger ones further outwards from the centre where the electric field is stronger. The two microparticle clouds are separated by a sharp boundary, as shown in figure 8.11. It should be stressed that the microgravity experiments are being carried out on board the International Space Station (ISS) under microgravity conditions. We hope that the forthcoming ISS data will reveal new aspects of numerous collective processes caused by charged macroparticles in a dusty plasma.

References

Alexandrov A F, Bogdankevich L S and Rukhadze A A 1984 *Principles of Plasma Electrodynamics* (Berlin: Springer)
Alfvén H 1954 *On the Origin of the Solar System* (Oxford: Clarendon)
Allen J E 1992 *Phys. Scripta* **45** 497
Annaratone B M *et al* 2001 *Phys. Rev.* E **63** 036406
Avinash K and Shukla P K 1994 *Phys. Lett.* A **189** 470
Backhouse T W 1885 *Meteorol. Mag.* **20** 133
Baines M J, Williams I P and Asebiomo A S 1965 *Mon. Not. R. Astron. Soc.* **130** 63
Barkan A, D'Angelo N and Merlino R L 1994 *Phys. Rev. Lett.* **73** 3093
Barkan A, Merlino R L and D'Angelo N 1995a *Phys. Plasmas* **2** 3563
Barkan A, D'Angelo N and Merlino R L 1995b *Planet. Space Sci.* **43** 905
——1996 *Planet. Space Sci.* **44** 239
Barnes M S, Keller J H, Foster J C, O'Neill J A and Coultas D K 1992 *Phys. Rev. Lett.* **68** 313
Benkadda S, Tsytovich V N and Vegra A 1995 *Commun. Plasma Phys. Control. Fusion* **16** 321
Bernhardt P A, Ganguli G, Kelley M C and Swartz W E 1995 *J. Geophys. Res.* **100** 23811
Bharuthram R and Shukla P K 1992a *Planet. Space Sci.* **40** 973
——1992b *Planet. Space Sci.* **40** 647
Birk G T, Kopp A and Shukla P K 1996 *Phys. Plasmas* **3** 3564
Bittencourt J A 1986 *Fundamentals of Plasma Physics* (Oxford: Pergamon)
Bliokh P, Sinitsin V and Yaroshenko V 1995 *Dusty and Self-Gravitational Plasmas in Space* (Dordrecht: Kluwer Academic)
Boeuf J P and Punset C 1999 *Dusty Plasmas: Physics, Chemistry and Technological Impacts in Plasma Processing* ed A Bouchoule (New York: Wiley) pp 1–76
Bouchoule A 1999 *Dusty Plasmas: Physics, Chemistry and Technical Impacts in Plasma Processing* ed A Bouchoule (New York: Wiley) pp 305–96
Brattli A, Havnes O and Melandsø F 1997 *J. Plasma Phys.* **58** 691
Charney J G 1947 *Geophys. Publ.* **17** 17
Chen F F 1965 *Plasma Diagnostic Techniques* ed R H Huddlestone and S L Leonard (New York: Academic) ch 4
Chen F F 1974 *Introduction to Plasma Physics* (New York: Plenum)
——1995 *Phys. Plasmas* **2** 2164
Chen L, Langdon A B and Lieberman M A 1973 *J. Plasma Phys.* **9** 311
Chen X and Tao X 1992 *Plasma Chem. Plasma Proc.* **12** 345
Cheng N, Zhu Z, Cheng C and Toksöz M 1994 *Geophysical Prospecting* **42** 303

Cho J Y N and Kelley M C 1993 *Rev. Geophys.* **31** 243

Chow V W, Mendis D A and Rosenberg M 1993 *J. Geophys. Res.* **98** 19 065

Chow V W and Rosenberg M 1995 *Planet. Space Sci.* **43** 613

Chu J H, Du J B and I L 1994 *J. Phys. D: Appl. Phys.* **27** 296

Chu J H and I L 1994 *Phys. Rev. Lett.* **72** 4009

Crapper G 1984 *Introduction to Water Waves* (Chichester: Harwood)

D'Angelo N 1965 *Phys. Fluids* **8** 1748

——1990 *Planet Space Sci.* **38** 1143

——1995 *J. Phys. D: Appl. Phys.* **28** 1009

——1997 *Phys. Plasmas* **4** 3422

——1998 *Phys. Plasmas* **5** 3155

D'Angelo N, Barkan A and Merlino R L 1996 *The Physics of Dusty Plasmas* ed P K Shukla, D A Mendis and V W Chow (Singapore: World Scientific) pp 93–101

D'Angelo N and Song B 1990 *Planet. Space Sci.* **38** 1671

de Angelis U 1992 *Phys. Scripta* **45** 465

de Angelis U and Forlani A 1998 *Phys. Plasmas* **5** 3068

de Gennes P G 1966 *Superconductivity of Metals and Alloys* (New York: Benjamin)

Daugherty J E, Porteous R K and Graves D B 1993 *J. Appl. Phys.* **73** 1617

Daugherty J E and Graves D B 1995 *J. Appl. Phys.* **78** 2279

Draine B T and Salpeter E E 1979 *Astrophys. J.* **231** 77

Dubin D H E 2000 *Phys. Plasmas* **7** 3895

Elskens Y, Resendes D P and Mendonça J T 1997 *Phys. Plasmas* **4** 4210

Epstein P S 1924 *Phys. Rev.* **23** 710

Farokhi B, Shukla P K, Tsintsadze N L and Tskhakaya D D 1999 *Phys. Lett.* A **264** 318

——2000 *Phys. Plasmas* **7** 814

Feuerbacher B, Willis R F and Fitton B 1973 *Astrophys. J.* **181** 102

Fortov V E, Kharpak A G, Kharpak S A, Molotkov V I, Nefedov A P, Petrov O F and Torchinsky V M 2000 *Phys. Plasmas* **7** 1374

Fortov V E, Molotkov V I, Nefedov A P and Petrov O F 1999 *Phys. Plasmas* **6** 1759

Fortov V E, Nefedov A P, Torchinsky V M, Molotkov V I, Petrov O F, Samarian A A, Lipaev A M and Khrapak A G 1997 *Phys. Lett.* A **229** 317

Fried B D and Conte S D 1961 *The Plasma Dispersion Functions* (New York: Academic)

Gallagher A 2000 *Phys. Rev.* E **62** 2690

Garscadden A, Ganguly B N, Haaland P D and Williams J 1994 *Plasma Sources Sci. Technol.* **3** 239

Glanz J 1994 *Science* **264** 28

Goertz C K 1989 *Rev. Geophys.* **27** 271

Goertz C K and Morfill G E 1983 *Icarus* **53** 219

Gradsteyn I S and Ryzhik I M 2000 *Tables of Integrals, Series and Products* 6th edn (New York: Academic) translated from the Russian by *Scripta Technika*

Guerra R and Mendonça J T 2000 *Phys. Rev.* E **62** 1190

Haaland P 1990 *J. Chem. Phys.* **93** 4066

Hamaguchi S and Farouki R T 1994 *Phys. Rev.* E **49** 4430

Harwit M 1988 *Astrophysical Concepts* (New York: Springer) p 405

Hasegawa A 1975 *Plasma Instabilities and Nonlinear Effects* (Berlin: Springer)

——1985 *Adv. Phys.* **34** 1

Hasegawa A and Mima K 1978 *Phys. Fluids* **21** 87

Havnes O 1988 *Astron. Astrophys.* **193** 309

Havnes O, Aslaksen T K and Melandsø F 1990 *J. Geophys. Res.* **95** 6581

Havnes O, Goertz C K, Morfill G E, Grün E and Ip W 1987 *J. Geophys. Res.* **92** 2281

Havnes O, Li F, Aslaksen T, Hartquist T W, Li F, Melandsø F, Morfill G E and Nitter T 1995 *J. Geophys. Res.* **100** 1731

Havnes O, Li F, Melandsø F, Aslaksen T, Hartquist T W, Morfill G E, Nitter T and Tsytovich V N 1996b *J. Vac. Sci. Technol.* A **14** 525

Havnes O, Nitter T, Tsytovich V N, Morfill G E and Hartquist T W 1994 *Plasma Sources Sci. Technol.* **3** 448

Havnes O, Trøim J, Blix T, Mortensen W, Næsheim L I, Thrane E and Tønnesen 1996a *J. Geophys. Res.* **101** 10 839

Hayashi H and Tachibana K 1994 *Japan. J. Appl. Phys.* **33** 804

Hill J R and Mendis D A 1981a *Moon and Planets* **24** 431

——1981b *Can. J. Phys.* **59** 897

Hollenstein C 2000 *Plasma Phys. Control. Fusion* **42** R93

Homann A, Melzer A, Peters S and Piel A 1997 *Phys. Rev.* E **56** 7138

Hopkins M B and Lawler J F 2000 *Plasma Phys. Control. Fusion* **42** B189

Horányi M and Goertz C K 1990 *Astrophys. J.* **361** 105

Howard J E, Dullin H R and Horányi M 2000 *Phys. Rev. Lett.* **84** 3244

Howard J E, Horányi M and Stewart G R 1999 *Phys. Rev. Lett.* **83** 3993

Ichimaru S 1973 *Basic Principles of Plasma Physics: A Statistical Approach* (London: Benjamin)

——1982 *Rev. Mod. Phys.* **54** 1017

Ichimaru S, Iyetomi H and Tanaka S 1987 *Phys. Rep.* **149** 91

Iizuka S, Saeki K, Sato N and Hatta Y 1985 *J. Phys. Soc. Japan* **54** 146

Ikezi H 1986 *Phys. Fluids* **29** 1764

Ishihara O 1998 *Phys. Scripta* T **75** 79

Ishihara O and Sato N 2001 *IEEE Trans. Plasma Sci.* **29** 000

Ivlev A V, Konopka U and Morfill G E 2000a *Phys. Rev.* E **62** 2739

Ivlev A V, Süterlin R, Steinberg V, Zuzic M and Morfill G E 2000b *Phys. Rev. Lett.* **85** 4060

Jana M R, Sen A and Kaw P K 1993 *Phys. Rev.* E **48** 3930

Jonker J H 1952 *Phillips Res. Rep.* **7** 1

Karpman V I 1975 *Nonlinear Waves in Dispersive Media* (Oxford: Pergamon)

Kaw P K and Sen A 1998 *Phys. Plasmas* **5** 3552

Kim K Y 1983 *Phys. Lett.* A **97** 45

Kim K and Kim D 2000 *J. Appl. Phys.* **87** 269

Kittel C 1956 *Introduction to Solid State Physics* (New York: Wiley) ch 11

Klimontovich Y L 1982 *Kinetic Theory of Nonideal Gases and Nonideal Plasmas* (New York: Pergamon)

Knudsen M 1991 *Ann. Phys.* **34** 593

Konopka U, Morfill G E and Ratke L 2000 *Phys. Rev. Lett.* **84** 891

Kortshagen U and Bhandarkar U 1999 *Phys. Rev.* E **60** 887

Krall N A and Trivelpiece A W 1973 *Principles of Plasma Physics* (New York: McGraw-Hill)

Kushner M 1988 *J. Appl. Phys.* **63** 2532.

Laframboise J G and Parker L W 1973 *Phys. Fluids* **16** 629

Lampe M, Joyce G, Ganguli G and Gavrishchaka 2000 *Phys. Plasmas* **7** 3851

Landau L D and Lifshitz E M 1960 *Mechanics* (Oxford: Pergamon)

——1971 *The Classical Theory of Fields* (Oxford: Pergamon)
——1989 *Statistical Physics* (Oxford: Pergamon)
Lapenta G 1999 *Phys. Plasmas* **6** 1442
Larichev V D and Reznik G M 1976 *Dokl. Akad. Nauk. USSR* **231** 1077
Laroussi M, Sayler G S, Glascock B B, McCurdy B, Pearce M E, Bright N G and Malott C M 1999 *IEEE. Trans. Plasma Sci.* **27** 34
Lee H C, Chen D Y and Rosenstein B 1997 *Phys. Rev.* E **56** 4596
Lesage G L 1782 *Nouveaux Memoires de l'Academie Royales des Sciences et des Belles—Letters* (Berlin: Springer) p 404
Liu J and Horton W 1986 *J. Plasma Phys.* **36** 1
Liu J, Juan W, Hsu J, Huang Z and I L 1999 *Plasma Phys. Control. Fusion* **41** A47
Luo Q Z, D'Angelo N and Merlino R L 1999 *Phys. Plasmas* **6** 3455
——2000 *Phys. Plasmas* **7** 2370
——2001 *Phys. Plasmas* **8** 31
Ma J X and Liu J 1997 *Phys. Plasmas* **4** 253
Ma J X and Yu M Y 1994a *Phys. Rev.* E **50** R2431
——1994b *Phys. Plasmas* **1** 3520
——1995 *Phys. Plasmas* **2** 1343
Madigan M, Martinko J M and Parker J 1997 *Biology of Microorganisms* 8th edn (Englewood Cliffs, NJ: Prentice-Hall)
Mahmoodi J, Shukla P K, Tsintsadze N L and Tskhakaya D D 2000 *Phys. Rev. Lett.* **84** 2626
Mamun A A 1998 *Phys. Scripta* **57** 258
Mamun A A 1999 *Astrophys. Space Sci.* **268** 443
Mamun A A, Cairns R A and Shukla P K 1996a *Phys. Plasmas* **3** 702
——1996b *Phys. Plasmas* **3** 2610
Mamun A A and Shukla P K 2000 *Phys. Plasmas* **7** 3499
Maxon S and Viecelli J 1974 *Phys. Rev. Lett.* **32** 4
Melandsø F 1996 *Phys. Plasmas* **3** 3890
Melandsø F, Aslaksen T and Havnes O 1993 *Planet. Space Sci.* **41** 321
Melandsø F and Shukla P K 1995 *Planet. Space Sci.* **43** 635
Melzer A, Homann A, Piel A and Schweigert I V 1998 in *Physics of Dusty Plasmas: Seventh Workshop* ed M Horányi, S Robertson and B Walch (New York: American Institute of Physics) pp 167–74
Melzer A, Schweigert I V and Piel A 1999 *Phys. Rev. Lett.* **83** 3194
Melzer A, Trottenberg T and Piel A 1994 *Phys. Lett.* A **191** 301
Mendis D A 1991 *Astrophys. Space Sci.* **176** 163
Mendis D A 1997 *Advances in Dusty Plasmas* ed P K Shukla, D A Mendis and T Desai (Singapore: World Scientific) pp 3–19
Mendis D A and Axford W I 1974 *Rev. Earth Planet Sci.* **2** 419
Mendis D A and Horányi M 1991 *Cometary Plasma Processes* ed A J Johnston (Washington, DC: Geophys. Mongr. No. 6) p 17
Mendis D A, Houpis H L F and Hill J R 1982 *J. Geophys. Res.* **87** 3449
Mendis D A and Rosenberg M 1994 *Ann. Rev. Astron. Astrophys.* **32** 419
Mendis D A, Rosenberg M and Azam F 2000 *IEEE. Trans. Plasma Sci.* **28** 1304
Mendonça J T, Shukla P K and Bingham R 2001 *Phys. Lett.* A **282** 288
Mendoza-Briceño C A, Russel S M and Mamun A A 2000 *Planet. Space Sci.* **48** 599
Merlino R L, Barkan A, Thompson C and D'Angelo N 1998 *Phys. Plasmas* **5** 1607

Messenger S 2000 *Nature* **404** 968
Meuris P 1997 *Planet. Space Sci.* **45** 1171
Meyer-Vernet N 1982 *Aston. Astrophys.* **105** 98
Mikhailovskii A B 1974 *Theory of Plasma Instabilities: Instabilities of a Homogenous Plasma* vol 1 (New York: Consultants Bureau)
Miswa T, Ohno N, Asano K, Sawai M, Takamura S and Kaw P K 2001 *Phys. Rev. Lett.* **86** 1219
Miyamoto K 1980 *Plasma Physics for Nuclear Fusion* (Cambridge, MA: MIT)
Mohideen U, Rahman H U, Smith M A, Rosenberg M and Mendis D A 1998 *Phys. Rev. Lett.* **81** 349
Molotkov V I, Nefedov A P, Putsyl'nik M Y, Torchinsky V M, Fortov V E, Kharpak A G and Yoshino K 2000 *JETP Lett.* **71** 102
Molotkov V I, Nefedov, Torchinskii V M, Fortov V E and Khrapak A G 1999 *Sov. Phys.–JETP* **89** 477
Montgomery D, Joyce G and Sugihara R 1968 *Plasma Phys.* **10** 681
Morfill G E and Thomas H 1996 *J. Vac. Sci. Technol.* A **14** 490
Morfill G E, Thomas H M, Konopka U and Zuzic M 1999a *Phys. Plasmas* **6** 1769
Morfill G E, Thomas H M, Konopka U, Rothermal H, Zuzic M, Ivlev A and Goree J 1999b *Phys. Rev. Lett.* **83** 1598
Morfill G E, Thomas H M and Zuzic M 1997 *Advances in Dusty Plasmas* ed P K Shukla, D A Mendis and T Desai (Singapore: World Scientific) pp 99–142
Nakamura Y, Bailung H and Shukla P K 1999 *Phys. Rev. Lett.* **83** 1602
Nambu M and Akama H 1985 *Phys. Fluids* **28** 2300
Nambu M, Vladimirov S V and Shukla P K 1995 *Phys. Lett.* A **230** 40
——1997 *Advances in Dusty Plasmas* ed P K Shukla, D A Mendis and T Desai (Singapore: World Scientific) pp 449–52
Nayfeh A H and Mook D T 1979 *Nonlinear Oscillations* (New York: Wiley)
Neufeld J and Ritchie R H 1955 *Phys. Rev.* **98** 1635
Nitter T 1996 *Plasma Sources Sci. Technol.* **5** 93
Northrop T G 1992 *Phys. Scripta* **45** 17
Northrop T G and Birmingham T J 1990 *Planet. Space Sci.* **38** 319
Nunomura S, Miswa S, Ohno N and Takamura S 1999 *Phys. Rev. Lett.* **83** 1970
Ockert M E, Cuzzi J N, Porco C C and Johnson T V 1987 *J. Geophys. Res.* **92** 14 696
Okuda H and Dawson J M 1973 *Phys. Fluids* **16** 408
Opik E J 1956 *Irish Astron. J.* **4** 84
Pandey B P, Avinash K and Dwivedi C B 1994 *Phys. Rev.* E **49** 5599
Perrin J and Hollenstein C 1999 *Dusty Plasmas: Physics, Chemistry and Technical Impacts in Plasma Processing* ed A Bouchoule (New York: Wiley) pp 77–180
Perrin J, Molinas-Mata P and Belenguer P 1994 *J. Phys. D: Appl. Phys.* **27** 2499
Pieper J B and Goree J 1996 *Phys. Rev. Lett.* **77** 3137
Pokhotelov O A, Onishchenko O G, Shukla P K and Stenflo L 1999 *J. Geophys. Res.* **104** 19 797
Popel S I, Yu M Y and Tsytovich V N 1996 *Phys. Plasmas* **3** 4313
Prabhuram G and Goree J 1996 *Phys. Plasmas* **3** 1212
Rahman H U, Mohideen U, Smith M A, Rosenberg M and Mendis D A 2001 *Phys. Scripta* T **89** 186
Rao N N 1993 *J. Plasma Phys.* **49** 375
Rao N N and Shukla P K 1994 *Planet. Space Sci.* **42** 221

Rao N N, Shukla P K and Yu M Y 1990 *Planet Space Sci.* **38** 543
Resendes D P 2000 *Phys. Rev.* E **61** 793
Resendes D P, Mendonça J T and Shukla P K 1998 *Phys. Lett.* A **239** 181
Resendes D P and Shukla P K 2001 *Phys. Scripta* T **89** 101
Rosenberg M 1993 *Planet. Space Sci.* **41** 229
Rosenberg M 1996 *J. Vac. Sci. Technol.* A **14** 631
Rosenberg M and Kalman G 1997 *Phys. Rev.* E **56** 7166
Rosenberg M and Mendis D A 1992 *J. Geophys. Res.* **97** 773
——1995 *IEEE Trans. Plasma Sci.* **23** 177
Rosenberg M, Mendis D A and Sheehan D P 1996 *IEEE Trans. Plasma Sci.* **24** 1422
——1999 *IEEE Trans. Plasma Sci.* **27** 239
Rosenberg M and Shukla P K 1998 *Phys. Plasmas* **5** 3786
——2000 *J. Geophys. Res.* **105** 23 135
Roth R M, Spears K G and Wong G 1985 *Appl. Phys. Lett.* **46** 253
Sagdeev R Z 1966 *Reviews of Plasma Physics* vol 4, ed M A Leontovich (Consultants Bureau, New York) p 23
Salimullah M and Shukla P K 1999 *Phys. Plasmas* **6** 686
Samaryan A A, Chernyshev A V, Nefedov A P, Petrov O F, Mikhailov Y M, Mintsev V B and Fortov V E 2000 *Sov. Phys.–JETP* **90** 817
Samsonov D and Goree J 1999 *Phys. Rev.* E **59** 1047
Samsonov D, Goree J, Ma Z W, Bhattacharjee A, Thomas H M and Morfill G E 1999 *Phys. Rev. Lett.* **83** 3649
Samsonov D, Goree J, Thomas H M and Morfill G E 2000 *Phys. Rev.* E **61** 5557
Samsonov D, Ivlev A V, Morfill G E and Goree J 2001 *Phys. Rev.* E **63** 025401(R)
Sato N, Uchida G, Kaneko T, Shimizu S and Iizuka S 2001 *Phys. Plasmas* **8** 1786
Sato N, Uchida G, Ozaki R, Iizuka S and Kamimura T 2000 *Frontiers in Dusty Plasmas* ed Y Nakamura, T Yokota and P K Shukla (Singapore: World Scientific) pp 329–36
Schamel H 1972 *Plasma Phys.* **14** 905
——1975 *J. Plasma Phys.* **13** 129
——1986 *Phys. Rep.* **140** 161
Schamel H, Das N and Rao N N 2001 *Phys. Plasmas* **8** 671
Schmidt M J and Gary S P 1973 *J. Geophys. Res.* **78** 8261
Selwyn G S 1993 *Japan. J. Appl. Phys.* **32** 3068
Selwyn G S, Singh J and Bennet R S 1989 *J. Vac. Sci. Technol.* A **7** 2758
Shukla P K 1992 *Phys. Scripta* **45** 504
——1996 *The Physics of Dusty Plasmas* ed P K Shukla, D A Mendis and V W Chow (Singapore: World Scientific) pp 107–21
——1999 *Phys. Lett.* A **252** 340
——2000a *Phys. Rev.* E **61** 7249
——2000b *Phys. Lett.* A **268** 100
——2000c *Phys. Rev. Lett.* **84** 5328
——2000d *Phys. Plasmas* **7** 1044
——2001 *Phys. Plasmas* **8** 1791
Shukla P K and Mamun A A 2001 *IEEE Trans. Plasma Sci.* **29** 221
Shukla P K and Morfill G M 1999 *Phys. Scripta* T **82** 119
Shukla P K and Rahman H U 1996 *Phys. Plasmas* **3** 430
Shukla P K and Rao N N 1996 *Phys. Plasmas* **3** 1770
Shukla P K and Rosenberg M 1999 *Phys. Plasmas* **6** 1038

Shukla P K and Salimullah 1996 *Phys. Plasmas* **3** 3858
Shukla P K and Silin V P 1992 *Phys. Scripta* **45** 508
Shukla P K and Stenflo L 1999 *Nonlinear MHD Waves and Turbulence* ed T Passot and P L Sulem (Berlin: Springer) pp 1–30
——2001a *IEEE Trans. Plasma Sci.* **29** 267
——2001b *Plasma Phys. Rep.* **27** 904
Shukla P K and Varma R K 1993 *Phys. Fluids* B **5** 236
Shukla P K and Verheest F 1999 *Astrophys. Space Sci.* **262** 157
Shukla P K, Yu M Y and Bharuthram R 1991 *J. Geophys. Res.* **96** 21343
Singh S V and Rao N N 1997 *Phys. Lett.* A **235** 164
Slattery W L, Doolen G D and DeWitt H E 1980 *Phys. Rev.* A **21** 2087
Smith B A *et al* 1981 *Science* **212** 163
——1982 *Science* **215** 504
Sodha M S and Guha S 1971 *Advances in Plasma Physics* vol 4, ed A Simon and W B Thompson (New York: Wiley) pp 219–309
Spitzer L Jr 1977 *Physical Processes in the Interstellar Medium* (New York: Wiley)
Stenflo L 1981 *Phys. Rev.* A **23** 2730
——1985 *J. Geophys. Res.* **90** 5355
Stenflo L and Shukla P K 2000 *Phys. Plasmas* **7** 3472
Stenflo L, Shukla P K and Yu M Y 2000 *Phys. Plasmas* **7** 2731
Stenflo L, Yu M Y and Shukla P K 1973 *Phys. Fluids* **16** 450
Sternglass E J 1954 *Sci. Pap. 1772* (Pittsburgh, PA: Westinghouse Research Laboratory)
Takahashi K, Oishi T, Shimomami K, Hayashi Y and Nishino S 1998 *Phys. Rev.* E **58** 7805
Talbot L, Cheng R K, Schefer R W and Willis D R 1980 *J. Fluid Mech.* **101** 737
Thomas E Jr and Watson M 2000 *Phys. Plasmas* **7** 3194
Thomas G E 1991 *Rev. Geophys.* **29** 553
Thomas H, Goldbeck, Hagel T, Ivlev A V, Konopka U, Morfill G E, Rothermel H, Süterlin and Zuzic M 2001 *Phys. Scripta* T **89** 16
Thomas H and Morfill G E 1996 *Nature* **379** 806
Thomas H, Morfill G E, Demmel V, Goree J, Feuerbacher B and Möhlmann D 1994 *Phys. Rev. Lett.* **73** 652
Thompson C, Barkan A, Merlino R L and D'Angelo N 1999 *IEEE Trans. Plasma Sci.* **27** 146
Tonks L and Langmuir I 1929 *Phys. Rev.* **33** 195
Tskhakaya D and Shukla P K 2001 *Phys. Lett.* A **279** 456
Tskhakaya D, Shukla P K and Tsintsadze N L 2001 *Sov. Phys.–JETP* **93** 301
Tsytovich V N 1997 *Sov. Phys.–Usp.* **40** 53
Tsytovich V N and Havnes O 1993 *Commun. Plasma Phys. Control. Fusion* **15** 267
Tsytovich V N, Khodataev Y K and Bingham R 1996 *Commun. Plasma Phys. Control. Fusion* **17** 249
Vanossi A, Rasmussen K Ø, Bishop A R, Malomed B A and Bortolani V 2000 *Phys. Rev.* E **62** 7353
Varma R K, Shukla P K and Krishan V 1993 *Phys. Rev.* E **47** 3612
Verheest F 2000 *Waves in Dusty Plasmas* (Dordrecht: Kluwer Academic)
Vranješ J, Petrović D and Shukla P K 2001 *Phys. Lett.* A **278** 231
Walch B, Horányi M and Robertson S 1994 *IEEE Trans. Plasma Sci.* **22** 97
Wang L 1999 *Commun. Mod. Phys. C: Commun. Plasma Phys. Control. Fusion* **1** 117
Wang X, Bhattacharjee A and Hu S 2001 *Phys. Rev. Lett.* **86** 2569

Washimi H and Taniuti T 1966 *Phys. Rev. Lett.* **17** 996
Weiland J 2000 *Collective Modes in Inhomogeneous Plasma* (Bristol: IOP Publishing)
Whiddington R 1912 *Proc. R. Soc.* A **86** 360
Whipple E C 1981 *Rep. Prog. Phys.* **44** 1197
Whipple E C, Northrop T G and Mendis D A 1985 *J. Geophys. Res.* **90** 7405
Wigner E 1938 *Trans. Faraday Soc.* **34** 678
Winske D, Gary S P, Jones M E, Rosenberg M, Mendis D A and Chow V W 1995 *Geophys. Res. Lett.* **22** 2069
Winske D and Jones M E 1994 *IEEE Trans. Plasma. Sci.* **22** 454
Winske D and Rosenberg M 1998 *IEEE Trans. Plasma Sci.* **26** 92
Winter J 1998 *Plasma Phys. Control. Fusion* **40** 1201
——2000 *Phys. Plasmas* **7** 3862
Wurden G A, Wurden A J and Gladstone I M 1999 *IEEE Trans. Plasma Sci.* **27** 142
Xu W, Song B, Merlino R L and D'Angelo N 1992 *Rev. Sci. Instrum.* **63** 5266
Yanagita S 1977 *Astrophys. Space Sci.* **49** L11
Zakharov V E 1972 *Sov. Phys.–JETP* **35** 908